

UNCLASSIFIED

NDIA

NDIA



**Proceedings of the 7th Annual TARDEC Ground Vehicle  
Survivability Symposium (U)**

March 26 - 28, 1996  
Naval Postgraduate School, Monterey, CA

Volume I - Unclassified Session Papers

**DISTRIBUTION STATEMENT A**  
Approved for Public Release  
Distribution Unlimited

May 1996

DTIC QUALITY INSPECTED 4

19991116 099

UNCLASSIFIED

# UNCLASSIFIED

## TABLE OF CONTENTS SESSION PAPERS

	Vol. No.	Page No.
<b><u>OPENING SESSION</u></b>		<b>1</b>
<b>King Auditorium, Tuesday, March 26, 1996</b>		
8:30 A.M. <b>Call to Order</b> Dr. Jack G. Parks, Symposium Chairman and Associate Director for Survivability, U.S. Army Tank-automotive and Armaments Command Research, Development & Engineering Center (TARDEC)	None Submitted	
8:35 A.M. <b>Welcome</b> RADM Marsha J. Evans, Superintendent, Naval Postgraduate School (Invited)	None Submitted	
8:45 A.M. <b>Presentation of Survivability Award</b> Dr. Jack Parks	None Submitted	
9:00 A.M. <b>TACOM Perspective</b> Dr. Richard E. McClelland, Technical Director, U.S. Army TARDEC	None Submitted	
9:25 A.M. <b>Keynote</b> Dr. Kenneth J. Oscar, Deputy Assistant Secretary of the Army for Procurement	None Submitted	
9:50 A.M. <b>Industry Perspective</b> Dr. Kenneth M. Krall, Vice President - Advanced Programs & Technology, Loral Vought Systems Corporation	Vol. 1	.3
10:45 A.M. <b>Armored Systems Modernization (ASM) Survivability Perspective</b> Major General John E. Longhouser, Program Executive Officer, Armored Systems Modernization	None Submitted	
11:10 A.M. <b>Armored Force Modernization ICT Initiatives</b> LTC Wilfred E. Irish, Chief Maneuver Division, Director of Combat Developments, U.S. Army Armor Center	Vol. 1	17
11:35 A.M. <b>Tactical Vehicle Survivability Perspective</b> Mr. John D. Weaver, Project Manager (PM), Light Tactical Vehicles	Vol. 1	45
12:00 A.M. <b>Defense Supply Center Business Processes - Meeting Customer Needs</b> COL Joseph M. Dougherty, USA, Director Land-Based Weapon System Group, Defense Supply Center	Vol. 1	57

UNCLASSIFIED



# UNCLASSIFIED

## HIT AVOIDANCE THREATS & COUNTERMEASURES SESSION

King Auditorium, Tuesday, March 26, 1996

Session Chairman: Mr. Thomas C. Winant, United Defense, L.P.

1:30 P.M.	<b>Threat Based Expert System Survivability</b> J. Mosley, PM, Armored Systems Integration	Vol. 1	89
1:50 P.M.	<b>ATGM Signatures Collected During Recent Live Firings</b> B. Figler & T. Spera Loral Infrared & Imaging Systems	Vol. 2	
2:10 P.M.	<b>Threat Exploitation of a LBR Anti-Tank Guided Missile</b> S. Buchholz & J. Kuppenheimer, Sanders, A Lockheed Martin Company	Vol. 2	
2:30 P.M.	<b>Effects of Countermeasures on Rocket Launched THSM</b> W. K. Fluhler, Dynetics, Inc. and C. Ochoa, U.S. Army Research Laboratory	Vol. 2	
3:10 P.M.	<b>Field Test Results of a Prototype Directed Missile Countermeasure Devise (DMCD)</b> J. O'Connell & J. Winter, U.S. Army CECOM and P. Kennedy, Northrop Grumman Corporation	Vol. 2	
3:30 P.M.	<b>ATIRCM Ground Vehicle ATGM Demonstration</b> S. Kelley, Sanders, A Lockheed Martin Company	None Submitted	
3:50 P.M.	<b>Focused Dispatch AWE-Laser Warning Receiver Demonstration</b> MAJ (P) J. Della Silva, PM, Armored Systems Integration	Vol. 1	101
4:10 P.M.	<b>The High Angular Resolution Laser Irradiance Detection System (HARLIDS)</b> M. Altman, Loral Infrared & Imaging Systems and A. Cantin, Defense Research Establishment Valcartier	Vol. 1	117
4:30 P.M.	<b>Integrated Survivability Analyses (ISA) - Real Time</b> B. Fatemi & J. Wiederrich, United Defense, L.P.	Vol. 1	127

## ARMOR TECHNOLOGY SESSION

Glasgow Auditorium, Tuesday, March 26, 1996

Session Chairman: Mr. Val Horvatich, United Defense, L.P.

1:30 P.M.	<b>Foreign Armor Protection Developments</b> W. Gstattenbauer, National Ground Intelligence Center	Vol. 2	
1:50 P.M.	<b>Ceramics for Armors - A Material System Perspective</b> E. Rapacki, U.S. Army Research Laboratory and G. Hauver, P. Netherwood, & R. Benck, Dynamic Science, Inc.	Vol. 1	139
2:10 P.M.	<b>CAV Armor Results</b> D. Schade, United Defense, L.P.	None Submitted	
2:30 P.M.	<b>Reactive and Semi-Reactive Armor for the Defeat of Advanced Medium Caliber Kinetic Energy Penetrators</b> D. Hackbarth & M. Zoltoski, U.S. Army Research Laboratory	Vol. 2	

UNCLASSIFIED

# UNCLASSIFIED

2:50 P.M.	<b>Ballistic Development of High Density Tungsten Carbide Ceramics</b> W. Gooch & M. Burkin, U.S. Army Research Laboratory and R. Palicka, C. Shih, & H. Mortensen, Cercom Inc.	Vol. 1	149
3:30 P.M.	<b>Evaluation of Hot Isostatically Pressed Targets as Armor Modules</b> G. Bulmash & W. Bruchey, U.S. Army Research Laboratory, W. Gurwell, Pacific Northwest National Laboratory, and B. Leavy, Dynamic Sciences, Inc.	Vol. 2	
3:50 P.M.	<b>Maturation of a Ceramic Faced Armor System</b> J. Drotleff, United Defense, L.P.	None Submitted	
4:10 P.M.	<b>Reactive Appliqué Armor for the Bradley M2A2/M3A2 Vehicle System</b> S. Chico, U.S. Army Armament Research, Development & Engineering Center (ARDEC)	Vol. 1	159
4:30 P.M.	<b>Anti-Mine Armor Development for the XM1114 HMMWV</b> D. Malone, O'Gara-Hess and Eisenhardt Armoring Company, D. Stevens, Southwest Research Institute, and J. Weaver, PEO-TMV-TACOM	Vol. 1	165

## ACTIVE PROTECTION AND SENSOR FUSION SESSION

King Auditorium, Wednesday, March 27, 1996

Session Chairman: Mr. Frank Stoddard, TRW Space and Electronics Group

8:30 A.M.	<b>Foreign Active Protection Systems</b> J. Shriver & R. Aiken, National Ground Intelligence Center	Vol. 2	
8:50 A.M.	<b>N-TAPS, A Near Term, Low Cost Active Protection System</b> F. Stoddard, J. Wehling, J. Lin, & D. Smith, TRW Space and Electronics Group	Vol. 1	177
9:10 A.M.	<b>Evaluation of Robust Kill Mechanism Designs fo Close-In Active Protection Systems</b> H. Fan, R. Fong, & S. Tang, U.S. Army Armament Research, Development and Engineering Center	Vol. 2	
9:30 A.M.	<b>SLID-Short Range Missile System for Active Defense</b> R. Hersh, Raytheon Electronic Systems	Vol. 1	187
10:10 A.M.	<b>Rockwell SLID Active Defense System</b> B. Fraser & W. Blonshine, Rockwell International Corporation	Vol. 1	197
10:30 A.M.	<b>A Tank-Mounted Active CM to Foreign Precision Guided Munitions (FPGM)</b> D. Walker, Office of the Test Director Precision Guided Weapons Countermeasures Test and Evaluation Directorate	Vol. 2	
10:50 A.M.	<b>Application of Fuzzy Logic to Threat Tracking in Active Defense Systems</b> S. Majowski, Delco Systems Operations	Vol. 1	205
11:10 A.M.	<b>An Approach to Prioritizing the ADHPM Threat</b> W. K. Fluhler, Dynetics, Inc.	Vol. 2	

# UNCLASSIFIED

# UNCLASSIFIED

11:30 A.M.	<b>The IDS Commander's Decision Aid (CDA)</b> R. Yannone, Sanders, A Lockheed Martin Company	Vol. 2	
<b><u>TOP ATTACK/MINE PROTECTION TECHNOLOGY SESSION</u></b>			213
Glasgow Auditorium, Wednesday, March 27, 1996			
Session Chairman: Mr. John Rowe, Office of the Program Manager, Armored Systems Integration			
8:30 A.M.	<b>Initiation Based Selectable Mode Shaped Charge and EFP Warheads</b> E. Baker, R. Campbell, & C. Chin, U.S. Army, Armament, Research, Development, and Engineering Center (ARDEC)	Vol. 1	215
8:50 A.M.	<b>EFP and Shaped Charge Concrete Penetration</b> E. Baker, T. Vuong, & B. Fuchs, U.S. Army, Armament, Research, Development, and Engineering Center (ARDEC)	Vol. 1	229
9:10 A.M.	<b>Trojan Horse: An EFP-Defeat Concept</b> J. May, Kaman Sciences Corporation	Vol. 2	
9:30 A.M.	<b>The Use of Momentum Transfer Armor of the Defeat of Explosively Formed Penetrators</b> Y. Huang & D. Hackbarth, U.S. Army Research Laboratory	Vol. 2	
9:50 A.M.	<b>Effectiveness of NERA Appliqué in Defeating Copper EFPs</b> Y. Huang, U.S. Army Research Laboratory	Vol. 2	
10:30 A.M.	<b>Energetic Grid Armor</b> J. Runyeon, R. Frey, W. Gooch, T. Havel, & M. Zoltoski, U.S. Army Research Laboratory	Vol. 2	
10:50 A.M.	<b>KSRAS: Kaman Smart Roof Armor System</b> J. May, Kaman Sciences Corporation	Vol. 2	
11:10 A.M.	<b>New Tire Penetration and Pressure Models for Improved Vulnerability Analyses of Wheeled Vehicles</b> R. Grote, L. Moss, & E. Davison, U.S. Army Research Laboratory	Vol. 1	243
11:30 A.M.	<b>Residual Capability Analysis of a Wheeled Vehicle Following Small Fragment Damage</b> S. Juarascio & J. Hunt, U.S. Army Research Laboratory	Vol. 1	253
<b><u>DETECTION AVOIDANCE SESSION</u></b>			263
Ingersoll Auditorium, Wednesday, March 27, 1996			
Session Chairman: Mr. Mark Pasik, General Dynamics Land Systems			
1:30 P.M.	<b>Signature Management Results from the ORSMC Program - Evolution of the Infrared Signature Management Suite</b> G. Snyder & S. Alitzer, U.S. Army CECOM	Vol. 2	
1:50 P.M.	<b>Neutralization of Side Attack Smart Mines Using the Second Generation ORSMC System</b> R. Gonzalez, U.S. Army CECOM	Vol. 2	

UNCLASSIFIED

# UNCLASSIFIED

2:10 P.M.	<b>Characterization of RSTA Threats to Crusader - Weapon Locating Radars</b> M. Scott & D. Foiani, IIT Research Institute and J. Herman, U.S. Army Research Laboratory	Vol. 2	
2:30 P.M.	<b>Validation Status of the TARDEC Visual Model (TVM)</b> G. Gerhart, R. Goetz, T. Meitzler, & E. Sohn, U.S. Army TARDEC	Vol. 1	265
3:10 P.M.	<b>Optimization of the Parameters of XPATCH for the Prediction of Radar Signatures of Ground Vehicles</b> J. Bennett, U.S. Army TACOM and G. BoBo, Keweenaw Research Center	Vol. 1	277
3:30 P.M.	<b>The TARDEC Visual Spectrum Analysis Model</b> D. Gorsich, J. Jones, R. Evans, & D. Thomas U.S. Army TARDEC	Vol. 1	287
3:50 P.M.	<b>Amphibious Assault Vehicle Survivability Enhancement by the use of Multispectral Camouflage Appliqués, MCAs</b> R. Peterson, USMC Program Office, Naval Surface Weapon Center and F. Manion, Monterey Bay Corporation	Vol. 1	297
4:10 P.M.	<b>Global Infrared Signatures: Optimization and Statistical System Assessment</b> W. Reynolds, Signature Research, Inc. and J. Petraska & M. Pasik, General Dynamics Land Systems Division	Vol. 1	307
<b><u>PENETRATION MECHANICS &amp; MODELING SESSION</u></b> <b>Glasgow Auditorium, Wednesday, March 27, 1996</b> <b>Session Chairman: Mr. Rodney Peterson, Naval Surface Warfare Center</b>			<b>315</b>
1:30 P.M.	<b>EM Effects on 38 - 100mm SC Jets</b> G. Filbey, U.S. Army Research Laboratory	None Submitted	
1:50 P.M.	<b>Scale Model Experiments with Ceramic Laminate Targets</b> C. Anderson, S. Mullin, & N. Blaylock, Southwest Research Institute and A. Piekutowski & K. Poormon, University of Dayton Research Institute	Vol. 1	317
2:10 P.M.	<b>A Simple Eroding Rod Penetrator Model</b> J. Dehn, U.S. Army Research Laboratory	Vol. 1	327
2:30 P.M.	<b>RHA Breakout Effects for Tungsten Penetrators</b> M. Normandia, Institute for Advanced Technology, U of Texas at Austin and D. Littlefield, Southwest Research Institute	Vol. 1	337
3:10 P.M.	<b>Modeling Ballistic Live-Fire Events</b> P. Deitz and R. Saucier, U.S. Army Research Laboratory	Vol. 1	347
3:30 P.M.	<b>Evaluation of a Full Scale Armored Multilayered Hull-Turret Assembly Using Model Analysis</b> A. Gupta, U.S. Army Research Laboratory	Vol. 1	357
3:50 P.M.	<b>The Determination of Shock Loads on Armor Vehicles During Threat Engagement</b> N. Gniazdowski & F. Gregory, U.S. Army Research Laboratory	Vol. 1	367

UNCLASSIFIED

# UNCLASSIFIED

4:10 P.M.	<b>Some Advances and Technical Needs in Computational Methods for Light Weight Armored Vehicle Structures</b> R. Namburu, U.S. Army Waterways Experiment Station	None Submitted	
<b><u>BEHIND THE ARMOR SESSION</u></b>			<b>375</b>
<b>Ingersoll Auditorium, Thursday, March 28, 1996</b>			
<b>Session Chairman: Mr. Mark Rzyzi, Office of the Program Manager, Armored Systems Integration</b>			
8:30 A.M.	<b>Estimating Ammunition and Ammunition Compartment Response in Support of Survivability Analyses</b> G. Gibbons, J. Watson, & F. Gregory, U.S. Army Research Laboratory	Vol. 1	377
8:50 A.M.	<b>Status of the Halon Replacement Program for Army Combat Vehicles</b> T. Treanor, U.S. Army Aberdeen Test Center	None Submitted	
9:10 A.M.	<b>Investigation of Fire Extinguishing Powders</b> A. Finnerty, U.S. Army Research Laboratory and L. Kieft	Vol. 1	393
9:30 A.M.	<b>Nuclear, Biological, and Chemical Contamination Survivability (NBCCS)</b> A. Blankenbiller & W. Magee, U.S. Army Chemical and Biological Defense Command	Vol. 1	403
10:10 A.M.	<b>Nuclear Protection Factors of the Composite Armored Vehicle (CAV)</b> K. Kerris & G. Ovrebo, U.S. Army Research Laboratory and J. Johnson, Oak Ridge National Laboratory	Vol. 1	409
10:30 A.M.	<b>Development of a Fallout Simulant</b> C. Heimbach, M. Oliver, & M. Stanka, U.S. Army Aberdeen Test Center	Vol. 1	419
10:50 A.M.	<b>Vulnerability Assessment of a Foreign Vehicle to Nuclear Radiation</b> R. Rydin, C. Ward, & R. Kehlet, National Ground Intelligence Center	Vol. 2	
11:10 A.M.	<b>The Electromagnetic Characterization &amp; Electronic Exploitation of a Foreign Vehicle</b> E. Shuff & C. Ward, National Ground Intelligence Center	Vol. 2	
11:30 A.M.	<b>A Shielding Analysis of the Leopard 2</b> D. Bash, U.S. Army Nuclear & Chemical Agency	Vol. 2	

UNCLASSIFIED

# UNCLASSIFIED

## SURVIVABILITY MODEL INTEGRATION AND SYSTEM

### SURVIVABILITY OPTIMIZATION SESSION

Glasgow Auditorium, Thursday, March 28, 1996

Session Chairman: Dr. William Jackson, TARDEC

#### *Survivability Model Integration*

8:30 A.M.	<b>The Hughes DSO Integrated Simulation Environment (ISE): A Signature Modeling and Analysis Tool Set</b> R. Bryant & M. Machacek, Hughes Delco Electronics Corporation	Vol. 1	431
8:50 A.M.	<b>Analysis of the Extended Survivability Suite</b> P. Janicki, TRW Incorporated & A. Anderson, Teledyne Brown Engineering	None Submitted	
9:10 A.M.	<b>Generic Performance Characterization and Modeling of Survivability Suites</b> M. Scott, IIT Research Institute	None Submitted	
9:30 A.M.	<b>Vehicle Survivability Analyses with the Model Linkage Process</b> F. Briglia, Teledyne Brown Engineering	Vol. 1	441

#### *System Survivability & Optimization*

10:10 A.M.	<b>The Threat Oriented Survivability Optimization Model (TOSOM)</b> A. Anderson, Teledyne Brown Engineering	Vol. 1	451
10:30 A.M.	<b>Order of Magnitude Trade-Offs Using Lanchester Equations</b> J. Reed, D. Hicks, D. Frederick, & W. Jackson, U.S. Army TARDEC	Vol. 1	461
10:50 A.M.	<b>TOSOM in Support of Crusader Survivability Suite Tradeoff Analyses</b> H. Griffis, Teledyne Brown Engineering	Vol. 1	471
11:10 A.M.	<b>Verification, Validation and Accreditation (VV&amp;A) Tests of the Bradley Simulator for the Anti-Armor Advanced Technology Demonstration (A2 ATD) Program</b> B. Jha, U.S. Army TARDEC and F. Wofford, U.S. Army Material Systems Analysis Activity	Vol. 1	481
11:30 A.M.	<b>Survivability Insight Gained by Analyzing Threat Technical and Operational Engagement Parameters</b> M. DeMent, Booz•Allen & Hamilton Inc.	None Submitted	

## POSTER PAPER PRESENTATIONS

Spanagel Hall, Room 101 A, Tuesday and Wednesday, March 26 & 27, 1996

P-01	<b>Configuration Management of Data for Signature, Countermeasures, and Armor Modeling of Systems for the Rapid Force Projection Initiative ACTD)</b> C. Kennamer, Nichols Research Corporation and E. Vandiver, U.S. Army Missile Command Research, Development, and Engineering Center	Vol. 1	491
------	---	--------	-----

UNCLASSIFIED

# UNCLASSIFIED

P-06	<b>In-Phantom Radiation Measurements Inside an M1A1 Tank Heavy Tank</b> M. Stanka, U.S. Army Aberdeen Test Center	Vol. 2	
P-07	<b>Advanced Concept Evaluation (ACE)</b> P. Buckley, PMC Incorporated and K. Lim, U.S. Army TARDEC	Vol. 1	499
P-08	<b>Wavelet and Fractal Analysis of Ground Vehicle Visual Signatures</b> D. Gorsich, C. Tolle, R. Karlsen, & G. Gerhart, U.S. Army TARDEC	Vol. 1	507
P-09	<b>Project Guardian: Tools for Optimizing Survivability on Ground Combat Vehicles</b> J. Cardenas, U.S. Army TARDEC	None Submitted	
P-10	<b>Ground Combat Vehicle Survivability Database</b> J. Olejar, C. Glausier, D. Brassard, K. Gantt, N. Funk, & M. Wunder, Booz•Allen & Hamilton Inc.	Vol. 1	517
P-14	<b>Off Normal Incidence Reflectance of High Performance Signature Reduction materials</b> W. Spurgeon, U.S. Army Research Laboratory	Vol. 2	
P-15	<b>Holographic Radar Testing of Road Wheels, Tracks and Signature Suppression Skirts</b> R. C. Sparling, Temeku Technologies	None Submitted	
P-21	<b>Survivability Issues Associated with Power Management in Future All-Electric Combat Vehicles</b> S. Fish, Institute for Advanced Technology	Vol. 1	531
P-22	<b>Computerized Wiring Damage Assessment - Ground Systems</b> M. Kolleck, Booz•Allen & Hamilton Inc. and J. Martin, SURVICE Engineering Company	Vol. 1	537
P-28	<b>Sensor Fusion Techniques Reduce Multipath Problems for Active Defense Systems</b> S. Majoewsky, DELCO Systems Operations	None Submitted	
P-30	<b>Integrated Survivability Analyses (ISA) - Real Time</b> J. Wiederrich & B. Fatemi, United Defense, L.P.	Vol. 1	547
P-31	<b>Damage Tolerance of Composite/Ceramic and Conventional RHA and Aluminum Versus 20mm Frag</b> T. Furmaniak, U.S. Army TARDEC	None Submitted	
P-32	<b>CAV Armor Results</b> D. Schade, United Defense, L.P.	None Submitted	

UNCLASSIFIED

**UNCLASSIFIED**

**OPENING SESSION**  
**King Auditorium**  
**Tuesday, March 26, 1996**

**UNCLASSIFIED**



**UNCLASSIFIED**

**THIS PAGE INTENTIONALLY LEFT BLANK**

**UNCLASSIFIED**

PROTECT

AFFORDABLE  
SURVIVABILITY

HORIZONTAL

INTEGRATION

An Industry Perspective Presentation  
Ground Vehicle Survivability Symposium

26-28 March 1996

K. M. Krall

**LOCKHEED**  
Vought Systems



# WHAT'S NEW

- Improved lethal mechanisms and enhanced standoff ranges
- Foreign businesses marketing APS kits
- Vehicular computer processing power expanding at a rapid pace
- Electronic defensive systems lighter and thus more attractive for rapid deployment forces



# CIS/RUSSIAN MILITARY ISSUES

## Performance Specifications of Tank Active Defense System

93UM0234A Moscow *TEKHNIKA I VOORUZHENIYE*  
in *Russian* No 9-10, Sep-Oct 92 (signed to press  
26 aug 92) pp 46-47

[Unattributed article: "Tank Active Defense System"]

[Text] This system installed in a tank is already successfully neutralizing antitank weapons at our test range.

Our automatic system makes your tank invulnerable.

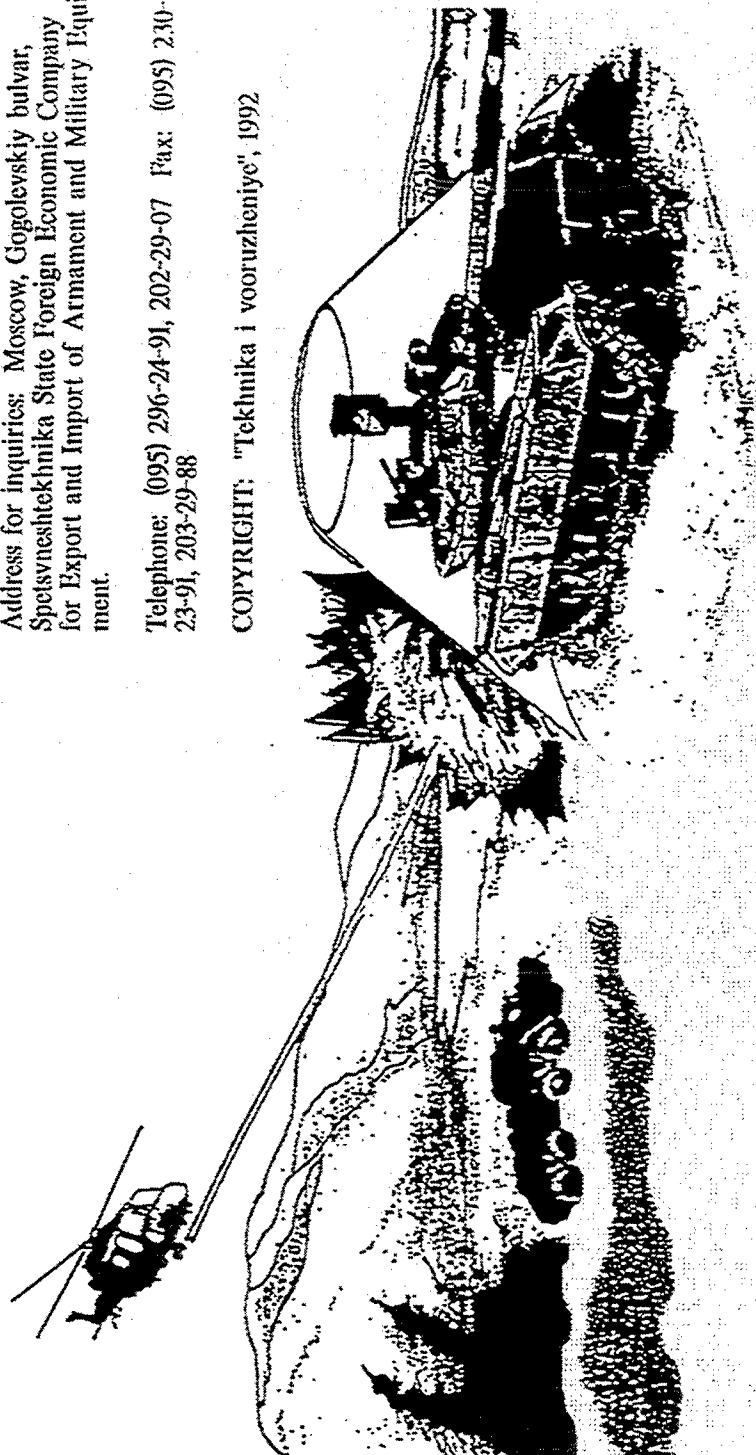
## Main Characteristics

Types of targets engaged	Antitank grenades and guided missiles, including hellborno (AT4, TOW, Hellfire)
Target detection	Radar
Operating mode	Automatic
Defended sector in azimuth	At least +/- 90°
Weight with antbullet armor	800-1,000 kg
Volume of electronic equipment within tank	30 dm³
Increase in tank survivability in battle	By several times
System reaction time	0.05 seconds

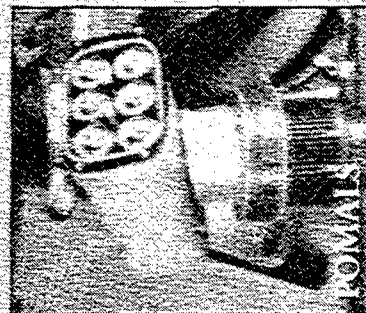
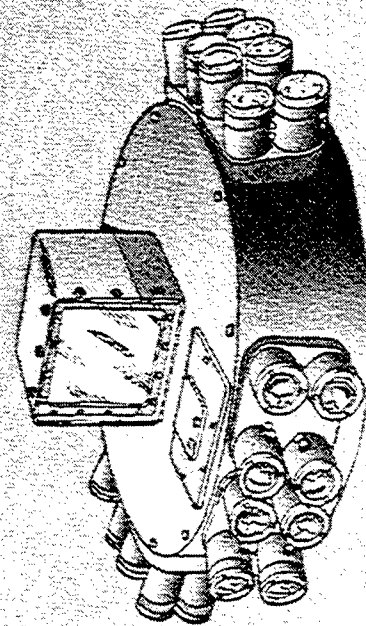
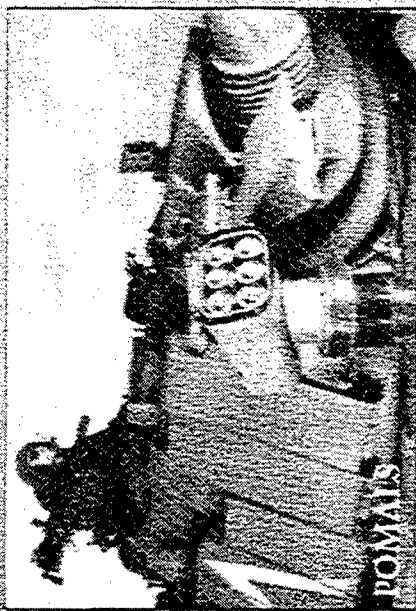
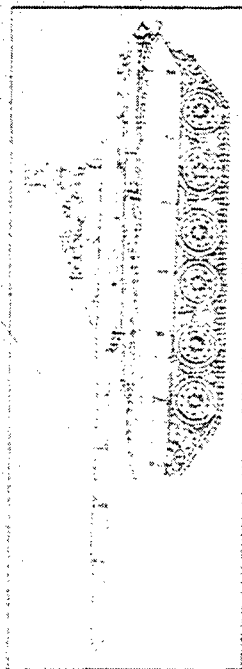
Address for inquiries: Moscow, Gogolevskiy bulvar, Spetsvneshtekhnika State Foreign Economic Company for Export and Import of Armament and Military Equipment.

Telephone: (095) 296-24-91, 202-29-07 Fax: (095) 230-23-91, 203-29-88

COPYRIGHT: "Tekhnika i vooruzheniye", 1992



# INITIAL DEPLOYMENT



INTERNATIONAL MARKETING OF DEPLOYED SYSTEMS



# **SOMETHING OBSERVATIONS**

- Survivability enhancement cost additions cannot substantially increase acquisition costs

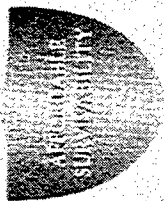
## **ESTABLISH COST TARGETS**

- Expanding the subsystems/components across missions and vehicles pays great dividends in capability per \$ spent

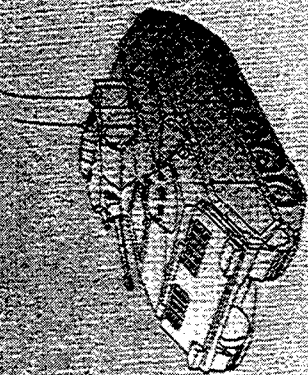
## **MAINTAIN COMMONALITY**

- Use of commercial technology must be accepted during the system concept formulation stage

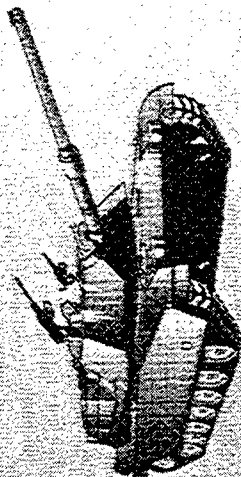
## **INSERT COSTS TECHNOLOGY**



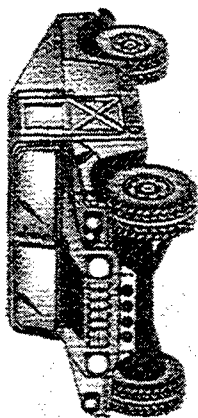
# HORIZONTAL INTEGRATION



M2/M3 - BRADLEY 4890 UNITS



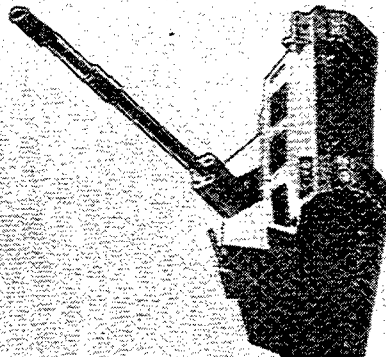
M1 - ABRAMS 5400 UNITS



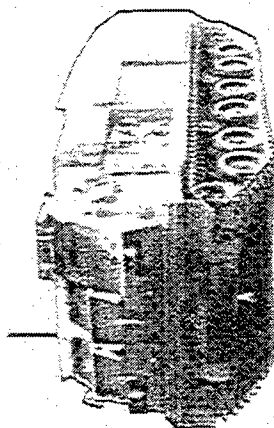
HMMWV  
SCOUTS/AVENGER 1610 UNITS



M270 MLRS 402 UNITS



PALADIN/  
CRUSADER 824 UNITS



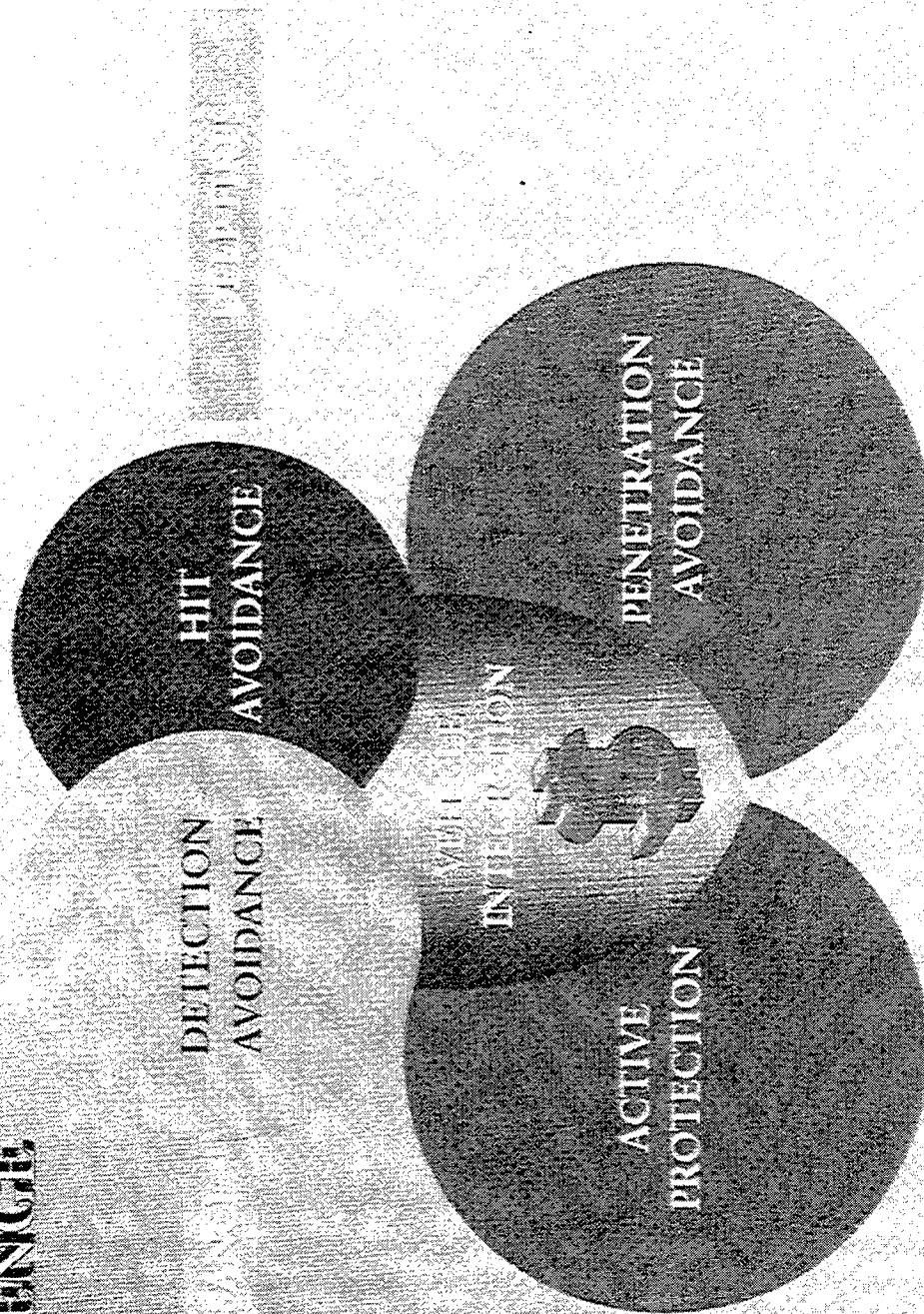
C2V

444 UNITS

SUBSTANTIAL QUANTITIES CAN BE CANDIDATES



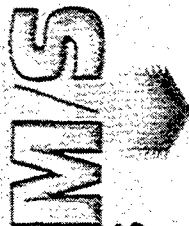
# A MULTIFACETED CHALLENGE



BALANCE COST/PERFORMANCE ACROSS THE VEHICLE FLEET AND  
MISSION OPERATIONS

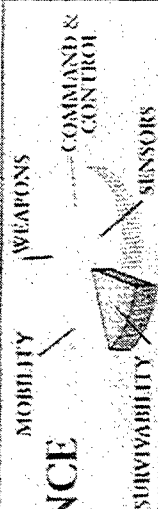
# METHODOLOGY TO ESTABLISH DESIGN COST TARGETS

SELECT MISSION/SCENARIOS  
QUANTIFY REPLACEMENT COSTS



SURVIVABILITY PAYOFF ANALYSIS

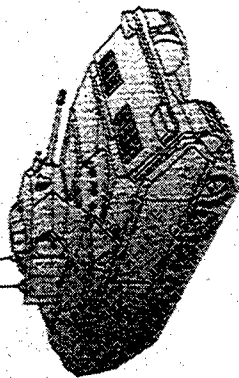
ESTABLISH MISSION PERFORMANCE  
VALUES



SUBSYSTEM SHOULD COST TARGETS



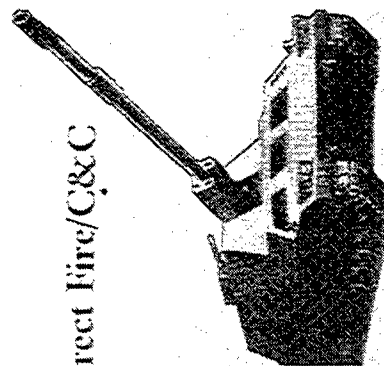
Reconnaissance



Direct Fire

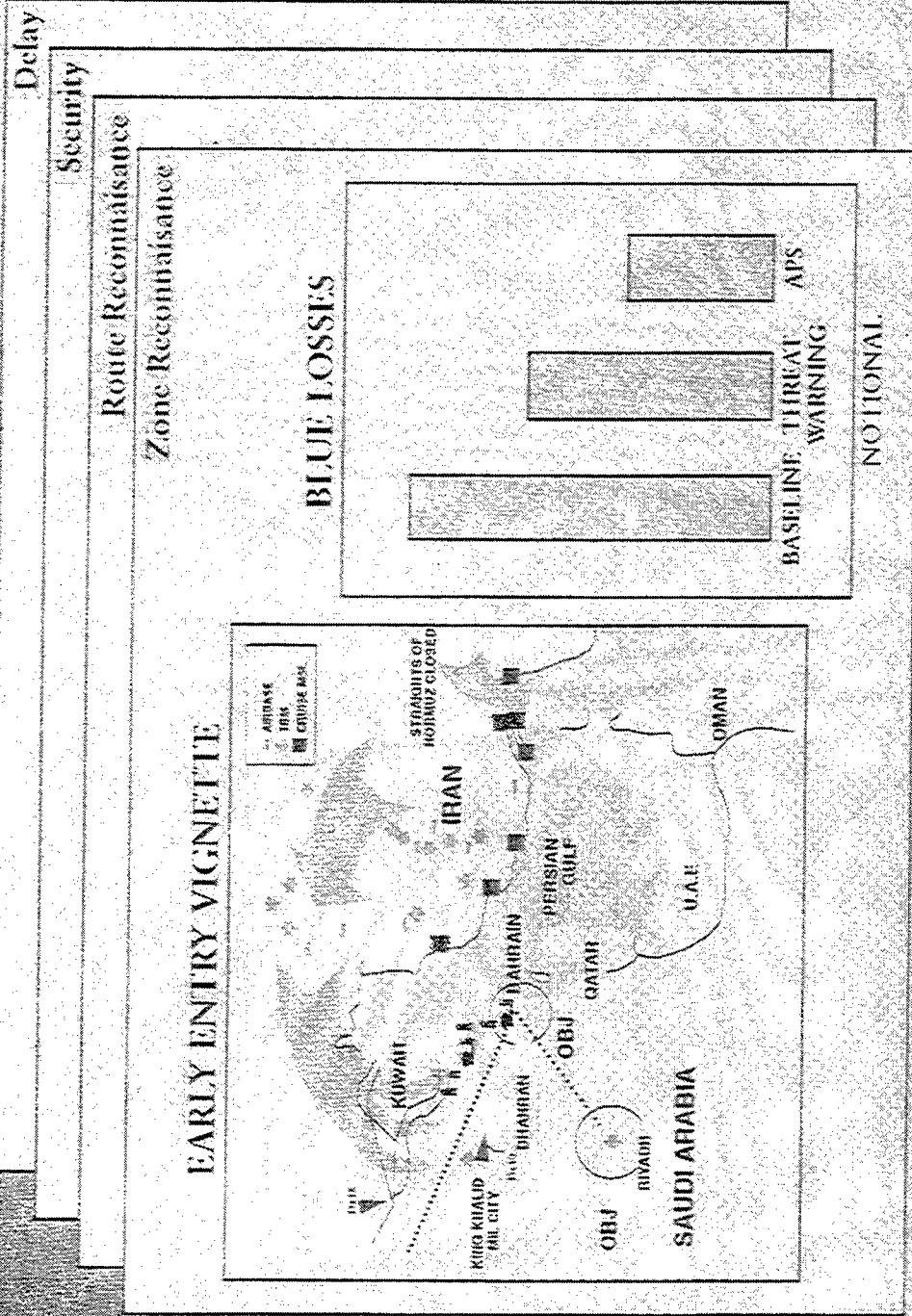


Indirect Fire/C&C



# SURVIVABILITY PAYOFF

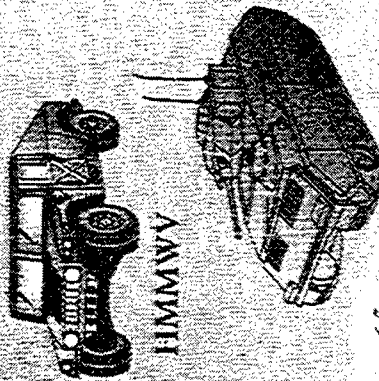
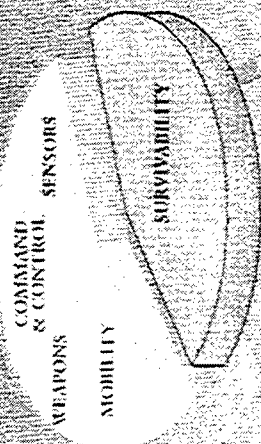
AVOIDABLE  
SURVIVABILITY



Force on Force

# COMPOSITE MISSION VALOR

## RECONNAISSANCE



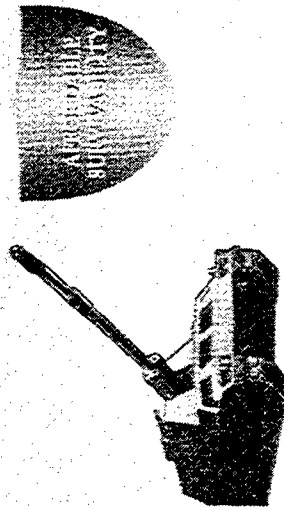
HMMWV

M3 - BRADLEY

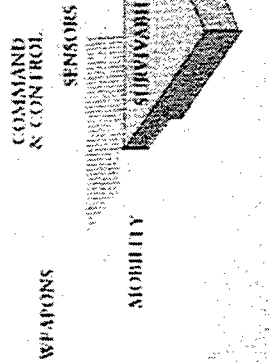
DETECTION AVOIDANCE	65
HIT AVOIDANCE	25
PENETRATION AVOIDANCE	0
ACTIVE PROTECTION	10

4 MISSIONS

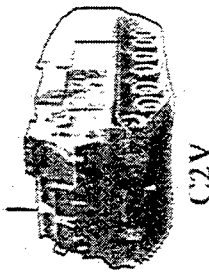
IMPORTANCE OF SURVIVABILITY AND  
PRIORITY OF SIGNATURE MANAGEMENT  
ARMOR, ELECTRONIC DEFENSE AND APS  
CAN BE ESTABLISHED



PALADIN/  
CRUSADER



M270



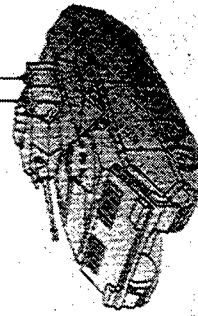
C2V

DETECTION AVOIDANCE	35
HIT AVOIDANCE	45
PENETRATION AVOIDANCE	10
ACTIVE PROTECTION	10

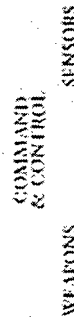
6 MISSIONS



ABRAMS



BRADLEY



DETECTION AVOIDANCE	10
HIT AVOIDANCE	25
PENETRATION AVOIDANCE	35
ACTIVE PROTECTION	30

6 MISSIONS



# COMMON ARCHITECTURE



TOP ATTACK  
COUNTERMEASURE

MISSILE WARNING



APS

SENSOR



CM

SIGNATURE  
SUPPRESSION

SMOKE  
DISPENSER



RADAR  
DETECTORS

SIGNATURE  
MANAGEMENT

DATA MGMT PROCESSOR

LASER WARNING

GPS

SINCGARS  
DIGITAL  
INTERFACE

DIGITAL DISPLAY

CORE

COMPONENTS

# COMMON SUBSYSTEMS

RADAR WARNING

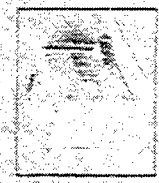
RADAR  
WARNING



IR  
CM

MISSILE

COUNTERMEASURES



MAXIMUM COMMONALITY ACROSS MISSIONS MUST BE SOUGHT

# **SOME THOUGHTS FOR TODAY'S AUSTERE TIMES**



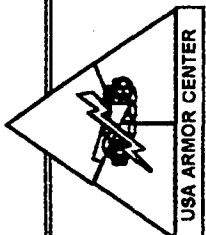
- Lethality and deployability needs demand increased vehicle survivability
- Achieving the proper combinations of armor, electronic countermeasuring and signature management across the Army ground systems will be challenging but can be done
- The government needs to organize/monitor subsystem requirements toward commonality selections across both VEHICLES AND MISSIONS
- Continued vigilance on affordability is crucial

**A STRONG NEED TO IMPROVE VEHICLE SURVIVABILITY CAN BE FULFILLED BY  
GOVERNMENT AND INDUSTRY WORKING AS A TEAM**

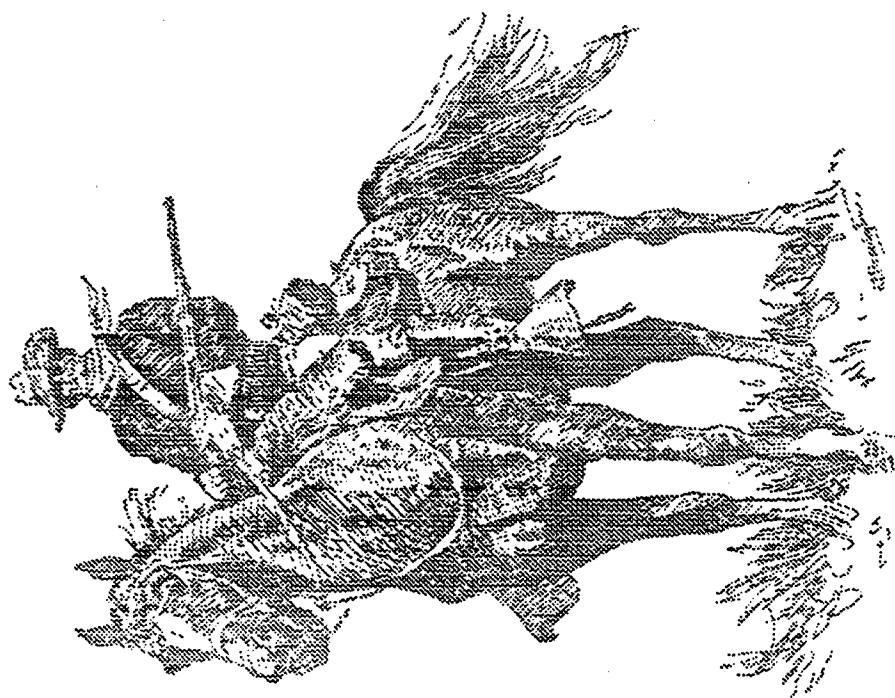
**UNCLASSIFIED**

THIS PAGE INTENTIONALLY LEFT BLANK

**UNCLASSIFIED**



# Armored Force Modernization ICT Initiatives



THE HOME OF MOUNTED WARFARE

3/1/96



# The Problem

USA ARMOR CENTER

No Concept For  
Fighting Armor in  
21st Century

No Holistic  
Approach to  
Armor Vehicle  
Modernization

Existing Plans For  
Armor Modernization  
Unaffordable

Aging Abrams  
Fleet / Increasing  
Cost of Operation

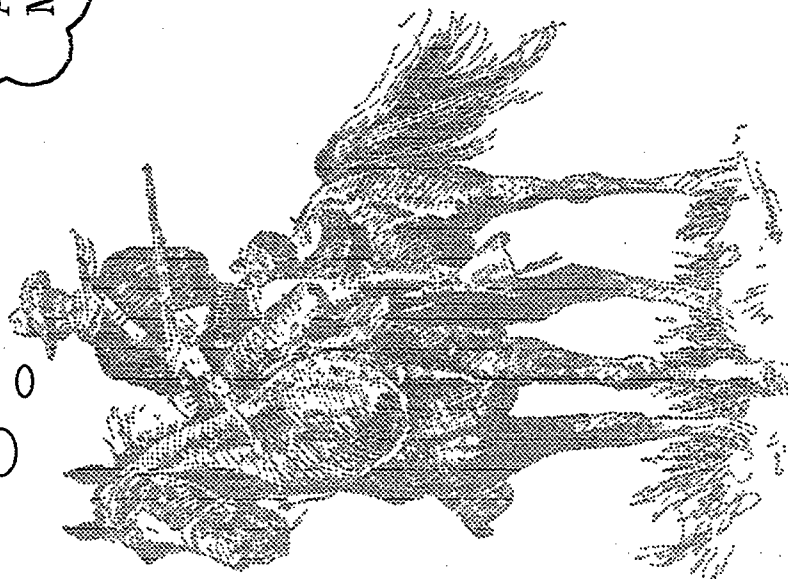
Tech Base Not  
Fully Aligned With  
Requirements

Development of  
Leap Ahead FMBT  
Technology  
Underfunded

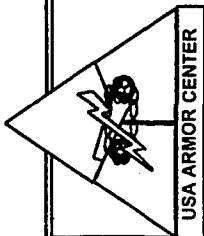
No Emphasis on  
FSV ... Mired in  
BFV Dev & Prod

Piecemeal  
Approach to Dev of  
Armor Force 21st  
Century

R&D \$ Do Not  
Result in Fielded  
Systems



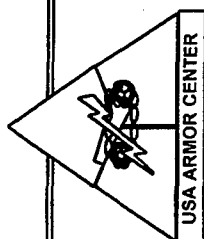
THE HOME OF MOUNTED WARFARE



# ATLANTA CAUCUS INITIATIVE

- Gather Senior Armor Leaders
- Review / Discuss Existing Plans
- Gain Consensus on the Problem / Issues
- Decide on a Single Strategy to Modernize the Armor Force
- Convert Decisions into a Long Range Plan to Include POM Input

THE HOME OF MOUNTED WARFARE

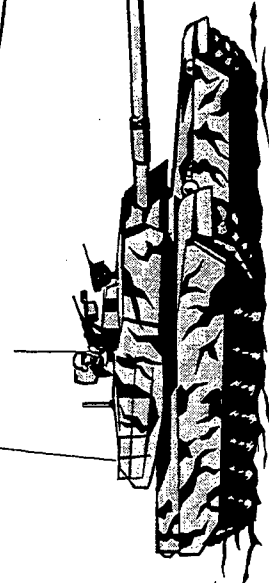


# Armored Force Modernization

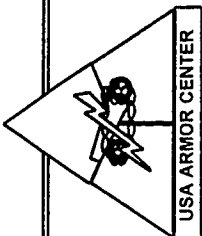
- Armor Integrated Concept Team Initiative
- *Develop Modernization plans based on guidance from Atlanta Caucus*
  - *Influence 98-03 POM Build*

using ICT Methodology  
described in TRADOC's new  
"Requirement Determination  
Pamphlet"

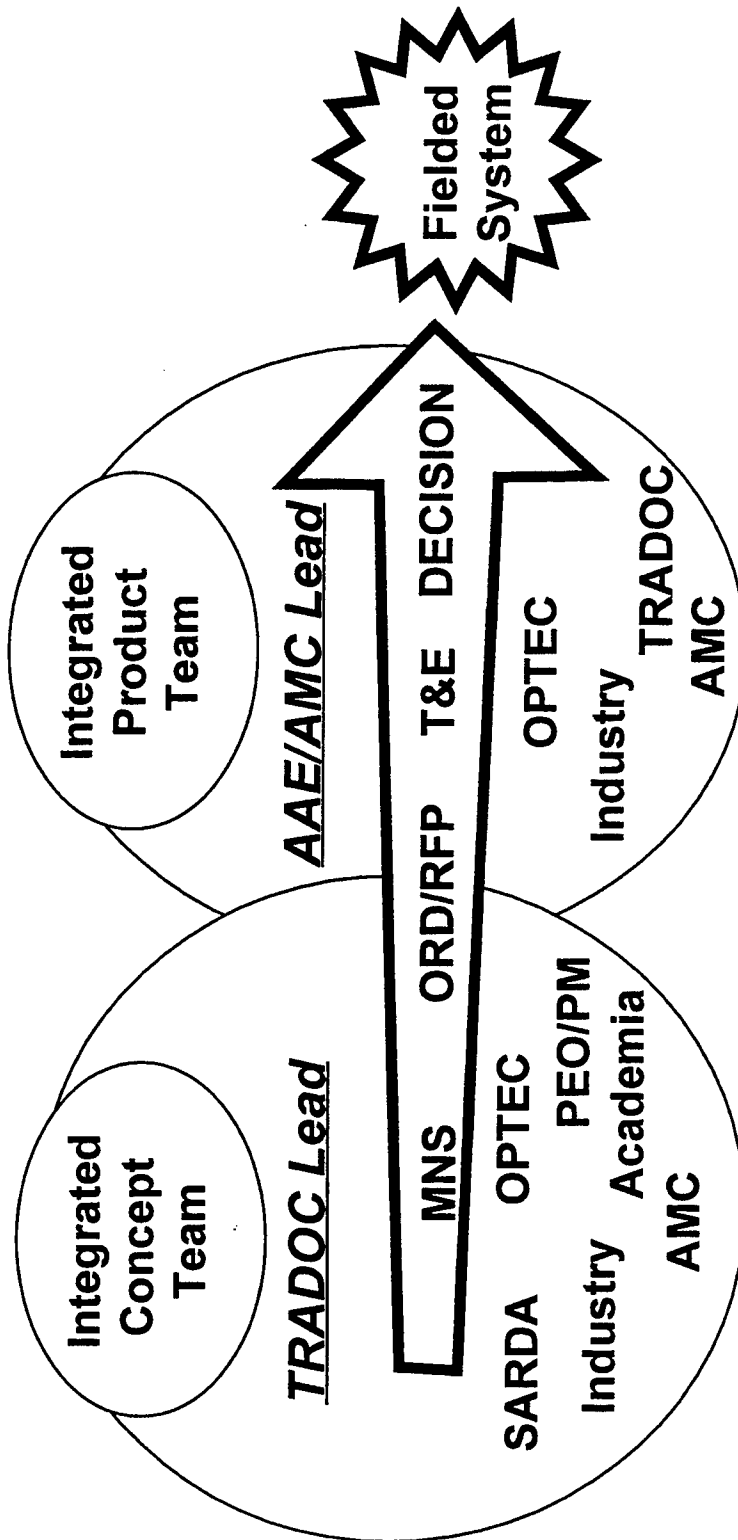
ATYPICAL  
ICTs



THE HOME OF MOUNTED WARFARE

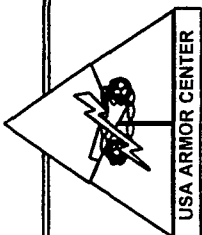


# Materiel Requirement Management



MS 0      MS I      MS II      MS III

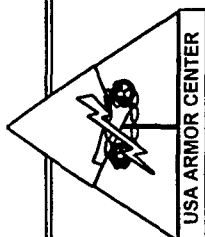
THE HOME OF MOUNTED WARFARE



# **INTEGRATED CONCEPT TEAMS**

- ***4 Integrated Concept Teams (ICTs)***
  - ***Future Main Battle Tank***
  - ***Current Fleet Modernization***
  - ***Guns and Ammunition***
  - ***Scouts***

THE HOME OF MOUNTED WARFARE



# ***Integrated Concept Team's Missions***

- ***Determine Force XXI conceptual implications based on 525-5***

***and the Armor branch concept***

**Concept**

- ***Identify operational capabilities required within constraints***

**Requirements**

- ***Provide cost, schedule, performance and risk assessment***

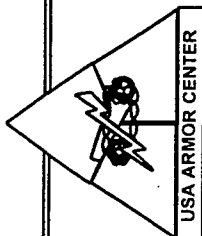
**Formulate a PROGRAM /PLAN**

**... ZERO**

**SUM**

**GAME**

**THE HOME OF MOUNTED WARFARE**

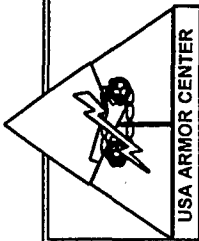


# ICT SCHEDULE

15 Jan  
Kickoff

21 Jan	TASK ANALYSIS (State the problem)	27 Jan
28 Jan	UNDERSTAND THE CONCEPTS ☆☆☆	3 Feb
4 Feb	REVIEW / DEVELOP REQUIREMENTS	10 Feb
11 Feb	☆☆ DEVELOP PROGRAM AND PLANS	17 Feb
18 Feb	FINALIZE ☆☆☆	24 Feb
25 Feb	BRIEF AND REPORT RESULTS ☆☆☆	2 Mar
3 Mar	☆☆☆☆ BRIEF CG TRADOC	9 Mar
10 Mar	☆☆☆☆ BRIEF DCG TRADOC ☆☆☆☆ BRIEF CG FORSCOM	16 Mar

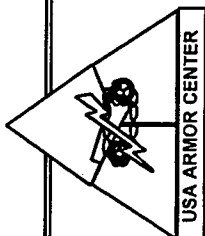
THE HOME OF MOUNTED WARFARE



# **Future Main Battle Tank (FMBT) Integrated Concept Team**

**THE HOME OF MOUNTED WARFARE**





# FMBT ICT Members

## Core:

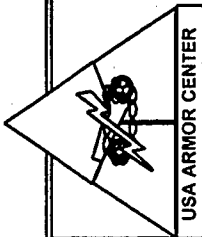
MAJ Harden	DFD	Mark Slominski	TARDEC
John Butler	DFD	MAJ Langhauser	PEO-ASM
Joe Schroeder	DFD	LTC Woznick	ARL
John Lewis	TARDEC	LTC Mingilton	PM-TMAS
Munira Tourner	TARDEC		

*Membership  
of 4 ICTs  
170 TOTAL*

## Subject Matter Experts

• Susanne Strohl	NVL	• Larry Puckett	TERM
• Dave Nielsen	AWWG	• Tom Hafer	SLID
• Barbara Moore	ARL	• Steve Caito	Hit Avoidance
• Ed LaRosa	ARDEC	• Dave Thomas	Survivability
• Dennis Ladd	EM Gun, ETC	• Gus Khalil	Electric Drives
• Mike Mattice	Lethality ATD	• Mark Ford	Compact Autoloader
• John Appel	SARD Perspective	• Nancy Saxon	Suspension
• John Gully	Hybrid Electric Drive	• Dan Bryant	Suspension
• Ted Zimmerman	TARDEC LNO to SARD	• Ernie Schwarz	Mobility, Engines
• Paul Lescoe	Robotics	• Dan Mariani	Crewman's Associate
• Pam Kaste	EM Gun, ETC	• Mark Feury	TARDEC
• Jennifer Hitchcock	Mobility, Engines	• Rao Yalamanchilli	TERM

THE HOME OF MOUNTED WARFARE



# Force XXI and Beyond

## “Army After Next”

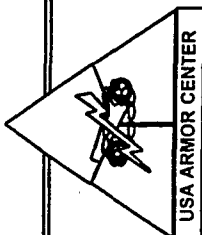
### Force XXI

1996      2000      2005      2010      2015      2020      2025

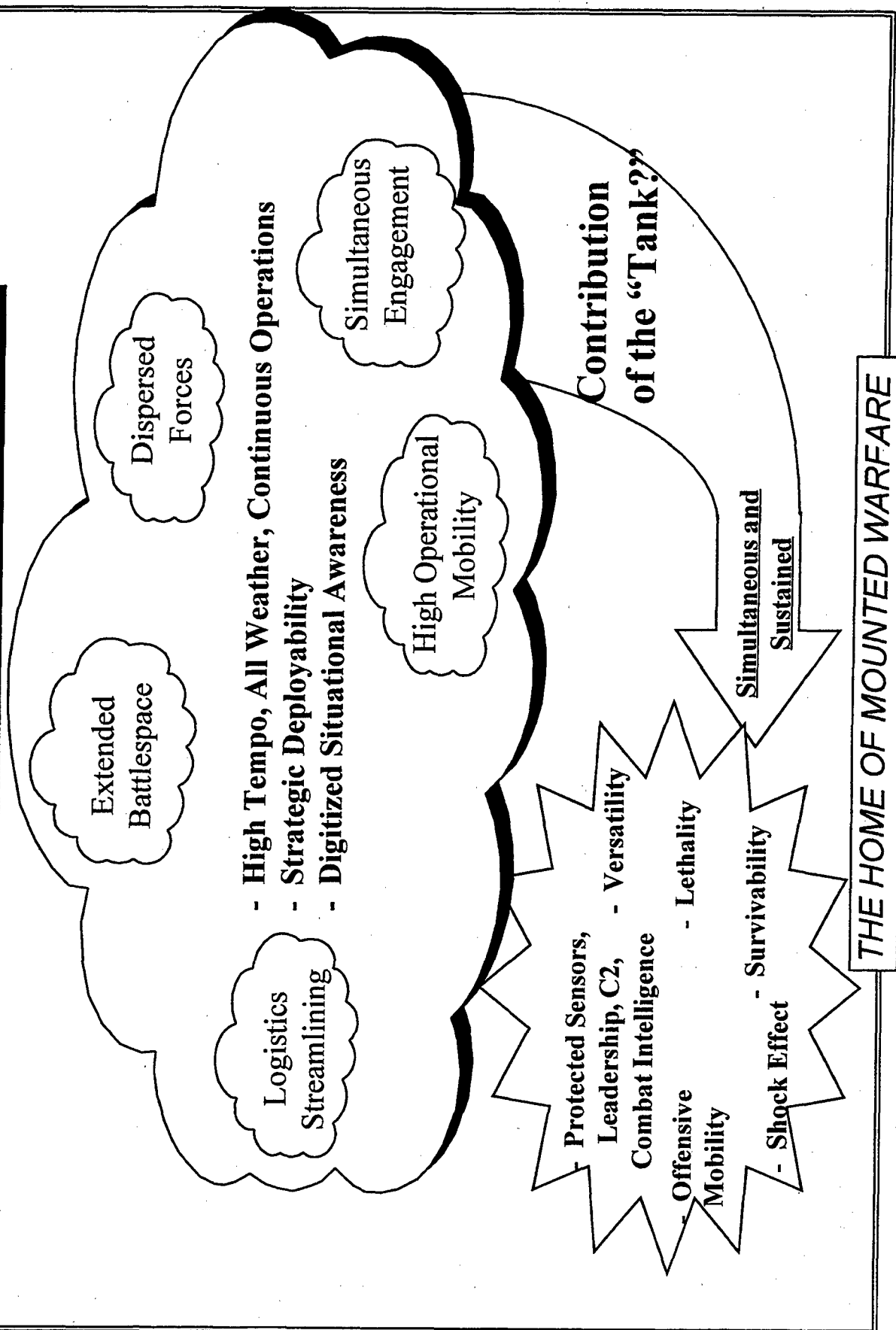
- **Force XXI:** Integration of Digital Communications Across Combined Arms to Improve Situational Awareness, Enhance Lethality and Survivability of Combined Arms Force, and Aid in Integration of Supporting Arms and Services
- Force XXI Modernization Objectives:
  - Project and Sustain
  - Protect the Force
  - Win the Information War
  - Conduct Precision Strike
  - Dominate the Maneuver Battle

- **Army After Next:** Revolution in Military Affairs Resulting From Integration of New Warfare Areas Created by Combination of New Technologies and New Operational Concepts and New Organizational Designs
- New Warfare Areas:
  - Precision Strike
  - Information Warfare
  - Dominating Maneuver
  - Space Warfare

THE HOME OF MOUNTED WARFARE



# Force XXI and Beyond

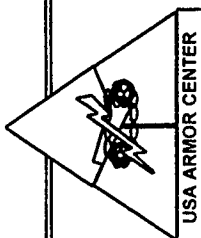


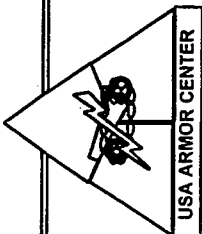
# Why a Future Combat System ?

- Must be Able to Fight Efficiently While Maintaining Battlefield Dominance Through:
  - **Lethality**: “One Shot, (At Least) One Kill” - At Longer Ranges
  - **Survivability** : Retain Friendly Combat Power
  - **Mobility** : Faster Force Level Movement
  - **Enhanced Command and Control** : Facilitates All of the Above
  - **Deployability**: Faster Generation of Combat Power in Theater
  - **Expanded Battlefield Role** : Non-Line of Sight Lethality, Self Protection vs Aircraft
- Improved Efficiency Reduces Logistic Tail, Improves Strategic Deployability and Operational Mobility:

*Without a Revolution in Logistics,  
There Will be no Force XXI !!!*

THE HOME OF MOUNTED WARFARE



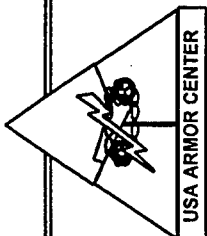


## FCS Program

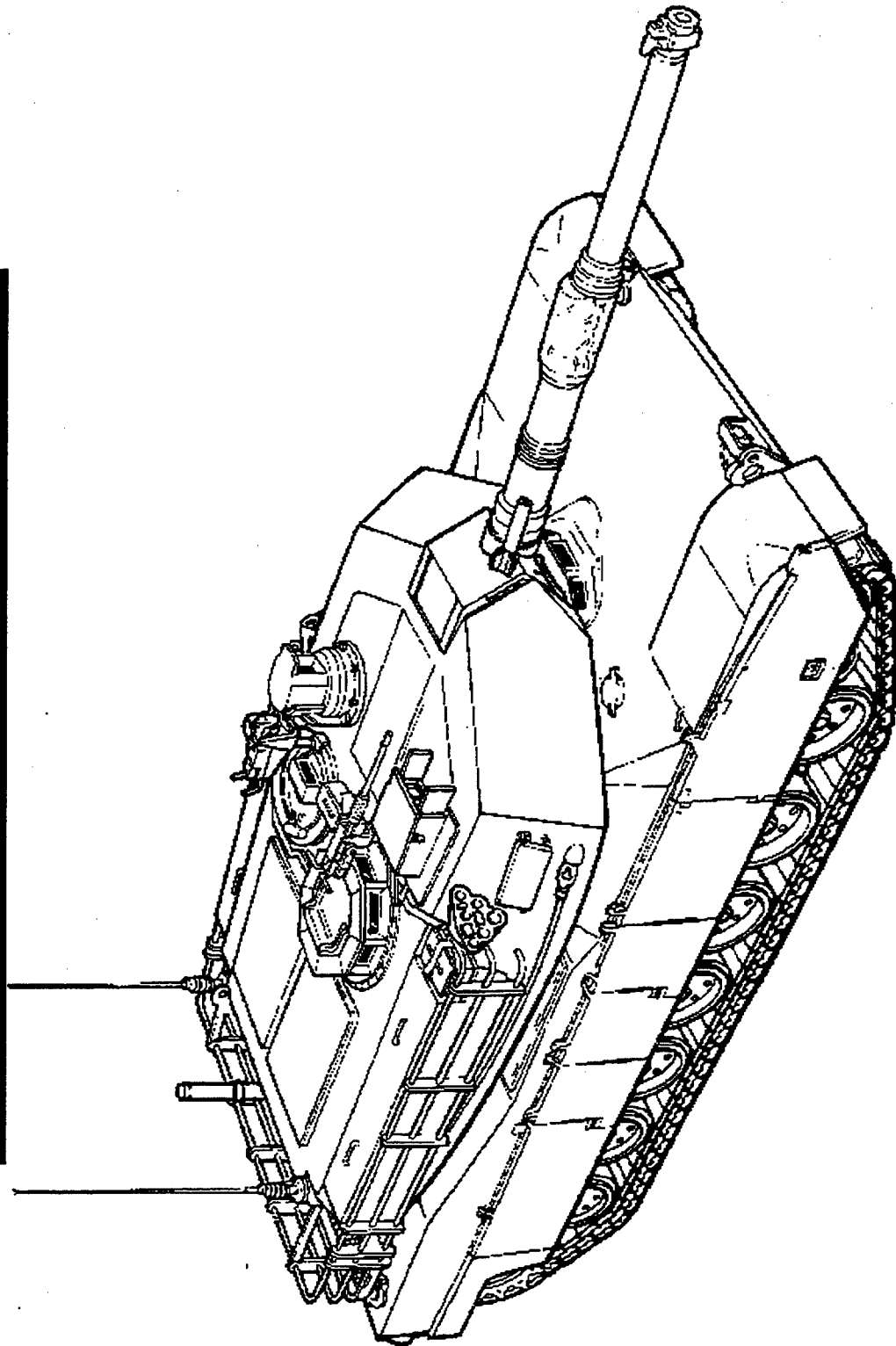
- New Start Required
- EM Gun:
  - *Increase Resourcing by 25% per Year*
- Prime Power Source:
  - *New Start Required in FY98*
- Tech Base Support:
  - *Continue Ongoing Efforts, Directed Toward FMBT*
  - *Additional Resources Needed for Follow-on Programs*

**HIGH RISK!!!**

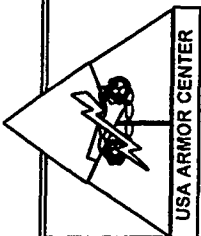
THE HOME OF MOUNTED WARFARE



## CURRENT FLEET MODERNIZATION INTEGRATED CONCEPT TEAM

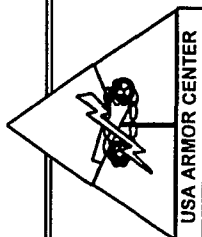


THE HOME OF MOUNTED WARFARE



# ABRAMS PROGRAM

- **M1:** Only safety related mods
- **M1A1:**
  - Establish Abrams Integrated Management (AIM) Program
  - Continued application of funded ongoing mods for safety, live fire, and Desert Storm Fixes
  - Installation of high payoff improvements
- **M1A2:**
  - M1A2 SEP and retrofit
  - Installation of high payoff improvements
  - AIM
- Establish dedicated PDSS for sustained software improvements
- Develop XM291 (120mm) gun; integrate on tank and install (if required)
- Continued development and integration of 120mm ammunition



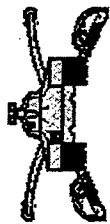
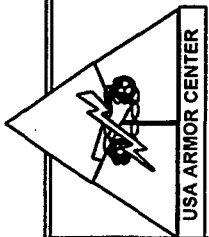
## HIGH PAYOFF IMPROVEMENTS

(Excluding guns and ammunition)

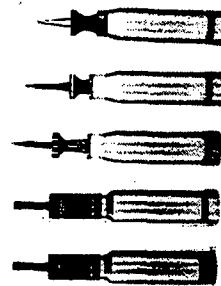
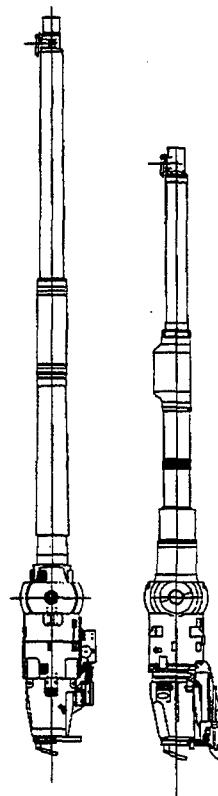
High Payoff Improvement	M1A1	M1A2
Vehicle Integrated Defense System (VIDS)	X	X
Armor Upgrade	X	X
M1A1 C <sup>2</sup> (Applique')	X	
Target Acquisition and Fire Control		X
Improved Fire Control	X	
Improved Driver's Vision Enhancement	X	
Battalion Countermine Set Improvements	X	X

THE HOME OF MOUNTED WARFARE

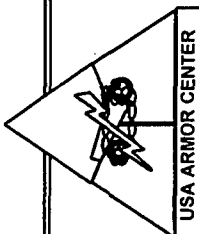




# Gun and Ammunition Integrated Concept Team



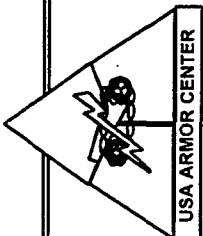
THE HOME OF MOUNTED WARFARE



# Recommended Gun/Ammunition Program

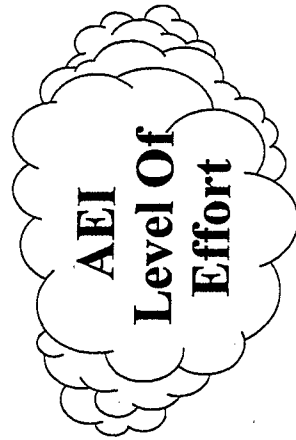
- Complete Procurement Of M829A2
- Complete Development And Procurement Of STAFF
  - Continue R & D For A Replacement With Improved Capabilities
- Increase Tech Base Efforts In Novel Penetrators, Pre-Cursors And Propellants. Add Integration Funds Necessary To Incorporate These Efforts Into The KE Program
- Complete Development Of XM291 (120mm)
- Increase The Technologies Necessary To Field A Tank Extended Range Munition (TERM) For Far Term (2004 - 2015)

THE HOME OF MOUNTED WARFARE

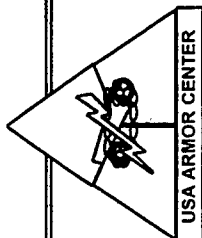


## Recommended Gun/Ammunition Program

- Develop And Procure Improved KE Service Round
- Procure Limited Quantities Of APERS For Contingency Operations
- Continue KE Training Round Procurement
- Develop/Procure Replacement Round With Increased Accuracy And Longer Range
- Continue CE Training Round Procurement
- Develop/Procure Replacement Emulating MPAT Service Round

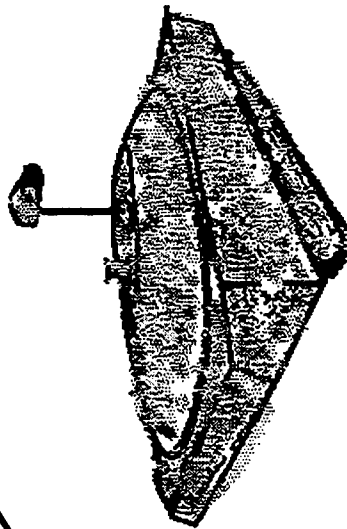


THE HOME OF MOUNTED WARFARE

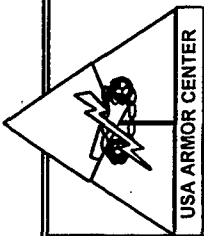


**Scout**

**ICT**



**THE HOME OF MOUNTED WARFARE**



## **Mounted Scouts In Force XXI and Beyond**

### Gain Information Dominance

- Reduce Unknowns
- Confirm/ Add to Knowledge Base

### Project The Force

- More Deployable
- Less Logistics

### Protect The Force

- Recon
- Counterrecon
- Security Force

### Shape The Battlespace

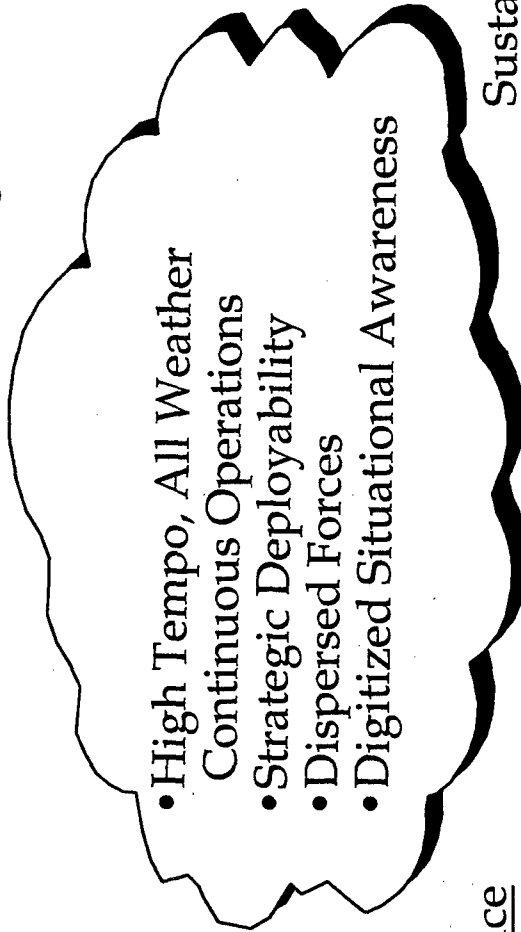
- Accurate, Timely Targeting
- BDA
- Force Enemy Action

### Decisive Attack

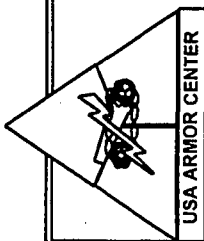
- Economy of Force Role Frees  
Main Force For Decisive Action

### Sustain and Transition

- Continuous RSTA



**THE HOME OF MOUNTED WARFARE**



# Scout ICT The End Game

**Either:**

**Do Not Meet  
Requirements**

**Cavalry Scout**

**Bn/Bde Scout**

**Near Term  
('98-'99)**

**M3A2ODS**

**UA HMMWV  
w/LRAS3 (accelerate)**

**Mid-Term  
( '00-'03)**

**M3A3  
M3A3+**

**Minor Mod AGS  
Minor Mod M113**

**Far Term  
( '04-'15)**

**M3A4**

**Or:**

**Meet  
Requirements**

**Cavalry Scout**

**Bn/Bde Scout**

**Recommended**

**M3A2ODS**

**UA HMMWV  
w/LRAS3 (accelerate) + DVE**

**M3A2ODS**

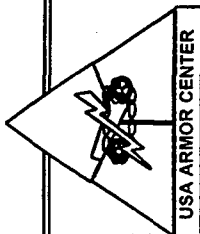
**~~M3A3  
M3A3+~~**

**Major Mod AGS**

**Major Mod M113  
New Start**

**Army  
FLCV  
TRACER**

**THE HOME OF MOUNTED WARFARE**



# “Armor” Funding Base Line

“Zero Sum  
Game”

## FCS:

- M1A3
- Tech Base (Selected)<sup>1</sup>

## AMMO:

- PM TMAS (Development)  
M829E3  
STAFF  
ATAS
- AMMO Procurement  
M829A2 KE  
M831A1 HEAT-TP-T  
M865 TP-T

## SCOUT:

- FSV
- M3A3 (Proc only)
- LRAS3
- M3A4

## Abrams:

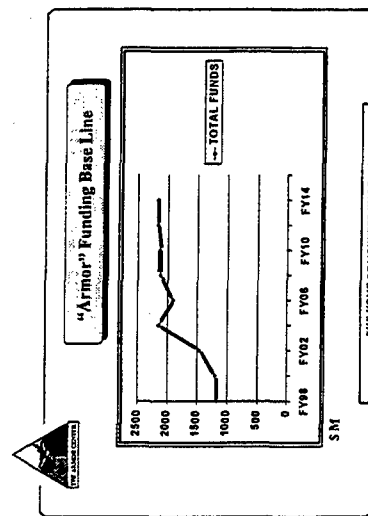
- M1A2 Production
- M1A2 SEP
- M1A2 Retrofit
- Abrams Tng Devices/Mods

## Supporting Programs:<sup>2</sup>

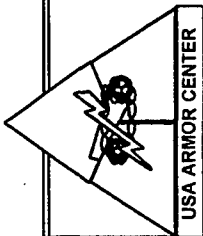
- CAV
- CTA Gun/Ammo
- ARPA Programs

<sup>1</sup> Further scrub of Tech Base required

<sup>2</sup> Applicable to other systems



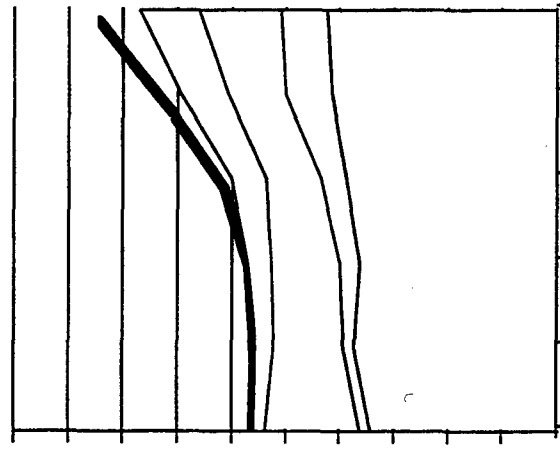
THE HOME OF MOUNTED WARFARE



# ICT REQUIREMENTS vs FUNDING (ZERO SUM)

FUNDING CUM

ICT REQ

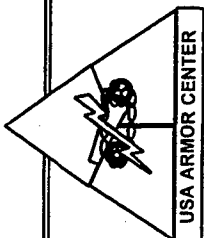


4 5 6 7 8 9 10 11 12 13 14 15

SCOUT ☐ GUN and AMMO ☐ FCS ☐ ABRAMS ☐

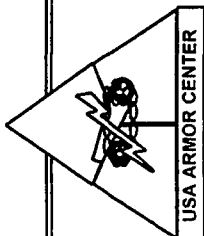
THE HOME OF MOUNTED WARFARE





# Recommendations

- Reorient Outyear Tank Production Funding Toward a FCS New Start
  - Complete M1A2 ("Identical Tanks") Production and Retrofit
  - Technology Insertion / Rebuild Program for Current Fleet
  - AEI Level of Effort to Tank Main Armament
- Reorient M3A3 Program toward Future Scout Vehicle New Start
- Conduct Independent Objective Industrial Base Analysis



## ***THE NEXT STEP***

- Submit Requirements Documents
- Focus TECH Base Efforts
- Influence 98-03 POM
- Armor FAA (April) Address additional M1A2 production issue
- Conduct Armor Caucus II June 2-3 1996

***THE HOME OF MOUNTED WARFARE***

**UNCLASSIFIED**

**THIS PAGE INTENTIONALLY LEFT BLANK**

**UNCLASSIFIED**



## *PEO Tactical Wheeled Vehicles*



# TACTICAL VEHICLE SURVIVABILITY A PERSPECTIVE



PM Light Tactical Vehicles

FEB94



## *The Armoring of Tactical & Wheeled Vehicles in the U.S. Army*



- Past
- Present
- Future

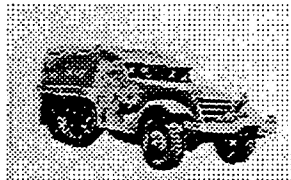
PM Light Tactical Vehicles



PERM



## *Early U.S. Efforts in Armoring Wheeled Vehicles*



WW II  
M-3



WW II  
M-8



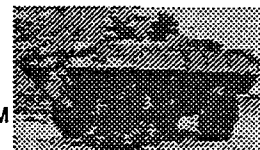
TWISTER



ARMORED LIMOSINE



KOREA  
M-20



VIETNAM  
V-100

PM Light Tactical Vehicles



PERM



## Present U.S. Forces Armoring of Wheeled Vehicles



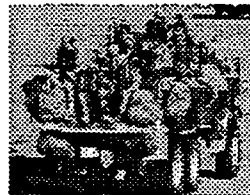
31 July 1994

VEHICLE HARDENING  
AND CONVOY OPERATIONS

US Army Transportation School  
Fort Eustis, Virginia

### SANDBAGS

"Sandbags are an effective means of reducing the effects of blast, preventing fire from reaching the driver, and providing protection from small arms fire and fragmentation. Sandbags are normally readily available and do not permanently impair the flexibility of the vehicles. Sandbags can be easily added or removed from the vehicle as the situation dictates. Commanders must consider the task at hand, recognizing that the weight of sandbags reduces the vehicle's capability to haul cargo."



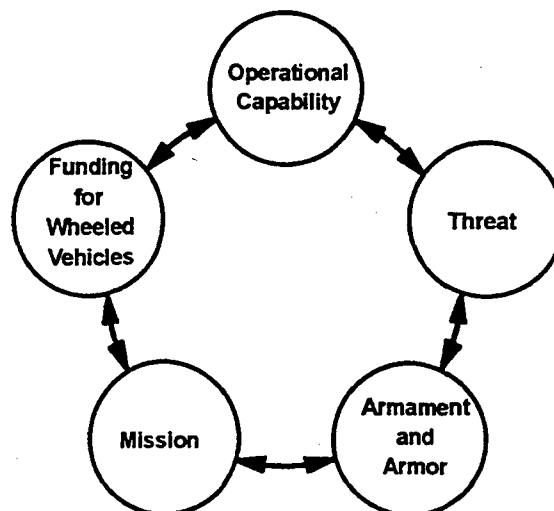
PM Light Tactical Vehicles



7220



## Why We Don't Have Wheeled Armored Vehicles or The Wheeled Vehicle Paradigm



PM Light Tactical Vehicles



7220



## Operational Capabilities The Traditional View



- Tied to Automotive Technology
  - Little R&D Applied to Wheeled Vehicles
- Wheeled Vehicles versus Tracked Vehicles
  - Lower Gross Vehicle Weight (GVW) and Payload Capability
    - High weights of armor and armament
  - Poorer Mobility
    - Track provides better ground pressure
  - Poorer Reliability, Availability, Maintainability and Durability in the Off Road Scenario
    - Robust designs of suspension and power trains for tracked vehicles
  - Easily defeated
    - Tire puncture

PM Light Tactical Vehicles



PERM



## Operational Capabilities the New View



- Tied to Automotive Technology
  - Still Little R&D Applied to Wheeled Vehicles
  - Commercial Automotive Components More Robust for Better Reliability.
- Wheeled Vehicles versus Tracked Vehicles
  - Lower Gross Vehicle Weight (GVW) and Payload Capability
    - Weights of armor and armament lower
    - Better tires, Central Tire Inflation & Power to Weight Ratio
  - Comparable Reliability, Availability, Maintainability and Durability in the Off Road Scenario
    - Commercial Demand for Better Reliability and an Interest in Off Road Operation
  - Not so Easily Defeated
    - Light Weight Armor, Run Flat Tires, Independent Suspension.

PM Light Tactical Vehicles



PERM



## Threat



- Historical Threat: Russia
  - Cold War Scenario
  - Major Conflict
  - Singular Identifiable Treat
  - Definable Battle lines
- Current: Multiple Threats
  - Multiple Scenarios
  - Major Conflict to Peace Keeping
  - Multiple Threats Depending on Theater
  - Undefined Order of Battle
  - Operation in a Highly Littered Battlefield
    - Mine and Sniper Threat Throughout the Area of Operation

PM Light Tactical Vehicles



PM



## Mission



- Historical
  - Non-Leathal Support Missions
    - Cargo Transport
    - Personnel Transport
    - C141 System Transport
  - Limited "Combat" Missions
    - HMMWV Armament Carrier and TOW Carrier

PM Light Tactical Vehicles



PM





## Mission



- Current
  - Traditional Non-Leathal Support Missions
  - Low Intensity and Operations Other Than War
  - Front Line Resupply / Recovery
  - Operation in High Treat Areas
    - Front Line Engagements
    - Operation in "Littered" Conditions Throughout the Theater
  - Tracked Vehicles are Not "Appropriate" in all Mission Scenarios

PM Light Tactical Vehicles



PM



## Cost



- Historically
  - Armoring a Wheeled Vehicle Can Cost More than the Vehicle Itself
  - Not Previously Justified based on Capability, Mission and Threat
- Current
  - Cost of Armor is Still High but Coming Down Relative to the Cost of the Wheeled Chassis
  - Now Justified based on Threat and Mission
  - Wheeled Platforms Provide a Lower Operational and Support as well as Transportation Cost than Track

PM Light Tactical Vehicles



PM



## Armament and Armor



- Historically
  - Armament
    - Lethal meant Big and Heavy and/or Very Expensive
  - Armor
    - Heavy and Expensive
- Current
  - Armament
    - Higher Lethality with Smaller Light Weight Weapons
  - Armor
    - Light Weight and Inexpensive Armor is Readily Available
    - Simulation and Optimization Technologies Permit Weight and Cost Optimization for Given Threats

PM Light Tactical Vehicles



7200



## Where We Are: What and Why



- ***The Traditional Wheeled Vehicle Paradigm Has Been Broken, We Now Have:***
  - Better, Light Weight and Affordable Armor and Armament
  - Better Automotive Technology
    - High Mobility
    - Greater RAM-D
  - New Missions
    - OOTW
    - Police Actions & Peace Keeping
  - Changing Threats
    - Littered Battlefield
    - Non-linear battle Lines

PM Light Tactical Vehicles



7200



## Where We Are: What and Why



- What We Do Not Have Is Army Commitment and Funding to Pursue the Solutions
- What Are We Doing to Meet the Needs of the Soldier?

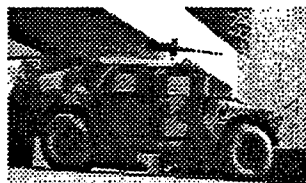
PM Light Tactical Vehicles



PERM



## Current Programs for Tactical and Wheeled Vehicle Protection



PM Light Tactical Vehicles



PERM



## High Mobility Multipurpose Wheeled Vehicle



### 12 Lb Mine Blast

M998 w/o Armor



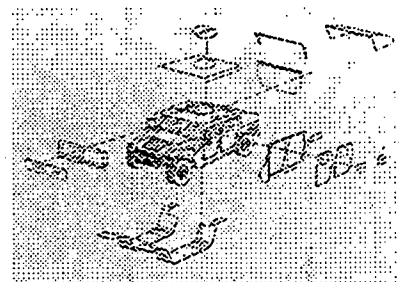
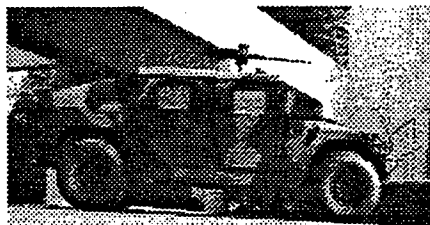
XM1114



PM Light Tactical Vehicles



## High Mobility Multipurpose Wheeled Vehicle - XM1114



#### Ballistic Protection:

- 360 degree, 7.62mm NATO AP
- Front Wheel:
  - 12 lbs Underbody mine blast protection
- Rear Wheel:
  - 4 lbs. Underbody mine blast protection
- Overhead:
  - 155mm @ 60 Meters

#### Developer and Manufacturer:

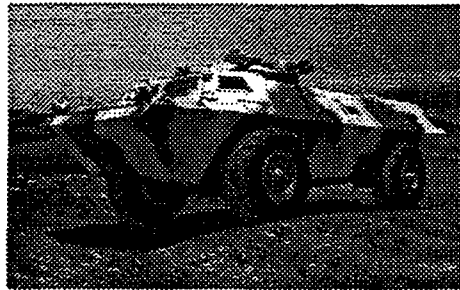
O'Gara-Hess and Eisenhardt  
Fairfield, OH

PM Light Tactical Vehicles





## Armored Security Vehicle



### o Requirements:

- Overall - 7.62mm Ball
- Crew Area:-
  - .50 Cal Ball & 7.62mm AP
  - .50 Cal AP With Add-On
  - Mine, Wheels - 12 lbs.
- Overhead - 60mm Mortar @ 10 Meters
- 155mm @ 15 Meters

### Developer and Manufacturer:

- Textron Marine & Land Systems
- New Orleans, LA

PM Light Tactical Vehicles



7284



## Tactical and Wheeled Vehicle Protection Kits



- Sand Bags
- Soft Protection, Ballistic Protective Blankets
- Hard Protection
- Emerging TRADOC Requirement
  - Requirement being staffed at HQ, TRADOC
- DA Emergency Requirement in Support of Bosnia
  - Soft Protection
    - Requirement: Equivalent to 1/2 inch Aluminum
  - Hard Protection
    - Requirement: 12 lbs. Mine Blast Protection - Front Wheel
    - 4 lbs. Mine Blast Protection - Rear Wheel
    - 7.62mm Ball Protection - 360 Degrees

PM Light Tactical Vehicles



7284





## Where Do We Need to Go? Future Initiatives



- Establish the Requirement for Armor on Wheeled Platforms to a Doctrinal Requirement
  - We Cannot Decide We Need It at Each Conflict and then Forget It After.
- Embed Protection Requirements into the Vehicle Requirement and Specification
  - Armored Models as Part of the Family of Vehicles or
  - Integrate Kits (Add on Armor) as part of the Inherent Design of the Vehicle.

PM Light Tactical Vehicles



PERM



## Where Do We Need to Go? Future Initiatives



- Allocate R&D Dollars to Wheeled Platforms to Design and Integrate Armor Protection
  - Take Advantage of Technology
    - New Design Tools
    - New Materials
    - Experience
  - In Concert with the Combat Vehicle Managers We Must Investigate Low Cost Low Weight Solutions
    - Transparent Armor
    - Metals & Ceramics
    - Combinations
    - Simulation

PM Light Tactical Vehicles



PERM



## Conclusions



- Wheeled Platform Armored Vehicle is a Concept Whose Time Has Come
- The Technology is Here to Provide Excellent levels of Protection and Low Weight and Low Cost
- The Missions and Associated Threats Require Wheeled Platforms to be Protected
  - For Combat and Support Missions

PM Light Tactical Vehicles



PERM



DEFENSE SUPPLY CENTER, COLUMBUS

COLUMBUS, OHIO

DEFENSE SUPPLY CENTER, COLUMBUS

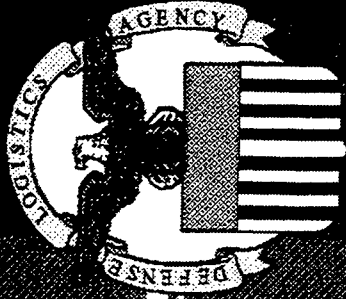
# 1996 TACOM GROUND VEHICLE SURVIVABILITY SYMPOSIUM

DEFENSE SUPPLY CENTER, COLUMBUS  
BUSINESS PROCESSES - MEETING CUSTOMER NEEDS

RADM ERNEST A. ELLIOT

26 MARCH 1996





DEFENSE SUPPLY CENTER, COLUMBUS

COLUMBUS, OHIO

DEFENSE SUPPLY CENTER, COLUMBUS

# AGENDA

MISSION

CONCEPT OF OPERATIONS

APPROACH TO WEAPON SYSTEM SUPPORT

NEW DLA MATERIEL MANAGEMENT

PHILOSOPHY

ENGINEERING - MEETING CUSTOMERS

READINESS NEEDS WITH AFFORDABLE

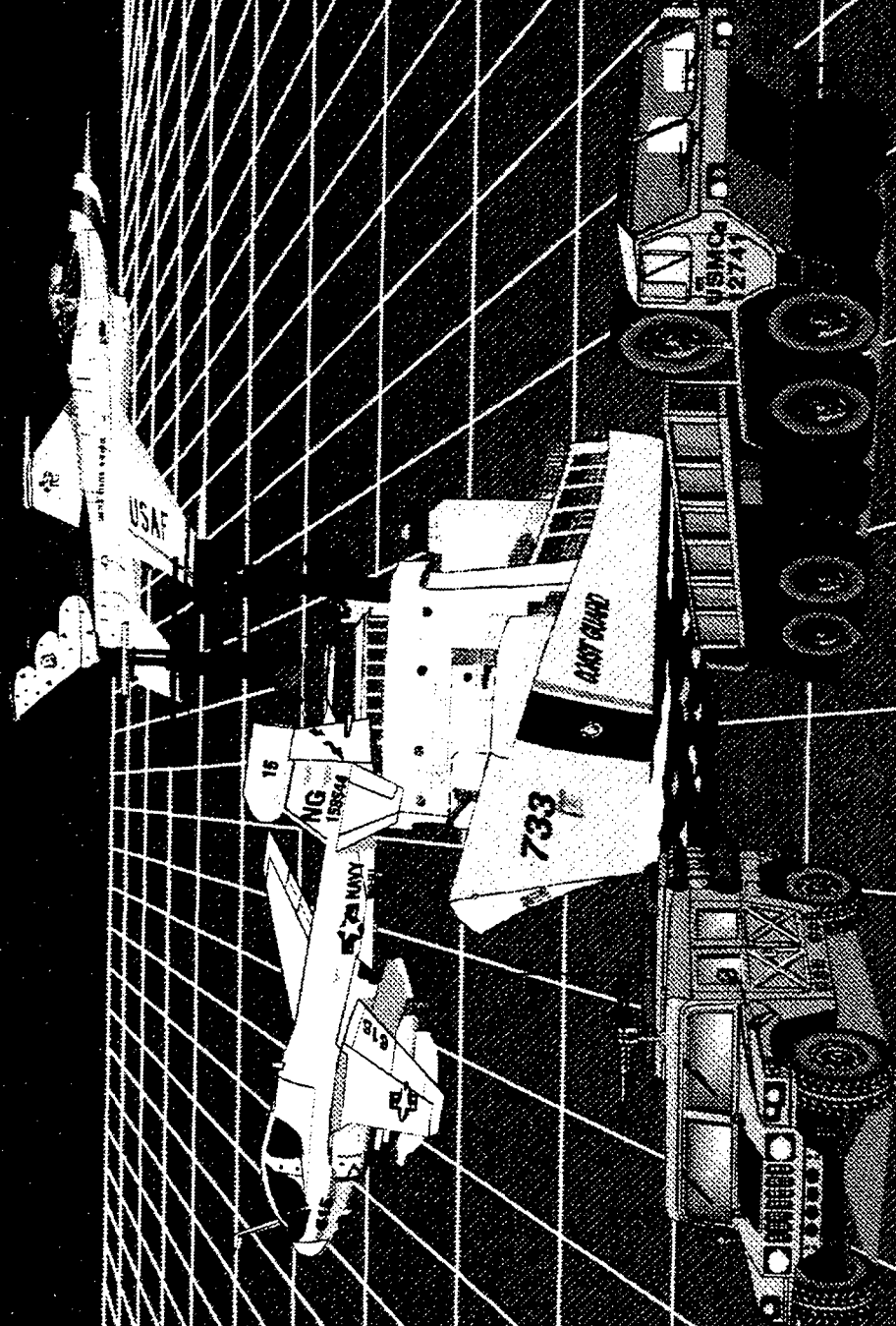
TECHNOLOGIES

HEAVY EQUIPMENT PROCUREMENT PROGRAM  
(HEPP)

SUMMARY

# MISSION

ENSURE THAT MATERIEL REQUIRED BY WAR  
FIGHTERS IS AVAILABLE WHEN & WHERE THEY  
NEED IT... AT THE LEAST POSSIBLE COST.



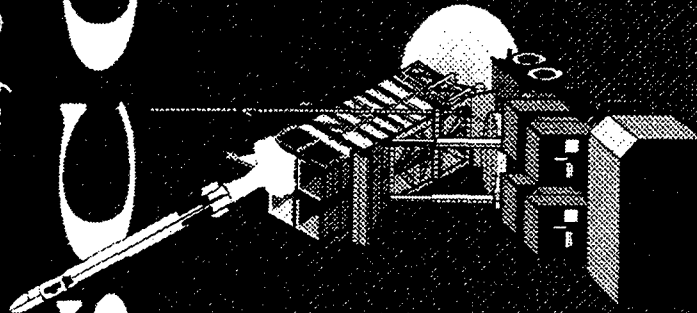
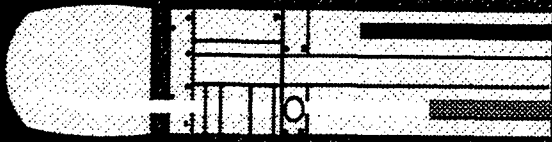
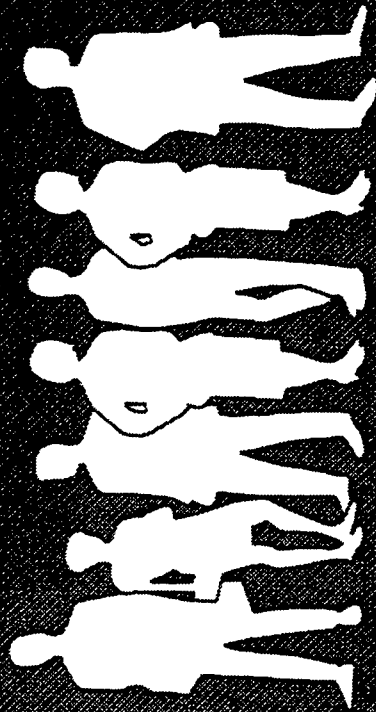


DEFENSE SUPPLY CENTER, COLUMBUS

COLUMBUS, OHIO

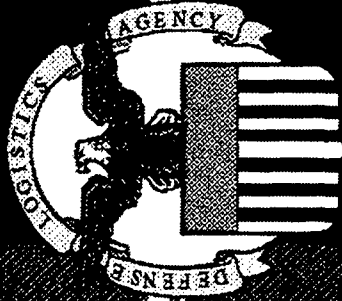
DSA

DEFENSE SUPPLY CENTER, COLUMBUS



MORE THAN 2,000 PEOPLE... RESPONSIBLE FOR OVER 737,000  
LINE ITEMS... MONITOR EVERYTHING FROM AIRFILTERS, TO  
VALVES & HOSES USED ON MAJOR WEAPONS SYSTEMS SUCH AS  
THE PATRIOT & TRIDENT MISSILE SYSTEMS.

MANAGING SUPPLY VALUE & COST PERFORMANCE



**DEFENSE SUPPLY CENTER, COLUMBUS**

**COLUMBUS, OHIO**

## **■ Concept of Operations**

**■ DEFENSE SUPPLY CENTER, COLUMBUS**

**DSCC MANAGES ASSIGNED ITEMS BY IDENTIFYING THE ENVIRONMENT IN WHICH THEY ARE APPLIED.**

**LAND SYSTEMS**

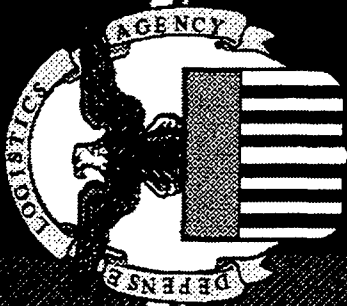
**AEROSPACE SYSTEMS**

**MARITIME SYSTEMS**

**COMMODITY APPLICATIONS**

**THIS CONCEPT ASSIGNS THE RESPONSIBILITY AND ACCOUNTABILITY FOR SUPPORT OF SPECIFIC WEAPONS SYSTEMS TO TEAMS OF FUNCTIONAL SPECIALISTS.**

**THESE SPECIALISTS PERFORM ALL ACTIVITIES REQUIRED TO EFFECTIVELY IMPROVE READINESS, SUSTAINMENT, AND SURVIVABILITY OF OUR CUSTOMERS' END ITEMS AROUND THE WORLD.**



**DEFENSE SUPPLY CENTER, COLUMBUS**

**COLUMBUS, OHIO**

**DSCC'S APPROACH**

**TO WEAPON SYSTEM SUPPORT**

**DEFENSE SUPPLY CENTER, COLUMBUS**

**LEVERAGES TARGETED INDUSTRIES**

**FOCUSES ON INDUSTRY THE WAY THEY RELATE TO US**

**MANAGES DIVERSE WORKLOAD IN MOST EFFICIENT, EFFECTIVE WAY**

**BETTER FOCUSED LONG - TERM RELATIONSHIPS WITH INDUSTRY**

**INCORPORATES BUSINESS PRACTICES OF PRIVATE INDUSTRY**

**MAXIMIZES ELECTRONIC COMMERCE**

**SERVES THE CUSTOMER BETTER**

**DRAMATIC IMPROVEMENT IN OUR ABILITY TO FORECAST**

**LONG - TERM RELATIONSHIP WITH CUSTOMERS**

**MORE RESPONSIVE TO CUSTOMERS' NEEDS**

**SERVES OUR PEOPLE BETTER**

**INCREASED OWNERSHIP/TEAMWORK**

**BETTER FOCUS OF RESPONSIBILITY AND ACCOUNTABILITY**

**IDENTIFICATION OF INTEGRATED PROCESS IMPROVEMENTS**

**MANAGES COMMODITIES ...**

**AND SUPPORTS WEAPONS SYSTEMS !**



**DEFENSE SUPPLY CENTER, COLUMBUS**

**COLUMBUS, OHIO**

**DEFENSE SUPPLY CENTER, COLUMBUS**



## **NEW DLA PHILOSOPHY**

**BUYING RESPONSE VICE INVENTORY (BRVI)**

**NO LONGER FOCUS ON BUYING, STOWING, ISSUING MATERIEL**

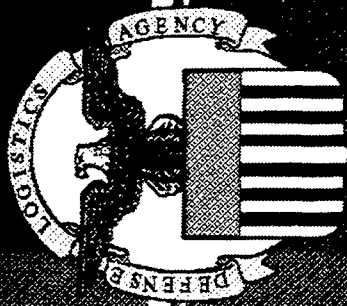
**WORK CLOSELY WITH CUSTOMERS TO PROVIDE TIMELY SUPPORT**

**SEEK OUT MOST RESPONSIVE AND COST-EFFECTIVE SOURCES**

**EMPHASIZING DIRECT VENDOR DELIVERY (DVD) AND PRIME  
VENDOR SUPPORT**

**MEETING SURGES IN DEMANDS - READINESS AND SUSTAINMENT**





DEFENSE SUPPLY CENTER, COLUMBUS

COLUMBUS, OHIO

DEFENSE SUPPLY CENTER, COLUMBUS

# DSCC CORPORATE CONTRACTING INITIATIVES OBJECTIVES

TEAMING WITH INDUSTRY TO:

- REDUCE OPERATING COSTS
- MINIMIZE LEADTIMES
- IMPROVE CUSTOMER SUPPORT



DEFENSE SUPPLY CENTER, COLUMBUS

COLUMBUS, OHIO

DEFENSE SUPPLY CENTER, COLUMBUS

DLA  
DEMANDS  
274 K

INITIAL KT  
9.5 K DMDS  
(3.5%)

W/KT MODS  
OSHKOSH  
92 K DMDS (34%)

# OSHKOSH LEADTIME IMPACT IN DAYS

AVERAGE LEADTIME    ALT    PLT    TOTAL

CURRENT	133	115	248
PROJ W/O EDI	30	10 DVD 90 STK	40/120
PROJ W/EDI	1	10 DVD 90 STK	11/91





DEFENSE SUPPLY CENTER, COLUMBUS

COLUMBUS, OHIO

DEFENSE SUPPLY CENTER, COLUMBUS

# OSHKOSH STATEMENT OF WORK SUMMARY

RESPONSE TIME: 10 DAYS DVD / 90 DAYS STOCK

DIRECT VENDOR DELIVERY

ELECTRONIC DELIVERY ORDERS

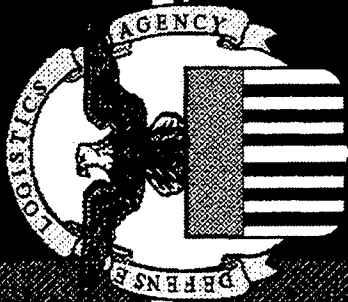
MAX/MIN DOLLAR LIMITS

QUARTERLY PERFORMANCE REVIEWS

ADD/DELETE NSNs

FIXED PRICE W/REDETERMINATION





DEFENSE SUPPLY CENTER, COLUMBUS

COLUMBUS, OHIO

DEFENSE SUPPLY CENTER, COLUMBUS

## DSCC AUTOMOTIVE INITIATIVE 2 BASIC ORDERING AGREEMENTS

FREIGHTLINER SP0700 - 95 - G - 0006

5 DAY STOCKED DELIVERY, 30 - 90 DAYS NONSTOCKED

HEAVY TRUCKS, PRIMARILY M915/M916 AND  
SMALL EMPLACEMENT EXCAVATOR

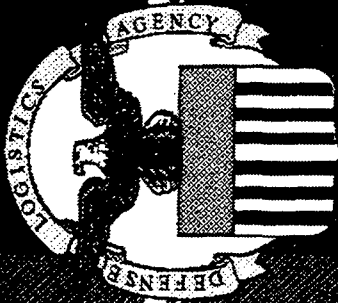
NAPA SP0700 - 95 - G - 0009

5 DAY STOCKED DELIVERY

LIGHT AND MEDIUM TRUCKS

BOTH FACILITATE CREDIT CARD AND EDI TRANSACTIONS  
THROUGH REQUISITION PROCESS

BOTH OFFER DISCOUNTS FROM OVER THE COUNTER SALES  
MILSTRIP, LOCAL PURCHASE, LOCAL PURCHASE - BOA



DEFENSE SUPPLY CENTER, COLUMBUS

COLUMBUS, OHIO

DEFENSE SUPPLY CENTER, COLUMBUS

## STANDING QUOTE SYSTEM

FEATURE OF ELECTRONIC BID BOARD  
OEM'S PRE-LIST PRICE, QUANTITY, TERMS BY NSN  
LISTING UPDATED ANY TIME  
RFQ MATCHES SOLE SOURCE NSN  
AWARD ISSUED  
ELIMINATED QUOTE COST AND NEGOTIATION TIME  
COMPANY PARTICIPATION:

AEROQUIP	LOADED
ABEX	LOADED
SIKORSKY	LOADED
BOEING HELICOPTERS	NEGOTIATING
BOEING DEFENSE/SPACE	NEGOTIATING
MCDONNELL - DOUGLAS	NEGOTIATING
SUNDSTRAND	NEGOTIATING
TEXTRON	NEGOTIATING



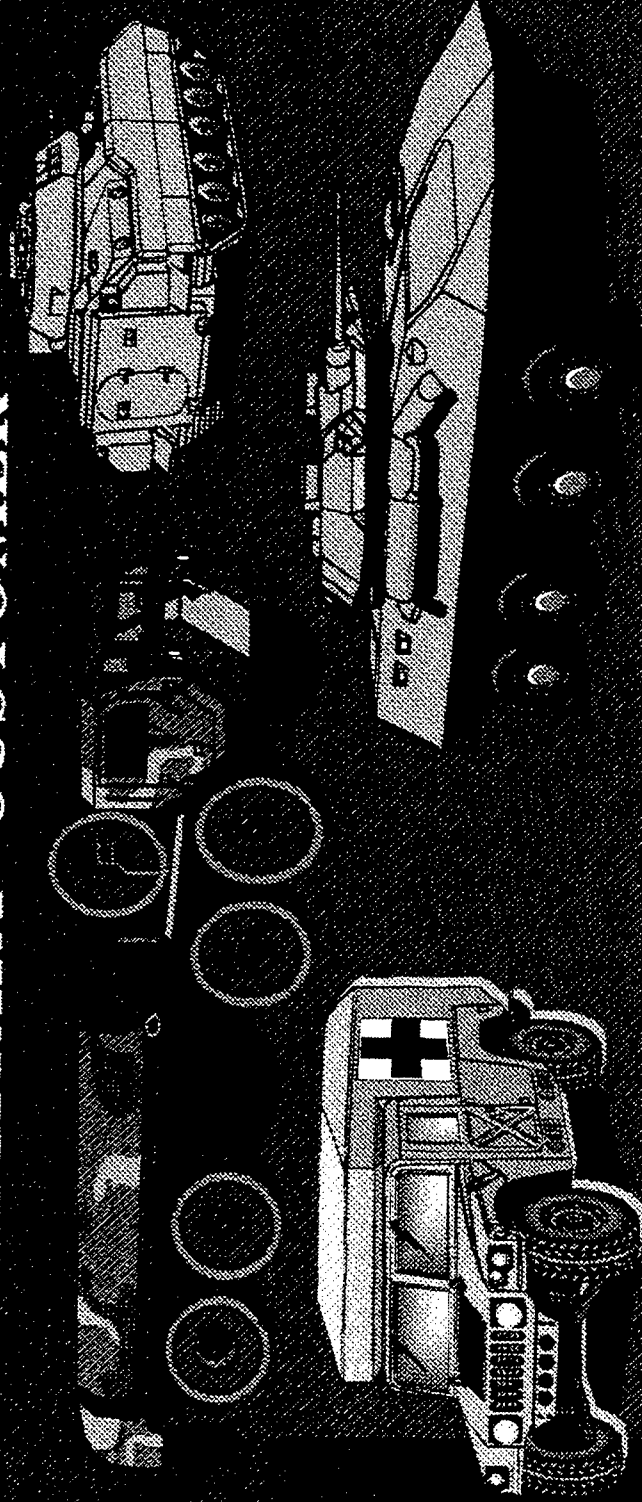
DEFENSE SUPPLY CENTER, COLUMBUS

COLUMBUS, OHIO

DEFENSE SUPPLY CENTER, COLUMBUS

# DSCC READINESS OFFICE

## MISSION SUPPORT TO THE MILITARY CUSTOMER





DEFENSE SUPPLY CENTER, COLUMBUS

COLUMBUS, OHIO

DEFENSE SUPPLY CENTER, COLUMBUS

# READINESS TEAM MISSION

SERVE OUR MILITARY CUSTOMERS IN MEETING  
THEIR READINESS AND SUSTAINABILITY  
OBJECTIVES THROUGH TECHNOLOGICAL  
ADVANCEMENTS. OUR GOAL IS TO PROVIDE  
THE RIGHT SOLUTION TO THE RIGHT PERSON  
AT THE RIGHT TIME FOR THE BEST VALUE.



DEFENSE SUPPLY CENTER, COLUMBUS

COLUMBUS, OHIO

DEFENSE SUPPLY CENTER, COLUMBUS

# READINESS TEAM FUNCTIONS

FOCAL POINT ON READINESS DEGRADERS

CAD/EDI3D MODELING AND ANALYSIS

DLA COORDINATING OFFICE FOR LAV AND M915

FUNCTIONAL TEST SHOP

ENGINEERING SUPPORT

ASSOCIATE MEMBER USAF AGE/PIWG

MEMBERS OF THE US MARINE LAV REVIEW BOARD

ESTABLISH NEW ITEMS OF SUPPLY

LEVERAGING RESOURCES THROUGH PARTNERSHIP





DEFENSE SUPPLY CENTER, COLUMBUS

COLUMBUS, OHIO

DEFENSE SUPPLY CENTER, COLUMBUS

# READINESS TEAM DRIVERS

DOD BUDGET  
BUYING POWER

INVESTMENT  
SQUEEZE

SAVINGS

CUSTOMER SATISFACTION



DEFENSE SUPPLY CENTER, COLUMBUS

COLUMBUS, OHIO

DEFENSE SUPPLY CENTER, COLUMBUS

# READINESS TEAM SUCCESS STORIES

LIGHT ARMORED VEHICLE (LAV)

BRAKE LINING SETS 2 1/2 AND 5 TON TRUCKS

BEAD BREAKER (TIRES)

ONE MAN HITCH





DEFENSE SUPPLY CENTER, COLUMBUS

COLUMBUS, OHIO

DEFENSE SUPPLY CENTER, COLUMBUS

# READINESS SAVINGS

LAV FUEL AND BRAKELINE

\$1.8M MAINTENANCE

BRAKE LINING SETS

\$1.3M MAINTENANCE

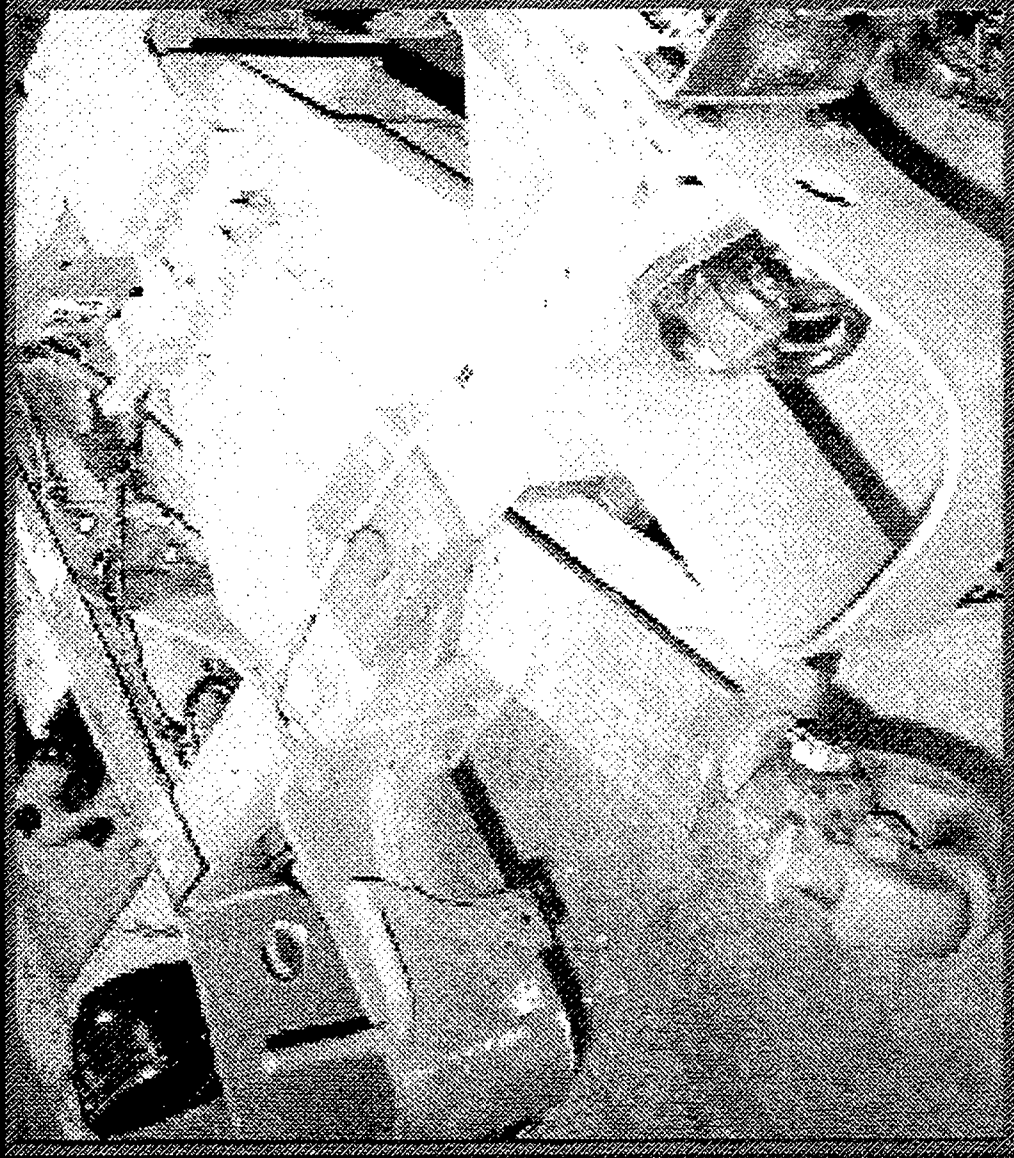
BEAD BREAKER TIRES,  
COTS REPLACEMENT

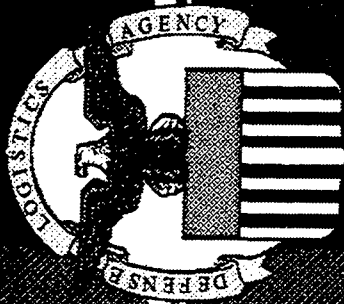
\$1.1M SUPPORT COST

ONE MAN HITCH

1 MAN YR/VEHICLE

# One - Man Hitch 2/12 & 5 Ton Trucks





DEFENSE SUPPLY CENTER, COLUMBUS

COLUMBUS, OHIO

DEFENSE SUPPLY CENTER, COLUMBUS

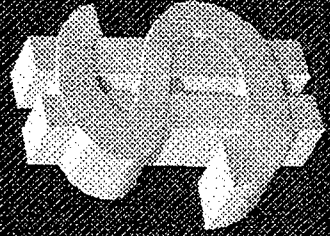
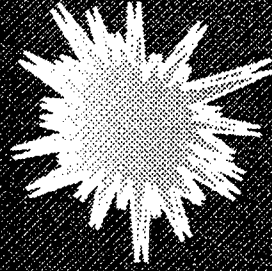
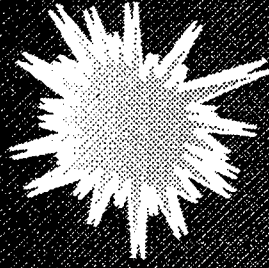
# READINESS TEAM IMPACT

MEET CUSTOMERS EXPECTATIONS

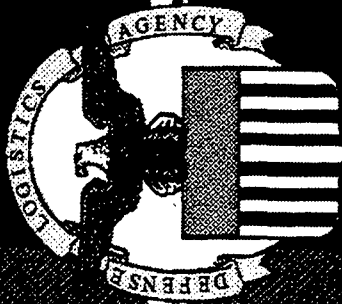
DEVELOP TRUST

IMPROVE READINESS

REDUCE COSTS



BEST BANG FOR BUCK!



DEFENSE SUPPLY CENTER, COLUMBUS

COLUMBUS, OHIO

DEFENSE SUPPLY CENTER, COLUMBUS

# PURSUING READINESS SUPPORT

CONTACT DSCC WEB SITE

<http://131.74.26.2:8888>

EMAIL: [cv00349@dcsc.dla.mil](mailto:cv00349@dcsc.dla.mil)

PHONE DSN 850-1796

FAX DSN 850-4419

\* ALL DSCC READINESS INVOLVEMENT WILL BE  
COORDINATED THROUGH THE APPROPRIATE ENGINEERING  
SUPPORT ACTIVITY

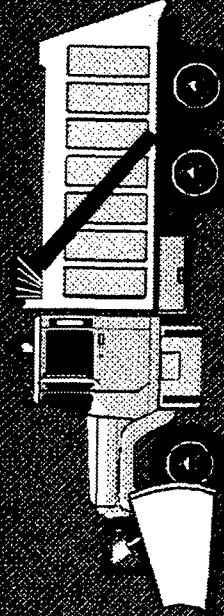
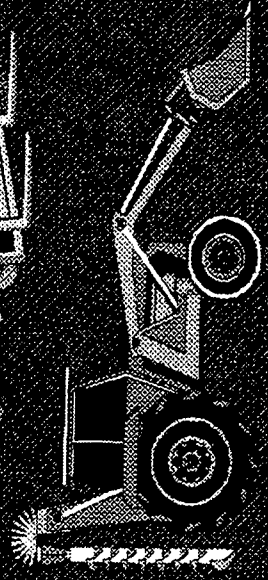
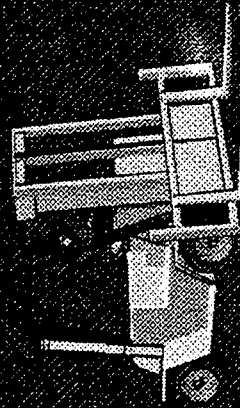
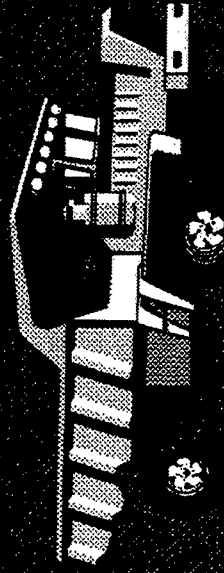


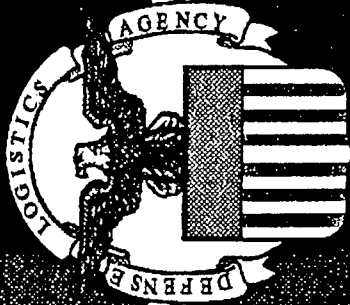
DEFENSE SUPPLY CENTER, COLUMBUS

COLUMBUS, OHIO

DEFENSE SUPPLY CENTER, COLUMBUS

# HEAVY EQUIPMENT PROCUREMENT PROGRAM (HEPP)





DEFENSE SUPPLY CENTER, COLUMBUS

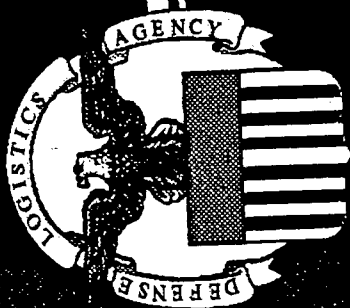
COLUMBUS, OHIO

DEFENSE SUPPLY CENTER, COLUMBUS

## BUSINESS INITIATIVE HEAVY EQUIPMENT PROCUREMENT PROGRAM

### ● PROGRAM OBJECTIVES

- ● CENTRALIZED ACQUISITION
  - ● ● CURRENT AND FUTURE REQUIREMENTS
  - ● ● LEVERAGES BUYING POTENTIAL
  - ● ● REDUCES DUPLICATION OF ACQUISITION EFFORTS
- ● STANDARDIZATION
  - ● ● REDUCES MAKES AND MODELS OF EQUIPMENT TO SUPPORT
  - ● ● ASSISTS IN INTERCHANGEABILITY
  - ● ● REDUCES INVENTORY LEVELS



DEFENSE SUPPLY CENTER, COLUMBUS

COLUMBUS, OHIO

DEFENSE SUPPLY CENTER, COLUMBUS

# BUSINESS INITIATIVE HEAVY EQUIPMENT PROCUREMENT PROGRAM

● WHAT DO YOU GAIN BY USING US?

- ● PRICE REDUCTIONS THROUGH REQUIREMENT  
CONSOLIDATION
- ● ACQUISITION METHODS TAILORED TO MEET YOUR NEEDS
- ● WARRANTY ON ALL EQUIPMENT
- ● FLEXIBILITY
  - ● ● COMMERCIAL EQUIPMENT
  - ● ● MODIFIED COMMERCIAL EQUIPMENT
  - ● ● MILITARY APPLICATION EQUIPMENT





DEFENSE SUPPLY CENTER, COLUMBUS

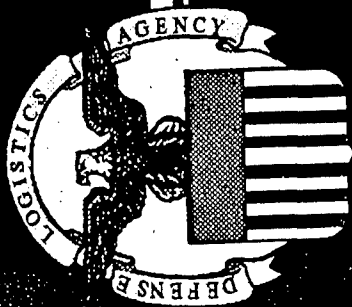
COLUMBUS, OHIO

DEFENSE SUPPLY CENTER, COLUMBUS

# BUSINESS INITIATIVE HEAVY EQUIPMENT PROCUREMENT PROGRAM

- TRACTORS (WHEEL AND TRACK)
- FIRE FIGHTING, CRASH/RESCUE VEHICLES
- ROAD CLEARING/CLEANING EQUIPMENT
- AIRFIELD MAINTENANCE EQUIPMENT
- CRANES AND CRANE SHOVELS
- EXCAVATION EQUIPMENT
- FORKLIFTS AND MATERIAL HANDLING EQUIPMENT
- SOIL PREPARATION EQUIPMENT
- WATER PURIFICATION UNITS
- RAIL MAINTENANCE EQUIPMENT
- CONVEYERIZED LINE DOCKS
- SNOW REMOVAL EQUIPMENT
- AUTOMATIC BUILDING MACHINES
- HAZARDOUS STORAGE BUILDINGS
- SMALL UNIT SHOWERS





# DEFENSE SUPPLY CENTER, COLUMBUS

COLUMBUS, OHIO

DEFENSE SUPPLY CENTER, COLUMBUS

## DSCC - HEAVY EQUIPMENT PROCUREMENT PROGRAMS HEAVY EQUIPMENT SAVINGS

GSA DSCC

FIREFIGHTING EQUIPMENT KOVATCH SAVINGS

1250 GPM PUMPER \$ 184,626 \$ 161,928 14 %

HEAVY RESCUE, 4 X 4 \$ 245,000 \$ 199,000 19 %

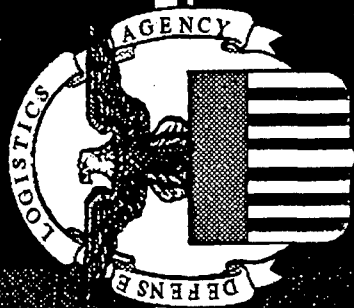
FULL TRACKED TRACTORS CATERPILLAR DEERE SAVINGS

SIZE T - 9/CAT D7H \$ 195,039 \$ 175,070 10 %

SIZE T - 7/CAT D6H DS \$ 136,557 \$ 121,151 11 %

SIZE T - 7/DEERE 750 BLT \$ 114,982 \$ 101,561 12 %

SIZE T - 4/DEERE 650G \$ 65,866 \$ 59,817 9 %



DEFENSE SUPPLY CENTER, COLUMBUS

COLUMBUS, OHIO

DEFENSE SUPPLY CENTER, COLUMBUS

## CUSTOMER SATISFACTION PARTNERS IN EXCELLENCE

### ● YOU :

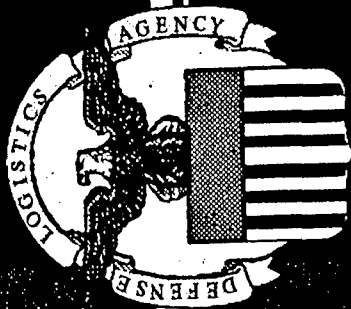
- ● DEFINE YOUR EQUIPMENT REQUIREMENTS
- ● PARTICIPATE IN TESTING AND EVALUATION, AS NECESSARY

### ● WE :

- ● PROVIDE ACQUISITION PLANNING ASSISTANCE
- ● ACT AS PURCHASING AGENT
- ● PERFORM CONTRACT ADMINISTRATION SERVICES

IF YOUR PARTICULAR REQUIREMENT ISN'T ALREADY COVERED BY ONE OF OUR CONTRACTS, WE'LL ADD IT.





# DEFENSE SUPPLY CENTER, COLUMBUS

COLUMBUS, OHIO

DEFENSE SUPPLY CENTER, COLUMBUS

## SUMMARY

- DLA / DSCC IS HERE TO PROVIDE  
✓ THE VEHICLES AND SPARE PARTS YOU  
NEED BETTER, FASTER, AND CHEAPER BY  
WORKING WITH THE MATERIEL DEVELOPER  
AND INDUSTRY.
- INFORMATION ON WWW  
<http://131.74.26.2:8888>
- CONTRACT INITIATIVES
- ENGINEERING EXPERIENCE  
READINESS/ COMBAT CAPABILITY
- HEAVY EQUIPMENT PROCUREMENT  
PROGRAM
- YOU ARE OUR CUSTOMERS AND  
CONTRACTORS
- WE WANT TO TEAM WITH YOU TO  
REDUCE DOD AND CONTRACTORS'  
LOGISTIC COSTS

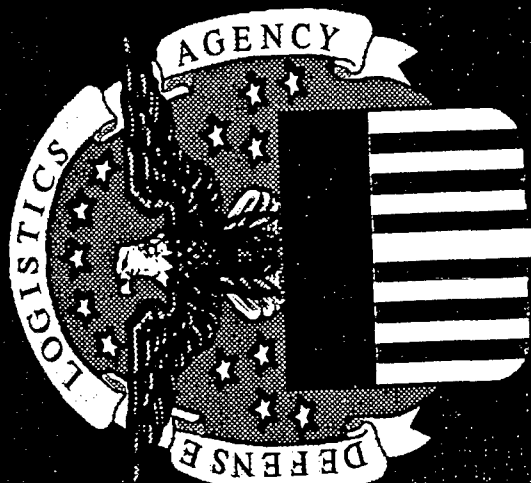


# DEFENSE SUPPLY CENTER, COLUMBUS

COLUMBUS, OHIO



DEFENSE SUPPLY CENTER, COLUMBUS



UNCLASSIFIED

THIS PAGE INTENTIONALLY LEFT BLANK

UNCLASSIFIED

UNCLASSIFIED

**HIT AVOIDANCE THREATS & COUNTERMEASURES SESSION**

King Auditorium  
Tuesday, March 26, 1996

Session Chairman: Mr. Thomas C. Winant, United Defense, L.P.

UNCLASSIFIED

UNCLASSIFIED

THIS PAGE INTENTIONALLY LEFT BLANK

UNCLASSIFIED

**(U) THREAT BASED EXPERT SYSTEM SURVIVABILITY (TBESS)**  
**A Practical Application of the Ground Combat Vehicle**  
**Survivability Database (GCVSD)**

**JEFFERY V. MOSLEY**  
**Office of the Project Manager for**  
**Armored Systems Integration**  
**ATTN: SFAE-ASM-AS**  
**Warren, MI 48397-5000**

**ABSTRACT(U)**

**(U) On 13 March 1995, the Program Executive Officer, Armored Systems Modernization (PEO-ASM) approved a new mission area for the Project Manager, Armored Systems Integration (PM-ASI): "To facilitate the use of Constructive, Virtual, & Live Modeling & Simulation (M&S), in support of DoD Acquisition Reform, and ASM program performance enhancement."**

**In support of the PEO's direction, PM-ASI has initiated several efforts to utilize M&S to enhance ASM programs, TBESS is one of those efforts. The objective of TBESS is to maintain comprehensive knowledge of threats to ASM systems in support of the identification of potential material survivability options. The TBESS process steps are:**

- (1.) characterize the ASM threat environment;**
- (2.) exploit threat capabilities;**
- (3.) identify ASM vulnerabilities and susceptibilities;**
- (4.) identify effective options for ASM system survivability; and**
- (5.) provide engineering level functionality of survivability options in support of Advanced Warfighting Experiments (AWE's) and ground combat vehicle (GCV) modernization.**

**The outcomes of the TBESS process include continuous review and update of ASM threat environments, the ability to identify countermeasures to mitigate threat environments, and the use of M&S to reduce design, test and evaluation cycles for identified technologies and components to enhance ASM system and force level survivability.**



**(U) THREAT BASED EXPERT SYSTEM SURVIVABILITY (TBESS)  
A Practical Application of the Ground Combat Vehicle  
Survivability Database (GCVSD)**

**JEFFERY V. MOSLEY  
Office of the Project Manager for  
Armored Systems Integration  
ATTN: SFAE-ASM-AS  
Warren, MI 48397-5000**

**(U) On 13 March 1995, the Program Executive Officer for Armored Systems Modernization (PEO-ASM) approved a new mission area for the Project Manager for Armored Systems Integration (PM-ASI): "To facilitate the use of Constructive, Virtual, & Live Modeling & Simulation (M&S), in support of DoD Acquisition Reform, and ASM program performance enhancement."**

**In support of the PEO's direction, PM-ASI has initiated several efforts to utilize M&S to enhance ASM programs, TBESS is one of those efforts. TBESS is a M&S application with its performance envelope or required performance defined by confidence limits (CLs). TBESS CLs are established by calibration of the current system design into a M&S application. Successful calibration is defined as verification of the application to physical tests, or to relevant in a M&S scenario results. The applications are then verified by their capability to predict the GCV system behavior, which are again comparable to physical tests.**

**All TBESS M&S applications are in the process of being accredited by PEO-ASM to support his programs. This paper will identify some specific applications already in use, and offer examples of additional uses and outcomes of the TBESS process.**

TBESS provides a cost benefit by reduction of the required resources to evaluate ASM GCVs and major sub-systems against survivability independent evaluation plan/ test evaluation plan (IEP/TEP) critical issues. IEP/TEP issues drive TEMPs. The TBESS process supports USER assessment of ASM GCV performance against critical operational issues (COIs). TBESS can identify potential vulnerability/susceptibility issues in operationally significant scenarios. It can be used as an evaluation tool for survivability concept and components. TBESS maximizes the use of virtual environments and virtual system integration to support resourcing decisions.

Next I will identify the process steps and tools which support TBESS for GCV enhancement, modernization demonstration and T&E. The objective of TBESS is to maintain and distribute comprehensive knowledge of threats to ASM systems and identify potential material survivability options.

The TBESS process steps are:

- (1.) Characterize the ASM threat environment;
- (2.) Exploit threat capabilities;
- (3.) Identify ASM vulnerabilities and susceptibilities;
- (4.) Identify effective options for ASM system survivability; and
- (5.) Provide engineering level functionality of survivability options in support of Advanced Warfighting Experiments (AWE's) and ground combat vehicle (GCV) modernization.

Characterize the ASM GCV threat environment. This is the nexus of TBESS, and is considered to be an intuitive step in analyzing system survivability. The initial data supporting threat environment characterization is provided by the System Threat Assessment Report (STAR).

The STAR is intended to provide the system combat and materiel developers an overview of the projected operational threat environment at the time of fielding. It is in this environment that the GCV system must perform and survive.

PM-ASI, as a complement to the STARs for ASM GCVs, has developed the Ground Combat Vehicle Survivability Database (GCVSD). The database contains a great deal of accurate and detailed data to support survivability analyses of GCVs. The database represents a major step to providing the required data in a consistent format. The time needed to identify data and obtain validated data is significantly reduced. The database provides data for both acquisition and engagement threats both conventional and non-conventional in nature. Characteristic, performance and descriptive data such as inventory listings are described in detail along with delivery systems for those specific threats.

The most important feature of the GCVSD is that it links potential survivability technology options to specific threats. The database is unique in that it includes descriptive information on GCV systems. The current U.S. GCV mix found in the database, represents a spectrum of armor and artillery combat systems.

The GCVSD serves as a data engine for detailed threat environment analysis. The assessed capabilities for threat systems and potential survivability options are not optimized for any given system. It is therefore a requirement that the data contained in the GCVSD be used to enhance threat articulation in operational scenarios for modeling and simulation.

Basic scenarios for M&S are obtained from TRADOC. It has been the experience of PM-ASI that these scenarios, to include their weapons, sensors, and munitions lists, are only a first step in assessing system survivability. This point is most evident in the area of non-conventional warfare such as chemical warfare (CW).

Through development of the TBESS process and in support of the GCV system survivability analysis, PM-ASI has developed a methodology using TRADOC scenarios to assess the CW threat to GCVs. see "Chemical Battlefield Challenge Level Estimates to the Advanced Field Artillery System (AFAS)." The report is dated 12 December 1994, and published by the Edgewood RD&E Center, APG Maryland. The methodology was developed with PM-ASI coordination of the efforts of ERDEC, NGIC, DIA, and DAMI-FIT to define the vapor concentrations for selected CW agents against specific battlefield targets over time.

This level of detailed analysis is required for chemical and biological agent filtering system designs. The methodology used the scenario information to identify the number of threat chemical munition rounds available for use against PM-ASI defined targets. The methodology included simulation of dynamic meteorological conditions.

This type of analysis is very important to the GCV development community. It utilizes validated threat density numbers along with assessed threat lethality data in operation scenarios. The CW analysis can provide initial assessment of NBC survivability IEP issues for developmental ground combat systems. Collateral efforts supported by ERDEC and the intelligence community included, review and re-definition of negligible and lethal toxicology values for chemical agents, and the reduction of a list of over thirty-three weaponizable agents down to a representative list of twelve. The later effort has a direct impact on chemical agent simulant testing for GCV system development.

The outcomes from threat environment characterization drive frequency of encounter determinations. Armed with this type of data, developers can perform trade-off analyses to identify threats of greatest consequence to their system. The data derived from trades study and analysis support downselect of system survivability design options.

The maintenance concept for the GCVSD supplies data for continuous threat analyses and trade studies, until final system design has been selected. Survivability options identified in the database can then be optimized to mitigate the threat(s) of greatest concern to the user and developer.

As I have stated, articulation of threat environment characteristics is of utmost importance to the successful implementation of the TBESS process. These characteristics must be integrated into a total threat environment for system survivability design and evaluation. This further supports cohesive and balanced survivability.

Threat exploitation in support of TBESS has been accomplished by PM-ASI in two complementary ways. First through intelligence Production Requests (PRs). PRs seek finished and in-process intelligence data on the threats of greatest consequence, which derived from step one of the TBESS process, to our GCV systems.

The second, given that PR processes are either not timely, or the level of detail is absent to support TBESS, is the development of standard methodologies to derive the needed characterizations. An example of PM-ASI's use of analysis to fill in for intelligence sources can be found in reports such as, "Armored Vehicle Susceptibility Analysis," dated January 1994. The report was prepared by DYNETICS INC, for OPM-SS and MICOM to identify current GCV susceptibilities to ADHPM and other precision guided munitions. The process used in developing the methodology to assess ASM GCV susceptibility to precision guided munitions, was coordinated with the established analysis community (AMSAA, TRAC), and the providers of finished intelligence (DIA, NGIC, & MSIC). TBESS leverages expert this experience! The assessed threat characteristics for GCV threats whether from PRs or independent analyses are a part of the GCVSD and are planned to be continually updated.

Specific characterizations required to support TBESS threat exploitation include sensor performance and timelines for threat engagement.

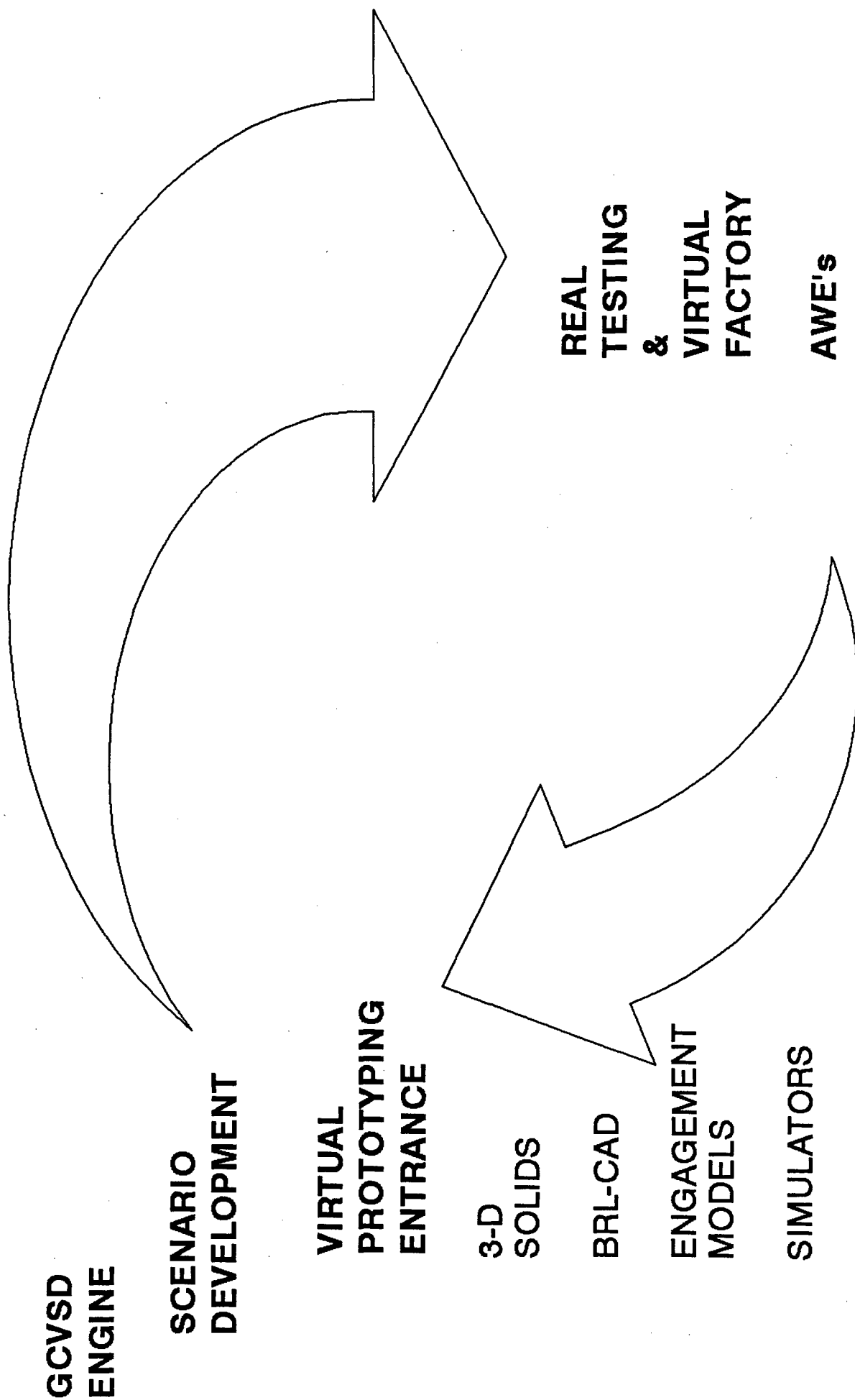
The third step of the TBESS process, identify ASM vulnerabilities and susceptibilities, utilizes the direct comparison of the assessed threat capabilities and aggregate environments against GCV design. The comparison is done initially in static conditions and then further assessed utilizing dynamic, and stochastic M&S. Analyses include not just ballistic, but NBC, electro-magnetic environmental effects (E3), information warfare vulnerability, and threat sensor susceptibility.

As stated in the beginning of this paper, TBESS is a PM-ASI initiative which uses M&S to enhance ASM program performance. PM-ASI has identified a M&S toolkit which identifies the minimally required M&S applications to assess GCV susceptibility and vulnerability. The toolkit has additional value in that it characterizes ASM lethality, mobility, and survivability capabilities. (SEE CHART and PROCESS DEFINITION)

Currently models, simulations, and methodologies exist to support accurate assessment of GCV system designs in all the preceding areas. Examples include NUSSE4- a single CW target effects model. ARL-SLAD/WSMR SEMI facility for E3 assessments. VAM/SQUASH models for ballistic vulnerability assessments. GENESIS 3.0/ALWSIM/CASTFOREM engagement models and force-on-force simulations. MODSAF for real time man in the loop simulations. The GCVSD again is a data engine to support timely assessment using these M&S applications.

The fourth TBESS step, identify effective options for ASM system survivability. The GCVSD serves here as a very comprehensive repository of survivability technologies and components. Survivability information is linked to threat performance. The effectiveness of each survivability option to each threat is verified either by constructive analyses or physical test and evaluation. In either case, the laws of mechanical and electromagnetic physics are not breached. In connection with each survivability option, there are benefits as well as burdens. The term burden may be related in terms of cost, weight, resource consumption, or sustainability. The benefits must not be termed only in direct mitigation of the above burdens, but they must be leveraged with GCV system capabilities and its operational use. The challenge for the system survivability designer is to balance the most operationally significant scenarios and their encounter or engagement parameters with tactics and doctrine against the performance of suites of survivability enhancements. The suites, as we will call them, must then be optimized in terms of susceptibility and vulnerability reduction to mitigate the threat environment and its most proliferated threats.

**THREAT BASED EXPERT SYSTEM SURVIVABILITY A PRACTICAL APPLICATION**



**SUPPORTS THE MODEL-TEST-MODEL PROCESS**

The known U.S. GCV survivability options can be grouped by avoidance category, (Detection, Acquisition/Hit, Penetration, and Kill).

Detection, acquisition, and hit avoidances relate to susceptibility reduction. The threats here are linked to sensors, visual, radar, acoustic, seismic, or pseudo-imaging. A potential M&S analysis tool here can be GENESIS version 3.0. This simulation can effectively model the effects of integrated susceptibility reduction suites against PGM sensors in a many on few scenario.

Penetration and kill avoidances relate to vulnerability reduction. The threats here are both conventional (ballistic) and non-conventional (E3 and NBC). The objective for the designer is, once a threat area has been quantified in terms of shock frequencies, penetration capabilities, or gravimetric densities, to produce designs which focus cost effective point defenses for the crew as well as for the survivability of the GCV system and its operational significant components.

The detailed data provided for each option in addition to application guidance, include description, performance, and production status. Expert points of contact for further information and assistance are also included in the GCVSD.

The survivability designer for future GCVs must seek to balance susceptibility and vulnerability reduction suites against not only postulated threats, but in full awareness of the current and proliferating ones as well. Care must be taken not to stove-pipe designs that do not clear out combined threats and multiple encounters.

The last step of the TBESS process, is to provide engineering level functionality of survivability options for GCV platform optimization. In today's acquisition environment GCV system developers are continually looking for ways to improve the quality of their systems. The ultimate outcome of which will be a GCV system which will be supportable and meet the user's operational needs.

TBESS provides the capability to assess system survivability enhancements impacts in total on concept and developmental systems in a virtual environment.



This can be done by parametrics, or by tethering virtual and real components to simulators. Actual field test conditions with user interaction can be accomplished at a fraction of present day physical test costs. In either case, this capability supports specific system level benefits and burdens to mobility, lethality, sustainment, and overall system level survivability.

PM-ASI has also sponsored the development of the tools for assessment, and is seeking accreditation for their use in GCV design and development to support ASM acquisition reform initiatives. Through use of the GCVSD and ASM M&S toolkit, program enhancements in the forms of reduced physical testing, expanded threat environment testing can be achieved at a cost of man months verses man years of effort. Use of TBESS M&S applications early in the initial design, or during a major system design change in a GCV system's engineering and development life cycle, allows the developer to capture the system's virtual configuration. This further supports design confidence, which will carry on into production, as configuration management of virtual systems feeds computer integrated manufacturing (CIM). The virtual link to CIM is value added to production facilities planning, product producibility, and serves to reduce production and manufacturing cost and time resource requirements.

The outcome of this step links technical and operational test environments.

A point must be made here that although M&S is a major part of TBESS, use of M&S alone is not recommended nor is it authorized by law in the design and T&E of combat systems. M&S as a design aid or tool is highly recommended to make maximum use of developer resources. The model-test-model concept represents great value added, given the commitment to update and calibrate models with physical test data. Used in this way, M&S is a reliable, maintainable, and creditable tool able to support design and development decisions. The TBESS process and tools are currently being used to support ASM major acquisition program milestone decisions.

The future of TBESS in ASM is to demonstrate its functionality and value added throughout the Army acquisition community. The fact that TBESS leverages the best available technology and process tools in an effective manner, makes it an excellent design aide for both the government and contractor community.

PM-ASI will seeks to improve the TBESS process, and support the verification, validation, accreditation and maintenance of its applications for ASM GCV system development.

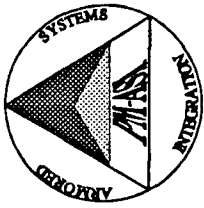
UNCLASSIFIED

THIS PAGE INTENTIONALLY LEFT BLANK

UNCLASSIFIED



# TARDEC Ground Vehicle Survivability Symposium



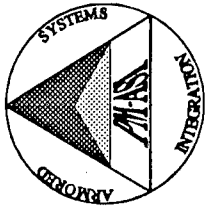
## Focused Dispatch Advanced Warfighting Experiment Laser Warning Receiver Demonstration

Major (P) Joseph Della Silva  
Office of the Project Manager, Armored Systems Integration  
26 March 1996



# Focused Dispatch Advanced Warfighting Experiment Laser Warning Receiver Demonstration

---

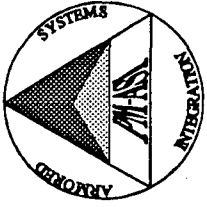


## Purpose

Present findings from the Laser Warning Receiver (LWR) Demonstration conducted during the Advanced Warfighting Experiment (AWE) Focused Dispatch, 14-30 August 1995



# Focused Dispatch Advanced Warfighting Experiment Laser Warning Receiver Demonstration

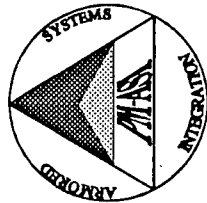


## Outline

- Objectives
- Background
- Demo Concept
- Key Players
- Demo Hardware
- Evaluation Concept
- Demo Results
- Conclusions



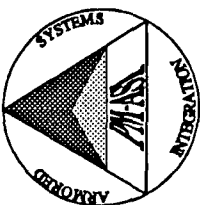
# LWR Demonstration Objectives



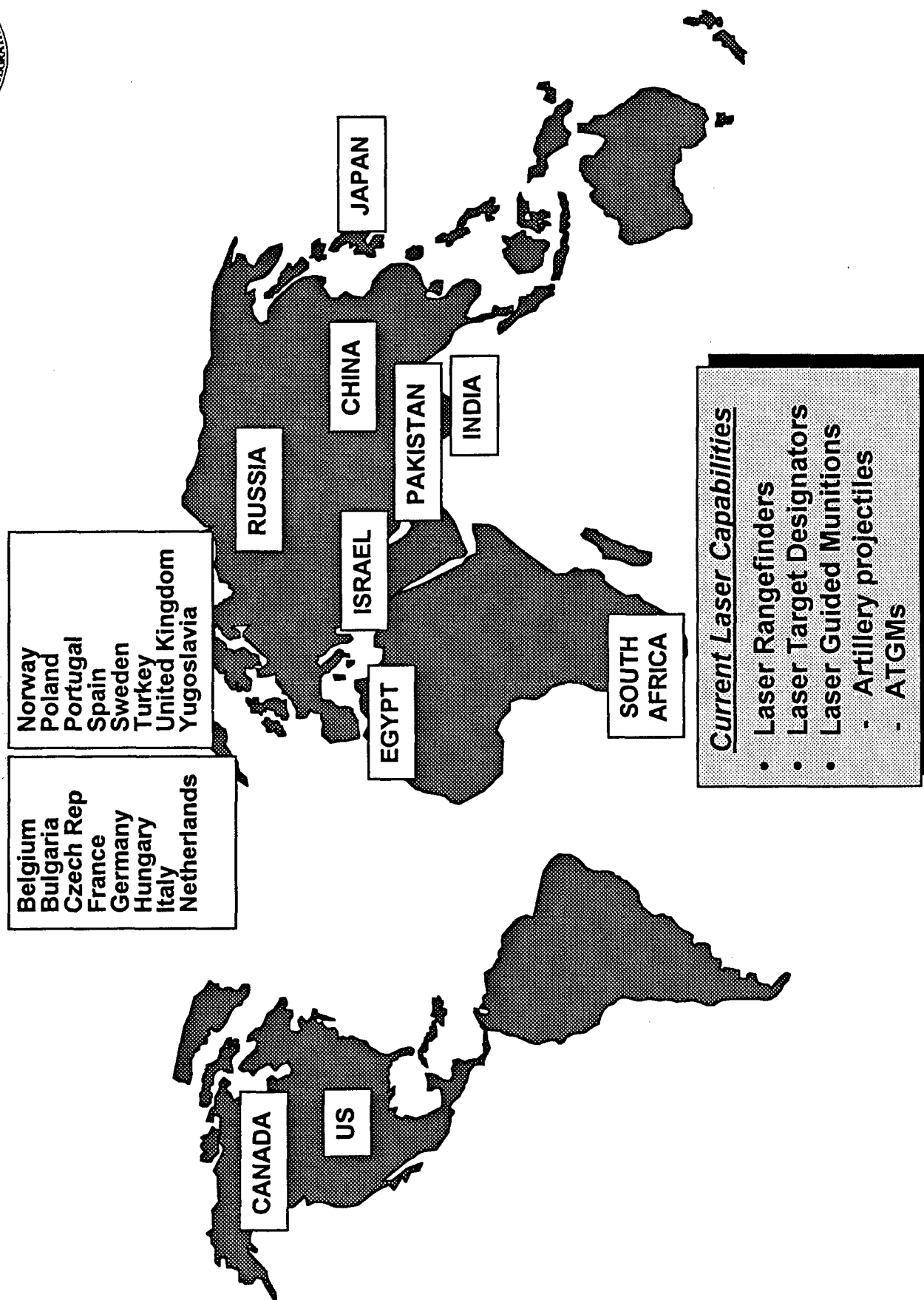
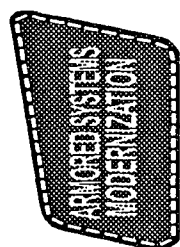
- Assess LWR's ability to enhance vehicle and crew survivability
- Collect experimental data to assess feasibility of placing LWRs on US Army Combat Vehicles

## Primary Areas of Concern

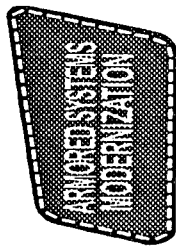
- Vehicle Survivability Benefits
- Tactics, Techniques, and Procedures (TTP)
- Soldier-Machine Interface (SMI)



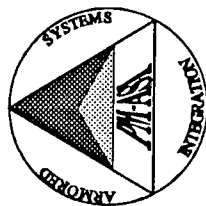
# Background Laser Threats to Ground Combat Vehicles







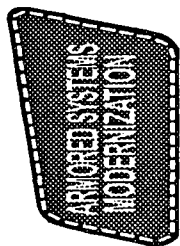
# Background



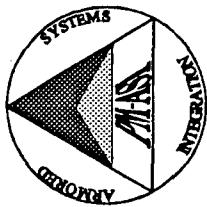
## Numerous LWR assessments conducted

	<u>Dates</u>
• LWR Concept Evaluation Program - Armor Center (Ft Knox)	FY91
• Vehicle Integrated Defense System (VIDS) demo - TARDEC	FY92
• Ground Wars Analyses of LWRs - PM-SS (Now PM-ASI)	FY92-FY93
• Ground Vehicle Survivability LWR Field Tests - CECOM	FY93
• Force Protection Concept Initiatives - MBBL (Ft Knox) <ul style="list-style-type: none"><li>- Distributed Simulation Development Test of VIDS</li><li>- Force Protection Evaluation Phase II</li></ul>	FY93 FY94
• Project Guardian EW Effectiveness Study - TARDEC/MBBL	FY94
• Integrated Protection System (IPS) Study - AMSAA	FY95

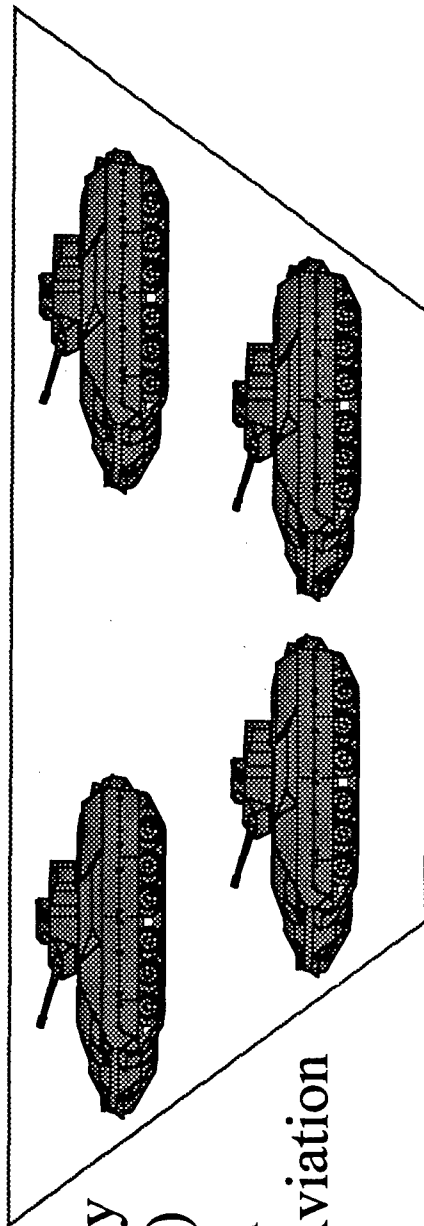
**All assessments confirmed LWR benefit, but no indication of the LWR's tactical utility or its benefit to a small unit**



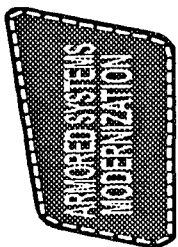
# LWR Demonstration Concept



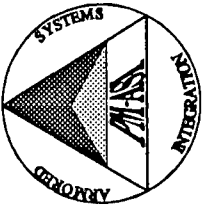
- Outfit a platoon of Bradley Fighting Vehicles (BFVs) with modified production AN/AVR-2A(V) Army Aviation Laser Detection Set



- LWRs detect MILES signals used to simulate threat weapon engagements
- Train BFV crews on LWR use, assess performance during three tactical scenarios:
  - ⇒ Deliberate Attack
  - ⇒ Movement to Contact
  - ⇒ Defense in Sector
- Collect data and soldier reactions on all laser engagements during each scenario



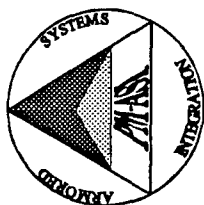
# Key Players



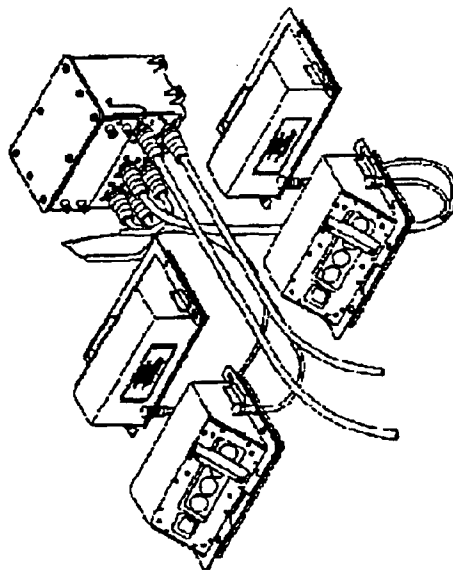
- US Army Infantry Center
  - Demonstration sponsor
  - Developed TTP
- Mounted Battlespace Battle Lab
  - Conducted demonstration
- PM Aviation Electronic Combat
  - Provided LWRs
- PM Bradley/UD(LP)
  - Provided LWR mounting hardware
- CECOM
  - Provided technical support
  - Conducted equipment training
- Hughes Danbury Optical Systems
  - Provided technical assistance
- PM Armored Systems Integration
  - Demo coordination
  - Provided data evaluation
- 2d Platoon, Co. B., 2-33 Armor
  - Provided soldiers to operate Bradleys with LWRs



# LWR Demonstration Hardware

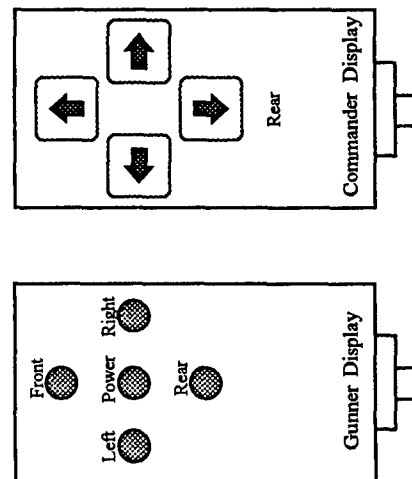


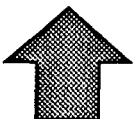
AN/AVR-2A(V) Laser Detecting Set

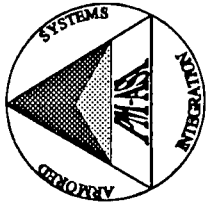


- Modified production version of the AN/AVR-2A(V)
  - 4 sensor heads provide 360 degrees field of regard
  - Each sensor provides quadrant location of MILES signals
- Custom- made display panels provide visual alert

LWR Display Panels



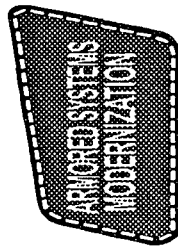
- Audio warning (tones) provided through BFV intercom system
- Threat detection: MILES used on tanks and ATGMs
- Countermeasure responses  Evasive maneuver  
Counterfire  
Simulated smoke



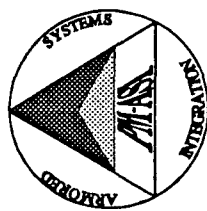
# Evaluation Concept

---

- **Soldier training prior to demo (all crews/backups):**
  - ⇒ LWR Training
  - ⇒ TTPs
  - ⇒ Data collection methods
  
- **Evaluation Methods Defined:**
  - ⇒ Given a lasing event:
    - ⇒ MILES simulates threat laser - kill or near miss
    - ⇒ LWR detects laser signal and alerts crew - Visual/Audio
  - ⇒ Vehicle commander reacts when either MILES or LWR detect threat lasing
  - ⇒ Reaction to threat alert continues for 30 seconds
  - ⇒ End of engagement, crew fills out data collection sheet



# Evaluation Concept (Continued)



- **LWR Concerns Identified:**

⇒ Vehicle Survivability:

1. Did the LWR aid target acquisition?
2. Did the LWR give crew the time needed to react?
3. Did the LWR enable crews to effectively counter multiple laser designations?

⇒ TTPs:

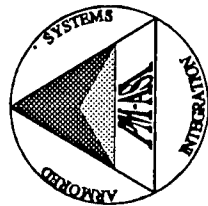
1. Did the LWR improve tactical performance?
2. Did the LWR improve platoon situational awareness?

⇒ SMI:

1. Were LWR displays adequate?
2. Were visual alerts/warnings sufficient?
3. Were audio alerts sufficient?



# LWR Demonstration Results



- Sixty seven laser engagements recorded throughout AWE
  - MILES alarmed on 19 engagements
  - LWR alarmed on 64 engagements\*
- Vehicle Survivability Impact:
  - Crews quickly identified targets and engaged, evaded, or employed smoke
  - Additional time to react
  - No data on multiple laser engagements

CM Option	# Laser Events (Total)	# Times CM Used	# Times CM Effective
Maneuver	67	55	44
Counterfire	67	54	Data Not Available
Smoke	67	44	37

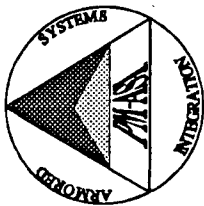
\* - Discrepancy due to LWR being more sensitive than MILES sensors



# LWR Demonstration Results

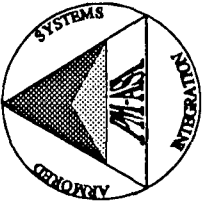
(Continued)

---



- TTP Impact
  - Improved ability to position weapons systems
  - Improved target acquisition ability to engage threats
  - Marked advantage in battlefield movement after contact made (no benefit before contact is made)
  - Improved platoon situational awareness
- SMI Assessments:
  - Displays adequate (soldiers prefer integration into sights)
  - Visual alerts good and clear
  - Audio alerts adequate, but would rather have vocal alert than tone
  - Must have both visual and audio alert





# Conclusions

---

## 1. Assessment of tactical utility/benefit of LWR to a small unit:



Soldier/System Survivability:

*Improved threat/target acquisition  
More time to react to threats*



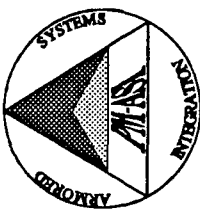
Unit tactical procedures:

*Improved ability to position vehicles  
Improved target acquisition  
(after contact)  
Enhanced maneuver capability  
(after contact)  
Improved situational awareness*



Soldier-Machine Interface:

*Simple displays adequate  
Visual and audio alerts needed*



## Conclusions (Continued)

---

### 2. Soldier recommendations:

- ☞ Improve direction of arrival (azimuth), would like range to target also
- ☞ Discriminate between rangefinders and designators
- ☞ Integrate with IVIS to enable generation of Contact Reports when lased
- ☞ Modify LWRs to give better protection outside vehicle
- ☞ Integrate LWR displays with vehicle/system displays
- ☞ Provide voice alert instead of audio tone

### 3. Focused Dispatch AWE reaffirmed LWR benefits at small unit level

UNCLASSIFIED

THIS PAGE INTENTIONALLY LEFT BLANK

UNCLASSIFIED

# UNCLASSIFIED

## The High Angular Resolution Laser Irradiance Detection System (HARLIDS)(U)

*by*

Michael P. Altman  
Loral Infrared & Imaging Systems  
Lexington, MA 02173

*and*

Dr. Andre Cantin  
Defense Research Establishment Valcartier  
Courcelette, Quebec, Canada

### ABSTRACT (U)

(U) In early 1995, Loral Infrared & Imaging Systems (LIRIS) designed, built, and tested the HARLIDS for EG&G Canada and the Defense Research Establishment, Valcartier (DREV), Canada. The system employs a nine element HARLID<sup>TM</sup> detector array and a grey code mask to establish the angle of arrival in each axis. The system is designed to detect laser rangefinders (LRF) and laser target designators (LTD). Laser irradiance levels were measured during characterization tests at DREV in September 1995. This system was installed upon a Canadian Forces Leopard main battle tank and underwent evaluation testing at the Canadian Government's QAG-16 Tank Trials in October 1995 at Gagetown, New Brunswick, Canada.

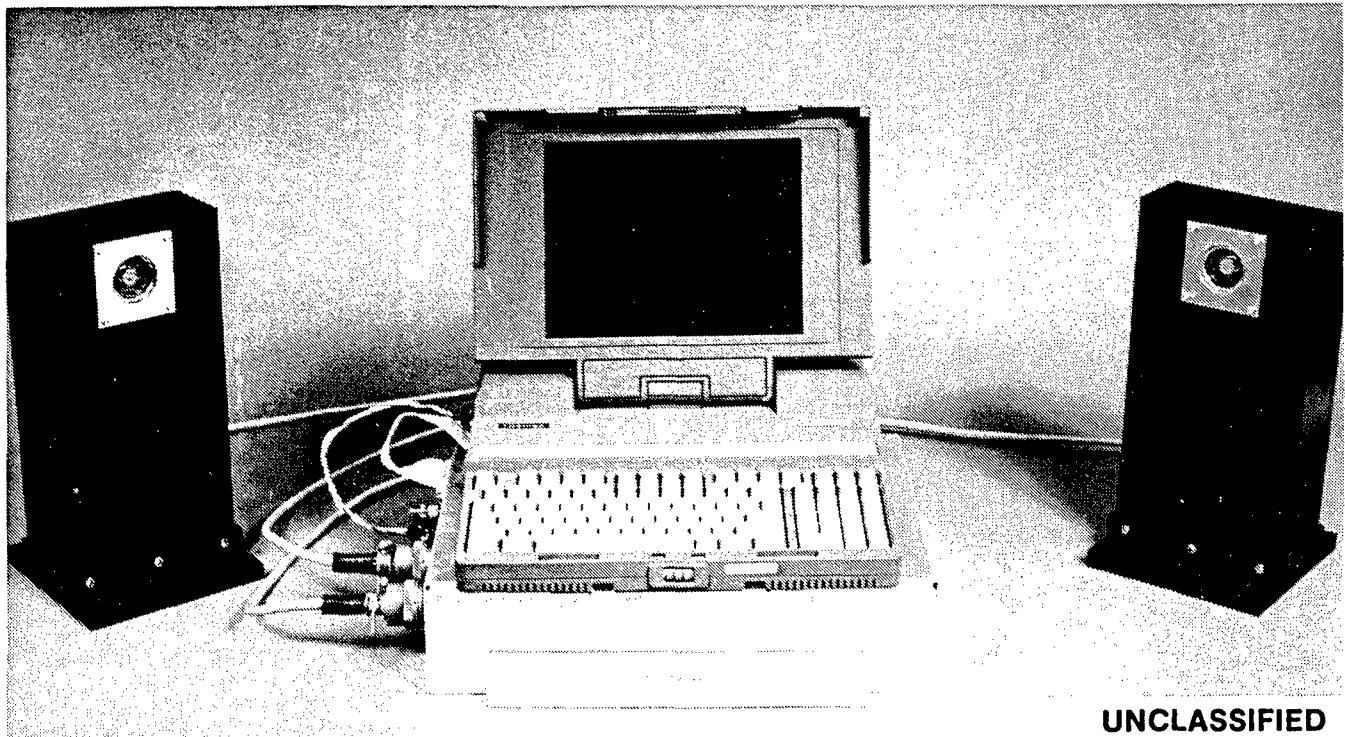
### (U) Introduction

(U) The HARLIDS Phase 1 program comprises the design, build, assembly, and test of 2 prototype HARLIDS laser warning receivers and a lap top personal computer (PC). The Phase 1 HARLID system is depicted in Figure 1. Each laser warning receiver consists of one HARLID detector module, one detection/discrimination electronics board, one protective glass window, one aluminum housing, and one cable. Two HARLIDS laser warning receivers, one interface box and one lap top PC were designed, built, and tested by LIRIS and delivered to EG&G Canada for DREV under contract from EG&G and the Canadian Government during the period November 1994 to July 1995. The LIRIS-owned laptop PC was loaned to DREV for 1 year to assist in field test trials in Canada. Irradiance levels from 1 mW/cm<sup>2</sup> to 10 W/cm<sup>2</sup> were measured during characterization tests at DREV in September 1995. This system was tested at the Canadian Government's QAG-16 laser warning receiver tank trials in October 1995 at Gagetown, New Brunswick, Canada.

UNCLASSIFIED

Distribution authorized to U.S. Government agencies only. Foreign Government Information to be protected and limited in accordance with the desires of the Canadian Government, March 4, 1996.

UNCLASSIFIED



UNCLASSIFIED

95359

Figure 1. (U) High Angular Resolution Laser Irradiance Detection System (HARLIDS)

(U) System Design

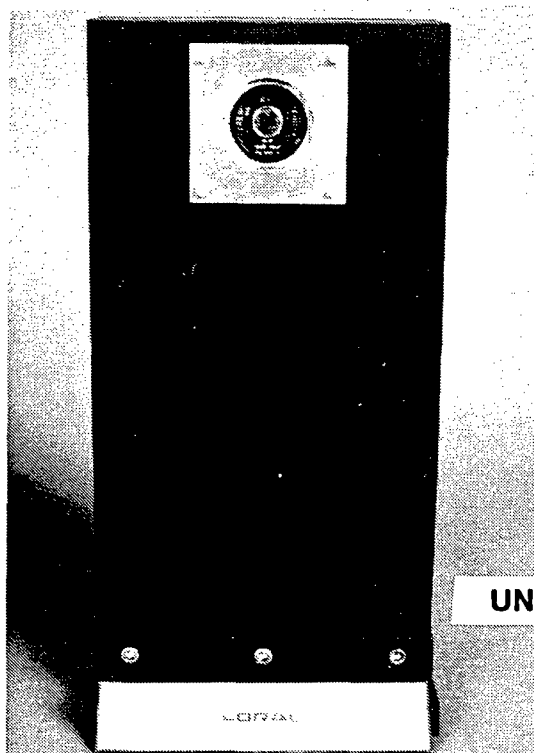
(U) The HARLIDS is designed to detect pulsed laser rangefinders and laser designators while providing angle of arrival information in azimuth. These rangefinder and designator systems exhibit irradiance levels from approximately  $100 \text{ W/cm}^2$  to  $100 \mu\text{W/cm}^2$ . The HARLIDS is designed with high and low sensitivity arrays to cover this large dynamic range. The HARLIDS Phase 1 program demonstrated the performance of the low sensitivity array.

(U) The HARLIDS consists of two HARLIDS laser warning receivers, an interface box, and a lap top personal computer. Each receiver houses one HARLID detector module mounted on a single HARLIDS electronics board shown in Figure 2 and Figure 3. DREV developed the patented, digital HARLID modules. A Canadian contract was awarded to EG&G Optoelectronics Canada to manufacture six of these modules. Two modules were provided to Loral for this program.

(U) Each HARLID detector module holds two arrays of silicon detectors. Each array consists of 9 detectors. Three detectors are reference detectors while the other six detectors are used to create a six bit word equal to the incident radiation's angle of arrival. This six bit word is created via a mask which transmits or blocks radiation over each detector depending on the angle of incidence. The three reference detectors have no blockage. The six bits translate to  $\pm 1^\circ$  accuracy in azimuth. Quadrant accuracy is provided in elevation. The HARLID module mask is illustrated in Figure 4.

UNCLASSIFIED

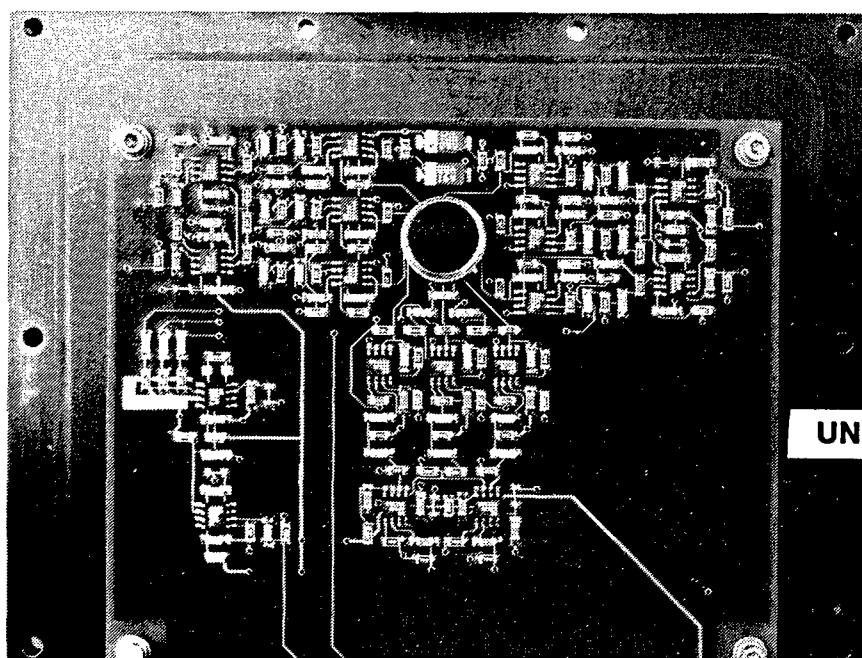
UNCLASSIFIED



UNCLASSIFIED

95356

Figure 2. (U) HARLIDS Laser Warning Receiver



UNCLASSIFIED

95358

Figure 3. (U) HARLID Detector Module and Electronics Board

UNCLASSIFIED

UNCLASSIFIED

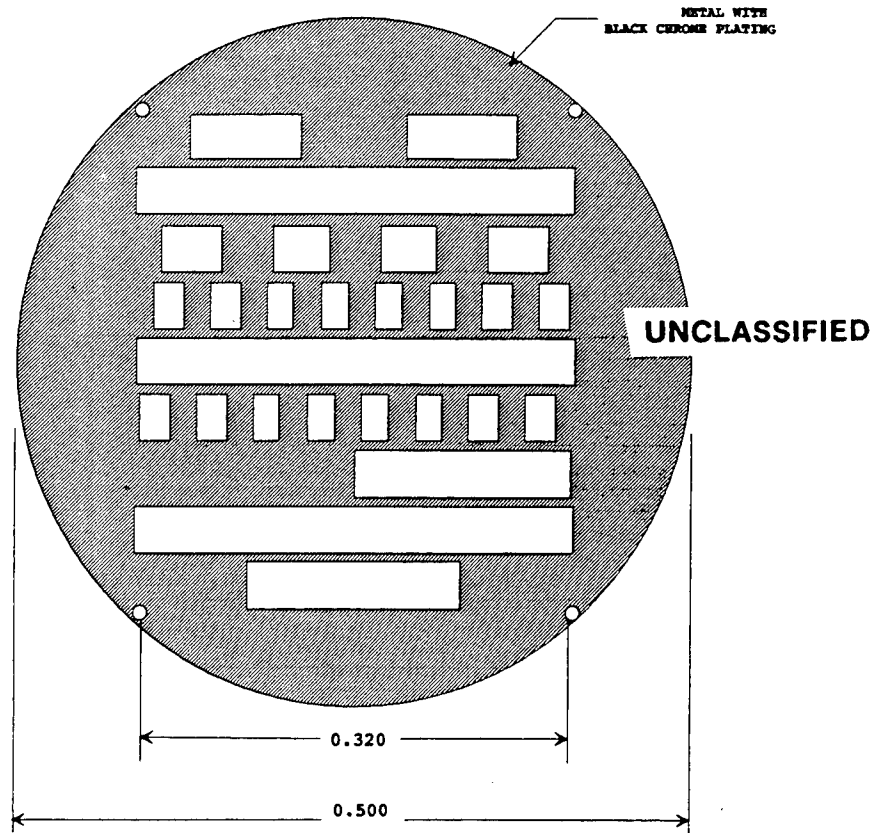


Figure 4. (U) HARLID Module Mask

(U) Each HARLID detector module provides a  $\pm 47^\circ$  azimuth by  $\pm 45^\circ$  elevation field of view. The field of view of the HARLIDS system is  $\pm 92^\circ$  azimuth and  $\pm 45^\circ$  elevation. Two HARLID detectors offer overlap coverage at  $\pm 2^\circ$ . The negative azimuth angles are assigned to positions to the left of the tank turret with  $0^\circ$  boresighted with the tank gun. Positive angles are assigned to the right side of the turret. The sensors are mounted on the tank turret at  $+45^\circ$  and  $-45^\circ$  azimuth with respect to the tank gun.

(U) System sensitivity is based upon a worst case solar background. The shot noise from direct solar irradiance results in a noise equivalent irradiance (NEI) value of  $61 \mu\text{W}/\text{cm}^2$ . The system is designed to a minimum detectable irradiance (MDI) value of  $590 \mu\text{W}/\text{cm}^2$  at the primary wavelength of interest.

(U) The HARLIDS system employs a high pass filter to attenuate unwanted background signals. In addition, solar backgrounds are also attenuated beyond 1 kHz. This is significant for helicopter applications where the sun may be viewed directly through the helicopter rotor, producing a modulated solar signal. The high pass filter also performs a second function: discrimination of threats from non-threats. Pulsed lasers exhibit pulse widths that are much shorter than non-threat sources. The high pass filter gates detections based upon their pulse widths. Detections that exceed the threshold setting are declared as threats. This discriminant is a key feature of the HARLIDS system.

#### (U) Electrical Design

(U) Figure 5 illustrates the HARLIDS functional block diagram.

UNCLASSIFIED

UNCLASSIFIED

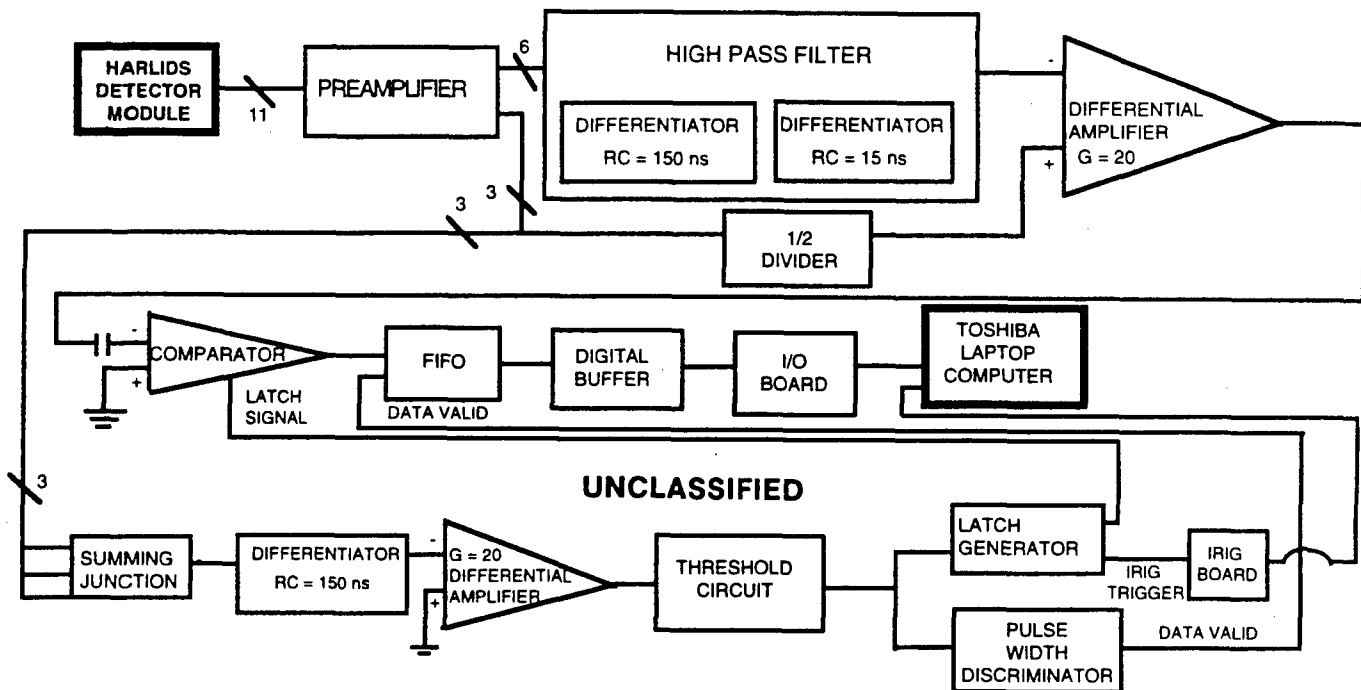


Figure 5. (U) HARLIDS Block Diagram

(U) The signal from each of the detectors (3 reference detectors and 6 signal detectors) is amplified by a preamplifier. The signal from the preamplifiers is differentiated with a passive network. The differentiated signal from each signal detector is subtracted from 1/2 of the signal from the nearest reference detector in the summing amplifier. The outputs of the 6 summing amplifiers go to the 6 signal comparators. These comparators are sampled by a logic pulse from the timing generator. These 6 outputs are stored in a FIFO (first in, first out memory) which also serves as the main computer interface.

(U) The signals from the 3 reference channels are summed in the reference summing amplifier. This summed reference signal is monitored by the overload comparator and amplified by a limiting amplifier and then detected by the reference channel comparator. The output of the reference channel detector is used to generate all the timing and logic signals associated with detection of a pulse and declaring it to be a laser pulse. A detected pulse generates an interrupt for the associated computer which then reads an 8 bit word. The 8 bits consist of the state of each of the 6 signal channels, plus the output of the overload comparator, plus a data valid signal which is the result of a pulse width measurement on the reference channel signal. Each of the major blocks is described in more detail below.

#### (U) Preamplifier

(U) The Analog Devices AD829 video operational amplifier was chosen as the preamplifier. This device has reasonable input referred noise (2 nV/Hz, 1.5 pA/Hz). The external compensation pin on this device has a number of interesting uses. For the preamplifier, the compensation pin is used as a feedback compensation which allows for a higher slew rate and

UNCLASSIFIED



## UNCLASSIFIED

(U) a better tolerance for source impedance variations than the standard compensation. The feedback components for this stage give it a flat response from DC to about 1 MHz with a single pole (6 dB per octave) roll off to frequencies over 10 MHz.

### (U) Differentiator

(U) Following each preamplifier is a differentiator network. At the output of this network, the frequency response measured from the preamplifier input is flat between 1 and 10 MHz, with a 2 pole (12 dB per octave) roll off below 1 MHz. This second order high pass filtering provides most of the rejection of non-laser sources by rejecting slowly varying signals.

### (U) Summing Amplifier

(U) Each of the signal channels is subtracted from 1/2 of the corresponding reference channel signal in a summing amplifier. This amplifier is an AD829 used open loop as a limiting amplifier by resistively loading the compensation pin. This converts the device into a non feedback voltage amplifier with a voltage gain approximately equal to  $50\Omega$  divided by the load resistor. The summing amplifiers use a  $5K\Omega$  load, so the summing amplifier gain is approximately 100. The bandwidth of the summing amplifier is set by the stray capacitance at the compensation pin, which is about 5 pF, and the load resistor. The bandwidth of the summing amplifiers is about 6 MHz.

### (U) Signal Comparator

(U) The comparator is a Maxim MAX900 quadruple comparator with output latches. This is a relatively low power part with a propagation delay of 7 ns and TTL level output. The summing amplifier output is AC coupled into the comparator using a long time constant (50  $\mu$ s) to reject the summing amplifier offset. The comparator output is fed through an EMI isolation resistor to the FIFO data input. These comparators have a nominal zero threshold; they are meant to compare 1/2 of the reference channel to the signal channel. Noise triggering, which is normally a problem with a zero threshold comparator, is prevented by the latch input. The latch input is only activated when a signal has been detected by the reference channel. Otherwise, all the signal comparators are held in the latched state and are therefore disabled.

### (U) Reference Summing Amplifier

(U) This amplifier, an AD848 video amplifier, sums the outputs of the three reference channel preamplifiers and provides a gain of about 3 for each channel, or a gain of about 10 if the signals from all three reference channels are the same. The input and output networks around this also duplicate the frequency response of the differentiators in the signal channel.

### (U) Reference Limiting Amplifier

(U) This amplifier is an AD829 connected as a limiting amplifier with a gain of about 30 and a bandwidth of more than 10 MHz. It is similar to the summing amplifiers in the signal path, but with lower gain and higher bandwidth.

## UNCLASSIFIED

### (U) Reference Comparator

(U) This comparator is the main signal detector for the electronics. It sees the summed signal from the three reference detectors with a total gain of about 250,000 V/A and a bandwidth from about 1 to 10 MHz. Loral has previously determined that this is near the optimum bandwidth for detection of laser pulse widths up to about 100 ns. This comparator has an input threshold set to about 50 mV. This threshold must be about 7 times higher than the worst case RMS noise at the comparator input. The latch input on this comparator is always active.

(U) Once a pulse is detected, the threshold of the reference detector drops to 0. This allows for more accurate timing of the pulse width and also provides positive feedback to ensure a minimum pulse width sufficient to operate the timing circuitry.

### (U) Mechanical Design

(U) Each HARLIDS receiver resides in a heavy aluminum housing. This housing serves a number of functions. It provides a rugged environment for the fragile electronics board and HARLID detector. It offers an EMI shield against sporadic outside noise sources that can interfere with the proper operation of the system. Finally, it offers height to the HARLID detector, in terms of an integral pedestal, to minimize field of view blockage when mounted on a tank. This is particularly important when detecting lasers that may be emanating from angles below the tank (e.g. when the tank is on a hill). This pedestal provides elevation so that the HARLIDS can have an unobstructed view over the tank turret.

(U) A protective outer glass window was designed to protect the HARLID detector module during field tests. Transmission tests revealed that the Barr glass demonstrated an inband transmission of 70% for both receivers. A holder was designed to mount both the protective glass window and standard two-inch square neutral density filters. While filters were not required for this phase of the program, the option for installing them at some other time was deemed useful.

(U) An interface box was designed to provide mechanical interface for all electrical connections between the receivers and the computer. The interface box provides connections for an external IRIG input. The AITG interface connector mates to the AITG card in the lap top computer. The AITG card provides IRIG-B information. The card can be synchronized with an external IRIG generator using the IRIG input port on the interface box. The PC-DIO-24 interface connector provides sensor information coming from cables 1 and 2 to the National Instruments I/O board (PC-DIO-24) residing in the laptop computer.

(U) It should be noted that each array is not boresighted with the mechanical centerline of the T-08 package of the HARLID detector module and therefore is not boresighted with the HARLIDS receiver. A 1.5° offset exists in azimuth. This offset is accounted for when generating the lookup tables for establishing system angle of arrival in the HARLIDS computer.

UNCLASSIFIED

## UNCLASSIFIED

### (U) Computer Interface

(U) The main components of the computer interface are the Toshiba 5200 lap top personal computer, the National Instruments PC-DIO-24 data I/O card (resident in the PC), the K-SYSTEMS IRIG-B card (AITG card also resident in the lap top PC), and two 256 by 9 bit FIFO's located in each receiver.

(U) The system was designed to perform as closely to real-time as possible. The system contains minimum hardware to buffer events. Due to the very tight cost constraints of the HARLIDS program, the system was designed around an existing lap top PC, I/O card and IRIG card. No additional means of buffering events was implemented. Under these conditions, software was written to minimize throughput. Activities were prioritized. The system and software were designed to respond to detection events as soon as possible. Other tasks were performed during periods of inactivity.

(U) When in the active state, the PC sends a request to each receiver to send the angle of arrival and threat type information to the computer. The PC then reads the buffer on the IRIG board. The receiver data and IRIG data are transmitted to the PC RAM via the I/O board. The system will confirm that the two receivers are in sync. This assures that both receivers are being read at the same IRIG time. If the FIFO's are not in sync, they will be reset.

(U) When in the inactive state, the PC writes the data in RAM into a file on the hard drive. This file is named by the user during program execution and is given a.log extension.

### (U) HARLIDS Phase 1 System Performance

#### (U) Subassembly Electrical Tests

(U) The subassembly electrical tests were executed with a test generator. This generator used an array of capacitors driven by a square wave generator to simulate narrow current pulses from the optical detectors. The major emphasis in testing was to characterize the accuracy of the amplitude comparison as a function of input signal to determine the effective dynamic range of the system. These tests indicated that the electronics for all nine detectors were functioning properly and that the system should meet its design goal of 30 dB optical (60 dB electrical) dynamic range.

#### (U) System Level Tests Performed By Loral

(U) Loral performed a functionality test with an LED to demonstrate the threat/non-threat pulsewidth discrimination capability of the system. An LED was driven with a function generator at pulsewidths typical of laser systems. The very low irradiance of the LED required that the source be placed less than 1 cm from the entrance aperture of the HARLIDS receiver. (This produced an extended, uncollimated optical field from which accurate angle of arrival measurements could not be derived.) The pulsewidth of the LED could be extended to demonstrate the threat and non-threat capability of the system. This was performed successfully at a demonstration for DREV and EG&G Canada on June 28th, 1995.

UNCLASSIFIED

## UNCLASSIFIED

(U) Limited false alarm testing was performed under solar background conditions with the sun in the field of view. The solar background shot noise is the dominant noise source when the sun is directly in the field of view of the HARLIDS receiver. Prior to this test, the threshold circuit was increased by a factor of two to account for the solar shot noise, which is expected to be twice the detector noise under worst case conditions.

(U) The solar shot noise test was performed at 12 noon on June 30 1995 in Lexington, Massachusetts, USA (latitude 42° 25'). This is close to worst case solar background conditions for this latitude. The test was performed just 10 days after the summer solstice.

(U) This test was performed for 15 minutes with both receivers directly viewing the sun. No detections (either threat or non-threat) were observed from either receiver during this time.

### (U) Results From DREV System Characterization Tests

(U) DREV characterized the HARLIDS system at their facility during the summer of 1995, upon receiving delivery from Loral. Angle of arrival measurement results are illustrated in Figure 6. DREV indicated that a four order of magnitude dynamic range had been measured using laser sources. Specifically, DREV reported that the system operated properly over a range of irradiances from 1 mW/cm<sup>2</sup> to 10 W/cm<sup>2</sup> at the primary wavelength of interest. These results are better than those reported during the electrical characterization tests.

(U) The HARLIDS was mounted on a Canadian Forces Leopard main battle tank and tested at Gagetown, New Brunswick, Canada, October 9th-27th, 1995. Technical evaluation included angle of arrival performance, off-axis detection, multiple threat discrimination, and false signal susceptibility. Threat sources included military laser rangefinders and target designators.

(U) The results analyzed to date indicate that the system displayed  $\pm 1^\circ$  angle of arrival accuracy during direct illumination and off-axis testing (up to 5 meters off-axis). The system showed no discrepancies when viewing threats that resided in the field of view of both receivers (overlap region). Front and backscatter tests displayed similar results.

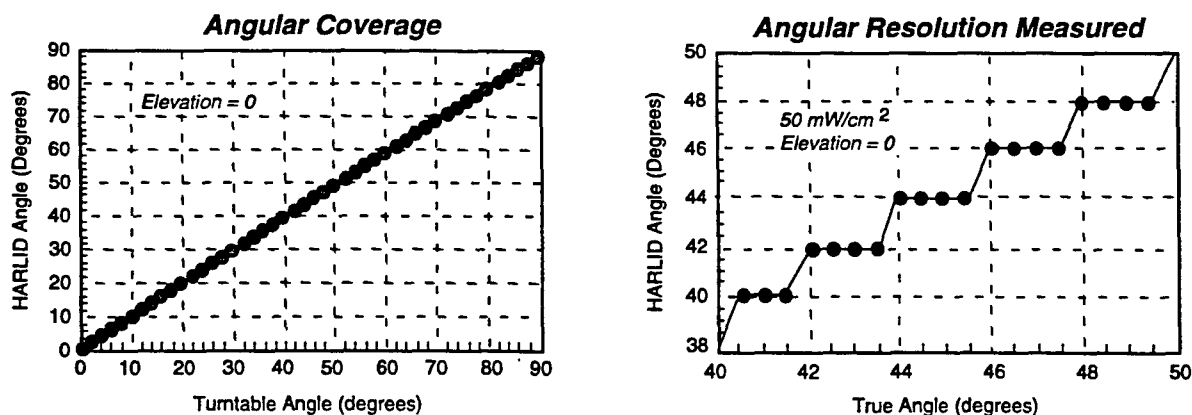
(U) The HARLIDS survived the rough tank environment, operating flawlessly during the 3 weeks of testing. The system remained mounted to the tank at night when temperatures dropped below 15°F. The system always operated the next morning.

### (U) Recommendations For Phase 2

(U) Phase 2 of the HARLIDS program is expected to demonstrate the performance of both high and low sensitivity arrays in a package suitable for helicopter installations. This requires that both arrays together must cover the 100 W/cm<sup>2</sup> to 100  $\mu$ W/cm<sup>2</sup> detection requirement.

UNCLASSIFIED

UNCLASSIFIED



UNCLASSIFIED

Figure 6. (U) HARLIDS Performance

(U) Due to the enhanced dynamic range capability demonstrated with the high sensitivity array, the low sensitivity array should only have to cover the  $100 \text{ W/cm}^2$  to  $10 \text{ W/cm}^2$  laser irradiance region. Some overlap of coverage between high and low sensitivity arrays is recommended. Still, this reduces the risk in providing a low sensitivity array with the same dynamic range performance as the high sensitivity array.

(U) Achieving the  $100 \mu\text{W/cm}^2$  sensitivity performance will be more difficult. Under worst case solar background conditions, the shot noise for this system is  $61 \mu\text{W/cm}^2$ . When the sun is not in the field of view, the NEI is lower and the requirement may be approachable with improvements to the electronics and a variable threshold circuit.

(U) The next generation of HARLIDS needs some type of first pulse logic to distinguish source irradiance from scattered signal. The present system has a crude form of this. A 100 microsecond lockout occurs whenever a valid pulse is received. However, this was incorporated to prevent throughput problems with the I/O card and not as a first pulse logic technique. The present technique appeared to work well during off axis ground irradiance tests. The system always pointed at the laser source.

UNCLASSIFIED

**UNCLASSIFIED**

## **INTEGRATED SURVIVABILITY ANALYSES (ISA) - REAL TIME (U)**

Bahram Fatemi, PhD  
and  
James Wiederrich, PhD  
United Defense L.P.  
Santa Clara, CA 95052

### **ABSTRACT (U)**

(U) Trends in ground vehicle weight and anti-armor penetration preclude armor as the sole solution for survivability. Vehicle survivability solutions require the proper selection of several survivability technologies to give the combined effect necessary to meet technical and cost requirements. This presentation gives an overview of the Integrated Survivability Analyses (ISA) approach being developed at United Defense to run in real time on engineering graphic workstations. This ISA approach accounts for the synergy and combined effect of survivability technologies, and the real time computation capability allows rapid evaluation of many design alternatives to be performed during the concept development phase. This ISA real time approach thus facilitates the selection of the proper mix of survivability technologies necessary to meet the technical and cost measures.

**UNCLASSIFIED**

Approved for public release

UNCLASSIFIED

UNCLASSIFIED

United Defense

FMC/BMY

# **Integrated Survivability Analyses (ISA) - Real Time**

Bahram Fatemi, PhD  
James L. Wiederrich, PhD  
United Defense  
Santa Clara, CA 95052

UNCLASSIFIED

UNCLASSIFIED

## **Why ISA?**

### **Armor Alone Won't Do It**

- Approaching Practical Weight Limits
- Increasing Anti-Armor Penetration

**Require Proper "MIX" of Survivability  
Technologies to Meet Technical &  
Cost Requirements**

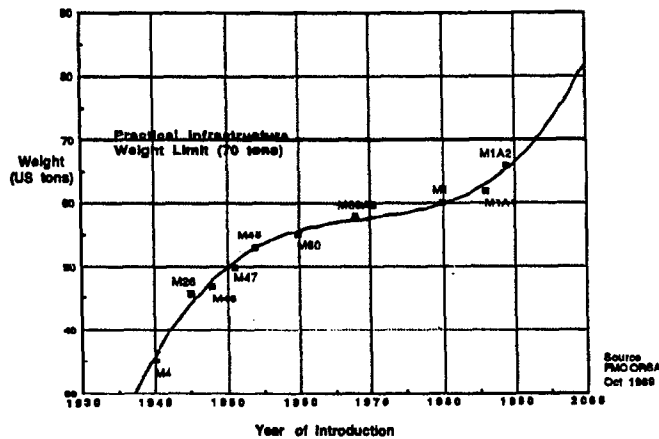
UNCLASSIFIED

UNCLASSIFIED

UNCLASSIFIED

UNCLASSIFIED

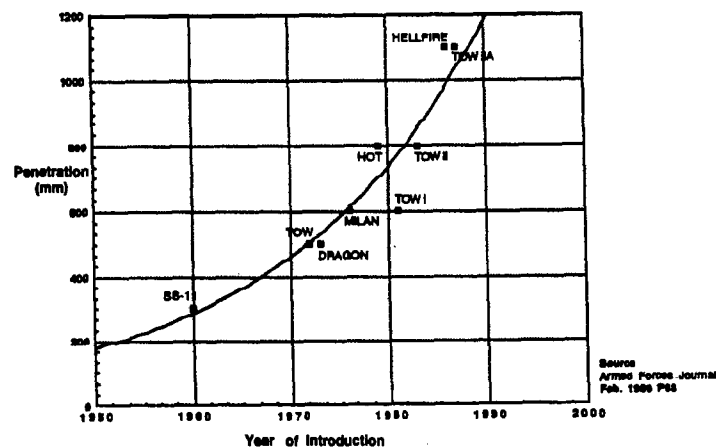
## US Tank Weight Trends



UNCLASSIFIED

UNCLASSIFIED

## Anti-Armor Penetration Trends



UNCLASSIFIED

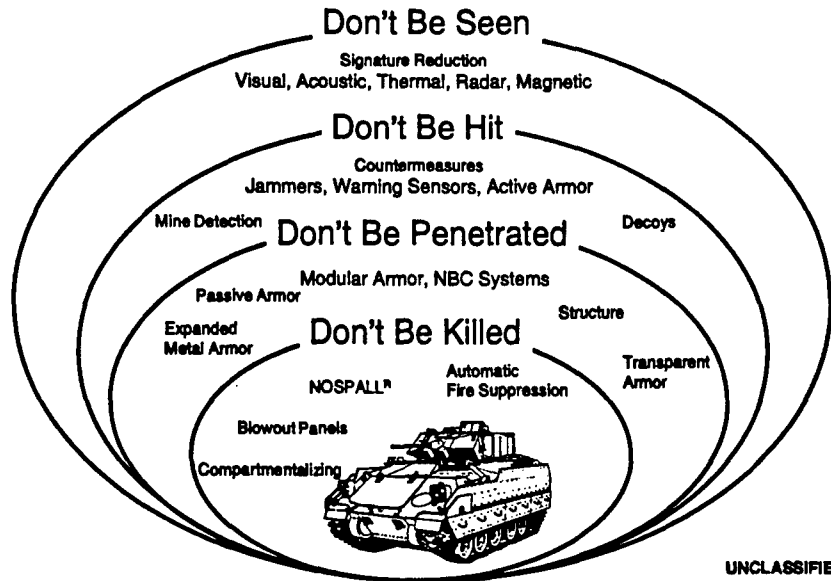
UNCLASSIFIED



UNCLASSIFIED

UNCLASSIFIED

## Layered Survivability



UNCLASSIFIED

## Ground Vehicle Survivability Focus

Survivability is the Combined Effect of:

- Detection Avoidance
- Acquisition / Hit Avoidance
- Damage Avoidance
- Kill Avoidance

Probability of Survival,  $P_s$

$$P_s = 1 - \{P_{\text{det}} \times P_{\text{acq/det}} \times P_{\text{hit/acq}} \times P_{\text{pen/hit}} \times P_{\text{kill/pen}}\}$$

UNCLASSIFIED

UNCLASSIFIED

UNCLASSIFIED

UNCLASSIFIED

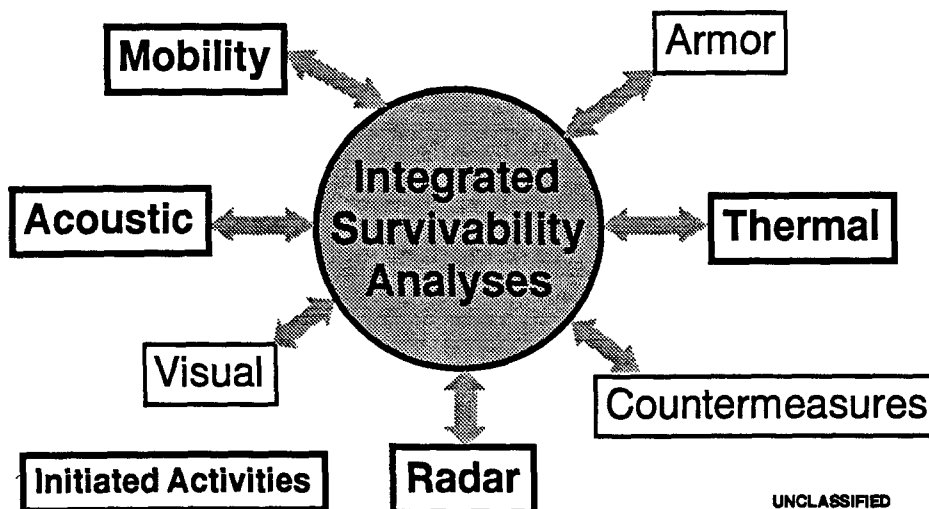
## Why ISA - Real Time ?

- Rapid Evaluation of Design Alternatives in Virtual Prototype
- Evaluate the Synergy and Combined Effect of Design Variables
- Visual and Graphical Presentation of Results
- Interactive Investigation of "What If" Scenario
- Applicable to Simulators and Virtual Environments

UNCLASSIFIED

UNCLASSIFIED

## Current UDLP ISA Activities



UNCLASSIFIED

UNCLASSIFIED

**UNCLASSIFIED**

UNCLASSIFIED

## **Real Time Thermal Signature Model**

- Dynamic Modeling of "Hot Spots" on the Bradley Fighting Vehicle
  - Roadwheel
  - Shock Absorber
  - Track, Sprocket and Idler
  - Gun Barrel
  - Exhaust Gas
- Thermal Model Validated Against UDLP's Lab Test Data
- Integrated into Dynamic Model of Vehicle to Provide Real-Time Transient Temperature Profile of Vehicle Hot Spots

UNCLASSIFIED

UNCLASSIFIED

## **Real Time Radar Signature Modeling**

- Predict the Radar Cross Section (RCS) of a Vehicle
- Basic Scattering Types Included are: Polygons, Cavities, Cylinder, Noise Sources and Wires
- RCS is a Function of Vehicle Position and Orientation and Position and Frequency of the Radar Sensor
- Integrated into Interactive Vehicle Dynamic Model to Provide Real-Time Prediction of RCS
- RCS Output Values Compare Favorably with Unclassified RCS Data Collected by UDLP

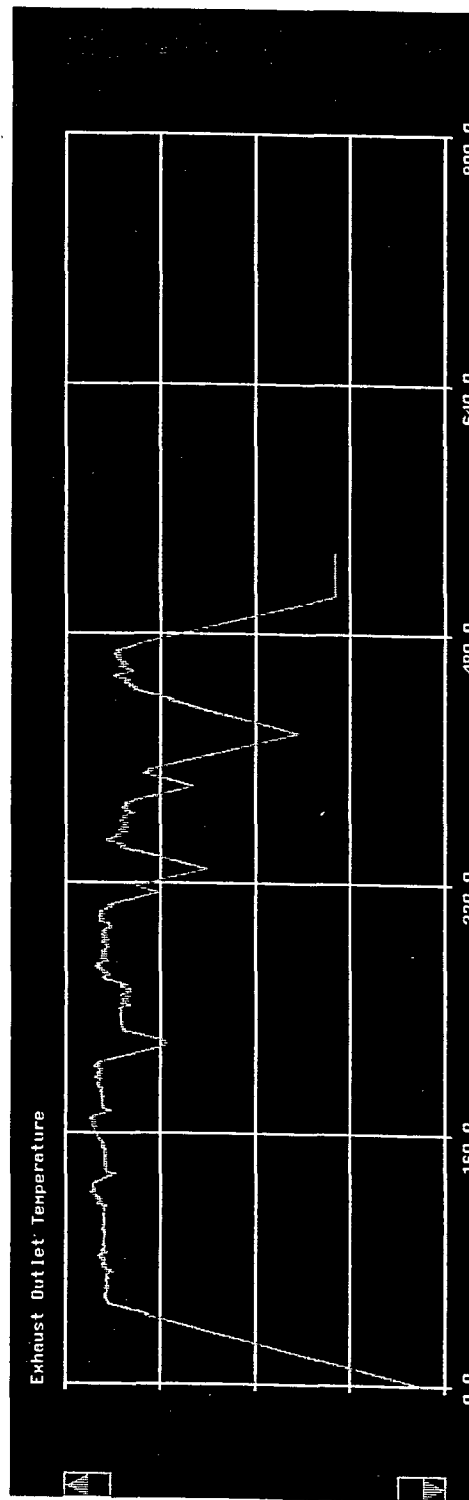
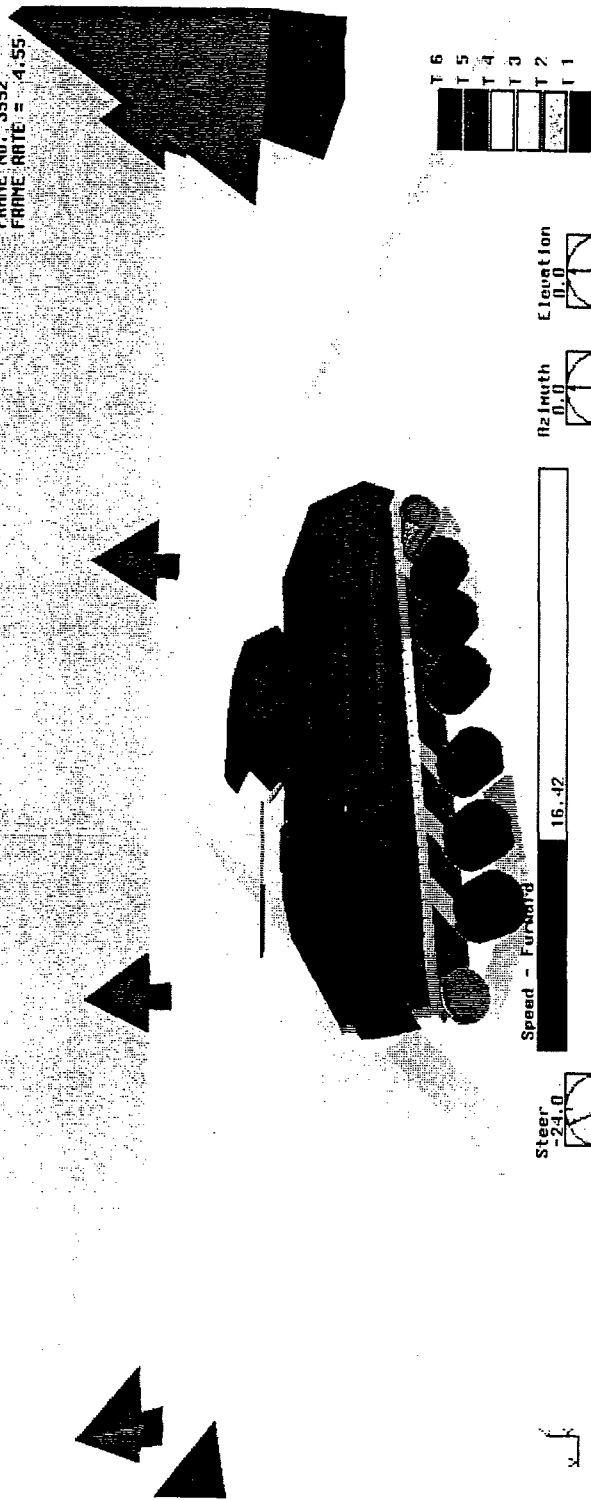
UNCLASSIFIED

**UNCLASSIFIED**

# Real Time Thermal Signature Model

Onboard Image Record I/O Display Analysis Type Radar Thermal Acoustic

TIME = 532.79999  
FRAME NO. = 3552  
FRAME RATE = 4.55



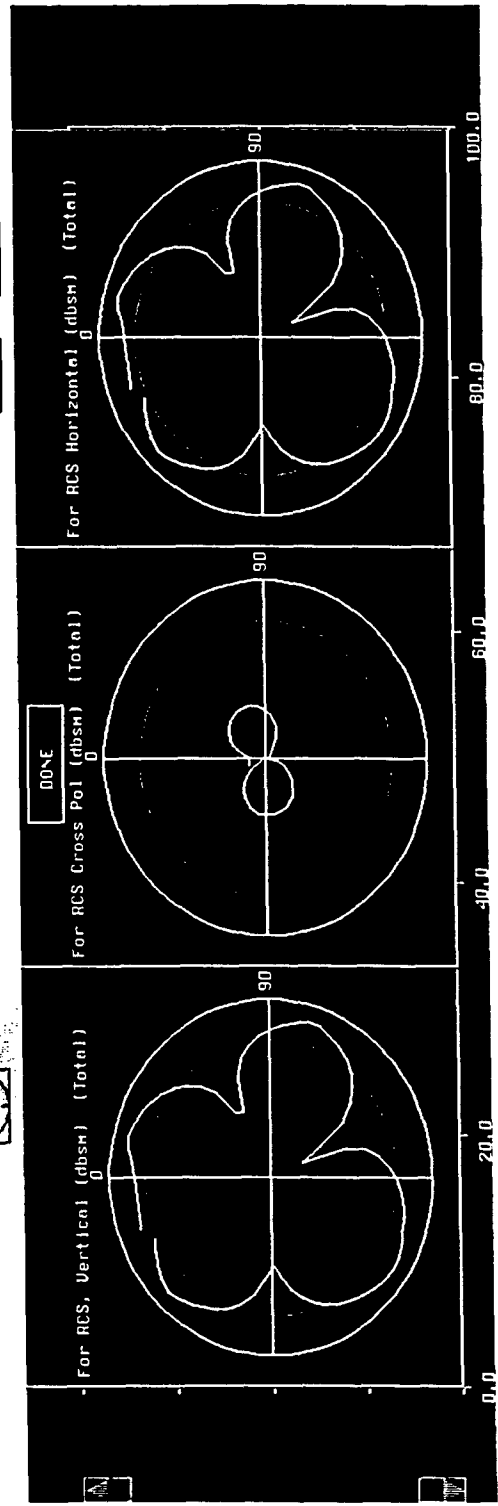
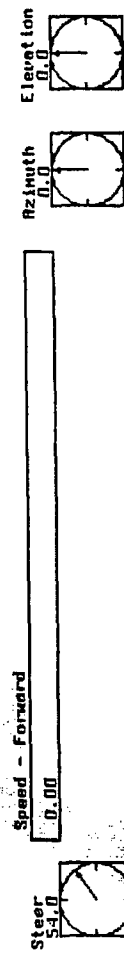
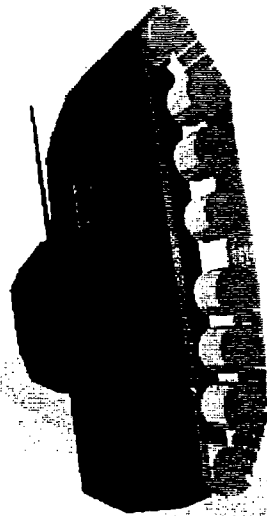
UNCLASSIFIED

UNCLASSIFIED

# Real Time Radar Signature Model

TIME = 84.95000  
 FRAME NO. = 433  
 FRAME RATE = 3.03

On Line Image Record I/O Display Analysis Type Radar Thermal Remote Io



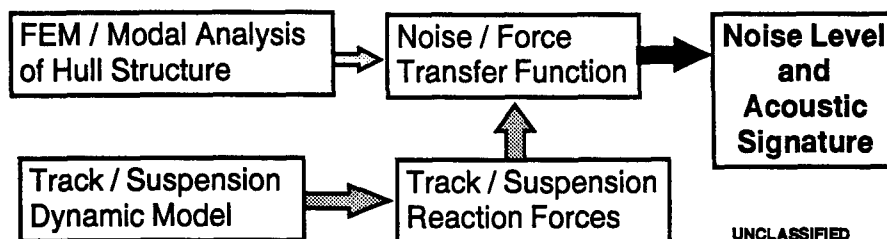
UNCLASSIFIED

UNCLASSIFIED

UNCLASSIFIED

## Real Time Acoustic Signature Modeling

- Procedure to Calculate Interior and Exterior Noise of Tracked Vehicles Based on Speed and Distance
- Acoustic Modeling Integrated into Dynamic Vehicle Model to Display Noise Level & Signature in Real-Time
- Good Correlation with Test Data from Quiet Components for Land Vehicles Contract



UNCLASSIFIED

UNCLASSIFIED

## Conclusions

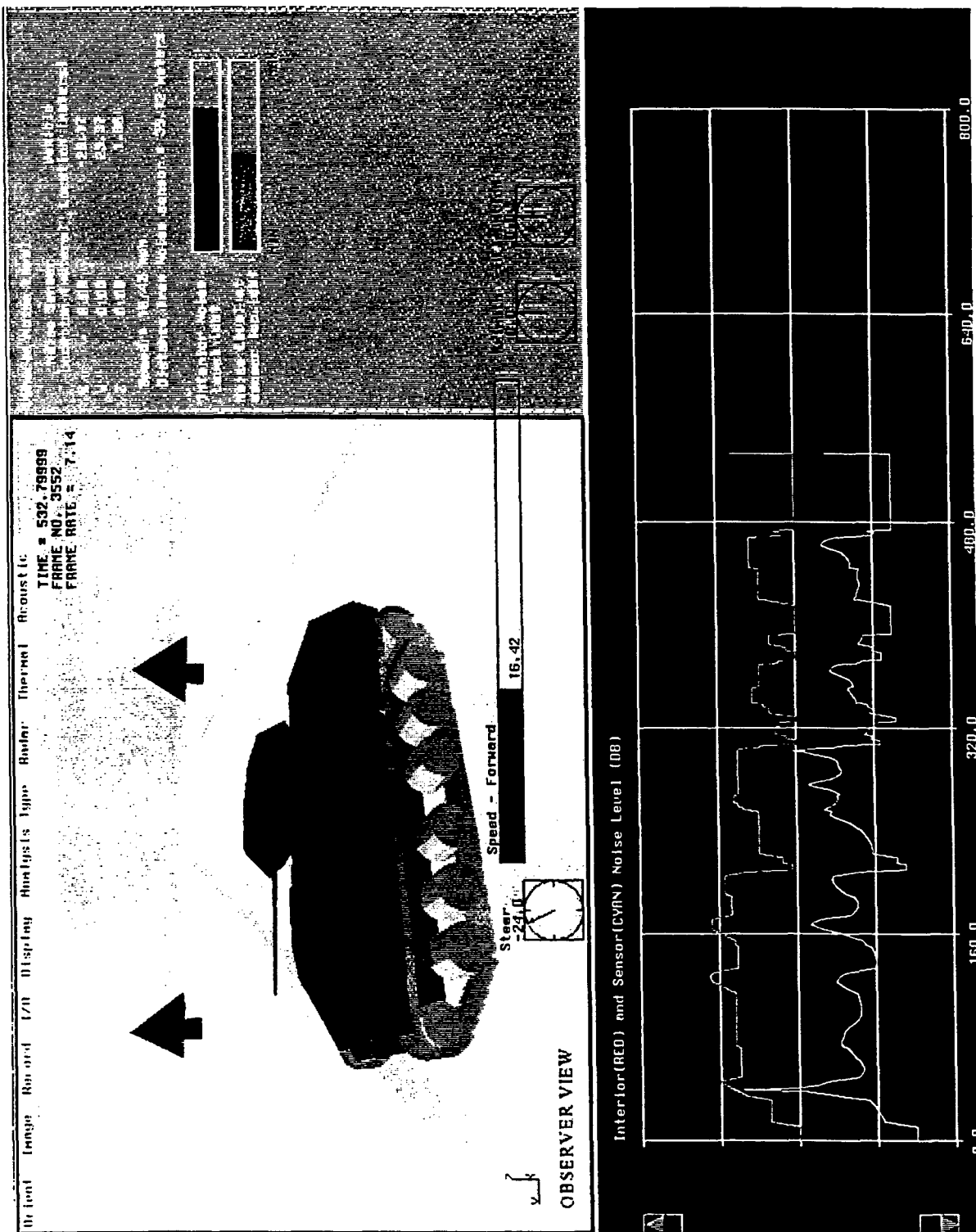
- ISA Approach is Being Developed for Vehicle Concept Evaluation
- Real Time Simulation of Vehicle Mobility and Thermal, Radar and Acoustic Signatures
- ISA Capability Facilitates Evaluating the Synergy and Combined Effect of Design Alternatives
- Methodology Allows Rapid Selection of the Proper Mix of Survivability Technologies to Meet Technical & Cost Requirements

UNCLASSIFIED

UNCLASSIFIED

# Real Time Acoustic Signature Modeling

UNCLASSIFIED



UNCLASSIFIED

UNCLASSIFIED

ARMOR TECHNOLOGY SESSION

Glasgow Auditorium  
Tuesday, March 26, 1996

Session Chairman: Mr. Val Vorvatich, United Defense, L.P.

UNCLASSIFIED



**UNCLASSIFIED**

**THIS PAGE INTENTIONALLY LEFT BLANK**

**UNCLASSIFIED**

# UNCLASSIFIED

## CERAMICS FOR ARMORS - A MATERIAL SYSTEM PERSPECTIVE (U)

E. J. Rapacki, U.S. Army Research Laboratory  
G.E. Hauver, P.H. Netherwood, and R.F. Benck, Dynamic Science, Inc.  
Aberdeen Proving Ground, MD 21005-5066

### ABSTRACT (U)

(U) The development of ceramic armor is a difficult challenge because the ballistic performance of ceramics is a material system problem, not just a material problem. Until system problems are solved, ceramics will perform below their full potential for ballistic protection. Recent studies have addressed the system problems. Sources of damage have been suppressed, the ceramic has been supported, and a weak interface layer has been introduced to manage the flow of failed projectile material at the surface of the ceramic. Using this approach, high-quality ceramics have sustained minimal damage while defeating long-rod projectiles launched at velocities from 1,600 to 2,000 m/s. The most recent studies have detected a weakness in support at the front of the ceramic. Minimizing this newly-found weakness is anticipated to reduce damage and therefore extend interface defeat to higher projectile velocities. The full potential of either laboratory targets or practical armor configurations has not yet been determined, but ballistic performance has continued to improve as system problems have been identified and solved.

### INTRODUCTION (U)

(U) Ceramics have been reported [1] to have no specific resistance to penetration by long-rod projectiles. Instead, their ballistic performance depends on damage which is influenced by response of the total system. A subsequent study [2] identified major sources of damage, introduced target features to suppress damage, and attempted to manage the flow of failed material from the attacking projectile. These efforts caused TiC to defeat a long rod of 93% tungsten heavy alloy (WHA), launched at a velocity of 1,600 m/s, with no penetration into the ceramic. However, moderate cracking of the TiC implied that support for the ceramic was marginal. A following study [3] introduced additional target refinements to support the ceramic, suppress damage, and manage flow of the projectile material at the front surface of the ceramic. WHA rods, launched at a velocity of 1,600 m/s, were then defeated by several high-quality ceramics, with no penetration, and relatively minor damage.

(U) Studies reported in the present paper have examined the flow of erosion products at the surface of different ceramics, the apparent dependence of flow on projectile velocity, and the transition from interface defeat to penetration. These studies are still in progress, but they have identified a problem with the current target system which would degrade the performance of ceramics, especially at higher velocities. This problem is related to the selection of target materials, and there are current efforts to refine the target system further.

UNCLASSIFIED

Approved for public release; distribution is unlimited

## CURRENT INVESTIGATION OF INTERFACE DEFEAT (U)

(U) The basic laboratory target is shown in Figure 1. This target is similar to the target reported in Reference 3, but the boundary configuration has been eliminated and the shock-wave attenuator has been improved in compensation. The side confinement is shrink fitted to the ceramic. This shrink fit improves lateral support and tends to suppress radial cracking, which is identified as one source of damage responsible for the transition from interface defeat to penetration. The shrink fit should also produce some strengthening of the ceramic [4,5]. The copper layer of the target suppresses the influence of shear failure at the back of the front steel confinement. Without effective suppression, shear failures can block the radial flow of material eroded from the projectile. If blockage occurs, there is a change from 90-degree radial flow to 180-degree flow. An associated increase of stress in the impingement area could be either the primary cause of penetration or a contributing factor. A weak target layer is situated between the copper and the ceramic. The function of this layer, usually graphite, is to accommodate the flow of erosion products and provide off-axis support at the front of the ceramic.

(U) The attacking long-rod projectile was varied during tests conducted to investigate the flow of erosion products during interface defeat. The variations were size, material, and velocity. For gas-gun launches at a nominal velocity of 1,600 m/s, the standard projectile was WHA with a diameter of 4.93 mm and a length-to-diameter (L/D) ratio of 20. A powder gun was used to launch larger WHA projectiles at velocities from 1,600 to 2,000 m/s. This larger projectile had a diameter of 6.18 mm and an L/D ratio of 20. The powder gun was also used for a short series of tests which compared flow behavior with projectiles of depleted uranium (DU) and WHA. DU and WHA projectiles had an L/D ratio of 15, and diameters of 5.29 and 5.38 mm, respectively.

(U) Ceramic tiles were recovered after tests with the smaller WHA projectile, launched at a nominal velocity of 1,600 m/s. Sectioned tiles of SiC, TiB<sub>2</sub>, and WC are shown in Figure 2. The feature of primary interest is microdamage under the impingement area in sectioned tiles of SiC and TiB<sub>2</sub>. Microdamaged material was not displaced to allow penetration. This result was repeated when the larger WHA projectile was launched at 1,600 m/s against SiC. However, at a velocity of 1,800 m/s, there was evidence of both interface defeat and extensive damage to the SiC, with partial penetration. At a velocity of 1,800 m/s, TiB<sub>2</sub> ceramic exhibited breakdown of the microdamaged region to a maximum depth of 4 mm, but interface defeat persisted, and ceramic 15 mm from the impingement area remained undamaged. At a velocity of 2,000 m/s, TiB<sub>2</sub> exhibited breakdown of the microdamaged region to a depth of nearly 8 mm, but interface flow still persisted and damage again was localized near the impingement area. The apparent absence of microdamage in WC ceramic is noteworthy. If other sources of damage are effectively suppressed, there should be no mechanism for penetration into WC at a velocity of 1,600 m/s. Tests with WC ceramic have not been conducted at higher velocities.

(U) An investigation of flow behavior was initiated to obtain information about the stability of microdamage which occurs under the impingement area. The target in Figure 1 does not permit radiographic observations. However, scarring of the copper interface layer provides indirect

information about flow in the adjacent weak layer located at the front surface of the ceramic. Copper layers recovered from targets with different ceramics are shown in Figure 3, ordered according to the quality of the flow. In the top row, the ceramics were  $B_4C$ ,  $Al_2O_3$  (Ebon A), and SiC; in the lower row, they were  $TiB_2$ , TiC, and WC. Microdamaged material in  $B_4C$  must have been displaced quickly. The resulting interface profile then directed the flow of erosion products across the weak layer and into the copper where flow was impeded. From left to right in the two rows, flow into the weak interface layer improved. With the final ceramic, WC, flow was well directed into the weak layer, leaving only grazing scars on the copper plate. The direction of flow undoubtedly depends on both the compression of the ceramic and the displacement of damaged material. WC ceramic produced well-directed flow because it had the highest modulus of all ceramics tested and sustained no obvious microdamage.

(U) The ordering in Figure 3 suggests that the laboratory target might have a design weakness which has a different influence on the behavior of each ceramic. Dehn [6] has reported computer modeling of interface defeat. His more recent computer modeling [7] treats interface defeat in a configuration similar to the laboratory target, and a plot of pressure at the ceramic as a function of radial distance is shown in Figure 4. This result suggests a gap in support at the front surface of the ceramic. Central support extends only slightly beyond the radius of the impinging projectile. This suggests that erosion products make a very sharp turn as flow enters the interface layer. The gap before pressure increases in the interface layer suggests an interval where the weak layer is unsupported by the copper layer. The radial distance at which pressure increases in the interface layer corresponds closely to the radius of the hole in copper plates recovered from tests with the better ceramics. With the poorer ceramics, the hole in the copper was enlarged by flow which turned through an angle significantly larger than  $90^\circ$ .

(U) Only limited information about flow can be inferred from examinations of recovered target components. Targets with aluminum confinement were introduced to permit flash-radiographic observations of flow at the ceramic. A representative target configuration is shown in Figure 5.  $TiB_2$  was used in the first observation because it was the best ceramic available in a size suitable for radiography. This test was conducted with the smaller (4.93 mm diameter) WHA rod, launched at a nominal velocity of 1,600 m/s. The first radiograph from this test is shown in Figure 6. The right side of the flow is not obscured by erosion products from the forward portion of the target and shows a sharp turn into the interface layer, in agreement with the behavior implied by Dehn's computer modeling. The compression of ceramic under the impingement area tends to direct the flow at an angle slightly larger than  $90^\circ$ . At the early time of this first radiograph, there is no evidence of impeded flow. The second radiograph (not shown) was recorded after radial cracks had propagated to the weak aluminum confinement which then failed, allowing penetration.

(U) SiC was also used in aluminum targets for flash-radiographic observations of interface flow. The initial tests were conducted with WHA long-rod projectiles, launched at a nominal velocity of 1,600 m/s. The flow patterns on copper plates, shown in Figure 3, suggested that the interface flow at SiC is not as well directed as the flow at  $TiB_2$ . This observation is supported by the radiographs from tests with WHA projectiles shown in Figure 7. At  $5.5 \mu s$  after the rod arrives at

SiC, flow is clearly directed across the weak layer of graphite and into the front confinement of aluminum. At  $7.7 \mu\text{s}$ , the flow problem continues. However, the more serious behavior is the displacement of microdamaged material and the onset of penetration. Penetration is actually occurring at  $5.5 \mu\text{s}$ , but it is much more obvious at  $7.7 \mu\text{s}$ . There is no computer modeling for a target with aluminum confinement, but the diameter of the penetration path through the aluminum plate at the front of the target is 2.3 times the diameter of the penetrator, so some gap in support at the front of the ceramic is inferred. In addition, the poorly directed and impeded interface flow may cause a higher central stress which contributes to the displacement of microdamaged ceramic from under the impingement area.

(U) Tests with flash-radiographic observations were also conducted with DU projectiles launched at a nominal velocity of 1,600 m/s. Radiographs from these tests are shown in Figure 8. At  $6.3 \mu\text{s}$  after the DU rod arrives at the SiC, flow is clearly directed across the interface layer. However, by  $7.9 \mu\text{s}$ , flow has become well directed into the weak interface layer. This suggests that the shear failure of DU results in more efficient flow into the weak layer intended to accommodate it. Although penetration is occurring, the depth is significantly less than the depth with WHA at nearly the same time. This is consistent with a lower central stress resulting from the less impeded flow of DU into the interface layer.

(U) An additional test with flash radiography was conducted at an obliquity of  $45^\circ$ . The ceramic in this test was Ebon A aluminum oxide. In Figure 3, the interface flow of WHA erosion products at Ebon A was more poorly directed than the flow at SiC. In compensation, DU was selected as the projectile material for the oblique test with Ebon A because its flow characteristics were judged superior to those of WHA. The launch velocity was again 1,600 m/s. The flash radiograph from this test, taken  $19.5 \mu\text{s}$  after the rod arrived at the ceramic, is shown in Figure 9. There appears to be total defeat at the interface, but this is not the true behavior. A faint darkening under the impingement area is penetration into the ceramic. Again, there apparently is a gap in support at the front surface of the ceramic, allowing microdamaged ceramic to be displaced. Flow at the ceramic is actually bifurcated, with a strong branch which moves along the interface, and a forward branch which displaces microdamaged material into the interface flow. The average Tate resistance for forward penetration is 9.4 GPa, which is relatively high for Ebon A, while resistance for flow into the interface is essentially zero. The strong, unimpeded interface flow could minimize stress in the impingement area, making this a relatively efficient mode of projectile defeat. However, a better selection of material for the front confinement should provide better support at the front of the ceramic and might prevent any forward penetration.

#### SUMMARY AND DISCUSSION (U)

(U) Targets for ballistic evaluations commonly allow the ceramic to be damaged by high shock stress and wave interactions, and damage is often aggravated by impedance mismatches and unfavorable geometries. Targets also commonly tend to provide weak support for the ceramic, allowing extensive propagation of cracks. Monolithic ceramic is reduced to discrete pieces which can be displaced, allowing penetration. These more obvious sources of damage are strongly influenced

# UNCLASSIFIED

by the target system. The system can be modified to suppress this damage effectively, allowing ceramic to be recovered for examination. It is then that microdamage is encountered, and its stability during impingement becomes a major consideration. If microdamaged ceramic remains in place, the projectile is defeated by flow at the surface of the ceramic. If microdamaged ceramic is displaced, penetration occurs.

(U) The influence of the system on the stability of microdamaged ceramic becomes important. Current evidence suggests that the present laboratory target contains material which provides less than optimum support close to the impingement area. When the system is optimized, the ceramic should become the final influence on interface defeat. Even at high velocities where the microdamaged region can no longer be stabilized, the system may still have an influence on the ballistic performance. As in the test at obliquity, the system may minimize the interface stress by maintaining a bifurcated flow with long-term stability. Many aspects of interface defeat remain to be investigated. The current state of the investigation clearly demonstrates that by controlling damage, ceramics can be effectively utilized for ballistic protection. Present results are encouraging, and interface defeat is believed to merit serious consideration for ceramic-armor applications.

## REFERENCES (U)

1. G.E. Hauver, P.H. Netherwood, R.F. Benck, W.A. Gooch, W.J. Perciballi and M.S. Burkins, "Variation of Target Resistance During Long-Rod Penetration into Ceramics," pp. 257-264, Proc. 13th Int. Symp. on Ballistics 3, Sundyberg, Sweden (1992).
2. G.E. Hauver, P.H. Netherwood, R.F. Benck and L.J. Kecskes, "Ballistic Performance of Ceramic Targets," Proc. Army Symp. on Solid Mech., Plymouth, MA, August 17-19 (1993).
3. G.E. Hauver, P.H. Netherwood, R.F. Benck and L.J. Kecskes, "Enhanced Ballistic Performance of Ceramics," Proc. 19th Army Science Conf., Orlando, FL, June 20-24 (1994).
4. J. Lankford, C.E. Anderson, Jr., G.R. Johnson and T.J. Holmquist, "Dynamic Compressive Failure of Ceramics Under Confinement," Proc. 1991 Combat Vehicle Survivability Conf., Vol. II, pp. 67-73, Gaithersburg, MD, April 15-17 (1991).
5. C.E. Anderson, Jr., J.D. Walker and J. Lankford, "Investigations of the Ballistic Response of Brittle Materials," SwRI Report 06-5117/002, prepared for the U.S. Army Research Office, Southwest Research Institute, San Antonio, TX, November (1995).
6. J. Dehn, "Modeling Armor that Uses Interface Defeat," Proc. 6th Annual TARDEC Combat Vehicle Survivability Symp., Vol. 1, pp. 443-448, Monterey, CA, March 28-30 (1995).
7. J. Dehn, Army Research Laboratory, private communication, October 12 (1995).

UNCLASSIFIED

UNCLASSIFIED

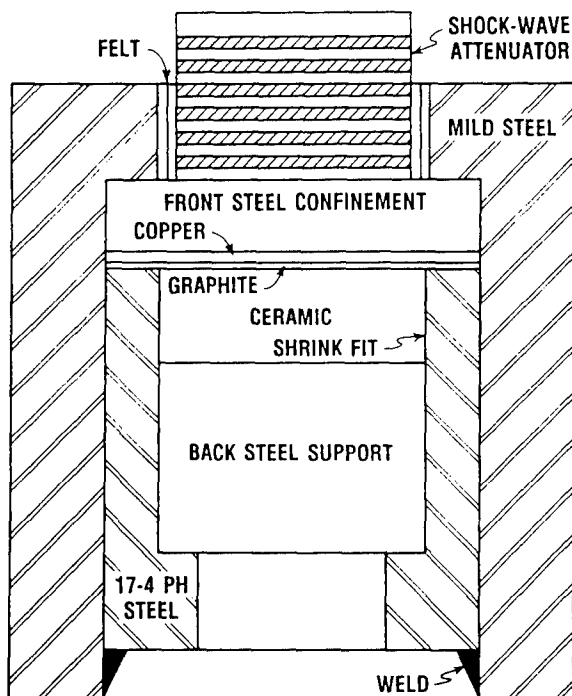


Figure 1. Basic laboratory target.

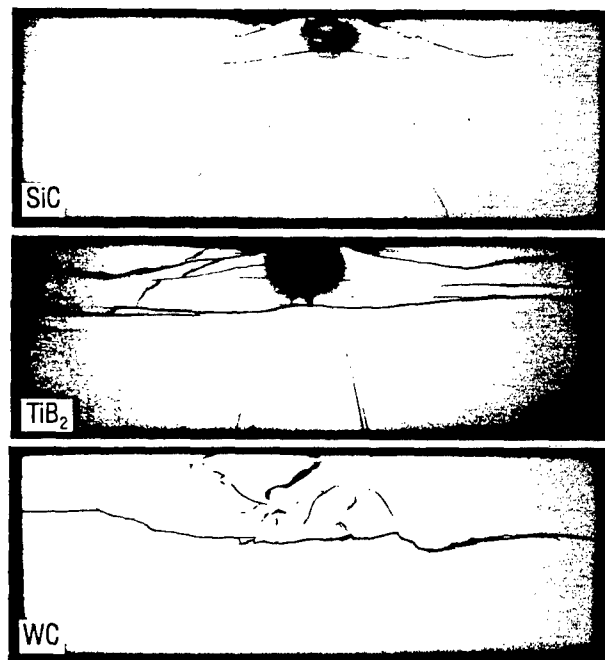


Figure 2. Ceramic tiles recovered and sectioned after interface defeat.

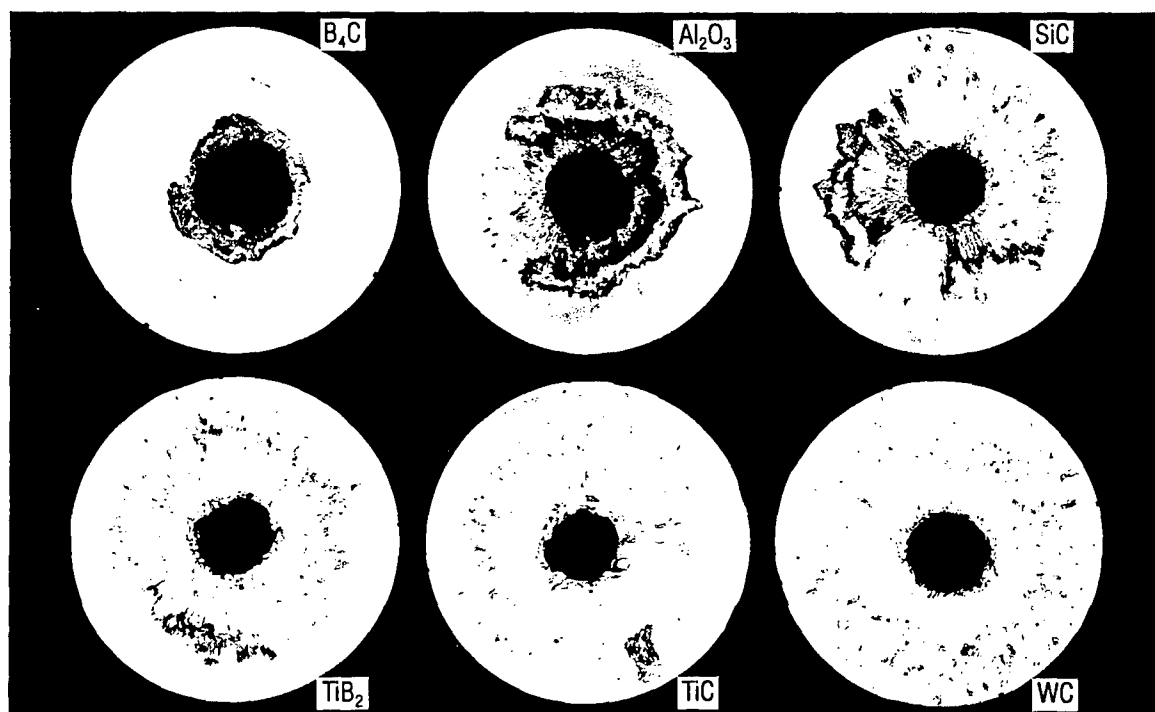


Figure 3. Copper layers from tests with different ceramics.

UNCLASSIFIED

UNCLASSIFIED

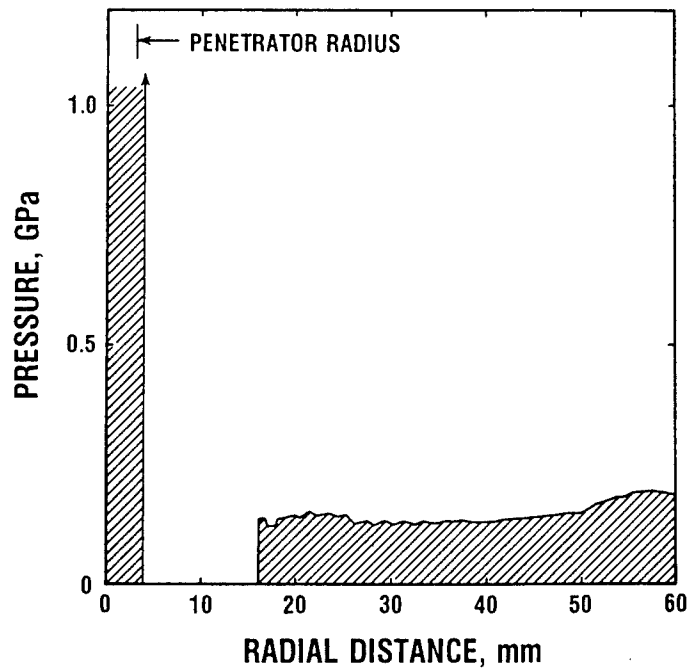


Figure 4. Computer modeling which shows a gap in support at the front surface of the ceramic.

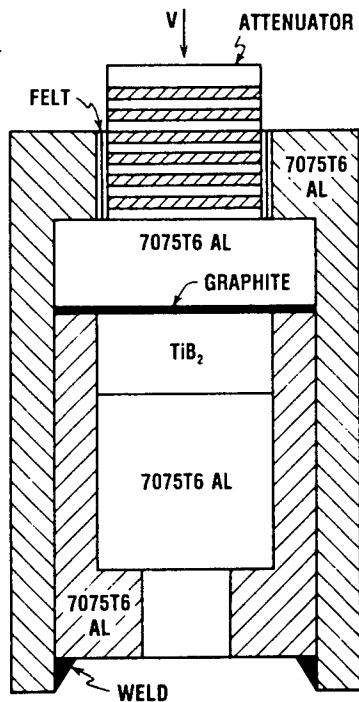


Figure 5. Ceramic target with aluminum confinement.



Figure 6. Flow at the surface of TiB<sub>2</sub> ceramic.

UNCLASSIFIED



UNCLASSIFIED

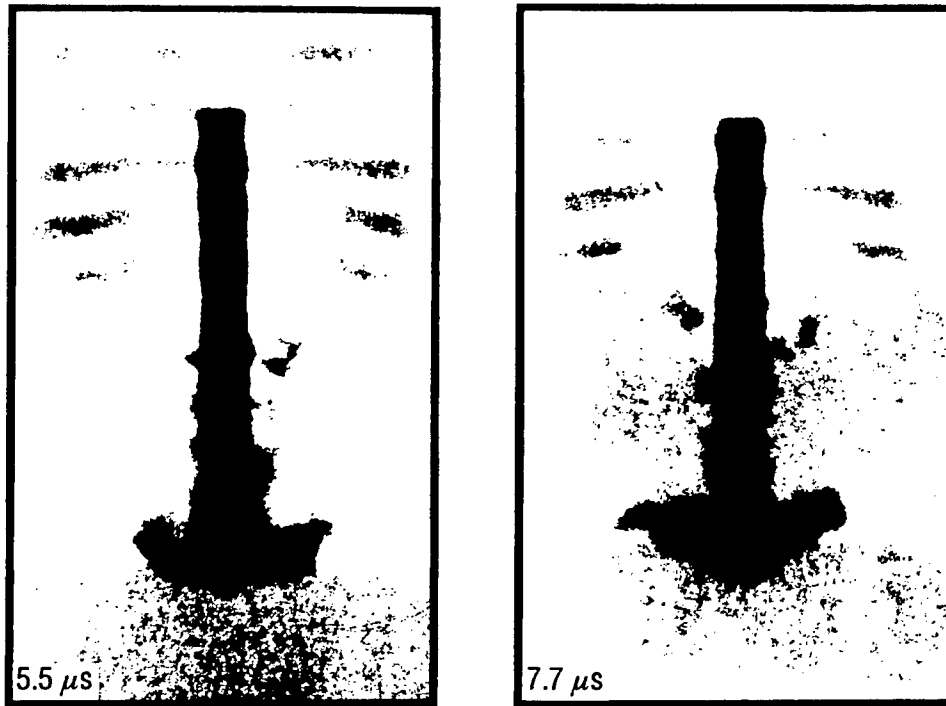


Figure 7. Interaction of WHA projectiles with SiC ceramics.

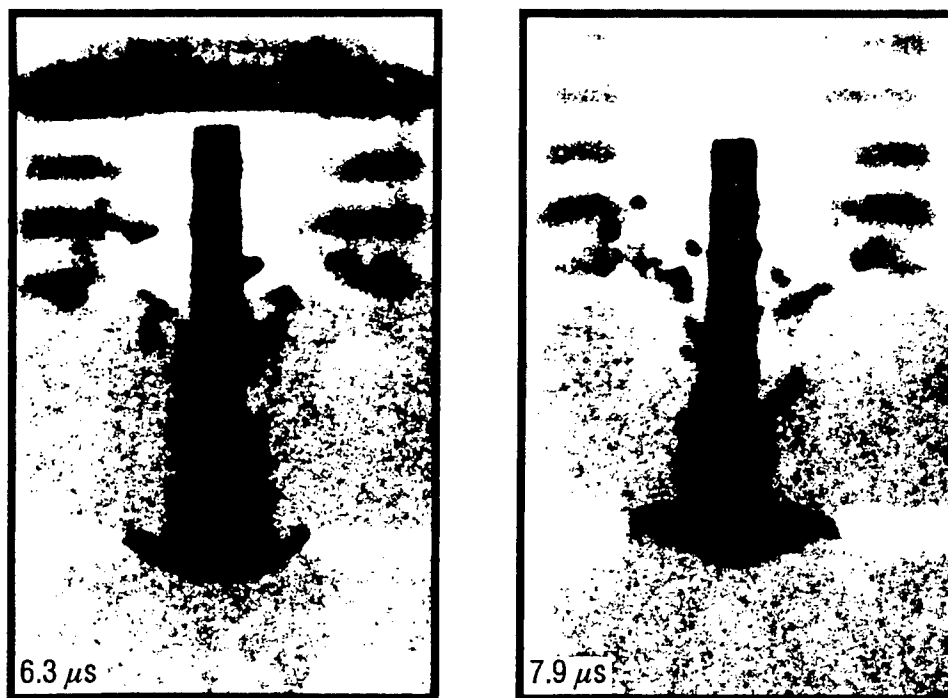


Figure 8. Interaction of DU projectiles with SiC ceramics.

UNCLASSIFIED

UNCLASSIFIED



Figure 9. Oblique interaction of a DU projectile with  $\text{Al}_2\text{O}_3$  ceramic (Ebon A).

UNCLASSIFIED

UNCLASSIFIED

THIS PAGE INTENTIONALLY LEFT BLANK

UNCLASSIFIED

# BALLISTIC DEVELOPMENT OF HIGH DENSITY TUNGSTEN CARBIDE CERAMICS

W.A. Gooch & M. S. Burkins  
U.S. Army Research Laboratory  
Aberdeen Proving Ground, MD 21005-5066

R. Palicka, C.J. Shih & H.H. Mortensen  
Cercom Incorporated  
Vista, CA 92083

## ABSTRACT

With increasing battlefield threats, current and future combat vehicles will require armor technologies which obtain maximum performance with compact structures and armors. The U.S. Army Research Laboratory, in cooperation with Cercom Inc., has developed a new class of high density ceramics which inherently provide high space efficiency and reduced susceptibility to damage accumulation effects in thick sections. While many ceramics were considered, this research has focused on high purity tungsten carbide (WC). This paper will present a survey of possible high density ceramics, document the mechanical properties of the currently-processed WC ceramic and baseline the ballistic performance against two laboratory kinetic energy penetrators.

## INTRODUCTION

With increasing battlefield threats, current and future combat vehicles will require armor technologies which obtain maximum protection with compact structures and armors. Additional requirements for stealth on the battlefield, new vehicle technologies such as composite structures, and increased performance of optical and sensor technologies will require new armor strategies.

The U.S. Army Research Laboratory (ARL) recently initiated development of a new class of ballistic ceramics known as high density ceramics. These ceramics are defined as any ceramic with a density greater than that of rolled homogeneous armor (RHA) steel ( $7.85 \text{ g/cm}^3$ ). While a significant number of ceramic oxides, nitrides and carbides meet this criteria, most of the ceramics are difficult to process or the costs are prohibitive. These ceramics are very interesting from an armor standpoint as very compact targets are possible. The tungsten carbide (WC) family of high density ceramics was selected as the prime ceramic of interest because of its  $15.6 \text{ g/cm}^3$  density, excellent mechanical properties and the potential unique applications in both the military and civilian markets. The WC materials, developed for armor applications, are pure ceramics and not ceramic/metal cermets, the latter being available for many years in large quantities for commercial markets. The tungsten carbide processing technology was developed by Cercom Incorporated of Vista, CA, and ballistically tested in the Armor Mechanics Branch of the Weapons Technology Directorate of ARL. These initial WC

Distribution authorized to U.S. Government agencies and their contractors - Critical Technology  
1 February 1996. Other requests should be referred to ARL.

ceramics are 99.6 weight-percent WC/W<sub>2</sub>C and are the first known materials of this type made in large tiles. The development of this ceramic will provide armored system developers with a very space efficient material for use in upgrading the protection of areas that have limited available space. The inherent high density of these tiles precludes their use against small arms threats, such as personnel armor, but make them attractive for use against higher-performing medium caliber and full-scale rods in applications such as backpack designs, add-on appliques, roof appliques, hatch appliques or hull and turret side armors.

## HIGH DENSITY CERAMICS

A review of possible ceramics of interest was undertaken by Cercom [1] and Table I lists important properties for nominally pure ceramics whose densities are greater than 7.85 g/cm<sup>3</sup>. Of the twelve ceramics listed, only two have been tested ballistically. Limited testing of hafnium carbide (HfC) was conducted by Hauver [2] in 1/5 scale tests to study dwell. Rupert et al [3,4] examined uranium oxide (UO<sub>2</sub>) ballistically in both sintered and hot isostatic pressed conditions. Nuclear Metals Incorporated of Concord, MA, developed the process for the production of depleted uranium ceramics. The work was successful in producing near-theoretical density UO<sub>2</sub> in 100-mm disks of thickness of 11.3-mm. The ballistic performance against Length/Diameter (L/D) 10 tungsten penetrators was as expected for thin ceramics, exhibiting low performance as compared to rolled homogenous armor (RHA) steel. Significant improvements were predicted by computer simulation for thicker cross-sections, but further work was discontinued because of the associated radiation limitations imposed by these uranium-based materials. Limited testing of high metal content WC

Table I. Elastic Properties and Melting Temperature of Selected High Density Ceramics

CERAMIC	DENSITY (g/cm <sup>3</sup> )	MELTING POINT (°C)	MODULUS (GPa)	HARDNESS (kg/mm <sup>2</sup> )	LONGITUDINAL WAVE VELOCITY (m/s)
MoB	8.77	2600	400	2350	6754
Mo <sub>2</sub> C	9.18	2522	533	1499	7620
NbN	8.31	2300	483	1525	7626
TaB	14.19	3090	400	3130	5309
TaC	14.40	3985	285	1720	4449
TaN	14.36	3087	576	--	6333
HfB <sub>2</sub>	11.19	3380	500	2900	6685
HfC	12.67	3890	360	3830	5330
HfN	13.39	3000	500	1600	6112
UO <sub>2</sub>	10.97	2850	--	--	--
WC	15.70	2800	696	2200	6600
W <sub>2</sub> C	17.20	2785	420	2150	4940

cermets were also conducted at ARL with 14.5-mm armor-piercing projectiles, but the performance was generally equal to equivalent areal weights of RHA. Significant toughness was evident from the metal matrix and the cermet did not crack.

The data in Table I established the direction for further development. The tungsten carbide family had both the highest density and modulus and exhibited a longitudinal sound speed about half that of lower density ceramics. The WC impedance was also about 2.5 times that for RHA. Large established commercial markets exist for cermet-based materials and WC ceramics have significant application in highly corrosive environments. Lastly, Cercom had developed the processing technology to densify large, high purity ceramics without metal sintering aids, important for ballistic grade ceramics. Within a short time, Cercom was successful in densifying high quality tiles of 100-mm x 100-mm size in thicknesses up to 25.4-mm, which were the first high purity WC ballistically tested. The process was scaled-up to 152-mm x 152-mm tile sizes in thickness up to 30-mm and 203-mm x 203-mm tiles were produced in thicknesses up to 12.7-mm. There is no processing limitation for production of WC armor tiles up to 40-mm in thickness for standard lateral sizes. Ditungsten carbide ( $W_2C$ ) was also densified in 152-mm x 152-mm size tiles of 26-mm thickness.

## HIGH PURITY TUNGSTEN CARBIDE

Tungsten and carbon form two simple compounds of interest, tungsten monocarbide (WC) and ditungsten carbide ( $W_2C$ ). Both ceramics have hexagonal crystal structures with a melting temperature of about 2800°C[1]. Traditional WC materials are, in fact, cermets, alloys of ceramics and metal binders that are sintered to form a hard dense material. These cermets contain eight to ten percent cobalt by weight, which is added as a liquid-phase sintering aid to allow the material to be fully densified at lower temperatures and pressures as compared to pure tungsten carbide. The cobalt addition reduces yield strength and hardness, but increases toughness.

Tungsten carbide cermets exhibit poor ballistic performance, as the resistance to penetration is governed by the percentage of metal content and location of the sintering aid in the microstructure. The specific material properties and structure that make tungsten carbide cermets valuable industrial materials inherently degrade their performance as ballistic materials. The physical, mechanical and thermo-mechanical properties of high purity tungsten carbide ceramics, however, provide a ballistic response similar to high quality ballistic ceramics of lower density. The majority of the ballistic testing was conducted with tungsten monocarbide.

The hot-pressed Cercom WC had a density of 15.6 g/cm<sup>3</sup> and the tiles were analyzed to be composed of WC and 2.8%  $W_2C$ , the latter a byproduct of the densification process. The nominal purity was 99.6% WC/ $W_2C$ . The tiles were densified without metal sintering aids which allow near-theoretical density tiles to be hot-pressed in large tile sizes. The grain size was between 0.3-1.4  $\mu$ m with an average grain size of 0.9  $\mu$ m. The crystal structure of WC and  $W_2C$  is hexagonal and matches other higher performing hexagonal ballistic ceramics such as  $\alpha$ -SiC,  $\alpha$ -TiB<sub>2</sub>, AlN, and  $\alpha$ -Al<sub>2</sub>O<sub>3</sub>.

The hot-pressed Cercom  $W_2C$  had an as-pressed density of about 16.02 g/cm<sup>3</sup>. Some WC was still present in the microstructure and a full density of 17.2 g/cm<sup>3</sup> was not achieved. The average grain size was about 11.2  $\mu$ m. Further improvement of  $W_2C$  is possible, but additional development has been halted, at present, to concentrate on WC. The measured quasi-static mechanical and elastic properties of the Cercom WC and available measured properties of  $W_2C$  are provided in Table II.

Table II. Measured Mechanical and Elastic Properties of Cercom WC and W<sub>2</sub>C

	WC	W <sub>2</sub> C
DENSITY (g/cm <sup>3</sup> )		
THEORETICAL	15.7	17.2
AS-PRESSED	15.6	16.0
HARDNESS (VICKERS-1-kg) (kg/mm <sup>2</sup> )	2200 ± 20	1720 ± 40
FLEXURAL STRENGTH (MPa)	1100 ± 130	--
CHARACTERISTIC STRENGTH (MPa)	1159	--
WEIBULL MODULUS	10.2	--
COMPRESSIVE STRENGTH (MPa)	4456 ± 150	--
K <sub>IC</sub> TOUGHNESS (MPa/m)		
SINGLE ETCH NOTCHED BEAM	7.56 ± 0.51	--
INDENTATION VICKERS	6.86 ± 0.19	--
TENSILE STRENGTH (MPa)	589 ± 57	--
CHARACTERISTIC STRENGTH (MPa)	617	--
WEIBULL MODULUS	10	--
ELASTIC MODULUS (GPa)	690.1	--
SHEAR MODULUS (GPa)	287	--
POISSON RATIO	0.20	--
SONIC VELOCITY (m/s)		
LONGITUDINAL	6858	--
TRANSVERSE	4300	--

When compared to traditional low-density ceramics, the compactness of the ceramic is a direct function of the inherent densities of materials. Table III provides a comparison of the densities and thickness for various ceramics for a given areal weight of 199.39 kg/m<sup>2</sup> of material. The latter weight represents what 25.4-mm (1-inch) of ballistic steel armor weighs and is a baseline for comparative purposes. As compared to steel, the tungsten carbide is approximately one-half the

Table III. Comparison of Ceramic Thicknesses

	DENSITY (g/cm <sup>3</sup> )	THICKNESS (mm)	AREAL DENSITY (kg/m <sup>2</sup> )
BALLISTIC STEEL ARMOR	7.85	25.40	199.39
TUNGSTEN CARBIDE	15.60	12.86	199.39
SILICON CARBIDE	3.22	61.92	199.39
ALUMINUM OXIDE (99.5%)	3.89	51.26	199.39
TITANIUM DIBORIDE	4.51	44.21	199.39

thickness for the same areal density; it is one-fifth that of silicon carbide, considered one of the best ceramic armor materials. The 99.5% aluminum oxide is presently utilized as a baseline ceramic for ballistic performance comparison; tungsten carbide is one-fourth its thickness. The remainder of this paper will document the ballistic performance of WC for two tungsten long-rods.

## TEST PROJECTILES

The L/D10 65-g and L/D 13 162-g tungsten projectiles, shown in Figure 1, have been used for many years as model scale rods for ballistic testing. The 7.8-mm x 78-mm L/D10 rod is a hemispherical-nosed right circular cylinder and is considered a quarter-scale laboratory rod. The 9.5-mm x 133-mm L/D13 rod is a right circular cylinder with a truncated conical nose and represents a medium caliber long-rod projectile. Table IV lists composition and typical mechanical property

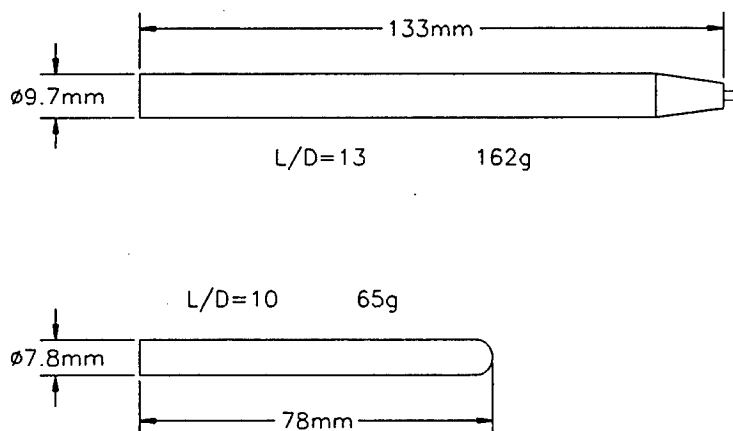


Figure 1. L/D10 and L/D13 Tungsten Rods

information on these penetrators. The baseline RHA penetration of these two rods have been documented by Gooch et al [5] and are governed by equations 1 and 2, where P is in mm and V is in km/s. These equations, based on work of Odermat and Frank, are accurate between 500-1800 m/s.

$$\text{L/D10 vs RHA:} \quad P = 171.5e^{-(1.379/V)^2} \quad (1)$$

$$\text{L/D13 vs RHA:} \quad P = 308.8e^{-(1.447/V)^2} \quad (2)$$

Table IV. Mechanical Properties for Model Scale Penetrators

Designation	L/D10 and 13 WA Rods
Composition (wt %)	93W-3Ni-2Fe
Density (g/cm <sup>3</sup> )	17.7
Hardness	40-45 R <sub>c</sub>
Yield Strength	1200 MPa
Ultimate Tensile Strength	1280 MPa
Elongation	8 %



## EXPERIMENTAL SETUP

The penetrators were fired from a laboratory gun consisting of a 40-mm L70 Bofors breech assembly with a 38-mm smoothbore barrel. A custom-built polypropylene sabot system was used to launch the projectiles. The gun was positioned 1.5 meters in front of the targets and an orthogonal flash radiographic system [6] was used to measure projectile velocity, pitch, and yaw. Propellant weight was adjusted to achieve the desired striking velocity and ballistic results with  $\geq 2^\circ$  total yaw were disregarded. The L/D10 rod was nominally fired at 1500 m/s which provides a baseline penetration into RHA of 73.6-mm. The L/D13 rod was nominally fired at 1550 m/s and the baseline penetration into RHA is 129.2-mm.

All the ballistic test data presented in this paper were conducted using the depth of penetration (DOP) technique developed by Woolsey et al [7]. The DOP technique is cost-effective, but only provides a relative performance indication; time-dependent effects, reported by Hauver et al [8] predominate in this methodology where no cover plate is used, interface effects are not minimized, and ceramic confinement is limited. Generally, the result of these factors are a rapid reduction in the relative performance as ceramic thickness increases, accompanied with an increase in the scatter of the ballistic data. While these factors are present in DOP testing of the lower-density technical ceramics, particularly for thicker tiles, they are much less important with high density ceramics. The optimum ceramic thickness for maximum ballistic performance in target designs, such as the DOP configuration, has been observed to be between 25 to 40-mm for the low density ceramics. This primarily relates to geometric considerations of the ceramic tile in its confinement, the sound speed of the ceramics and time for reflection from the ceramic back and side interface.

The DOP target configuration used in this paper is shown in Figure 3. All tests were shot at  $0^\circ$  obliquity and the target had no cover plate, but was confined laterally by a steel frame in which the ceramic tile was epoxied. The depth of penetration into the rear RHA plate ( $P_R$ ) was measured for each impact. The L/D10 tests were conducted on 102-mm square tiles and the joint thickness varied between 1 to 2-mm. Subsequent work by Burkins et al [9], on examining the sources of variance in DOP data led to the determination that the bond thickness is a source of variability in the ballistic data. This has led to a modification in the assembly procedures for all subsequent DOP testing. The bond thickness is now maintained at 0.5-mm for both the side confinement and the rear interface. The L/D13 tests were conducted on 152-mm square tiles, using the newer DOP technique.

## BALLISTIC CHARACTERIZATION

Ballistic performance of armors or elements of armors are characterized by dimensionless factors which compare the areal density (mass/area) and thickness of the material to baseline RHA. Many variations and terminologies exist, but Frank [10] developed and described a concise set of mass and space effectiveness factors whose conventions are in use at ARL. Since the DOP technique determines the equivalent RHA performance of the ceramic relative the semi-infinite penetration of the rod, the ballistic characterization of the ceramic can be defined by the mass effectiveness ( $e_m$ ), the space effectiveness ( $e_s$ ) and the armor quality factor ( $q^2$ ) as described by equations 3; the small  $e$  indicating that the performance indices are elemental rather than system effectiveness. The term ( $P_{RHA} - P_R$ ) relates the baseline RHA penetration of the rod to the residual RHA penetration depth and represents how much baseline RHA penetration was removed by ceramic thickness  $T_{CER}$  at the same

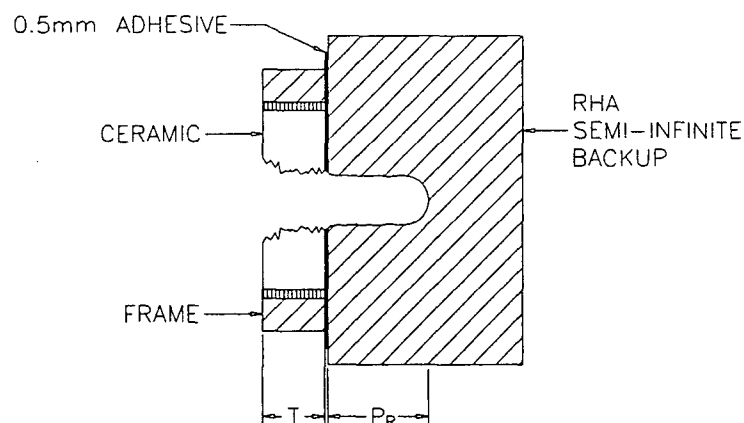


Figure 2. DOP Target Configuration

impact velocity. The ceramic mass effectiveness can then be related to  $e_s$  by the ceramic density ( $\rho_{CER}$ ) and the RHA density ( $\rho_{RHA}$ ). RHA has an  $e_M$  and  $e_s$  of 1 and higher indices indicate better ballistic performance. The quality factor has significance for armor designers as this factor relates both the mass and space factors. Values over 1 indicate armors or materials which are thinner and/or lighter than the baseline RHA performance and high values indicate superior armors or materials.

$$e_s = \frac{P_{RHA} - P_R}{T_{CER}} \quad e_m = \frac{(P_{RHA} - P_R) \times \rho_{RHA}}{T_{CER} \times \rho_{CER}} = e_s \times \frac{\rho_{RHA}}{\rho_{cer}} \quad q^2 = e_m \times e_s \quad (3)$$

## EXPERIMENTAL RESULTS/DISCUSSION

### L/D10 DOP Tests Versus WC

The initial ballistic tests of the WC were conducted on the then available 102-mm x 102-mm tiles of three thicknesses. This lateral size is not considered optimum for the L/D10 rod and 152-mm x 152-mm tiles would provide increased performance. Table V documents the WC DOP test data and comparative DOP data for 102-mm and 152-mm square Coors 99.5% aluminum oxide are shown. For the alumina data, the  $P_R$  represents the average value for multiple tests at each thickness and the data has been corrected to a 1500 m/s baseline. The 152-mm x 152-mm AD995 alumina data are more complete and illustrates the inherent performance degradation problem of low-density ceramics when impacted by medium caliber rods in a DOP target configuration. The mass and space effectiveness are optimum for tiles between 25 and 40-mm in thickness and thicker tiles begin to lose performance as time dependent factors predominate. The material has failed and mass and space effectiveness rapidly decrease as the penetrator encounters, essentially, granulated ceramic. As the RHA penetration performance of a rod increases, this ceramic design problem becomes greater for the armor designer, as the residual penetration becomes larger as the ceramic gets thicker. As with many armor designs, the target is driven by the space factor, not the mass factor. While Hauver et al [11] and Prifti et al [12] have been successful in overcoming time dependent effects in ceramics, the total mass and/or space effectiveness values are still low if the total parasitic mass or space is included in the effectiveness calculations. The problem resides with the low density of the ceramics for these high performance applications in simple armor designs.

Table V. L/D10 DOP Ballistic Test Data

SIZE (mm)	CERAMIC	CERAMIC THICKNESS (mm)	CERAMIC AREAL DENSITY (kg/m <sup>2</sup> )	AVERAGE P <sub>R</sub> (mm)	e <sub>m</sub>	e <sub>s</sub>	q <sup>2</sup>
RHA	NONE	0	0	73.6	1.00	1.00	1.00
102	AD995	12.7	49	59	2.32	1.15	2.67
		38.1	148	27	2.46	1.22	3.01
		50.8	198	30	1.74	0.86	1.49
152	AD995	10.0	39	64	1.94	0.96	1.86
		20.0	78	50	2.38	1.18	2.80
		25.4	99	40	2.67	1.32	3.52
		30.0	117	33	2.73	1.35	3.69
		40.0	156	24	2.51	1.24	3.11
		50.0	195	22	2.08	1.03	2.14
		50.8	198	30	1.73	0.86	1.49
102	WC	6.35	99	63	0.84	1.67	1.40
		12.7	198	45	1.13	2.25	2.54
		25.4	396	5	1.36	2.70	3.67

The initial tungsten carbide ballistic test data shown Table V demonstrated two important factors, even for this less than optimum DOP target. First, the mass and space factors were still increasing, which means an optimum thickness has not been reached. More importantly, the space effectiveness was double that of the alumina at the same thickness even though the areal mass was four times as great. Further analysis with thicker WC tiles is not possible because the residual penetration of the L/D 10 tungsten rod is approaching zero. For this reason, the L/D10 rod was replaced with the higher performing L/D13 tungsten rod.

#### L/D 13 DOP Tests Versus WC

Table VI documents twelve DOP tests for three thicknesses of WC. The tile sizes were 152-mm square and the bond lines were maintained at a constant 0.5-mm. The effectiveness factors for each test have been determined from the impact velocity and no corrections have been applied. These twelve tests represent a consistent set of data and demonstrate a number of interesting observations. First, the ballistic performance for the 10 and 20-mm WC tiles was very similar with the mass effectiveness near 1.55 and the space effectiveness near 3.0. The 20-mm tiles were just slightly better performers. The 30-mm WC tiles demonstrated significantly better performance than would be predicted from the thinner tiles and an optimum size may not yet have been reached. As with the L/D10 rods, however, the residual penetration is approaching zero and a higher performing rod will have to be utilized to determine the optimum tile thickness for tungsten carbide.

For 30-mm tiles, the mass effectiveness was over two and the space effectiveness was over four. The space effectiveness factors are the highest measured to date in a DOP test. The quality factors were also very high, although many high performance ceramics can exceed these values for

thinner tiles because their mass effectiveness values are higher. The high space factors in these L/D13 tests mean that the rod is being stopped in a ceramic thickness that is about one-fourth its length.

Table VI. L/D13 DOP Ballistic Test Data for WC

SIZE (mm)	CERAMIC THICKNESS (mm)	CERAMIC AREAL DENSITY (kg/m <sup>2</sup> )	IMPACT VELOCITY (m/s)	AVERAGE P <sub>R</sub> (mm)	e <sub>m</sub>	e <sub>s</sub>	q <sup>2</sup>
RHA	0	0	1550	129.2	1.00	1.00	1.00
152	10.3	160.1	1531	95.0	1.53	3.05	4.68
	10.3	160.1	1543	97.0	1.54	3.02	4.65
	10.2	158.1	1552	99.0	1.50	2.99	4.49
	10.2	159.3	1554	99.0	1.52	3.01	4.57
152	20.1	314.2	1541	62.0	1.65	3.28	5.41
	20.2	314.6	1545	62.0	1.65	3.29	5.44
	20.1	314.2	1554	69.0	1.52	3.02	4.61
	20.2	315.0	1561	71.0	1.49	2.96	4.40
152	30.2	471.5	1543	7.0	2.02	4.01	8.10
	30.2	470.7	1543	5.8	2.04	4.05	8.26
	30.0	467.6	1543	7.7	2.03	4.03	8.17
	30.1	470.3	1549	11.4	1.97	3.91	7.68

#### L/D13 DOP Tests Versus W<sub>2</sub>C

A series of four 152-mm x 152-mm ditungsten carbide DOP tests were conducted on a single thickness of about 26-mm. Table VII documents the DOP performance of this ceramic. The mass performance was about equal to its weight in RHA which provided a space factor of just over two. The performance did not approach that exhibited by the WC tiles and can be attributed to the much higher grain size and lower than expected density.

Table VII. L/D13 DOP Ballistic Test Data for W<sub>2</sub>C

SIZE (mm)	CERAMIC THICKNESS (mm)	CERAMIC AREAL DENSITY (kg/m <sup>2</sup> )	IMPACT VELOCITY (m/s)	AVERAGE P <sub>R</sub> (mm)	e <sub>m</sub>	e <sub>s</sub>	q <sup>2</sup>
RHA	0	0	1550	129.2	1.00	1.00	1.00
152	26.0	420.3	1549	72.0	1.07	2.19	2.3
	26.1	420.2	1555	73.0	1.06	2.18	2.3
	26.1	420.2	1560	72.0	1.09	2.25	2.5
	26.0	420.4	1574	72.5	1.12	2.31	2.6

## CONCLUSIONS

This paper documents the development of a new class of ballistic ceramics known as high density ceramics. These ceramics have been defined to be any ceramic whose density is greater than that of rolled homogeneous armor steel ( $7.85 \text{ g/cm}^3$ ) and are very interesting from an armor standpoint, as very compact targets are possible. The WC family of high density ceramics was selected as the prime ceramic of interest because of its  $15.6 \text{ g/cm}^3$  density, excellent mechanical properties, and the potential applications in both the military and civilian markets. The tungsten carbide processing technology was developed by Cercom Incorporated of Vista, CA, who succeeded in producing high purity WC ceramics in large tile sizes.

Ballistic testing with L/D10 and 13 rods demonstrated very high space effectiveness factors and further testing is planned with higher performing rods in the future. The development of this ceramic will provide armored system developers with a very space efficient material for use against higher-performing medium caliber and full-scale rods in applications such as backpack designs, add-on appliques, roof appliques, hatch appliques or hull and turret side armors.

## REFERENCES

1. Schneider, S., Engineered Materials Handbook, Vol.4, Ceramics and Glasses, ASM International, 1991
2. Hauver, G., Private Communication
3. Rupert, N., Schoon, R., Evaluation of High Density Ceramics for Ballistic Applications. Conference on Dynamic Loading in Manufacturing and Service, Melbourne, Australia, 1993
4. Rupert, N., Burkins, M.S., Gooch, W., Walz, M., Levoy, N., Washchilla, E., Development of High Density Ceramic Composites for Ballistic Application, International Conference on Advanced Composite Materials, Wollengong, Australia, 1993
5. Gooch, W., Burkins, M. S., Frank, K., Ballistic Performance of Titanium against Laboratory Penetrators, 1<sup>ST</sup> Australasian Congress on Applied Mechanics, Melbourne, Australia, 1996
6. Grabarek, C. and Herr, L., X-Ray Multi-Flash System for Measurement of Projectile Performance at the Target, BRL Technical Note 1634, September 1966
7. Woolsey, P., Mariano, S., and Kokidko, D., Alternate Test Methodology for Ballistic Performance Ranking of Armor Ceramics, 5th Annual TACOM Armor Conference, Monterey, CA, 1989
8. Hauver, G., Gooch, W., Netherwood, P., Benck, R., Perciballi, W., and Burkins, M., Variations of Target Resistance During Long-rod Penetration into Ceramics, Proc. 13th International Symposium on Ballistics, Stockholm, Sweden, 1992
9. Burkins, M. S., Gooch, W., Ceramic Testing Methodology, ARL Workshop, June, 1995
10. Frank, K., Armor-Penetrator Performance Measures, ARBRL Report MR-03097, 1981
11. Hauver, G., Netherwood, P., Benck, R., Ballistic Performance of Ceramic Targets, 13<sup>TH</sup> Army Symposium on Solid Mechanics, Plymouth, MA, 1993
12. Prifti, J., Woolsey, P., Gooch, W., Perciballi, W., Advanced Ceramic/Metallic Armor Systems for Defeat of Long Rod Penetrators, Second Ballistic Symposium on Classified Topics, Johns Hopkins University, 1993

Unclassified

**Reactive *Applique* Armor  
for the  
Bradley M2A2/M3A2 Vehicle Systems**

Stephen Chico  
U.S. Army Armaments Research  
Development and Engineering Center  
Picatinny Arsenal, NJ 07806-5000

**ABSTRACT (U)**

(U) In April 1995, a reactive armor tile system was Type Classified for use on the Bradley Fighting Vehicle. The unique properties of this armor are its ability to be mounted on a light armor vehicle and provide a high level of protection against shaped charge threats while remaining relatively insensitive to burning from small arms threats. Mounting tiles on a light combat vehicle requires special design considerations to prevent blast effects of the tile from damaging the vehicle while providing maximum protection. The armor system achieves its performance through the internal design and the use of a low-flammability explosive. A performance specification is being used for the procurement of the armor tiles and extensive qualification testing has been conducted. This paper will discuss the design and performance characteristics of the armor tiles as well as the scope of the performance specification and specific test results. On 31 July 1995, a contract was awarded to Martin Marietta Ordnance Systems for the production of Reactive Applique Armor Tiles to be used on the Bradley Fighting Vehicle.

**(U) Introduction**

(U) The U.S. Army Armament Research Development and Engineering Center (ARDEC) has been involved with the testing and Type Classification of three reactive armor tile systems since 1985. The first system was for use on the M60A3 Tank which is currently in use by the U.S. Marine Corps. An Army developed system of tiles for the Bradley Fighting Vehicle was Type Classified in December 1987. Recently, a reactive armor tile system developed to a performance specification and supplied by Lockheed-Martin as the prime contractor with Rafael of Israel as the major subcontractor has been type classified (April 1995). ARDEC was responsible for the design and execution of the qualification testing for each system.

Unclassified

Distribution authorized to the Department of Defense and DoD contractors only: Critical Technology, March 1996.  
Other requests shall be referred to Commander US Army Armaments Research Development and Engineering  
Center, AMSTA-AR-CCH-C, Picatinny Arsenal, NJ 07806-5000

(U) In 1986, work began on the development of a Reactive Armor tile system for the Bradley Fighting Vehicle as part of the block modification A2 upgrade. The armor system for the Bradley presented a greater challenge than the armor systems developed for tanks. The thinner hull of the Bradley would not be able to withstand the blast impulse as well as the thicker steel hulls of a tank. In addition, the thinner hull places more of the burden of stopping the shaped charge jet on the tile. These design considerations led to tile configurations that have multiple internal cassettes to increase the tiles effectiveness and segmented explosive elements which limit the blast effects.

(U) At the beginning of this development program Reactive Armor was a relatively new and unknown product. Due to the explosive content of the tile, all the standard ammunition tests were performed as well as several non-standard tests devised by the test community. This extensive testing ensures the safety of the soldier under all anticipated conditions.

(U) System Characteristics:

<u>Nomenclature</u>	<u>Dimensions</u>	<u>Weight</u>	<u>Area Density</u>	<u>Qty per Vehicle</u>
M3A1	12"x 13"x 3"	36 lbs.	33.7 lb/sqft	26
M4A1	12"x 2.5"x 5.5"	6 lbs.	12.0 lb/sqft	9
M5A1	13"x 14.3"x 12.2"	84 lbs.	67.7 lb/sqft	55
M6A1	7"x 10.2"x 8"	30 lbs.	53.6 lb/sqft	7
M7A1	7"x 10.2"x 8"	23 lbs.	41.1 lb/sqft	8

The tiles can be mounted on those Bradley's with an A2 block modification upgrade (and all subsequent upgrades) by the crew in the field using brackets and bolts supplied in an installation kit. Installation time is estimated at 2-3 hours. The total system weight is approximately 6,500 lbs.

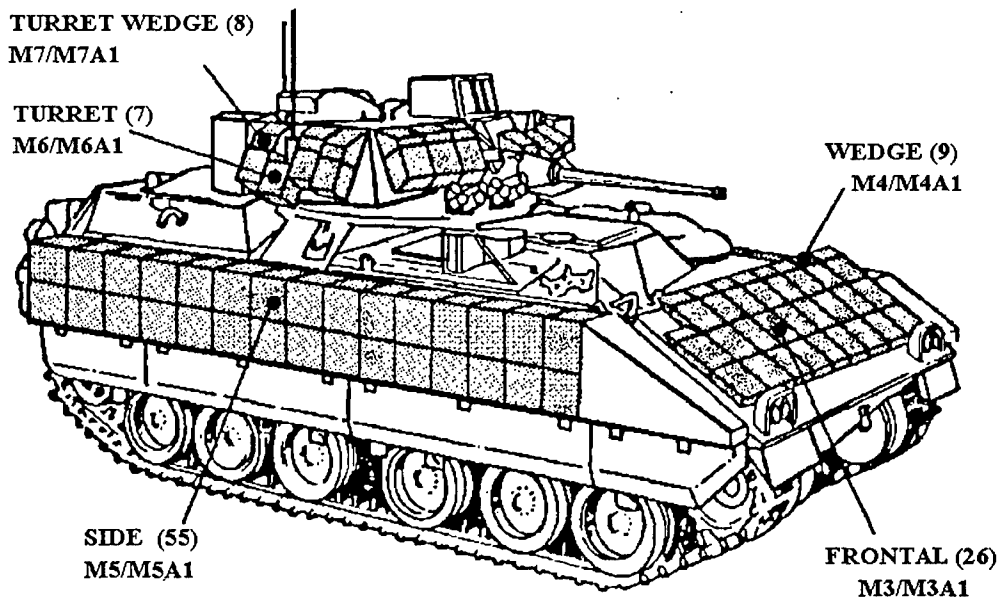


Figure 1

Bradley Vehicle with Applique Armor

Unclassified

(U) Performance Criteria

(U) The tile system is required to provide 360° of protection against penetration by Hand Held Heat (HHH) anti-tank weapons and 60° of frontal arc protection against the Anti-Tank Guided Missile (ATGM) threat.

(U) The performance specification was designed to test the effectiveness of the tiles as built and to ensure the protection level is not degraded after the tiles are subjected to various environments. In addition, the tiles must not detonate, deflagrate or present a safety hazard as a result of testing.

(U) During the pre-qualification test program, the armor tile's sensitivity to burning became an issue. Additional criteria for the tiles to be insensitive to small arms threats were established. This presented the designers with a new challenge in that the tiles had to maintain performance against shape charge threats yet be insensitive to initiation from small arms threats. With the addition of the no-burning criteria, one of the three contractors withdrew from the program and the other failed to meet performance requirements. Lockheed Martin remained as the only potential supplier. The Lockheed-Martin/Rafael design was qualified in a six month test program conducted at Aberdeen Proving Ground and ARDEC. Based on the successful results of these tests the armor tiles were type classified-standard in April 1995 meeting all the criteria outlined in the performance specification.

(U) Qualification Test Program

(U) As experience was gained with reactive armor, the test quantities required to qualify the armor systems were reduced. The M60 tile system required 728 tiles for qualification. There were only two tile configurations with the only difference being in tile size. Therefore, many tests did not need to be repeated. The number of tiles used in the qualification of the Bradley TDP design was well over 2,000. The large number of tiles required is attributed to the fact that the Bradley armor system consists of five different tile designs. Not only are the tiles different sizes, but the internal configurations for each are different. The tiles built to the performance specification have the same external dimensions as the previously developed Army TDP tiles and as such consist of five separate designs. A quantity of 1280 tiles were tested to qualify this design. This quantity may again seem high, but each tile is different in size, weight and internal configuration such that the environmental tests must be conducted on each design and in sufficient quantity to ensure it will meet the required performance with an acceptable reliability. The quantity of tests had to be balanced against the production costs and the time and cost of testing.

(U) Qualification Tests

(U) Shaped Charge Armor Protection was conducted on new tiles to develop a performance baseline. The tiles were statically tested against shaped charge warheads in the orientation they would be mounted on the vehicle using armor plates identical to the construction of the vehicle.



The shot lines for this test were at worst case angles and through the center of volume of the tiles. The turret tiles were tested against the HHH surrogate threat. The Front and Side tiles were tested against the ATGM surrogate threat.

(U) Mapping Evaluation was conducted using the same procedure as the baseline performance tests except that the shot-lines through the tiles were at non-optimal locations, primarily along the edges of the tiles or suspected vulnerable areas of the tiles. Ten out of twenty-six (26) shots were conducted within 1/2" of the tiles edge, four of which passed and only one of the remaining five penetrated beyond the first 1" witness plate. This data was collected primarily for inclusion in overall vehicle vulnerability models.

(U) Junction tests were also conducted to determine the performance in situations where the shaped charge jet passes through multiple tiles. Nine tests were conducted and all passed.

(U) Enhanced Performance. Tiles were tested against threats that were known to exceed their protection capabilities to determine how effectively the tiles reduced the performance of the larger threats.

(U) Collateral Damage and Sympathetic Detonation testing were conducted to determine the effect detonation of a tile would have on the surrounding tiles. Collateral damage is conducted by initiating a tile in an array with a threat warhead. The criteria is that only the initiated tile and one additional tile may be destroyed. For sympathetic detonation, a tile is initiated with a detonator and no additional tiles may detonate or deflagrate. The tiles passed this requirement.

(U) Hazard Classification: the standard hazard classification tests were conducted for the armor tiles per TB 700-2. The resulting hazard classification for the tiles is 1.4D.

(U) Small Arms Sensitivity. Tiles were subjected to various small arms fire in either bursts or single shots depending on the threat and the expected range of engagement. The number of rounds per tile was determined by considering the dispersion and expected range of engagement for each threat. The criteria was that no tiles detonate or deflagrate for the smaller threats and that only 10% combined are allowed to flame for the larger threats. Shaped charge performance tests conducted on tiles damaged by small arms threats showed that the undamaged areas of the tiles maintain their protection capability.

(U) Corrosion Test. Tiles and tile components were subjected to 336 hours of 5% salt spray to determine the tiles' resistance to corrosion. The sealed tiles exhibited very little corrosion and no internal corrosion. Some of the internal components that were tested individually were corroded.

(U) Drop Tests. Tiles were dropped a distance of 40-feet in a packaged and palletized condition. In all cases there was some minor denting of the tiles. Tiles were also dropped a distance of 7-feet both bare and packaged. Again there was minor tile denting. There was no safety hazard caused by dropping the tiles.

(U) Safety Tests

(U) Safety tests were conducted to determine if various events would cause the tiles to detonate, deflagrate or otherwise cause a safety hazard.

(U) A Vehicle Impact Test was run to simulate a collision between a vehicle with tiles and another vehicle. In this test a 500-lbs. wedge shaped weight was dropped 40-feet onto tiles temperature conditioned to both hot (160°F) and cold (-65°F) temperatures. Tiles were crushed, dented and or severed, but there were no explosive reactions.

(U) Drill Tests were conducted to evaluate the hazard of accidental drilling into a tile. Tiles were drilled with bits ranging from 1/8" to 3/4" at approximately 500 RPM. The worst case reaction for any tile was heavy smoke with no visible flame.

(U) Heat Exhaust testing was conducted to determine their reaction should a vehicle such as an M1 tank park near a Bradley uploaded with tiles. Torpedo heaters were used to raise the temperature of single tiles to 250°F and maintain that temperature for one hour. The worst case reaction was that some tiles showed evidence that the explosive melted.

(U) Cutting Torch tests were conducted to evaluate the potential hazard from a cutting torch. Tiles were subjected to being cut by an oxygen-acetylene torch both starting from the edge and starting in the center. All tiles flamed between 10 to 30 minutes, but no violent reactions occurred.

(U) Arc Welding tests were conducted to evaluate the hazard should an unsuspecting soldier try to weld something to a tile. Tiles were subjected to arc welding (200-300 amps) for 15 seconds. Of the 10 tiles tested all smoked and five exhibited visible flaming although all flames were extinguished within two minutes.

(U) Lightning Strike. Tiles were subjected to two simulated lightning strikes each per tile per Test Method T02 of MIL-STD-1757A. The lightning strike is a multi-component waveform with a peak current of 200,000 amps. Out of 10 tiles tested (20 strikes) only one tile exhibited some smoking (2nd strike).

(U) Vehicle Vibration. Tiles were subjected to simulated vehicle vibration at both hot and cold temperatures. The tiles were then performance tested. All the tiles met the performance criteria after the vibration tests.

(U) SEQUENTIAL ENVIRONMENTAL TESTS

(U) Tiles were sequentially subjected to loose cargo vibration and 7-foot drop while packaged. The tiles were unpackaged and then subjected to temperature storage, temperature shock, temperature humidity, loose cargo vibration, 7 -foot drop and water immersion tests. Three temperature groups of tiles were subjected to these tests. Each group contained 12 of each type of tile. At the end of the sequence the tiles performance was tested at their respective group temperature. Of the 180 performance tests conducted three penetrated beyond the acceptable criteria. Two of these penetrations were 1/16" and the third was 1/8".

(U) CONCLUSIONS:

(U) The results of the qualification testing demonstrate that a reactive armor tile system can be used to increase the survivability of relatively thin hulled combat vehicles. The armor tile system developed for the Bradley Fighting Vehicle greatly enhances its survivability against the proliferation of shaped charge threats while remaining insensitive to small arms threats. The performance of the tile system is not affected by the anticipated battlefield environments and the tiles do not present a safety liability to the soldiers.

(U) References.

Final Report for the Production Qualification (PQT) of the Generic Applique Armor for Bradley Fighting Vehicle System - A2 (BFVS-A2), Vendor Evaluation - Qualification for Production (Phase III - Qualification Tests), March 1995, Land Systems Division, Live Fire Vulnerability Directorate. U. S. Army Combat Systems Test Activity, Aberdeen Proving Ground, MD Report No. CSTA-7658.

UNCLASSIFIED

Classified by: \_\_\_\_\_

**ANTI-MINE ARMOR DEVELOPMENT FOR THE XM1114 HMMWV (U)**

Dennis J. Malone  
O'Gara-Hess and Eisenhardt Armoring Company  
Fairfield, Ohio 45014

David J. Stevens  
Southwest Research Institute  
San Antonio, Texas 78228

John D. Weaver  
PEO-TWV-TACOM  
Warren, MI 48397-5000

**ABSTRACT (U)**

(U) TACOM has recently developed the XM1114, an uparmored version of the High Mobility Multi-purpose Wheeled Vehicle (HMMWV), for use in combat situations as well as in peace keeping missions. The XM1114 is based on the ECV (Enhanced Capacity Vehicle) HMMWV and is designed to protect the occupants from armor-piercing projectiles, artillery fragments and landmines, up to and including anti-tank mines. The design of the anti-mine armor system is discussed in this paper and the experimental results from a test using an anti-tank mine are shown to compare well to the predicted results.

(U) INTRODUCTION

(U) To support peacekeeping missions and to provide the U.S. Army with a low-profile, high speed, high mobility, reconnaissance vehicle, TACOM has recently developed a series of uparmored High Mobility Multi-purpose Wheeled Vehicles (**HMMWVs**), including the XM1109, based on the M1097 HMMWV,

UNCLASSIFIED

Approved for public release; distribution is unlimited.

and, the XM1114, based on the ECV HMMWV. The design threats for both vehicles include armor piercing projectiles, anti-tank mines, and artillery fragments. These vehicles and their protective systems are designed and fabricated by the O'Gara-Hess and Eisenhardt Armoring Company (**OHEAC**), working in conjunction with the HMMWV manufacturer, AM General (**AMG**); Southwest Research Institute (**SwRI**) has supported OHEAC in the design and analysis of certain protective, structural, and weapon system components of the XM1114, the XM1109, and field-installable kits for the HMMWV family of vehicles.

(U) The HMMWV is a unique vehicle, carefully designed to optimize a number of characteristics, including overall weight, payload, range, durability, and performance (i.e., speed, mobility, extreme terrain capability, etc). In some ways, the HMMWV resembles a modern aircraft more than its predecessor, the Jeep. The body of the HMMWV is fabricated mostly with riveted and bonded aluminum sheet; steel is used only for critical structural members, such as the frame rails, body attachment mounts, and turret supports; and, the vehicle was designed "close to the teeth", i.e., the effects of modifications must be carefully considered. To develop an armor system for such a unique, light-weight, tactical vehicle, one must minimize the effects of the extra weight on the payload and the load-bearing elements of the body and frame. In addition, any reduction in ground clearance should be minimized to maintain mobility and rough terrain capability. And finally, the armor system should be removable or easily accessed so that NBC decontamination can be performed.

(U) In this paper, the design process of the anti-mine armor system for the XM1114 is presented. The results from a recent anti-tank mine test are discussed and compared to the numerically predicted deflections. Several XM1114 vehicles are currently undergoing operational endurance testing.

(U) DESIGN APPROACH

(U) The overall design goals of the armor system are to prevent fatalities and to minimize the number and extent of injuries, when a pressure-activated anti-tank mine is detonated under a tire. The loss of vehicle mobility is expected; however, weapon systems should still function. To minimize casualties, the occupants must be protected from: blast overpressures, gross deformation of the vehicle, fragments created by vehicle breakup, and structural motions (accelerations) imposed on the crew through the seat and seat base. The protection from structural motion is provided by both the armor system and collapsible seat brackets, designed and supplied by an outside contractor;

UNCLASSIFIED

since this paper is concerned with the armor system, the seat bracket will not be discussed further.

(U) As mentioned above, to develop a successful anti-mine armor design for a light tactical vehicle, a number of issues must be considered, including: weight, ground clearance, durability, and NBC decontamination. The armor system for the XM1114 was designed to bolt on and off, to facilitate NBC decon and to allow easier repair for accident or maneuver-induced damage. In terms of overall geometry, the armor covers the floor area of both sides of the HMMWV and extends into the forward and rear tire wells. On the exterior sides, the anti-mine armor bolts into the footwell structure located below the two armored doors. In the interior, the armor is bolted to a series of specially designed resilient mounts, which are, in turn, attached to the steel frame rails; the frame rail is not drilled or welded and the effect of the attachments on the fatigue life of the frame rails has been shown to be minimal. Finally, the armor system also attaches to aluminum panels inside the crew compartment, to create a semi-monocoque construction.

(U) In addition to providing areal coverage, the anti-mine armor must also be able to withstand the blast loads from the mine, without excessive deformations. The loads acting on an armor surface will be a function of the distance from the mine and the angle of obliquity of the surface to the direction of the blast. For instance, for the left front portion of the armor system (the driver's compartment), the schematic in Figure 1 shows that the blast will act most strongly on the angled portion of the floorwell, and with less intensity on the horizontal portion of the armor and the firewall section of the armor. Based on this geometry and the explosive weight of the anti-tank mine, blast pressure histories on the exposed surfaces can be estimated using TM-855-1, "Fundamentals of Protective Design for Conventional Weapons," and DOE/TIC-11268, "A Manual for the Prediction of Blast and Fragment Loadings on Structures" (Bowles et al. 1992).

(U) To maximize blast and flexural resistance while minimizing weight and the impact upon ground clearance, a layered plate system was devised for the cross section of the armor system in the footwell region and a single layer was used for the horizontal and firewall armor sections, as shown in Figure 2 (which is not to scale). While the details of the geometry, materials, and welding process are proprietary, it can be said that the inner and outer plate and the tubes are steel and are welded together in such a way that the heat affected zones (HAZs) are in areas of relatively low stress.

(U) To define the required material strength, ductility, thickness, and weight of the layered plate approach, and to investigate the effects of the weld-induced

## UNCLASSIFIED

HAZs, PRONTO, a Lagrangian Finite-Element hydrocode developed by Sandia National Laboratories (Taylor and Flanagan 1987), was used to optimize the system for controlled deformation and energy absorption. A number of iterations were performed using two dimensional models as shown in Figures 2 through 5, which present different views of the armor system at different times of the analysis. The design was continually modified until an acceptable combination of deformation and system weight were achieved. The predicted reactions from the PRONTO analyses were also used to determine the forces that must be resisted by the resilient mounts used to attach the armor to the steel frame rails; these forces, in turn, determined the mechanical requirements for the system of attaching hardware.

### (U) ANTI-TANK MINE TEST

(U) During the summer of 1995, the XM1114 HMMWV was successfully tested with an anti-tank mine at the Aberdeen Proving Grounds. The mine was placed in soil, under the front left tire, and remotely detonated. High speed footage of the event, as well as data from a remote pressure gage, confirmed that the mine went "high-order".

(U) Figures 6 and 7 present the exterior of the XM1114 before and after testing, respectively. While Figure 7 shows that considerable damage occurred in the engine compartment, the amount of damage and deformation in the underbody armor system was quite small, with the driver's compartment staying intact. Additionally, all crew compartment doors remained closed and latched during the test, functioning to transfer the blast-induced loads throughout the armor system and enhancing crew survivability. As Figure 8 shows, the interior of the vehicle was likewise in good shape, with little intrusion into the driver's space. The peak deflection, at the center of the slanting floorwell, was approximately 1.75", which agrees quite well with the predicted value of 1.45". Measurements from the instrumented HYBRID 3 anthropomorphic dummy showed that the driver would survive the blast.

### (U) CONCLUSION

(U) The anti-mine armor system on the XM1114 was successfully designed through careful consideration of the issues that were most important to the U.S. Army, including weight, ground clearance, vehicle performance and durability, and, most importantly, sufficient protection levels for the anti-tank mine threat. State-of-the-art hydrocode analysis was combined with the practical design experience of the team members to create a system that

UNCLASSIFIED

effectively and efficiently defeated the mine during testing. The design approach and the resulting armor system were proven through mine tests and endurance tests of the XM1114 and they can be directly and confidently extended to other tactical wheeled vehicles.

(U) REFERENCES

Bowles, P.K., et al., *A Manual for the Prediction of Blast and Fragment Loading on Structures*, Report No. DOE/TIC-11268, US Army Engineer Division, Huntsville, AL, 1992.

*Fundamentals of Protective Design for Conventional Weapons*, TM5-855-1, HQ Dept. of the Army, Washington, D.C., Nov 3, 1986.

Taylor, L.M., and Flanagan, D.P., 1987. *PRONTO 2D, A Two-Dimensional Transient Solid Dynamics Program*, SAND86-0594\_UC-32, Sandia National Laboratories, Albuquerque, New Mexico.

UNCLASSIFIED



UNCLASSIFIED

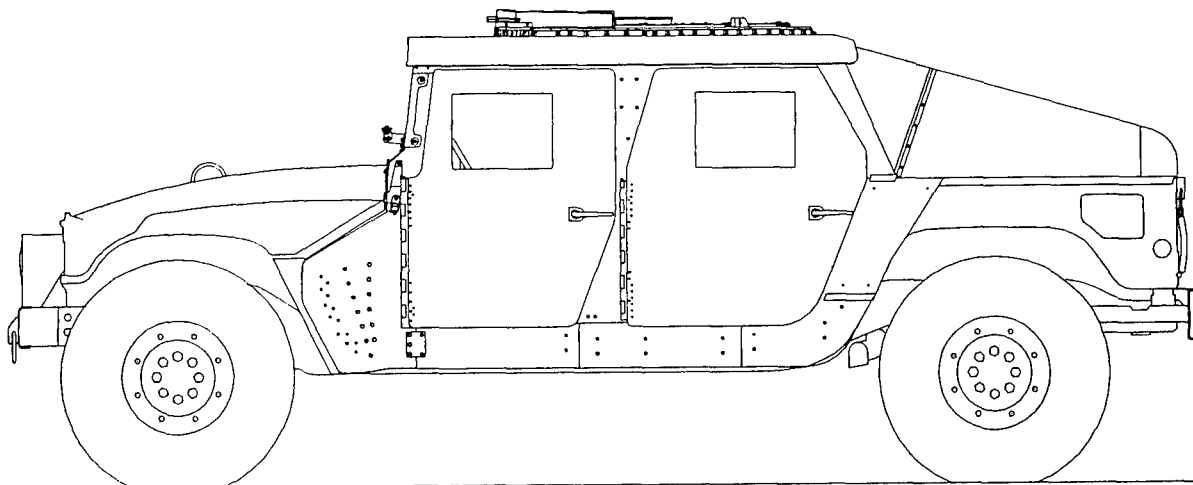


Figure 1. (U) Schematic of an Up-Armored HMMWV (XM1114).

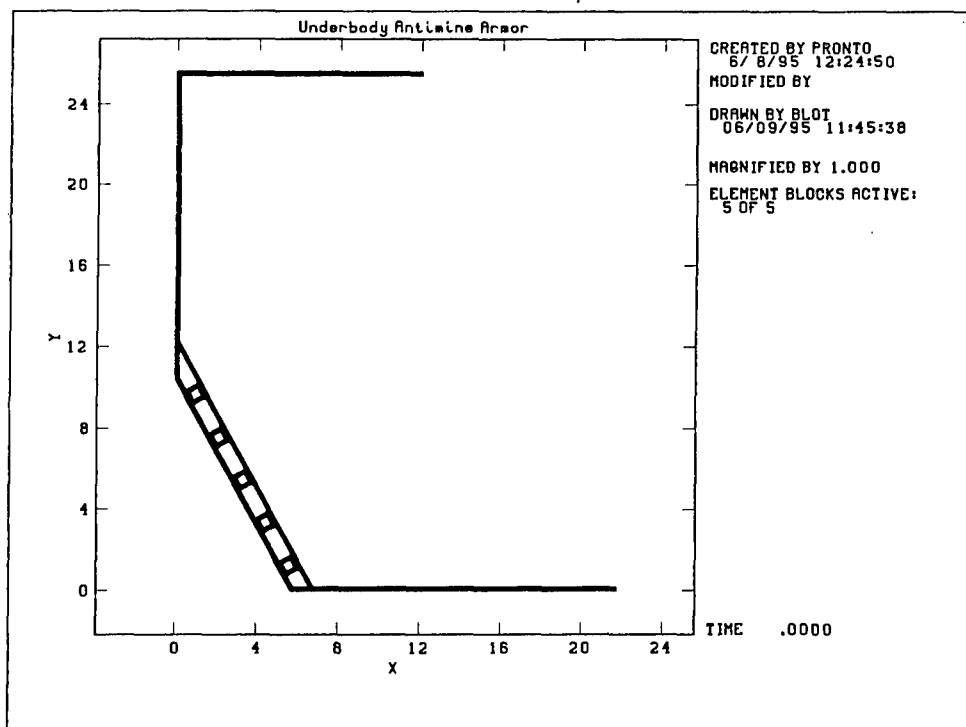


Figure 2. (U) Side View of Antimine Armor System for the XM1114, Time = 0.0 msec.

UNCLASSIFIED

UNCLASSIFIED

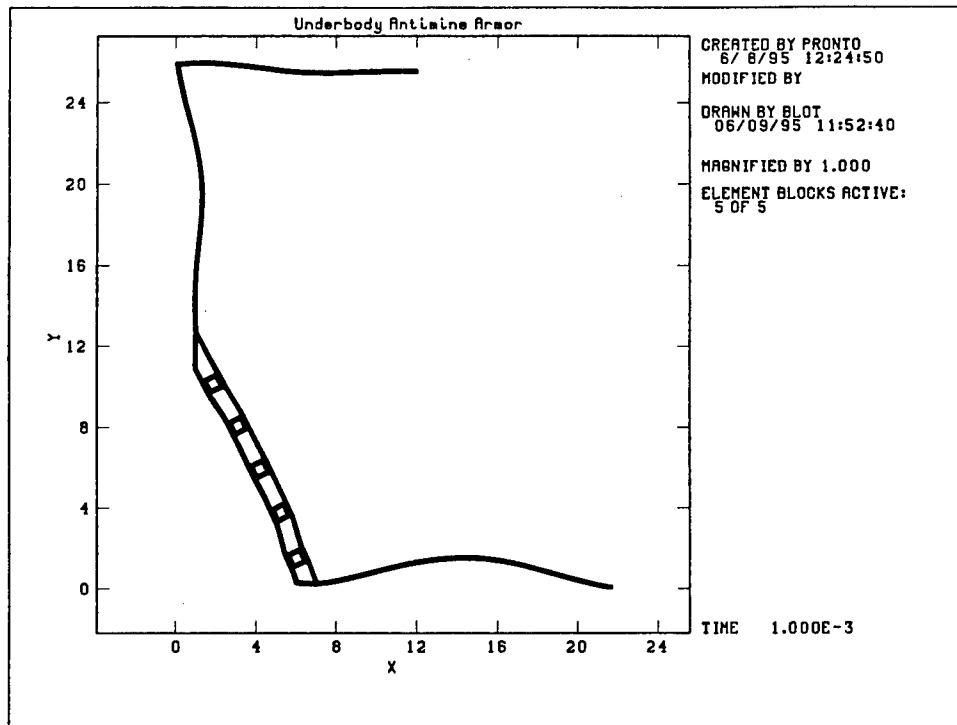


Figure 3. (U) Side View of Antimine Armor System for the XM1114, Time = 1.0 msec.

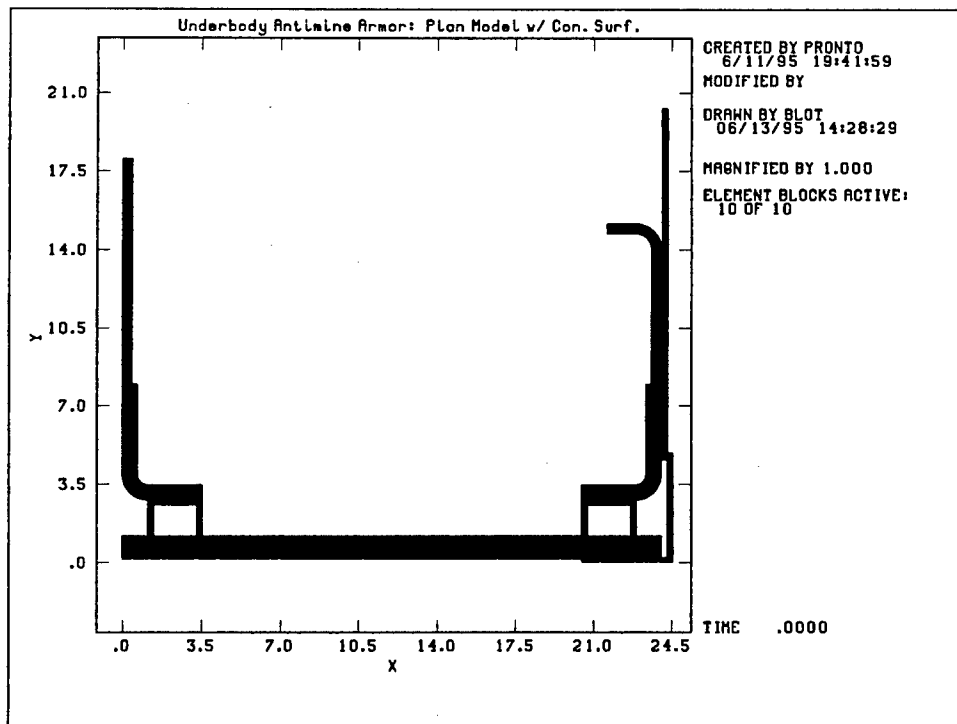


Figure 4. (U) Top View of Antimine Armor System for the XM1114, Time = 0.0 msec.

UNCLASSIFIED

UNCLASSIFIED

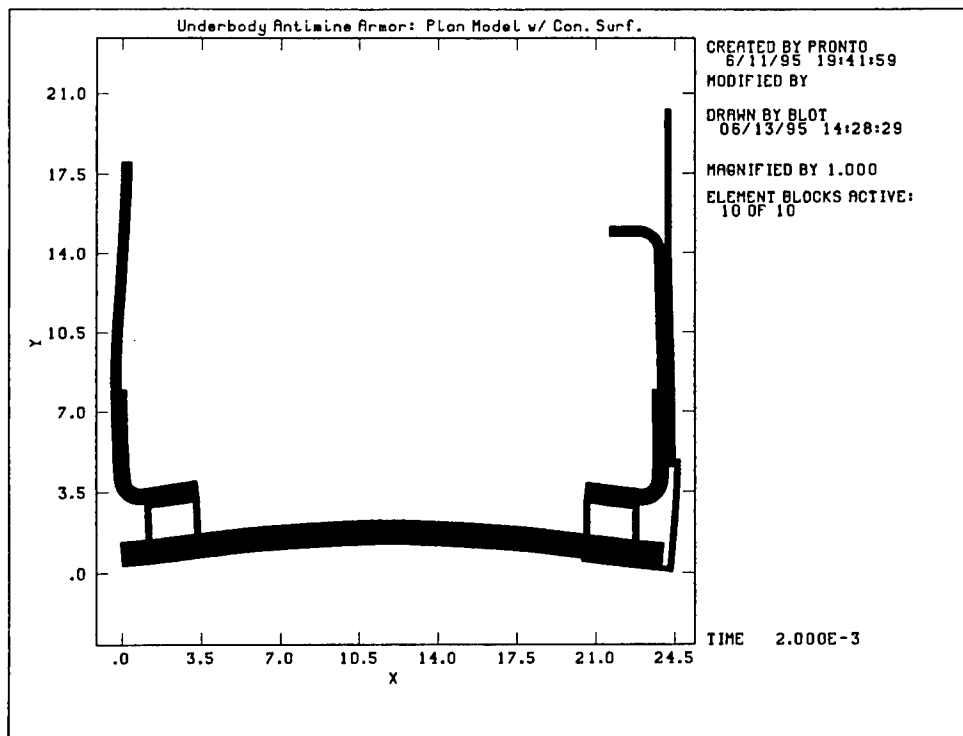


Figure 5. (U) Top View of Antitank Armor System for the XM1114, Time = 2.0 msec.



Figure 6. (U) XM1114, Prior to Antitank Mine Test

UNCLASSIFIED

UNCLASSIFIED

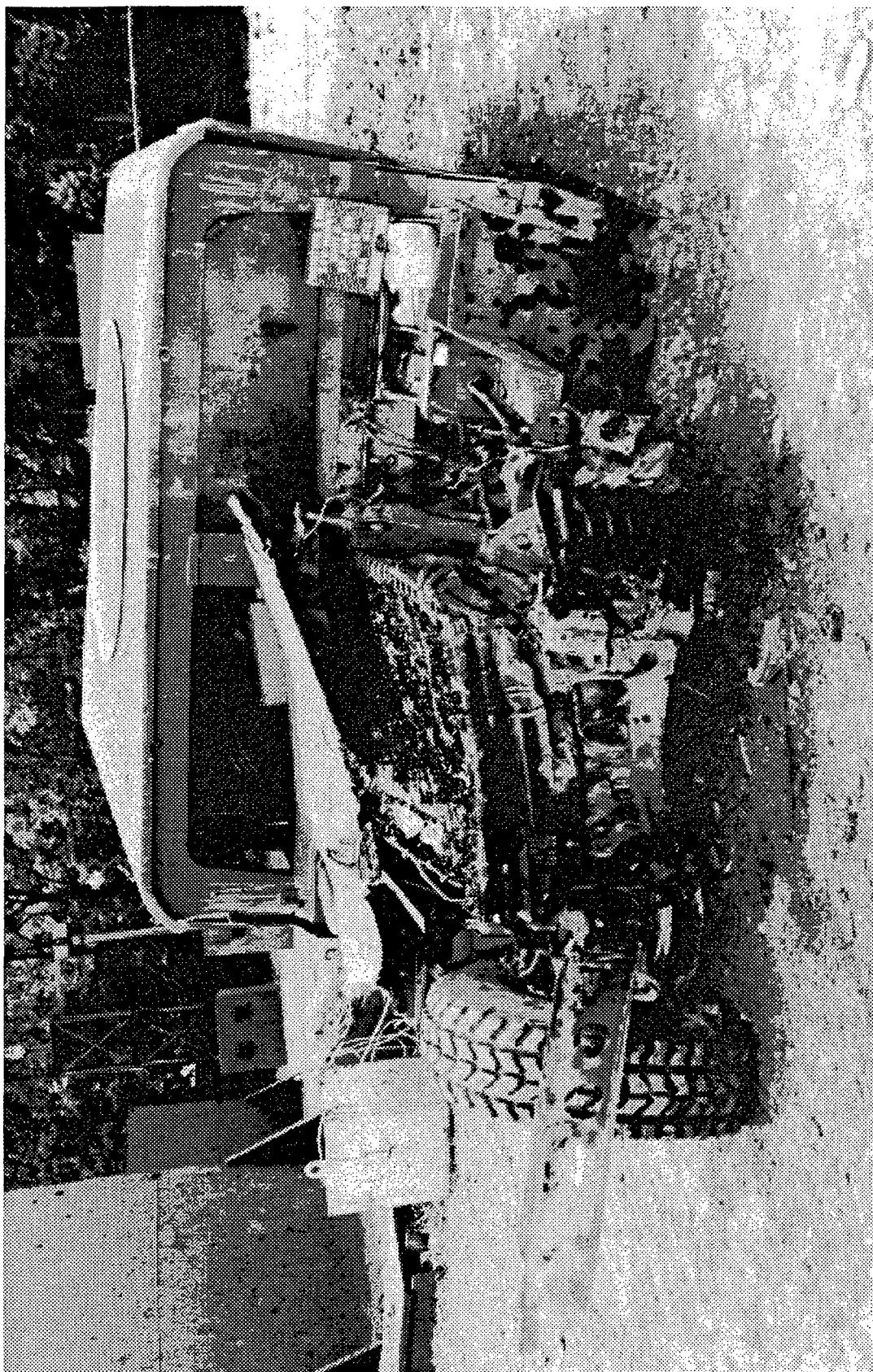


Figure 7. (U) Exterior of XM1114, After Antitank Mine Test

UNCLASSIFIED

UNCLASSIFIED



Figure 8. (U) Interior view of XM1114, After Antitank Mine Test

UNCLASSIFIED

UNCLASSIFIED

**ACTIVE PROTECTION AND SENSOR FUSION SESSION**

**King Auditorium**

**Wednesday, March 27, 1996**

**Session Chairman: Mr. Frank Stoddard, TRW Space and Electronics Group**

UNCLASSIFIED

**UNCLASSIFIED**

**THIS PAGE INTENTIONALLY LEFT BLANK**

**UNCLASSIFIED**

UNCLASSIFIED

**N-TAPS, A Near Term, Low Cost Active Protection System (U)**

Mr. Frank J. Stoddard

Dr. John W. Wehling

Dr. Jane M. Lin

Mr. David P. Smith

TRW Space and Electronics Group  
One Space Park  
Redondo Beach, CA 90278

**ABSTRACT (U)**

(U) The proliferation of lethal threats to armored vehicles is generating interest in nontraditional means for their protection. In particular, active protection systems (APS) have the potential to provide needed protection without compromising tactical and strategic mobility. An APS is defined as one that intercepts and destroys the effectiveness of an incoming threat before it reaches the targeted vehicle. Recent significant advances in computing and sensor technologies have eliminated obstacles to development of an effective APS that hampered earlier attempts.

(U) These advances are being exploited in the Near-Term Active Protection System (N-TAPS) that will be demonstrated under the TACOM Integrated Defense System (IDS) program. This paper reviews historical attempts to develop an APS, describes the N-TAPS concept and its enabling technology and discusses plans for proof-of-concept demonstration testing.

(U) Introduction

(U) In recent years, highly lethal modern threats to armored vehicles have proliferated throughout the world. This proliferation is of particular concern because even the most advanced armor technologies cannot provide the required protection without significantly degrading vehicle tactical and strategic mobility. Furthermore, electronic warfare techniques cannot provide robust means for defeating all of the threats of interest.

(U) As a result, a different approach is needed, one that provides the necessary protection at a reasonable cost without compromising vehicle capabilities. The only known concept for achieving this goal is an APS. The need for APS was established in the Operational Requirements Document (ORD) for the Anti Tank Guided Missile Defense System (ADS) of 10 March 1995. Also, APS was identified in the Project Guardian Study as a potential means for providing protection against the widest range of threats at an affordable cost. Recently, APS was one of only two survivability suites selected for further development under the TARDEC Integrated Defense System (IDS) program.

Distribution authorized to Department of Defense and DoD contractors only.

Other requests should be referred to:  
U.S. Army Tank-Automotive RD&E Center  
ATTN: AMSTA-TR-R  
Warren, MI 48369-5000

9600931 O1 .004



(U) An APS protects a targeted asset by intercepting and destroying the effectiveness of the threat before it reaches its target. As such, APS complements armor and other survivability systems and has the potential to improve survivability without compromising strategic and tactical mobility.

(U) Various APS architectures have been proposed. In general, an APS consists of sensor and countermeasure subsystems for which the principal development challenges are in meeting requirements for small size, light weight, fast reaction, low cost, minimal collateral damage and high effectiveness. A summary of the various options that have been proposed for each component of an APS for armored vehicle defense is provided in Figure 1. The specific combination of features selected for a given application is strongly influenced by vehicle survivability requirements, threats to be countered, attack scenarios, vehicle integration and operability constraints, level of technology available, kill mechanism required to defeat the threats, and cost considerations.

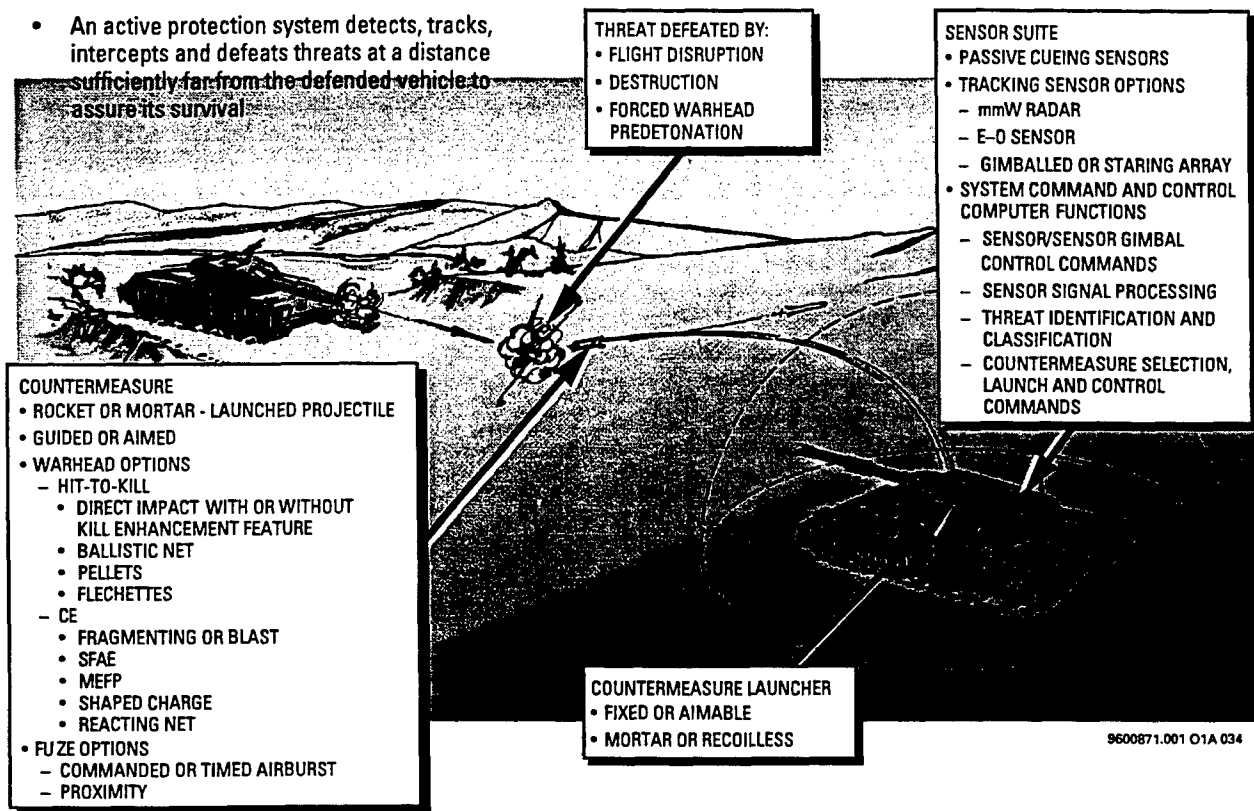


**Figure 1. What Is an Active Protection System?**

(U) It is important to realize that subsystem requirements are strongly coupled. For example, if the kill mechanism selected requires precision delivery to be effective against the threat, as is true of a hit-to-kill countermeasure, then a high precision tracking sensor is required. If, on the other hand, the selected countermeasure has a large kill effectiveness volume, threat tracking accuracy requirements can be relaxed. Also, the sensor power requirement is influenced by the threat detection range capability needed. It is increased when the required intercept range is increased or a slower responding countermeasure is used. Such considerations, strongly influence optimal selection of APS sensor component type, size, power, signal processor throughput, beam agility, and overall cost.

9600931 O1 .004

## UNCLASSIFIED

(U) As a general rule, attempts to fashion a fielded APS system from existing components are doomed to failure. The requirements for an effective APS and the constraints imposed by armored vehicle integration and operation are so stringent that only a bottoms-up integrated systems approach will result in a viable system.

(U) In the following, a brief history of U.S. attempts to develop an APS for armored vehicles is presented. Then the TRW Near-Term Active Protection System (N-TAPS) concept conceived under TARDEC funding is discussed along with the developing technology that will enable it to be economically fielded. Following that, the proof-of-concept brassboard N-TAPS to be demonstrated under IDS is described.

### (U) Historical Review

(U) Considerable U.S. research and development activity has been devoted to APS since the early 1950s. Most of this effort has focused on Naval and anti-ballistic missile (ABM) applications. An example of one of the few operational APSs is the Naval Phalanx system. Another operational system is the Patriot, which although developed as an anti aircraft missile system, was used in an area-defense APS role against SCUD missiles in the Gulf War. Examples of ABM systems that have been demonstrated successfully but not yet deployed include the Exoatmospheric Re-entry Vehicle Interceptor System (ERIS) and the Extended Range Interceptor (ERINT).

(U) A much more modest effort has been devoted to the armored vehicle APS application. Work began in 1952 when development of Dynamic Armor was initiated at Picatinny Arsenal. Dynamic Armor was originally a concept involving sensing incoming threat projectiles and destroying them with linear shaped charges detonated in the path of the projectile before it reached the targeted vehicle. This in-house Army program eventually was named Dash-Dot. It suffered from lack of funding until 1957 when it came under the supervision of the Ordnance Tank Automotive Command (OTAC, now known as TACOM). OTAC had overall responsibility for the program with Picatinny Arsenal and Ballistic Research Laboratory (BRL) directing development of the explosive countermeasures and the Diamond Ordnance Fuze Laboratory directing development of the sensing system. Dash-Dot originally utilized distributed-staring optical sensors (see Figure 2) to detect the threat and trigger a linear shaped-charge segment attached to the side of a tank hull and oriented to fire upwards. The resulting shaped-charge jet sheet was intended to intercept and destroy the threat before it contacted the vehicle. Practical difficulties were encountered, however, in implementing the system. Among these difficulties were sympathetic detonations among neighboring shaped-charge segments, difficulties with obstacles damaging the low-mounted linear charges, collateral damage and operational effectiveness of the optical sensors. Apparently as a result of these difficulties, Army recommendations were made in 1959 to reorient Dash-Dot. The new recommended approach incorporated a radar sensor and a lethal mechanism consisting of fragments, flechettes, or explosive pellets directed outward from the vehicle along the approximate trajectory of the incoming threat. Work on Dash-Dot was later abandoned.

(U) In the meantime, private industry became interested in this application. In 1957, United Aircraft Corporation conceived a system called Flyswatter under its own funds. Their study culminated in an unsolicited proposal to TACOM (still called OTAC at that time) in 1959. In 1960, the concept was updated and a revised proposal was submitted but was not funded, although the concept was considered to have merit.

(U) In 1959, Sanders Associates studied a concept for defeat of antitank missiles under a contract from Frankford arsenal. Their study concluded that their concept, which consisted of a tribeam

9600931 01 .004

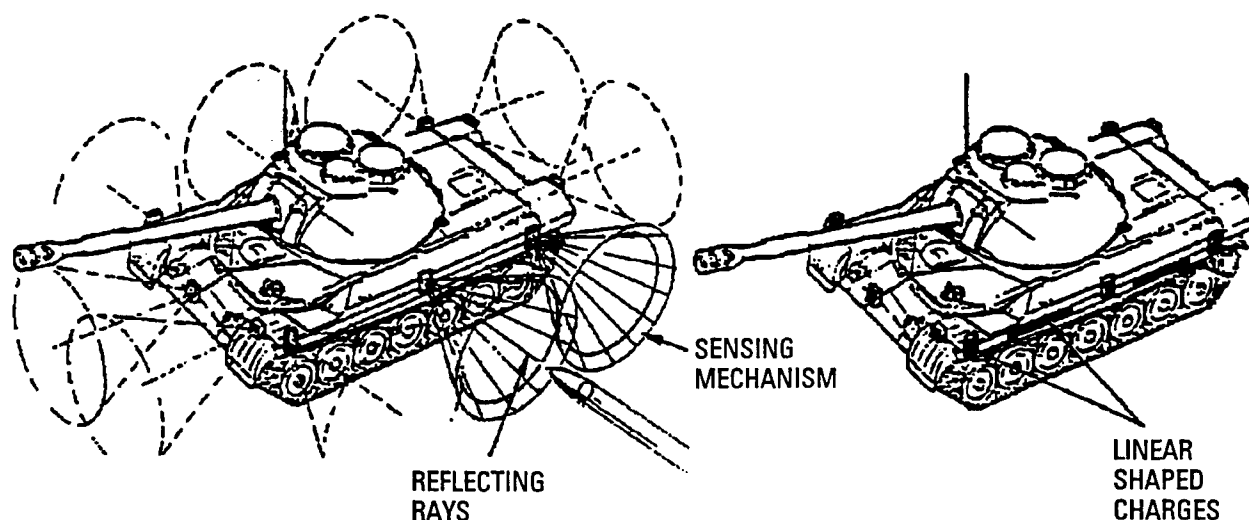


**Figure 2. Dash-Dot System Concept**

(U) scanning pulse Doppler radar coupled with three turreted high rate-of-fire 58 millimeter (mm) shotguns was feasible.

(U) After 1959, interest in active protection systems ebbed. Little activity existed until 1967, when TACOM awarded United Aircraft Corporation a contract to study a Dynamic Armor concept. This system, which was judged feasible, consisted of a coherent pulsed Doppler nonscanning interferometer radar, a weapon system computer, and an aimable pancake-shaped shotgun that projected a cloud of fragments when the threat passed a given standoff range threshold. The system was designed to cover a quadrant in azimuth and a 60-degree sector in elevation. As a result, four systems were required to provide the vehicles with 360-degree coverage in azimuth, one on each corner of the hull.

(U) These early efforts were abandoned by the late 1960s. At that time, system implementation was stymied by the then primitive state of the needed sensor and computer technology as well as concerns about collateral damage and operational effectiveness. The result was another hiatus in significant APS activity that lasted from 1968 to 1981.

(U) In 1981, interest in APS technology revived at TACOM. At that time, TRW won a small competitive contract for threat defeat mechanism studies. Testing and system studies followed with other companies and Army Laboratories becoming involved as well. Between 1981 and 1986 considerable progress was made on limited funds in understanding APS requirements, system design issues, the effectiveness of various mechanisms to defeat direct-fire threats, and technology development needs.

(U) In 1984, General Dynamics received a contract from TACOM to study an active armor protection concept originally conceived under corporate funding. Their concept was similar to that proposed earlier by United Aircraft, but it differed in the details of its implementation. Full 360-degree azimuthal protection of the defended vehicle was achieved by four subsystems, each of which protected a 90-degree quadrant. Each subsystem consisted of a planar array 60 GHz mmW Doppler radar that detected and tracked the threat, a weapon system that launched the countermeasure on command. The countermeasure was a fragmenting warhead that achieved kill of a chemical energy threat by forcing the predetonation of its warhead at a distance great enough from

9600931 O1 .004

UNCLASSIFIED

(U) the vehicle that it would sustain little damage. Predetonation was forced by penetration of the threat warhead by fragments produced upon explosion of the countermeasure. Countermeasure detonation timing was controlled by a variable time-delay fuze with the appropriate time delay set by computer command before the countermeasure was launched.

(U) The scope and pace of APS technology development in the U.S. increased considerably in 1986 with the initiation of the DARPA Armor/Anti-Armor program. It funded further development and demonstration of the General Dynamics system. Delco was also funded under that program to demonstrate a similar system. This DARPA program continued until 1993, at which time the effort transitioned to TACOM which funded additional General Dynamics and Delco development and demonstration activities until 1994.

(U) In the period between 1986 and 1994, TACOM continued to fund TRW and other companies to explore APS concepts and technologies that were not part of the DARPA-funded efforts. In addition, alternative explosive countermeasure work applicable to APS was initiated at ARDEC and ARL, and coordinated with TACOM.

(U) During this period, the TRW work focused on APS concept definition studies and technology demonstrations exploiting the latest advances in solid state millimeter wave radar technology at W-band frequencies, the latest commercial signal processing technology, and large kill-effectiveness-volume countermeasures. The objective of this effort was to develop a system concept and demonstrate the necessary technology for a minimum development and production cost, all-weather APS that would be both effective against both overhead and direct-fire threats while being compatible with vehicle integration and operability constraints, and capable of implementation in the near term. The result was the Near-Term Active Protection System, N-TAPS.

(U) In 1994, DARPA initiated the Small, Lightweight, Interceptor Device (SLID) program with Allied Signal, Rockwell and Raytheon. In 1995, Rockwell and Raytheon were selected to continue into a flight demonstration phase.

(U) In recent years, evidence of Russian progress in APS development has surfaced. Specifically, the Drozd and Arena systems have become known.

(U) Concern about foreign and domestic progress in APS and its potential proliferation sparked interest in a counter APS (CAPS) program which was initiated in 1994 by MICOM.

(U) Also in 1994, TARDEC initiated the Integrated Defense System (IDS) Program. The competitive procurement was won by a team led by United Defense Limited Partnership (UDLP) with Lockheed Sanders, TRW, Dynetics, Hughes Danbury Optical Systems (HDOS), and Loral Infra Red Imaging Systems (LIRIS) as subcontractors. The IDS program has two major components that will be further developed and demonstrated. One is a system for integrating and managing electronic warfare and passive countermeasures. That effort is led by Lockheed Sanders. The other is N-TAPS, with that effort led by TRW.

(U) The following sections describe the N-TAPS concept, its enabling technologies, its current status and plans under the IDS program.

(U) N-TAPS Concept

(U) Consideration of the requirements that an APS must satisfy for various vehicles, threats and

9600931 01 .004

## UNCLASSIFIED

(U) attack scenarios leads to the conclusion that a single universal APS that will be effective in all cases is unlikely. Instead, a flexible system having modules that can be tailored to a specific application is highly desirable. Also, for increased effectiveness, it is highly desirable to provide a layered system. With a layered system, the overall effectiveness of the APS can be very high even though the effectiveness of the system for each layer is significantly lower. The advantage of this approach is that the APS development task is easier and less expensive than for the single layer system. As a practical matter, a two layer system sharing a common vehicle-mounted sensor and command subsystem with inexpensive expendable countermeasures appears to be the optimum system. The inner layer system would provide the capability to defeat threats inside of 10 to 15 m from the defended vehicle while the outer layer system would reach out to about 50 m for direct fire threats and up to about 250m for overhead threats. Dash-Dot, the General Dynamics and Delco DARPA-funded systems, Drozd and Arena are examples of inner-layer systems while SLID is an example of an outer-layer system.

(U) With these considerations in mind, N-TAPS in its most effective form is two-layer system comprised of a family of low cost, near-term-technology components that can be tailored to a specific armored vehicle application and developed quickly to improve vehicle survivability. It would provide full hemisphere protection against overhead and direct-fire threats but could be tailored to operate in a reduced zone if a specific application does not require full coverage.

(U) An example of an N-TAPS outer layer concept for a tank is shown in Figure 3. In this concept, the entire system is housed in an armored box that bolts up to the rear of the turret. The system consists of a sensor and command subsystem and a countermeasure subsystem.

(U) The sensor and command subsystem is comprised of passive cueing sensors, a small, digitally controlled, low power tracking radar that is cued by the passive sensors to reduce active emission times, and a very high throughput, commercial technology radar signal processor (RSP). The radar consists of an array of monolithic microwave integrated circuit (MMIC) transceiver modules operating at millimeter wave frequencies. The module array is mounted on a very high rate electrical gimbal assembly and is protected by a bullet-proof radome. The RSP controls the radar and its gimbal, processes the passive-sensor and radar outputs, classifies the threat, analyzes its trajectory, controls the countermeasure gimbal, commands firing of the countermeasure that intercepts the threat and provides countermeasure air burst fuze function time commands that are transmitted to the countermeasure via the radar.

(U) In addition to its APS role, the radar system could perform several additional important tasks currently requiring use of a number of additional sensors. Included are measurements of gun muzzle velocity, projectile trajectory, site-to-crest terrain mapping and local area surveillance.

(U) The countermeasure subsystem consists of a lightweight, fast response, erectable, recoilless launcher containing a number of countermeasures. When not in use, the countermeasure subsystem is housed in an armored well. The countermeasures are spin-stabilized ballistic projectiles boosted by a short duration burn, high impulse, solid propellant rocket motor. Stringent requirements for threat tracking accuracy by the radar system, launcher pointing accuracy and countermeasure aimpoint dispersion are avoided by equipping the countermeasure with a variety of warheads having large kill effectiveness volumes. Examples of candidate warhead types include multiple explosively formed projectiles (MEFP), radial shaped charges, large diameter deployable passive or explosive nets, spin-dispersed buckshot clouds, flechettes, and solid fuel-air explosives. The warhead to be selected depends on a variety of factors related to the type of threats involved, collateral damage potential, engagement scenarios, etc. The system has the potential to utilize a

9600931 O1 .004

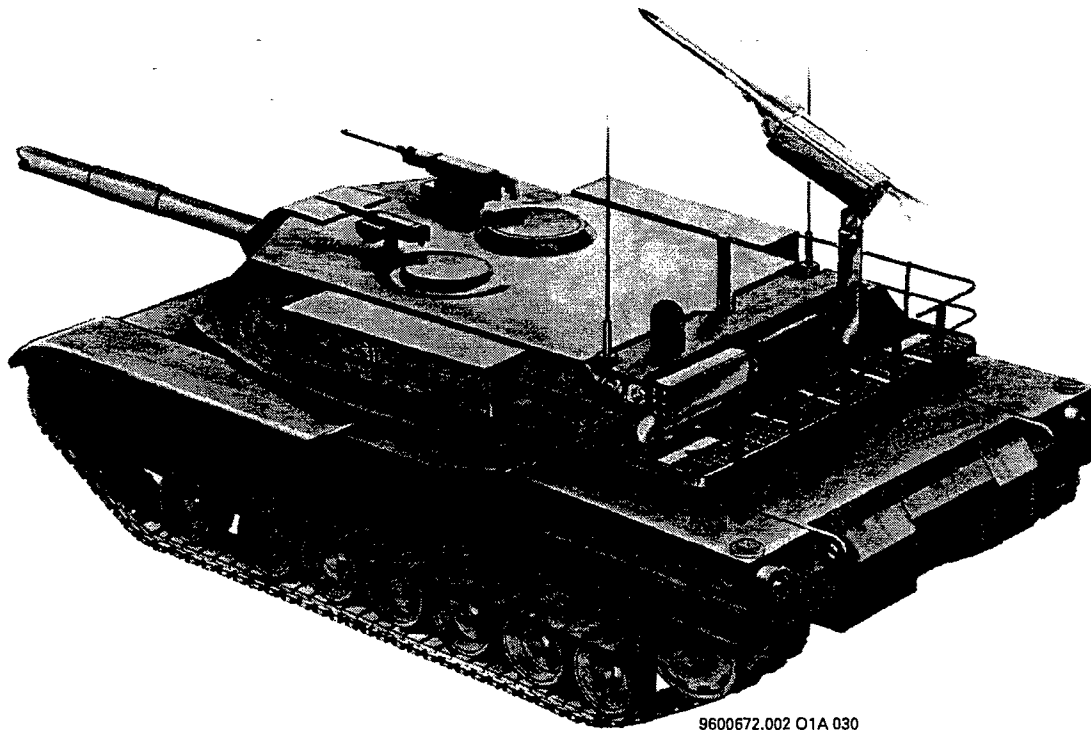


**Figure 3. IDS/N-TAPS Outer Layer Operational Concept**

(U) number of different warheads on a selectable basis depending on the circumstances of the attack. Also, some of the warhead options can be used in an offensive role if that proves desirable. Overall size of the countermeasure is about 18 in. long with a 4 in. diameter. Its total weight is about 20 lbs.

(U) An inner layer defense system could be added to the vehicle to backstop the outer layer system. Inner layer concepts include rapidly deployed barriers to shield portions of the vehicle as needed and aimable MEFP or radial shaped charge warheads mounted on the vehicle or deployed a short distance away from it.

(U) Enabling Technologies

(U) The key technologies required for a viable N-TAPS include: 1) a high throughput RSP; 2) a miniaturized, high performance all weather sensor producible in quantity at low cost; 3) advanced warheads; 4) high rate gimbals; and 5) small high performance rocket motors. Of these, the first two have been the missing link until very recently. Within the last year, it has become possible, and TRW is constructing a unit to demonstrate it, to produce an RSP from commercial components, and (U) will consist of five to eight VME cards that will approach a 4 GFLOPS throughput capacity. It will have sufficient computing power to handle not only the APS application but also all other major vehicle computational needs.

(U) Recent advances in MMIC technology under the MAFET Thrust II program at TRW is

9600931 O1 .004

(U) providing the required low cost advanced sensor capability needed for N-TAPS. Under MAFET Thrust II, mmW chip technology developed under the MMIC program, TRW funds and TRW commercial projects will be further improved. This work covers the frequency spectrum from Ka to W-band.

(U) For N-TAPS we have selected W-band as the baseline because it provides the best combination of technological maturity, compatibility with N-TAPS performance requirements, and small size. The latter feature is critical in minimizing radar gimbal power requirements needed to produce the high beam scanning rates required for N-TAPS. It is anticipated, however, that some added radar system functions may require a different frequency and this can be readily accommodated without compromising the APS function.

(U) Eventually, the need for a radar gimbal may be eliminated if a solid state phased array radar proves feasible and can be produced at low cost. In the near term, however, use of either a gimbal or a distributed staring array are the only protocol options.

(U) The progress in W-band MMIC chip technology, including that planned for near-term projections are illustrated in Table 1. As the Table shows, significant progress has already been made in improving transmitter power and reducing receiver noise figure. Transmitter power level, currently at 70 mW, is expected to grow to 250 mW under MAFET Thrust II. With adequate funding, it is believed that 1 W capability could be provided by the year 2000.

**Table 1. (U) Progress W-Band MMIC Chip Technology**

Year	Transmitted Power (mW)	Noise Figure (dB)
1994	10	12
1996	70	8
1997 Goal	250	5
2000 Projection	1000	5

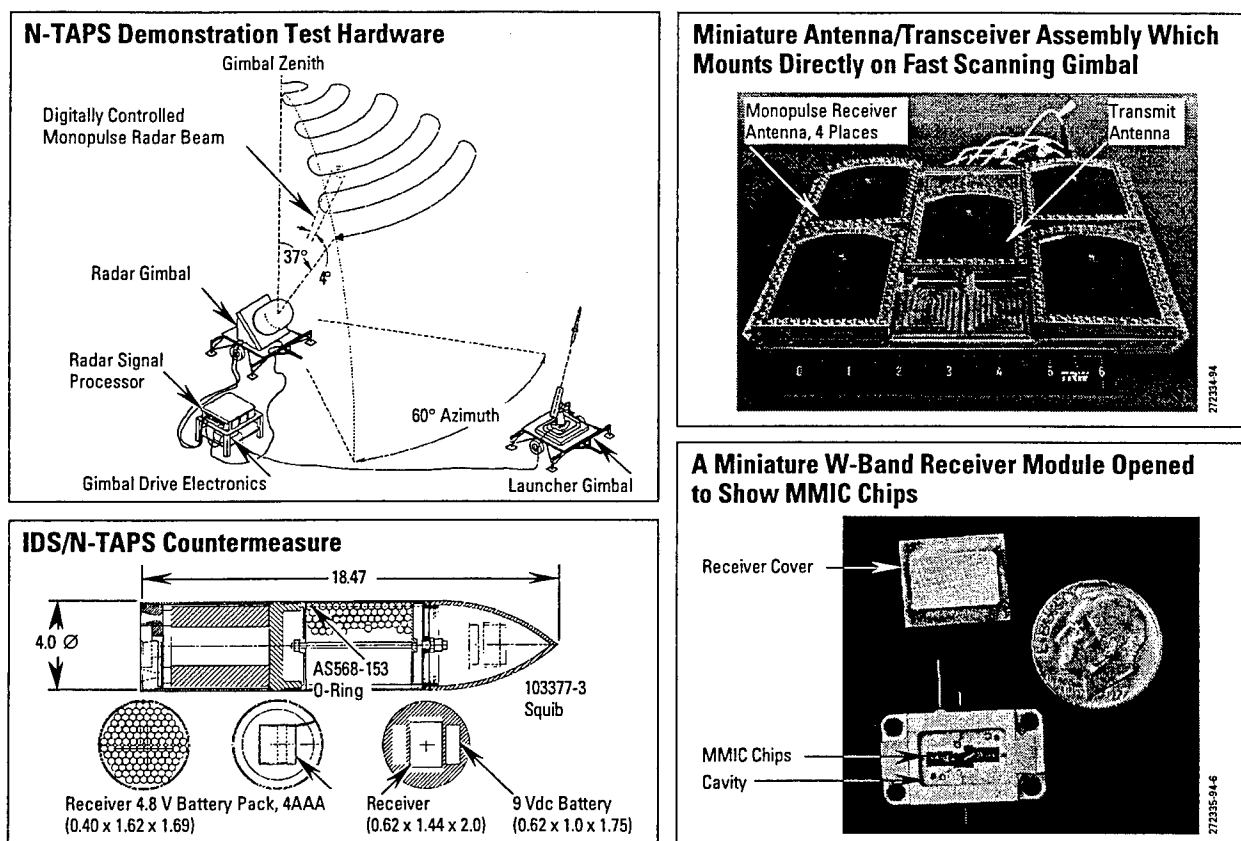
(U) High powers can be produced at lower frequencies. For example, the MAFET Thrust II goal is 3 W at Ka-band. Eye safety concerns, however will probably limit N-TAPS power emissions to 1 to 2 W, so the higher power capability may not be usable. Also, the much larger antenna at Ka-band frequencies results in prohibitive radar gimbal power requirements. As a result, W-band appears to be the optimum frequency selection for the N-TAPS radar at this time.

(U) Significant progress has already been made on developing the technology for low cost manufacturing. For example, TRW has developed and automated assembly line with capability to assemble modules operating from Ka-band to W-band frequencies. This capability is required for large volume, low cost production of N-TAPS radars.

#### (U) IDS/N-TAPS Demonstration

(U) Under the IDS program, TRW plans to demonstrate defeat of ATGMs using a brassboard outer-layer N-TAPS originally designed and fabricated under the TARDEC/TRW N-TAPS contract for field-test demonstrations involving an overhead threat. It is important for the reader to realize that this hardware was designed exclusively to meet field test requirements using as much existing equipment as possible in order to meet a firm 15-month development and test schedule. It was not designed for mounting on a vehicle and, in fact, cannot be. It does however fulfill its

9600931 O1 .004



9600871.002 O1A 034

**Figure 4. IDS/N-TAPS Demonstration**

(U) purpose of being a proof-of-concept demonstrator.

(U) Some details of the test equipment are shown in Figure 4. The W-band radar transceiver/antenna assembly is a unique FM/CW amplitude monopulse design comprised of pill box antennas mounted on a thin wave guide plate to which a MMIC transmitter and four receiver modules are mounted. A receiver module, which is comparable in size to the transmitter module, is shown in Figure 4, illustrating its small size. An important feature of the radar design is that there are no external wave guide runs. The result is an extremely rugged design that can be mounted directly to a high rate gimbal system which has routinely subjected the radar to accelerations exceeding 200 g's with no resulting damage.

(U) For IDS, the radar is being upgraded with higher performance transmitter and receiver modules that have recently become available. No other changes to the radar hardware are planned at this time.

(U) Future vehicle-configured radars would incorporate further anticipated MMIC module improvements and be of a different, miniaturized configuration specifically designed for the vehicle, not a demonstration field test, application.

(U) The demonstration radar gimbal is a hydraulically actuated, "wobble-plate" designed originally to produce a high rate spiral scan about the zenith with a 74 degree field of regard. It was not intended for direct-fire threats so for IDS, the gimbal base will be tilted to provide the capability

9600931 O1 .004



## UNCLASSIFIED

(U) to cover a 60 degree azimuth by 90 degree elevation sector with a raster scan, suitable for tracking ATGMs.

(U) The radar gimbal is an expedient design that is bulky. A vehicle-configured gimbal would be much smaller, of a different design with a lower power requirement and would utilize electric actuation.

(U) The radar system is digitally controlled by a custom designed high rate RSP. It generates the radar wave form which is under software control and, is easily modified as required for optimized testing. It also controls the radar gimbal, processes the radar data to generate Kalman-filtered trajectory data which are processed to generate a fire control solution for aiming the countermeasure launcher gimbal, launching the countermeasure and controlling the countermeasures' fuze timing.

(U) The current RSP was designed in 1994 by TRW. Rapid advances since then make it possible to design a significantly higher performance RSP now. To demonstrate this, TRW is building and will demonstrate this year an RSP in a VME chassis that will be upgradeable to a throughput approaching 4 GFLOPS, sufficient for an advanced N-TAPS.

(U) The N-TAPS/IDS countermeasure is illustrated in Figure 4. It is a small, spin-stabilized ballistic round with a non-explosive warhead. It has a modified production solid propellant rocket motor with performance near that required for a fielded system. It is compatible with a number of advanced warheads currently under development but for IDS, a non-explosive spin-dispersed buckshot warhead has been baselined for low cost demonstration reasons. Warhead function time is controlled by the RSP via a radio communication link. Once warhead deployment is commanded, a small squib fires, forming the release of the ball pack which disperses and forms a cloud of buckshot in the path of the incoming threat. Other types of warheads can be fitted to this round, as required, for follow-on demonstrations. It is anticipated that an operational version of this countermeasure could be produced at very low cost.

### (U) Concluding Remarks

Recent advances in computing and mmW radar technology make it possible to produce an advanced, very compact, low-production cost system capable of meeting the stringent requirements for active protection of armored vehicles. A brassboard proof-of-concept version of such a system was produced under the TARDEC/TRW N-TAPS contract and is being upgraded under the IDS Program. We plan to demonstrate the capability of this system to defeat ATGMs in 1996.

### (U) Acknowledgments

(U) This work is supported by U.S. Army Contract DAAE07-95-C-R043 to United Defense Limited Partnership and Subcontract No. Y25-Y-0007 to TRW. Contract direction is provided by U.S. Army TACOM.

9600931 O1 .004

UNCLASSIFIED

## SLID - SHORT RANGE MISSILE SYSTEM FOR ACTIVE DEFENSE (U)

Rodney R. Hersh  
Raytheon Electronic Systems  
Tewksbury, Massachusetts 01876-0901

### ABSTRACT (U)

(U) The Small Low-cost Interceptor Device program is developing an autonomous active defensive system for vehicle and limited area defense. This paper describes the Raytheon SLID system design and the development efforts performed to date on the SLID contract, DAAA21-94-C-0007.

### INTRODUCTION

(U) The Small Low-cost Interceptor Device (SLID) is an ARPA sponsored, ARDEC managed program to demonstrate a short range defense against such as HEAT, ATGMs, artillery and mortar rounds, as is depicted in Figure 1. This system is intended to provide both an active defense capability for armored vehicles and a limited area defense capability against top attack targets. The SLID program has completed two phases of concept definition and refinement, one phase of risk reduction and hardware demonstration, and is now in a system demonstration phase. Two competing concepts are being developed; they will be tested against both ATGMs and indirect fire targets. A DEMVAL program is being planned to transition this system to field prototypes this phase of the program.

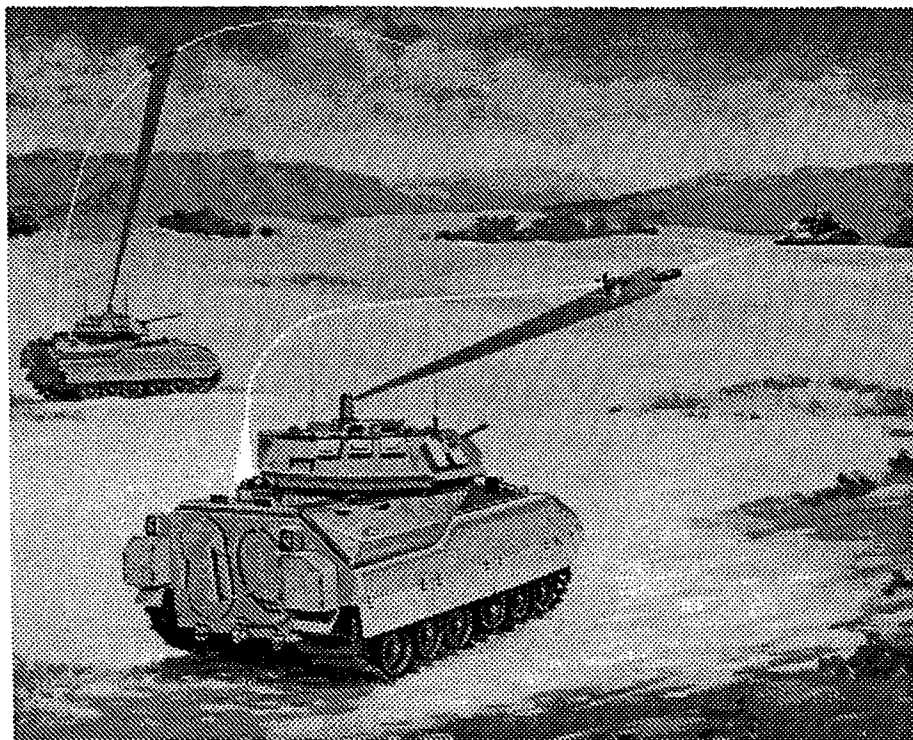


Figure 1. (U) The SLID System

UNCLASSIFIED

**SYSTEM CONCEPT**

(U) The SLID system is being designed to detect, track and engage a variety of missile and ordnance threats that may attack the host platform or defended area. While the SLID program first addressed the problem of active defense for armored vehicles against HEAT rounds and ATGMs, it has expanded to include the problem of limited area defense for high value targets against top attack rounds such as artillery and mortars. Table I lists representative threats that the SLID system is being designed to counter. The threats can be divided into three categories, direct fire guns, ATGMs, and top attack projectiles. Each category has a unique requirement that affects the SLID system design. The direct fire threats such as HEAT and LAW drive the system response time and preclude manual operation, the ATGMs determine the maximum range for threat detection, while the top attack projectiles drive the surveillance sector for threat warning. System performance goals are a hit-to-kill capability against all threats and nominal 100 and 250 meter intercept ranges against the anti-armor and top-attack threats respectively. The zone of defense should be a 10 meter circle for the anti-armor mission and at least 25 meters for the top-attack defense mission.

**Table I. (U) Representative SLID Threats**

UNCLASSIFIED			
Class/Threat	Range (m)	Max Vel. (m/s)	Type
Heat	1000 - 2500	3500	Gun
ATGM			
TOW	< 4000	400	Rocket
Hellfire	< 5000	400	Rocket
Dragon	< 1000	95	Boosted
AT-6	< 5000	500	Rocket
Projectiles			
Mortar	1 - 4 km	250	Gun
Arty	2 - 10 km	300	Gun
LAW/RPG	< 400 m	150	Boosted

(U) Raytheon has designed a fully autonomous system that performs all functions required for threat warning, threat assessment, engagement planning, and guided intercept. Figure 2 shows a block diagram of the system, and Figure 3 shows the system operation flow. The Raytheon design is comprised of three main subsystems, the fire control system, which includes the threat warning and tracking sensors and the system computer, the launcher, and the SLID projectile. The fire control system provides the initial threat cue (an external cue from another asset such as a radar is possible) for the tracking sensors. The target is acquired and tracked to determine if it is a threat to the host platform; a decision of hostile initiates engagement planning which includes launcher preparation and intercept planning. A SLID projectile is then vertically launched, a pitchover maneuver commanded, the booster motor ignited, and the projectile is guided to intercept. Projectile maneuvers for the intercept are accomplished with small, divert rocket motors. A small warhead has been included for kill enhancement.

Membership Values

Name	Height	Crisp	Fuzzy
Bill	6'8"	1	0.99
Joe	6'2"	1	0.80
Tom	5'11"	1	0.65
Sam	5'6"	0	0.50
Burt	4'2"	0	0.05

Figure 1 Membership functions in the set "tall"

(U)The previous simple example illustrates the concept of fuzzy membership sets, but in order for this to be applicable to real-world problems, several additional concepts must be introduced. Suppose the same five people used in the example above play golf. A membership function can be generated by ranking the players from 1.0 (always plays golf) to 0.0 (never plays golf). This is shown in Figure 2.

Name	Height	Golfer
Burt	4'2"	0.85
Joe	6'2"	0.70
Bill	6'8"	0.50
Sam	5'6"	0.40
Tom	5'11"	0.05

Figure 2 Membership functions in the set "golfer"

Now suppose it is desired to find the membership function indicating how the five people in these examples fit into the combined category of "tall golfer"?

Name	Height	Golfer	Tall	Tall Golfer
Joe	6'2"	0.70	0.80	0.70
Bill	6'8"	0.50	0.99	0.50
Sam	5'6"	0.40	0.50	0.40
Burt	4'2"	0.85	0.05	0.05
Tom	5'11"	0.05	0.65	0.05

Figure 3 Membership functions in the set "tall golfer"

As can be seen in Figure 3, the membership function element for a given person in the combined classification of "tall golfer" is the smaller of the membership elements of the two original classifications (i.e. "tall" and "golfer"). The person who most closely matches "tall golfer" is then the one with the highest combined membership function element. Thus it is Joe who best represents the idea of "tall golfer" even though he is neither the tallest nor the most avid golfer of the group. This is the basic operation used in fuzzy inference logic.

(U)At this point, the reader who is not already familiar with fuzzy logic might well ask "This is nice, but how can anything useful be made from it?" The usefulness can be appreciated by substituting IF-THEN rules for the "categories" used in the brief description presented above.

UNCLASSIFIED

Thus the rule for the example shows would be "if TALL and GOLFER then TALL GOLFER". The first practical application of fuzzy reasoning to an engineering problem was made in 1973 by Mamdani and Assilian of London University. They applied several IF-THEN rules to control a small toy steam engine. The entire controller was built from simple statements like the following:

IF steam pressure is a little to high AND it is not changing much,  
THEN reduce heat a little.

IF steam pressure is about right AND it is not changing much  
THEN don't change anything.

IF steam pressure is a little too high AND pressure is increasing  
THEN reduce heat a little

(U)In order to operate a fuzzy control system or a fuzzy filter in practice, three steps are required. The first step is "fuzzification". This means taking a (crisp) variable that is known to have a value within given limits, and assigning membership function elements that best represent it. The second step is to combine several of these variables according to the IF\_THEN rules describing the physical system to be controlled. The third step is "defuzzification" used to assign a single output value to the result.

(U) Methodology

(U)For purposes of testing various ideas relating to the application of fuzzy inference to problems in AP, sample code was written to run on the same processor as the original Kalman filter tracking software. In this way, everything developed during this investigation is available for use within the framework of the existing APP. The first modules developed were a Fuzzification module, a Defuzzification module, and a 2-variable fuzzy inference engine. These basic building blocks allow the conversion of ordinary crisp variables into the fuzzy realm, operating on them through the use of fuzzy inference logic, and provide conversion back to crisp variables for use elsewhere in the APP software.

(U)It was decided to develop a simple one-dimensional filter in order to study the possible application of fuzzy methodology to improving Kalman filter initialization. Such a test case is easy to compare with more traditional ways of extracting useful information from noisy input data. A common assumption in the literature is that fuzzy control "...is deterministic, and does not retain any state information from one iteration to the next." This perceived limitation can easily be overcome by defining a (fuzzy) state output vector and including it as additional input to the inference engine.

(U) Software

(U)A practical AP system must provide full hemispherical coverage for the host GCV. Covering an entire hemisphere with membership bins to appropriate accuracy becomes impractical due to the large memory and processing capability this would require. In addition, such a solution would be extremely inefficient, since the percentage usage of this vast amount of hardware would be extremely low, due to the small area of incoming projectiles compared to the 2-PI steradians of the protected hemisphere. Therefore, the test filter was designed around a position "error" term in an attempt to make the calculations independent of the absolute position.

(U)With the exception of Doppler range rate, all outputs of the Delco AP system sensor(s) measure position (range, azimuth angle, and elevation angle). In addition, the time between measurements is also provided to the APP. Thus a system that computes an expected target

UNCLASSIFIED

position based on the current state vector and time elapsed from the previous measurement, and then compares that position with the new sensor input is really independent of the actual location. All that is required for processing is the delta between the expected position and the latest sensor measurement. This is the same philosophy used by the Kalman filter algorithm, but in the case of a fuzzy logic filter it has the effect of reducing the number of membership function bands of the fuzzy variables to a reasonable number. For this investigation, fuzzy variables with five bands were used.

(U) Another problem encountered when applying the test filter to a measurement is how to determine when to stop processing the input data stream using fuzzy techniques and to use the filter output to initialize the Kalman tracking filter. To this end, a "confidence" variable was introduced in an attempt to estimate when the fuzzy system has accumulated enough trust in the sensor data to allow the Kalman filter to begin tracking the projectile. This is similar to the familiar covariance matrix of the Kalman algorithm. It soon became apparent that from a computational perspective, the compliment of "confidence" (dubbed "concern") was more useful, so it was used instead.

(U) Simulation Results

(U) Two examples of the operation of the sample filter are shown below. Figure 4 shows the response to an arbitrary made-up waveform. Figure 5 shows the response to actual crossrange data taken from an ATGM test flight.

UNCLASSIFIED

UNCLASSIFIED

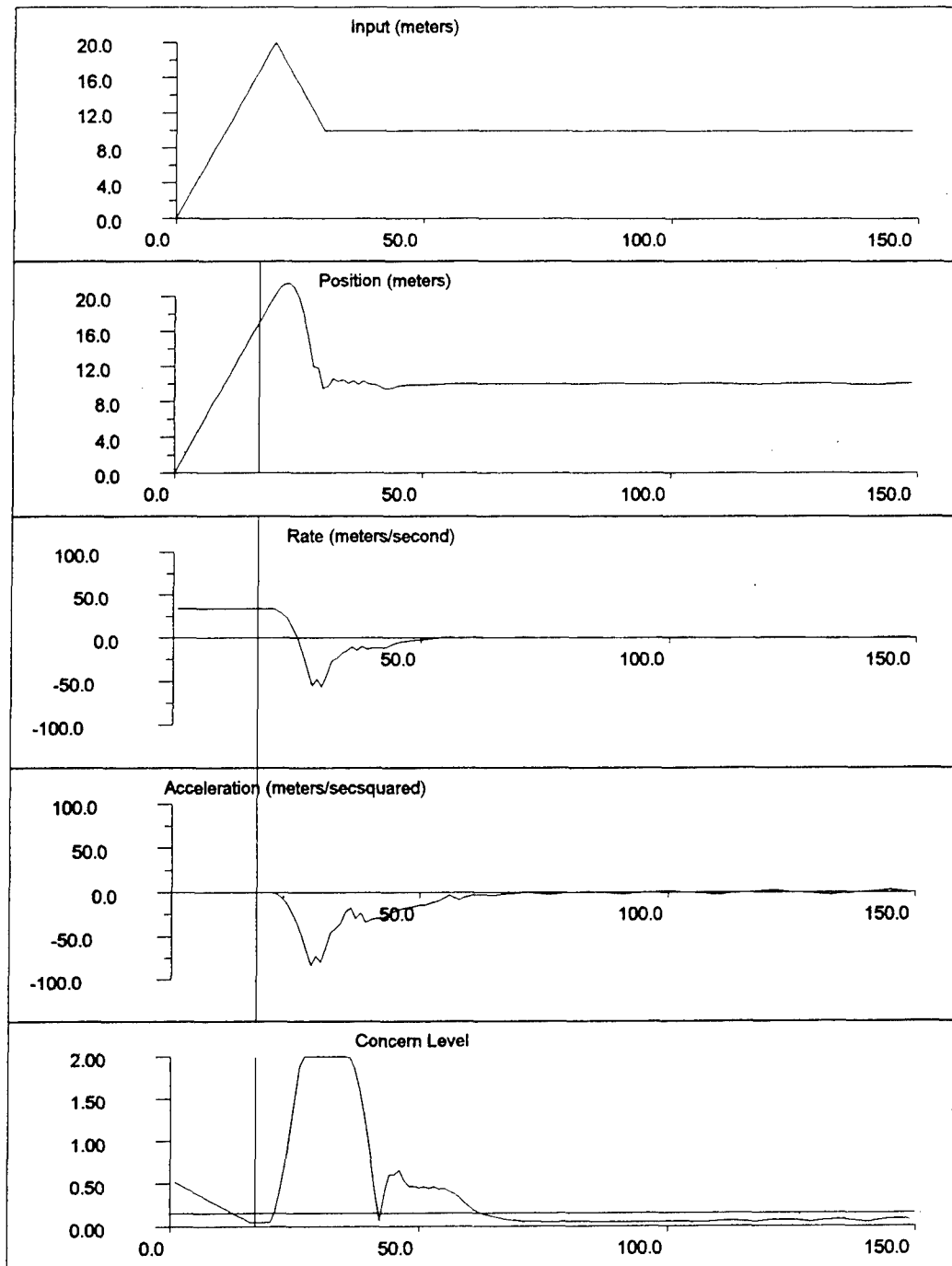


Figure 4 Fuzzy test filter response to triangle input.

UNCLASSIFIED

UNCLASSIFIED

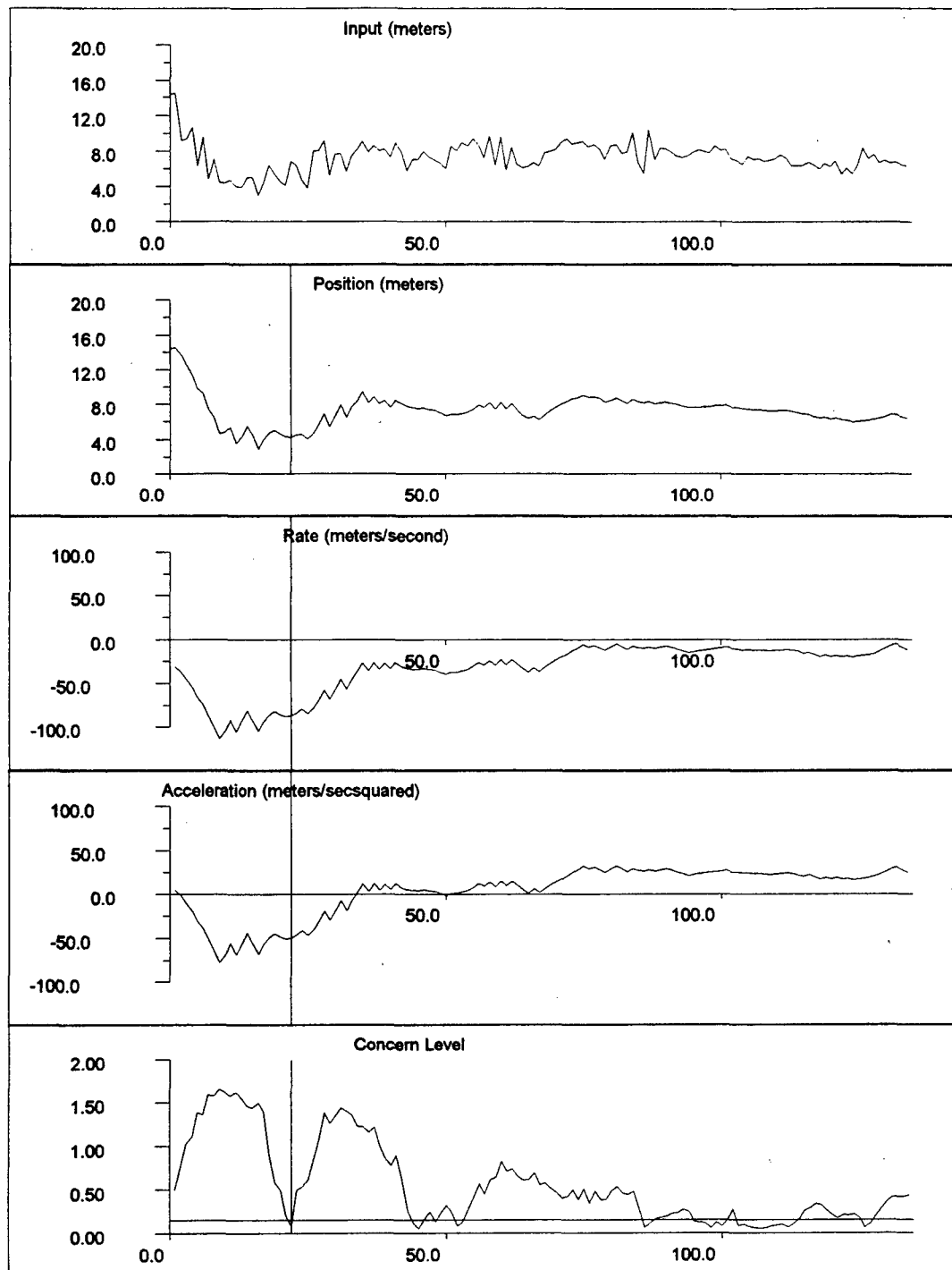


Figure 5 Fuzzy test filter response to actual ATGM sensor crossrange input.

UNCLASSIFIED



(U) Conclusion

(U)The software used for this experiment was a simple 1-dimensional filter. Such a filter is a reasonable choice since the ultimate application will be to perform a 1-dimensional filter on each separate sensor measurement, rather than implement a full 3-dimensional tracker. It was shown that the filter that was constructed did indeed perform well. The concepts of a state vector for past history retention and the confidence/concern variable were also shown to function as expected.

(U)Since a fuzzy system is a collection of rules that are each applied to a varying degree based on input data, quite a bit of knowledge about the physics of the situation can be incorporated. The Delco APP currently classifies threats into four categories (ATGM, gun-launched HEAT, KE rod penetrators, and Top Attack weapons). Fuzzy logic measurement pre-processors can easily make use of the ballistic characteristics of each type to further enhance the Kalman filter initialization process.

(U)At this time, what is still left to be done is the integration of four of these fuzzy measurement pre-filters with the Kalman tracking filter of the APP. Once this is accomplished in the near future, quantitative measurements can be made of the number of sensor measurements required for the tracking filter to reach a given accuracy. Results with and without the fuzzy initialization can then be compared.

UNCLASSIFIED  
DISTRIBUTION LIMITED TO U.S. GOVERNMENT AND ITS CONTRACTORS

Anti-Armor Warhead  
Classified by: Tech. SCG, 9 FEB 95  
Declassify on: OADR

**Initiation Based Selectable Mode Shaped Charge and EFP Warheads (U)**

E.L. Baker\*, R. Campbell and C. Chin  
U.S. Army, Armament Research, Development and Engineering Center  
Picatinny Arsenal, NJ, USA 07806-5000

**ABSTRACT (U)**

(U) A variety of initiation based selectable mode shaped charge and EFP warheads have been computationally designed and experimentally demonstrated. Modern shaped charge and explosively formed projectile (EFP) warheads are typically designed for hard target penetration of a small lethal area. However, greater lethality can be achieved for soft target encounters by using lower penetration capability over a larger lethal area. Initiation based selectable mode technology incorporates multiple detonators and variable initiation timing in order to produce both heavy target and soft target penetration modes on a selectable basis. Selectable detonator technologies have been developed to be both economical for warhead development and practical for system integration. This effort has successfully developed and demonstrated a variety of initiation based selectable mode warhead devices including shaped charges and non-axisymmetric "clothespin" EFP warheads that produce either deep penetration for hard targets or increased lethal area cross penetration patterns for soft target encounters. This new initiation based selectable mode warhead development capability is now available and currently being used for development of tactical warhead systems.

(U) INTRODUCTION

(U) The ARDEC Energetics and Warheads Division has a long history of anti-armor warheads research, development, design, and application. Modern shaped charge and explosively formed projectile (EFP) warheads are typically designed for hard target penetration of a small lethal area. However, greater lethality could be achieved for soft target encounters by using lower penetration capability over a larger lethal area, depending on the target properties. Recent emphasis has been placed on the development of selectable mode warheads in order to attain increased performance over a wider variety of target types. Future munition systems will employ selectable warheads in order to achieve high lethality over a range of targets such as tanks, personnel carriers, armored artillery, aircraft and personnel using a single munition in a highly

UNCLASSIFIED  
DISTRIBUTION LIMITED TO U.S. GOVERNMENT AND ITS CONTRACTORS

UNCLASSIFIED

DISTRIBUTION LIMITED TO U.S. GOVERNMENT AND ITS CONTRACTORS

(U) controlled manner. To date, two main methods of providing selectable mode functionality are being developed: mechanical methods and explosive initiation based methods. The design and development of mechanical based selectable mode warhead systems is relatively mature. Initiation based selectable mode technology is a more recent development that incorporates multiple initiation and variable initiation timing in order to produce both heavy target and soft target penetration modes on a selectable basis. The ARDEC Target Defeat Program has developed and demonstrated highly advanced initiation based selectable warhead technology. This development includes selectable initiation firing sets, selectable initiation modeling and design capability, and technology demonstrations on shaped charge and EFP warheads.

(U) FIRING SET TECHNOLOGY

(U) Firing set requirements differ significantly for warheads development and tactical system application. Warheads development firing sets must be flexible in use for a number of different applications and normally be reusable in order to reduce costs over time. Tactical system firing sets must be weight efficient and cost effective from a disposable viewpoint.

(U) Warheads Development Firing Sets

(U) Based on typical warhead geometries and high explosive detonation velocities, it was calculated that a 100ns simultaneity for a groups of detonators would be sufficient for most warhead development. Reusable warheads development firing sets were developed based on RP2 bridgewire detonators. High speed smear photography was used to measure the simultaneity of detonator sets. An electronic configuration attaining just under 100ns simultaneity for a 10 detonator set was achieved. Two additional firing sets were built, as it was determined that multiple sets of detonators would be required at specific time intervals in order to meet advanced selectable mode design requirements. It proved more difficult to control times between detonator sets than to achieve required simultaneity. Specific detonator set timings had to be iteratively adjusted in order to attain final detonator set firing times within 100ns of the desired firing times. Figure 1 presents a smear photograph of multiple detonators fired at multiple times.

(U) System Application Firing Sets

(U) Exploding Foil Initiators (EFIs) are appropriate for system application as they are lightweight, relatively inexpensive and require significantly less energy than other types of initiators. EFIs are currently used in a number of DoD munitions and are commercially available. A feasibility study was conducted in order to determine if firing sets based on EFIs would be suitable for application to tactical initiation based munitions (ref. 1). Table 1 presents projected volume and weight requirements for various multiple initiation firing sets. Both multiple initiation at a single firing time and multiple initiation at multiple firing times were considered. The study indicated that EFI based firing sets using existing technology is both feasible and currently attainable for most projected selective initiation munitions.

UNCLASSIFIED

DISTRIBUTION LIMITED TO U.S. GOVERNMENT AND ITS CONTRACTORS

UNCLASSIFIED  
DISTRIBUTION LIMITED TO U.S. GOVERNMENT AND ITS CONTRACTORS

(U) NON-AXI SELECTABLE EFP TECHNOLOGY

(U) Previous axisymmetric selectable initiation EFP (ref. 2) work demonstrated the feasibility of both designing and producing initiation based selectable mode EFPs. Fly over top attack munitions have been found to produce extremely high lethality, as they can attack more vulnerable target regions. Non-axisymmetric EFPs are typically desired for fly over top attack munition geometries as they are normally more amenable to horizontal munition shoot down configurations. No known initiation based selectable mode efforts had previously addressed non-axisymmetric warhead configurations.

(U) Hard Target Mode

(U) A previously developed full scale non-axisymmetric "clothespin" EFP warhead was chosen for initiation based selectable mode development. The design was originally developed using iterations of DYNA3D high rate finite element computer modeling and experimentation. The iron strip-like liner folds into a final projectile configuration resembling the shape of a clothespin. Figure 2 presents a diagram of the EFP warhead geometry. Figure 3 presents DYNA3D computer modeling of the EFP formation and final geometry comparison to a flash x-ray experimental result. The final EFP is a robust single high velocity (1.9km/s) projectile suitable for hard target penetration.

(U) First Generation Soft Target Mode

(U) The first generation soft target mode was developed using experimentation and subsequently modeled in order to develop a computational design capability. A five detonator array was simultaneously fired along the rear surface of the EFP. Short standoff flash x-rays revealed that a four fragment configuration was produced. A 3/8" steel target plate placed at a 20 ft standoff revealed that a three hole target pattern was produced. Figure 4 presents the initiation configuration, flash x-ray trace, and final target hole configuration. Subsequent DYNA3D modeling revealed that although four fragments were formed, the two initially outside fragments converged together at the axis center, whereas the two initially center fragments separated away from the axis. The two fragments converged together on the axis form a single penetration hole, explaining the three hole target pattern. Figure 5 presents the DYNA3D simulation that explained the presence of only three target holes.

(U) Second Generation Soft Target Mode

(U) The modeling capability was subsequently used to develop a second generation "cross fragment" configuration. The DYNA3D modeling could only be used for the early fragment formation process, as high mesh distortion quickly ended the ability to model further in time with a Lagrangian description. However, DYNA3D was still used as a design tool for the placement and timing of detonators, as the early mass velocity direction and liner deformation were good indicators of final fragment configurations. It was found that precise timing of

UNCLASSIFIED  
DISTRIBUTION LIMITED TO U.S. GOVERNMENT AND ITS CONTRACTORS

(U) multiple detonator sets at multiple firing times was required to obtain a desirable cross fragment pattern using only surface detonators. A final 2pt + 2pt + 4pt multiple point multiple time firing configuration was designed. The design was computationally verified to produce the desired six fragment cross pattern using the CTH Eulerian finite difference program. Figure 6 presents the DYNA3D and CTH simulation results. An experimental demonstration was subsequently performed. As predicted, flash x-rays revealed a six fragment configuration with two of the fragments converged together on the axis. A five hole target pattern was produced in the desired cross configuration. Figure 7 presents the original detonator array configuration, flash x-ray and resulting target pattern.

(U) SELECTABLE SHAPED CHARGE TECHNOLOGY

(U) The BRL 81mm shaped charge was chosen as a shaped charge baseline for initiation based selectable mode development. The design has been extremely well characterized and a high performance wave shaped version was previously developed for hard target attack (ref. 3). Figure 8 presents CALE modeling of the jet formation process. The wave shaped design has a 9.8 Km/s jet tip velocity and produces 8.5 charge diameters (CDs) of penetration at an 8CD standoff into steel rolled homogenous armor (RHA).

(U) Hard Target Mode Wave Shaper Replacement

(U) One application of multiple detonators is the replacement of existing mechanical wave shapers. Current mechanical detonation wave shaping practice is to place a disk of non-detonating material (wave shaper) within an explosive charge. The detonation wave is shaped by propagating around the mechanical wave shaper. Theoretically, similar detonation wave shaping can be produced by placing a ring of detonators at the wave shaper position. The replacement of mechanical wave shaping with initiation based wave shaping could significantly reduce the explosive charge head height, considerably reducing warhead weight and volume. Figure 9 presents a diagram illustrating the concept. Testing was conducted using detonator arrays to replace the mechanical wave shaping using the BRL 81mm. A ten detonator array successfully produced a straight jet of good ductility, whereas lower numbers of detonators produced radial jet dispersion. Figure 10 presents flash x-rays of jets produced by four and ten detonator arrays. The results clearly demonstrate the feasibility of mechanical wave shaper replacement with detonator arrays.

(U) First Generation Selectable Shaped Charge

(U) Again, the first generation soft target mode was developed using experimentation and subsequently modeled in order to develop a computational design capability. A series of tests were conducted using two diametrically opposed detonators simultaneously fired on the charge outside diameter. The test series consisted of positioning the detonators at high, middle and base (low) axial positions on the charge. Figure 11 presents a diagram of the detonator configurations and resulting jet flash x-rays. The jets produced were fan shaped, that is thin in one plane and

UNCLASSIFIED  
DISTRIBUTION LIMITED TO U.S. GOVERNMENT AND ITS CONTRACTORS

(U) spread in a perpendicular plane. A definite trend of spray (fan) angle versus detonator axial position was noted. As the detonators are moved toward the liner base, the jet spray angle increases. At the liner base, the spray angle is approximately 180 degrees. Figure 12 presents a typical long standoff "line" fragment pattern produced on a target plate. The charges were simulated using the three dimensional Eulerian hydrocode, CTH. The simulation results closely reproduced the experimental spray angle trends. Figure 13 presents a comparison of the two detonator high and two detonator mid CTH results.

(U) Second Generation Selectable Shaped Charge

(U) Again, the modeling capability was subsequently used to develop a second generation "cross fragment" configuration. CTH was used to investigate a variety of initiation concepts. Again, it was found that precise timing of multiple detonator sets at multiple firings times was required to obtain a desirable cross fan jet formation using only surface detonators. A final 2pt + 2pt multiple point multiple time firing configuration was designed. Figures 14 and 15 present CTH simulation results of the cross fan jet formation at 30 $\mu$ s. An experimental demonstration was subsequently performed. Due to testing equipment concerns, the cross fan jet design was shot at long standoff without flash x-rays into a target plate. Figure 16 presents the resulting cross fragment target pattern.

(U) CONCLUSIONS

(U) The ARDEC Target Defeat Program has successfully developed and demonstrated highly advanced initiation based selectable warhead technology. This development includes selectable initiation firing sets, selectable initiation modeling and design capability, and technology demonstrations. The technology demonstrations included a variety of initiation based selectable mode warhead devices including shaped charges and non-axisymmetric "clothespin" warheads that produce either deep penetration for hard targets or increased lethal area penetration patterns for soft target encounters. As part of this effort, the ability to design initiation configurations to produce predefined cross fragment patterns has been demonstrated. In addition, the replacement of mechanical wave shaping with initiation based wave shaping has been successfully demonstrated. The initiation based selectable mode warhead technology developed under the Target Defeat Program is now available and currently being applied to tactical munition systems.

(U) REFERENCES

- (U) 1. E. Homentowski, "Multipoint Fireset Weaponization", *U.S. Army Armament Research, Development and Engineering Center Technical Report*, Picatinny Arsenal, NJ, 1996.
- (U) 2. E.L. Baker and T. Vuong, "Massively Parallel Computation of Multimode Warhead Mechanics", *Proceedings of the 19th Army Science Conference*, Orlando, FL, June 1991.

UNCLASSIFIED  
DISTRIBUTION LIMITED TO U.S. GOVERNMENT AND ITS CONTRACTORS

UNCLASSIFIED  
DISTRIBUTION LIMITED TO U.S. GOVERNMENT AND ITS CONTRACTORS

(U) 3. E.L. Baker, "A Parametric Optimization of Shaped Charge Wave Shaping", *Proceedings of the SCS 1992 Eastern Multiconference, Government and Military Simulation Conference*, Orlando, FL, April 1992.

(U) TABLES

UNCLASSIFIED

Configuration	Volume(cc)	Weight(gm)
1 point	35	80
2 point	40	90
4 point	45	100
8 point	55	130
12 point	60	170
2pt + 2pt	50	120
2pt + 2pt + 2pt	60	150
4pt + 2pt + 2pt	70	160

Table I. (U) Projected volumes and weights of tactical system application selective initiation firing sets.

(U) FIGURES

UNCLASSIFIED

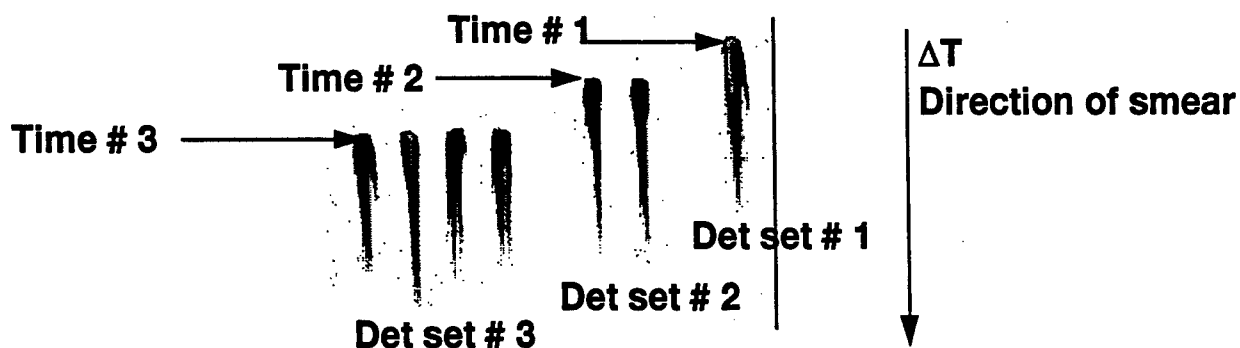


Figure 1. (U) A 1-2-4 multiple detonator multiple firing time sequence.

UNCLASSIFIED  
DISTRIBUTION LIMITED TO U.S. GOVERNMENT AND ITS CONTRACTORS

UNCLASSIFIED

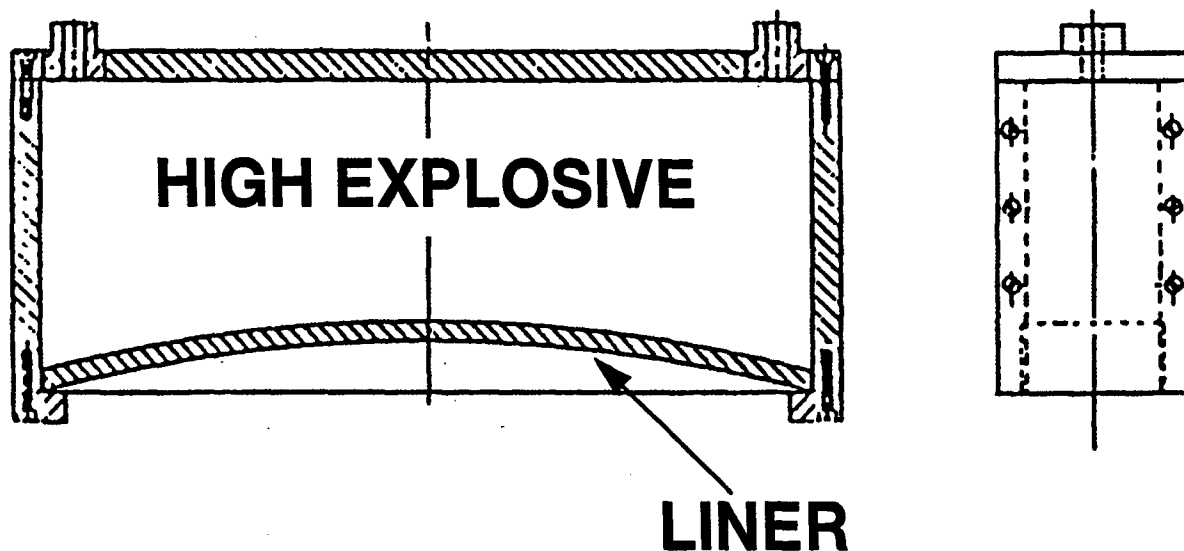


Figure 2. (U) Non-axi EFP warhead geometry.

UNCLASSIFIED

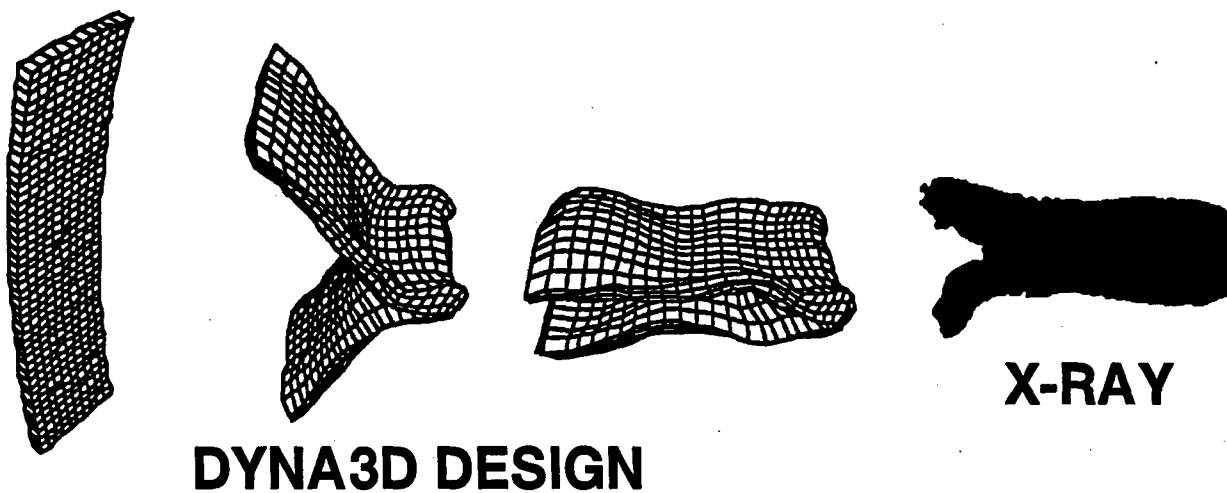


Figure 3. (U) DYNA3D EFP formation and comparison to x-ray.



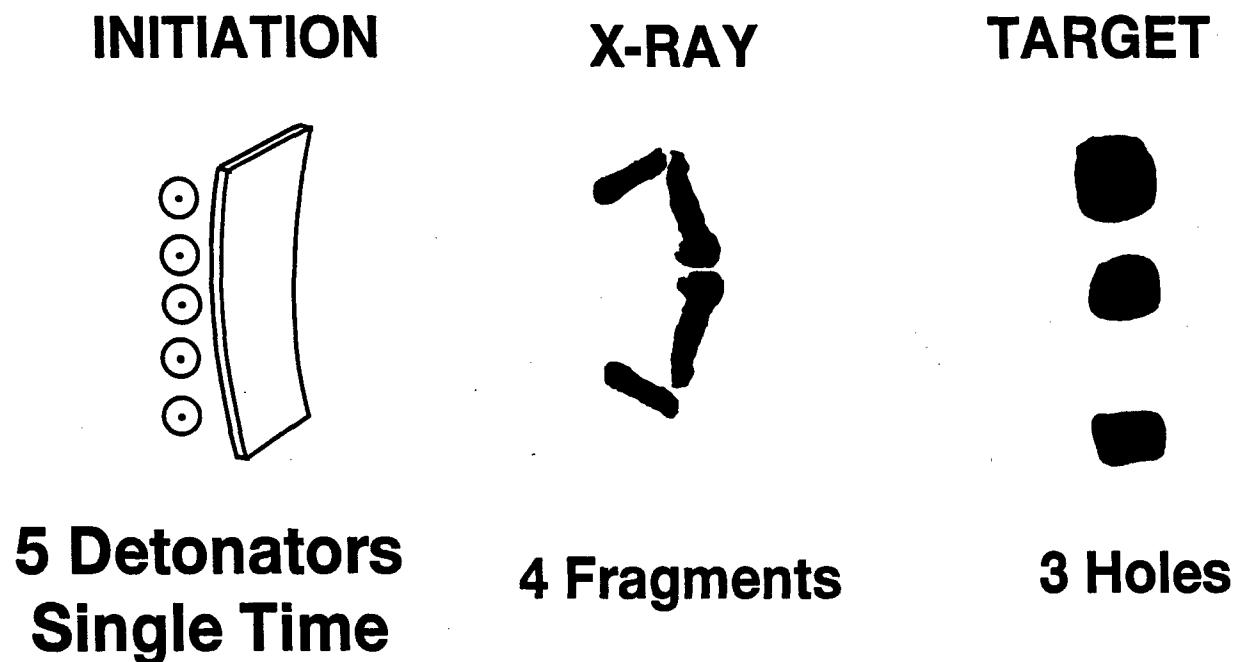


Figure 4. (U) First generation soft target mode.

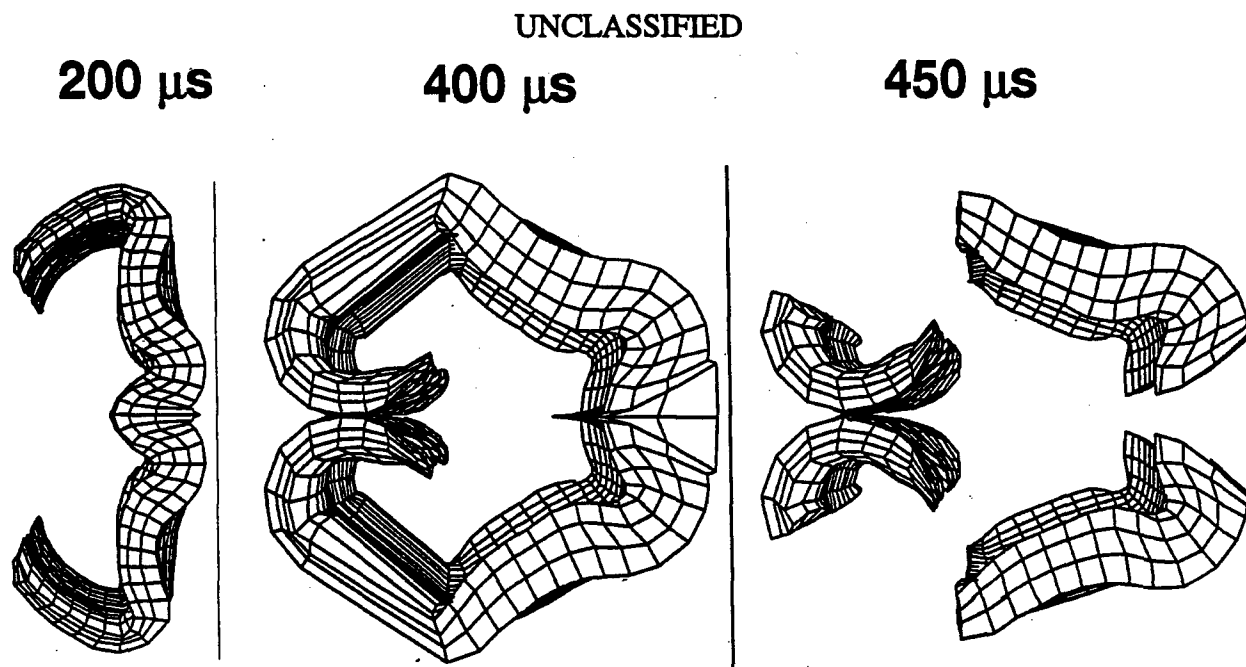
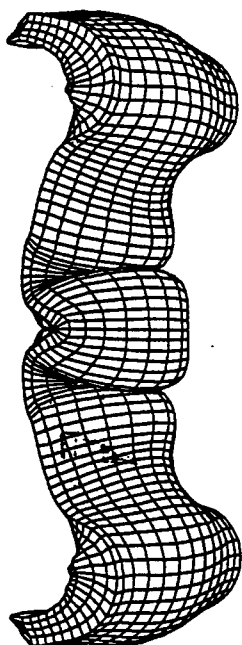


Figure 5. (U) First generation soft target mode DYNA3D simulation.  
UNCLASSIFIED

**Lagrangian**



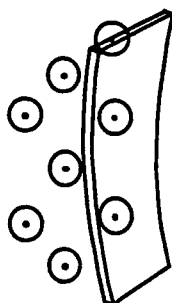
**Eulerian**



Figure 6. (U) Second generation soft target mode DYNA3D and CTH simulations.

UNCLASSIFIED

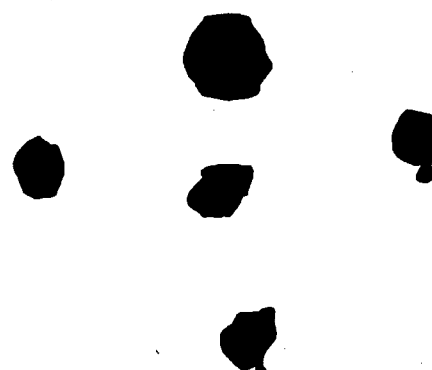
**INITIATION**



**X-RAY**



**TARGET**



**8 Detonators  
3 Times**

**Fragments**

**5 Holes**

Figure 7. (U) Second generation soft target mode.

UNCLASSIFIED

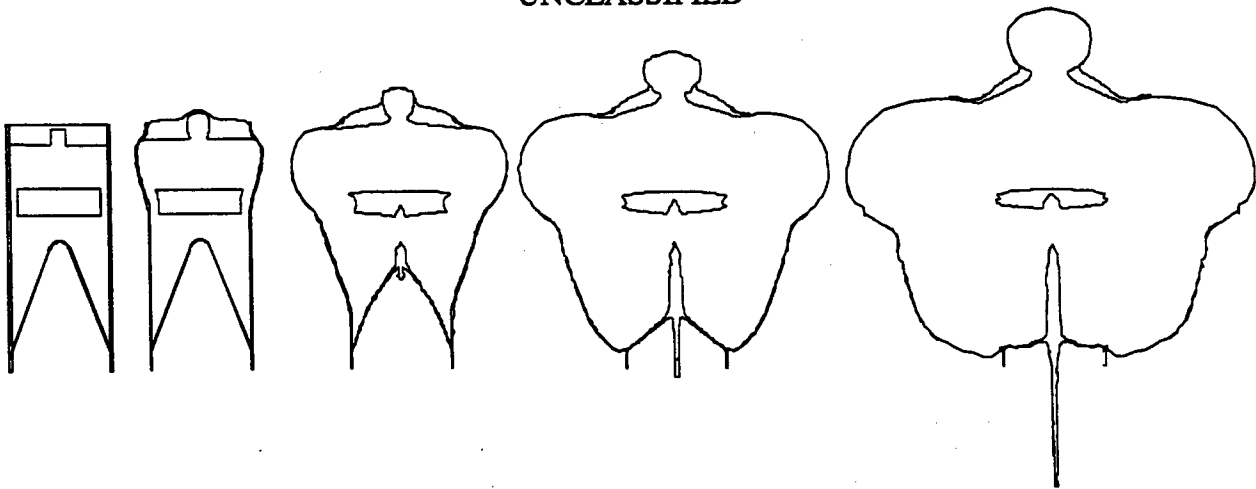
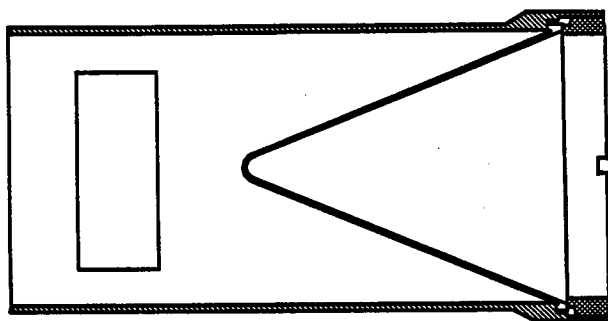
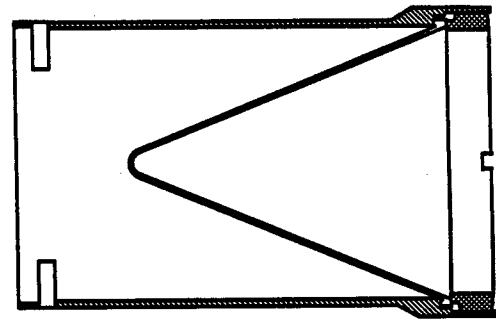


Figure 8. (U) CALE modeling of the jet formation process, 10 $\mu$ s intervals.

UNCLASSIFIED



**Wave Shaper**



**Initiation Replacement**

Figure 9. (U) Mechanical versus initiation based wave shaping.

UNCLASSIFIED

**4 Detonator x-ray**



**10 Detonator x-ray**



Figure 10. (U) Flash x-rays of jets produced by four and ten detonator arrays.

UNCLASSIFIED

UNCLASSIFIED  
DISTRIBUTION LIMITED TO U.S. GOVERNMENT AND ITS CONTRACTORS

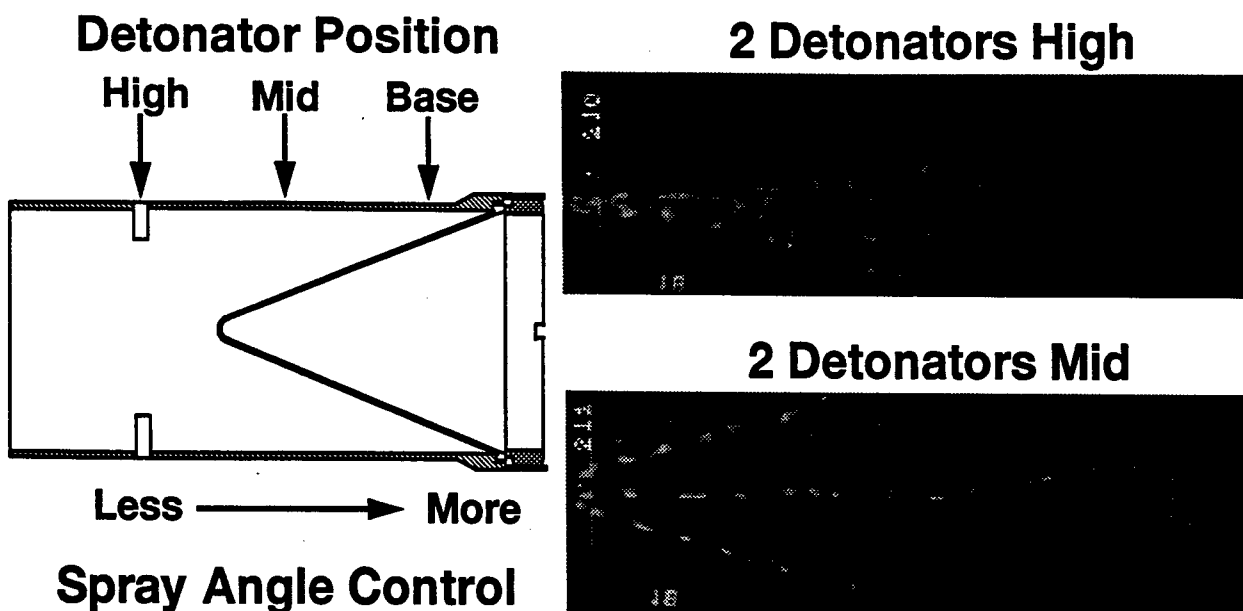


Figure 11. (U) First generation soft target mode configurations and resulting jet flash x-rays.

UNCLASSIFIED

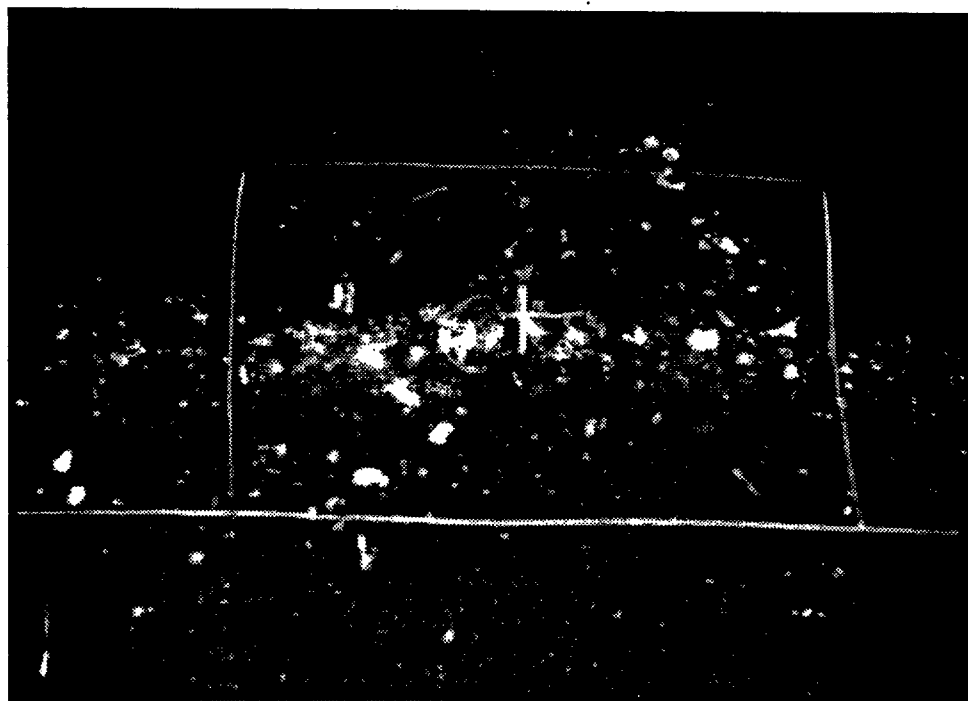


Figure 12. (U) First generation soft target mode line pattern produced on a target plate.

UNCLASSIFIED  
DISTRIBUTION LIMITED TO U.S. GOVERNMENT AND ITS CONTRACTORS

UNCLASSIFIED  
DISTRIBUTION LIMITED TO U.S. GOVERNMENT AND ITS CONTRACTORS  
UNCLASSIFIED

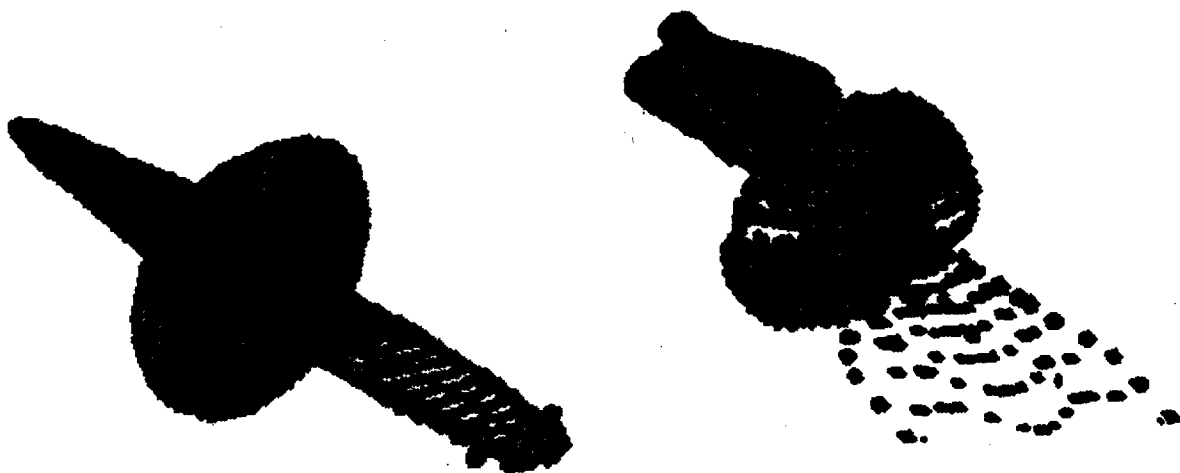


Figure 13. (U) Two detonator high (left) and two detonator mid (right) CTH results.

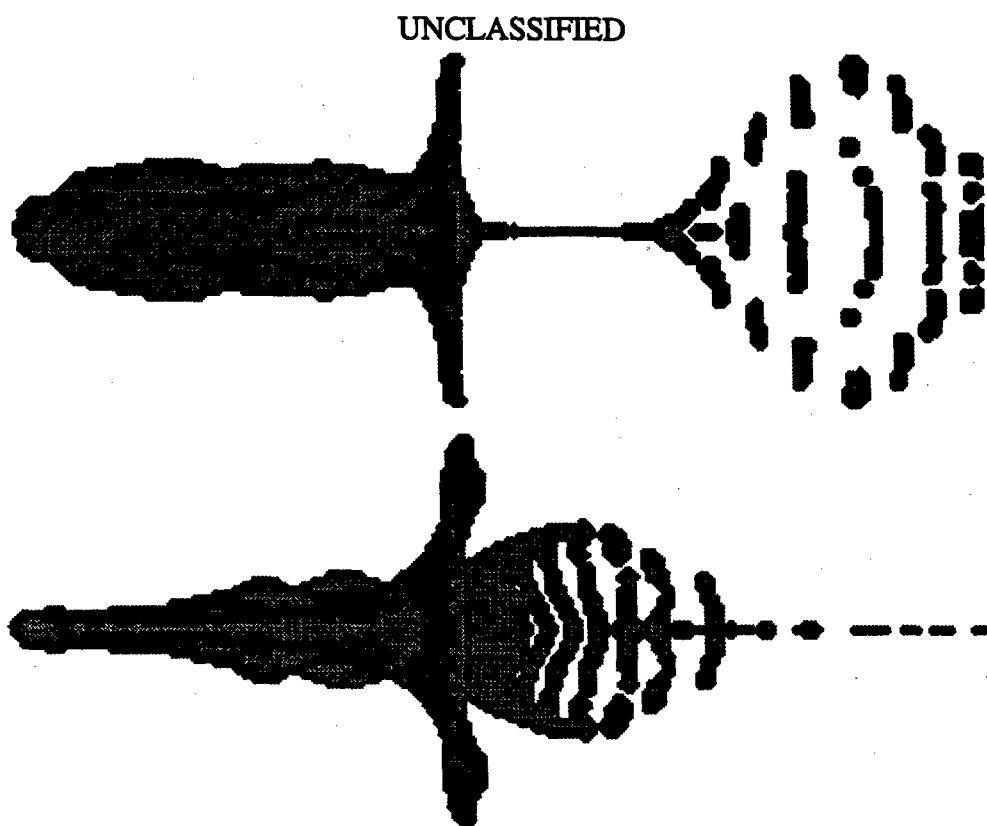


Figure 14. (U) YZ (top) and ZX (bottom) views of cross fan jet formation CTH simulation at 30  $\mu$ s.

UNCLASSIFIED  
DISTRIBUTION LIMITED TO U.S. GOVERNMENT AND ITS CONTRACTORS

UNCLASSIFIED  
DISTRIBUTION LIMITED TO U.S. GOVERNMENT AND ITS CONTRACTORS  
UNCLASSIFIED

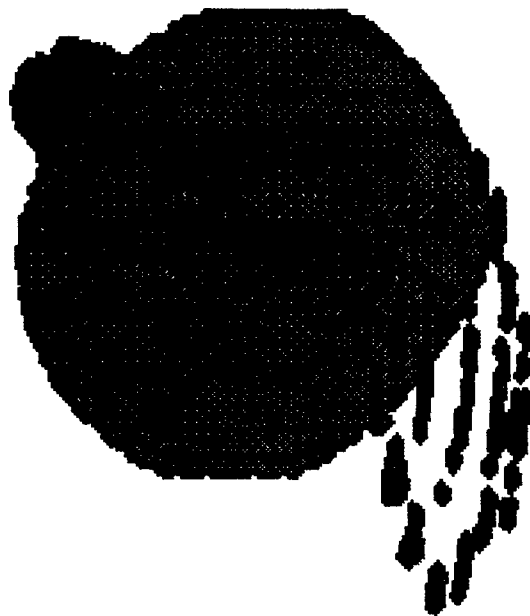


Figure 15. (U) CTH simulation result of cross fan jet formation at  $30\mu\text{s}$ .

UNCLASSIFIED

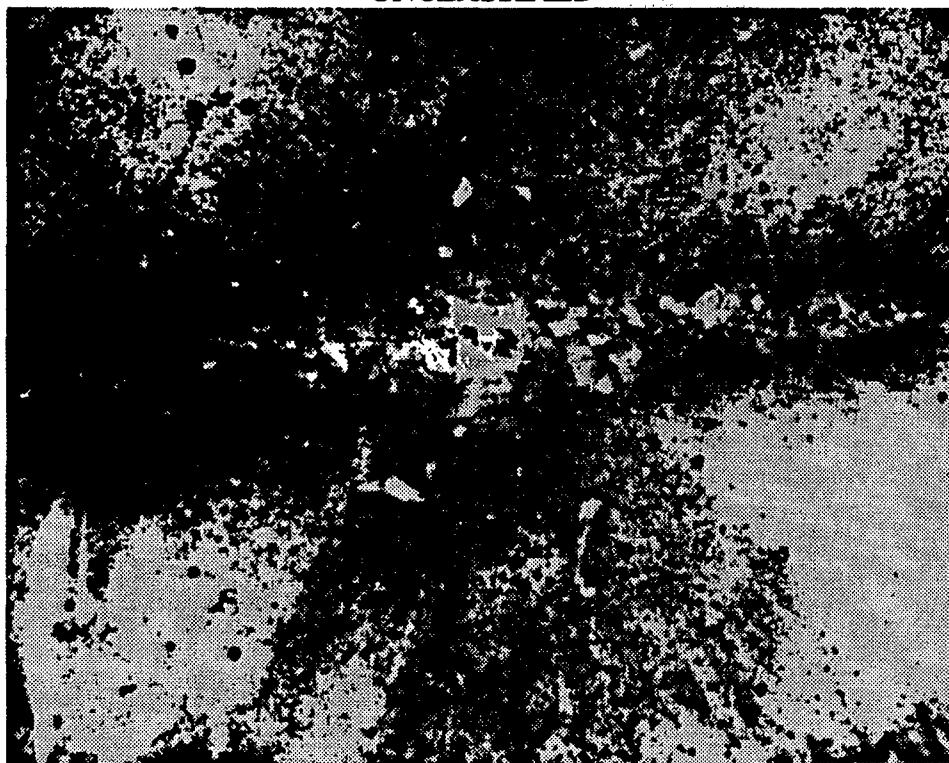


Figure 16. (U). Cross fan jet target pattern

UNCLASSIFIED  
DISTRIBUTION LIMITED TO U.S. GOVERNMENT AND ITS CONTRACTORS

**UNCLASSIFIED**

**THIS PAGE INTENTIONALLY LEFT BLANK**

**UNCLASSIFIED**

UNCLASSIFIED  
DISTRIBUTION LIMITED TO U.S. GOVERNMENT AND ITS CONTRACTORS

Anti-Armor Warhead  
Classified by: Tech. SCG, 9 FEB 95  
Declassify on: OADR

**EFP and Shaped Charge Concrete Penetration (U)**

E.L. Baker\*, T. Vuong, B. Fuchs  
U.S. Army, Armament Research, Development and Engineering Center  
Picatinny Arsenal, NJ, USA 07806-5000

**ABSTRACT (U)**

(U) Tantalum lined explosively formed projectiles (EFPs) and copper lined shaped charges were test fired against controlled concrete targets. The concrete targets were designed so that the penetration did not perforate the targets. In order to develop a modeling capability for the development of anti-concrete warheads, a series of gun fired tantalum projectile concrete penetration experiments was also performed using the same concrete target configuration. The gun fired experiments were simulated using the arbitrary Lagrange Eulerian (ALE) high rate finite difference computer program, CALE. After some concrete model calibration, the CALE simulations agreed well with the gun fired tantalum projectile experimental results. Simulation of the EFP penetration using the same concrete model parameters was subsequently performed. Analytic simulation of the shaped charge jet penetration was also performed. This new simulation capability and baseline concrete penetration data is now being used for the development of more advanced anti-concrete warheads.

(U) Introduction

(U) The ARDEC Energetics and Warheads Division has long history of anti-armor warheads research, development, design, and application. Recent emphasis has been placed on the development of anti-concrete warheads for a variety of applications including demolition, urban warfare, and hardened bunker defeat. In response to this emphasis, the ARDEC Target Defeat Program is developing anti-concrete warhead technology. As a part of this technology development, a database of gun launched projectile concrete penetration and baseline warhead concrete penetration performance has been generated using highly controlled concrete targets. The gun launched projectile data has been used to develop a concrete penetration modeling capability for the development of anti-concrete warheads. The modeling capability was verified by successfully simulating the EFP and shaped charge experiments.

UNCLASSIFIED  
DISTRIBUTION LIMITED TO U.S. GOVERNMENT AND ITS CONTRACTORS



UNCLASSIFIED  
DISTRIBUTION LIMITED TO U.S. GOVERNMENT AND ITS CONTRACTORS

(U) Continuum Modeling

(U) High rate continuum modeling of penetration is now routinely done using explicit time integration of either a Lagrangian description or an Eulerian description of the conservation equations. In a Lagrangian description, the computational mesh distorts with the material movement, whereas in an Eulerian description materials essentially advect through a stationary mesh. Normally, the Lagrangian description has an advantage of computational speed, but can be impractical or unphysical for penetration calculations which include high distortion and material flow. Typically, the computational time step becomes small where the computational mesh becomes extremely distorted. In addition, erosion routines (dropping of elements) are normally required. An Eulerian description can accommodate high distortion and flow behavior, but often requires fine zoning for adequate phenomenon resolution, as well as the added computational burden of mixed cell calculations and material interface reconstruction. The DYNA (ref. 5) and EPIC (ref. 6) computer programs are examples of second order explicit Lagrangian description continuum models. The CTH (ref. 2) and MESA (ref. 3) computer programs are examples of second order explicit Eulerian description continuum models. A new class of arbitrary Lagrange Eulerian (ALE) continuum models is now emerging. An ALE description allows the use of either a pure Lagrangian description, a pure Eulerian description, or an intermediate description including both mesh movement and material advection through the mesh. This intermediate ALE description can provide the user with a large variety of modeling options in order to improve computational run time and physical phenomenon resolution. CALE (ref. 9) is a relatively new two dimensional ALE finite difference program that is now becoming widely used. CALE may be run in a pure Lagrangian mode until a prescribed cell distortion level is reached. At this point, material advection is allowed for the distorted cells, and a mesh relaxation algorithm is used to maintain a relatively smooth mesh. In addition, the mesh relaxation algorithm may be weighted by materials or pressure. In this way, mesh is continually moved into high weighted regions of interest. This allows a smaller number of total cells to be used, while resolving regions of interest. The result is improved resolution of physical phenomenon with a reduced computation time. To date, very little penetration modeling and almost no concrete penetration using ALE methodology has been done (ref. 4). Previous work (ref. 1) assessed the applicability of CALE to concrete penetration modeling using several test problems where gun fired penetrator experimental results were available. The success of that effort prompted the broader development of an ALE concrete penetration modeling capability using CALE. As a part of this development, it was decided that a relatively large database of penetration experiments would be beneficial.

(U) Controlled Projectile Penetration

(U) A series of tantalum projectile concrete penetration experiments were completed for ARDEC at the U.S. Army Waterways Experiment Station in Vicksburg, Mississippi. The experiments included tantalum projectiles penetrating concrete targets with and without a thin circular steel plate cast into the concrete at a small depth from the target surface. The steel plate thickness (1.6cm) and depth (3.8cm) was chosen to simulate typical concrete reinforcement. Three types of tantalum projectiles were fabricated using bar stock tantalum. Figure 1 presents a

UNCLASSIFIED  
DISTRIBUTION LIMITED TO U.S. GOVERNMENT AND ITS CONTRACTORS

(U) schematic of the tantalum projectiles. The concrete targets were fabricated using the well characterized and controlled SAC-5 concrete (ref. 7) and ASTM1024 steel plates. The targets were allowed to cure for at least 90 days in order to assure appropriate concrete characteristics. Figure 2 presents a schematic of the concrete targets. Projectile velocities of approximately 0.8, 1.0, 1.5, and 1.8 Km/s were selected for the projectile velocities. The concrete targets were designed so that the penetrators did not perforate the targets. Figures 3 and 4 present photographs of typical experimental results. Continuum modeling of concrete penetration has been used for some time (ref. 8). One traditional method of modeling comparison and calibration has been the use of hole profiles. After some material modeling investigation, it was decided to use a readily available (ref. 9) concrete material model. A tabulated yield stress versus pressure was used to model the concrete strength behavior, along with the TEPLA-F porous equation of state. The initial concrete porosity, density and strength behavior were modified to reflect available material properties of the actual SAC-5 concrete used in the testing. The experimental series was simulated using an initial mesh resolution of approximately 1mm in the projectile impact region. The tantalum material was weighted higher than surrounding materials, so that higher local resolutions were achieved in and near the tantalum. After initial modeling, it was apparent that some significant discrepancies to the experimental results existed. Part of the discrepancy appeared to be related to the absence of a formal damage model. As no damage state variables were saved, previously failed material would "heal" itself when recompressed, subsequently displaying material strength. This behavior was particularly obvious along the axis of symmetry. The inclusion of the newly developed Tipton-Stienberg damage model overcame this deficiency. After some additional calibration, the agreement to experimental results was quite good. Figure 5 presents material boundaries at 0, 50, 100, and 200 microseconds for the TANT94-7 test simulation. Figure 6 presents a comparison of the final (2000 microsecond) simulation result to the experimental hole profile for the TANT94-7 test. Table 1 presents a summary comparison of the controlled projectile computational and experimental results. As the concrete penetration capability was developed for application to anti-concrete warheads, it was decided to verify the capability by simulating EFP and shaped charge concrete attack. The EFP concrete attack simulation was performed using the same concrete targets and the newly developed concrete model parameters.

(U) Explosively Formed Projectile Penetration

(U) Three identical EFP concrete attack experiments were performed. The experiments consisted of ARDEC 4.5" EFPs shot at a two meter standoff against the same concrete targets with the thin circular steel plate reinforcement simulant. The ARDEC 4.5" EFP is extremely well characterized, having been used for several hundred experiments over a 10 year period. The design has been developed using two and three dimensional Lagrangian modeling with the DYNA2D and DYNA3D computer programs. The final penetrator shape and velocity (2.08 Km/s) has been experimentally verified using flash x-rays at both ARDEC and ARL. The penetrator formation and final shape from DYNA2D, as well as a flash x-ray are presented in figure 7. The DYNA2D shape and experimental velocity were used as input to the CALE penetration modeling. Figure 8 presents the EFP penetration modeling at 0, 50, 100, and 200

UNCLASSIFIED  
DISTRIBUTION LIMITED TO U.S. GOVERNMENT AND ITS CONTRACTORS

UNCLASSIFIED  
DISTRIBUTION LIMITED TO U.S. GOVERNMENT AND ITS CONTRACTORS

(U) microseconds. The completely damaged concrete contour is shown with a dark line. The three EFP penetration experiments were performed for simulation verification. Figure 9 presents a photograph of the experimental setup. Figure 10 presents a photograph of a resulting target. The three resulting hole profiles were very similar, indicating good reproducibility of both the warheads and target behaviors. Figure 11 presents a comparison of the final (2000 microsecond) simulation result to the three experimental hole profiles for the EFP penetration. Excellent agreement between simulation and experimentation resulted.

(U) Shaped Charge Jet Penetration

(U) Three identical shaped charge concrete attack experiments were performed. The experiments consisted of BRL 81mm shaped charges shot at a five charge diameter standoff against the same concrete targets with the thin circular steel plate reinforcement simulant. The BRL 81mm shaped charge is also extremely well characterized, having been used at ARDEC for several hundred experiments over a 20 year period. The jet characteristics have been experimentally determined using flash x-rays, presented in figure 12. Figure 13 presents the CALE computational jet formation at 0, 10, 20, 30, 40, and 60 microseconds. On the whole, the experimental jet characteristics compare well with the ALE continuum modeling. From previous CALE modeling it is known that the jet tip velocity (8.5Km/s), computational onset of jet particulation (170 $\mu$ s from formation) and accumulated jet length (850mm to 3.5Km/s) matches the experimentation reasonably well, but that the total number of jet particles is significantly under predicted. For this reason, analytic modeling of shaped charge jet penetration was done. However, ALE continuum modeling of jet penetration is continuing to be studied. Using the included jet tip velocity, break-up time, a virtual origin standoff of 447mm and a penetration cutoff jet velocity of 3.5 Km/s, the predicted target penetration including the steel disk thickness is 1238mm. The actual penetration was 1181mm. The predicted penetration cutoff jet velocity using the experimental penetration is 3.8 Km/s. Figure 14 presents a photograph of the experimental setup. Figure 15 presents a photograph of a resulting target. The three resulting hole profiles were again very similar, indicating good reproducibility of both the warheads and target behaviors. Figure 16 presents a comparison of the experimental hole profiles to analytic hole depth. The analytic hole depth is in quite good agreement with the experimentation.

(U) Conclusions

(U) After some initial material model limitation, the calculations ran extremely smoothly to very late times (several milliseconds). The benefits of ALE technology are clearly demonstrated by the achievement of high local mesh resolution, while maintaining a relatively small overall mesh size. This work has concentrated on material model investigation and parameterization with emphasis placed on the concrete behavior using a large set of controlled projectile penetration experimental results. The inclusion of the newly developed Tipton-Stienberg damage model has allowed much more physically realistic results to be achieved. The resulting concrete material model has produced good agreement with the controlled projectile experiments. The resulting model has been validated to produce good agreement with EFP

UNCLASSIFIED  
DISTRIBUTION LIMITED TO U.S. GOVERNMENT AND ITS CONTRACTORS

(U) concrete attack experiments. Traditional analytic shaped charge jet penetration formulation has also been validated to produce good agreement with shaped charge concrete attack experiments. This new simulation capability and baseline concrete penetration data is now available, and currently being used for the development of more advanced anti-concrete warheads.

(U) References

(U) 1. E.L. Baker and T. Vuong, "Arbitrary Lagrange Eulerian (ALE) Continuum Modeling of Concrete Penetration by Tantalum Rods", *Proceedings of the SCS 1995 Eastern Multiconference, Military and Government Simulation Conference*, Phoenix, AZ 1995 (April).

(U) 2. R.L. Bell et al., "CTH User's Manual and Input Instructions Version 1.024", *CTH Documentation*, Sandia National Laboratories, Albuquerque, NM. 1991.

(U) 3. S.P. Clancy and S.T. Bennion, "MESA, The Main Program", *Los Alamos National Laboratories Report LA-CP-91-173*, 1991.

(U) 4. M. Finger, K. Sinz et al., "Joint DoD/DOE Munitions Technology Development Program FY-94 Progress Report: Concrete Modeling for Penetrating Munitions", *Lawrence Livermore National Laboratory Report UCRL-ID-103482-94*, 1994.

(U) 5. J.O. Hallquist, "User's Manual for DYNA2D -- An Explicit Two-Dimensional Hydrodynamic Finite Element Code with Interactive Rezoning", *Lawrence Livermore National Laboratory Report UCID-18756 Rev 2.*, 1984.

(U) 6. G.R. Johnson and R.A. Stryk, "User Instructions for the 1991 Version of the EPIC Research Code", *U.S. Air Force Wright Laboratory Report WL/MN-TR-91-53*, 1992.

(U) 7. S. Joy and J. Ehrgott, "Material Characterization of SAC-5 Concrete", *Geomechanics and Explosion Effects Division Internal Report*, U.S. Army Engineer Waterways Experiment Station, 1994.

(U) 8. J.J. Osborn and D.A. Matuska, "Dynamic Response of a Kinetic Energy Penetrator", *Eglin Air Force Base Technical Report AFATL-TR-78-24* 1978 (March).

(U) 9. R. Tipton, "CALE User's Manual", *CALE Documentation*, Lawrence Livermore National Laboratory, Livermore, 1991.

UNCLASSIFIED  
DISTRIBUTION LIMITED TO U.S. GOVERNMENT AND ITS CONTRACTORS

UNCLASSIFIED  
DISTRIBUTION LIMITED TO U.S. GOVERNMENT AND ITS CONTRACTORS

(U) Tables

UNCLASSIFIED

Projectile	Velocity (m/s)	Test Name	Tunnel Depth (cm)		Plate Hole Diameter (cm)	
			COMP	EXP	COMP	EXP
TA1	884.	TAN94-1	14.0	15.7	2.4	2.8
TA1	1084.	TAN94-2	21.6	22.7	2.5	2.9
TA1	1453.	TAN94-3	30.4	34.3	3.0	2.8
TA1	1717.	TAN93-3	32.5	35.8	3.4	3.1
TA1	858.	TAN94-10	16.9	17.8	No Plate	
TA1	1109.	TAN94-8	25.1	26.7	No Plate	
TA1	1415.	TAN94-9	31.2	31.8	No Plate	
TA1	1812.	TAN93-8	35.2	40.9	No Plate	
TA2	1056.	TAN94-4	15.6	21.3	2.6	2.8
TA2	1450.	TAN94-5	22.9	25.4	3.0	3.0
TA2	1475.	TAN93-6	22.9	25.0	3.0	3.2
TA3	1101.	TAN94-6	23.0	22.6	3.8	3.7
TA3	1480.	TAN94-7	28.1	27.9	4.2	4.3
TA3	1770.	TAN93-7	31.4	33.8	5.0	4.5

Table I. (U) Summary of the computational (COMP) and experimental (EXP) results.

(U) Figures

UNCLASSIFIED

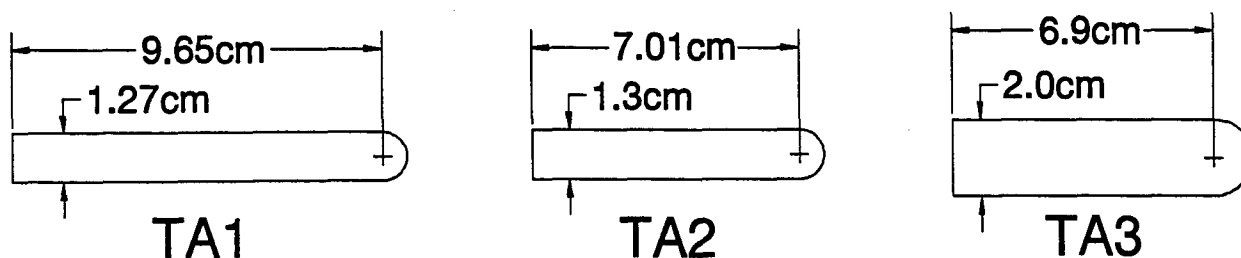


Figure 1. (U) Tantalum projectile geometries.

UNCLASSIFIED  
DISTRIBUTION LIMITED TO U.S. GOVERNMENT AND ITS CONTRACTORS

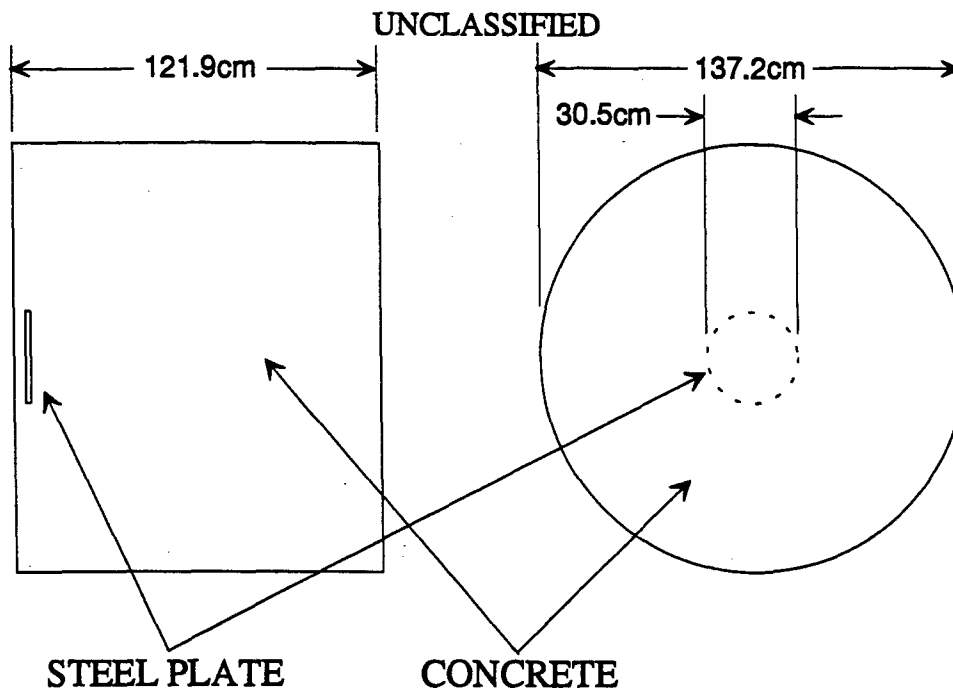


Figure 2. (U) Concrete target geometries.

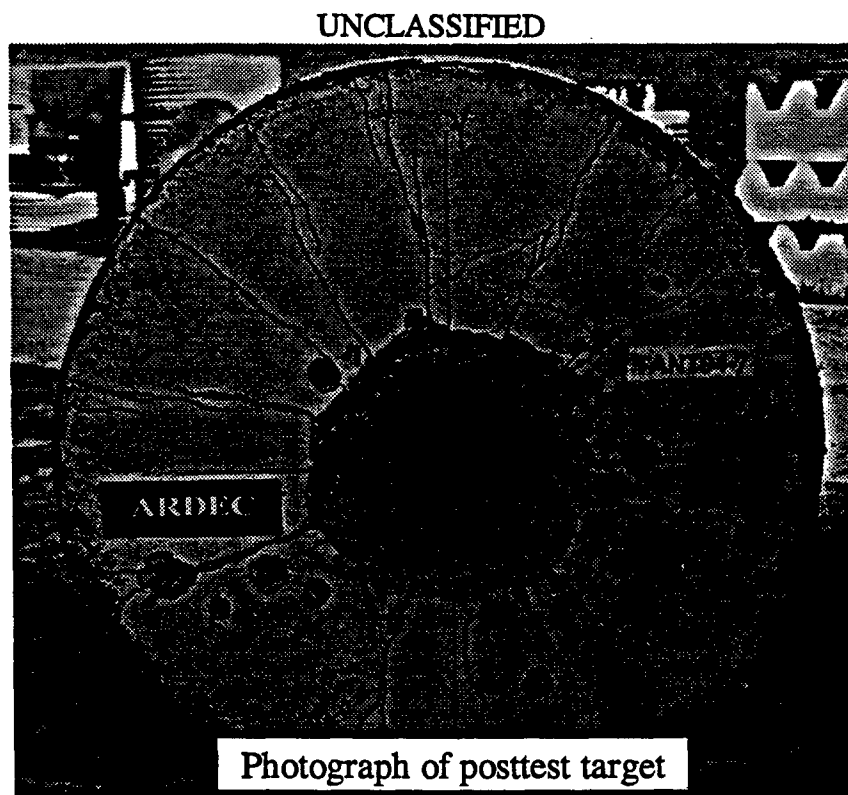


Figure 3. (U) Photograph of typical experimental result.

UNCLASSIFIED

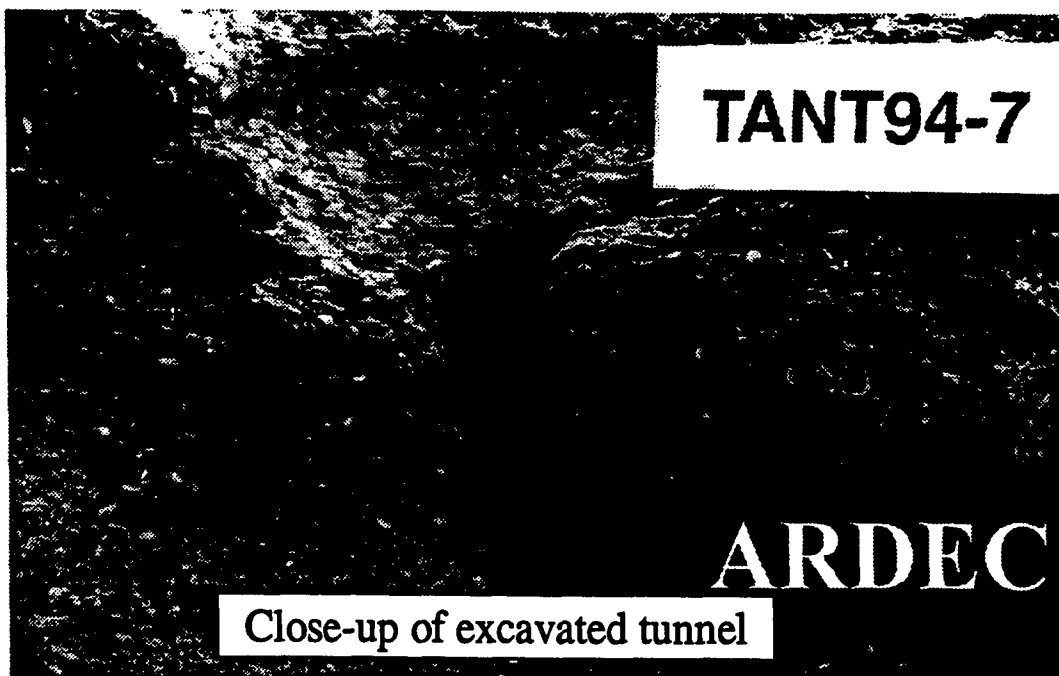


Figure 4. (U) Photograph of typical experimental result.

UNCLASSIFIED

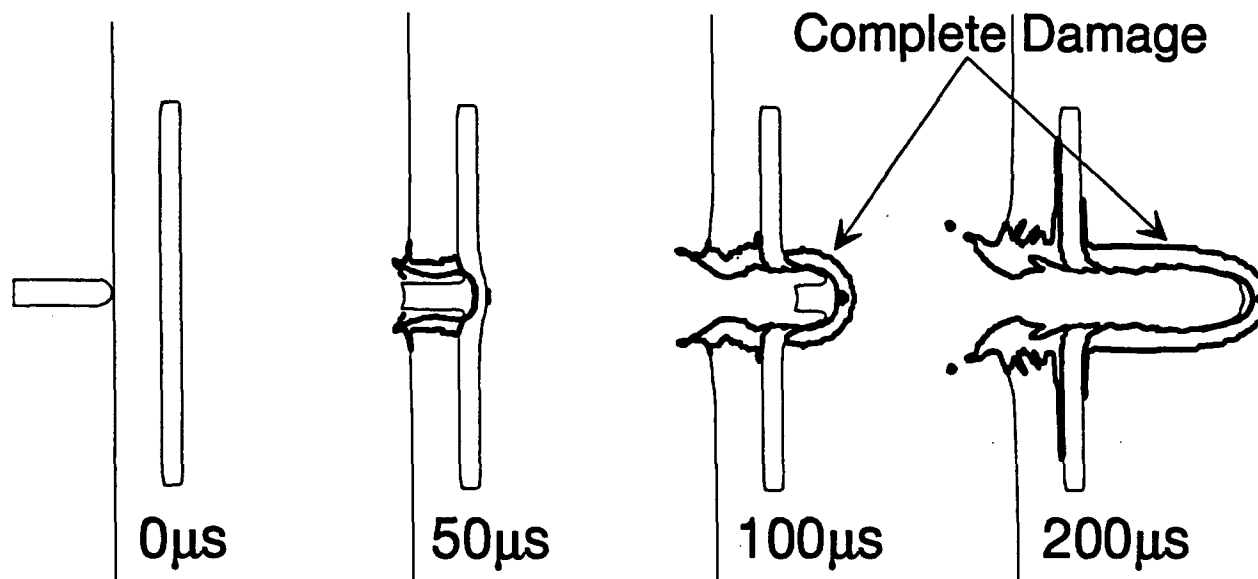


Figure 5. (U) Material boundaries at 0, 50, 100 and 200 microseconds.

UNCLASSIFIED

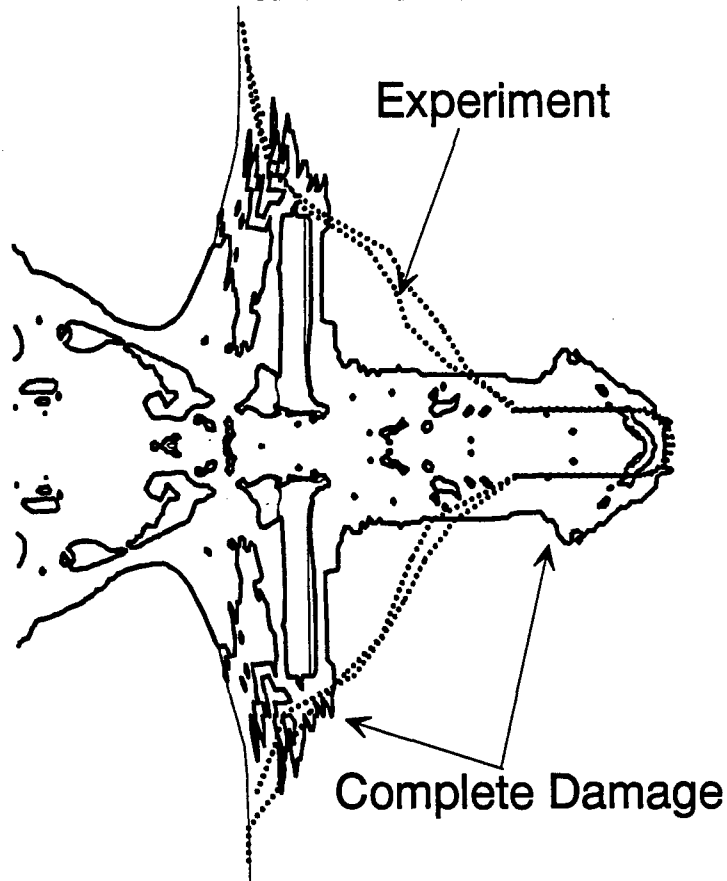


Figure 6. (U) Computational and experimental hole profile (0 and 90 degrees) for TANT94-7.

UNCLASSIFIED

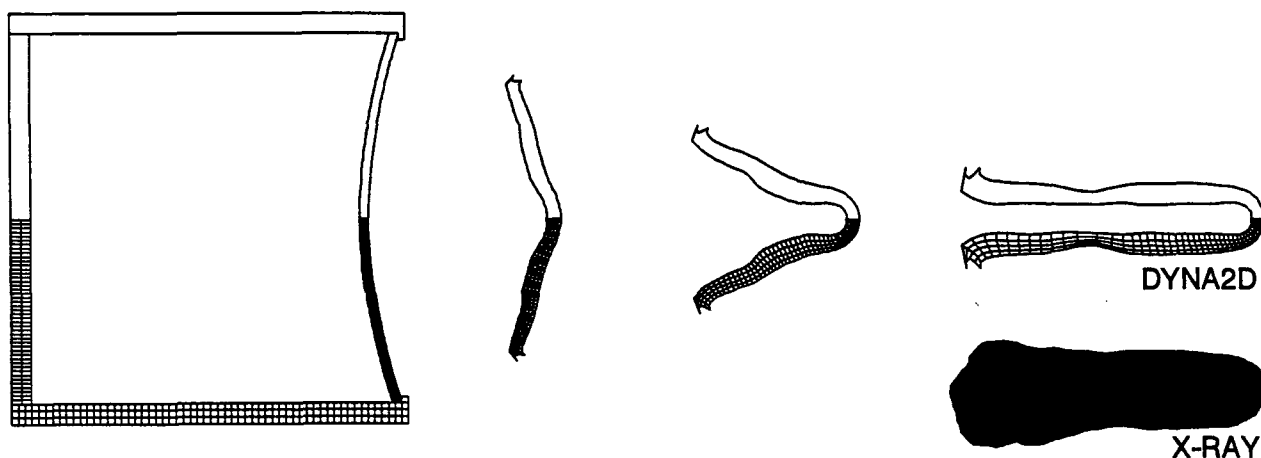


Figure 7. (U) Penetrator formation and final shape.



UNCLASSIFIED

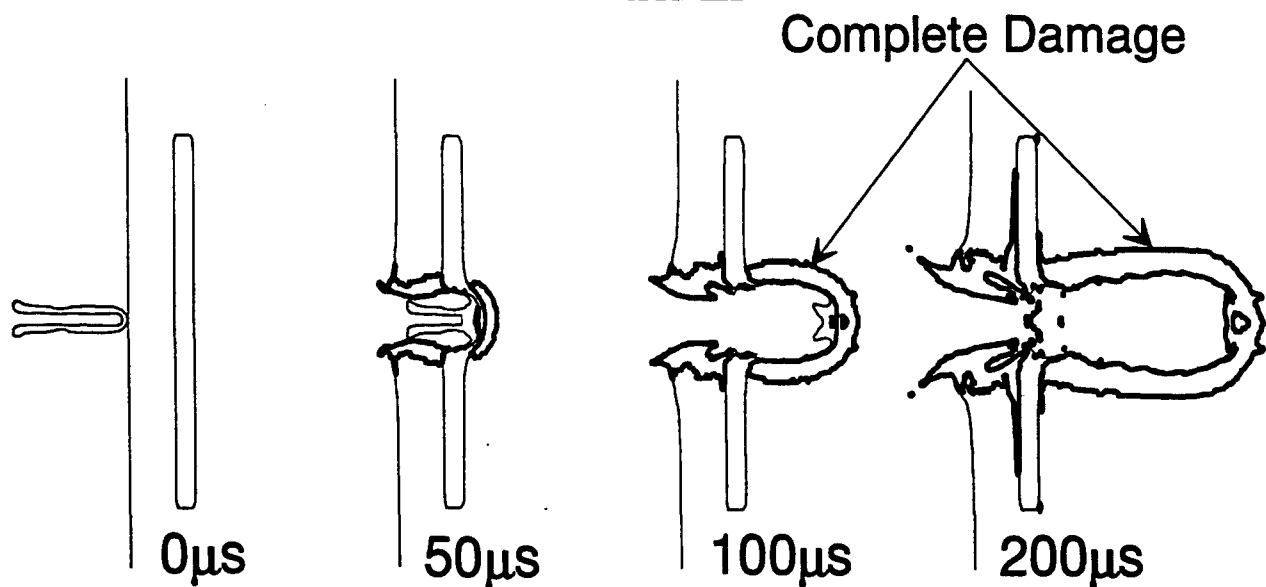


Figure 8. (U) CALE EFP penetration modeling at 0, 50, 100 and 200 microseconds.

UNCLASSIFIED

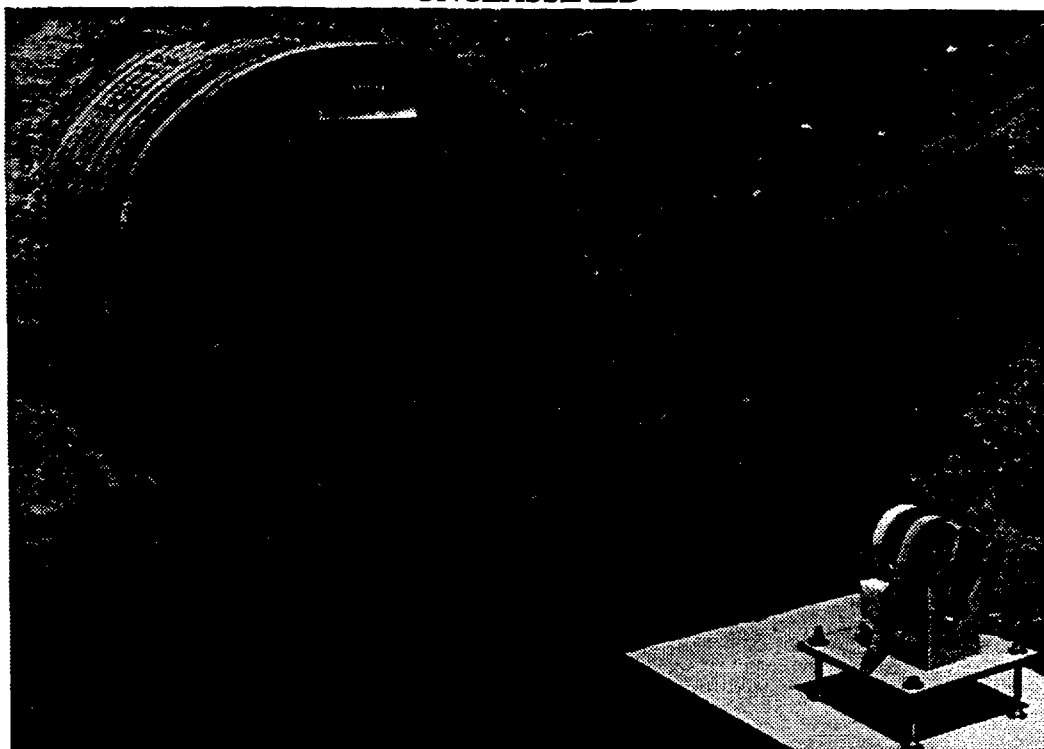


Figure 9. (U) Experimental setup for EFP concrete attack.

UNCLASSIFIED

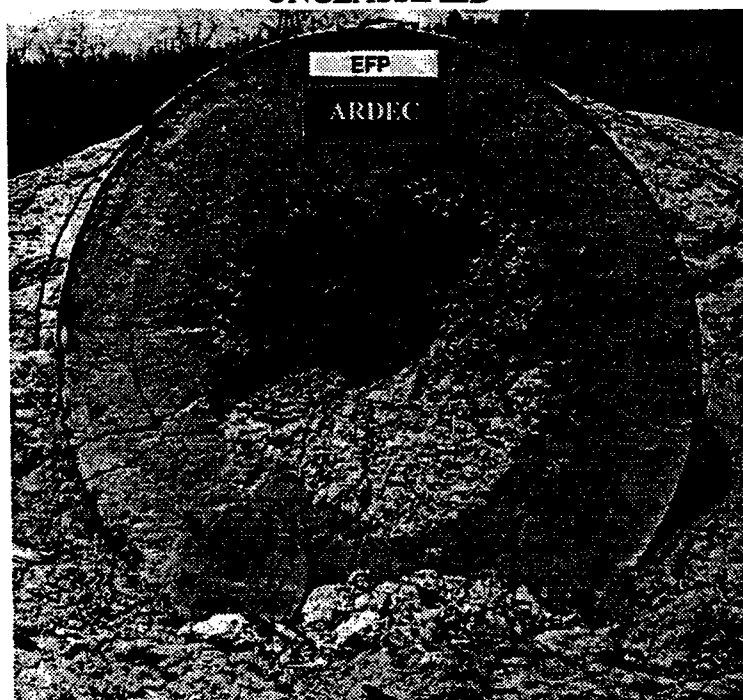


Figure 10. (U) Resulting target from EFP concrete attack.

UNCLASSIFIED

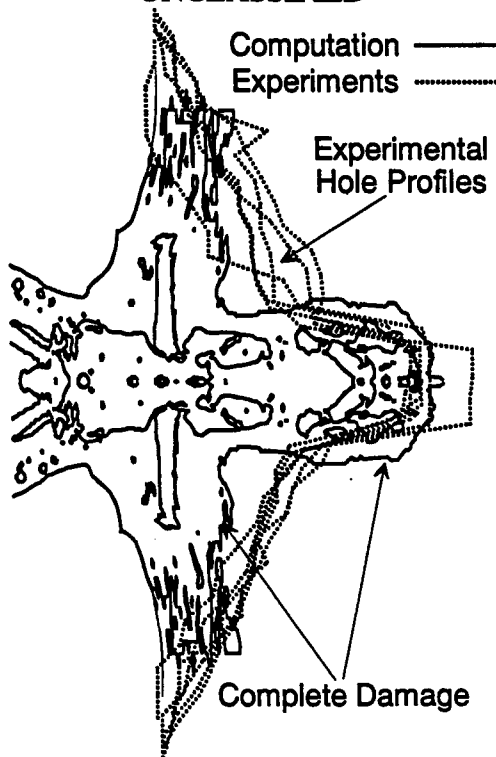


Figure 11. (U) Comparison of EFP penetration simulation to experimental hole profiles.

UNCLASSIFIED

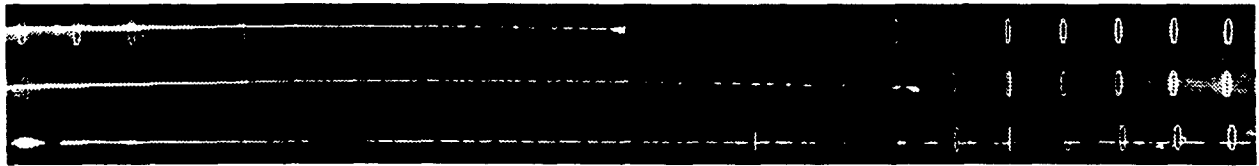


Figure 12. (U) Flash x-rays of shaped charge jet at 132 $\mu$ s, 162 $\mu$ s and 262 $\mu$ s.

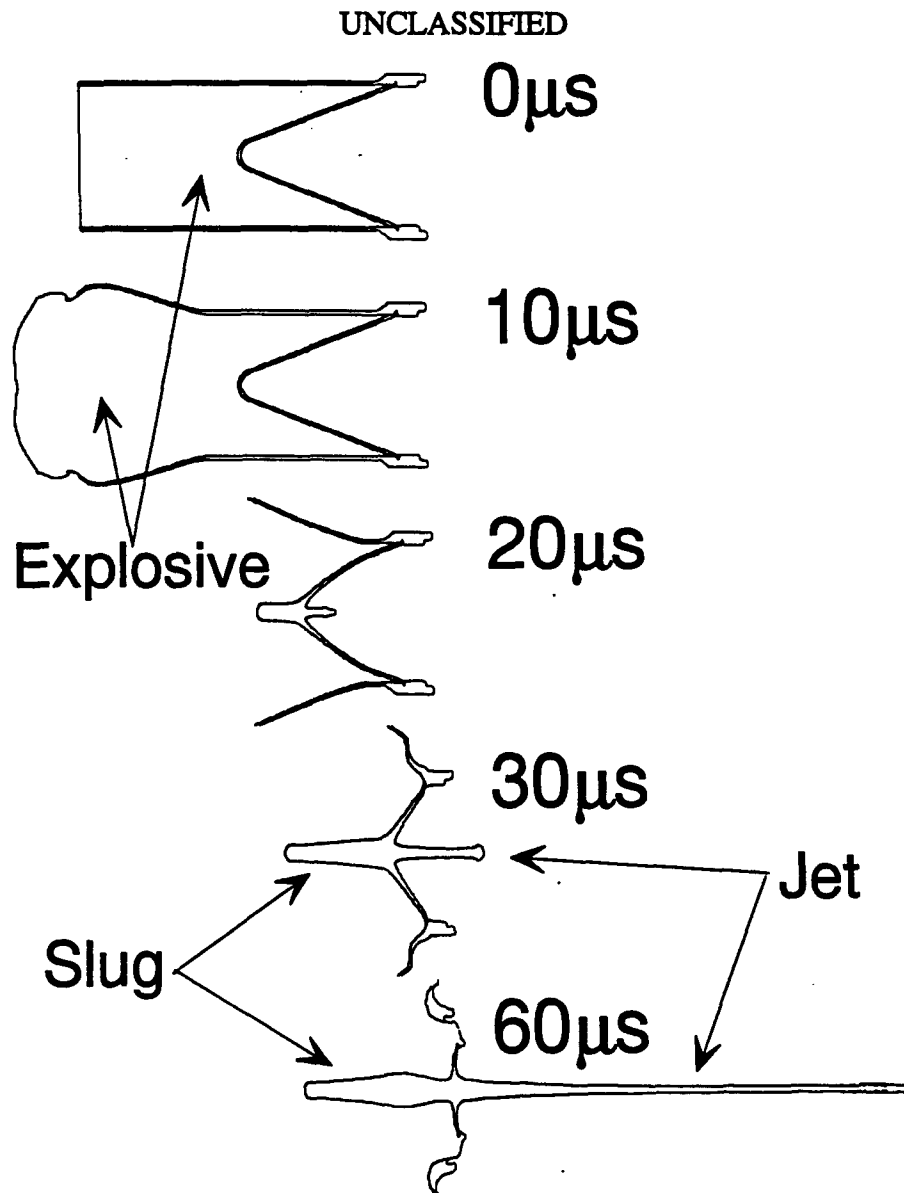


Figure 13. (U) CALE modeling of shaped charge jet formation.

UNCLASSIFIED  
DISTRIBUTION LIMITED TO U.S. GOVERNMENT AND ITS CONTRACTORS

UNCLASSIFIED

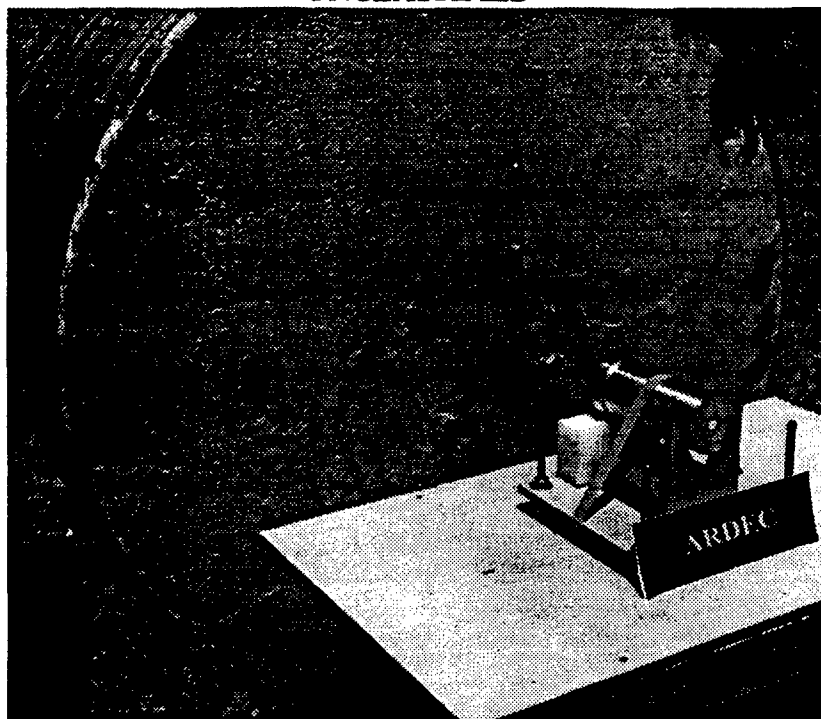


Figure 15. (U) Experimental setup for shaped charge concrete attack.

UNCLASSIFIED

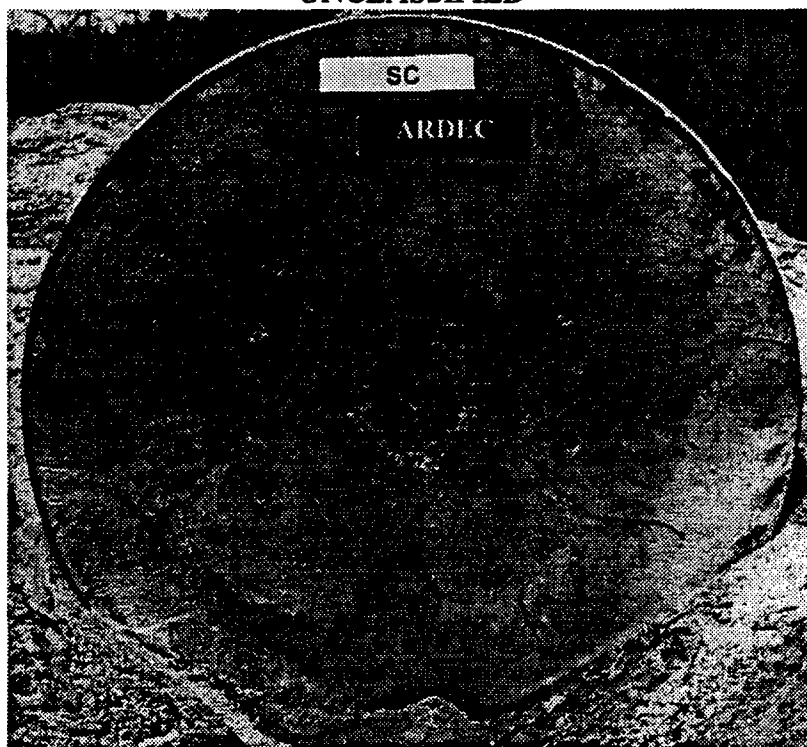


Figure 16. (U) Resulting target from shaped charge attack.

UNCLASSIFIED  
DISTRIBUTION LIMITED TO U.S. GOVERNMENT AND ITS CONTRACTORS

UNCLASSIFIED

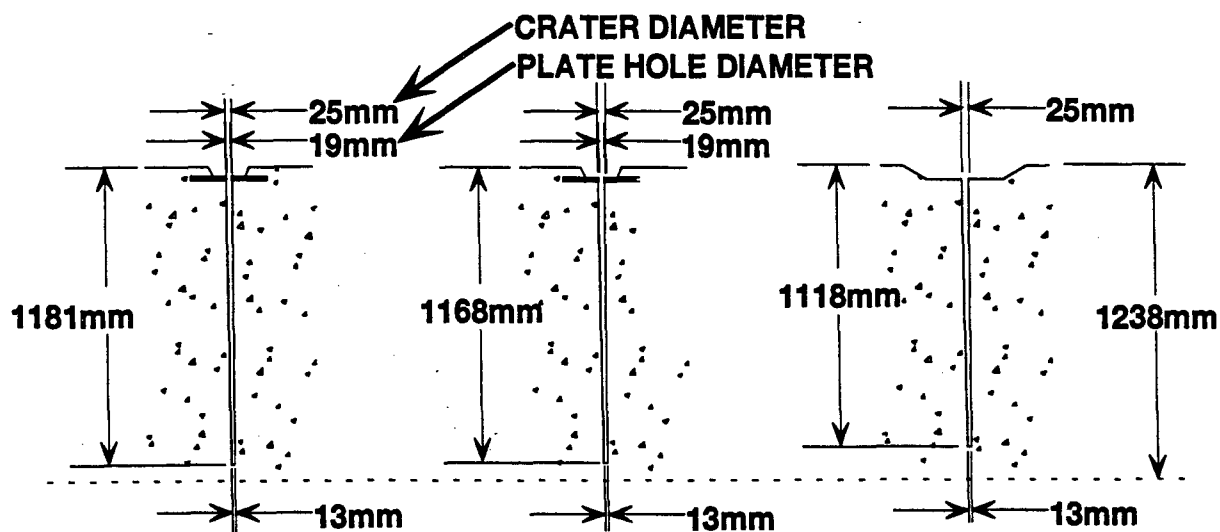


Figure 17. (U) Comparison of the three experimental hole profiles to analytic hole depth.

## NEW TIRE PENETRATION AND PRESSURE MODELS FOR IMPROVED VULNERABILITY ANALYSES OF WHEELED VEHICLES (U)

Ricky L. Grote, Linda L. C. Moss, and Edwin O. Davisson  
U.S. Army Research Laboratory  
Aberdeen Proving Ground, MD 21005-5068

### ABSTRACT (U)

(U) An improved methodology was developed for the U.S. Army Research Laboratory's Ballistic Vulnerability/Lethality Division to conduct vulnerability analyses of wheeled vehicles subjected to attack from small steel and tungsten fragments less than 0.65 g (10 gr). Sequential statistical methods were used to collect and compute the velocity at which 50% of the fragments are expected to perforate the target,  $V_{50}$ . Also the traditional THOR penetration equations were improved upon for tires. Methodology was developed to predict tire deflation with and without an on-board Central Tire Inflation System and to determine the level of damage required to render a tire or tires nonfunctional within given time limits.

### 1. (U) INTRODUCTION

(U) The U.S. Army Research Laboratory's Ballistic Vulnerability/Lethality Division (BVLVD) reviewed the current methodologies used to conduct vulnerability analyses of wheeled vehicles subjected to attack from steel and tungsten fragments. This internal audit revealed that there was a lack of experimental data that would defend the use of existing tire probability of kill functions (now called probability of component dysfunction,  $P_{cd}$ ) and support the use of current penetration equations when "small" fragments are considered. Additionally, the capability of an on-board Central Tire Inflation System (CTIS) had never been considered explicitly in determining the level of damage required to render a tire or tires nonfunctional within given time limits.

(U) Consequently, an experimental program plan was developed with the goal of producing sufficient data to substantiate the current tire vulnerability methodology or to allow for development of new methodology, if necessary. The tire vulnerability modeling process proceeded by answering the following questions in order:

1. Do small fragments have the ability to perforate tires?
2. What are the effects of multiple perforations in a single tire?
3. If tires are perforated, what is the resulting deflation rate?
4. If the target has a CTIS, how does CTIS performance influence deflation rate?
5. What are the effects of perforations in multiple tires on a vehicle with a CTIS?

(U) The experimental plan was developed to directly address these five questions. The ability to model fragment perforation of tires was to be addressed by adding small steel and tungsten fragment data to an existing data set for the development of an improved and more general penetration equation and by determining  $V_{50}$  ballistic limits for various tire cross sections. The remaining questions which pertain directly to the validity of the existing  $P_{cd}$  functions were to be resolved via experimental firings at pressurized tires mounted on a vehicle with a CTIS and theoretical development of governing equations. A Soviet BM-21 multiple rocket launcher was selected as the target vehicle for several reasons: it was available, it contained a CTIS, and additional tires were available for testing.

### 2. (U) TARGET VEHICLE

(U) The BM-21 MRL consists of a launcher assembly mounted on a URAL-375 chassis. The launcher assembly contains 40 firing tubes for high-explosive-fragmenting munitions. Most of the discussion will focus on the URAL-375, since the tires and the CTIS are part of this truck. The URAL-375 is a 4.5-ton, three-axle 6x6 cross country vehicle that may be used on surfaced roads, earthen roads, and on roadless terrain. The URAL-375 also incorporates the use of adjustable inflation tires and a CTIS for increased mobility. The service manual (USSR, undated) for this vehicle provides guidance for tire pressure settings and driving speeds for various road surface conditions.

## 2.1 (U) Tire Characteristics.

(U) The tires mounted on the BM-21 are 14.00×20 adjustable inflation tires, model 01-25. These tires consist of 10 plies, are tubed, and have the typical cross-country tread design. The tire cross-sectional thickness varies both in the tread and sidewall areas. The sidewall ranges from about 1.52 cm (0.6 in) to 2.54 cm (1.0 in) and the treads vary from about 5 cm (2 in) to 6.6 cm (2.6 in) with the area between the tread lugs around 2.54 cm (1.0 in).

## 2.2 (U) CTIS Characteristics.

(U) Soviet-designed tire-inflation systems were first included on pure transport vehicles in 1958. Two basic types of CTIS's were implemented in vehicle designs. The oldest type, introduced on the ZIL-157 and resident on the BM-21, is more complex and offers more flexibility to the operator (Warner 1987). This system contains control valves that can isolate any individual tire or set of tires. The pressure in the tires with open control valves can then be adjusted either up or down through the use of a three-way slide valve that has positions for inflate, deflate, and neutral (Warner 1987). The newer design does not have the cab-mounted valves for each tire. In this case, air supplied through use of the three-way valve is fed into a manifold and onto each axle of the vehicle from a common supply. The GAZ-66, ZIL-131, URAL-1320, and KrAZ-25TB are known to use this system.

## 3. (U) V<sub>50</sub> BALLISTIC LIMITS

### 3.1 (U) V<sub>50</sub> Experimental Plan.

(U) The intent of the ballistic limit experiments was to answer, at least in part, the first question listed in the introduction: Do small fragments have the ability to perforate typical combat vehicle tires? V<sub>50</sub> is that velocity at which 50% of the fragments are expected to perforate the target. The V<sub>50</sub> ballistic limit data are very useful in that they provide a quick notion of what threat mass and velocity are required to defeat a target. It can also be used in some penetration equations to provide predictions of residual velocity. The experimental matrix included a range of small fragment sizes, 0.13 to 0.37 g (2 to 5.7 gr), and tire thicknesses of 1.52 to 6.6 cm (0.6 to 2.6 in).

(U) A single tire was used for the V<sub>50</sub> and penetration equation portions of this effort. The tire was cut into 16 wedge-shaped sidewall pieces and 8 tread sections. Each section was rigidly clamped to a test stand so that the rubber would be somewhat rigid.

(U) The experimental setup for the V<sub>50</sub> and penetration equation work consisted of a 5.56-mm gun, four velocity breakscreens, and a stand to hold the tire sections. A piece of photo paper taped to the front of the tire section was used for checking fragment orientation at impact.

(U) The experimental procedure followed for the V<sub>50</sub> work was the Up and Down Method, which is described in Darcom Pamphlet 706-103 (U.S. Army Materiel Development and Readiness Command 1983), AMC Pamphlet 706-111 (U.S. Army Materiel Command 1969), and JMEM Surface-to-Surface Manual JTCG/ME-61S1-3-4 (Joint Technical Coordinating Group for Munitions Effectiveness 1982). Basically, the velocity is increased or decreased incrementally depending on whether or not perforation is achieved. Experimentation stops when a specified number of firings have been conducted or when a zone of mixed results is achieved.

### 3.2 (U) V<sub>50</sub> Analysis and Results.

(U) The DiDonato and Jarnagin procedure was implemented to obtain unique maximum likelihood estimates of the mean and the asymptotic standard deviation of the perforation distribution for various threat masses against target thicknesses (McKaig and Thomas 1983). The V<sub>50</sub>, also known as the ballistic limit, is the mean of the perforation distribution. The asymptotic standard deviation of the perforation distribution and the standard deviation of V<sub>50</sub> were also determined. The standard deviation of V<sub>50</sub> is a measure of the accuracy of V<sub>50</sub>. Simply stated, if additional data sets were provided with the same mass against the same target thickness, the V<sub>50</sub> calculated could vary from the one computed for the previous data set. The standard deviation of V<sub>50</sub> indicates the amount of variability in the V<sub>50</sub> estimate.

(U) Unique maximum likelihood estimates are possible as long as two restrictions hold. The first restriction requires a zone of mixed results, in which the lowest velocity that perforated the target is smaller than the highest velocity that did not perforate. The second restriction requires that the average velocity for the perforated data is greater than the average velocity for the nonperforated data. When these restrictions did not hold, the standard deviation of the V<sub>50</sub> calculation was not possible. The V<sub>50</sub> and asymptotic standard deviation estimates were then obtained using a nonparametric method. This method used the three highest velocities that did not perforate with the three lowest velocities that did

perforate. There were 279 firings conducted to obtain the data required for the  $V_{50}$  calculations. Of these, 131 data points from perforating shots could also be used in support of the penetration equation development.

(U) Comparing the perforation capabilities of steel and tungsten, given the same fragment mass against the same tire thickness, demonstrated that tungsten has a lower  $V_{50}$  than steel, more than 100 m/s lower (see Table 1). This is not surprising since tungsten has a higher density ( $17.7 \text{ g/cm}^3$ ) compared to steel ( $7.8 \text{ g/cm}^3$ ).

Table 1. (U) Some  $V_{50}$  Comparisons

Mass (g) [gr]	Tire Thickness (cm)	$V_{50}$ (m/s)			
		Steel		Tungsten	
		Mean	Std. Dev.	Mean	Std. Dev.
0.13 [2]	1.52 Sidewall	550	*	330	6.74
	2.54 Sidewall	704	27.54	471	6.00
	2.54 Between Lugs	N/A	N/A	434	2.20
0.26 [4]	1.52 Sidewall	399	14.16	293	*
	2.54 Sidewall	621	11.07	413	5.94
	2.54 Between Lugs	624	52.52	382	8.73

(U) N/A = 0.13 g between lugs was not tested.

\* (U) Standard Deviation  $V_{50}$  estimate not available, since there was not a zone of mixed results.

#### 4. (U) PENETRATION EQUATIONS

##### 4.1 (U) Penetration Equations Experimental Plan.

(U) Danish (1968, 1973) had already developed penetration equations from experimental data that included steel right circular cylinder (RCC) fragment simulators ranging in mass from 0.32 to 7.78 g (5 to 120 gr) fired against various tire thicknesses. The intent of the experimental design developed for this effort was to supplement the work of Danish with smaller RCC firings, from the  $V_{50}$  work, and with approximately 50 firings of real fragments so that the validity of the penetration equations could be extended to the smaller fragment regime. The mass of the real fragments ranged in size from 0.05 to 0.36 g (0.77 to 5.5 gr). They were fired against the sidewall, lugs, and between lugs. For the development of the penetration equation, the procedure required that all firings produced fragments that perforated the tire sections. Experiments were conducted with different striking velocities so that a range of overmatches was achieved for each fragment mass and target thickness combination.

##### 4.2 (U) Penetration Equations Analysis and Results.

(U) In the 1960s, The Johns Hopkins University developed a set of empirical penetration equations based on steel fragments fired against various materials, including rubber. This effort, called Project THOR (The Johns Hopkins University 1961), predicts residual velocity and residual mass given the following independent variables: target thickness, average impact area of fragment, fragment striking mass, obliquity, and fragment striking velocity. Coefficients were computed for each of the different target materials. The forms of the equations are as follows:

$$V_r = V_s - 10^a (TA)^b M_s^c (\sec \theta)^d V_s^e \quad (1)$$

and

$$M_r = M_s - 10^f (TA)^g M_s^h (\sec \theta)^i V_s^j \quad (2)$$

where  $V_r$  = residual velocity (fps)  $M_r$  = residual mass (gr)  
 $V_s$  = striking velocity (fps)  $M_s$  = striking mass (gr)  
 $T$  = thickness of target (in)  $\theta$  = obliquity angle (deg)  
 $A$  = average impact area (in<sup>2</sup>)  $a, b, c, d, e, f, g, h, i, j$  = empirically determined coefficients.

(U) Danish (1968, 1973) realized that the use of rubber as a target material for tires was inappropriate, since tires have nylon threading in addition to rubber. Therefore, he used the THOR form to update coefficients for the penetration of steel fragments against tires.

(U) Danish claimed that during his experimentation, fragment mass did not degrade when perforating tires. This claim was substantiated in the very early firings conducted as part of the ballistic limit work. Thus, only a residual



velocity penetration algorithm was deemed necessary. The experiments conducted by Danish included 641 fragments with the range of mass size from 0.32 to 7.78 g (5 to 120 gr). Both bias-ply and radial tires were included in the combined data set, since statistical analysis showed they were not significantly different.

(U) Our goal was to augment Danish's data with smaller fragments and to account for fragment material differences. Data for the algorithm development included data from 131 firings that perforated the target in the ballistic limit experiment and 36 additional firings of real fragments along with 641 data from Danish's experiments. This provided a total of 808 data points for the development of a THOR-type penetration equation.

(U) The THOR form (Equation 1) is nonlinear, and the coefficients could be determined using nonlinear least squares. However, the nonlinear least squares simply performs a fit, and it is difficult to test for the significance of the estimators. Except asymptotically, nonlinear regression does not provide the ideal statistical properties of unbiased and minimum variance estimators, as linear regression. Also, there are no exact statistical tests on model parameters for nonlinear regression (Myers 1990).

(U) Although the THOR form is a nonlinear equation, it is intrinsically linear, since it can be transformed into a linear form:

$$\log (V_s - V_r) = a + b \log (TA) + c \log (M_s) + d \log (\sec \theta) + e \log (V_s). \quad (3)$$

(U) Thus, the statistically significant variables and their corresponding coefficients can be estimated through the use of multiple linear regression. The original THOR project conducted by the Johns Hopkins University proceeded in this manner. Variables considered in the current analysis included the original THOR variables, separating the variables thickness and area, and three variables that might account for threat material differences. They are  $K$  = shape factor ( $\text{cm}^2/\text{gm}^{2/3}$ ),  $D$  = density of material ( $\text{g}/\text{cm}^3$ ), and  $E$  = modulus of elasticity (megapascals). However, only one of these three variables is necessary to describe material differences. The correlation between density and modulus of elasticity is 1.00; therefore, we dropped elasticity, since density is an easier variable to obtain. The correlation between density and shape is  $-0.76$  (in log scale). Either one (but not both) could be used in the model. The adjusted  $R^2$  value ( $R^2_{\text{adj}}$ ) using either variable is 0.783.  $R^2$  is the ratio of the variation of the regression sum of squares for a given regression model to the variation of the total sum of squares for a given data set. The closer this ratio is to unity, the more efficient the model is at prediction. The adjustment to  $R^2$  accounts for the degrees of freedom in the model, and thus, allows for proper comparisons among models with different numbers of independent variables. The variance inflation factors, eigenvalues, and conditioning index for shape or density with the other significant variables are well within the rule-of-thumb criteria (Myers 1990) for checks of ill-conditioning. These are measures of correlation between the regressor variable to enter the model and the variables already in the model when performing a stepwise regression procedure.

(U) Shape was chosen over density since shape factor is more intuitive to a vulnerability analyst as an indication of a fragment's ability to penetrate. For example, a rod will perforate a target easier than a sphere of the same mass and velocity. Using shape also meant that a vulnerability analyst would only need typical arena data for fragmenting munitions and would not have to research material properties such as density.

4.2.1 (U) Obliquity. The final form of the tire penetration equation does not include a term for target obliquity, since all firings were conducted at a  $0^\circ$  obliquity. It was felt that obliquity would not be a significant parameter for a "soft" target except for the increase of the target line-of-sight thickness. Danish (1968) had conducted four firings with 3.9-g (60 gr) steel fragment simulators at an obliquity of  $60^\circ$  and came to the same conclusion about the significance of obliquity.

(U) To further investigate the effect of obliquity, sixteen additional firings that perforated the 1.52-cm sidewall target were conducted at a  $45^\circ$  obliquity. Three were steel and 13 were tungsten RCC fragment simulators; both types were 0.26 g (4 gr). Using the penetration equation, a check for consistency was conducted by changing the line-of-sight thickness (by multiplying thickness by  $\sqrt{2}$ ) and using the new model to predict the residual velocity. The standardized residuals are all within  $\pm 2.2$ . Generally, if the residuals are random and within  $\pm 3.00$ , the model is in check.

4.2.2 (U) Real versus Simulated Fragments. Both real and simulated tungsten fragments were included in the data set of 808 points, providing a good opportunity to determine whether there is a significance between the two for developing penetration equations. The total number of 112 tungsten fragments included 45 real and 67 simulated fragments. An indicator variable in the regression analysis revealed that there is no significant difference between real and simulated fragments.

4.2.3 (U) Multiple Barriers. The penetration equations developed under the original THOR project were for perforation of a single target plate. Over the years, the THOR equations have been applied recursively to successive

plates even though the additional plates are beyond the limits of the data from which the equations were generated. Much of the error associated with this practice comes from the fact that fragments are deformed and change shape when they perforate metal plates. Thus, the shape of the fragments at successive plates would be changed from the original.

(U) Bely et al. (1992) showed that, theoretically, implementing a recursive algorithm will not provide an unbiased estimate of the final residual velocity. Their analysis showed that the residual velocity underpredicted approximately 50 m/s for each metal plate perforated. However, tires are "soft" targets, and it was shown via experimentation that fragment mass did not change upon perforation; therefore, it is possible that successive barriers may be handled by the penetration equation in either a recursive fashion or by increasing the thickness term. In an attempt to gain insights into this issue, a small excursion was conducted. Eighteen firings were conducted at the sidewall of an intact tire. These 18 firings resulted in two 0.32-g (5 gr) and five 0.97-g (15 gr) steel fragment simulators that perforated when fired at the 1.52-cm area of the sidewall. The intent was to perforate both sidewalls of the tire and to record striking and residual velocities. The tire was not inflated so that a single tire could be used for this excursion.

(U) The penetration equation was first implemented in a recursive manner to check agreement with the experimental data. The residual velocity computed from the equation after penetration of the first side of the tire was used as the striking velocity for the second tire barrier. The predicted versus observed plot for the final residual velocity revealed no bias in the prediction, and the data fit well around the perfect fit line. When the tire thickness was doubled as input into the penetration equation, the predicted residual velocity consistently overpredicted the actual value. Although this excursion was taken on a very small sample, it does allow us to see that there are no gross errors for recursively estimating a fragment through multiple barriers, when the target is "soft" relative to the fragment.

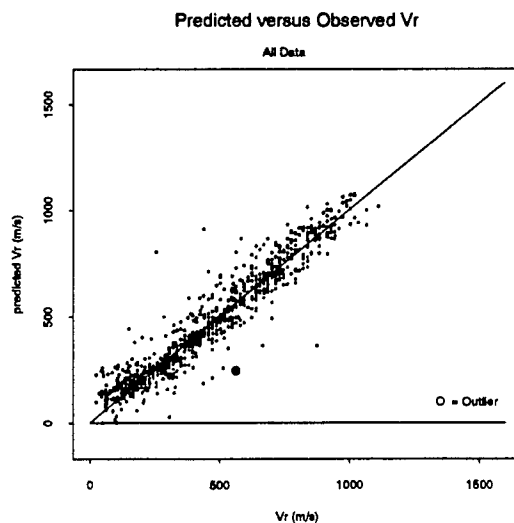
4.2.4 (U) Coefficients and Goodness-of-Fit. The significant variables and their coefficients solved in the linear form were transformed back into the original form as

$$V_r = V_s - 10^{1.479} K^{0.411} M_s^{-0.191} T^{0.732} V_s^{0.350}. \quad (4)$$

(U) The fit of the equation to the experimental data is reasonable as given by an adjusted  $R^2$  of 0.783. The standard error, also known as the square root of the residual mean square error (MSE),  $\sigma_{\log(v_s - v_r)}$ , is 0.102. Both the  $R^2$  and the standard error are comparable to Danish's original fits with values of  $R^2 = 0.752$  and standard error = 0.096.

(U) Figure 1 presents a predicted versus observed residual velocity plot, which shows that there is reasonable agreement between the Equation 4 and the observed data set. If the model were a perfect representation of the data, all points on the graph would fall on the solid, perfect fit line. It is obvious, by inspection, that the points do tend to cluster around the perfect fit line, with slight overpredictions when  $V_r$  is close to 0. (These overpredictions close to 0 can be corrected with the incorporation of  $V_{50}$  to the THOR penetration equations. This is addressed in the expanded ARL report [Grote et al. 1996].) One datum, with a standardized residual of -11.1, is encircled as an outlier. This was also an influential point and therefore was omitted in this final fit. Other points that appear to stray from the perfect fit line have smaller standardized residuals in the logarithmic scale. Omitting them did not substantially change the equation and thus were not highly influential. Therefore, they remained in the data set for the model development.

UNCLASSIFIED



UNCLASSIFIED

Figure 1. (U) Predicted versus Observed Residual Velocity, All Data.

## 5. (U) TIRE DEFLATION AND CTIS PERFORMANCE

### 5.1 (U) Deflation and CTIS Experimental Plan.

(U) The objective of the tire deflation effort was to determine how quickly tires would become inoperable in the absence of a functional tire inflation system. A set firing matrix was not developed prior to initiation of this effort due to the uncertainty of what combination of number of fragment perforations and sizes of fragments would be required to deflate the tires within the time limits prescribed by traditional A-, B-, and C-kills. Traditional A-, B-, and C-kills correspond to time to failure criteria of 5, 20, and 40 minutes, respectively. This, of course, also held true for CTIS performance evaluation.

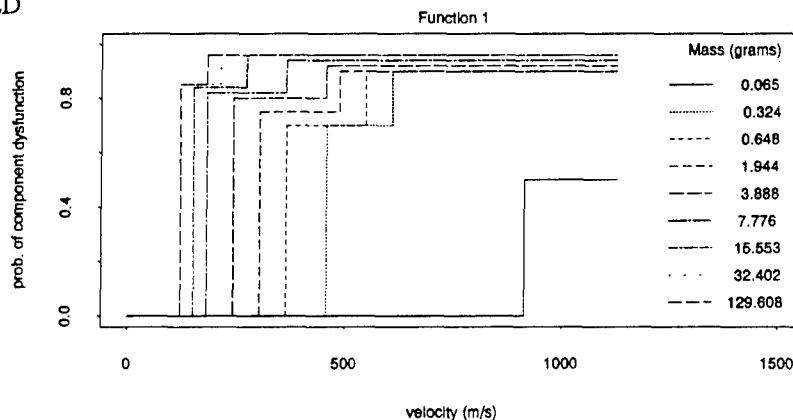
(U) The experimental setups for the tire deflation and CTIS performance work were identical as far as instrumentation and ballistics were concerned. The differences were in the configuration of the BM-21's tire inflation components. In both cases, the front driver's side tire (designated as Tire 1) was used as the target tire. It was decided that the target tire would remain stationary during the firing process for each experiment since Bodt and Schall (1991) showed that motion of a tire was insignificant and otherwise would require a rather sophisticated setup. Furthermore, the vehicle had to remain stationary during the tire deflation time to allow for collection of pressure-time data. A pressure gauge was installed in line with the air hose connected to Tire 1. This allowed for monitoring of the tire pressure before and during experimentation. Guns ranging in size from 5.56 mm to 12.7 mm were used to fire fragments and fragment simulators ranging in size from 0.13 g to 13.4 g. The setup also contained a stripper plate for the plastic sabots used to hold the fragments, two "sky screens" to measure velocity, a steel barrier placed behind the front tire to protect engine components of the BM-21 rocket launcher. Prior to conducting each tire deflation experiment, the CTIS was activated to inflate Tire 1 to approximately 3.2 kg/cm<sup>2</sup> (45 psi). The valve to Tire 1 located in the truck cab was then closed to isolate the tire from the rest of the inflation system. This was done to allow the tire to deflate as if it were on a vehicle that did not have a CTIS.

(U) The evaluation of the CTIS performance required a different valve configuration and required that the engine be running throughout each experiment. All tire valves remained in the open position for each CTIS experiment. The CTIS was configured in this manner to represent the CTIS design currently in use. This effectively meant that all of the tires could deflate if a single tire were perforated.

### 5.2 (U) Tire Deflation Analysis and Results.

(U) The single-tire deflation experiments were conducted to determine the validity of the functions that were being used for tires for describing the probability of component dysfunction given a hit ( $P_{cdh}$ ) at the 40-minute time criterion. These functions are provided as inputs to vulnerability codes for use in determining the probability of causing component dysfunction given a hit by a fragment of a certain size and velocity. If the existing functions were found to be invalid, new functions or models were to be developed that could be implemented in vulnerability codes. The  $P_{cdh}$  functions are "step functions" that correlate fragment mass-velocity combinations to a  $P_{cdh}$  value. Figure 1 graphically represents one of the two-step  $P_{cdh}$  functions. "Two-step" means that for each mass, there are two velocity steps that give different  $P_{cdh}$  values. Note that the  $P_{cdh}$  values provided are for single fragment impact on a single tire. There is no ability to account for the effect of multiple fragment impacts. Also note that this function is indicating that a single fragment as small as 0.06 g (1 gr) has the potential to cause tire dysfunction. It is easy to understand why tires have been shown as being quite vulnerable in many vulnerability analyses.

UNCLASSIFIED



UNCLASSIFIED

Figure 2. (U) An Example of a Step Function for the Probability of Component Dysfunction Given a Hit.

(U) The first assessment of the experimental data collected reveals that the existing functions dramatically overestimate the vulnerability of tires to single fragment attacks. A few experimental results are provided below to illustrate the point about the inadequacy of the existing  $P_{cd/h}$  functions:

1) It took five to six perforations, of a single 14.00 × 20 tire, by 0.26-g (4 gr) steel fragment simulators to deflate the tire within 40 minutes.

2) 25–26 perforations by 0.26-g (4 gr) steel fragment simulators were required for deflation within 5 minutes.

(U) Thus, it was clear that not only were the  $P_{cd/h}$  functions invalid, but a completely new approach would be needed to account for the effects from multiple fragment perforations. The new approach was to develop a model, utilizing regression analysis of the experimental data and engineering calculations, that would calculate tire pressure as a function of time, number of perforations, and fragment size.

(U) Starting with the ideal gas law and experimental results on gas effusion, Equation 5 can be derived (see Grote et al. [1996] for derivation) as

$$P(t) = P(0) e^{-t(\text{constant} \cdot Hn)(R \cdot T/V)} \quad (5)$$

where

$P$ = tire pressure (kg/cm <sup>2</sup> )	$H$ = area of a hole (cm <sup>2</sup> ) (assumes equal size holes)
$P(0)$ = initial tire pressure (kg/cm <sup>2</sup> )	$T$ = absolute temperature (K)
$t$ = time (s)	$R$ = universal gas constant (84.73 kg · cm <sup>3</sup> /mole · K)
$n$ = number of perforations	$V$ = total volume of system (cm <sup>3</sup> ).

(U) The model (5) is based on ideal conditions uncomplicated by irregularly shaped holes of varying depths which can change the nature of the air flow. Experiments do not provide a direct measure of the hole area or shape characteristics. To make a link from the shot conditions of the experiments to the functional description of the tire pressure, a slightly altered version of Equation 5 is used, incorporating the hole area into a new constant  $C$ :

$$P(t) = P(0) e^{-t(C)(R \cdot T/V)}, \quad (6)$$

where

$$C = \{ 0.10205 (\Sigma P_a) + 0.19662 \Sigma (P_a/n)^2 \}$$

and

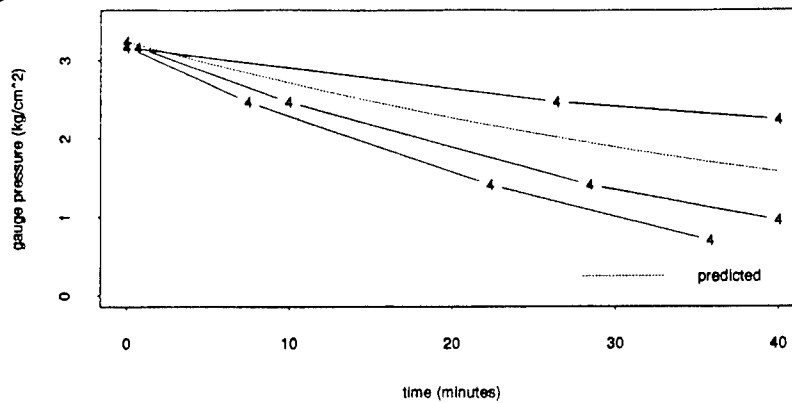
$$P_a = \text{presented area of a fragment at impact.}$$

(U)  $C$  is not a function of the tire volume ( $V$ ), the time ( $t$ ) of the measurement, the initial tire pressure, or temperature. It is the only degree of freedom in Equation 6 for fitting to experimental data, and it is an implicit function of variables related to hole geometry, number of holes, exposed area, and possibly other damage characteristics.

(U) The empirical value for  $C$  starts with the basic exponential equation:  $P_i(t) = P_0 e^{(-t \cdot C_i)}$ . For each of the  $i = 58$  data sets, the  $C_i$  parameter was determined from a regression in logarithmic form:  $\ln(P_i(t)) = \ln(P_0) - t \cdot C_i$ . The  $R^2$  for each was at least 0.95. A common  $C$  was determined for the entire data set based on tire damage characteristics. Mass and shape of fragment do not characterize the damage, but instead the fragment itself. However, the average fragment presented area and the cumulative presented area on the tires do characterize damage. Both are statistically significant in a multiple regression analysis and were included as independent variables. The overall fit for  $C$ , which is forced through the origin, has an  $R^2 = 0.957$ . Figure 3 shows the fit of the Tire Deflation Model (Equation 6) for four fragments, 0.26 g (4 gr) each, perforating the tire. The three replications of the experiment illustrate the amount of experiment-wise variability in the deflation rate.

(U) The data upon which the tire deflation model was based were for fragments of identical size. Experimental excursions were conducted, showing the adequacy of the deflation model for tires of various sizes, for deflation caused by perforation with multiple fragments of various sizes, and for perforation by much larger fragments. A comprehensive discussion of these excursions is presented in Grote et al. (1996).

UNCLASSIFIED



UNCLASSIFIED

Figure 3. (U) Example of Tire Deflation Fit for Four Fragments, 0.26 g Each.

### 5.3 (U) CTIS Performance Analysis and Results.

The capability of an on-board CTIS has never been explicitly modeled in a vulnerability analysis. Thus, additional experiments were conducted to determine the effect a CTIS could have on the ability of fragments to deflate some or all of the tires on the BM-21. After an appropriate engine speed was determined, 45 experimental firings were conducted. Some interesting results that point out the significance of a CTIS are as follows:

- 1) The CTIS was able to maintain the maximum tire pressure in all six tires of the BM-21 when a single tire was perforated 35 times by 0.26-g (4 gr) steel RCC fragment simulators.
- 2) Eleven perforations of a single tire, with 0.97-g (15 gr) steel fragment simulators, caused pressure in all tires to drop to 2.46 kg/cm<sup>2</sup> (35 psi) in 1,227 s (~20 minutes) and 2.11 kg/cm<sup>2</sup> (30 psi) in 2,400 s (40 minutes).
- 3) A single perforation of a tire by a 13.4-g (207 gr) steel fragment simulator, fired from a 0.50-caliber gun, resulted in a rapid drop in pressure that leveled off at about 2.5 kg/cm<sup>2</sup> (38.6 psi).

(U) Experimentation never proceeded beyond the number of perforations mentioned in 2 and 3 above because once the tires were deflated, with those numbers of holes, they could not be reinflated by the CTIS. Since sufficient experimental data could not be obtained to develop an empirical model for CTIS performance, theoretical models were sought.

(U) As a first approximation of the CTIS system, the tires were all assumed to be instantaneously in equilibrium with each other, and one pressure function sufficient for all tires. In effect, there would be one large tire with a volume equal to the sum of the volumes of the individual tires. The reservoir tank which is generally held at ~7.1 kg/cm<sup>2</sup> (100 psi) prior to a leak represented another volume. When the CTIS is set in the inflate mode and the engine speed is constant, the compressor provides a constant number of molecules per unit time to the reservoir.

(U) A reservoir tank for both this model and subsequent more complex models appeared to be unnecessary, since the higher starting pressure almost instantaneously equilibrated with the tire pressures. Inclusion of the tank might be needed if the volume in the tank were not such a small fraction of the tire volumes or if the tank pressure were allowed to rise far beyond a fixed cut-off pressure. Without the reservoir, the air from the compressor is assumed to move directly into the tire compartment.

(U) This simplified model yields a closed-form solution:

$$P(t) = m_1/c - (m_1/c - P_0) e^{-t(c \cdot R \cdot T / V_t)}, \quad (7)$$

<p>where</p> <p><math>P</math> = tire pressure (kg/cm<sup>2</sup>), gauge pressure</p> <p><math>m_1</math> = number of moles/time from compressor</p> <p><math>P_0</math> = initial tire atmospheric (gauge) pressure (kg/cm<sup>2</sup>)</p> <p><math>c</math> = rate constant for air leaking from tires to atmosphere (and is estimated by the regression C-value)</p>	<p><math>t</math> = time (s)</p> <p><math>T</math> = temperature (K)</p> <p><math>V_t</math> = volume of tire (cm<sup>3</sup>)</p> <p><math>R</math> = universal gas constant (84.73 kg · cm / mole · K).</p>
---	---

(U) As long as the leak rate of each tire is small or the damage to each tire is essentially the same, this simplified form gives very satisfactory results. However, when some tires have many holes and some have few or no holes, the individual tires can have quite different pressure histories. Note that if the flow rate from the CTIS ( $m_1$ ) is set to zero in Equation 7, it can be reduced to the tire deflation model. A complete derivation is omitted for brevity.

(U) An extensive effort was put forth in an attempt to try to preserve the simplicity of this closed-form model. We believed the less information required about a target vehicle, the easier implementation would be in vulnerability codes. Selective application of the simplified CTIS model to groups of tires with similar damage and the tire deflation model to tires with extensive damage could not capture the complexity of a flow in which the CTIS compressor air is dynamically allocated according to relative pressures in the tires.

(U) A complex model having separate air lines from each tire to a common junction which then connected to the compressor was proposed. The model was simplified a bit by assuming the hoses connecting the tires to the common junction were all of the same length and had the same flow characteristics. The value of the constant that characterized these hoses was determined by fitting the model to data for which one, two, and three hoses had been disconnected from the tires.

(U) This model leads to a system of seven coupled, first-order, linear differential equations. A closed-form solution is a complicated sum of seven exponential terms and provides no more insight than a solution obtained by numerical methods. The software developed used a simple Runge-Kutta technique to generate pressure histories for each of the seven functions. Systems with a different number of tires can be used in the program by changing the number of tires in the input

$$P_i'(t) = (RT/V_i) [c_h(P_0(t) - P_i(t)) - c_i P_i(t)], \quad i = 1, \dots, n \quad (8)$$

$$P_0'(t) = (RT/V_0) [m_1 - c_0 P_0(t) - \sum c_i (P_0(t) - P_i(t))], \quad i = 1, \dots, n. \quad (9)$$

(U) To use this model, the analyst must be able to provide the number of tires connected to the CTIS, the initial tire pressures, the volume of each tire, deflation constants from the regression formula for each tire, a constant used in characterizing the flow rate from tires to the junction, the compressor capacity in moles of gas per second, the air reservoir volume (not critical — can be approximated), the air temperature, and the atmospheric pressure.

#### 6. (U) REAL BOMBLET EXPERIMENTS

(U) Three real bomblets were provided to the U.S. Army Research Laboratory for the purposes of verifying the results and models already obtained and to provide insight into the bomblet's lethality against wheeled vehicles that have an on-board CTIS. The bomblets were detonated at different locations close to the side of the BM-21 target. General results show an overprediction for one of the experiments, an underprediction for another experiment, and a very snug fit for the third experiment; therefore, no adjustment was made to the model to create a better fit.

#### 7. (U) SUMMARY AND CONCLUSIONS

(U) The ability of small steel and tungsten fragments to perforate tires was fully characterized, for a wide range of tire thicknesses, via the ballistic limit characterizations and the development of a residual velocity penetration equation. A residual mass algorithm was not developed since there appeared to be no erosion of the fragments upon perforation of the tire targets. Small excursions were conducted to determine how target obliquity and multiple target barriers should be handled when applying the residual velocity algorithm.

(U) The issues of tire deflation and the effect of central tire inflation systems were addressed through the development of three models. First, in the absence of a CTIS, Equation 6 should be applied to each tire individually. This equation was developed via theoretical derivation and regression analysis of experimental data. When the vulnerability of a vehicle that has a CTIS is to be analyzed, the complex CTIS model presented in section 5 should be implemented. The simplified model, Equation 7, provides a good representation when the tire damage is minimal or all tires are damaged to "nearly" the same degree. It is a very difficult task to determine how "nearly" should be defined. Additionally, it is difficult to deflate all tires within standard time criteria of 5, 20, and 40 minutes when minimal damage has occurred.

(U) An issue that was not explicitly stated in the introduction, is the extensibility of the work conducted as part of this effort to vehicles other than the BM-21 and the URAL-375. Both the tire deflation and the CTIS models are in a general form that allows for application to any other vehicle. To apply these models to other vehicles, certain parameters about the vehicles must be known. For the tire model in Equation 6, the volume of each tire and the initial tire pressure must be

known. Of course, a minimum tire pressure must also be provided to determine whether a particular tire would be considered nonfunctional. Additionally, the CTIS model requires the number of tires connected to the CTIS, an airflow rate from the compressor and air tanks to the system of tires, and information concerning the connecting hoses.

(U) Another issue for extensibility, which is not so obvious, concerns the use of the penetration equation that was developed. Tire thickness is a major parameter in the penetration equation, yet most target descriptions have tires with uniform thickness profiles. The differences in tire thickness were considerable over the tread and sidewall areas of the BM-21 tires, not to mention variability that exists from tire to tire. This leads one to believe that to accurately apply the penetration equation to any tire, the thickness profile of the sidewall and tread areas will be required. This further implies that the geometric target descriptions of tires will have to be more detailed than those that currently exist.

(U) The series of real bomblet experiments was an unexpected bonus. These experiments clearly pointed out the need for the development of the complex CTIS model and provided data towards the validation of the same model. The experiments also showed that bomblets can cause numerous perforations of tires at "close" distances. The effect of greater ranges from bomblet to target and multiple bomblets was beyond the scope of this effort.

#### 8. (U) REFERENCES

(U) Bely, D., B. A. Bodt, and R. N. Schumacher. "Real Bomblet Penetration Evaluation," BRL-TR-3400, U.S. Army Ballistic Research Laboratory, Aberdeen Proving Ground, MD, September 1992 (UNCLASSIFIED).

(U) Bodt, B., and J. Schall. "Survivable Tire System (STS) Test Analysis: Stage 1 Survivability," BRL-TR-3226, U.S. Army Ballistic Research Laboratory, Aberdeen Proving Ground, MD, 1991 (UNCLASSIFIED).

(U) Chambers, J. M., and T. J. Hastie. "Statistical Models in S," Wadsworth & Brooks/Cole Advanced Books & Software, AT&T Bell Laboratories, Pacific Grove, CA, 1992 (UNCLASSIFIED).

(U) Danish, M. B. "Perforation of Truck Tires by Compact Steel Fragments," BRL-MR-1926, U.S. Army Ballistic Research Laboratory, Aberdeen Proving Ground, MD, 1968 (UNCLASSIFIED).

(U) Danish, M. B. "Perforation of Radial Truck Tires by Compact Steel Fragments," BRL-MR-2269, U.S. Army Ballistic Research Laboratory, Aberdeen Proving Ground, MD, 1973 (UNCLASSIFIED).

(U) Grote, R. L., L. L. C. Moss, and E. O. Davisson. "New Tire Penetration and Pressure Models for Improved Vulnerability Analyses of Wheeled Vehicles," ARL report in publication, 1996 (UNCLASSIFIED).

(U) Joint Technical Coordinating Group for Munitions Effectiveness. "Joint Munitions Effectiveness Manual-Surface to Surface, Fragmentation and Terminal Effects Data for Surface to Surface Weapons," JTCG/ME-61S1-3-4, Revision 1, July 1982 (UNCLASSIFIED).

(U) McKaig, A., and J. Thomas. "Maximum Likelihood Program for Sequential Testing Documentation," BRL-TR-2481, U.S. Army Ballistic Research Laboratory, Aberdeen Proving Ground, MD, 1983 (UNCLASSIFIED).

(U) Myers, R. H. Classical and Modern Regression with Applications, Second Edition, PWS-Kent Publishing Company, Boston, MA, 1990 (UNCLASSIFIED).

(U) The Johns Hopkins University. "The Resistance of Various Metallic Materials to Perforation by Steel Fragments; Empirical Relationships for Fragment Residual Velocity and Residual Weight (U)," Project THOR Technical Report, No. 47, for the Ballistic Analysis Laboratory Institute for Cooperative Research, April, 1961 (UNCLASSIFIED).

(U) U.S. Army Materiel Command. "Experimental Statistics - Section 2 - Analysis of Enumerative and Classificatory Data," AMC Pamphlet 706-111, 1969 (UNCLASSIFIED).

(U) U.S. Army Materiel Development and Readiness Command. "Selected Topics in Experimental Statistics With Army Applications," DARCOM Pamphlet 706-103, 1983 (UNCLASSIFIED).

(U) USSR. "Model URAL-375D Truck," Service Manual Seventh Edition, USSR, Moscow, undated (UNCLASSIFIED).

(U) Warner, D. R. "Ground Transport Vehicles (Current and Projected)—Eurasian Communist Countries," DST-1150S-280-87, Foreign Science and Technology Center, Charlottesville, VA, 1987 (UNCLASSIFIED).

# UNCLASSIFIED

## RESIDUAL CAPABILITY ANALYSIS OF A WHEELED VEHICLE FOLLOWING SMALL FRAGMENT DAMAGE (U)

Stephanie S. Juarascio  
James E. Hunt  
U.S. Army Research Laboratory  
Aberdeen Proving Ground, Md 21005-5066

### ABSTRACT (U)

(U) This paper highlights the use of recent advancements in the modeling of fragment effects for assessing damage to wheeled vehicles.

(U) The development of new tire penetration and pressure models by the U.S. Army Research Laboratory (ARL) has resulted in significant advances in the capability to accurately model the vulnerability of wheeled vehicles to small fragments. These models have been embodied within the ARL's Stochastic Analysis of Fragment Effects (SAFE) approximation method. SAFE has been implemented under the Modular Unix-Based Vulnerability Estimation Suite (MUVES) environment. SAFE has been used to predict damage to wheeled vehicles following interaction with fragments generated from one or multiple fragmenting munitions. Some comparisons of SAFE results with field experiments will be presented.

(U) Traditionally, a loss in wheeled vehicle mobility has been assessed given the loss of some combination of tires. Existing truck performance data suggest that flat tires may not prevent the vehicle from moving but instead limit its maximum controllable speed and the maximum distance over which it may be driven. Available data from truck performance tests and recommended travel speeds given reduced tire pressures have been used to develop criteria upon which to base estimates of top speed given tire damage.

(U) This paper discusses the vulnerability modeling process, the application of the experimentally and theoretically derived tire penetration and pressure models, and the use of existing data to assess reduced capability of a damaged vehicle to move. Implications for the use of this vulnerability data within force level and effectiveness models will be presented within the context of the general findings of wheeled vehicle vulnerability studies.

### (U) INTRODUCTION

(U) Vulnerability has been described as the characteristics of a system that cause it to suffer a loss or reduction in capability as a result of having been subjected to a hostile battlefield environment. Until recently, tire vulnerability has been modeled as the dominant characteristic causing loss of mobility in wheeled vehicles normally operating within the range of hostile artillery. New experimental data suggest that this may not be true. The focus of this paper is how new methodology for assessing tire damage can be used to support an assessment of the potential for reducing top speed of a wheeled vehicle.

(U) The Survivability Lethality Analysis Directorate (SLAD) of the U.S. Army Research Laboratory (ARL) conducted an experimental program in 1994 that resulted in new physically based, mathematical models which provide a solid basis for predicting perforation of small steel and tungsten fragments through tires and for predicting pressure-time histories of damaged tires on vehicles with and without central tire inflation systems (CTIS). Results of these experiments indicated that to deflate a single typical truck tire within 40 minutes, 5-8 perforations by small fragments would be required. The experimental data also showed that a CTIS can have a profound affect on the amount of damaged required to deflate all connected tires (ref. 1). These data implied that probability of kill functions used in

UNCLASSIFIED



## UNCLASSIFIED

previous studies significantly over-estimated the lethality of a single fragment against a tire. The new tire vulnerability models developed from this experimental effort have been incorporated into SLAD's best methodology for analyzing fragment effects, the Stochastic Analysis of Fragment Effects (SAFE) model (ref. 2).

### (U) Vulnerability/Lethality Methodology Background

(U) Standard effectiveness data developed utilizing Joint Technical Coordinating Group for Munitions Effectiveness (JTCG-ME) methods are generated from data based on single-fragment, expected-value models such as the Vulnerability Analysis of Surface Targets (VAST) (ref 3). Vulnerable Area ( $A_v$ ) data generated using VAST were intended to describe the lethality of a single fragment against a component. The generation of single-fragment  $A_v$ s is not a straightforward process that explicitly models the physical processes involved in a damage event. Effectiveness models employing the use of  $A_v$ s include the Matrix Evaluator Computer Program, and Complex Targets Computer Program (ref. 4,5,6). These models utilize  $A_v$  data to assess a probability of achieving various types of system level kills, standards for which have been defined by the JTCG-ME (ref. 7). Ultimately, what is provided to both the high-resolution Training and Doctrine Command (TRADOC) Analysis Center's battle model CASTFOREM (ref. 8) as well as the simple fractional damage effectiveness model ARTQUIK (ref. 9) is a quantity called a lethal area (ref. 10). Lethal area, which is used to quantify a system level kill, is often used to determine parameters for the Carleton damage function. The Carleton function, an exponential square fall-off function, is used to perform an assessment of the outcome of a target/threat interaction. The use of the single-fragment methodology which serves as a basis for these techniques does not provide an accurate burst point assessment. Although single-fragment, expected-value techniques introduce significant error into the development of data intended for burst point assessment, the task of modeling target-damage/loss-of-capability resulting from potentially thousands of fragment impacts could not possibly have been accomplished on the computers of the 1960's using the simulation techniques that can be used today.

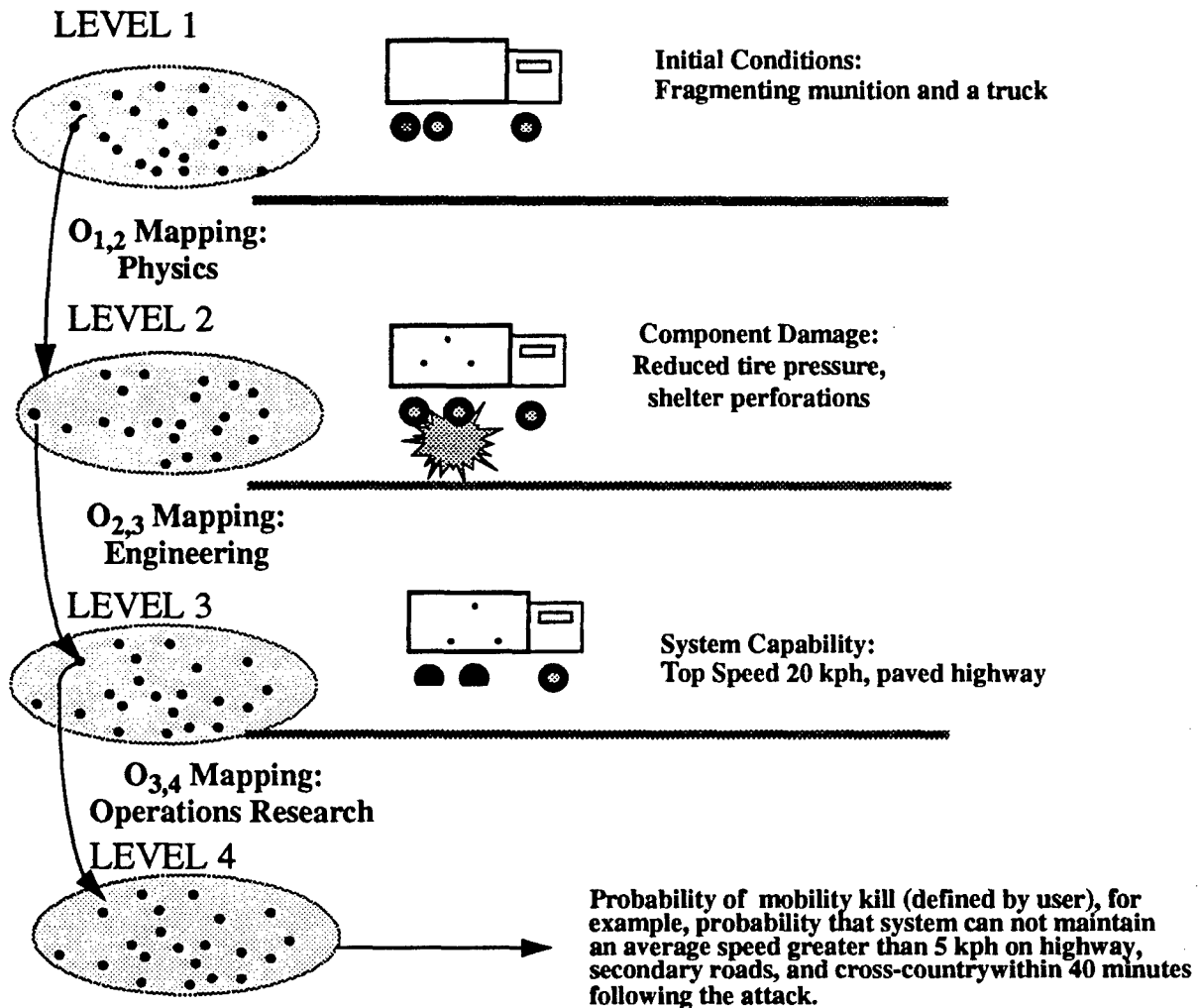
(U) The vulnerability/lethality (V/L) Taxonomy was first introduced by Deitz in the late 1980's to clarify the process of vulnerability modeling and is composed of the four levels depicted in Figure 1 (ref. 11,12). Each level is composed of points, a point representing a vector of information. Level 1 contains vectors describing the initial target/threat conditions. Level 2 contains component damage state vectors. Level 3 contains vectors describing system capability. Each point at each level is comparable to a real world event. Points are mapped sequentially from one level to the next using stochastic operators. Levels are not composed of probabilities, although the information within each level might be used to assess a probability. SAFE has been implemented to analyze the vulnerability of a truck to fragmenting munitions. This process resulted in the development of Level 2 damage vectors which were then used to assess remaining system capability.

### (U) SAFE MODEL DEVELOPMENT

(U) The Stochastic Predictor of Artillery Effects (SPRAE) model, the predecessor of SAFE, was developed to provide the capability to stochastically analyze effects of fragmenting munitions and to support live-fire pre-shot estimates. It combined and improved on existing methodologies from the VAST program and the Surface-to-Air Missile Site Mean Area of Effectiveness (SAMSMAE) program (ref. 13). These latter deterministic models divided the vulnerability process into a calculation of component  $A_v$  for a set of attack directions followed by burst point and lethal area analysis using  $A_v$ s.  $A_v$ s were produced using parallel rays for a spectrum of fragment masses and velocities. The SPRAE model corrected deficiencies in the  $A_v$  approach by calculating component probability of kill ( $P_k$ ) values directly at a specified burst point using radially emanating ray-tracing techniques. Rays were produced prior to generating initial fragment distribution. Each ray could contain multiple, partial or no fragments. Since component  $P_k$  values were calculated for each ray and the survivor rule summed over all rays, no multiple hit damage methodology was possible.

(U) The SAFE model enhances fragment analysis by explicitly modeling fragment trajectories and allows the capability to simulate and evaluate component damage resulting from multiple fragment impacts. This approach has allowed for the incorporation of physically based component damage models that require fundamental target/threat interaction information such as the number, size, and locations of holes in a component. SAFE provides a stochastic approach for vulnerability modeling which is superior to the previous approach. It has been implemented under MUVES, which provides use of Boolean operators for fault tree modeling of system capability (ref. 14).

UNCLASSIFIED



UNCLASSIFIED

Figure 1. (U) Abstraction of the Vulnerability Process

**(U) SAFE Model Comparisons to Field Experiments**

(U) Level 2 vulnerability metrics produced using SAFE have been compared to data obtained through experimentation and testing. Some of these results are presented here. Comparative efforts are currently on-going.

(U) A variety of fragment data has been collected and compared to predictions made with SAFE. Three experimental shots were fired in which a fragmenting munition was detonated at 1) one foot from the center of the rear tires of a truck, 2) six inches from the middle tire, and 3) three feet from the center of the front and rear tires (Table 1). Data collected during these experiments included the number of fragment perforations through tires, residual tire pressure as a function of time and number of perforations through aluminum plates at distances of approximately 20 and 30 feet.

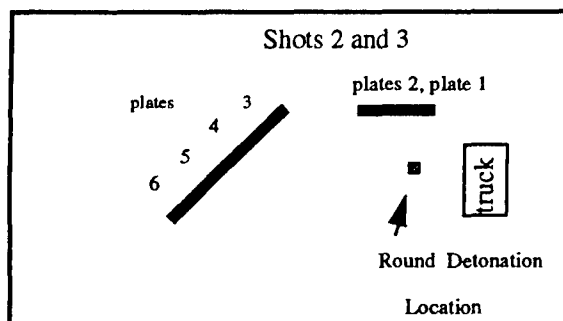
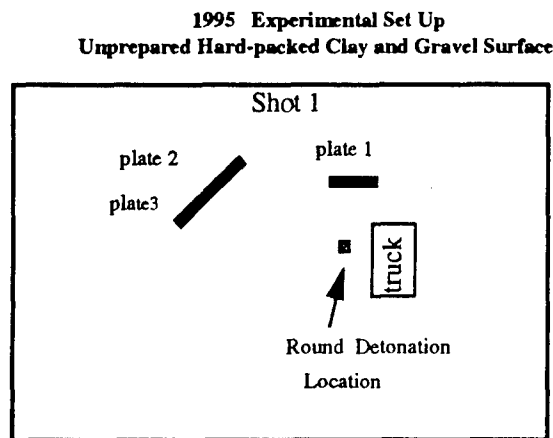
(U) Comparison to empirical data indicated that SAFE predictions of perforations through tires were good, with the observed number falling within one standard deviation of the predicted mean in all but two of nine tires. In each of these two cases, the predicted mean was slightly higher than the observed (Table 1: shot 1 - rear tire and shot 2 - middle tire). In these two cases, the number of holes counted is probably somewhat smaller than actual since perforations caused by small fragments are difficult to find. Tire deflation data were also compared to the prediction of the new tire deflation algorithm. These comparisons showed good agreement across trends (ref. 1). It was suspected that the hard-packed clay and gravel detonation surface caused fragment ricochet and flying debris which increased the number of

# UNCLASSIFIED

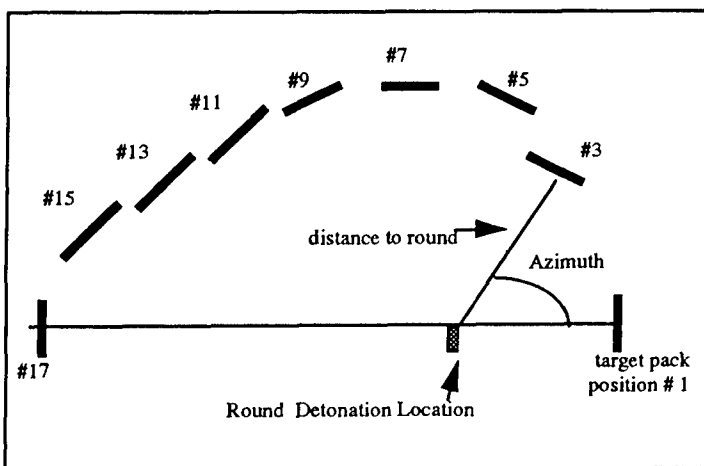
impacts and perforations through aluminum plates above what was predicted as shown in Table 1. Comparison to data collected on a prepared surface supports this presumption by showing good agreement to data obtained during a fragment damage demonstration conducted in 1990. These demonstration tests consisted of an arena of aluminum target packs placed at different distances from the round detonation location. In these arena tests, the round was detonated on a prepared plywood surface. As shown in Table 1, the observed number of holes (prepared surface) is within one standard deviation of the mean assessed from the distribution of outcomes predicted by SAFE. Additional data are being collected which will facilitate the investigation of the differences in predicted and data observed in the 1995 experimental set up.

UNCLASSIFIED

Table 1: (U) SAFE Predicted vs. Observed Number of Holes in Aluminum Plates



1990 Fragment Tests on Prepared Plywood Surface



Passenger Side Tires:	Holes in Tires	
	Predicted Mean, Sigma	Observed Number
Shot 1		
front	1.4, 1.1	1
middle	38.7, 5.2	35
rear	38.9, 4.3	32
Shot 2		
front	2.1, 1.4	0
middle	118.6, 6.7	91
rear	13.6, 3.2	13
Shot 3		
front	6.8, 2.3	5
middle	23.9, 3.3	26
rear	2.8, 1.6	2

Distance to Plate Number:	Round (ft)	Holes in Aluminum Plates	
		Predicted Mean, Sigma	Observed Number
Shot 1			
1	20	3.1, 1.6	33
2	30	1.3, 1.1	19
3	30	1.3, 1.4	9
Shot 2			
1	20	3.3, 1.6	11
2	20	7.2, 2.3	25
3	30	1.7, 1.2	9
4	30	1.6, 1.2	no data
5	30	1.8, 1.3	5
6	30	1.8, 1.3	2
Shot 3			
1	20	4.4, 1.8	10
2	20	4.7, 1.9	5
3	30	1.4, 1.1	8
4	30	1.2, 1.0	4
5	30	1.5, 1.2	9
6	30	1.6, 1.2	9

Arena Position (#), Distance to Round (ft)	Holes in Target Pack	
	Predicted Mean, Sigma	Observed Number
1, 10.8	10.8, 2.8	13
3, 18.7	8.9, 2.4	7
5, 24.3	5.9, 2.2	6
7, 24.9	5.9, 2.0	6
9, 28.5	4.6, 2.0	5
11, 29.5	4.5, 2.0	3
13, 31.2	4.0, 1.8	4
15, 35.4	3.3, 1.7	2
17, 44.0	2.1, 1.4	1

UNCLASSIFIED

UNCLASSIFIED

## UNCLASSIFIED

### (U) APPLICATION OF SAFE TO ASSESS WHEELED VEHICLE DAMAGE AND CAPABILITY

(U) The vulnerability process begins with a description of the target and the threat. A geometric computer model of the URAL-375D six-wheeled vehicle was developed from an actual vehicle using the Constructive Solid Geometry (CSG) technique. The CSG model consists of simple geometric solids combined together with Boolean operators to create complex three-dimensional objects. The threat is characterized by its elements that cause lethal effects against an enemy target. In the analysis of the fragment damage to the vehicle, required elements include fragmentation characteristics and fragment penetration capabilities. The fragment characterization provides basic statistical information that permits the modeling of fragment trajectories, masses, and velocities. Fragment penetration capability is described using penetration equations that provide the means to determine penetration through various barrier materials of the CSG model and to assess residual fragment mass and velocity.

(U) Penetration equations form one of the basic elements needed to complete the  $O_{1,2}$  mapping. The other basic element required to complete the  $O_{1,2}$  mapping is a model which describes the response of critical components given interaction with a damage mechanism; in this case, a fragment or a number of fragments. Typically this is done using a probability of component dysfunction assessment which relies on the use of component kill criterion. Component kill criteria have traditionally been developed for the case where a component is hit by a single fragment. The data and analysis emerging from the tire vulnerability investigation showed that the use of single fragment kill criterion is invalid for tires. The tire investigation showed that a single fragment even as large as 200 grains can not "kill" the tire tested when a CTIS is used to reinflate the damaged tire. Because fragmenting munitions generate multiple fragments, however, the possibility exists that a tire may be exposed to multiple fragment impacts generated from either a close-in burst or from a number of rounds detonating at some range from the target. Given multiple fragment perforations, the residual tire pressure may drop to unacceptably low levels.

(U) What is an "unacceptably" low tire pressure? This depends upon the circumstances such as whether the truck is traveling on the highway or in snow where recommended tire pressures vary considerably, 3.2 kg/cm<sup>2</sup> and 0.5-0.7 kg/cm<sup>2</sup>, respectively. As long as the truck can still move with some speed, it does not meet the criterion for a standard "Mobility kill." It may not, however, be able to travel at top speed with reduced tire pressure. The ability to model the physical phenomena associated with a tire damage event provides a mechanism for allowing a more detailed look at the potential for degrading the vehicle's top speed. Use of the old single fragment kill criterion did not provide such a basis. This also holds true for modeling of leaker systems such as fuel tanks. The old single fragment methodology did not provide a means for measuring the residual capacity of the fuel tank due to fragment perforations. The new leaker methodology which has been incorporated into SAFE provides a physical basis for performing these transformations or mappings. A reduction in fuel capacity (a Level 2 metric) can then be related to a maximum run time or travel distance (a Level 3 metric). Both reductions in speed and travel distance can be used within the context of a battle model to logically determine the system's battlefield utility. When battle modeling is not the end use of vulnerability estimates, quantifiable, and measurable thresholds at Level 3 can be used to assess a "battlefield kill." This would result in the specific quantification of what is meant by "kill". The most fundamental flaw in the older vulnerability processes was the use of expected loss-of-function values as probabilities within battle models and to support decision making processes. Quantification of thresholds specifying a precise definition of what is meant by a "kill," and an assessment of the frequency with which these thresholds are achieved through the use of stochastic modeling, provide a means for assessing a true probability of kill. Explicitly accounting for fragment damage to components within SAFE has opened a new avenue of approach for performing vulnerability analyses.

(U) **Level 1 Initial Target Conditions:** The Russians are known to be the world leaders in off-road mobility, which in part has been achieved through the use of the CTIS and the development of tire technology for running tires at very low tire pressures (ref. 15, 16). The top speeds shown in Table 2 were obtained from system engineering specifications pertaining to the maximum permissible tire-inflation pressures for typical Russian wheeled vehicles which utilize variable tire pressures to maximize off-road mobility. Because the response of the system to damage depends upon its configuration, initial conditions must be defined. Typically, a CTIS is off and only turned on for a period of time to adjust tire pressure. For the purpose of this example, the CTIS is off at the time of the target/threat interaction. This is the best case configuration for vehicle survivability. Fragment damage occurring to the air tanks given that the system is open (either inflating or deflating the tires) would result in a rapid loss of air pressure throughout the system as has been observed (ref. 1).

UNCLASSIFIED

# UNCLASSIFIED

UNCLASSIFIED

**Table 2: (U) Recommended Top Speed for a Russian Vehicle with CTIS**

Terrain Conditions	Tire Inflation Pressure: kg/cm <sup>2</sup> (psi)	Top Speed (km/hr)
Paved Highway	3.2 (45)	75
Secondary Roads- gravel or crushed stone	2.5 (35)	60
Wet earthen roads or dry ploughed land	1.4-1.7 (20-25)	20
Dry loose sand	0.7-1.2 (10-17)	20
Water covered grassland	0.5-0.7 (7-10)	10

UNCLASSIFIED

**(U) Mapping from Level 1 to Level 2 :** Residual tire pressure depends upon the number and size of tire perforations and the status of the CTIS. Details of the algorithm are presented in a companion paper (ref. 17). Modeling the use of the CTIS to reinflate or maintain pressure in the tires following damage requires assumptions regarding the reaction of the crew. For this example, it will be assumed that the crew will react to a loss in tire pressure (observable from a gauge in the cab of the vehicle) by turning on the CTIS. However, it will also be assumed that the crew will not turn on the CTIS in the event that the air tank has been perforated (also observable from a gauge in the cab). Damage to the CTIS air compressor and air tanks is evaluated in a binary fashion, and as such these components are either "killed" or "not killed." In order to evaluate the residual tire pressure, damage to these components must first be evaluated. If the air tank and compressor are still operable, the CTIS algorithm provides tire pressure as a function of time following the ballistic event. If the air tank or the air compressor is killed, CTIS capacity is set to zero. Setting CTIS capacity to zero is equivalent to having no capability to inflate the tires. The new tire deflation algorithm provides an assessment of residual tire pressure for each tire as a function of time for the cases with and without CTIS capability.

**(U) The CSG model of the truck includes components and structures of the engine, the fuel system, the transmission, the CTIS, the suspension, the steering system, the brake system, the starter system, the mainframe, the cargo bed, the cab, and associated vehicle structures.** Like the air tank and compressor, most critical components are evaluated in a binary fashion: "killed" or "not killed." The exceptions are the tires, which are evaluated in terms of residual tire pressure, and the fuel tank, which can be evaluated in terms of its residual capacity. In the analysis of damage states resulting from fragment impact or perforation, usually those components typically thought of as non-critical, such as the vehicle skin, shelter skin, or cargo bed, are considered only in terms of the shielding they provide to critical components. SAFE can be used to assess damage to these types of components for input to special studies. Such an example is on-going work that SLAD is doing to develop techniques to analyze the penetration of chemical agents through fragment-generated holes in U.S. communications shelters.

**(U) Level 3 Metrics for Truck:** A measure of the engineering capability that the system possesses is provided at Level 3. By definition, a Level 3 metric must be observable, quantifiable, and measurable. For instance, the loss of a cooling system may result in an overheated engine which can cause engine shutdown (if only temporarily). This translates to a loss of capability at Level 3 (speed is reduced to zero). This specific loss of capability can be mapped into the Level 4 loss of mobility as traditionally defined: the system is incapable of performing controlled movement. Level 3 metrics for a truck have been defined to fall within three basic capability categories: Move, Function, and Communicate. An example set of Level 3 metrics within each of the categories for a basic truck follows:

<b>Move:</b>	<b>Maximum speed</b>	<b>Communicate: Transmit/receive voice communications</b>
	<b>Maximum travel distance</b>	
	<b>Minimum turning radius</b>	<b>Function: Maximum load capacity</b>
	<b>Minimum stopping distance</b>	<b>Maximum towed load capacity</b>
	<b>Maximum negotiable grade</b>	

UNCLASSIFIED

## UNCLASSIFIED

(U) The tire deflation algorithm provides a means for assessing residual tire pressure (the  $O_{1,2}$  mapping) and engineering specifications (shown in Table 2) and provides a means for assessing a reduction in maximum speed ( $O_{2,3}$ ) given reduced tire pressure. The precision with which residual tire pressure is mapped into maximum speed is limited by the level of granularity associated with the mapping operator. The granularity associated with the Level 3 entity "Maximum speed" was specified to be: 75 kph (at tire inflation of 2.5-3.2 kg/cm<sup>2</sup>) which represents no degradation in maximum speed; 60 kph (at tire inflation of 1.7-2.5 kg/cm<sup>2</sup>); 20 kph (at tire inflation of 0.7-1.7 kg/cm<sup>2</sup>); 10 kph (at tire inflation of 0.5-0.7 kg/cm<sup>2</sup>); and 5 kph (at tire inflation less than 0.5 kg/cm<sup>2</sup>). These speed "bins" were defined on the basis of recommended tire inflation levels with the exception of the 5-kph bin which was based on data obtained at Aberdeen Test Center (ref 16).

(U) Although damage to other critical components may degrade other capabilities within the Move category, critical component damage is modeled only to the level that damage is determined to either result in the loss of subsystem function or not. For example, while a bent steering rod might degrade turning radius and/or reduce maximum speed, this level of damage may not result in a loss of capability to steer. Furthermore, this type of damage is not expected to occur as a result of fragment damage. A fragment may clip a steering rod, either cutting it or cutting it to the point where its use will cause it to break. Such damage would be mapped into a total loss of capability to steer the system. Loss of the steering system maps into Level 3 as a total loss in the capability to make turns of any radius, which subsequently maps into traditional loss of mobility at Level 4 (system can not perform "controlled" movement on the battlefield although it may have the capability to accelerate and decelerate). A prerequisite to achieving a finer level of granularity at Level 3 is the development of a finer  $O_{1,2}$  mapping operator which considers the potential for damage which does not result in the total loss, but rather a degradation in capability. Currently, SAFE provides a precise  $O_{1,2}$  operator which permits the evaluation of damage to leakers such as the fuel system, cooling system, and lubrication system. Through the use of detailed target geometry modeling and explicit ray-tracing, SAFE also provides the capability to evaluate damage to small individual components supporting the function of such systems as the engine. Loss of or damage to some components of the engine such as spark plugs or pistons may result in a degradation to engine power, which may result in a reduction in speed as well as a reduction in the maximum negotiable grade. The level of detail that the analyst must go to should be decided on the basis of the types of damage expected by the threat mechanisms. In the case of fragmenting munitions, it is not at all likely that a piston or combinations of pistons will be the only major components of the engine damaged since a direct or close-in hit will likely result in collateral damage to other engine components. From distant burst points, there may be some small probability that a fragment may damage one of these components in isolation, which could perhaps result in some amount of degradation to the engine. Currently, there is work on-going within SLAD to consider how damage to components of different types of engines may degrade rather than kill engine functioning. Because the likelihood of degrading the engine with small fragmenting munitions is small, expending significant levels of effort to precisely map loss of engine power as a function of or damage to engine components may not be necessary. On the other hand, the vulnerability of fluid reservoirs of the cooling system, lubrication system, and fuel system are of significant concern due to the likelihood of fragment perforation. Loss of fluid will affect the functioning of the system as a function of time. The next step in the development of Level 3 metrics is to exploit the use of the SAFE to model degradation to the capability of a truck to move as a function of time following the damage event. Given the current mapping operators which are in place, a more accurate description of the Level 3 entities which can be analyzed under the move category is as follows:

Move:	Maximum speed
	Maximum travel distance
	Capability to turn (more granular description of turning radius)
	Capability to stop (more granular description of stopping distance)

(U) Maximum negotiable grade (or some less granular description of this capability) has not been included in the above list since there are currently no operators defined for assessing a loss of this capability. Loss of such a capability would be inherent given a maximum speed of zero or a maximum travel distance of zero. The above quantities can currently be assessed for specified points in time following an attack. Multiple time points may be assessed as desired. Maximum speed is set to zero given loss of the engine, transmission, suspension, or crew. When damage occurs to the tires only, a reduction in speed can be assessed according to the speed bins previously prescribed. Discussion on the modeling and granularity of capability to carry and/or pull a load and to communicate is the subject for another paper.

UNCLASSIFIED

# UNCLASSIFIED

(U) Consider some example results in which fragment damage to the URAL-375D is mapped into remaining capability using stochastic modeling. Each assessment will be made at a single point in time, 40 minutes after the target/threat interaction. Given a specific burst point of a round, the first damage assessment process might yield four different Level 2 results. First, no critical components were damaged or killed other than a brake line and tires. Damage to the brake line resulted in a kill of the braking system, and tire damage resulted in a maximum sustainable tire pressure of 1.5 kg/cm<sup>2</sup>. Tire damage maps into Level 3 as a reduction in maximum speed = 20 kph, and the loss of the braking system maps into a loss in the capability to stop the vehicle. Consider the same initial conditions again, and because of the stochastic nature of the event, the damage assessment may yield a slightly different result: 1) the fuel filter was killed, 2) the CTIS air tank was perforated, and 3) tire damage resulted in a maximum sustainable tire pressure of 1.4 kg/cm<sup>2</sup>. Mapping this damage vector from Level 2 to Level 3 yields: maximum speed = 0 kph and maximum travel distance of zero. A third damage vector also provides different results: fragment damage to the fuel tank results in loss of fluid and loss of fuel tank capacity (from 250 liters to 125 liters). This damage maps into a Level 3 reduction in maximum travel distance of 1/2 (or approximately 170 km). A fourth damage vector might produce no damage, which translates into no loss in capability at Level 3. This process can be continued over X-iterations from which the frequency of occurrence of the various damage vectors is assessed as shown in Table 3. This process could also be repeated for a number of initial conditions at Level 1 to further populate the space at Level 2 and Level 3. The distribution of results might then be drawn on by the operational modeling community to support battle modeling and acquisition decisions.

UNCLASSIFIED

Table 3: (U) Example Level 3 Outcomes and Probability Assessment

Capability Vectors/Distribution						
Wheeled Vehicle Capability	vector 1	vector 2	vector 3	vector 4	vector 5	vector 6
Maximum Speed (kph)	20	0	0	75	20	75
Maximum Travel Distance (km)	350	0	170 km	350	350	350
Capability to turn	not lost	not lost	not lost	not lost	not lost	not lost
Capability to stop	lost	not lost	not lost	not lost	not lost	not lost
frequency of occurrence is used to assess probability, P(V#)	0.60	0.10	0.10	0.10	0.06	0.04
cumulative probability	0.60	0.70	0.80	0.90	0.96	1.00

UNCLASSIFIED

## (U) EFFECTIVENESS AND FORCE-LEVEL MODELING IMPLICATIONS

(U) Traditionally, a loss in wheeled vehicle mobility has been assessed to occur given the loss of any major subsystem critical to its capability to move, including the engine, the fuel system, the cooling system, the lubrication system, the steering system, the transmission, the tires (or some combination of tires), and the crew (at least one member of the crew is required to drive the vehicle). The loss of mobility has been defined to mean that the vehicle is "incapable of performing controlled movement on the battlefield." To support such an assessment, component kill criteria are selected specifically to perform this mapping (a Level 2 to Level 4 mapping). Component kill criteria and component contribution to mobility may be weighted using scenario considerations. Data developed in this way have a very limited range of applicability yet are typically used to support a wide range of analytical studies. The development of Level 2 and Level 3 vulnerability data provides the means for building a base of data which does not contain inappropriate perturbations.

(U) One example of how Level 3 vulnerability data may be used is in direct support of evaluating required operational capabilities of a major weapon systems. The "survivability move" is a requirement that has been established for some major U.S. systems and is defined in terms of how fast and over what distance the system must be able to move. Vulnerability assessments of maximum speed and maximum distance provide the information that a decision maker needs to evaluate this requirement. The difficulty is that speed and distance of the vehicle may be affected by more than vehicle damage. Terrain may influence the speed with which the system may move. Thus it must be considered. The most efficient way to factor such elements into an evaluation is through the O<sub>3,4</sub> mapping process.

UNCLASSIFIED

# UNCLASSIFIED

(U) **Establishing a Threshold for Kill at Level 3 Data:** Users of vulnerability data that rely on the use of a single estimate, such as the probability of mobility kill,  $P(M)$ , can obtain this information from Level 3 vulnerability data. The problem with such an approach is that there may be a multitude of outcomes at Level 3 that the user is not prepared to deal with, and the bottom line is that as customers, these modelers may still want the standard mobility and function/firepower kill estimates. These assessments can be made from the data at Level 3 simply by defining threshold values, at Level 3 instead of Level 2, at which system capabilities map into the standard kill definitions. As noted earlier, loss of the capability to turn the truck would map directly into the standard definition of mobility kill as do maximum speed and maximum travel distance of zero. However, loss of the capability to stop a wheeled vehicle may not be included in the mapping to mobility kill because this capability has not traditionally been thought of as an important one. While true in some cases, the conduct of military operations in the mountains would add a certain significance to this capability. Maximum speed and maximum travel distance present the problem that there may be some Levels above absolute zero which could map into a mobility kill. But here, the user is required to make a conscious decision regarding the most appropriate modeling decision for the set of circumstances that he or she is required to assess. Once a kill is "quantified" to mean, for example, a reduction in speed to less than 10 kph and a maximum travel distance of less than 12 km, the probability of occurrence can be assessed from the data in Table 3 to be  $P(M) = P(\text{vector } 2) + P(\text{vector } 3) = 0.20$ . Furthermore, if reduction in speed to less than 10 kph, maximum travel distance of less than 12 km, and a loss the capability to stop are used to assess a mobility kill,  $P(M)$  can easily be updated:  $P(M) = 0.20 + 0.60 = 0.80$ .

(U) **Averaging over Possibilities:** Now consider a scenario such as described in Table 4 in which the composition of the road network and average traveling speeds on different roads types have been specified. Evaluation of reduced speed given tire damage within the context of a specific scenario can be used to develop a weighted  $P(M)$  on the basis of some user-specified criteria. For example, vector 1 in Table 3 shows a residual capability to travel at a maximum speed of 20 kph, which exceeds the average required for trails and off-roads. It does not meet the required average for primary roads, so a wheeled vehicle could be scored as a kill in both scenario 1 and 2.

UNCLASSIFIED

**Table 4: (U) Road Network Composition and Average Speed on Various Terrain Types for Undamaged Truck**

Percentage of Road Network Composition (%), Average Travel Speed (kph)				
Scenario	Primary Roads	Secondary Roads	Earthen roads (trails)	Off-Roads
S 1	10% , 40	30% , 22	10% , 12	50% , 10
S 2	35% , 60	60% , 20	5% , 6	0% , 2

UNCLASSIFIED

(U) Using the percentage of road type comprising the network and average speed as the required threshold value for determining a kill, then  $P(M)$  can be assessed for each vector outcome and averaged in a number of ways to suit the use:

$$\begin{array}{ll}
 \text{vector 1: } P(M|\text{Scenario 1}) = 0.1 + 0.3 = 0.4 & P(M|\text{Scenario 2}) = 0.35 \\
 \text{vector 2: } P(M|\text{Scenario 1}) = 0.1 + 0.3 + 0.1 + 0.5 = 1.0 & P(M|\text{Scenario 2}) = 0.35 + 0.60 + 0.05 = 1.0 \\
 \text{vector 3: } P(M|\text{Scenario 1}) = 0.1 + 0.3 + 0.1 + 0.5 = 1.0 & P(M|\text{Scenario 2}) = 0.35 + 0.60 + 0.05 = 1.0 \\
 \text{vector 4: } P(M|\text{Scenario 1}) = 0.0 & P(M|\text{Scenario 2}) = 0.0 \\
 \text{vector 5: } P(M|\text{Scenario 1}) = 0.1 + 0.3 = 0.4 & P(M|\text{Scenario 2}) = 0.35 \\
 \text{vector 6: } P(M|\text{Scenario 1}) = 0.0 & P(M|\text{Scenario 2}) = 0.0
 \end{array}$$

(U) Scenario averages can be calculated by weighting the probability of mobility kill determined from each vector by the frequency of its occurrence,  $P(V)$ , found in table 3:

$$\begin{aligned}
 P(M|S1) &= (.40)(.60) + (1.0)(0.1) + (1.0)(0.1) + 0 + (.40)(.06) + 0 = 0.46, \text{ and} \\
 P(M|S2) &= (.35)(.60) + (1.0)(0.1) + (1.0)(0.1) + 0 + (.35)(.06) + 0 = 0.43.
 \end{aligned}$$

(U) The probability of kill averaged over both scenarios, where scenario 1 and scenario 2 are equally likely:  $P(M) = 0.45$ .

UNCLASSIFIED



# UNCLASSIFIED

## (U) SUMMARY

(U) Results of the tire investigations showed that multiple fragment impacts were required to deflate tire pressure and invalidated the use of the single-fragment vulnerable and lethal area heuristics for evaluating tire loss. Although the effort behind the tire investigations could have been accomplished years ago, it could not have been applied until the development of a stochastic model for artillery against ground systems. SAFE, which embodies the tire deflation algorithm and sophisticated leaker model, provides the vulnerability analyst with a means of investigating in detail fragment damage to weapon and combat support systems and increasing the fidelity with which system-level vulnerability analyses can be performed. The V/L taxonomy is a structure which should be used to ensure proper physical mappings from one state to the next and as a means for establishing knowledge gaps upon which to base recommendations for future work. It is well known and has been documented that older vulnerability techniques used to produce vulnerable and lethal area data do not model physical processes and do not produce output which can be compared to data obtained from field experiments, Live-Fire Tests, and actual battlefield events (ref. 11,12). Unfortunately, the use of heuristics, which assumes that damage due to individual fragments can be assessed independently, adds significant error to the weapon system evaluation.

## (U) REFERENCES

1. Rick Grote, Ed Davisson, Linda Moss, "New Tire Penetration and Pressure Models for Improved Vulnerability Analyses of Wheeled Vehicles (U)", ARL report in progress.
2. James E. Hunt, "An Indirect-fire MUVES Approximation Method (U)", Proceedings of the 6th Annual Combat Vehicle Survivability Symposium, held in Monterey, CA, 28-30 March 1995; also available on the World Wide Web at the site <http://web.arl.mil/~jehunt/safe.html>.
3. D.L. Nail, "Vulnerability Analysis for Surface Targets (VAST), an Internal Point-Burst Vulnerability Assessment Model-Revision I (U)", CSC TR-82-5740, August 1982.
4. Matrix Evaluator Computer Program, User and Analyst Manual (U), 61 JTCG/ME-72-11, August 1973.
5. Modifications to ARTQUIK and SAMSITE Computer Programs (U), OP-SS/MEWG-94-1, 29 April 1994.
6. Complex Targets Computer Program (U), Volume II, Analysts Manual, 61 JTCG/ME-75-14-2, June 1979.
7. The Joint Technical Coordination Group for Munitions Effectiveness (JTCG/ME), "Target Vulnerability (U)", 61A1-3.
8. D.C. Mackey, D.S. Dixon, K.G. Jensen, T.C. Loncarich, J.T. Swaim, "CASTFOREM Methodologies (U)", U.S. Army TRADOC Analysis Command, TRAC-WSMR-TD-92-011, April 1992.
9. "Simplified Artillery Projectile Effectiveness Model - ARTQUIK Computer Program User Manual (U)", 61 JTCG/ME-8-8, 1 October 1990.
10. K.A. Myers, "Lethal Area Description (U)", BRL Technical Note No. 1510, July 1963.
11. Dr. Paul H. Deitz, Mr. Aviars Ozolins, "Computer Simulations of the ABRAMS Live-Fire Field Testing (U)", Memorandum Report BRL-MR-3755, May 1989.
12. Dr. Paul H. Deitz, Mr. Richard Saucier, "Modeling Ballistic Live-Fire Events (U)", Proceedings of the Annual Ground Vehicle Survivability Symposium, held in Monterey, CA, March 25-28, 1996.
13. Robert Schumacher, "SAMSMAE, A Computer Code for Determining Mean Areas of Effectiveness for Multiple Component Targets (U)", ARBRL-TR-02295, February 1981.
14. Phillip J. Hanes et al., "Modular Unix-Based Vulnerability Estimation Suite (MUVES) Analysts Guide (U)", BRL-MR-2954, December 1991.
15. Donald R. Warner, "Ground Transport Vehicles (Current and Projected) -- Eurasian Communist Countries (U)", Defense Intelligence Agency, DST-1150S-280-90, 21 November 1990.
16. D. Warner, "Russia: Run Flat Capabilities of Tactical Tires (U)", NGIC, 1100-55B-94, 11 November 1994.
17. Rick L. Grote, Linda L. C. Moss, Edwin O. Davisson, "New Tire Penetration and Pressure Models for Improved Vulnerability Analysis of Wheeled Vehicles(U)", Proceedings of the Annual Ground Vehicle Survivability Symposium, held in Monterey, CA, 25-28 March 1996.

UNCLASSIFIED

**UNCLASSIFIED**

**DETECTION AVOIDANCE SESSION**

**Ingersoll Auditorium  
Wednesday, March 27, 1996**

**Session Chairman: Mr. Mark Pasik, General Dynamics Land Systems**

**UNCLASSIFIED**

**UNCLASSIFIED**

THIS PAGE INTENTIONALLY LEFT BLANK

**UNCLASSIFIED**

## **Validation Status of the TARDEC Visual Model (TVM)**

G. Gerhart, R. Goetz, T. Meitzler and E. Sohn  
US Army Tank-Automotive Research, Development and Engineering Center (TARDEC)  
Warren, MI 48397  
gerhartg@cc.tacom.army.mil

### **ABSTRACT**

The TARDEC Visual Model (TVM) represents a fundamental advance in predicting man-in-the-loop visual and infrared target acquisition performance for both sensor and target signature applications. TVM applies recent results from computational neural science to model the human visual system's response to color and brightness, motion, spatial patterns, and ambient illumination. It uses a "front end" module to feed an improved model for field-of-regard and field-of-view search and detection in addition to observer population performance.

This paper describes in detail some examples of the verification and validation efforts for TVM during the last year. The results show clearly that TVM correlates quite well with empirical data for high contrast targets. Low contrast targets are more difficult to correlate with empirical data. This result appears to originate in part from the fact that the detection process involves higher levels of discrimination using cognitive information.

### **1.0 INTRODUCTION**

The TVM model development began with the Army Target Acquisition Model Improvement Program (TAMIP) which occurred during the FY92-94 time frame. The primary emphasis initially was predicting human observer acquisition performance against low contrast targets. During the FY94-95 time period TARDEC began an ambitious joint CRDA with General Motors Corporation to apply TVM to the design and evaluation of collision avoidance countermeasures for automobiles. The goal was to perform a proof of principle demonstration of early vision computation models for driver automotive tasks.

The TVM software and documentation was delivered to TARDEC on 31 January 1995. Since that time both AMSAA and TARDEC have been involved in an extensive verification and validation phase to complete beta testing and eventually distribute the software to the user community. TARDEC and OptiMetrics Inc. are currently involved with an ACT II Battle lab proposal to extend TVM to automatic target cueing. This program also develops comprehensive software engineering tools to rapidly prototype applications of the basic methodology in an object oriented environment. This feature is particularly important for configuring both classified and unclassified versions of the software code.

### **2.0 CVM METHODOLOGY**

#### **2.1 Background**

Recent studies show that simple image metrics do not give good predictive results when applied to highly resolved targets in complex background scenes. These ad hoc formalisms typically use first or perhaps second order statistics to incorporate target texture and background clutter into their analysis. In addition some empirical human observer models calculate probabilities of acquisition for detection, recognition and identification tasks. These latter models are usually based upon a relatively small set of observer test data and inevitably are extended beyond their capabilities to a diverse set of end applications.

The TVM human visual processing model is built upon vision research reported during recent years.<sup>1,2,3,6,7</sup> This work shows that the very early human visual system performs a multi-dimensional analysis of retinal images in terms of spatial-temporal modulation of color and luminance. These results clearly show why traditional size and contrast models fail to provide accurate predictions of vehicle detectability. Developments in visual psychophysics<sup>4,5,6</sup> have provided models of behavioral response to visual stimuli which have been tested and incorporated into TVM for detection and discrimination tasks. TVM also incorporates an extension to the traditional search modeling for representing false alarm behavior.<sup>8,9</sup>

## **2.2 Theory**

TVM processing is organized into three sequential stages. The first stage simulates early visual processing. The second stage computes a visual information metric. The third stage predicts search and target acquisition performance.

## **2.3 Early Visual Processing**

Figure 1 illustrates the processing sequence in the early vision module. The input to the model is either a sequence of digitized video images (dynamic analysis) or a single digitized image (static analysis). First, the software simulates temporal sampling and filtering; the outputs are three images representing the low pass or stationary component, and two bandpass images. Second, the software simulates color vision processing which reorganizes the output of the red/green/blue sensitive (RGB) cones into a single luminance (black-white) and two color opponent components (red-green and yellow-blue). Only the luminance component of the temporal bandpass images are carried forward from the output of the temporal high pass filters, whereas all three luminance/color opponent components of the temporal low pass image are utilized in the low pass filter analysis. Third, the software simulates the spatial pattern analysis performed at individual neural receptive fields which are essentially two-dimensional spatial filters that respond to contrast and color gradients at different size scales and orientations. TVM analyzes the image planes at multiple resolutions, sampling the gamut of receptive field sizes at one octave increments (i.e. factors of 2). Each receptive field acts as a two-dimensional spatial filter, bandpass in one orientation and low pass in the other. TVM represents the set of possible orientations with two orthogonal filters: horizontal and vertical.

The signal processing represented in Fig. 1 is essentially phenomenological in character<sup>10</sup>. The detailed steps in the sequential processing are fairly well known and form the basis of a predictive model. This sequence of events<sup>10</sup> defines a receptive field signal to

noise ratio (S/N) model based upon the individual band pass filter output signals. A subsequent pooling over the respective channels forms a composite system S/N where each channel is weighted by the number receptive fields for that particular band pass filter. An RSS S/N metric includes both internal noise and background clutter. The predictive nature of this portion of TVM requires that the signature metric be calibrated to human observer data and subsequently validated by an independent data set. The statistical module then predicts both probabilities of detection and false alarm for foveal acquisition and field of regard search.

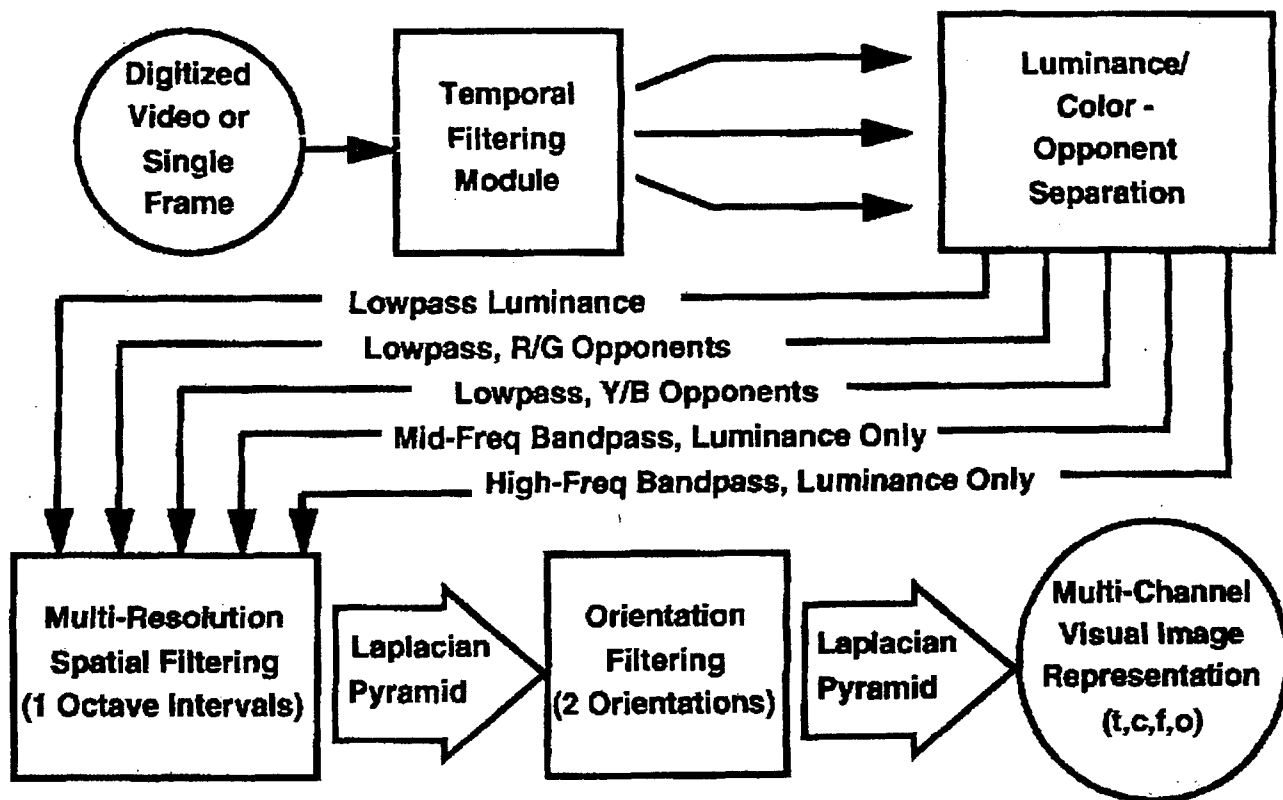


Figure 1: TVM Early Vision Model

### 3.0 TVM VERIFICATION

Several case studies are presented which explore the dynamic, color, visualization and statistical decision modules of TVM. Additional analysis explores the sensitivity of the  $d'$  calculations to both edge and texture cue features.

#### 3.1 Dynamic Model

Figure 2 illustrates an example of the output from the dynamic portion of the early vision model used in our verification study. The top row is a black and white rendition of a full color image showing three frames from a video sequence where two tanks are moving across a grassy field. The bottom row shows the application of the three temporal filters to the middle frame in the top row where the left image depicts the application of the low pass filter while the other two images illustrate the output from the two band pass filters. The low pass filtered

image preserves color but is slightly blurred due to motion blur as compared to the original image. The two high pass filters reject the temporal zero frequency component and consequently, they have very good static clutter rejection capabilities because the background scene is stationary in time. As you see the primary cues are due to the perimeter edges where the vehicle is covering and uncovering portions of the background scene. The S/N ratio for these two images is very large and explains why static targets that blend well with the background are quite conspicuous when they begin to move or change in some temporal fashion.

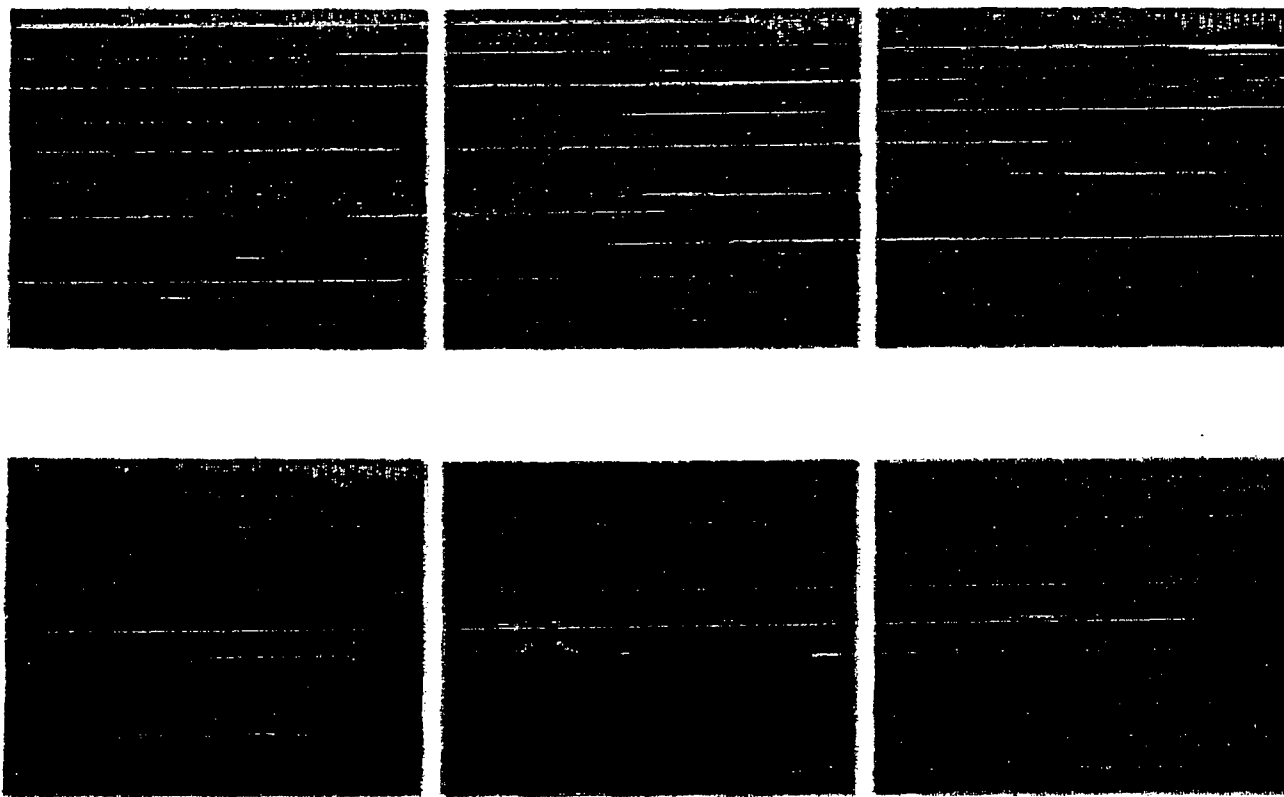


Figure 2: Verification of the TVM dynamic model

### 3.2 Color Opponent Model

Figure 3 is an additional case study representing a qualitative test for color-opponent axis decomposition in the TVM model. An original Ishahara red/green color blindness chart was scanned into its three red, green and blue color components. TVM performs the linear transformation to color opponent space with the results displayed below. Note that the numbers are not discernible in the two B/W images while several numbers are clearly visible with different contrast ratios in the R/G and B/Y color planes. If the observer is not R/G color blind, he will see the integers 3 and 5 with a greater contrast than 5 and 17 in the composite image. He will see the numbers 3 and 15 because masking effects will not allow him to see

the lower contrast numbers 5 and 17. If on the other hand the observer is R/G color blind, he will not see the numbers 3 and 15, and will thus respond that 5 and 17 are visible but at a lower color contrast. Consequently, TVM correctly predicts that the B/W plane has no contribution to the visibility of either set of integers since luminance contrast would easily mask the visibility of the two color channels. Also the relative contrast difference between the two color channels at least qualitatively predicts why the Ishahara test pattern discerns between R/G color blindness and normal observers.

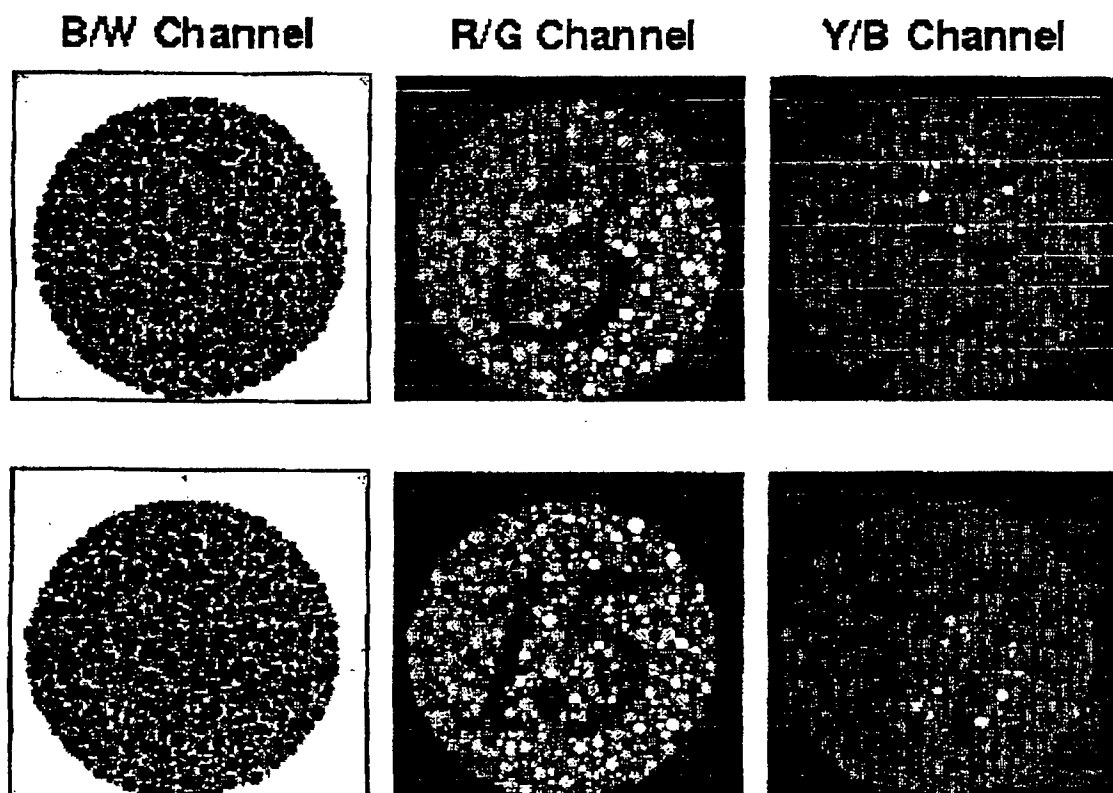


Figure 3: Ishahara calibration test for red/green color blindness.

### 3.3 Correlation Between the Visualization and $d'$ Calculations

Figures 4 and 5 represent a qualitative comparison between outputs from the visualization and statistical decision modules in TVM. Figure 4 shows a portion of the original target/background scene at the top and a sequence of images where various levels in the Laplacian pyramid have been matched with respect to a standard background region. The latter was arrived at by patching in portions of the original background in a seamless fashion over the target area so it was undetectable by a human observer.



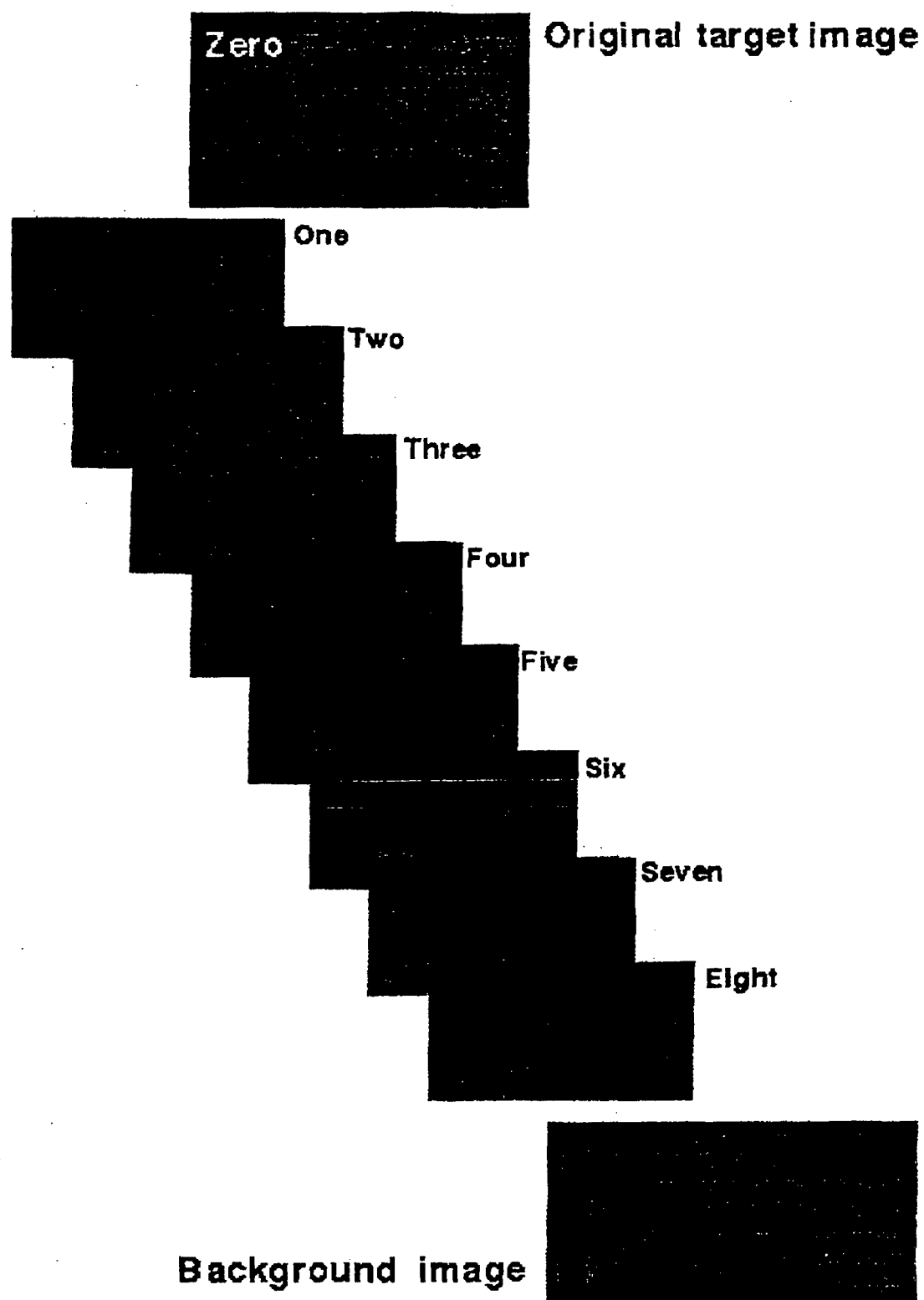


Figure 4 Laplacian pyramid analysis.

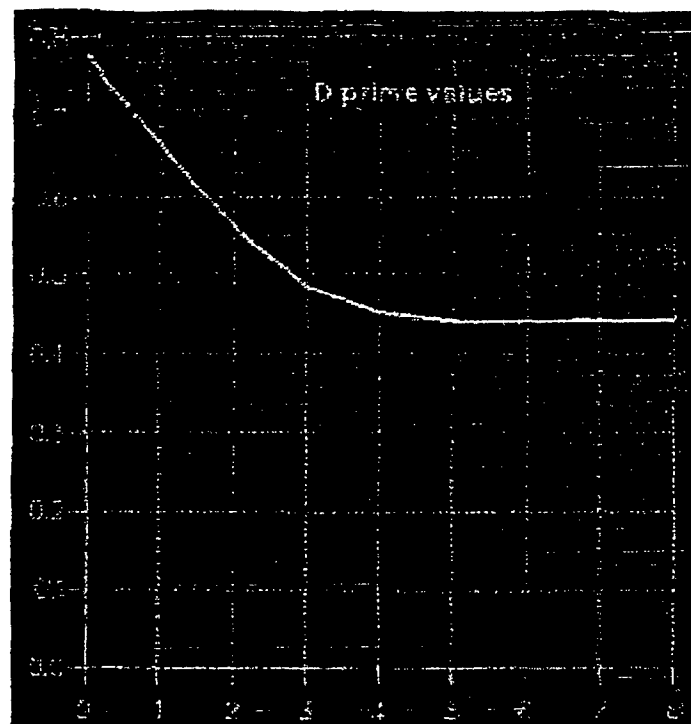


Figure 5. A graph of  $d'$  as a function of the number of levels matched to the background in the Laplacian pyramid.

The series of eight images in Fig. 4 represents the eight levels in the corresponding Laplacian pyramid. All of the various color opponent and orientation channels for each level have been matched relative to the local background scene by setting their corresponding S/N ratios equal to zero. The process begins with the highest spatial frequency and works its way down by factors of two to the lowest spatial frequency level. The image labeled one in Fig. 4 refers to the aggregation of all channels in the top level of the pyramid, image two the two top levels, etc.. As one can see the top three or four levels contain essentially all of the informational differences between original target and the standard background scene without the target.

Each of the corresponding eight images in Fig. 4 are obtained by using the TVM visualization module. After the S/N ratio is set equal to zero for each channel, TVM inverts the target acquisition equations and produces a corresponding image of the original scene minus the missing information. In this fashion a vehicle designer can determine which cue features on the target correspond to specific regions in the Laplacian spatial frequency decomposition. Figure 5 contains a graph of  $d'$  as a function of the number of levels in the pyramid matched to the background scene. Note that this curve levels off between three and four correlating quite well with imagery in Fig. 4. TVM thus gives a good qualitative comparison between the resulting imagery from the visualization module and the statistical decision module  $d'$  outputs.

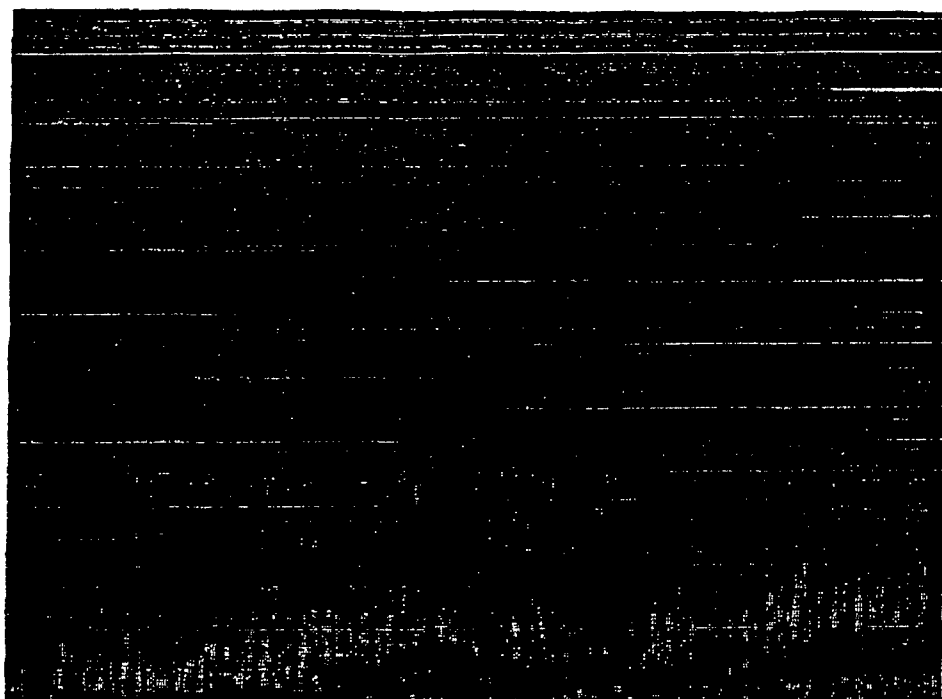


Figure 6a High contrast M1 target image.

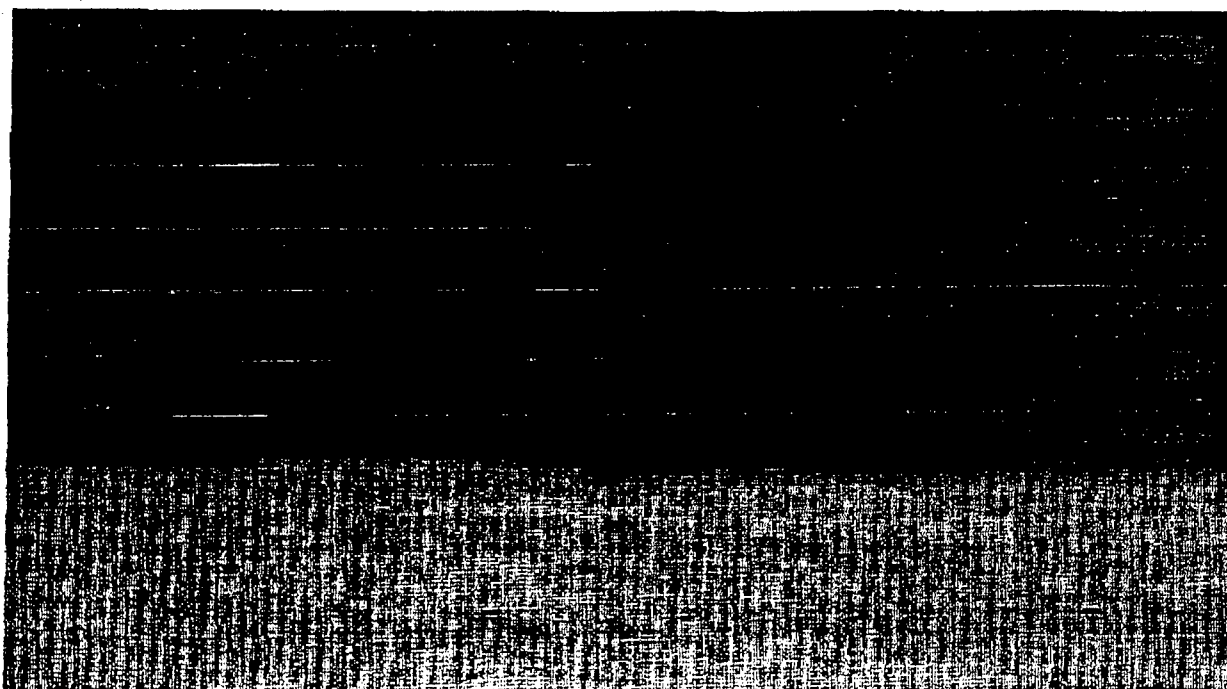


Figure 6b Enhanced zoom of the M1 target area.

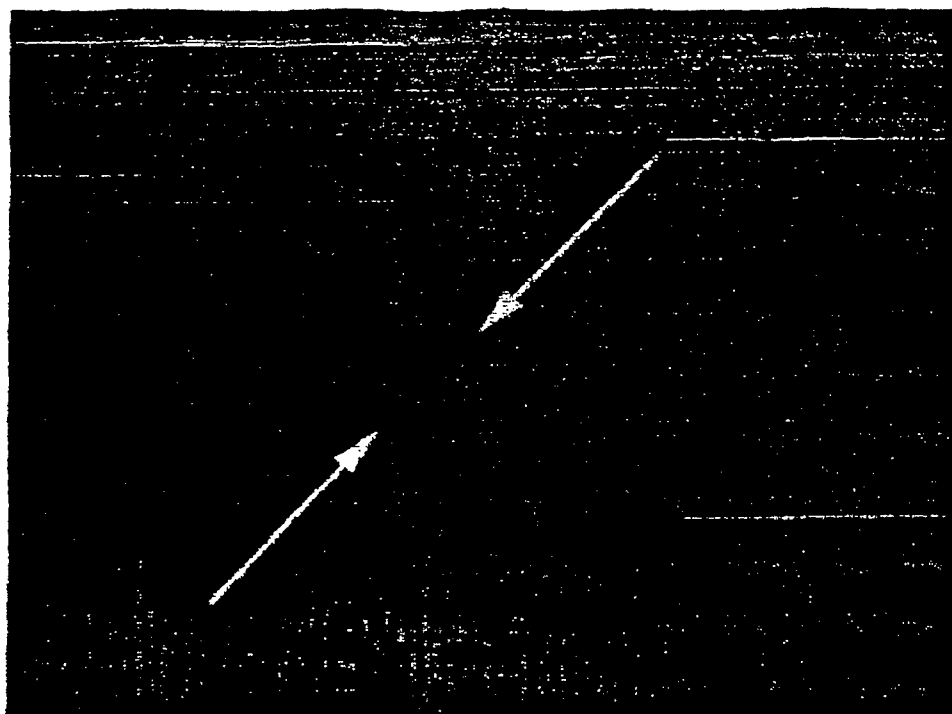


Figure 7a Low contrast M1 target image.

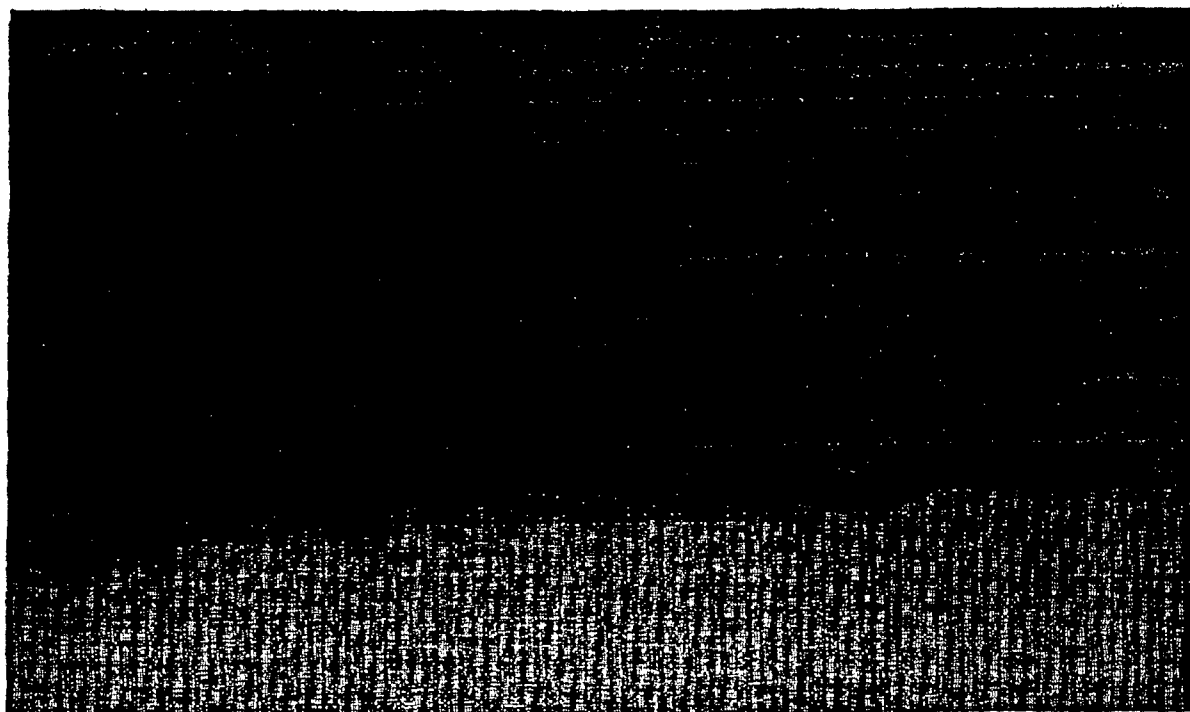


Figure 7b Enhanced zoom of the M1 target area.

Figure 6a was used in an additional study to predict  $d'$  for a side view of a M1 in a tree line portion of the background. The target has a woodland camouflage pattern which is fairly conspicuous and has an empirical observer  $d' = 3.2$ . TVM, however predicts a  $d'$  of approximately 1.8. This particular example illustrates that TVM is not consistent in making good absolute predictions for  $d'$  and the resulting probabilities of detection and false alarm. An examination of Fig. 6b shows that the target region has well defined perimeter edges and internal contrast gradients relative to the local background. The perimeter edges allow the observer to easily segment the target region using texture differences.

An analogous study of Figs. 7a and 7b gives somewhat different results. In this example the target edges have a lower contrast than in Fig. 6 while the target texture matches the background much better. TVM predicts a  $d'$  of approximately 1.4 which matches the experimental value quite well.

A subsequent analysis of these results indicates that the multiresolution S/N model in TVM accounts quite well for the edge content of the target region. Figure 4 clearly shows that the important target cue features originate from the higher spatial frequency channels. The latter are weighted more heavily in TVM because the density of visual receptive fields is much larger for the higher spatial frequency channels. As a result the model works fairly well for Fig. 7 where the texture match is quite good and does not contribute significantly to target detection. In Figure 6, however, it appears that TVM is not adequately taking into account the large target/background texture differences which are clearly evident in this scene. The larger predicted  $d'$  is essentially due to the over all higher edge contrast in this image while the texture differences are largely accounted for in the TVM signature metric.

In general the future development of TVM will focus in two broad areas. The first will involve the development of a more robust signature metric that will be based upon the present multiresolution S/N model and the incorporation of some elements of human cognition. The latter is essential because the acquisition of low contrast targets appears to involve higher level discrimination of specific cue features. The appearance, for example, of a particular shape, edge contour, etc. will often short circuit the "normal" detection process by allowing the observer to insert cognitive information from his recollections of the target. In addition the discrimination of specific cue features may very well limit the applicability of signal detection theory in the predictions of the statistical decision module.

#### 4.0 SUMMARY

This paper has described some of the many studies that the authors have investigated during our verification of the TVM model. The consensus to date by both AMSAA and TARDEC is that TVM early vision model is essentially complete and valid. Additional work needs to be done, however, in correlating the outputs of the statistical decision module with the results of empirical field tests. Some doubts do exist on the robustness of various field test data used to validate TVM. Various factors including the reproducibility of the test conditions and small amounts of observer data are serious limitations to our ability to make good statistical correlations between empirical and theoretical results.

The TVM model appears to correlate much better with laboratory test data where the observer testing is conducted under more controlled conditions and the larger volume of data

leads to better discrimination between statistically significant parameters. TARDEC is completing the construction of a new dual use human perception laboratory which we will utilize to both calibrate and validate TVM performance. In addition this facility will be important in augmenting available field test data and providing the means to guide the direction of future development of the TVM model.

TARDEC is currently involved in a phase II effort to enhance the TVM signature metrics and improve the performance of the model for low contrast targets. This effort should be concluded during the 2nd quarter of FY96 with a subsequent evaluation phase to determine the robustness of the improved model for a variety of target/background scenes.

## 7.0 REFERENCES

1. Blakemore, C., (ed.) [1990] *Vision: Coding and Efficiency*, Cambridge U. Press.
2. Boynton, R.M. [1992] *Color Vision*, Optical Society of America.
3. DeValois, R.L. and DeValois, K. [1990] *Spatial Vision*, Oxford U. Press.
4. Graham, N.V.S. [1989] *Visual Pattern Analyzers*, Oxford U. Press.
5. Green, D.M. and Swets, J.S. [1966] *Signal Detection Theory and Psycho physics*, John Wiley & Sons.
6. Landy, M.S. and Movshon, J.A. (eds.) [1991] *Computational Models of Visual Processing*, MIT Press.
7. Macmillian, N.A. and Creelman, C.D. [1990] *Detection Theory: A User's Guide*, Cambridge U. Press.
8. Nicholl, J. [1994] A Mathematical Framework for an Improved Search Model, IDA Paper P-2901, Institute for Defense Analysis.
9. Washburn, A.R. [1980] *Search and Detection*, Military Operations Research of America.
10. G. Witus, M. Cohen, T. Cook, M. Elliott, J. Freeling, P. Gottschalk, and G. Lindquist, *TARDEC Visual Model Version 2.1.0 Analysts' Manual*, Report OMI-552 30 January 1995.

UNCLASSIFIED

THIS PAGE INTENTIONALLY LEFT BLANK

UNCLASSIFIED

UNCLASSIFIED

OPTIMIZATION OF THE PARAMETERS OF XPATCH FOR THE PREDICTION OF  
RADAR SIGNATURES OF GROUND VEHICLES (U)

John G. Bennett  
U.S. Army Tank-automotive and Armaments Command  
Warren, MI 48397-5000

and

Geralyn BoBo  
Keweenaw Research Center  
Houghton, MI 49931

ABSTRACT (U)

(U) To use XPATCH to predict the radar signature of a ground vehicle, we must balance computer run time with accuracy of the prediction. In this paper, we demonstrate our techniques to achieve this balance by selecting an optimum set of five of the XPATCH input parameters for the predictions of the signature of the M2A2 Bradley Fighting Vehicle. We optimize this set of parameters subject to a maximum allowable run time for the prediction of the radar cross section of the vehicle over the desired range of azimuth and elevation angles and subject to a minimum desired accuracy. The results show the effects of each parameter on run time and on accuracy.

(U) Background

(U) Developed by Demaco, Inc., for the Air Force, XPATCH predicts radar signatures by a technique based upon ray tracing. Input parameters, adjustable by the user, control how XPATCH performs this ray tracing. The user must select these parameters, either deliberately or by accepting default values. In this paper, we examine how five of these parameters affect run time and the predicted signature. Moreover, we discuss techniques to achieve a balance between run time and accuracy.

UNCLASSIFIED

Further dissemination only as directed by U.S. Army TACOM, 4 Mar 96, or higher DoD authority.



(U) Techniques

(U) Table 1 lists the five parameters studied and their default values. The first two parameters determine how XPATCH creates a binary space partition, and the other four parameters control the ray tracing.

(U) A Silicon Graphics Indigo 2 computed all the runs for this work. Table 2 lists an inventory of the computer's hardware. We chose as our sample geometry a 59,930 facet model of the M2A2 Bradley Fighting Vehicle, an actual Army vehicle exhibiting the typical complexity of ground vehicles. We predicted the radar cross section (RCS) of the vehicle at 35 GHz. A typical study of the RCS of a vehicle would require at least 1000 RCS predictions.

(U) Variation with Azimuth and Elevation Angles

(U) We began our study by examining the variability in run time due to variation in azimuth and elevation angles with all input parameters fixed. We set all parameters to their default values except the number of waves per wavelength. We set the number of waves per wavelength at 5 instead of its default value of 10 in order to reduce run time enough to make 100 runs in a reasonable time. For azimuth and elevation angles, we randomly chose pairs between 0 and 360 degrees azimuth and between 0 and 80 degrees elevation. Figure 1 plots these azimuth elevation pairs.

(U) To examine the relationship between elapsed time and the CPU time, we plotted these times against each other for the 100 azimuth-elevation pairs, Figure 2, and fitted the points by linear regression. Elapsed time was equal to CPU time plus an overhead of 55 seconds per run.

(U) Figure 3 displays a histogram of elapsed times for the 100 runs. Elapsed time varied by more than a factor of 2 and averaged 28.8 minutes with a standard deviation of 5.4 minutes.

(U) Effects of Variation of Input Parameters

(U) For our study of the effects of input parameters, we chose an azimuth-elevation pair with an average elapsed time, namely, an azimuth of 356.0 degrees and an elevation of 30 degrees. Keeping all other parameters at default values, we set each parameter at 0.25, 0.5, 1, 2 and 4 times its default value. For this study, we used a default value of 5 for the number of rays per wavelength instead of the XPATCH default of 10.

(U) Ray Tracing Parameters

(U) The number of rays per wavelength exhibited the strongest influence on CPU time, Figure 4. CPU time increased with the 1.9 power of the number of rays per wavelength. The

maximum number of bounces had a moderate influence on CPU time, Figure 5. CPU time increased only as the log of the maximum number of bounces. With increases in NSCALE above the default value of 5, CPU time remained constant, Figure 6.

(U) Facet Geometry Parameters

(U) Maximum tree depth, Figure 7, showed a similar lack of influence on CPU time for values above the default value. CPU time showed only a slight linear dependence on maximum number of facets per voxel, Figure 8.

(U) Selection of Optimum Parameters

(U) To select optimum parameters, we examined the dependence of the predicted RCS on the parameters together with the dependence of the CPU time. Figures 9 through 13 show these dependencies. Unfortunately, for the azimuth-elevation pair we studied, the RCS changed only slightly as we varied the input parameters. Nonetheless, we reached the following tentative conclusions:

Maximum tree depth and maximum facets per voxel should be set at their default values of 20 and 10. The default maximum tree depth was at a knee of the CPU time curve. And RCS was independent of facets per voxel.

RCS reached an asymptotic value at 10 rays per wavelength, the XPATCH default value. But run time would be 2 hours per point at this value. We must perform additional runs to determine loss of accuracy from ray tracing at 5 or fewer rays. In particular, we should select an azimuth-elevation pair at which the RCS is lower.

NSCALE should be set at the default value, 5, a knee in the CPU time curve. Also, in the vicinity of 5, the RCS was independent of NSCALE.

The maximum number of bounces should be set at least at the default value, 50. This value was at a knee of the RCS curve.

(U) Acknowledgment

We would like to thank Mr. Jack Jones, U.S. Army Tank-automotive Armaments Command, for converting the geometry of the M2A2 vehicle from BRL-CAD into the facet format required by XPATCH.

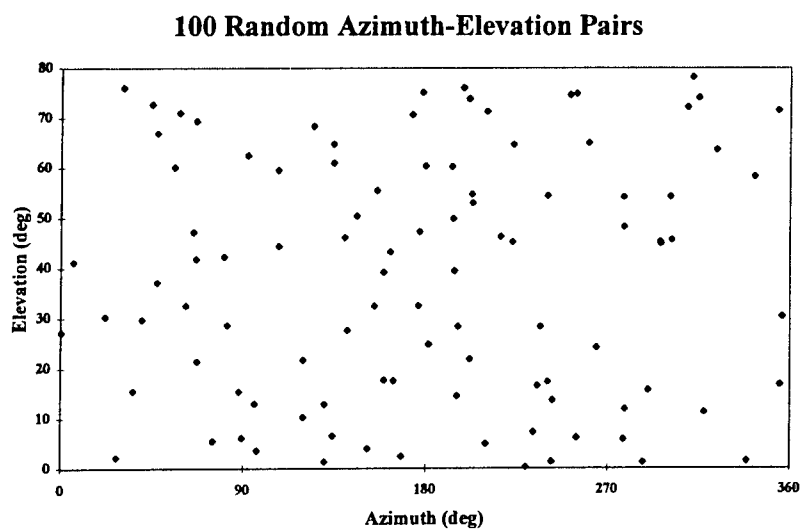
**Ray Tracing**  
**Maximum Bounces (50)**  
**Rays per Wavelength (10, 5 in this study)**  
**NSCALE, zone size in rays (5)**

**Facet Geometries**  
**Maximum Tree Depth (20)**  
**Maximum Facets per Voxel (10)**

(U) Table 1. Five input parameters for XPATCH with default values in parenthesis.

**150 Mhz IP22 Processor**  
**FPO: MIPS R4010**  
**CPU: MIPS R4400**  
**Data Cache Size 16 Kbytes**  
**Instruction Cache Size 16 Kbytes**  
**Secondary Unified Instruction/Data Cache Size 1 Mbyte**  
**Main Memory Size 64 Mbytes**  
**Graphics Board: GUI Extreme**  
**Integral SCSI Controller 1: Version WD33C93B rev D**  
**Integral SCSI Controller 1: Version WD33C93B rev D**

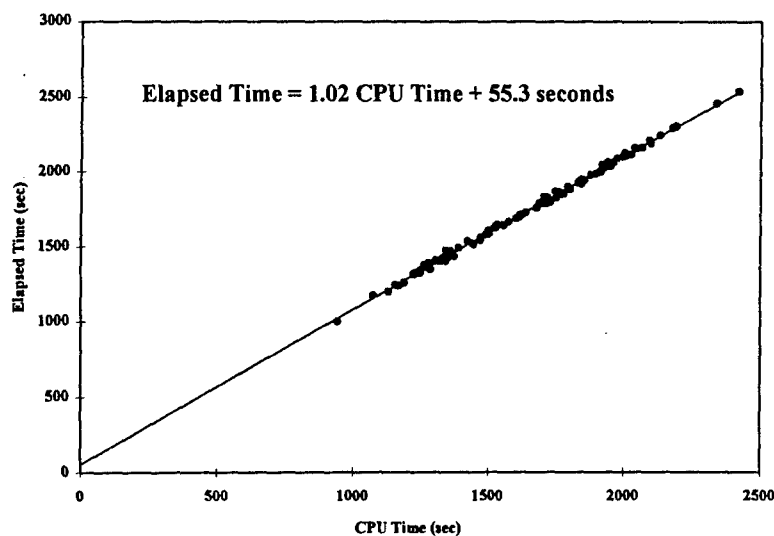
(U) Table 2. Hardware parameters of the computer.



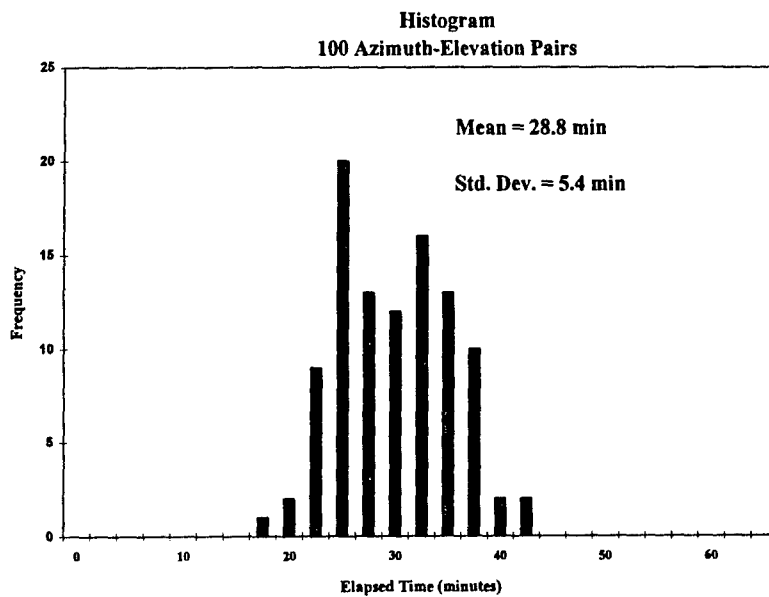
(U) Figure 1. A random selection of 100 azimuth-elevation pairs.

UNCLASSIFIED

### Elapsed Time vs. CPU Time

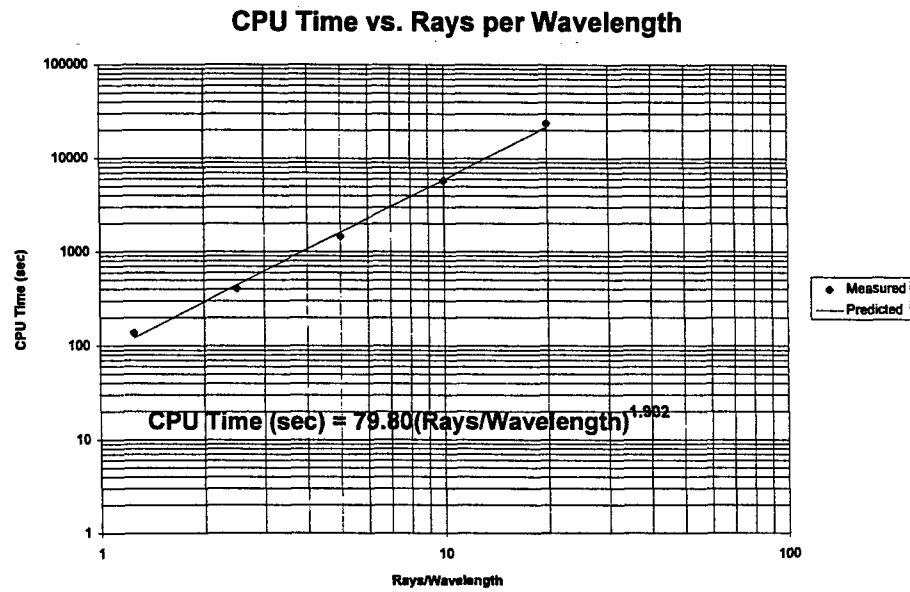


(U) Figure 2. Elapsed time versus CPU time with linear regression fit to the data.

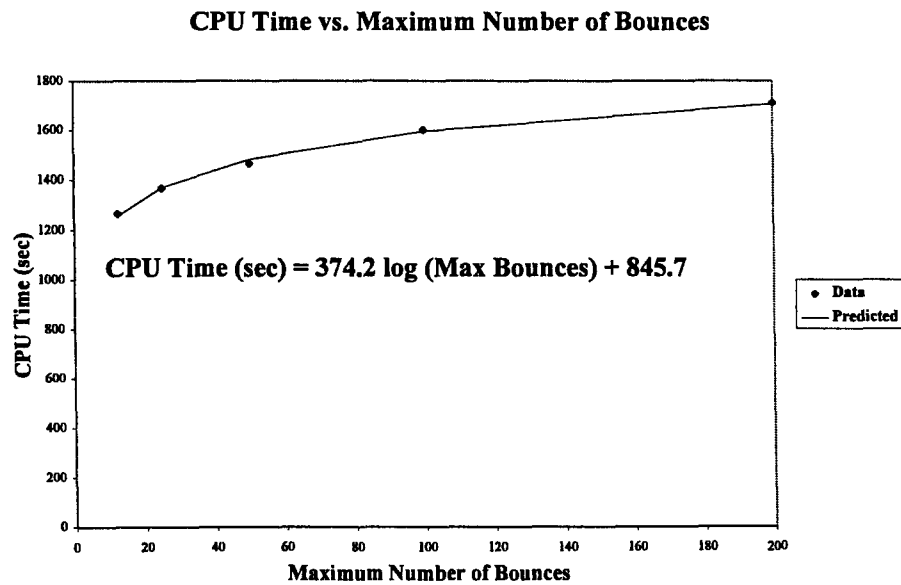


(U) Figure 3 Histogram of the elapsed times for 100 azimuth-elevation points.

UNCLASSIFIED



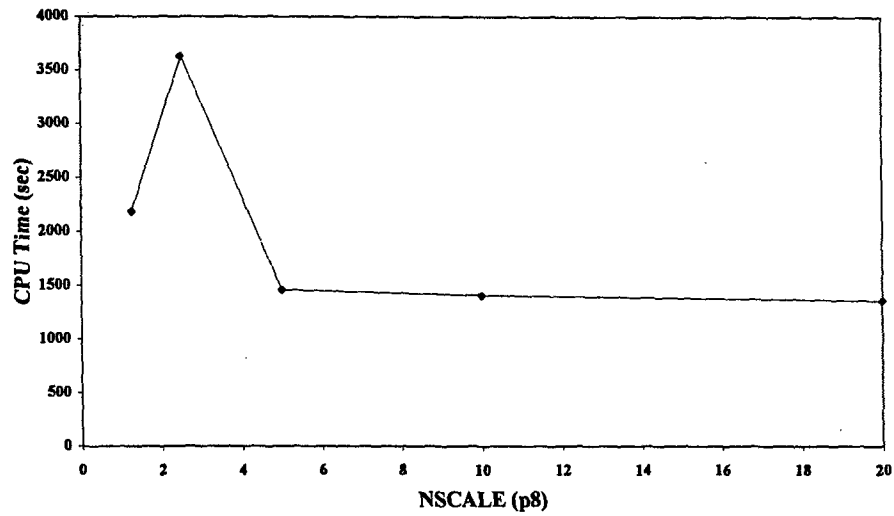
(U) Figure 4. CPU time versus rays per wavelength with a linear regression fit.



(U) Figure 5 CPU time versus Maximum number of bounces with curve fit to the data.

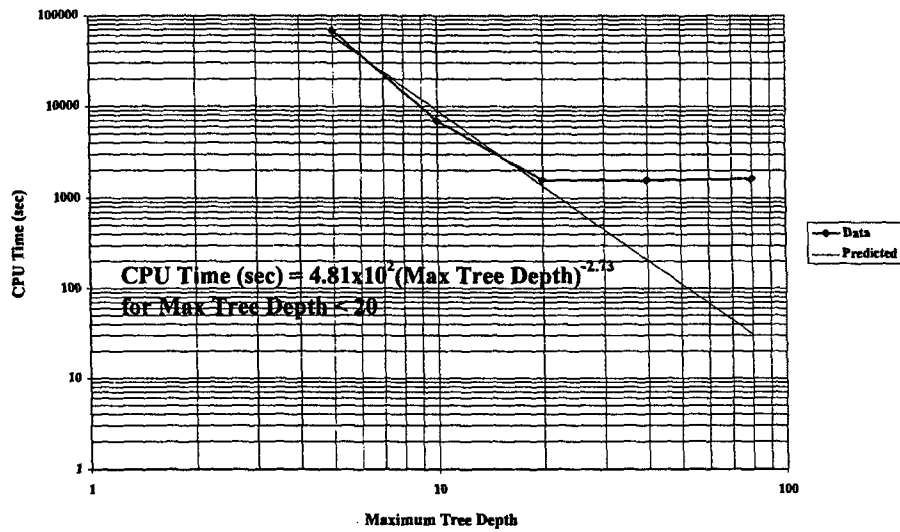
UNCLASSIFIED

### CPU Time Versus NSCALE



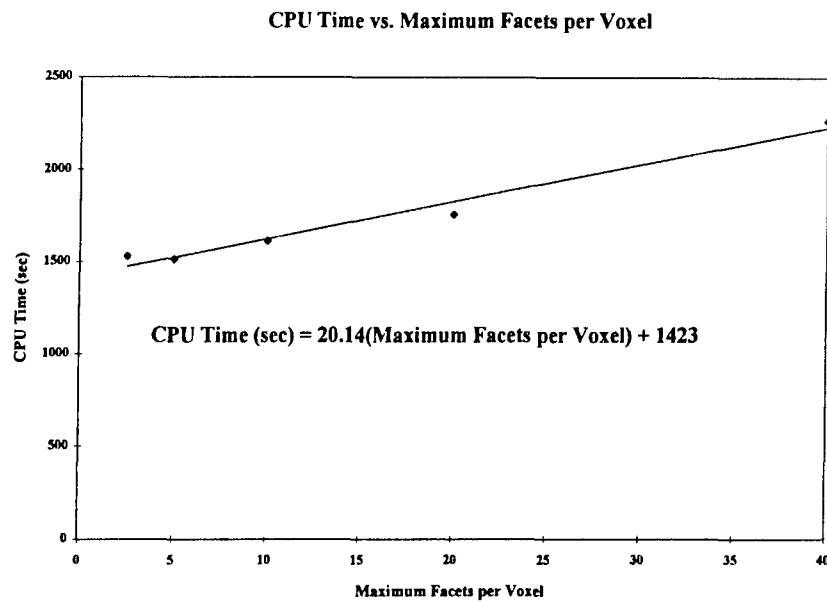
(U) Figure 6. CPU time versus NSCALE.

### CPU Time vs. Maximum Tree Depth

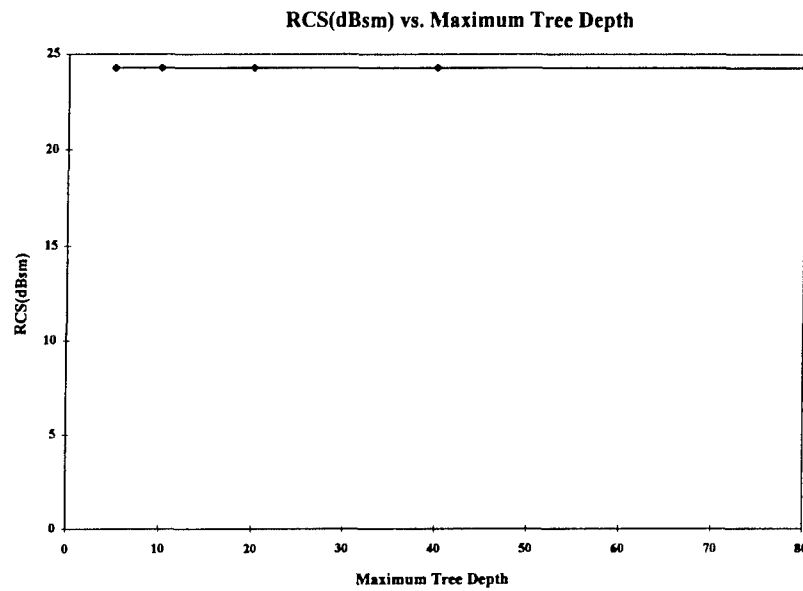


(U) Figure 7. CPU time versus maximum tree depth.

UNCLASSIFIED

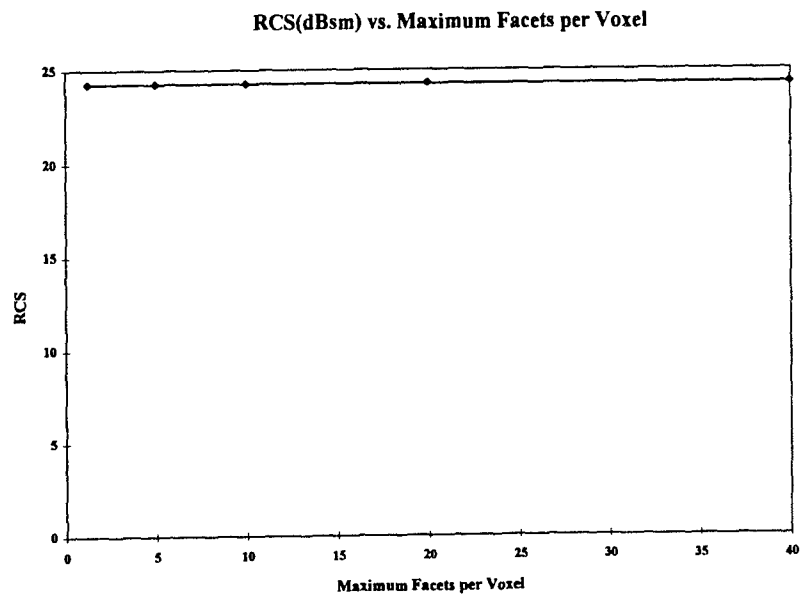


(U) Figure 8. CPU time versus maximum number of facets per voxel.

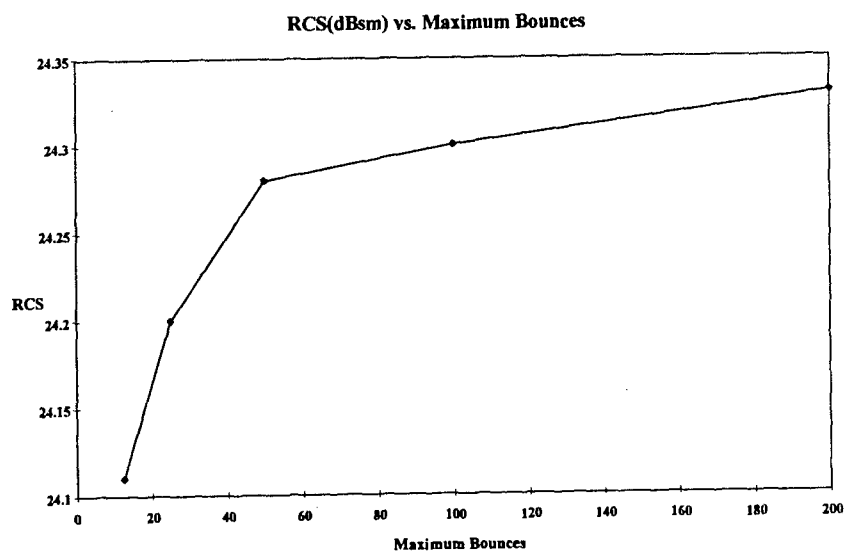


(U) Figure 9. RCS versus maximum tree depth.

UNCLASSIFIED



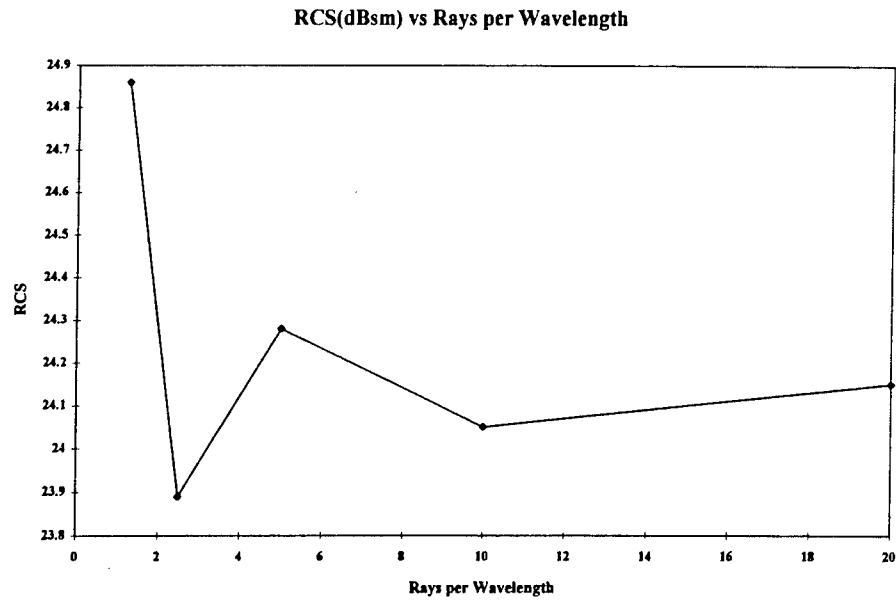
(U) Figure 10. RCS versus maximum facets per voxel.



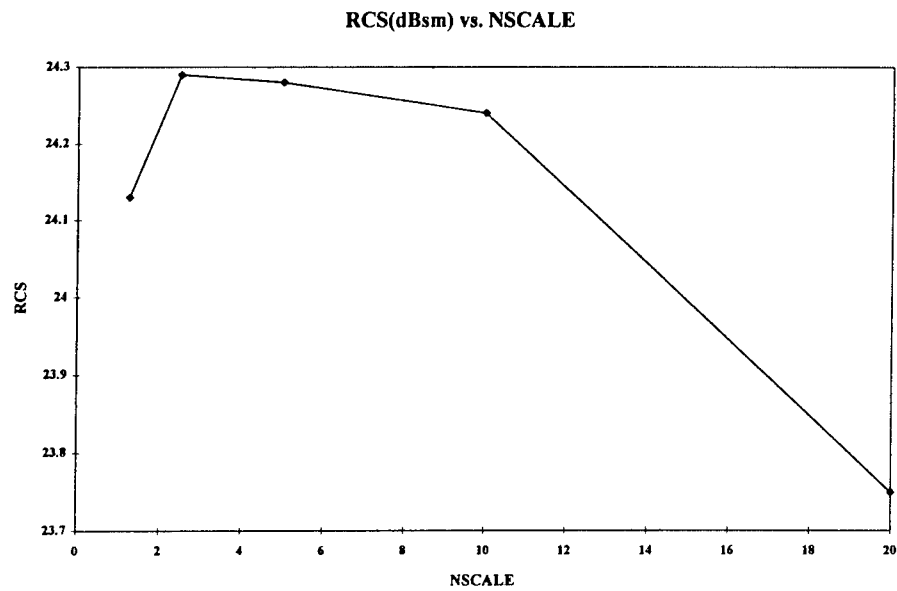
(U) Figure 11. RCS versus maximum number of bounces.

UNCLASSIFIED





(U) Figure 12. RCS versus number of waves per wavelength.



(U) Figure 13. RCS versus NSCALE.

## The TARDEC Visual Spectrum Analysis Model (U)

By David Gorsich, Jack Jones, Roger Evans and David Thomas  
 U.S. Army Tank-automotive and Armaments Command  
 Research, Development & Engineering Center  
 Survivability, MS263  
 Warren, MI 48397-5000

### ABSTRACT (U)

(U) There are two types of visual models, empirical and theoretic ones. Most are empirical due to their computational efficiency and the need for only photorealistic pictures. However there is a great Military need for theoretical visual modeling, or modeling based on the physical theories of light. TARDEC's model is focused on being able to model narrow spectral band visual signatures of vehicles. The Visual Spectrum Analysis Model is broken into a local and global component. To model the local characteristics of light reflectance from various surfaces, the bi-directional reflectance distribution function (BRDF) must be incorporated into the vehicle geometry. The paper discusses how this has been done and some of the follow-on validation work on the local model. Validation of the global model is also discussed. Included are explanations of the rendering process which incorporates the BRDF, a discussion of the Graphical User Interface (GUI) and tools included in the model. One of most important tools is the camouflage mapper which enables the user to map camouflage patterns directly onto a three-dimensional model. Finally, future work and applications of the model to perception analysis using the TARDEC Visual Model (TVM) is mentioned.

### (U) INTRODUCTION

(U) This paper presents continued efforts toward developing a physically reasonable visual model for the U.S. Army. Models like XPATCH and PRISM, which predict the radar and thermal signatures of ground vehicles, have become indispensable in the design and modification of military vehicles. However, no similar simulation model has appeared suitable for visual or near-IR tasks.

(U) There are two types of visual models, empirical and theoretic. Empirical models tend to focus on creating visual images that look good and are computationally efficient. Theoretic models focus on having physical validity and keeping with the physical laws of light reflectance. Our goal is to present a near-real-time, easy to use, theoretical tool which produces photometric values of faceted or polygonal objects

(U) One goal of signature reduction in thermal modeling is to reduce thermal contrast. Similarly, the reduction of glints is a key goal in visual modeling. The angles where the glint will appear for each surface point, whether it is a mirror, diffuse paint or a special surface, is defined in the model by a bi-directional reflectance distribution function (BRDF) and the geometry of the vehicle. This BRDF is the heart of the model, and it is this function which makes the model different from a simple radiosity or ray tracing solution to the rendering problem. Most rendering software packages, such as the software used by Pixar to do the movie Toy Story, use only two parameters to define the reflective characteristics of a surface: a specular component and a diffuse component. That is one of the reasons the images still have a plastic appearance to them. Approximating the characteristics of light reflection from a surface by a specular number and diffuse number does not give real world numbers like actual luminance values. The software Radiance by Greg Ward comes close to rendering an object correctly, but it does

not have arbitrary BRDF capability, mainly due to a lack of BRDF data. Also, Radiance was designed to model light in building interiors, not vehicles in a battlefield, so there is less attention to glints, special coatings and the sky.

(U) Currently, the only way to determine true luminance values of a vehicle in a background is experimentally. There are a number of problems when trying to do other types of modeling using computer imagery without experimental data. For example, the TARDEC Visual Model, which models the human visual system, needs to have some data on the image regarding the background-to-sky luminance and background-to-target luminance ratios. Other models like Oracle by British Aerospace use luminance ratios as key numbers to determine the detectability of objects in backgrounds. The main problem is the fact that calculations using RGB values are physically meaningless since they are device dependent.

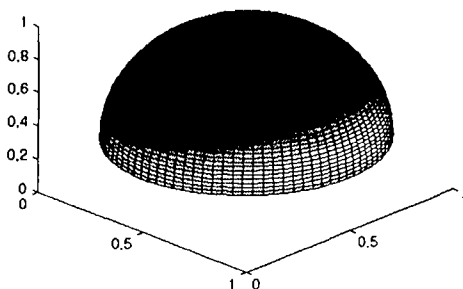
#### (U) THE LOCAL MODEL

(U) The TARDEC Visual Spectrum Analysis Model is broken up into two key components: a local model and a global model. The local model is the key to the entire rendering process. It defines how light reflects from each point on the surfaces of a vehicle. Essentially, the local model is the BRDF model with a geometry attached so it is oriented in space via a unit normal vector and position. The local model code is modular, and can be taken out and changed without affecting the rest of the model. This is a key issue, since the model is still being tested with the Sandford-Robertson BRDF model [6] which defines the BRDF using four variables:

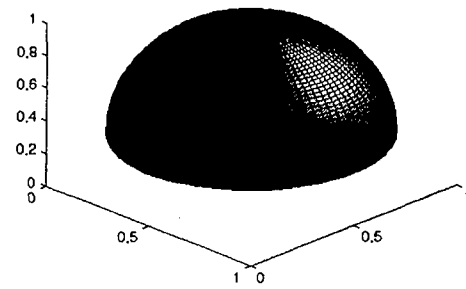
b = grazing angle fall-off coefficient  
e = specular lobe width coefficient

$\rho(\lambda)$  = diffuse total spectral reflectance  
 $\epsilon(\lambda)$  = spectral total hemispheric reflectance

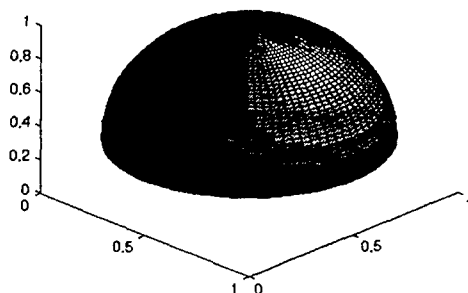
(U) The parameters above are generated by fitting the model to measured BRDF data. Approximating the BRDF with only four parameters greatly reduces the computer storage space and computational resources required in the initial stages of testing. The bi-directional reflectance function itself is hard to come-by. Usually, it is not an actual function, but a large volume of measured data. The BRDF is a three-dimensional cube of data which represents the reflectivity of light from one point on a surface, and only for one wavelength! Adding a discrete portion of wavelengths from the visual spectrum makes the BRDF a four-dimensional data set. Accessing the data from a hard-drive for every surface point is very slow and inefficient, so the data itself is modeled by a function. One way to model the data set is to do a singular value decomposition. This way, the data can be reduced to a smaller parameter set and a function created. This is essentially what the Sandford-Robertson model does. Unfortunately, the model has some problems and does not account for polarization and non-isotropic surfaces. The Sandford-Robertson model, like the Cook-Torrance model, assumes the BRDF can be broken into a specular function and a diffuse function. The model assumes only one specular lobe. After initial validation, a more sophisticated BRDF model will be introduced into the local model. Models like the Beard-Maxwell model break down the function into reflections from the first surface and scattering from within the volume. These models incorporate polarization but do not handle glossy coatings well [3]. Below are several plots of the Sandford-Robertson BRDF of CARC 383 green paint.



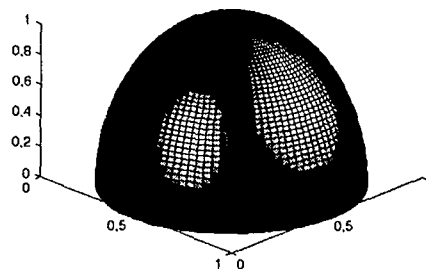
(U) Figure 1



(U) Figure 2



(U) Figure 3



(U) Figure 4

Figure 1 shows the BRDF at an incident glint angle of 5 degrees. Figure 2 is at an incident angle of 25 degrees. Figure 3 demonstrates the problem with the Sandford-Robertson model at incident angles near 90 degrees. The reflected lobe should be more centered around the top of the hemisphere. The incident angle for this Figure is 85 degrees. Figure 4 is an example of a conceptual non-isotropic BRDF with two lobes at different reflected angles for an incident angle of 45 degrees. The other BRDF in Figures one through three is isotropic. The Sandford-Robertson model cannot deal with BRDFs of this form. The ratios of reflectance were modeled using a series of simple cosine functions dependent on angle.

(U) Once the Sandford-Robertson parameters for a material surface are obtained, the BRDF must be evaluated for a particular wavelength and set of incoming and outgoing radiance vectors. The BRDF is a three-dimensional data set that varies with wavelength and angles of incidence. The value of the BRDF is given by  $R(\lambda, p, v, v')$ , where  $\lambda$  is the wavelength,  $p$  the point on the polygon,  $v$  the outgoing vector and  $v'$  the incoming vector. The point  $p$  endows the BRDF with a surface normal.

(U) Using the BRDF, the radiance reflected from incoming radiance is determined from:

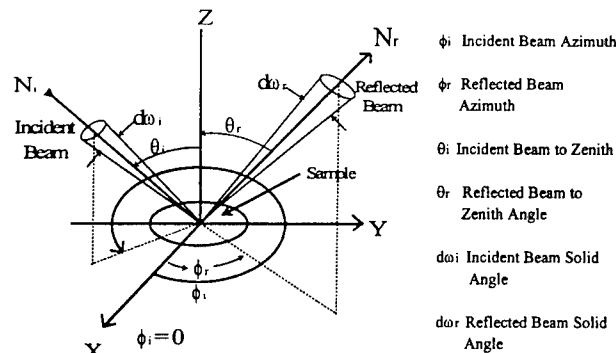
$$L(\lambda, p, v, v') = \int_{2\pi} R(\lambda, v, v') L(\lambda, p, v') (N \cdot v') dv'$$

where:

$L(\lambda, p, v')$  is the incident radiance  
 $N$  is the normal of the surface  
 $L(\lambda, p, v, v')$  is the reflected radiance in watts per steradian  
 $dv'$  is the differential solid angle around direction  $v'$   
 $v$  is the outgoing radiance unit vector  
 $v'$  is the incoming radiance unit vector  
 $N$  is the surface normal unit vector

Since  $N$  and  $v'$  are unit vectors, the dot product is simply the cosine of the angle between the two vectors. Since the reflectance point is actually a very small microsurface, when the angle between the incident ray  $v'$  and the normal is greater than  $90^\circ$ , the ray is considered to be blocked and contributes nothing (we assume no translucent or transparent points). The local geometry for the BRDF is seen in Figure 5.

## CONCEPT OF BIDIRECTIONAL REFLECTANCE



(U) Figure 5

The integral is approximated by a summation of projected areas of variable size. The sky is considered a hemisphere and is broken into sky patches using the solid angle or steradian. The area of each patch is

$$dA = r^2 \sin\theta d\theta d\phi$$

where theta runs from 0 to 90 degrees and phi from 0 to 360 degrees around the surface. Theta is defined to be the angle between the surface normal and the vector  $v'$ . So the differential solid angle is

$$d\omega = dA / r^2 = \sin\theta d\theta d\phi$$

Since radiance is defined as the power per unit projected area perpendicular to the ray per unit solid angle in the direction of the ray, the projected area of the hemisphere patch is used given by

$$dA = \cos\theta d\omega$$

which is the projected solid angle, where again theta is the angle between the normal vector and the sky patch center. The radiance from the sky patch is averaged to one value,  $L(\lambda, p, v')$ . Therefore the radiance reflected from the microfacet due to the sky is approximated by:

$$L(\lambda, p, v) = \sum_{\theta, \phi} R(\lambda, v, v') L(\lambda, p, -v') \cos\theta d\omega$$

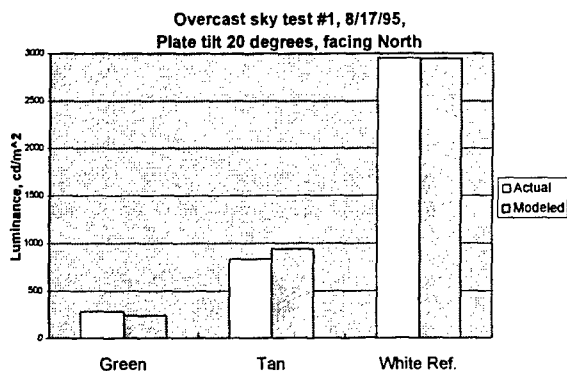
where  $v$  and  $v'$  are functions of theta and phi. Theta prime is the angle from the zenith or 0 degrees to the horizon or 90 degrees. The positive x direction is set as North and the positive y direction is West.

(U) The CIE (International Commission on Illumination) provides sky models which give a typical luminance distribution of a clear or cloudy sky, given the zenith (straight up) luminance and sun position. The sun position can be calculated using latitude, longitude, and time of the year. These sky models were used to provide a realistic sky hemisphere.

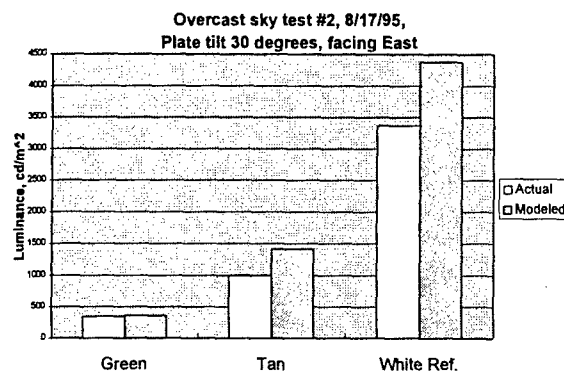
(U) The local model code was developed in C++, with separate modules for the sky, sun, BRDF, and sky/sun integration. This modular, object-oriented design allows easy module replacement, for example, for the evaluation of a different BRDF model.

(U) The local model was validated with luminance measurements of a plate at various normals on days with a clear sky and a cloudy sky. The plate was one square foot in size, and painted with standard Army camouflage CARC green and tan. A Spectralon plate was used as a white reference. Spectralon is 98% diffuse with a constant reflectance over the visual band. The BRDFs for the CARC paints had been measured and modeled by Surface Optics using the Sandford-Robertson BRDF model, so the values for  $b$ ,  $e$ ,  $\rho(\lambda)$ , and  $\epsilon(\lambda)$  were known [10].

Figures 6, 7 and 8 show the variation of the model output against measured luminance values with two different plate normals, or plate tilts. Measured luminance data was taken with a Minolta CS-200 colorimeter.

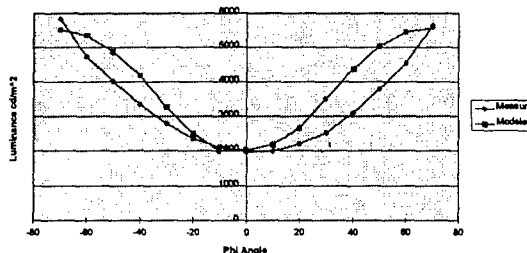


(U) Figure 6



(U) Figure 7

Modeled-vs-Measured Luminance Values for Different Plate Tilts



(U) Figure 8

(U) Other sources of error include the following: an approximated sun intensity, the lack of a ground lighting model, errors in the sky model, errors in the BRDF model and errors in the measurements due to surface dirt and wear. The majority of the errors come from the model of the sky and the sun intensity. Solutions to these problems will come from using actual measured sun luminance values and a cloud effects addition to the sky model. The CIE sky models assume a completely clear or cloudy sky, and the sky is rarely perfectly clear or cloudy. In figure 8, notice the error in the measured versus modeled luminance occurs at a plate tilt of 45 degrees, an angle giving a large glint.

(U) The local model does not give consideration to emission from a point (only reflection), polarization, coupling of wavelengths (phosphorescence) or time dependent light behavior (luminescence), but it is possible to incorporate these characteristics of light into the model at a later time.

#### (U) THE GLOBAL MODEL

(U) The facet-lighting calculations described above work well for a single panel, but are not adequate for modeling a vehicle. Facet blocking must be evaluated in order to provide self-shadowing; for example, the shadow of the gun barrel on the hull of a tank. Also, methods for the application of camouflage patterns to a vehicle geometry are required for a useful visual simulation.

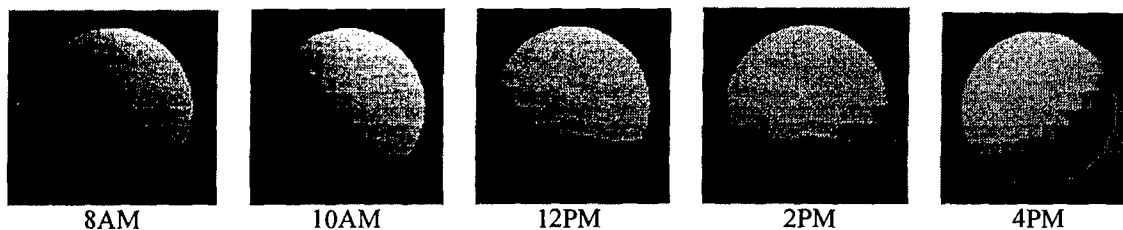
(U) The visual model extends the reflectance point to a polygon which has a spatial position and boundaries in addition to the surface normal. The reflectance points are located at the polygons' centroids. The normals for the polygons are stored in the facet file. The area of the polygon is determined by selecting a point

inside the polygon and forming triangles that have areas that are easily found and then summed. Source code from Joseph O'Rourke's Computational Geometry was used [4]. Polygons are distributed based on the camouflage pattern and the original geometry.

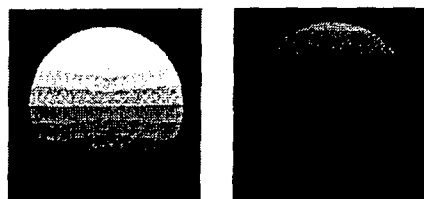
(U) If the polygons were connected with each other to make up a sphere, then there would be no question of whether a reflectance from a vertex was blocked by another polygon. There is no polygonal blocking. The radiance from a polygon contributes to the illuminance of the eyepoint if the angle between the normal and the eyepoint direction is less than  $90^\circ$ . But any global illumination model must deal with polygon blocking from the reflectance point to the eyepoint and blocking of sky patches by other polygons. The introduction of a blocking function,  $V$ , and an adaptive subdivision of the polygons is used [8]. The blocking function simply checks to see if a polygon "sees" the eyepoint. Essentially it is an intersection routine. With the blocking function, the total illuminance to the eyepoint is given by:

$$\sum_{\omega} R(\lambda, v, v') L(\lambda, v, -v') V(v, v') G(v, v') (dA/e)$$

(U) The global model was tested on a sphere seen in Figure 9. The sphere did not require the blocking function. All the geometries were evaluated with Warren, Michigan as the location and most use August 17, 1995 as the date, since a limited amount of measured data was available for this scenario. While these images may not compete in "realism" with those coming out of Hollywood, it should be kept in mind that our needs require the generation of photometric or radiometric data with measured environmental and surface properties. The attractiveness will increase as self-shadowing, and other physically-proper enhancements are added to the model. Averaging techniques such as Gouraud shading can be used, but they have a tendency to cover up flaws in the data, such as too-large facets in a shadow boundary area. A sphere works well for testing because it provides the full range of viewing angles and has no self-shadowing. The white level used in converting from luminance data to imagery is  $3000 \text{ cd/m}^2$  for the sunny-day runs, and  $1000 \text{ cd/m}^2$  for the cloudy-day runs. The sphere tests in Figure 9 use the Sandford-Robertson model for green CARC paint, and the view is looking northward at the sphere. There are five spheres in figure 9, each representing a different time of day. The times are, starting from left to right, 8:00, 10:00, 12:00, 14:00, and 16:00. The difference in the sun angle is easily seen. Figure 10 shows tests with ideal diffuse surfaces on sunny and cloudy days at 12:00.



(U) Figure 9



(U) Figure 10

(U) Figure 11 shows the simple "ktank" geometry at 8 AM. The results will improve greatly when self-shadowing is added by the evaluation of facets blocking other facets' view of light sources. Unfortunately, this will

also greatly increase run times. The blocking function was tested, but only to a limited extent, since the "ktank" has such a simple geometry.

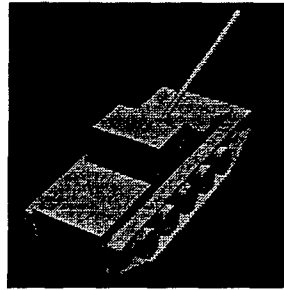


Figure 11

(U) After the vehicle has been properly evaluated, a composite image will be created by combining the vehicle data with a calibrated background image. The placement and size of the vehicle, and the lighting conditions should be set to match those of the background data. TARDEC's RTISR (Real-Time Imaging Spectral Radiometer) camera is capable of taking imagery where every pixel covers the whole visual spectrum.

#### (U) The Camouflage Mapping Tool

(U) A visual simulation model for combat vehicles necessarily must address the application of camouflage patterns. A popular approach, especially in commercial rendering packages, is texture mapping, where two dimensional images are mapped onto three dimensional surface geometry. Although this method is acceptable in most virtual reality applications, its dependence upon sophisticated hardware, lack of bi-directional capability, and certain dynamic abnormalities (such as morphing and false rotation), inspired an alternative approach.

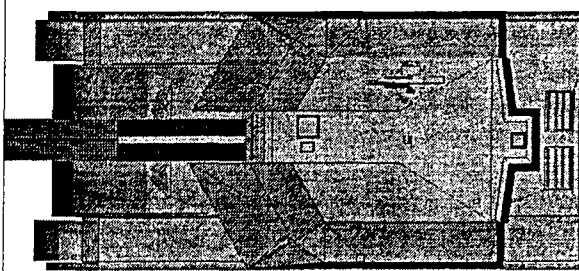
(U) The uniqueness of TARDEC's visual model is the procedural use of the BRDF rather than a simply diffuse face, as typically used with the radiosity method. So the question of how BRDFs are assigned to so many reflectance points is asked. The reflectance points are assigned BRDFs by the camouflage pattern. An algorithm for applying the camouflage pattern was developed so the basic requirements of a camouflage pattern would be met dynamically with any underlying geometry. This algorithm has been implemented using the discretization code written by Jones [8] which divides FRED faceted geometry based on a metric, in this case, the edges of the camouflage pattern. Thus a polygon is assigned a BRDF.

(U) The camouflage GUI follows the Faceted Region Editor (FRED) style. Within FRED, the camouflage pattern, decals and dirt can be incorporated into the geometry of the vehicle and edited directly in computer three space. The data structure is similar to the FRED \*.fac data structure. In fact, the geometry for the visual model including the camouflage pattern is FRED read and writable; however, that will likely not be the case as the structure matures to incorporate double precision and additional signature parameters. The existing FRED translators were modified to retain the information (such as vertex normals and colors) necessary to produce the more realistic Gouraud shaded images for our radiance model front end GUI.

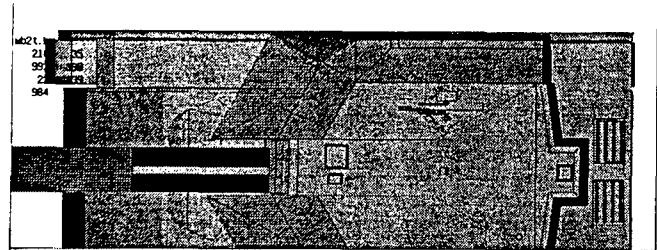
(U) As an alternative to texture mapping, the GUI contains a way to create "overlay polygons", which are advantageous since the rendering is hardware independent, BRDF parameters are easily attached, and they won't deform since the rendering is the same as for any other type of polygon. Figure 13 illustrates how the user selects rectangular regions on both the rendered geometry and a scanned camouflage pattern map by clicking on the desired lower-left and upper-right corners within each image. The system then lays the map on the graphics as seen in Figure 14. After selecting the desired BRDF, the user traces a pattern, Figure 15, and the system produces the overlay polygons, Figure 16. This process is repeated for every pattern and from each aspect. In Figure 17, another part of the camouflage pattern has been applied. The process will later be automated so the user will not even have to trace the pattern.



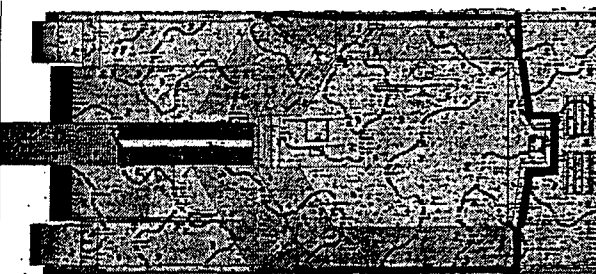
(U) To map the pattern onto a three-dimensional geometry, the traced pattern is transformed from screen space to world coordinates, where the Z of the screen is set at the near clipping plane. This closed area is then extruded to the far clipping plane to form a solid. The overlay polygons are obtained by taking the boolean intersection between the "visible" polygons and the extruded space.



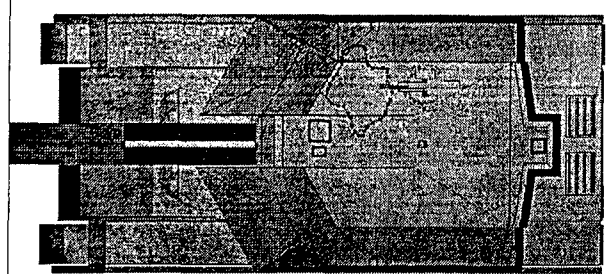
(U) Figure 12



(U) Figure 13



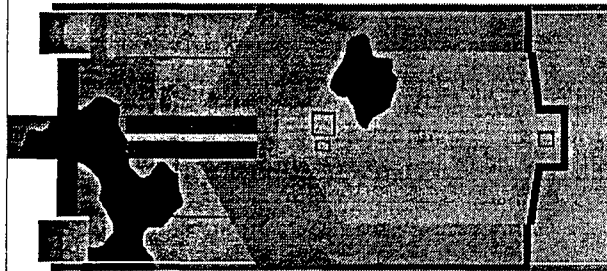
(U) Figure 14



(U) Figure 15



(U) Figure 16



(U) Figure 17

(U) By camouflaging vehicles in this way, old camouflage patterns can be used and mapped onto new vehicle designs in a three-dimensional way, quickly speeding up design of the pattern and reducing cost. And having the pattern embedded into the geometry is computationally very effective.

(U) CONCLUSIONS AND FUTURE DIRECTIONS

(U) The on-going development of the TARDEC Visual Spectrum Model has been very exciting. The opportunity to help the United States Army in the design of vehicles which are less observable in the visual spectrum is tremendous. There has been quite a great deal of work done in visual modeling in the computer graphics world which is helping to quicken the development of our model. The key to our model is the BRDF function, so often overlooked by the commercial sector. The work done so far in validating the model and approach has been successful, but further validation work is required. More detailed testing will be performed in the summer of 1996, with a variety of coatings with known BRDFs and test geometries. Measurements will be taken with a hand-held colorimeter and with a calibrated spectral camera system, and their measurements will be compared with model outputs. TARDEC will soon be receiving a tabletop-sized goniometer to take measurements of surfaces to get the raw BRDF data. This data will then be modeled, reduced and used in the local visual model. The ability to model the data is very dependent on the complexity of the data itself. Other areas of future research are in finishing the self-shadowing and inter-reflections. In doing this, additional machines will be used in parallel. Also, being able to insert the rendered vehicle in a background in a continuous and physically reasonable way still needs to be finished. Further development of the camouflage mapping tool will also be a key area of development.

(U) References

- [1] A. S. Glassner, *Principles of Digital Image Synthesis*, Morgan Kaufmann Publishers, 1995.
- [2] C. Shlick, "A Survey of Reflectance Models," *Computer Graphics Forum*, Volume 13, (1994), number 2, pp. 121-131.
- [3] K. K. Ellis, "First-Principles Coatings Reflectance Model Validation," 1995 Ground Target Modeling and Validation Conference.
- [4] J. O'Rourke, *Computational Geometry in C*, Cambridge University Press, 1994.
- [5] Ashdown, Ian, *Radiosity: A Programmers Perspective*, Academic Press Professional, 1993.
- [6] B. Sandford and L. Robertson, "Infrared Reflectance Properties of Aircraft Paints (U)," *Proc. IRIS Targets, Backgrounds and Discrimination*, 1985.
- [7] D. Thomas, R. Evans, D. Gorsich, J. Rakowski, J. Crosby, M. Hagen, "A Visual Signature Model and Analysis Tool," 1995 Ground Target Modeling and Validation Conference.
- [8] J. Jones, D. Gorsich, T. Gonda, G. Bobo, "Automated Adaptive Thermal Discretization," 1995 Ground Target Modeling and Validation Conference.
- [9] M.F. Cohen, J.R. Wallace, *Radiosity and Realistic Image Synthesis*, Academic Press Professional, 1993.
- [10] Surface Optics Corporation, *Army Camouflage Paint Data Base*, 1993.

**UNCLASSIFIED**

THIS PAGE INTENTIONALLY LEFT BLANK

**UNCLASSIFIED**

## Unclassified

### AMPHIBIOUS ASSAULT VEHICLE SURVIVABILITY ENHANCEMENT BY THE USE OF MULTISPECTRAL CAMOUFLAGE APPLIQUES, MCAS

Rodney Peterson,  
USMC Program Office, Naval Surface Weapon Center, NSWC  
and  
Francis M. Manion  
Monterey Bay Corporation

#### ABSTRACT

The USMC are developing high speed Amphibious Assault Vehicles, AAVs. Because of their speed, these AAVs are more survivable, but worldwide availability of Advanced Guided Munitions, AGMs, using thermal imagers could still pose a threat. To counter this threat, the NSWC- USMC Program Office is considering Multispectral Camouflage Appliques, MCAs, to reduce the thermal signature of the AAVs.

This task looked at the signature aspect of the threat posed by line-of-sight AGMs and generic top attack smart munitions seekers to AVs, and the thermal signature presented by these AVs. AVs are constructed of lightweight materials which can result in detectable thermal signatures. The surface temperatures for the lightweight materials were calculated and compared to the thermal signatures of an AV demonstrator. The agreement was good and the calculations served as a basis for the design of MCAs for AVs. Two MCA approaches were fabricated and installed on an AV demonstrator vehicle. TOW thermal images were then taken to define the signature reduction achieved.

The thermal images of the AV demonstrator, with MCAs attached, show that the thermal signature was suppressed and muted and that "hot spot" cues were masked. The MCAs were effective, easy to fabricate, straightforward to install, adaptable, and yet light and easy to carry. These results indicate that MCAs appear to be a low cost means to synergistically complement the high water speed survivability of AAVs.

#### INTRODUCTION

The U.S. Marines are developing Advanced Amphibious Assault Vehicles, AAVs, as a modern replacement for AAV7A1s. These AAVs will be high water speed vehicles enabling landing operations with transports positioned further from shore. Because of their speed, the AAVs are more survivable, but worldwide availability of Advanced Guided Munitions, AGMs using thermal imagers could still pose a threat. To counter this threat, the USMC Program Office is investigating the feasibility of MCAs to reduce the thermal signature of AVs. This report is a short summary of the NSWC/USMC task performed under contract N00167-94-0060.

This task required: 1) analysis of the thermal signature of an amphibious assault vehicle, 2) the design of signature reduction appliques and 3) the experimental measurement of the signature reduction obtained. A primary consideration in this evaluation was that the applique logistic burden be light and their installation straight-forward, since these appliques could be installed just before entering combat to ensure that the combat thermal signatures of USMC assault vehicles are not compromised.

Unclassified



**Figure 1: The Propulsion System Demonstrator at High Water Speed**

Advanced Amphibious Assault Vehicles are not as yet available as test beds for the camouflage applique evaluation. However, the Propulsion System Demonstrator, PSD, was available having served its purpose in demonstrating among other measures, high water speeds. as shown in Figure 1.

This demonstrator makes an excellent test bed for signature reduction experiments since; (1) it is available as a test bed, (2) its thermal signature data has been recorded and (3) it incorporates many of the features of the future Amphibious Assault Vehicles, (such as many different light weight materials). These materials can greatly influence the thermal or far IR signature of the vehicle. For these reasons the PSD was selected as the test vehicle for the MCA signature reduction evaluation.

There are five (5) sections in the remainder of this report: 1) The AV Survivability Challenge, 2) Thermal Characteristics of PSD, 3) MBC's MCA Signature Reduction Technique, 4) PSD MCA Installation and Test Results, and the 5) Summary.

#### THE AV SURVIVABILITY CHALLENGE

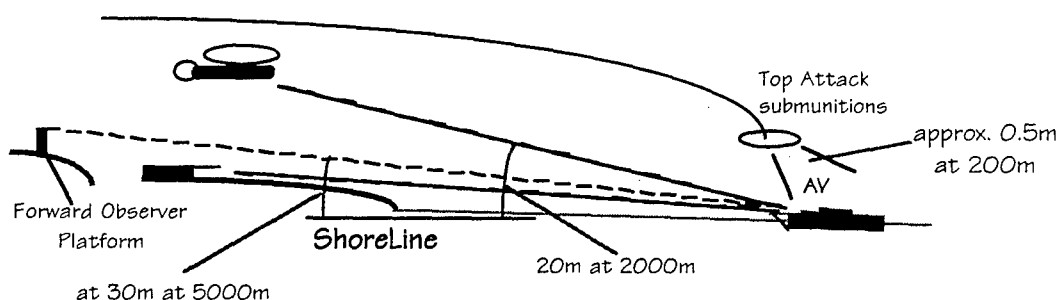
Amphibious Vehicles are most vulnerable as they approach the shoreline. This vulnerability is increased by the extended launch distance and the short timelines of defensive AGMs.

Increased defensive weapon range (AGM range) makes it necessary to take measures to protect the sea-going transports. In order to reduce this vulnerability AVs, are being designed with a three-fold increase in sea-going speed. Nevertheless, this increase in speed is not sufficient for survivability when the shoreline defenses use AGMs. Thus, AVs must have signatures management in order to delay (or eliminate) their acquisition until they are inside the shoreline defensive timelines. The survivability synergism between increased AV speed and their reduced signature will be demonstrated graphically .

Most shoreline defenses will engage the AV with low LOS, be they guns, missiles or heliborne ATGMs . However, AGMs of particular concern are those that dispense "top attack" submunitions. The defensive weapon LOSs are shown in Figure 2. The low angle aspect of the AV and the AV's topside signatures are of primary concern.

Unclassified

## Line-Of-Sight Angles



$$\text{LOS Angles} = \Delta \text{ Height} / \Delta \text{ Range}$$

$$\text{LOS Angle} = 0.006 \text{ to } 0.01 \text{ radians}$$

or about 0.4 to 0.6 degrees

**Figure 2: AGM Lines-Of-Sight, (LOS), When Engaging Approaching Amphibious Vehicles**

Figure 2 is a notional sketch of the L-OS signature of the AVs that are important in their sea-going phase. In land engagements similar signature aspects are important but with a more exposed and reconfigured vehicle. AGMs produce a two part problem: 1) Low LOS acquisition and 2) Top Attack munition end-games.

The lines-of-sight angles are small. The example shows an L-O-S angles of 0.4 to 0.6 degree. The defensive platforms tend to remain low for their own survivability. Even top attack munitions need to be directed by an acquisition platform. Therefore low LOS are the initial acquisition mode and the low LOS AV signature aspect of the AV is most important in the Sea Mode. This does not mean that signature reduction to defeat the top attack munition end game is not important.

### Survivability Synergism between Reduced AV Signature and Increased AV Speed

At 25kts the AV travels at about 13m/s. A range of 4000m requires 310s to traverse, and a range of 2000m, 155s. Thus the vehicle must not be detected until just inside 800m from shore to beat a defender's 60s timeline. The signature management approach is to delay or eliminate detection and to defeat acquisition and lock-on by the submunitions, i.e. remove hot spots and acquisition cues, such as straight edge contrast.

Figure 3 illustrates the vulnerability reduction achieved by increasing the speed of the AV. There are two parameters critical to the shoreline defense; 1) engagement distance and 2) time required to detect, acquire and launch and fly a munition. This chart plots distance versus time, to illustrate the AV's relative vulnerability as it is inside the defensive engagement distance with a time from shore longer than the AGM's minimum time.

In Figure 3, a constant AV velocity is a straight line whose slope depends on the AV speed. The slope identified as the "Velocity of AV" characterizes the vulnerability situation of AV. AV Vulnerability to AGMs is indicated by the area bounded by the "Velocity of AV" line, "AGM Max. Range", and the "AGM Min. Time" lines. The right side boundary is an arbitrary maximum time. This vulnerability indicator is the sum of the gray cross-hatched areas.

Unclassified

3

### Increasing AV Speed Reduces Potential Vulnerability

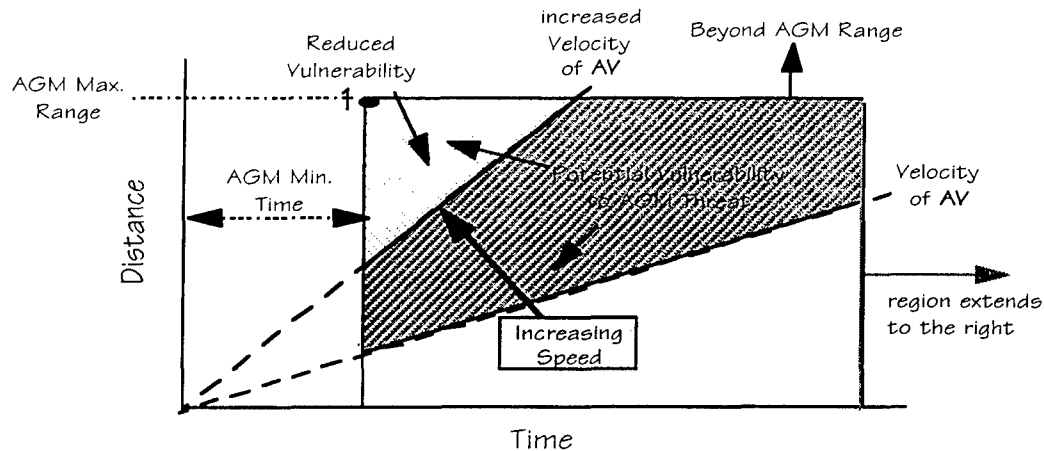
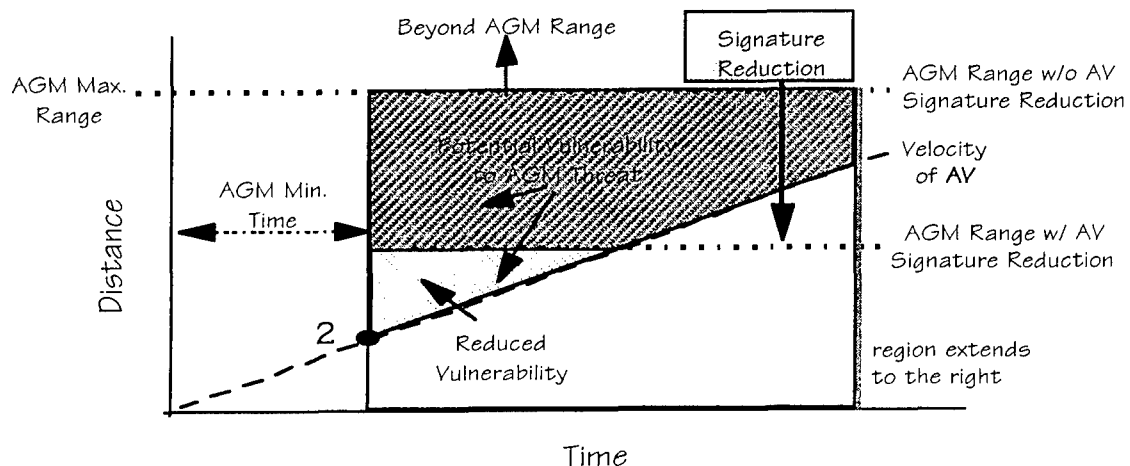


**Figure 3: Increased Speed Reduces AV Vulnerability to AGMs**

This vulnerability measure area includes the two gray cross-hatched areas in this figure. As the AV's velocity is increased (in this example by increased slope), this vulnerability measure is reduced to just the light gray cross-hatched area. The dark gray cross-hatched area has been eliminated.

Figure 3 illustrates the vulnerability reduction obtained of increasing AV speed. If the AV was fast enough that its velocity line would intersect the AGM Max. Range at the AGM Min. Time point, the vulnerability would be zero. This point is marked by "1" on the figure. Simply stated, at this point when the AV was detected, it was already inside the AGM's timeline.

### Decreasing AV Signature Reduces Potential Vulnerability



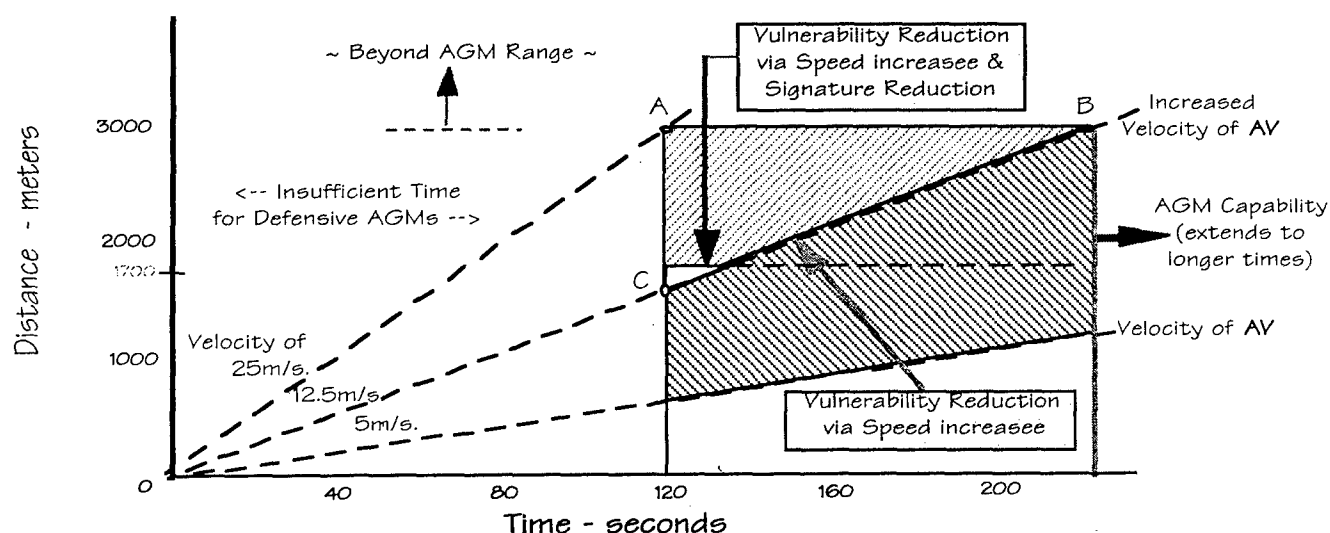
**Figure 4: Reduced Signature Reduces AV Vulnerability to AGMs**

Figure 4 illustrates the vulnerability reduction achieved by reducing the signature of the AV. Again, the AV vulnerability is characterized by the the sum of the gray cross-hatched areas, and reduced vulnerability by the removal of the dark gray cross-hatched area from the notional vulnerability measure. This vulnerability reduction is achieved by means of a reduced AV signature. This is similar to the previous chart except instead of increasing the AV speed, the

AV's signature is reduced such that the "AGM Max. Range " (or AGM Range without Signature Reduction) dashed line is dropped down to the "AGM Range w/ AV Signature Reduction" dashed line.

Figure 4 illustrates the value of signature reduction. If the AV's signature could be reduced to the range where the "Velocity of AV" line intersects the "AGM Min. Time", point "2" on the figure, then the AV's vulnerability would be zero. Simply stated, when the AV was detected, it was already inside the AGM's timeline.

### Demonstrating the Survivability Synergism of Signature Reduction with Speed Increase



**Figure 5: Survivability Synergism of Reduced Signature Reduces AV Speed Increase**

Figure 5 was developed to demonstrate the synergism between increase speed and signature reduction in reducing the AV's vulnerability to AGMs. It is a combination of the two previous figures. However, notional distance and time dimensions are assigned. Assuming defensive AGM maximum range of 3000 meters and the AGM minimum time of 60 seconds, a region of AGM Capability is defined. These are notional characteristics but useful to illustrate the AV vulnerability and vulnerability reduction.

Overlaid on this distance - time region are notional AV sea-going velocity lines of 25m/s (48+kts), 12.5m/s (24+kts) and 5m/s (9.5+kts). At a speed of 25m/s the AV can be acquired by the AGM at 3000m but the AGM does not have time to engage since the AV is closing too fast, point "A" on the figure. At 12.5m/s the AGM has time to engage the AV from 3000m, point "B", to 1500m, point "C". At 5m/s (9.5+kts) the AGM has time to engage the AV until the AV is but 600m from shore. AV's vulnerability is indicated by the area above the dashed 5m/s velocity line, the sum of the gray cross-hatched and non hatched areas.

If the AV's speed was increased from 5m/s to 12.5m/s, its vulnerability measure is reduced by the elimination of the dark gray cross-hatched area. However if the AV's signature was reduced, along with this speed increase, such that the AGM could not acquire until 1700m, then the vulnerability measure is reduced to only the non hatched area. The survivability synergism of



## Unclassified

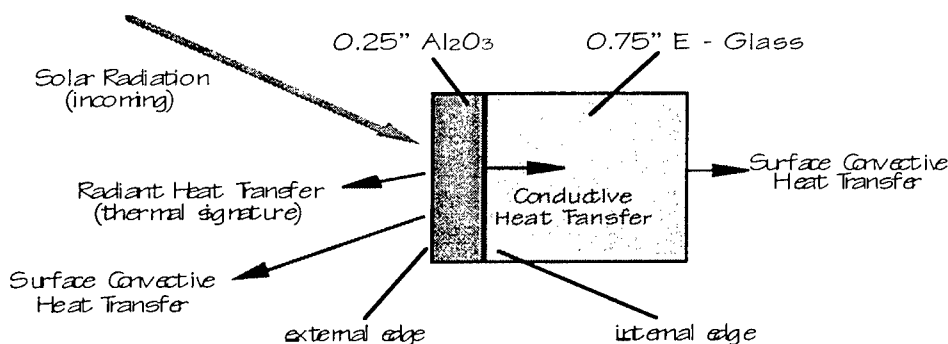
Increased Speed and Signature Reduction is self evident. Increased speed eliminates the dark gray cross-hatched area and then synergistically signature reduction eliminates the light gray cross-hatched area. The remaining vulnerability is the non hatched area, which remains here only for the purpose of illustration.

AV developers must realize that weapons developers are working hard to extend the AGM range and reduce its timeline. Thus signature reduction efforts must continually strive to avoid hostile detection until the AV is inside potential AGM timelines.

### THERMAL CHARACTERISTICS OF PROPULSION SYSTEM DEMONSTRATOR

The PSD was constructed of E-Glass, Aluminum, AD 94 Alumina, and thin Aluminum skinned Balsa. Except for Aluminum, these lightweight materials are very poor heat conductors, thus heat from solar radiation tends to intensify at the surface. The thermal diffusivity of Al is 3.66 ft<sup>2</sup>/hr. whereas the other materials range from 0.02 to less than 0.01 ft<sup>2</sup>/hr. Thermal diffusivity is a measure of how fast the heat absorbed at the surface is conducted away from the surface and into the body of the material.

AVs require lightweight materials for bouyancy which tend to have low heat conduction. These materials respond differently to time varying solar loads than say Aluminum plates, their surface heating is much faster and they cool faster.



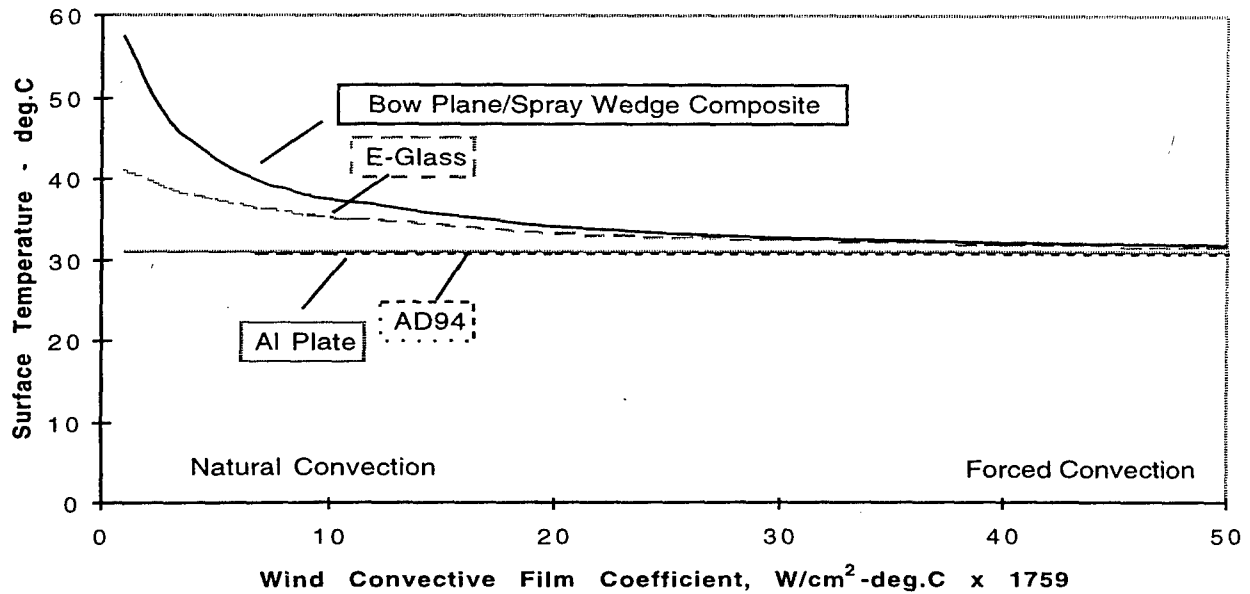
Typical PSD Material Section  
Heat Transfer Balance

Figure 6: Simple One-Dimensional Heat transfer Model

To define the surface heating of the PSD, a simple one-dimensional model was analyzed. Thermal equilibrium requires that heat absorbed from solar radiation be balanced by the heat conducted into the material, the heat convected away from the surface (by wind), and the heat radiated away from the surface. The heat conducted into the material will ultimately depend on the heat transfer away from the inside surfaces. Interior surface radiation was ignored because interior surfaces tend to radiate back and forth to each other since there is no cold sink.

The only way the surface temperatures of lightweight materials can be kept somewhat near the background is for a strong convective heat transfer component from the wind. In the Sea-Mode the wind will help but in the Land-Mode the PSD's radiant signature is a problem. This heat transfer (actually heat balance) model is used to estimate the surface temperatures of the many different materials of the PSD.

# Surface Temperature vs. Wind Effect



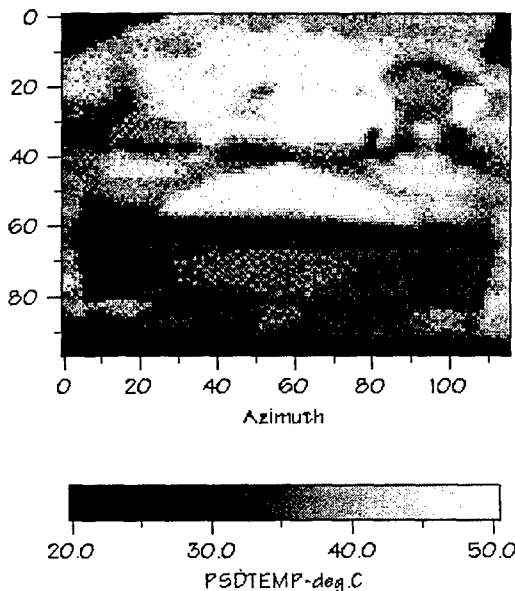
**Figure 7: Thermal Characteristics of PSD Materials with High Solar Radiation**

Figure 7 shows the results of the one-dimensional heat transfer analysis. This is for high solar load,  $80mw/cm^2$ . PSD surface temperatures also were calculated for low solar load, high and low convection and for zero heat conduction as well as for the material dependent heat conduction. Figure 7 indicates that the thin skinned Balsa Bow Plane approaches  $50^\circ C$  when there is little or no wind. Grayscale thermal images were provided by the NSWC Marine Program Office. These images included a calibration temperature scale. MBC used this scale to generate an array of temperatures, a value for every pixel, 11,252 pixels in the cropped image of Figure 8.

## Thermal Image Data

Array 97 by 116 pixels

- Mean Temperature =  $36.12^\circ C$
- Max. Temperature =  $50.6^\circ C$
- Min. Temperature =  $19.7^\circ C$
- Std. Dev. =  $8.75^\circ C$



**Figure 8: Thermal Image of the PSD with High Solar radiation**

The test condition shown in Figure 8 are for high solar load, ambient air at  $30^\circ C$  (about  $86^\circ F$ ), a sky

temperature of 20°C and low to no wind. Note, that the Spray Wedge surface temperature appears to approach 50° C. The Spray Wedge is that part of the Bow Plane that is much thicker, i.e. more resistive to internal heat conduction. This PSD image also included the hot exhaust which was not analyzed in detail.

#### MCA SIGNATURE REDUCTION TECHNIQUE

Thermal signatures depend on; the actual surface temperature ( $T_{\text{surface}}$ ), surface emissivity ( $e$ ), and the reflected surface temperature, ( $T_{\text{reflected}}$ ). The apparent surface temperature is,

$$T_{\text{apparent}}^4 = eT_{\text{surface}}^4 + (1 - e) T_{\text{reflected}}^4.$$

The thermal signature is the apparent surface temperature,  $T_{\text{apparent}}$ . If the surface emissivity were 1.0, the thermal signature would be the surface temperature. Typical surfaces have emissivities of 0.8 to 0.9. Thus for these emissivities, the thermal signature is dominated by the actual surface temperature.

MBC's MCA material is highly IR reflective, meaning it has a very low emissivity ( $e$ ). Thus the apparent temperature is made more dependent on the reflected surface temperature and less on the actual surface temperature. With MCAs of low emissivity or high IR reflectance installed, the signature is mostly the reflected surface and not the actual surface. If the reflected surface is background the AV appears as mostly background. This is the MCA signature reduction approach. For AV fronts, sides and rear surfaces (seen in low acquisition angles) highly reflective MCA materials are used, to reflect nearby background and hide the vehicle.

However MCAs on topside surfaces reflect the sky. Thus the MCA reflectance must be carefully selected so that the net radiant topside signature matches the look-down background. MCAs can be made reversible for Sea-Mode and for Land-Mode, since their visual colors as well as their IR reflectances will have to be different.

If the sky temperature is known with certainty, a perfect background match could be achieved, but since the sky varies from say -20°C to +20°C, an intermediate IR reflectance is selected to minimize the PSD's relative IR contrast. This intermediate reflectance was determined by minimizing the contrast temperature over the -20°C to +20°C range. If this range is less, the contrast signature is then reduced.

A special highly reflective IR material was prepared to cover the engine exhaust, to suppress a very detectable cue the front of the PSD.

#### PSD MCA INSTALLATION AND TEST RESULTS

The PSD was templated to define the sizes of the various MCA components. It was decided to bond the MCA material on a Coroplast™ board for easy mounting. Therefore the templates were used as guides for the Coroplast™ cutouts. The MBC manufactured IR reflective material was then bonded to these Coroplast™ boards. The MCA boards were then fastened to the PSD using commercial hook & loop fasteners. The MCA material for top side signature reduction was USA forest green with far IR reflectances of 72% and 55%. These MCA materials were cut into irregular shapes, and mixed on Coroplast™ test boards. The boards were not completely covered, so that there were 3 different IR reflectances being mixed on these boards. This ensured a mottled pattern, avoiding all straight edges that would aid in detection of the PSD.

The MCAs were attached, on the hot areas shown in the PSD thermal image on Figure 8 ; the Bow Plane , the Spray Wedge, the ventilation louvers, the hatches, (both outside and inside, since an open hatch is very detectable), the top and the front- face of the turret, and topsides of the rear deck.



Figure 9a: Coroplast™ mounted MCAs Attached

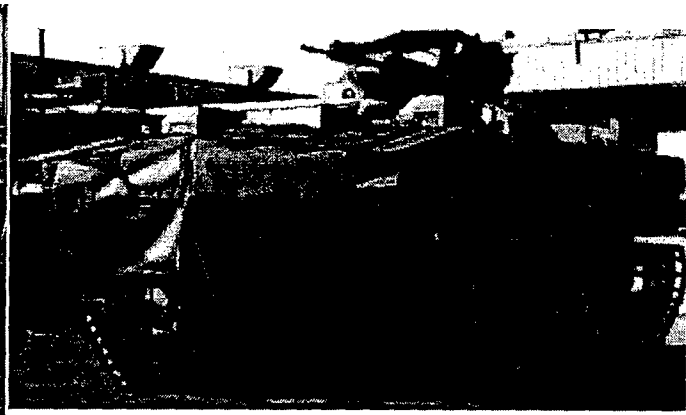


Figure 9b: MCA Tarp Attached

**Figure 9: PSD with Multispectral Camouflage Appliques attached.**

Figure 9 presents the PSD with MCAs attached. There were two approaches to apply the MCAs to the PSD. Coroplast™ mounted MCAs and a Bow Plane Tarp with MCAs (IR reflective material) bonded to the Tarp. This MCA does not use the Coroplast™ backing.

Figure 9a is a grayscale image, in the visible band, of the PSD with the Coroplast™ MCAs attached. Since the PSD was in the process of being repaired, no appliques were mounted on its side skirts which were removed from the vehicle. A second MCA approach used Texilene backing and bonded the IR reflective MCAs to this material.

This approach is shown in Figure 9b, and covers the same Bow Plane. The Tarp is 105" by 100" weighting less 5lb. The MCA Tarp has grommets for tiedown straps or bungee cords. The tarp could also be attached by means of hook and loop fasteners. Either method allows for quick and easy installation and removal. The tarp can be made reversible for sea or land use.

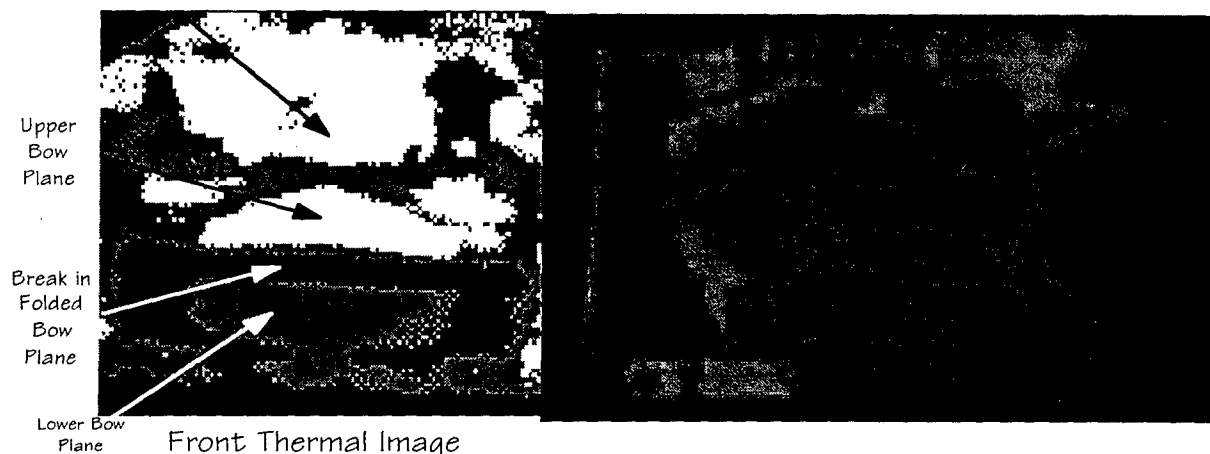


Figure 10a. PSD Thermal Image w/o MCA Covering.

Figure 10b: PSD Thermal Image with MCA Tarp.

**Figure 10: Side by Side of PSD Thermal Images**

Figure 10 is a side by side comparison of thermal images of the PSD front view uncovered (Figure 10a) and with the MCA Tarp (Figure 10b).

## Unclassified

The Figure 10b image is the thermal picture of the MCA Tarp covered PSD from the TOW FLIR in wide field of view. The scene is similar to the previous (visible band) picture of the MCA Tarp covering the PSD. Figure 10a shows glaring white (hot) and black (cold) sections of the uncovered PSD that are strong acquisition cues.

The Figure 10b image shows that the PSD with MCA Tarp masks these contrasts and presents a muted image to the hostile observer. The Spray Wedge hot triangle is masked as is the hot lower front of the turret (exhaust pipe heat radiation). This image was recorded on a clear cool day. The sky temperature was cold. The MCA section on the upper surface are darkest because they reflect the cold sky. Those on the lower part of the Spray Wedge are reflecting the local surface temperature which was between 5 °C and 10°C, 41° F and 50° F. This comparison alone shows the MCAs are a viable signature reduction technique.

### SUMMARY

This is a summary of the accomplishments of this developmental task.

- Signature reduction enhances the worth of increased speed in vehicle survivability. Quickness in coming ashore minimizes the chance of detection but low signatures along with speed reduces this chance to almost nil.
- Amphibious Vehicles need lightweight materials for buoyancy. These have thermal signature characteristics that can spotlight the vehicle for thermal imagers. Heat transfer calculations show the basis for these thermal signatures. These calculations can be used to design MCAs to hide these surface temperatures.
- MCAs demonstrated that they were effective in masking the PSD thermal hot spots and cues.
- The MCA Tarp is easily fabricated, it is adaptable to the many situations the USMC may be assigned, and yet it is light and easy to carry. It is the preferred MCA approach.

### REFERENCES

1. "Amphibious Clout Spells Success for Warfighter", Lt. Col. T. C. Linn, USMC, pg. 20, National Defense, Journal of the American Preparedness Association, April 1994.
2. Task 1 Technical Report: Data Collection, Contract Number N00167-94-C-0060, 13 July 1994.
3. Infrared Handbook, Figure 3-111, Infrared Information Analysis Center, 3rd printing 1989.
4. Tasks 2 and 3 Technical Report: Design Options and Tradeoff Analysis, and Draft MCA Specifications, Contract Number N00167-94-C-0060, 25 August 1994.

### ACKNOWLEDGEMENT

The work report here was performed under NSWC/USMC contract N00167-94-0060. The authors would like to thank Steve Ouimette of NSWC USMC Program Office and United Defense of York, PA for their assistance in the use of the PSD.

UNCLASSIFIED

GLOBAL INFRARED SIGNATURES: OPTIMIZATION AND STATISTICAL SYSTEM  
ASSESSMENT (U)

William R. Reynolds  
Signature Research, Incorporated  
Calumet, MI 49913

Jeffrey W. Petraska  
Mark A. Pasik  
General Dynamics Land Systems Division  
Sterling Heights, MI 48310

ABSTRACT (U)

(U) The diversity of ground vehicle thermal signatures is directly a consequence of the operational environment. Permutations of independent infrared (IR) signature parameters in the operational environment including diurnal and seasonal meteorological variations, background composition, operating profiles, etc., define the global IR signature. Signature management necessitates optimization of the global signature given multispectral constraints, thus the requirement to statistically evaluate signature performance with respect to trade studies, goals, and specifications. A practical approach is derived for the optimization and statistical system assessment of the global signature. A GDLS case study, including global signature calculations using PRISM, least squares optimization, and statistical analysis is presented.

(U) Introduction

(U) A ground combat vehicle is required to operate under extreme conditions in a number of diverse environments. For example, Operation Desert Storm used armored fighting vehicles to support a desert operation. The U.S. peace keeping mission in Bosnia currently requires armor support in the European theater. These radically different backgrounds, weather and operational conditions present unique design challenges to the engineer tasked to integrate low observables (LO) technology into ground combat vehicles. Successful system integration of LO requires the maximum survivability benefit over a wide spectrum of operational conditions.

(U) Our approach to thermal management using passive technologies is to minimize the global thermal signature over a representative sample of conditions, typically represented by diurnal cycles, that have been selected as "representers" of the ensemble of all conditions that will be encountered. The global thermal signature is quantified by the average signature measure over all meteorological inputs, background types, operational profiles, and seasonal and diurnal variations that the vehicle may encounter [1]. Examples of signature measures are probability of detection, search time, contrast temperature, or other measures of detectability. For simplicity the contrast temperature,  $\Delta T$ , which is the difference between the average radiometric temperature of the vehicle and the average radiometric temperature of the background, is universally used in the signature community. In addition, the root mean square (rms) temperature of the vehicle, which is the rms temperature variation across the vehicle surface, is also employed because of the increased sophistication of threat systems.

UNCLASSIFIED

(U) Estimates of the global signature are obtained using thermal models such as PRISM and the representer input data set. The model-based approach to estimating the global thermal signature mitigates the difficult and expensive task of obtaining measured data in the field. Representer inputs to the model have been selected using cluster analysis of 12 months of measured meteorological data obtained at 7 minute intervals for each diurnal cycle [2,3]. The objective of the representer approach is to obtain a statistically good global signature estimate using a minimum of input data to the model. For example, if the same signature approximation can be obtained using 2 or 3 diurnal cycles as opposed to using 30 diurnal cycles for each month then a significant savings in analysis is realized.

(U) With the establishment of a methodology to obtain global signature estimates the process of reducing the vehicle signature is quantified. A signature treatment can be modeled and the impact on the global signature can be computed. Parameters of the signature treatment, emissivity for example, can be varied until a minimum signature is obtained. The capability to optimize a treatment, subsystem and system using a model based approach is extremely important and is the basis of modern LO design. It is too costly and complex to try to optimize system level design using field testing. The cummulation of the following problems are nearly insurmountable:

- (U) uncontrolled environment,
- (U) no repeatability,
- (U) long lead times (one year for seasonal variations),
- (U) test hardware fabrication and maintenance, and
- (U) intensive resource requirements (expensive).

#### (U) Approach

(U) The model based optimization process can proceed at the system, subsystem or component level since thermal models such as PRISM do not have the capability to iterate on design parameters. It is often advantageous to optimize at the sub-system level where possible. The optimization process proceeds as follows:

1. (U) Select the representer input data set that will approximate the global operation of the system.
2. (U) Create a valid representation of the treatment, subsystem, or system for the model.
3. (U) Run the model and compute the integrated or sum square error (SSE) measure of merit,  $\Delta T$  for example.
4. (U) Re-run the model as required to minimize the SSE for the design parameter(s) of interest.

#### (U) Case Study

(U) A familiar problem is to find the optimal emissivity value for the various surfaces of a ground vehicle. In addition, if stand-off plates are added to the system the thermal response can be tuned to minimize contrast using the additional degrees of freedom. The edges of the stand-off are open to promote natural convection between the plate and the vehicle surface. The thermal

## UNCLASSIFIED

(U) mass, solar absorptivity and thermal emissivity are free parameters of the system. In addition to all of the scenario, meteorological, and operational conditions impacting the vehicle surfaces, the plate also exchanges heat with both the terrain and sky as a function of the surface normal angle.

(U) One solution to the problem is obtained by defining a simple thermal representation of a vehicle surface with and without a stand-off plate. The emissivity level of the external surface is varied in increments of 0.05 until the SSE,  $\epsilon$ , in (1) is minimized for each of the geometric orientations being considered.

$$SSE = \epsilon = \sum_{i=1}^{n=288} (T_i^v - T_i^b)^2 \quad (1)$$

(U) where  $T_i^v$  is the average vehicle temperature and  $T_i^b$  is the average background temperature of the  $i^{\text{th}}$  time sample of a 24-hour diurnal cycle, which consisted of 288 data points in our analysis. A rms contrast temperature is computed from the SSE in (1) by

$$T_{rms} = \sqrt{\frac{\epsilon}{n-1}} \quad (2)$$

(U) In this case the surface normal is examined for five orientations, north, south, east, west and vertical.

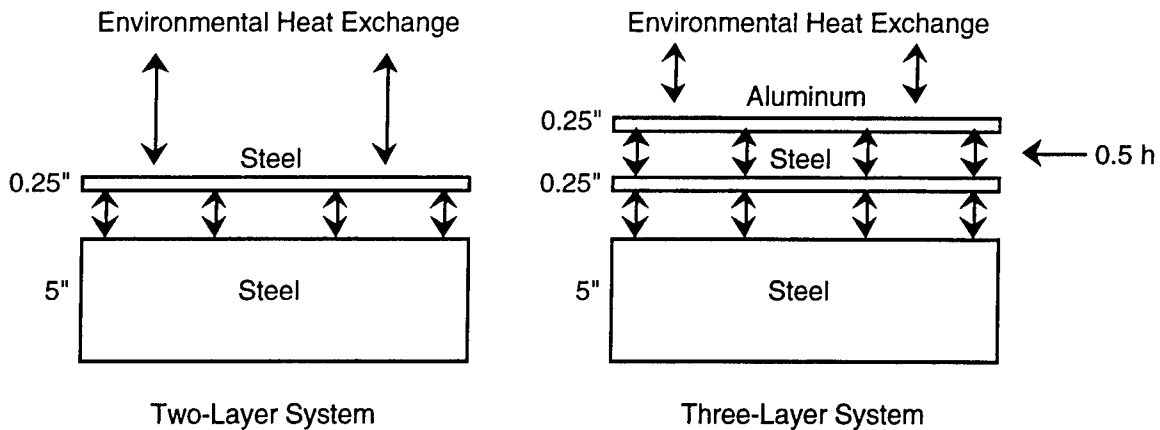
(U) Three diurnal cycles from an Aberdeen Proving Ground data collection were selected to represent the meteorological environment in which the flat plate system would be optimized. The days are described as a cloudy spring day, partially cloudy summer day and a clear fall day. A tall grass or weedy type background was selected for the model. In the background data files adjustments were made for the living and dormant condition of the vegetation in response to the seasonal variations.

(U) The various external surfaces of the ground vehicle are simulated with a flat plate system comprised of two flat steel plates shown in Figure 1. In the three-layer system the outermost aluminum stand-off plate, 0.25 inches thick, is exposed to the ambient environment and participates in convective and radiative heat exchange with the environment. The middle plate, which represents the vehicle skin, is also 0.25 inches thick. It exchanges radiation with the plates above and below, and is also subjected to convection at half of the level as the exterior surface. The retarding of the convection coefficient simulates the reduced flow that might be expected in the two-dimensional channel. In addition, as the air in the channel picks up heat the convection becomes less efficient. The two-layer system is identical to the three-layer system, except for the absence of the stand-off plate. In this case the vehicle surface (0.25" steel plate) is completely exposed to radiative and convective heat exchange with the environment.

(U) In both systems the bottom plate, approximately 5 inches thick, represents the large thermal mass of a vehicular system. This plate serves as a heat sink and is connected to the environment by radiation exchange with the middle plate. Convection is not considered between these layers. The emissivity of the inner surfaces of both plates is initially set to 0.94.

UNCLASSIFIED





UNCLASSIFIED

Figure 1. (U) Conceptual Drawings of the Two-Layer and Three-Layer Panel Systems.

(U) PRISM was modified to compute and output the SSE for each of the diurnal cycles. Initially, 12 emissivity levels were run simultaneously. A second input file having still lower emissivities was created if the global minimum was not obtained.

(U) The SSEs for the horizontal two-layer system are reproduced in Table I with the total SSE in the fifth column. Four  $\Delta T$ s per hour of the simulation elapsed time were used for the total of 96 points per diurnal cycle to compute the SSE. The minimum SSE value in each column is shaded.

Table I. (U) SSE Values for the Horizontal Two-Layer System.

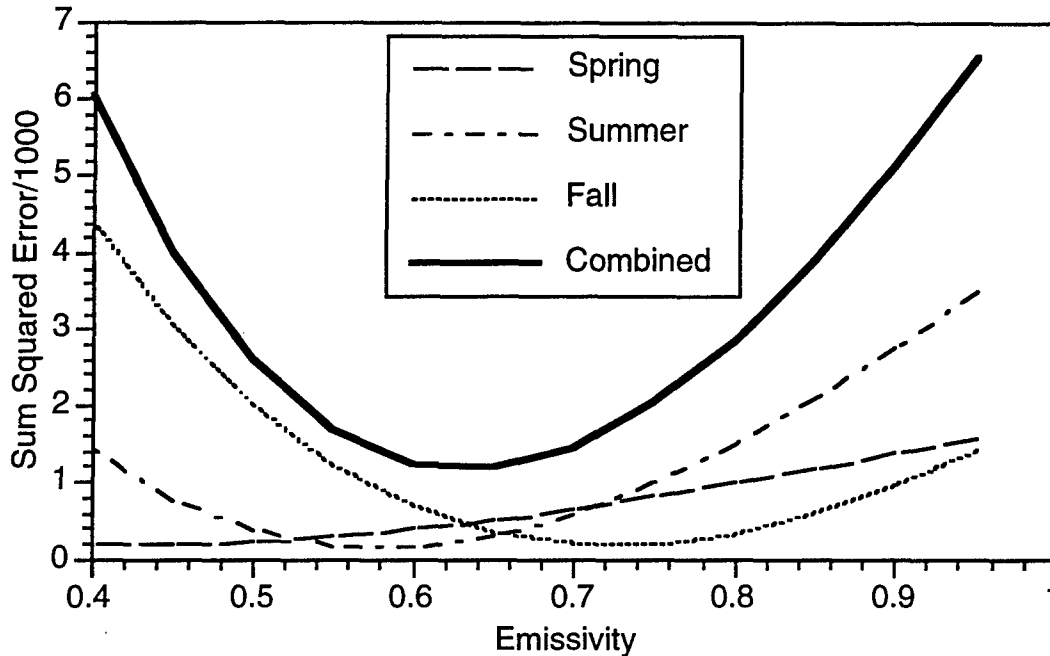
Emissivity	Spring Day ( $\times 10^{-3}$ )	Summer Day ( $\times 10^{-3}$ )	Fall Day ( $\times 10^{-3}$ )	Total ( $\times 10^{-3}$ )
0.95	1.492	3.121	1.122	5.734
0.90	1.331	2.553	0.779	4.663
0.85	1.139	1.903	0.436	3.478
0.80	0.959	1.331	0.197	2.488
0.75	0.793	0.847	<b>0.080</b>	1.720
0.70	0.643	0.467	0.101	1.211
0.65	0.510	0.205	0.280	<b>0.995</b>
0.60	0.398	<b>0.089</b>	0.640	1.119
0.55	0.309	0.115	1.208	1.633
0.50	0.246	0.333	2.015	2.594
0.45	<b>0.213</b>	0.762	3.094	4.069
0.40	0.214	1.437	4.489	6.140

UNCLASSIFIED

(U) The data in Table I shows that the global optimum emissivity level for the horizontal two-layer system is 0.65. Table I also shows that the optimal emissivities for the spring, summer, and fall diurnal cycles are 0.45, 0.55, and 0.75, respectively, suggesting that as the solar loading increases the optimal emissivity also increases. It is more likely, however, that the trend is due to the reduced amount of long-wave thermal energy that is received as the cloud cover is reduced. The clear sky, particularly at night, will tend to cause a large negative contrast due to the reduced reflective component of radiosity.

UNCLASSIFIED

(U) It is also important to note that the global optimal emissivity in Table I is not 0.58, the average of the three optimum diurnal emissivities. The slope or the rate at which the optimal value is approached with respect to the independent variable has skewed the global optimal away from the average. This effect can be observed in Figure 2, which is a plot of the analogous data for the three-layer configuration. The SSE cusp for the summer day is much steeper at the higher emissivity levels than the fall day.



UNCLASSIFIED

Figure 2. (U) The SSE for the three-layer system as a function of the emissivity for each of the diurnal cycles and the combined global values.

(U) Further analysis was performed to find the optimal emissivities on the three-layer system as a function of time of day and orientation. Optimal emissivities for both daylight (solar) and night (non-solar) portions of the diurnal cycle were computed for horizontal plates, as well as for two cases where the surface normal was rotated 45 degrees from vertical. Diurnal optimal emissivities were also calculated for vertical plates facing north, south, east, and west. Table II contains the summary results of these experiments.

Table II. (U) Optimal Emissivities for the Three-Layer Panel System.

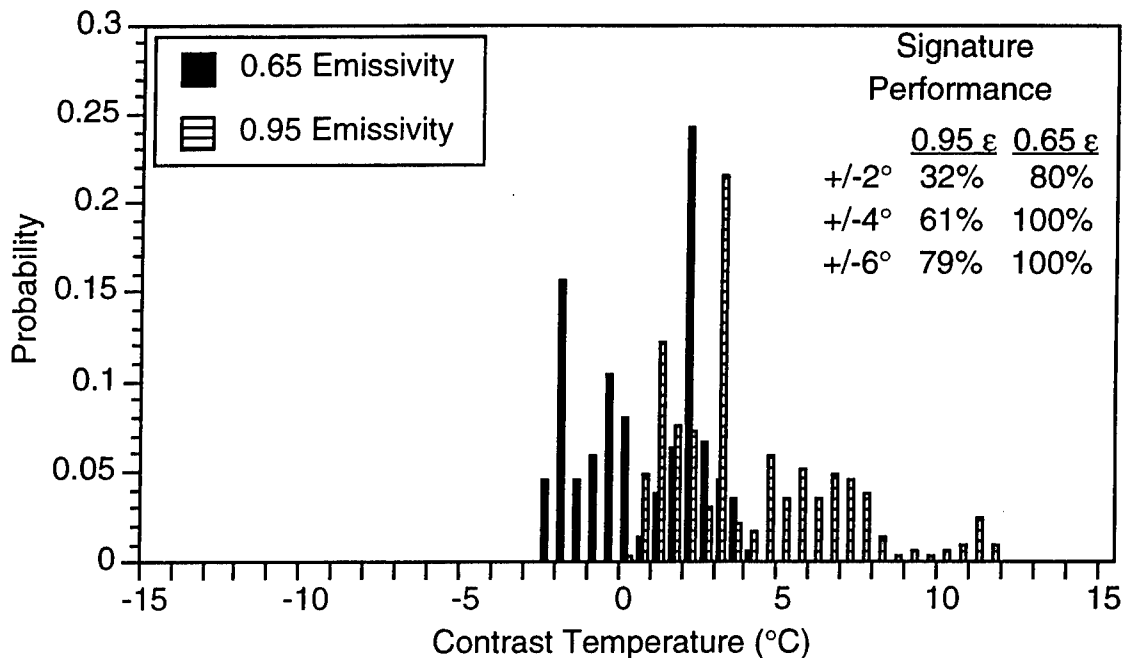
Surface Normal	Day				Night				Diurnal			
	sprg	sumr	fall	com	sprg	sumr	fall	com	sprg	sumr	fall	com
Vertical	0.45	0.55	0.70	0.60	<.45	0.70	0.90	0.80	<.45	0.55	0.70	0.65
North									<.45	0.70	>.95	0.75
East									<.45	0.50	0.65	0.55
45° Elv. South									<.45	0.55	0.50	0.50
South	<.45	0.90	0.45	0.50	<.45	0.45	0.55	0.45	<.45	0.75	0.45	0.50
45° Elv. West									<.45	0.55	0.60	0.55
West	0.45	0.50	<.45	0.45	<.45	<.45	0.55	0.45	<.45	0.45	0.45	0.45

UNCLASSIFIED

UNCLASSIFIED

(U) If it is assumed that the vehicle azimuth over the mission life is random, that any direction is equally probable, then the optimal emissivity for a vertical stand-off surface is 0.56, the average of the combined north, east, south, and west values highlighted in the last column of Table II. In summary, the optimal emissivity for vertical surfaces is about 0.10 less than for horizontal surfaces.

(U) To quantify the impact of changing the emissivity to the optimum value the simulation contrast temperatures were examined statistically for the horizontal three-layer system. Figure 3 contains the histograms of both the 0.95 emissivity and 0.65 optimal stand-off plate emissivity levels. The signature performance measure, defined to be the percentage of time within selected  $\Delta T$  intervals, shows that for the standard 0.95 emissivity the stand-off plate signature is within  $\pm 2$  degrees C 32 percent of the time. The 0.65 optimal emissivity stand-off achieves  $\pm 2$  degrees C or less 80 percent of the time. Similar improvements are seen for signature levels of  $\pm 4$  and  $\pm 6$  degrees C. It can be observed in Figure 3 that the general impact of emissivity changes on the system is to translate histogram along the contrast axis.



UNCLASSIFIED

Figure 3. (U) Histogram of contrast values for an aluminum stand-off three-layer system.

(U) Re-running the configurations in Table II for the two-layer system yielded exactly the same global optimal emissivity values. In fact,  $T_{rms}$  was slightly higher for the horizontal three-layer system than for the two-layer system, 2.2 versus 1.9 degree C, whereas the three-layer  $T_{rms}$  was slightly lower with the panels in the vertical orientations. In comparison, for the two-layer configuration  $T_{rms}$  is 4.5°C when the emissivity is 0.95, the approximation of a standard CARC coating. The use of an optimal coating emissivity reduces the rms contrast temperature a full 2.6 degrees.

(U) The impact of the thickness of the outer panel on the signature was examined for the horizontal two-layer system. By varying the thickness (and the thermal mass) of the outer layer, the system signature might be further reduced. The SSEs for the horizontal two-layer system with a 0.55 emissivity are plotted in Figure 4 and show that the system is relatively insensitive to modest changes in the thermal mass. In fact, a 12 fold increase in thickness from 1 mm to 12 mm provided negligible  $T_{ms}$  difference.

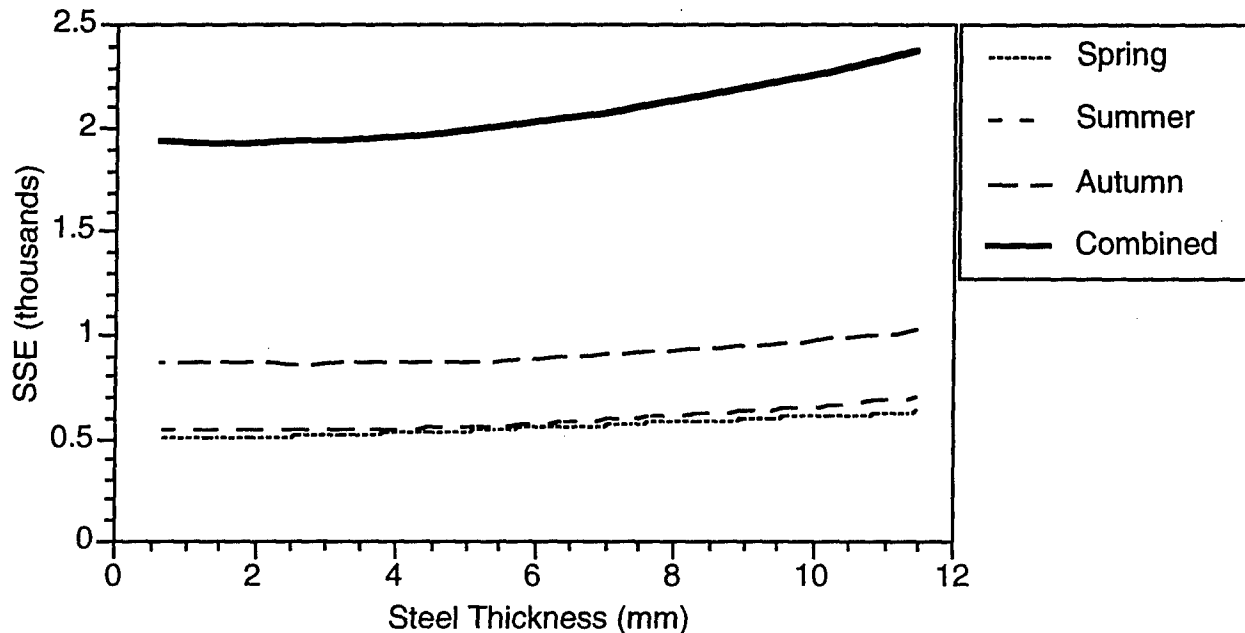


Figure 4. (U) Sensitivity of the SSE to perturbations in thickness (thermal mass) where the surface emissivity is 0.55.

#### (U) Summary and Conclusions

(U) In general, the optimization methodology described above, whether implemented at the component, subsystem or system level plays an important role in the design cycle. The above example provides insight into the complexities of fine-tuning a conceptually simple technology.

(U) The thermal signature histogram is an efficient method of describing a thermal signature in the sense that the relevant complexities of the signature are preserved.

(U) It is demonstrated theoretically that passive emissivity control is a powerful technology for signature control if carefully utilized. The following points highlight some of the results:

- (U) The optimal emissivity for vertical and horizontal surfaces are different.
- (U) The orientation of a vertical surface impacts the optimal emissivity dramatically.
- (U) Within limits the signature is relatively insensitive to material thickness.
- (U) The two-layer and three-layer systems yield identical global optimal emissivity values.
- (U) Emissivity shifts effect a translation in the IR signature histogram.

UNCLASSIFIED

(U) References

1. (U) LaHaie, A.M.L., Beckwith, J.P., Wilburn, D.K., and Reynolds, W.R., "IR/SRM, A Signature Rating Model," Final Report, TACOM Rept. No. 13474, Jan, 1990.
2. (U) Hilgers, J.W., Reynolds, W.R. and Petraska, J.W., "Principal Component Analysis of Measured Meteorological Parameters for Weighted Thermal Signature Assessment," Proc. Fifth Ground Target Modeling and Validation Conference, Mich. Tech Univ., 1995.
3. (U) Hilgers, J.W., Reynolds, W.R. and Petraska, J.W., "Parameter Normalization in Meteorological Data Characterization for Thermal Signature Analysis," , Proc. Sixth Ground Target Modeling and Validation Conference, Mich. Tech Univ., 1996.

UNCLASSIFIED

UNCLASSIFIED

**PENETRATION MECHANICS & MODELNG SESSION**

Glasgow Auditorium  
Wednesday, March 27, 1996

Session Chairman: Mr. Rodney Peterson, Naval Surface Warfare Center

UNCLASSIFIED

UNCLASSIFIED

THIS PAGE INTENTIONALLY LEFT BLANK

UNCLASSIFIED

UNCLASSIFIED

## SCALE MODEL EXPERIMENTS WITH CERAMIC LAMINATE TARGETS

Charles E. Anderson, Jr.<sup>†</sup>, Scott A. Mullin<sup>†</sup>, Andrew J. Piekutowski<sup>‡</sup>,  
Neil W. Blaylock<sup>†</sup>, Kevin L. Poormon<sup>‡</sup>

<sup>†</sup>Southwest Research Institute  
San Antonio, TX 78228-0510

<sup>‡</sup>University of Dayton Research Institute  
Dayton, OH 45469-0182

### ABSTRACT

Ballistic impact experiments were performed on ceramic laminate targets at three scale sizes—nominally 1/3, 1/6, and 1/12—to quantify the effects of scale on various responses, in particular, the ballistic limit velocity. The experiments were carefully designed and controlled so that the different scale sizes were high fidelity replicas of each other. A variety of responses were measured. Some of the measured quantities showed little or no dependence on scale size, whereas other quantities, particularly the ballistic limit velocity, were found to vary with scale size. The results for the ballistic limit velocity were extrapolated to estimate full-scale response from the subscale tests.

### INTRODUCTION

Scale models are commonly used in experimental investigations. At ordnance velocities, scaled projectiles and targets are generally used to limit the cost of experiments. In addition, since gun systems are kinetic-energy limited, smaller projectile masses must be used to obtain impact velocities greater than 2.0 km/s. However, there has been a reluctance on the part of many applied researchers to accept scale model data in lieu of full-scale data for actual projectile-target interactions. This reluctance is generally attributable to a belief that full-scale performance cannot be predicted accurately from subscale data. Unfortunately, documentation to either support or refute this belief is essentially nonexistent.

Important parameters, such as geometry, material properties, and impact conditions, can be formed into nondimensional terms, referred to as Pi terms; for example, see Ref. [1]. According to the principles of similitude modeling, when Pi terms (those relating geometry, material characteristics, and initial conditions) are kept invariant between two different experiments, the experiments will display "similar" response. In other words, the values of the response Pi terms will be equal between the experiments. The most common approach to satisfy the requirements imposed by the Pi terms is to develop a replica model. A replica model is one in which the same materials are used in the model as the prototype—within the context of this article, "prototype" refers to the full-scale test articles and experiment—with the only difference being geometric size. The model is constructed so as to mimic the arrangement of the prototype, with corresponding materials at corresponding locations. The size of a replica model relative to the prototype is described by the geometric scale factor, denoted by  $\lambda$ . For example, the  $\lambda$  in this work will represent subscale sizes between 1/12 and 1/3. One feature of replica scaling is that velocity is invariant; i.e., for ballistic impact testing, model and prototype projectiles are fired at the same velocity. However, the concept of a replica model contains some inherent issues that may lead to distortions in the subscale model and limit its ability to reproduce full-scale results. In a replica model, the model

UNCLASSIFIED



law results in conflicting requirements on the Pi terms involving strain rate and fracture toughness, thereby making it impossible to keep Pi terms involving these parameters invariant (see Ref. [1] for a more detailed discussion).

Recent work [1-3], including the present effort, has focused specifically on issues related to scaling of ballistic penetration ( $V > 1$  km/s). In these studies, attention has been paid to materials, fabrication, experimental procedures, and terms that distort as scale size changes. The work in Refs. [1-3] is concerned with steel (RHA) targets; in the study discussed here, the targets were ceramic laminates. Approximately 36% of the thickness of the target was ceramic; the remainder was armor steel. Ballistic tests were conducted at three scale sizes with two targets of different thickness. The test methodology was designed to permit the determination of the ballistic limit velocities. Additionally, a variety of other measurements was performed: hole diameters and crater height on the impact side of the target, bulge height on the exit side, penetration depth for targets not perforated, and residual projectile length and velocity for targets perforated. The overall objective was to determine the magnitude of the scale effect (if any).

## EXPERIMENTS

**Projectiles.** Full scale was defined in terms of a long-rod tungsten alloy penetrator with a hemispherical nose, length-to-diameter ratio of 20, and a diameter of 2.54 cm. This was called the prototype projectile for the purpose of defining the subscale projectiles; no full-scale tests were conducted. Subscale projectiles were designed to replicate the prototype at three scale sizes: 1/3.15, 1/6.30, and 1/12.60. The tungsten alloy used for the tests, WN008FH manufactured by GTE (90% tungsten, 8% nickle, and 2% iron), has a density of  $17.19 \text{ g/cm}^3$ . Dimensions for the projectiles are listed in Table I. There is a factor of four between the smallest and largest of the subscale projectiles.

Table I. Nominal Projectile Dimensions and Masses

Scale Size, $\lambda$	Diameter, $D$ (cm)	Length, $L$ (cm)	Mass, $M$ (g)
1/3.15	0.8063	16.12	158.9
1/6.30	0.4032	8.064	19.82
1/12.60	0.2016	4.032	2.433

**Targets.** A schematic of the target is shown in Fig. 1. Thickness proportions of the steel/ceramic/steel layers were selected as 3:4:4. Total target thickness is represented by the parameter  $T$ . The target is analogous to a range target used for testing and evaluation; however, to avoid certain proprietary issues, the targets used in this study were not replicas of the range target. All components of the targets were sized for geometric scaling between the three scale sizes. The steel was 4340 steel, hardened to  $R_c 30 \pm 2$ ; the ceramic was 99.5% pure aluminum oxide manufactured by Ceredyne. Fiberfrax, a non-asbestos, cloth-like (glass) insulating material (density of  $0.1 \text{ g/cm}^3$ ) manufactured by Carborundum, was used to isolate the ceramic tiles from the front and back steel plates. Targets were fabricated by welding mild steel side plates and angle iron to the front and back 4340-steel plates. Weld lines are depicted in Fig. 1 by the closely spaced hash lines or by the heavy black fill. Two target sets were designed; the elements in the second target set were 50% thicker than the elements in the first target set. Table II provides the dimensions of the various elements in the two target sets.

UNCLASSIFIED

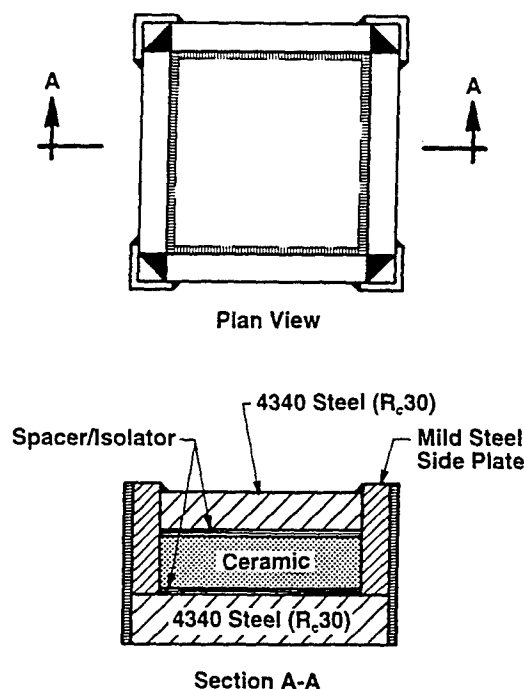


Figure 1. Schematic of target configuration.

Table II. Dimensions for Ceramic Laminate Targets

	1/3.15	1/6.30	1/12.60	1/3.15	1/6.30	1/12.60
	Target 1 Thicknesses (cm)			Target 2 Thicknesses (cm)		
Front plate: 4340 Steel	3.810	1.905	0.953	5.715	2.858	1.429
Layer 2: Fiberfrax	0.635	0.318	0.159	0.635	0.318	0.159
Ceramic: 99.5% Al <sub>2</sub> O <sub>3</sub>	5.080	2.540	1.270	7.620	3.810	1.905
Layer 4: Fiberfrax	0.635	0.318	0.159	0.635	0.318	0.159
Base Plate: 4340 Steel	5.080	2.540	1.270	7.620	3.810	1.905
Side Plates: Mild Steel	2.540	1.270	0.635	2.540	1.270	0.635
Angle Iron: Steel	5.1x5.1x0.95	2.5x2.5x0.64	1.3x1.3x0.32	5.1x5.1x0.95	2.5x2.5x0.64	1.3x1.3x0.32

**Experimental Data.** Projectiles were launched from a two-stage light-gas gun. The two smaller projectiles were launched from a 50/20-mm system; a 75/30-mm system was used for the larger projectile. Velocities were determined using a laser "break" beam system. Projectile yaw and pitch were obtained by orthogonal flash X-rays prior to impact, and combined to give the total impact inclination  $\gamma$ . The primary objective of the test series was to determine the ballistic limit velocity  $V_{BL}$  for each target thickness and scale size. Additionally, parameters were measured so that the effect of scale on other target responses could be determined. Details of the experimental results are provided in Ref. [4].

UNCLASSIFIED

The 1/12.6-scale tests were plagued by excessive projectile yaw. This was largely attributed to the mass of the sabot with respect to the projectile mass since any asymmetry in the opening of the sabot would be sufficient to perturb the flight of the projectile. Although projectile yaw confounds data analysis, attempts were made to account explicitly for the effects of yaw in the analysis.

## DATA ANALYSIS

### Ballistic Limit

Several methods were used to determine the ballistic limit velocity. One of the preferred ways for determining  $V_{BL}$  is to fit the experimental data to the Lambert equation [5]:

$$V_r = \begin{cases} 0, & 0 \leq V_s \leq V_{BL} \\ a(V_s^p - V_{BL}^p)^{1/p}, & V_s > V_{BL} \end{cases} \quad (1)$$

where  $V_r$ ,  $V_s$ , and  $V_{BL}$  are the residual, striking (impact), and limit velocities, respectively. The parameters found through a nonlinear regression fit to the experimental data are the slope  $a$ , the exponent  $p$ , and the limit velocity  $V_{BL}$ . The experimental data points, along with the results of the curve fits, are plotted in Fig. 2 for the  $T/L = 0.945$  target set. Excessive projectile inclination at impact is denoted by an open symbol. The maximum velocity that could be achieved for the 1/3.15-scale projectile launch package was 2.33 km/s, and this velocity was not sufficient to perforate the thicker ( $T/L = 1.378$ ) target. The ballistic limit velocities are given in Table III for cases where sufficient data existed to apply Eqn. (1).

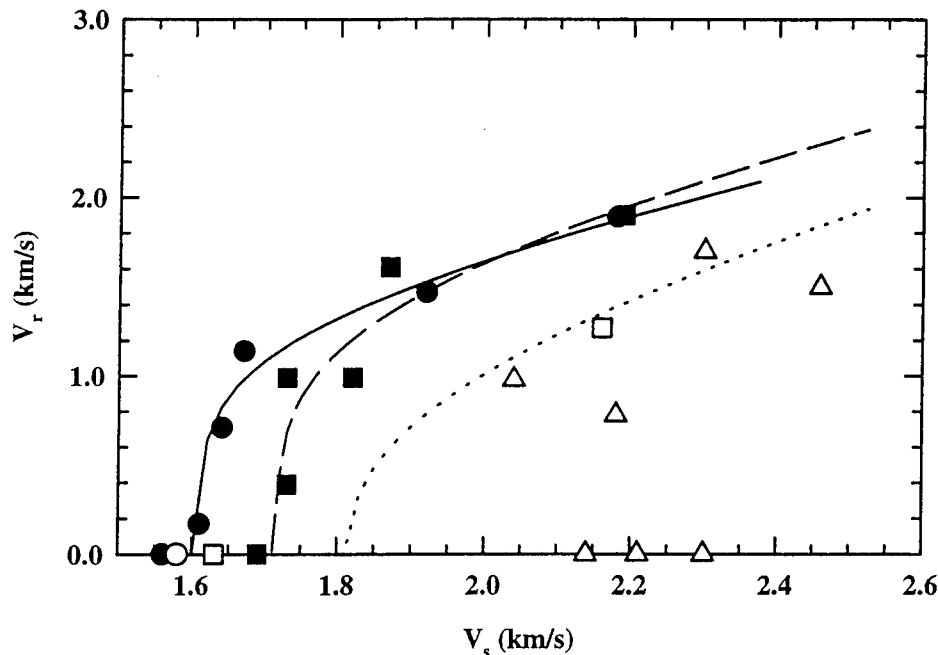


Figure 2. Residual velocity vs impact velocity for  $T/L = 0.945$  target. (Open symbols represent large impact inclination.)

Table III. Estimates of Ballistic Limit Velocities (km/s)

Scale Size $\lambda$	$T/L = 0.945$			$T/L = 1.378$		
	Eqn. (1)	Perf/No Perf	$V + \Delta V$	Eqn. (1)	Perf/No Perf	$V + \Delta V$
1/3.15	1.61	1.59	1.65	—	> 2.33	2.46
1/6.30	1.72	1.71	1.69	2.54	2.57	2.54
1/12.6	1.82	< 2.04	< 2.14	—	> 2.39 < 2.72	2.77

A second method to estimate the ballistic limit velocity examined the perforation (perf) versus no perforation (no perf) data as a function of impact velocity. In several cases, perforation occurred with only a small increase in impact velocity beyond a "no perf" datum, thereby providing a reasonably good estimate of the ballistic limit velocity. The estimates for the ballistic limit velocity using this procedure are also listed in Table III.

The last procedure applied is the least precise of the three methods, but it permits an estimate for the limit velocity for targets not perforated and permits a correction to be approximated for impact inclination. For those projectiles that did not perforate the target, a velocity increment necessary to achieve perforation was estimated. We will refer to this procedure as the ( $V + \Delta V$ ) method. The procedure makes use of the semi-infinite normalized penetration curve as a function of velocity, i.e.,  $P/L$  vs  $V$ . Using the slope of the  $P/L$  vs  $V$  curve, the increment in velocity necessary to achieve a small increment in penetration can be accurately estimated. However, target bulging and failure create uncertainties in a methodology that is based on "semi-infinite" penetration. To allow for less confinement in a finite target, the  $\Delta V$  needed to achieve perforation is modified. The details are provided in Ref. [4]. Additionally, Bjerke, *et al.* [6], provide the basis for a first-order estimate of the effects of impact inclination (yaw). Again, the details are provided in Ref. [4].

The  $V + \Delta V$  method was applied to both target sets. The method gives reasonable answers (within 0.05 km/s) for  $V_{BL}$  for the cases where Eqn. (1) and the perf/no perf methods could be applied; see Table III. For the 1/3.15-scale and the 1/12.6-scale tests, for which  $T/L = 1.378$ , the  $V + \Delta V$  method provided the only estimate for  $V_{BL}$  (although the perf/no perf procedure was used to place constraints on acceptable values). As already noted, the 1/12.6-scale experiments were plagued by excessive yaw.

We now want to place uncertainties on the estimates for the ballistic limit velocities. Methodologies have been developed to permit estimates of the ballistic limit velocity from a relatively small number of tests [7]. Central to these methodologies is the recognition that over a specified velocity range, either a partial or a complete penetration of a target may occur—a zone of mixed results—with the percent of complete penetrations over this range increasing as the impact velocity increases. Experience has shown that the zone of mixed results is 0.020 to 0.050 km/s wide for metallic armor materials. That is, the ballistic limit velocity is  $\pm 0.010$  to  $\pm 0.025$  km/s about some mean velocity, usually referred to as  $V_{50}$ , which for purposes here is considered to be synonymous with  $V_{BL}$ . For example, in Ref. [8], the ballistic limit velocities were determined for two different target thicknesses within  $\pm 0.010$  km/s with a very small number of tests.

With the preceding paragraph as background, results of Table III, combined with a review of all of the data, permit an estimate of the ballistic limit velocities and the associated uncertainties, Table IV. Typically, for cases where perf/no perf data exist, the limit velocity is taken to be the average of the two impact velocities, and the uncertainty is the distance between this average and either data point. To be conservative, we have doubled this uncertainty. A similar analysis has been applied to the data in Table III, subject to the constraints imposed by "perf/no perf". The uncertainties in Table IV reflect at least, we believe, a  $2\sigma$  value for  $V_{BL}$ .

**Table IV. Ballistic Limit Velocities and Uncertainties (km/s)**

Scale Size $\lambda$	$T/L = 0.945$	$T/L = 1.378$
1/3.15	$1.60 \pm 0.04$	$2.40 \pm 0.10$
1/6.30	$1.71 \pm 0.04$	$2.55 \pm 0.04$
1/12.6	$1.90 \pm 0.16$	$2.70 \pm 0.04$ - 0.10

## ANALYSIS OF SCALING EFFECTS

Analysis of the experimental data seeks to determine whether there is a systematic difference in response as a function of scale, beyond that attributable to measurement uncertainty. A large body of evidence exists for a fundamental energy scaling principle in which some critical energy is a constant [9]:

$$E_c = \text{constant}, \quad (2)$$

where  $E_c$  has units of energy per unit area. Examples include detonation of explosives, spall strength, failure of brittle structures, aspects of shear banding, and fragmentation [4]. For the case here, we write Eqn. (2) in the form:

$$\rho_p V_{BL}^2 l = \text{constant}, \quad (3)$$

where  $l$  is some characteristic length, such as projectile length or target thickness. Length scales as the geometric scale factor  $\lambda$ , which then suggests

$$V_{BL} \propto \lambda^{-1/2}. \quad (4)$$

The ballistic limit velocities with their uncertainties are plotted versus the inverse square root of the scale size in Fig. 3. Over a scale factor of four, the observed differences between the ballistic limit velocities are greater than the uncertainties in the determination of  $V_{BL}$ . The results of Fig. 3 indicate that  $V_{BL}$  increases as the scale size decreases, and that  $V_{BL}$  is approximately linear with respect to  $\lambda^{-1/2}$ .

A linear least-squares regression fit was performed as a function of  $\lambda^{-1/2}$ . Data points were weighted by the inverse of their uncertainty prior to the regression analysis. Results of the regression analyses are, with  $V_{BL}$  in km/s:

$$V_{BL} = 1.30 + 0.165\lambda^{-1/2} \quad T/L = 0.945 \quad (r^2 = 0.995) \quad (5a)$$

$$V_{BL} = 2.12 + 0.166\lambda^{-1/2} \quad T/L = 1.378 \quad (r^2 = 0.983) \quad (5b)$$

The linear least-squares fits to the data are shown as the dotted lines in Fig. 3. Note that the slopes in Eqns. (5) are independent of the impact velocity. Of course, Eqns. (5) applies *only* to the materials and geometries, i.e., projectile and target configuration, tested.

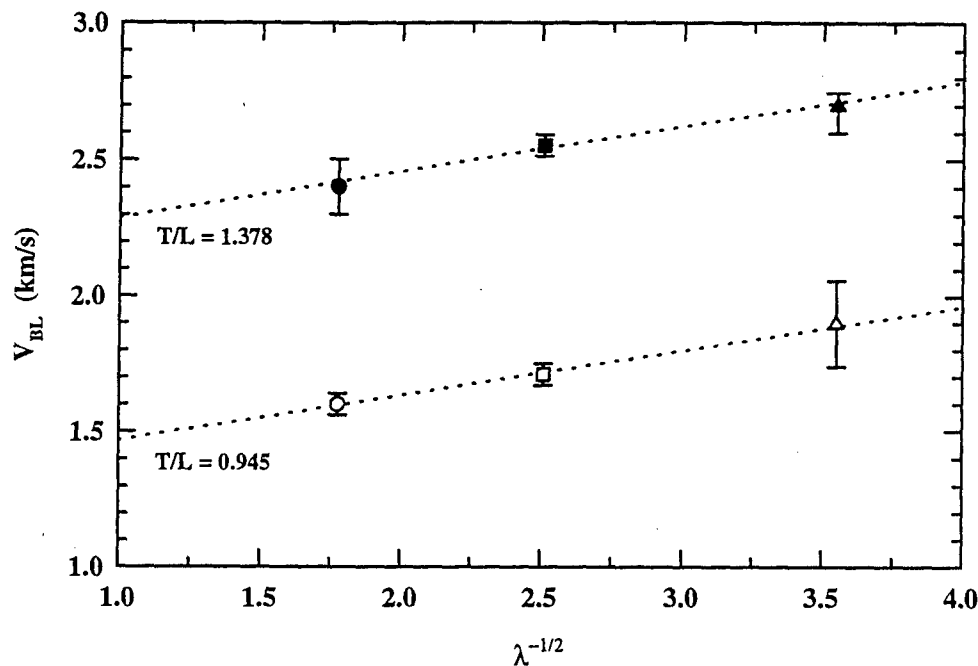


Figure 3. Ballistic limit velocities versus scale size

It is possible to extrapolate the subscale data to full scale to estimate the ballistic limit velocity at full scale. Setting  $\lambda = 1$  in Eqns. (5) gives 1.46 km/s and 2.29 km/s for the two target thicknesses, respectively; thus,  $V_{BL}$  for full scale is significantly lower than would be predicted by each subscale test. These targets have not been built or tested at full scale, so we do not have confirmation of the full-scale prediction. However, it appears that the apocryphal stories are true that subscale results are different than full-scale results in armor penetration experiments. In fact, the results here show that subscale tests will overestimate the effectiveness of an armor system.

## SUMMARY AND DISCUSSION

A series of tests at three scale sizes was performed to determine the ballistic limit of two ceramic laminate targets; the second target was 50% thicker than the first and therefore required higher impact velocities for perforation. Other measures of ballistic performance were recorded in addition to the ballistic limit. Because of the small quantity of comparable data, the effect could

not be quantified. These measurements included penetration depth in targets not perforated, residual projectile length and velocity for perforated targets, and the bulge height on the target rear plate. For all of these measures, target resistance to penetration appeared to increase as the scale size became smaller. For example, 1/12-scale targets had lower normalized residual velocity, less penetration depth, and lower bulge height than comparable 1/3-scale targets tested with approximately the same impact velocity.

The scale size effect could be quantified for the ballistic limit velocity since the test series was specifically designed to determine this response parameter. (Parenthetically, we note that the scale size dependency of the response variables described in the previous paragraph are consistent with a ballistic-limit-velocity scale effect.) It was found that  $V_{BL}$  decreased with increasing scale size. For the two ceramic laminate targets tested in this study,  $V_{BL}$  changed by approximately 120 m/s for a factor of two change in the scale size [Eqn. (5)]. Since the scale sizes were varied over a factor of four, a reasonable extrapolation can be made to estimate full-scale response. For example, for the impact conditions and types of targets and projectiles tested here, this study indicates that 1/6-scale targets could overpredict full-scale response by approximately 15%.

What is the underlying cause of the scale effect? It was demonstrated in Ref. [1], using numerical simulations, that strain rate hardening cannot be used to explain differences of more than 5% over a scale factor of 10. Lending support to the computational study is an experimental investigation by Wen and Jones [10] where they found geometrically similar responses over a scale factor of four, even when using strain rate sensitive materials (albeit the experiments were performed at a considerably lower impact velocity).

It was suggested in Ref. [1] that a possible explanation for the scale size effect is the difference in absolute time available for damage or failure to evolve. Failure of the target and projectile depend upon the stress state and accumulation of damage. The stress state at the various scales is very nearly the same, since the stresses are primarily a function of impact velocity (with only a little dependence on strain rate). On the other hand, damage accumulates with time. In these scale model experiments, time scales as  $\lambda$ , which means that events happen faster in the subscale models (for example, time is reduced by a factor of four in going from the 1/3-scale tests to the 1/12-scale tests).

If differences in damage evolution are to be a plausible explanation of the scaling effect, it must be demonstrated that the characteristic failure times are approximately the same as the loading times. We offer the following example. It is observed experimentally that the spall strength of metals, e.g., Armco iron and 6061-T6 aluminum, decreases by a factor of two as the pulse width changes from 0.05-0.10  $\mu$ s to 0.30-0.40  $\mu$ s, which implies that a characteristic damage time for spallation (a wave propagation phenomenon) is on the order of several tenths of a microsecond [11]. The failure mode of the targets in the present work is not spallation, but order-of-magnitude estimates can be made of the failure time for the experiments reported here. It might be expected, for ballistic experiments, where the operative mechanism is large-field plastic flow, that characteristic damage times might be an order of magnitude longer than for spallation, i.e., on the order of a few microseconds. An estimate of the loading time is obtained from nominal steady-state penetration. For the order-of-magnitude estimates here, the erosion rate of the projectile is approximately one-half the impact velocity, e.g., 1.0 km/s. Since the projectile opens a cavity approximately 2.0 projectile diameters, a characteristic loading time is estimated to be on the order of 4 to 16  $\mu$ s as the scale factor changes from 1/12 to 1/3. Clearly, these order-of-magnitude estimates are heuristic, but it appears plausible that characteristic loading and failure times are similar.

Therefore, we postulate that the root cause of the differences in ballistic response as a function of scale size is due to differences in damage history and failure. For example, we noted that the 1/3-scale targets had a scab ring surrounding the exit hole; such a feature was not observed at the other scales. Another example concerns the "interior damage ring," described in Ref. [4], that exists on the back face of the front steel target element. Full-scale tests of a proprietary target have been performed where an isolation material (analogous to the Fiberfrax used in the tests reported here) was placed between the steel and the ceramic. The same damage feature was observed, but in the full-scale tests, this feature exhibits considerably more damage (not just bulging). In some of the full-scale tests, this ring actually scabbed, having the appearance of a spall ring [12]. In the experimental study of Ref. [3], considerably more damage (tearing and scabbing) is observed around entrance and exit holes at the 1/3.15-scale size than for the smaller scales, particularly for the oblique targets.

Atkins postulated, for situations in which extensive plastic flow precedes and accompanies fracture, that geometric nonscaling is a consequence of work done in opening and driving cracks [13]. He examined very low velocity impact problems and demonstrated experimental support for his postulate. Even if Atkins' work is extended to include other failure mechanisms (e.g., ductile void growth and coalescence, and shear localization), there are essential differences between Atkins' explanation and the one given here. For ballistic problems, the energy dissipated in plastic work dominates the mechanics; energy losses in fracture are very small relative to the plastic work, and therefore, geometric scaling should be satisfied within experimental variability (in low velocity impacts, energy absorbed in fracture processes is significant relative to energy dissipated in plastic flow, as Atkins has demonstrated). In Atkins nomenclature, the nondimensional variable  $\xi$ , which is essentially a measure of the ratio of energy dissipated in plastic work to that dissipated in fracture, is large for ballistic impact problems; therefore, geometric scaling distortion cannot be determined from the energy arguments of Atkins. Instead, it is the details of damage evolution that are important because damage scales as absolute time instead of scaled time; thus, small targets do not have the same amount of "damage" at homologous times. This is particularly important near a threshold condition such as the ballistic limit. The next paragraph describes one way in which the two postulates can be differentiated.

Further study is warranted where the focus is investigation and understanding of the origins of the scale effect. An ancillary question is whether it is the failure of target material or projectile material, or both, that needs to be invoked to account for the experimentally observed differences. Another relevant question is whether the scale effect saturates at some point. Equations (5) were extrapolated to full scale by setting  $\lambda$  equal to 1.0. But at some point, assuming that the scale effect is caused by a damage rate effect, the absolute times will be sufficiently long that damage will saturate. Therefore, further increases in scale size will not result in more damage; experimental results should then be independent of scale size. Where the scale effect saturates, if it does, remains to be determined, and is also an open research question.

## ACKNOWLEDGEMENTS

This work was performed under contract DAAL03-91-C-0021 with the U. S. Army Research Office. A number of people at SwRI provided considerable assistance in various aspects of this research effort. Mr. Bruce Morris was responsible for the design and fabrication of the targets. Ms. Suzanne Royal assisted in data reduction. The authors would like to acknowledge the support and encouragement of Dr. Thomas Kiehne, formerly of the Defense Advanced Research Projects Agency, and now at the Institute for Advanced Technology, Mr. Billy Hogan of Los Alamos National Laboratory, and Mr. René Larriva of Interferometrics. Lastly, the authors would like to acknowledge



the contribution of Dr. Dennis Grady, of Sandia National Laboratories, who provided the key suggestion for plotting the ballistic limit velocity as the inverse square root of the scale size, and pointing out other examples of the energy scaling relationship.

## REFERENCES

1. C. E. Anderson, Jr., S. A. Mullin, and C. J. Kuhlman, "Computer simulation of strain-rate effects in replica scale model penetration experiments," *Int. J. Impact Engng.*, **13**(1), 35-52 (1993).
2. L. Magness, Jr. and W. Leonard, "Scaling issues for kinetic energy penetrators," *Proc. 14th Int. Symp. on Ballistics*, Vol. 2, 281-289, Québec City, 26-29 September (1993).
3. S. A. Mullin, C. E. Anderson, Jr., N. W. Blaylock, B. L. Morris, Jr., A. J. Piekutowski, and K. L. Poormon, "Scale model penetration experiments: Finite-thickness steel targets," SwRI Report 3593/003, Southwest Research Institute, San Antonio, TX (1995).
4. C. E. Anderson, Jr., S. A. Mullin, A. J. Piekutowski, N. W. Blaylock, and K. L. Poormon, "Scale model experiments with ceramic laminate targets," *Int. J. Impact Engng.*, **18**(1), 1-22 (1996).
5. J. A. Zukas, T. Nicholas, H. G. Swift, L. B. Greszczuk, and D. R. Curran, *Impact Dynamics*, Chapter 5, John Wiley & Sons, Inc., New York (1982).
6. T. W. Bjerke, G. F. Silsby, D. R. Scheffler, and R. M. Mudd, "Yawed long-rod armor penetration," *Int. J. Impact Engng.*, **12**(2), 281-292 (1992).
7. ——"Elements of terminal ballistics, Part 2, Collection and analysis of data concerning targets," AMCP 706-161, Army Material Command Engineering Design Handbook Series, U. S. Army Material Command (1962).
8. C. E. Anderson, Jr., V. Hohler, J. D. Walker, and A. J. Stilp, "Time-resolved penetration of long rods into steel targets," *Int. J. Impact Engng.*, **16**(1), 1-18 (1995).
9. D. E. Grady, Sandia National Laboratories, private communication (1994).
10. H.-M. Wen and N. Jones, "Experimental investigation of the scaling laws for metal plates struck by large masses," *Int. J. Impact Engng.*, **13**(3), 485-505 (1993).
11. L. Davison and R. A. Graham, "Shock compression of solids," *Physics Reports* (Review section of *Physics Letters*), **55**(4), 255-379 (1979).
12. W. Gooch, Army Research Laboratory, private communication (1994).
13. A. G. Atkins, "Scaling in combined plastic flow and fracture," *Int. J. Mech. Sci.*, **30**(3/4), 173-191 (1988).

UNCLASSIFIED

A SIMPLE ERODING ROD PENETRATOR MODEL (U)

J. T. Dehn  
U. S. Army Research Laboratory  
Aberdeen Proving Ground, MD 21005-5066

ABSTRACT (U)

(U) Following a brief history of the two main rod penetrator models, a simple model of eroding rod penetration is presented. which extends the older of the models to the eroding rod case. The model which is presented here is quite simple. It can serve as a convenient way to organize known results, and could become a tool for making qualitative engineering predictions.

(U) INTRODUCTION

(U) The penetration of armor by projectiles has been a subject of study for centuries. As part of this effort many workers have developed one-dimensional models to describe impacts at zero degrees obliquity (refs. 1 and 2). Among these models there are two main traditions. One uses Newton's law of motion and represents the opposing target force by some function of the velocity. The other uses a modified form of Bernoulli's conservation equation, together with supplementary equations.

(U) The first type may be called the lagrangian or Poncelet tradition after its founder (refs. 3 and 4). In this tradition one assumes that the force applied to the center of mass of the rod by the target has the form

$$F = -(a + bV + cV^2) \quad (1)$$

namely, a quadratic form in the penetrator velocity,  $V$ , with constant coefficients  $a$ ,  $b$ , and  $c$ . The equation of motion for a projectile with constant mass,  $m_0$ , (the only case so far considered) is  $m_0 \dot{V} = F$ , where  $\dot{V} = dV/dt$ .

(U) The second type may be called the eulerian or hydrodynamic tradition. Models of this type employ a special form of Bernoulli's conservation law for fluid flow. In its most common form Bernoulli's law is

$$p_1 + .5\rho V_1^2 + \rho gh_1 = p_2 + .5\rho V_2^2 + \rho gh_2 \quad (2)$$

where  $p_i$ ,  $V_i$  and  $h_i$  are the pressure, velocity and height of the fluid (of constant density  $\rho$ ) at points  $i=1$  and  $2$  in the earth's gravitational field which has constant acceleration,  $g$ . A special form is often

UNCLASSIFIED

UNCLASSIFIED

called the "modified Bernoulli equation", namely,

$$.5\rho_p(v-u)^2 + Y_p = .5\rho_t u^2 + R_t \quad (3)$$

Here there are two "fluids" involved, the projectile with constant density,  $\rho_p$ , and the target with constant density,  $\rho_t$ . The velocity of the rear of the projectile is  $v$ , while  $u$  is the velocity of the point where the projectile and target touch (the stagnation point). In Eq. (3) a Galilean transformation has been made from the laboratory system of coordinates to a system moving with constant velocity,  $u$ . The constancy of  $u$  is required in order to preserve the form of Bernoulli's energy conservation law. The projectile and target strengths or "resistances" are  $Y_p$  and  $R_t$  respectively.

Usually,  $Y_p$  and  $R_t$  are taken to be constants, so, since everything else is constant, the velocity,  $v$ , must also be constant. Therefore, Eq. (3) is a relation between six constants. It was first applied to rods by Hill, Mott and Pack in 1944 (ref. 5), building on earlier work in the United States and England dating from 1941.

(U) In 1967, Tate began a series of open literature publications (refs. 6-10) which extended the procedure of reference 5. In his first paper he spoke of an "almost steady state" and noted that, "Strictly one cannot use Bernoulli's equation because the process is unsteady....". He took  $v$  and  $u$  to vary slightly with time. Hence the name "quasi-steady-state".

(U) Since 1967, Tate's work has been used by a number of people who applied his formulas to penetration of semi-infinite targets from high impact speed to zero velocity of the remnant rod. To achieve agreement with experiment, some of these authors found they had to make Tate's "resistance" a function of time (ref. 11). Past criticisms and recent discussions of Tate's model have been summarized by Anderson and Walker (ref. 12), who also presented favorable comparisons with CTH code calculations and experiments.

(U) More recently, Walker and Anderson (ref. 13) started with Euler's momentum equation and derived a form of Eq. (3) which contains five additional terms, none of them including Cook's (ref. 14) three added terms to account for target compression, heating and shock wave dissipation. In their derivation they appealed to CTH code calculations and to fairly elaborate considerations taken from cylindrical geometry. In addition, their "critical" parameter  $\alpha$  which (multiplied by the crater radius) in some sense describes the extent of the plastic zone in the target, is required to be a function of both time and impact speed. The crater radius is also required to be a function of impact speed. All of this may be true, but it could be daunting to a journeyman engineer. Their model is commendable and reduces to Tate's model when the crater radius and the extent of the plastic zone vanish, but it is not simple.

UNCLASSIFIED

UNCLASSIFIED

(U) A SIMPLE MODEL

(U) Introduction

(U) Newton's law for the motion of the center of mass of a body is

$$d(m\dot{S})/dt = m d\dot{S}/dt + \dot{S} dm/dt = F \quad (4)$$

where it has been assumed that the mass lost from the nose of the rod comes to rest on the cavity wall. Here  $\dot{S}$  is used instead of  $V$ .

(U) The speed of the center of mass,  $\dot{S}$ , is related to the penetration speed (rod nose speed),  $\dot{P}$ , and  $\dot{R}$  (rod rear speed) as follows:  $\dot{S} = \dot{P} - \dot{\ell}/2$  and  $\dot{S} = \dot{R} + \dot{\ell}/2$  where  $\dot{\ell} = \dot{m}/(\rho_p A_p) < 0$ . Thus,  $\dot{R} > \dot{S} > \dot{P}$  in general and  $\dot{R} = \dot{S} = \dot{P}$  only when there is no erosion ( $\dot{\ell} = 0$ ). Addition of these equations gives

$$\dot{S} = (\dot{P} + \dot{R})/2. \quad (5)$$

which is the time derivative of the definition of the center of mass,  $S = (P + R)/2$ . The center of mass is a mathematical point half way between the nose and rear of this uniform rod. The fact that the center of mass is a mathematical point and not a material point is clear for objects like a hoop. It is also true for idealized "one-dimensional" objects such as we are describing here. The rod length at any time is  $\ell = P - R = - (R - P)$  where  $P$  is the position of the rod nose and  $R$  is the position of its rear. For a rod of constant, uniform density,  $\rho_p$ , and cross-sectional area,  $A_p$ , the mass at any time is  $m = \rho_p A_p \ell$  so

$$\dot{m} = \rho_p A_p \dot{\ell} = -\rho_p A_p (\dot{R} - \dot{P}) \quad (6)$$

is the mass erosion rate.

(U) The Constant Velocity Ratio Approximation

(U) The constancy of  $u$  and  $v$  in Eq. (3) and so of their ratio  $\delta = \dot{R}/\dot{P} = v/u$  was assumed by Birkhoff et al. (ref. 15) with  $Y_p = R_t = 0$ . However, it is approximately true for many long rod penetrations of interest, as one can see by examining relevant experimental data (refs. 6, 11, 16 and 17) obtained using flash x-rays during multiple firings under identical conditions. Fig. 1 is taken from Anderson, Jr. et al. (ref. 11) for a tungsten alloy projectile with fineness ratio 20 striking a steel target at 1,500 m/s. Straight-line slopes which almost pass through most of the measured positions (solid circles) could be drawn, illustrating the approximate constancy of the velocities and so of their ratio over most of the penetration. The use of an approximately constant ratio  $\delta$  can be preferable to the assumption of approximately constant  $\dot{R}$  and  $\dot{P}$  separately. It is possible for  $\dot{R}$  and  $\dot{P}$  to change substantially with time while  $\delta = \dot{R}/\dot{P}$  remains constant, provided  $\dot{R}$  and

UNCLASSIFIED

UNCLASSIFIED

$\dot{P}$  change by the same fractional amount. For example, If  $\dot{R} \rightarrow 0.7\dot{R}$  and  $\dot{P} \rightarrow 0.7\dot{P}$ ,  $\delta$  remains unchanged. Approximately the same fractional change occurs in many cases of interest, as is evident from the approximate parallelism of curves calculated for  $\dot{R}$  and  $\dot{P}$  as they decrease with time (Fig. 2). If we look at Fig. 1, we see that the data are not sufficient to tell us about the behavior of the ratio,  $\delta = \dot{R}/\dot{P}$ , toward the end of the penetration. Fig. 2 shows calculated velocities of rod nose (bottom curve) and rear (top curve) as a function of time (HULL code simulations for 65 g tungsten alloy rods with  $\lambda_0/d_0 = 20$  striking Rha steel targets at 1,500 m/s). The rear of the rod does not start to decelerate until reached by a shock wave. The ratio of the rear and nose speeds,  $\delta$ , is about 2 for most of the penetration and becomes  $\delta = 1$  by the end of the penetration, near 170  $\mu$ s.

(U) In cases like this where  $\delta$  varies from some value greater than one, approaching unity at the end of the penetration, one can use an average value for  $\delta$  to describe the entire penetration in a simple model. Cases where the nose velocity reaches zero before the tail velocity cannot be treated by using an average  $\delta$ , since  $\delta$  diverges.

(U) Derivation of the Equation of Motion

(U) Now insert constant  $\delta$  in Eq. (6) which becomes

$$\dot{m} = -\rho_p A_p (\dot{R} - \dot{P}) = -\rho_p A_p (\delta - 1)\dot{P} = -\mu\dot{P} \quad (7)$$

where the constant mass erosion rate coefficient,  $\mu = \rho_p A_p (\delta - 1)$ . An integration of Eq. (7) gives  $m = m_0 - \mu P$ . In addition, from Eq. (5) and the definition of  $\delta$ ,  $\dot{S} = (\dot{P} + \dot{R})/2 = \dot{P}(1 + \delta)/2 = \dot{P}\epsilon$  where  $\epsilon = (1 + \delta)/2$ . Substitution of  $m = m_0 - \mu P$ ,  $\dot{m} = -\mu\dot{P}$ ,  $\dot{S} = \epsilon\dot{P}$ , and  $d\dot{S}/dt = \epsilon d\dot{P}/dt = \epsilon \dot{P} d\dot{P}/dP$  by the chain rule in Eq. (4) gives

$$(m_0 - \mu P)\epsilon \dot{P} d\dot{P}/dP + \epsilon \dot{P}(-\mu\dot{P}) = F = -(a + c\dot{P}^2) \quad (8)$$

where the force applied to the rod by the target has the Poncelet form ( $b=0$  in Eq. 1, viscosity neglected). The speed of the rod nose,  $\dot{P}$ , is used instead of the speed of the center of mass, since the force exerted by the target depends on how fast the nose is moving. Rearranging Eq. (8) gives

$$(m_0 - \mu P)\epsilon \dot{P} d\dot{P}/dP = -(a + \bar{c}\dot{P}^2) \quad (9)$$

where  $\bar{c} = c - \epsilon\mu$ . Here  $\bar{c}$  may be called the reduced inertial coefficient. The term  $c\dot{P}^2$  represents the inertial resistance of the target, while  $\epsilon\mu\dot{P}^2$  includes the fact that mass is also being lost. The loss of rod mass produces a decrease in deceleration. From Eq. (4) with  $F=0$ , namely,  $m d\dot{S}/dt = -\dot{S}\dot{m}$ , mass loss ( $\dot{m} < 0$ ) always produces an acceleration ( $d\dot{S}/dt > 0$ ) with or without an applied force. In Eq. (9) the constant term  $a$  is proportional to the target yield strength. Here the form  $a = 3A_t Y_t$  will be used, following Tabor (ref. 18) who observed that the target yield strength,  $Y_t$ , at least for a metal, is approximately equal to a constant,  $C_m$ , multiplied by its Brinell hardness,  $H_B$ . The inertial coefficient is assumed to have the form  $c = 0.5\rho_t A_t$ .

UNCLASSIFIED

UNCLASSIFIED

(U) SOLUTIONS IN THE P-P PLANE

(U) The General Case

(U) An integration of Eq. (9) gives

$$P = (m_o/\mu) [1 - [(a + \bar{c}P_o^2)/(a + \bar{c}P^2)]^\beta] \quad (10)$$

where  $\beta = .5\epsilon\mu/\bar{c}$ , and  $P_o$  is the value of  $P$  a few microseconds after impact when the model begins to apply. In Eq. (10)  $m_o = \rho_p A_p \ell_o$  is known. The constants  $a$  and  $c$  are also known except for  $A_t$ . The constant  $\bar{c} = c - \epsilon\mu$  with  $\mu = \rho_p A_p (\delta - 1)$  and  $\epsilon = .5(\delta + 1)$ . Then  $\epsilon\mu = .5\rho_p A_p (\delta^2 - 1)$ . That leaves two unknown constants,  $\delta$  and  $A_t$ . If data like that shown in Fig. 1 are known, then  $\delta$  can be estimated and  $\epsilon$  and  $\mu$  calculated.  $A_t$  can also be estimated from experiment, determining all the constants in Eq. (10).

(U) When target crater measurements are made, usually only crater diameters (or crater radii,  $r_t$ ) at the original target face are reported. Generally these increase with striking speed. However, in the present model, the ratio  $k = A_t/A_p$  will be taken to be independent of both time and striking speed. It is the effective area of the crater bottom opposing the rod nose during most of the penetration. It should not vary much with striking speed except in special cases when there is a shatter gap in the  $P_f, \dot{S}_o$  plane. Then  $A_t$  should increase suddenly as  $\dot{S}_o$  reaches the critical speed for shatter and then decrease again to another constant value. The ratio of the radii,  $(r_t/r_p) \geq 1$  and for many cases of interest it is  $\geq 2$ . Then the ratio of the areas is  $A_t/A_p = k \geq 4$ .

(U) Since this simple model uses an average value of  $\delta = \dot{R}/\dot{P}$ , it can be called an average-velocity-ratio model. Since  $A_p$  and  $A_t$  (or the radii  $r_p$  and  $r_t$ ) are measured in another dimension, it can be called quasi-one-dimensional. And since it relies on experimental data to determine its parameters, it can be called semi-empirical.

(U) Solutions in the  $P_f/\ell_o, V_I$  Plane

(U) When  $\dot{P} = 0$  in Eq. (10), the final penetration depth in a semi-infinite target per unit original length of penetrator is

$$P_f/\ell_o = [1/(\delta - 1)] [1 - [1 + (V_I/\gamma)^2]^{-\beta}] \quad (11)$$

since  $m_o = \rho_p A_p \ell_o$  and  $\mu = \rho_p A_p (\delta - 1)$ . Here  $\gamma = \delta[a/\bar{c}]^{1/2}$  introduces no new

UNCLASSIFIED

UNCLASSIFIED

where  $k=A_c/A_p$  and  $\rho_t/\rho_p=7.85/17.65=.445$ . The value  $k=4.5$  gives  $\beta=1/2$  which will be used to describe Fig. 3. Walker and Anderson (ref. 13) quote data which says that the ratio of the crater area at the top of the crater (the face of the target) to the projectile cross-sectional area increases with striking speed. In the present model  $A_c$  is the area at the bottom of the crater which opposes the projectile during most of the penetration, a quantity which is usually smaller than the area of the top of the crater. Here  $A_c=kA_p$  is assumed to be independent of time and striking speed.

(U) It is difficult to estimate even an approximate value of the inflection point,  $V_{II}$ , from Fig. 3. However, one can calculate a value from Eq. (15), using  $\delta=\sqrt{2}$ ,  $\rho_t=7.85g$  and  $Y_c=.6 \times 10^{10}$  dynes/cm<sup>2</sup> = .6 GPa for steel. One obtains  $V_{II}=.94 \times 10^5$  cm/s = .94 km/s. By putting this value in Eq. (13) with  $\beta=1/2$ , one finds  $\gamma=\sqrt{2}(.94) \approx 1.33$  km/s. Then Eq. (11) becomes

$$P_f/\ell_o = 2.4 \left[ 1 - \left[ 1 + (\dot{S}_o/1.33)^2 \right]^{-1/2} \right] \quad (17)$$

which approximately fits the data in Fig. 3.

(U) Table 1 shows  $P_f/\ell_o$  versus  $V_c$  for a fit to Fig. 3 by an arbitrary function chosen by Silsby (ref. 20) together with values calculated from Eq. (17). Silsby's function  $P_f/\ell_o = [1.255 + .08\dot{S}_o] / [1 + 109 \exp(-3.42\dot{S}_o)]$  was chosen to fit the experimental data over the range  $0.5 < \dot{S}_o < 4.5$  km/s.

Table 1. (U)  $P_f/\ell_o$  according to Eq. (17) with  $\delta=\sqrt{2}$ ,  $A_c=4.5A_p$  compared with Silsby's function.

$\dot{S}_o$ (km/s)	0	0.5	1.0	1.5	2.0	2.5	3.0	3.5	4.0	4.5	5.0	$\infty$
Silsby	.01	.06	.29	.84	1.27	1.42	1.49	1.53	1.57	1.62	1.66	$\infty$
Eq. (17)	0	.15	.48	.81	1.07	1.28	1.43	1.55	1.64	1.72	1.78	2.4

Eq. (17) agrees with Silsby's function within 16% above  $\dot{S}_o=1.00$  km/s, the range of principal military interest. The agreement for lower striking speeds could be improved by including the viscous term  $b\dot{P}$  in Eq. (9), or by making  $A_c$  vary with striking speed. Such complications are not worthwhile in

UNCLASSIFIED

UNCLASSIFIED

parameters. Much of the data which has been obtained for semi-infinite targets can be plotted in the  $P_f/\ell_o, V_I$  plane described by Eq. (11) where  $V_I$  is the impact speed with  $V_I = \dot{R}_o = \delta \dot{P}_o$ . The slope of Eq. (11) is

$$d(P_f/\ell_o)/dV_I = [(\rho_p A_p \epsilon)/(a \delta^2)] [V_I / [1 + (V_I/\gamma)^2]^{\beta+1}] \quad (12)$$

which vanishes as  $V_I \rightarrow 0$  and  $V_I \rightarrow \infty$ . Eq. (11) is an s-shaped curve with an inflection point at the coordinates

$$V_{Ii} = \gamma/[1 + 2\beta]^{\frac{1}{2}} \quad (13)$$

and

$$P_{fi}/\ell_o = [1/(\delta-1)] [1 - [1 + 1/(1+2\beta)]^{-\beta}] \quad (14)$$

using Eq. (13) in Eq. (11). The subscript i indicates inflection point.

(U) Recall that  $\beta = .5\epsilon\mu/\bar{c}$  so,  $\bar{c} = c - \epsilon\mu = \epsilon\mu/(2\beta)$ , from which one can find  $\epsilon\mu$  in terms of  $c$  and  $\beta$ , namely,  $\epsilon\mu/(2\beta) = c/(1+2\beta) = \bar{c}$ . Thus,  $\bar{c}(1+2\beta) = c$  can be put into Eq. (13), with  $\gamma = \delta[a/\bar{c}]^{\frac{1}{2}}$  to obtain  $V_{Ii} = \delta(a/c)^{\frac{1}{2}}$  independent of  $\beta$ . Moreover,  $a = 3A_t Y_t$  and  $c = .5\rho_t A_t$ , so

$$V_{Ii} = \delta [6Y_t/\rho_t]^{\frac{1}{2}} \quad (15)$$

independent of both  $A_t$  and  $\beta$ .

(U) A Particular Example

(U) Figure 3 shows data from Sorensen, et al. (ref. 19) for semi-infinite steel (rolled homogeneous armor) targets struck by tungsten alloy rods at impact speeds from 0.5 to 5.0 km/s. The rods had masses which varied by more than an order of magnitude (from less than 100 g to 2,000 g), and their fineness ratios ( $\ell_o/d_o$ ) varied from 9 to 30. In spite of these variations, a plot of  $P_f/\ell_o$  versus  $\dot{S}_o$  shows all the data falling approximately on a single curve.

(U) From Fig. 1 one can estimate  $\delta = \dot{R}/\dot{P} \approx 2$  during most of the penetration. To estimate a suitable average value of  $\delta$  to describe the whole penetration, this paper recommends using the geometric mean of  $\delta = 2$  and  $\delta = 1$ , namely,  $\delta = [(2)(1)]^{\frac{1}{2}} \approx 1.4$ . So the factor  $1/(\delta-1) = 1/(\sqrt{2}-1) \approx 2.4$  in Eq. (11). In this case,  $\epsilon\mu = .5\rho_p A_p (\delta^2 - 1) = .5\rho_p A_p$ , so

$$\beta = .5\epsilon\mu/\bar{c} = .5(.5\rho_p A_p)/[.5\rho_t A_t - .5\rho_p A_p] = .5/[k\rho_t/\rho_p - 1] \quad (16)$$

UNCLASSIFIED



UNCLASSIFIED

view of the approximate nature of this simple model. At a low striking speed like 0.5 km/s in Table 1, the experimental penetration,  $P_f$ , is only .06 of the initial rod length,  $l_0$ . That is,  $P_f$  is about half a rod diameter for the rods in Fig. 3 with fineness ratios between 9 and 30. The craters are so shallow that entrance phase phenomena dominate the motion. Since this simple model neglects entrance phase phenomena, it is not surprising that its predictions are poor for low impact speeds.

(U) SUMMARY

(U) It has been shown that a simple lagrangian model of eroding long rod penetration can be based on Newton's second law, using a Poncelet force and a reasonable approximation for the mass erosion rate. This model has been illustrated by an example and found to agree approximately with experiments. It is conceptually simple and easy to use. However, it is limited to cases of finite  $\delta$ .

(U) There are many other cases of penetration to which this simple model could be applied, including penetration versus time data. Some of these cases with better agreement for low striking speeds will be considered in a later paper.

(U) ACKNOWLEDGEMENTS

(U) The author wishes to thank his colleagues Hubert Meyer, Gordon Filbey, Steven Segletes, and Graham Silsby for their many helpful suggestions.

(U) REFERENCES

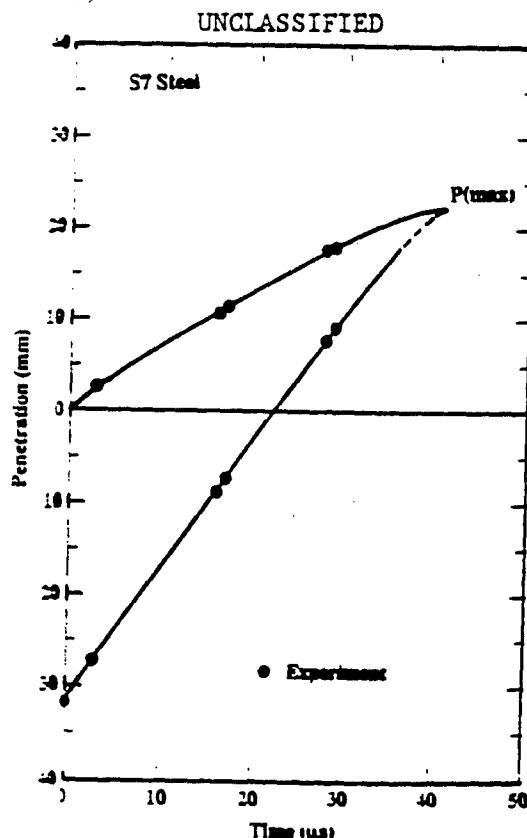
1. M. E. Backman and W. Goldsmith, The Mechanics of Penetration of Projectiles into Targets. Int. J. Eng. Sci. **16**, pp. 1-99 (1978). (U)
2. W. Johnson, Impact Strength of Materials, Crane-Russak, New York (1972), cc. 9-10. (U)
3. J. V. Poncelet, Cours de Mechanique Industrielle. Paris (1829). (U)
4. H. P. Robertson, The Mechanics of Armor Perforation. NRDC Armor and Ordnance Report No. A-227 (OSRD No. 2043), (1943). (U)
5. R. Hill, N. F. Mott and D. C. Pack, Penetration of Armour by High Velocity Projectiles and Munroe Jets. A. C. 6064 (1944). (U)
6. A. Tate, A theory for the deceleration of long rods after impact. J. Mech. Phys. Solids **15**, 387 (1967). (U)
7. A. Tate, Further results in the theory of long rod penetration. J. Mech. Phys. Solids **17**, 141 (1969). (U)
8. A. Tate, A comment on a paper by Averbuch and Bodner concerning the mechanics of plate perforation by a projectile. Int. J. Eng. Sci. **17**, (1979). (U)
9. A. Tate, Long rod penetration models - Part I. A flow field model for high speed long rod penetration. Int. J. Mech. Sci. **28**, 535 (1986). (U)
10. A. Tate, Long rod penetration models-Part II. Extensions to the hydrodynamic theory of penetration. Int. J. Mech. Sci. **28**, 599 (1986). (U)

UNCLASSIFIED

UNCLASSIFIED

11. C. E. Anderson, Jr., J. D. Walker and G. E. Hauver, Target resistance for long-rod penetration into semi-infinite targets. Nucl. Eng. and Design **138**, (1992). (U)
12. C. E. Anderson, Jr. and J. D. Walker, An examination of long-rod penetration. Int. J. Impact Engng. **11**, 481 (1991). (U)
13. J. D. Walker and C. E. Anderson, Jr., A time-dependent model for long-rod penetration. Int. J. Impact Engng. **16**, 19 (1995). (U)
14. M. A. Cook, Mechanism of cratering in ultra-high velocity impact. J. Appl. Phys. **30**, 725 (1959). (U)
15. G. Birkhoff, D. P. MacDougall, E. A. Pugh and G. I. Taylor, Explosives with lined cavities. J. Appl. Phys. **19**, 563 (1948). (U)
16. E. Perez, Etude experimentale et theorique de la penetration de cibles metalliques semi-infinies par des projectiles metalliques de grande allongement et de vitesse superieure a 2000 m/s. Sciences et Techniques de L'Armement **56**, 11 (1982). (U)
17. C. E. Anderson, Jr., V. Hohler, J. D. Walker and A. J. Stilp, Time-resolved penetration of long rods into steel targets. Int. J. Impact Engng. **16**, 1-18 (1995). (U)
18. D. Tabor, The Hardness of Metals. The Clarendon Press, Oxford (1951). (U)
19. B. R. Sorensen, K. D. Kimsey, G. F. Silsby, D. R. Scheffler, T. M. Sherrick and W. S. De Rosset, High Velocity Penetration of Steel Targets. Int. J. Impact Engng. **11**, 107-119 (1991). (U)
20. G. Silsby (private communication). (U)

Fig. 1. (U)  $l_0/d_0 = 20$   
tungsten alloy rod  
striking  $\sigma$  steel target  
at 1,500 m/s. Positions  
of rod nose (top curve)  
and tail (bottom curve)  
versus time. Data from  
ref. 11.



UNCLASSIFIED

UNCLASSIFIED

UNCLASSIFIED

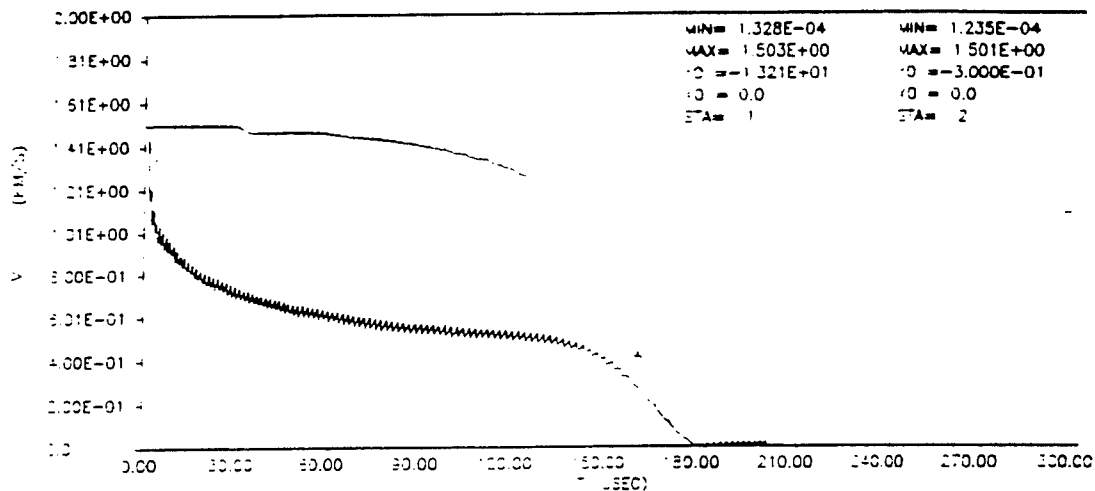


Fig. 2. (U)  $l_0/d_0 = 20$  tungsten alloy rod striking  $\sigma$  steel target at 1,500 m/s. Velocities of rear (top curve) and nose (bottom curve) versus time. HULL code simulation.

UNCLASSIFIED

UNCLASSIFIED

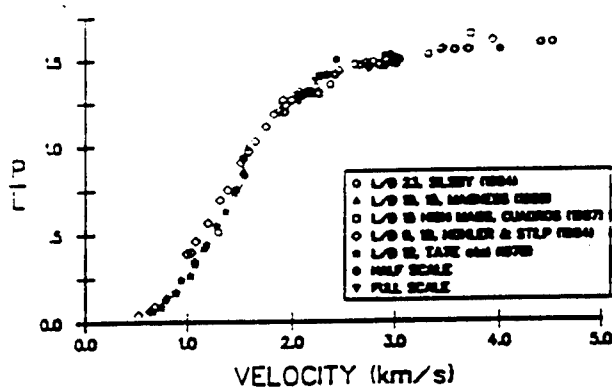


Fig. 3. (U) Tungsten alloy rods of various sizes striking steel targets at different velocities. Penetration per unit rod length versus impact velocity.

UNCLASSIFIED

UNCLASSIFIED

# UNCLASSIFIED

## RHA BREAKOUT EFFECTS FOR TUNGSTEN PENETRATORS (U)

Dr. Michael J. Normandia  
Institute for Advanced Technology, The University of Texas at Austin, Austin, Texas 78759

David L. Littlefield  
Southwest Research Institute (SwRI), San Antonio, Texas 78228

### ABSTRACT (U)

(U) An experimental investigation has been conducted to generate penetration data just below the ballistic limit velocity of finite thickness targets. Thirteen experiments were conducted impacting 76.2 mm thick 4340 steel (nominal BHN 330) with 70 g,  $l/d = 5.5$ , tungsten alloy (X-11) penetrators. Nine impacts were within 14% below the ballistic limit velocity estimated experimentally to be 1.69 km/s. Eight additional experiments were conducted using the same penetrator and 64.3 mm thick RHA (nominal BHN 302) at 30-degrees obliquity (a line-of-sight thickness of 74.2 mm). Five impacts were within 4% below the ballistic limit velocity estimated experimentally to be 1.62 km/s.

(U) These data were generated to quantify changes in target resistance as the rear target surface is approached, specifically to validate backface and breakout algorithms used in the Walker-Anderson analytic penetration model [Ref. 1]. Using this data, we determined how the dimensionless parameter,  $\alpha$ , which denotes the extent of the plastic flow field in the target, degrades once it impinges on the target rear surface. The subsequent degradation in target strength matches the data adequately. Agreement between the backface model calibrated at 0-degrees obliquity with hardened 4340 steel was good when used for RHA targets at 30-degrees obliquity. However, the functional form of the degradation used results in a discontinuous slope for target strength. Other functional forms are being examined based on a modified spherical cavity expansion model [Ref. 6,7] which shows that the extent of the plastic zone is continually altered by the presence of a free surface. This results in a gradual decrease in target resistance at an increasing rate as the rear surface is approached.

### (U) INTRODUCTION

(U) A set of experimental data is presented in which finite thickness 4340 and RHA steel targets were impacted with  $l/d = 5.5$ , tungsten-alloy penetrators at both normal incidence and 30-degrees obliquity. The experiments were conducted near the ballistic limit velocity by approaching it from below in small enough increments to examine the breakout region with sufficient detail to provide a rigorous test for penetration models or numerical codes.

UNCLASSIFIED

(U) Rear target surface effects on penetration resistance are an important part of any analytic penetration model used to calculate residual penetrator characteristics [Ref. 1,2,3]. A typical breakout algorithm in an engineering model gradually reduces the target strength as a free surface or target interface is approached. Some criterion for plugging should also be included. The lack of appropriate data with which to test the assumptions of the algorithms used limits the modeler, and hence, the robustness of the model. Material failure models in hydrocodes are also difficult to validate, and hence nominal agreement with residuals is typically acceptable.

(U) The large amount of residual penetrator data available is often of limited use in calibrating engineering penetration models. This is due to large scatter, an extremely steep slope of the residual versus striking velocity curve near the ballistic limit velocity, and the lack of precise residual mass measurement techniques which typically rely on x-radiographs and analyses based on an assumed shape for the residual penetrator. The data presented here are very near to and mostly just below the ballistic limit velocity, which provide the modeler with a more complete data set with which to infer how target strength degrades as the rear surface is approached.

#### (U) EXPERIMENTAL TEST SETUP AND DATA

(U) The experiments were conducted using a 29 mm, smooth-bore powder gun during 1988 at the Abex Research Center Ballistics Impact Facility, located in Mahwah, NJ, but have not, until now, been reported publicly. Three separate velocity measurement techniques were used for these experiments: a laser velocimeter, an orthogonal view, infrared shadowgraph camera triggered by a laser, and a high-speed Fastax streak camera. The first two systems gave an instantaneous digital readout which was later verified by development of both the Fastax and infrared film, which also provided data on penetrator pitch and yaw. The accuracy between the velocity measurement systems was typically within 2 to 3%, on average.

(U) The penetrators used for all of these experiments were flat-nosed, right-circular cylinders made of a X-11 tungsten alloy with a density of 18.5 g/cc with the following nominal characteristics: weight of 70 g, aspect ratio (l/d) of 5.5, diameter of 9.55 mm, and length of 52.8 mm. Thirteen ballistic impact experiments were conducted using 203 mm in diameter by 76.2 mm thick 4340 steel (BHN 330 nominal) to establish a penetration profile near the rear target surface. The targets were impacted at velocities just below the ballistic limit velocity which was determined from these experiments to be 1.69 km/s. An additional 8 ballistic impact experiments were conducted at 30-degrees obliquity using the same penetrator and 64.3 mm thick RHA targets with a nominal hardness of BHN 302. Both targets have similar thicknesses, 76.2 mm and 74.2 mm and have line-of-sight-thickness to penetrator diameter ratios of approximately 8. The experimental geometry is depicted schematically in Figure 1.

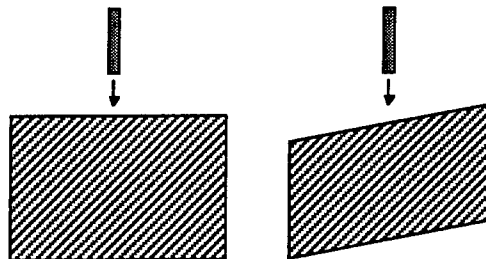


Figure 1. (U) Schematic diagram of experimental impact conditions using 70 g, X-11 tungsten alloy penetrator, 9.55 mm in diameter by 52.832 mm long shown impacting 76.2 mm thick 4340 steel (BHN 330) at normal incidence (on the left) and 64.3 mm thick RHA (BHN 302) at 30-degrees incidence (on the right).

UNCLASSIFIED

(U) The experimental data are summarized in Table I for the 0-degree 4340 targets and in Table II for the 30-degree RHA targets. The data was sorted by impact velocity for clarity.

Table I. (U) Data for X-11 impacting 76.2 mm thick 4340 BHN 330 steel at 0-degrees.

Test	Impact Velocity, km/s	Impact Velocity/vbl, (vbl = 1.69 km/s), km/s	Normal Penetration Depth, mm	Maximum Bulge Height, mm	Net Penetration, (Depth-Bulge) mm	p/l
1	1.020	0.603	36.07	0.000	36.07	0.6827
2	1.459	0.863	55.98	2.921	53.06	1.004
3	1.476	0.874	50.83	0.000	50.83	0.9620
4	1.516	0.897	58.93	3.861	55.07	1.042
5	1.570	0.929	63.70	4.928	58.78	1.112
6	1.572	0.930	59.33	2.565	56.77	1.075
7	1.615	0.955	64.52	5.029	59.49	1.126
8	1.626	0.962	68.83	8.433	60.40	1.143
9	1.663	0.984	67.06	5.537	61.52	1.164
10	1.668	0.987	72.72	3.810	68.91	1.304
11	1.719	1.02	76.94 *	9.068*	76.94*	1.456
12	1.966	1.16	>76.2	n/a	>76.2	n/a
13	2.032	1.20	>76.2	n/a	>76.2	n/a
14	1.655		>71.12 **	n/a	>71.12	n/a
15	1.697		>71.12 **	n/a	>71.12	n/a

\* Penetration includes 0.74 mm witness plate penetration of 7.24 mm thick target plug with 9.068 mm bulge.

\*\* The targets used in tests 14 and 15 were 71.12 mm thick and both were perforated.

Table II. (U) Data for X-11 impacting 64.3 mm thick RHA BHN 302 steel at 30-degrees.

Test	Impact Velocity, km/s	Impact Velocity/vbl, (vbl = 1.62 km/s) km/s	Normal Penetration Depth, mm	Bulge Height (Max.), mm	Net Normal Penetration, (Depth-Bulge) mm	Line-of-Sight Penetration-Bulge, mm	p/l
1	1.557	0.961	55.52	6.248	49.28	57.87	1.095
2	1.563	0.965	57.89	7.061	50.83	59.78	1.132
3	1.576	0.973	60.25	7.849	52.40	61.72	1.168
4	1.595	0.984	63.65	9.398	54.25	64.10	1.213
5	1.607	0.992	PLUG INTACT		56.39	65.11	1.232
6	1.636	1.010	>64.29	n/a	>64.29	>74.23	>1.405
7	1.640	1.013	>64.29	n/a	>64.29	>74.23	>1.405
8	1.658	1.024	>64.29	n/a	>64.29	>74.23	>1.405

(U) The experimental data from Table I are depicted graphically in Figures 2 and 3 for the 4340 steel. Shown are the measured hole depth from the top surface and the net penetration (hole depth - bulge). These latter values were used to compare with analytic penetration models. A data curve fit is also shown in Figure 3 for easier comparison with analytic model calculations. The exponential curve fit depicted in Figures 3 and 4 is given by the expression

$$p \text{ (mm)} = 36.3345 * \exp [0.0328 v \text{ (km/s)}^{5.8654}]; \quad 1 \text{ km/s} < v < 1.7 \text{ km/s.} \quad (1)$$

This curve fit results in an extrapolated ballistic limit velocity of 1.7 km/sec. Also shown is a semi-infinite penetration curve calculated using the traditional Tate model with  $Y_p = 2 \text{ GPa}$  and  $R_q = 5.32 \text{ GPa}$ , which was computed using a spherical cavity expansion analysis [Ref. 6].

UNCLASSIFIED

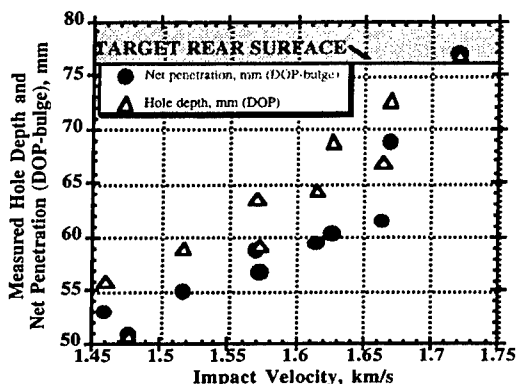


Figure 2. (U) Experimental data depicting measured hole depth (DOP) and net penetration (DOP - bulge) vs. impact velocity for X-11 impacting 203 mm diameter by 76.2 mm thick, 4340 BHN 330 steel.

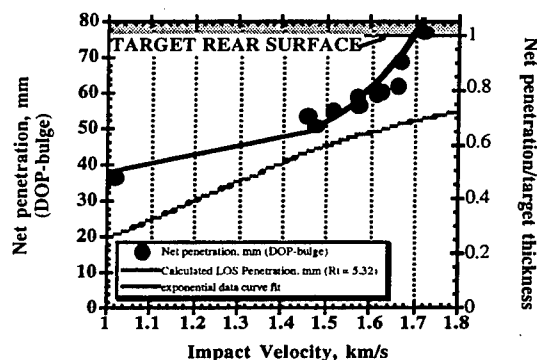


Figure 3. (U) Normalized experimental data depicting net penetration vs. impact velocity for X-11 impacting 76.2 mm thick 4340 BHN 330 steel with curve fit and calculated semi-infinite penetration.

(U) There is one data point with an impact velocity significantly below the ballistic limit velocity. This experiment was conducted in an attempt to remove rear surface effects and to approximate semi-infinite behavior. Unfortunately, the experimental impact velocity of 1.02 km/s included the existence of a non-deforming penetrator regime making it penetrate deeper than a fully eroding penetrator using a target resistance of  $R_t = 5.32$  GPa.

(U) One of the three tests which resulted in target perforations resulted in a witness plate penetration of 0.74 mm caused by an intact target plug with a thickness of 7.24 mm and a bulge of 9.068 mm. This velocity was estimated to be just above the ballistic limit velocity estimated to be 1.69 km/s. In Figure 4, we depict the data normalized by the ballistic limit velocity and expand the velocity scale. In Figure 5 the data is shown for the RHA targets impacted at 30-degrees obliquity and normalized by the experimentally estimated ballistic limit velocity of 1.62 km/s.

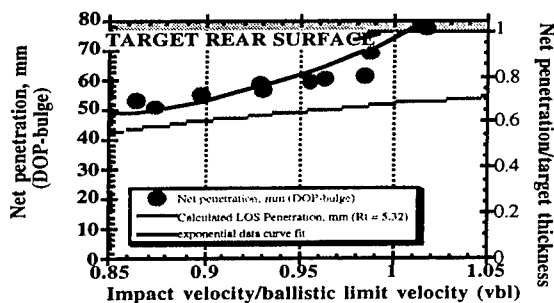


Figure 4. (U) Expanded view of experimental data near ballistic limit velocity for X-11 impacting 76.2 mm thick 4340 BHN 330 steel where velocity is normalized by 1.69 km/s.

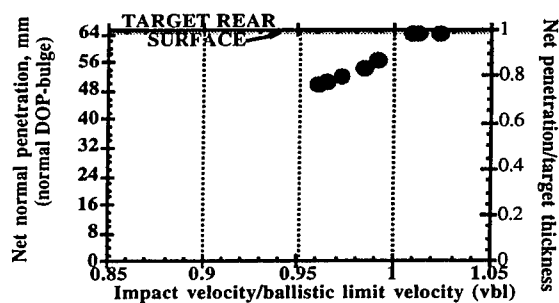


Figure 5. (U) Experimental data (net normal penetration - bulge) near ballistic limit velocity for X-11 impacting 64.3 mm thick RHA where velocity is normalized by 1.62 km/s.

## (U) ENGINEERING MODEL APPROXIMATIONS

(U) We utilize standard Tate-Alekseevskii [Ref. 4,5], Bernoulli-type, steady state penetration models to illustrate the effect of model parameters on data as the rear target surface is approached. We calculate the effective target strength,  $R_t$  required to match each penetration data point. In Table III and in Figure 6, we compare the computed values of  $R_t$  with no breakout model with the predictions based on a semi-infinite nominal target strength,  $R_{\infty}$  of 5.32 calculated

# UNCLASSIFIED

using a spherical cavity expansion model. This value agrees with those used in the literature Ref. [8]. Notice that the magnitudes of  $R_t$  are substantially below the semi-infinite value. When normalized by the ballistic limit velocity, however, both data sets show a consistent degradation in strength as the rear target surface is approached. Recall that both targets have similar line-of-sight thicknesses, 76.2 mm and 74.2 mm.

Table III. (U) Calculated  $R_t$  values for each penetration data point for X-11 impacting 76.2 mm thick 4340 (BHN 330) at 0-degrees and 64.3 mm thick RHA (BHN 302) at 30-degrees.

Test	Impact Velocity, km/s	Impact Velocity/vbl, km/s	Net Line-of-Sight Penetration, mm	Computed Target Strength, $R_t$ GPa	$R_t/R_{t\infty}$ ( $R_{t\infty} = 5.32$ GPa)
4340-1	1.020	0.603	36.07	-	-
4340-2	1.459	0.863	53.06	4.09	.770
4340-3	1.476	0.874	50.83	4.43	.832
4340-4	1.516	0.897	55.07	4.09	.770
4340-5	1.570	0.929	58.78	3.86	.726
4340-6	1.572	0.930	56.77	4.11	.772
4340-7	1.615	0.955	59.49	3.93	.739
4340-8	1.626	0.962	60.40	3.86	.725
4340-9	1.663	0.984	61.52	3.84	.721
4340-10	1.668	0.987	68.91	3.03	.569
4340-11	1.719	1.02	76.94*	2.33	.438
4340-12	1.966	1.16	>76.2	-	-
4340-13	2.032	1.20	>76.2	-	-
RHA-1	1.557	0.961	57.87	3.92	.737
RHA-2	1.563	0.965	59.78	3.73	.701
RHA-3	1.576	0.973	61.72	3.56	.669
RHA-4	1.595	0.984	64.10	3.36	.632
RHA-5	1.607	0.992	65.11	3.29	.618
RHA-6	1.636	1.010	>74.23	2.49	.468
RHA-7	1.640	1.013	>74.23	-	-
RHA-8	1.658	1.024	>74.23	-	-

\* Penetration includes 0.74 mm witness plate penetration of target plug.

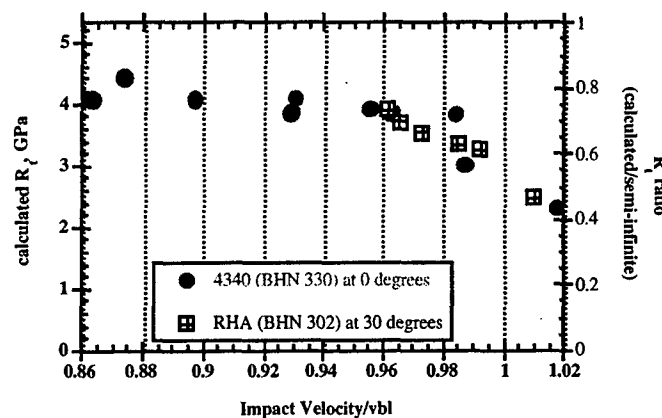


Figure 6. (U) Calculated  $R_t$  values for each penetration data point for X-11 impacting 76.2 mm thick 4340 (BHN 330) at 0-degrees (filled circles) and 64.3 mm thick RHA (BHN 302) at 30-degrees (open squares).

UNCLASSIFIED



(U) The values of  $R_t$  required to match the data just above the ballistic limit velocity ( $v/v_{bl} = 1.02$  for 4340 and 1.01 for RHA), were less than 50% of the semi-infinite value of 5.32 GPa. This strongly suggests that computed residual penetrator characteristics near, and above, the ballistic limit velocity are likely to be affected substantially if one utilizes a value of  $R_t$  as calibrated using semi-infinite data. Calibrating model parameters with specific penetration data from finite targets is also likely to result in errors as different values are required to match each data point. The only obvious solution is to include an algorithm which accounts for the presence of a free surface and degrades the value of target strength continually as the rear surface is approached.

#### (U) WALKER-ANDERSON MODEL PARAMETERS

(U) We calibrate a breakout algorithm in the Walker-Anderson penetration model using this specific data set. This model is often referred to as an unsteady Tate-Bernoulli penetration model. Breakout is modeled by degrading the value of a critical parameter in the model as the rear surface is approached. The parameter  $\alpha$  denotes a ratio of the radius of the plastic zone to the radius of the crater. The shape of the plastic zone is assumed to be spherical ahead of the penetrator. This parameter is used to determine a value for the target resistance  $R_t$ , given as

$$R_t = \frac{7}{3} \ln(\alpha) Y_t \quad (2)$$

where  $Y_t$  denotes the target flow stress. The value for  $\alpha$  used in the central region of the target is estimated from cavity expansion theory. As the rear surface is approached, this value of  $\alpha$  is degraded according to the empirical relationship:

$$\alpha = \alpha_0 - (\alpha_0 - 1) \left[ \frac{x - [T - R_c(\alpha_0 - 1)]}{R_c(\alpha_0 - 1)} \right]^n \quad (3)$$

where  $R_c$  is the crater radius,  $T$  is the target thickness,  $x$  is the position of the projectile/target interface measured from the front target surface,  $\alpha_0$  is the value attained for  $\alpha$  when the plastic zone just touches the rear surface, and  $n$  is a free parameter. This expression for  $\alpha$  is used only when the plastic zone impinges on the rear surface of the target, i.e., when  $T - R_c(\alpha_0 - 1) \leq x \leq T$ . The parameter  $\alpha$  attains the value of  $\alpha_0$  for  $x = T - R_c(\alpha_0 - 1)$  and 1.0 for  $x = T$ . In principle, reducing the value of  $\alpha$  as the projectile approaches the rear of the target is equivalent to reducing the value for  $R_t$ , as has already been suggested by the results given in Table III using the traditional Tate model.

(U) The free parameter,  $n$ , in Eq. (3) can be adjusted to match experimental data. Changing this parameter alters the functional form of the target resistance near the rear surface. Shown in Figure 7 is a plot of  $\alpha$  versus the normalized thickness ( $x/T$ ) for several values of the parameter  $n$  [Ref. 3]. The values of  $\alpha_0$  and  $R_c$  used were 5 and 0.25, respectively. As is evident from the figure, when  $n < 1$  the value of  $\alpha$  degrades very quickly when the plastic zone just touches the rear surface and then continues to degrade at a reducing rate. This is contrasted with the case where  $n > 1$ , where the degradation is more gradual at first, then accelerates continually, with the degradation being the largest just before the projectile exits the target.

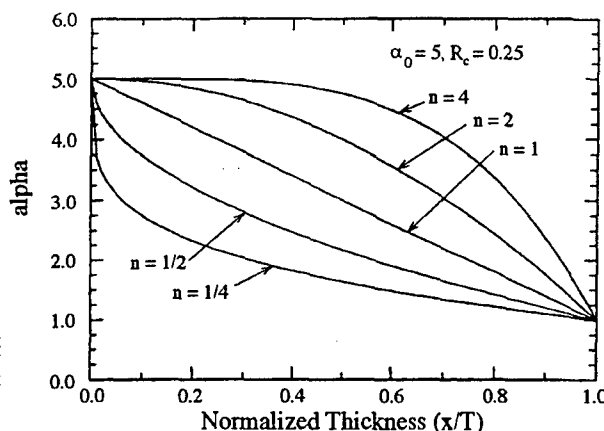


Figure 7. (U) Variation of  $\alpha$  with  $(x/T)$ , [Ref. 3].

(U) Shown in Figure 8 is a graph of net penetration versus impact velocity for the 4340 targets. The penetration depth from the experiments is reproduced here using the data in Table I, along with the regression line that corresponds to the data. The extrapolated portion of the line extends from the highest velocity at which no breakout occurred—from 1.67 km/s to 1.72 km/s.

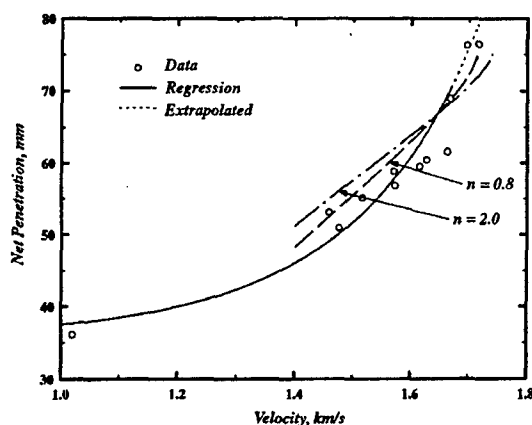


Figure 8. (U) Penetration versus impact velocity from the experiments and calculations.

(U) Results from calculations are also shown for two specific values of the parameter  $n$ : 0.8 and 2.0. In both calculations, the target flow stress  $Y_t$  was adjusted so that the predicted penetration depth matched the regression line at an impact velocity of 1.65 km/s. The resulting values for  $Y_t$  were 1.29 and 1.15 GPa for  $n = 0.8$  and 2.0, respectively. These are both within the range that would be expected for the dynamic flow stress of 4340 steel. The results for the curve with  $n = 0.8$  provides a reasonable match to the experimental data. The ballistic limit velocity is estimated to be 1.72 km/s which is close to the value suggested by the regression line plotted in Figure 8.

(U) The breakout model described above has been used to model residual velocity data obtained from other experiments with finite-thickness RHA targets [Ref. 3]. Results from that analysis suggested that the proper value of  $n$  was 2 for those particular targets. The results for  $n = 2.0$  do not match the current data set as well. The slope of the line is different from the regression line and the estimated ballistic limit velocity is computed to be 1.75 km/s. Thus, for the particular data set presented here, a value of  $n = 0.8$  reasonably captures the physics involved in breakout mechanics, at least in an empirical sense.

(U) The parameter  $n$  is principally used as a curve fitting constant. Results for different values for  $n$  also mimic the behavior of possible breakout failure mechanisms that might occur in the target. For example,  $n > 1$  is consistent with a ductile failure mode in which only a small portion of the plastic zone is involved with the target rear surface in the early stages of breakout. This causes the initial effects of breakout on target resistance to be small (e.g., see Figure 7 for  $n > 1$ ). On the other hand,  $n < 1$  mimics a plugging type of failure mode, where a significant and more rapid loss in target strength is expected when the plastic zone is relatively further from the rear surface. It is not unreasonable to expect that  $n$ , and the mode of failure, varies for different target materials. The RHA used in Reference 3 was much thicker (~460 mm) and softer (BHN 269) than the steels used in these experiments. Since the harder targets used here would be more subject to a plugging-type of failure, it might be expected that a smaller value of  $n$  is required to match the data.

(U) We use the Walker-Anderson model with the breakout algorithm to calculate the plastic zone size and target resistance as a function of time as the projectile penetrates the target. In Figure 9, the plastic zone parameter,  $\alpha$ , and the target resistance parameter,  $R_t$ , are plotted as a function of penetration depth for an impact velocity of 1.75 km/s, which is less than 4% above the ballistic limit velocity of 1.69 km/s for the target. Results are shown for two values of  $n$ ; 0.8 and 2.0. Two different measures of the target resistance  $R_t$  are also shown:  $R_{t1}$ , which is determined using Eq. (2), and  $R_{t2}$ , which is the functional form of the target resistance used in the traditional Tate model [Ref. 4], namely,

$$R_{t2} = Y_t + \frac{1}{2} \rho_p (v - u)^2 - \frac{1}{2} \rho_t u^2 \quad (4)$$

The subscripts, p and t, denote projectile and target materials, respectively;  $\rho$  is the density,  $u$  is the projectile/target interface velocity, and  $v$  is the projectile tail velocity. We use Eq. (4) to compute  $R_{t2}$  from the Walker-Anderson model. Since  $u$  and  $v$  vary with time in the model,  $R_{t2}$  also changes with time, as opposed to a constant value for  $R_{t2}$  when used in the traditional Tate model.

(U) The results using the breakout algorithm are shown in Figure 9. The presence of the rear target surface begins to affect the plastic zone size and target resistance after the projectile has penetrated about 41 mm, when  $(x/T) = 0.54$ , or 3.7 penetrator diameters from the target rear surface. When  $n = 2$ , the degradation in  $R_t$  and  $\alpha$  is gradual at first, then falls off sharply as the penetrator breaks through the target at 76.2 mm. On the other hand, when  $n = 0.8$ , both  $R_t$  and  $\alpha$  drop sharply at 41 mm, and decay more gradually as the projectile approaches the rear surface.

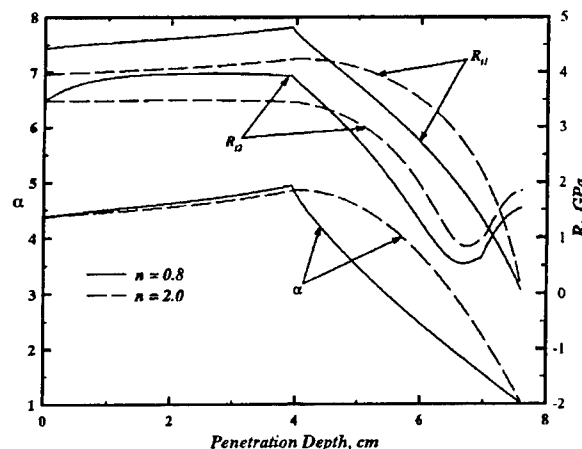


Figure 9. (U) Calculated values for  $\alpha$  and  $R_t$  as a function of penetration depth for an impact velocity of 1.75 km/s.

(U) The discontinuity in the slopes for  $R_t$  and  $\alpha$  at a depth of 41 mm does not appear to be physically realistic. This suggests a different form for Eq. (3) may be needed to adequately model the degradation in  $\alpha$ . It does, however, correctly indicate that the target resistance falls off quite dramatically when the projectile tip is still a considerable distance from the target rear surface. A rapid change in slope is a possible result of the formation of a plug which begins to move ahead of the projectile. This also results in an increase in the rate of penetration as observed both in the analytical model and in numerical code computations [Ref. 3].

(U) On the other hand, Satapathy, Normandia, and Bless [Ref. 5], use a modified spherical cavity expansion theory to suggest that the rear surface limits the extent of the elastic zone. This enters into the boundary conditions used to determine the location of the plastic zone. The effect of the finite boundary is felt long before it impinges on the rear target surface. The consequences of this are that  $R_t$  begins to degrade much sooner than 4 penetrator diameters from the rear target surface and that this degradation would be more gradual, increasing as the rear surface is approached, similar to  $n > 1$  in Figure 7.

(U) In Figure 10 results are shown for the line-of-sight penetration as a function of velocity for the oblique RHA targets tested. The experimental results given in Table II are shown on the graph, along with the analytical predictions for  $n = 0.8$  and  $2.0$ . In each of the analytical predictions, the target flow stress was adjusted so the penetration depth agreed with the experimental value at an impact velocity of  $1.6 \text{ km/s}$ , which were  $1.30$  and  $1.17 \text{ GPa}$  for  $n = 0.8$  and  $2.0$ , respectively. When  $n = 0.8$ , the predicted penetration depth is consistent with the experimental result; the slope of the line is reasonably close to the value suggested by the data. It is difficult, however, to make firm quantitative assessments due to the limited experimental data. Nevertheless, the curve for  $n = 0.8$  matches the data better than when  $n = 2.0$ . These observations are also consistent with the results shown in Figure 6; they suggest that the same degradation model for  $R_t$  might be used for both normal and oblique data.

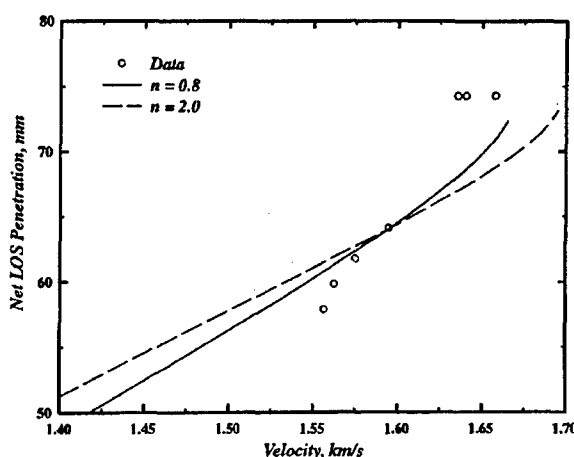


Figure 10. (U) Line-of-sight penetration versus impact velocity for the RHA target.

## (U) SUMMARY

(U) Experimental data were presented which details the behavior of finite thickness targets for impact velocities which are near, but below the ballistic limit velocity. The presence of the rear target surface of both RHA (BHN 302) and 4340 (BHN 330) steel provide a continually degrading value of target resistance as the impact velocity approaches the ballistic limit from below. The Walker-Anderson model is calibrated to this data set and matches both sets of data

## UNCLASSIFIED

reasonably well. However, the functional form chosen to degrade the extent of the plastic zone results in a slope discontinuity in target strength. Other functional forms are being evaluated based on a modified spherical cavity expansion model which shows that the plastic zone is affected before it actually impinges on the target rear surface due to the fact that the elastic zone is finite [Ref. 6].

### (U) ACKNOWLEDGMENTS

(U) This work was supported by the U. S. Army Research Laboratory (ARL) under contract DAAA21-93-C-0101. The authors gratefully acknowledge ARL for supplying the RHA to Abex for testing under contract DAAA15-86-C-0014 with ARL/TACOM.

### (U) REFERENCES

(U) [1] Walker, J. D. and Anderson, Jr., C. E., "A Time-Dependent Model for Long-Rod Penetration," *Int. J. Impact Engng.*, vol. 16 (1), pp. 19 - 48, 1995.

(U) [2] Contiliano, R., McDonough, T. B., and Swanson, C.V., "Application of the Integral Theory of Impact to the Qualification of Materials and the Development of a Simplified Rod Penetrator Model," A.R.A.P. 368, November 1978.

(U) [3] Anderson, Jr., C. E., and Littlefield, D. L., "Pretest Predictions for Long-Rod Interactions with Armor Technology Targets," SwRI Technical Report No. 07-5117, April 1994.

(U) [4] Tate, A., "A Theory for the Deceleration of Long Rods After Impact," *J. Mech. Phys. Solids*, vol 15, p. 387, 1967.

(U) [5] Alekseevskii, V. P., "Penetration of a Rod into a Target at High Velocity," *Combustion, Explosion and Shock Waves*, vol. 2, pp. 63-66, 1966, translation from the Russian.

(U) [6] Satapathy, S., Normandia, M. J., and Bless, S. J., "Finite Target Thickness Effects in Metals and Ceramics as revealed by Cavity Expansion Analysis," to be presented, ASME conference, Baltimore, MD, June 1996.

(U) [7] Normandia, M. J., Satapathy, S., Littlefield, D. L., Walker, J. D., and Anderson, Jr., C. E., "Modified Cavity Expansion Analysis For Modeling Finite Target Penetration," to be published, 16th International Symposium on Ballistics, San Francisco, CA, October 1996.

(U) [8] Anderson, Jr., C. E., Walker, J. D., and Hauver, G. E., "Target Resistance for Long-Rod Penetration," *Nuclear Engng. & Design*, vol. 138, pp. 93-104, 1992.

UNCLASSIFIED

## MODELING BALLISTIC LIVE-FIRE EVENTS

Dr. Paul H. Deitz and Mr. Richard Saucier

Army Research Laboratory, Aberdeen Proving Ground, MD 21005-5068

### ABSTRACT (U)

(U) This paper explains the need for a stochastic vulnerability model to support the analysis of live-fire testing. The history of the development and use of such a model over the last decade is summarized by demonstrating the need for new methodologies and the establishment of the SQuASH vulnerability model. A brief review is made of the various assessment efforts made to compare SQuASH model outputs with various Abrams Live-Fire Test results. This has led to a model improvement plan for upgrading SQuASH. The incorporation of the upgraded model into the MUVES suite of vulnerability codes and its application to the upcoming Armored Gun System (AGS) Live-Fire program are described.

### (U) INTRODUCTION

(U) Nearly a decade ago, the US began a new form of vulnerability experimentation called *Live-Fire Testing* (LFT) (ref. 1). In LFT, a complete vehicle such as a tank or armored personnel carrier is placed in full battle readiness, engine running, full load of fuel and ammunition, and fired at with an overmatching threat. Only the absence of a live crew compromises actual encounter realism. Congressional legislation had been passed recognizing that in spite of design limits defining absolute protection, systems should nevertheless be tested according to threats expected to be encountered. Many such threats could be overmatching. The issue was to mitigate and ameliorate such events. In addition, LFT can uncover vulnerabilities not foreseen by vehicle designers and improve survivability.

(U) The first live fire tests occurred against the M113 armored personnel carrier.<sup>†</sup> For the most part, these results were non-controversial. By 1985, testing had begun on the more modern Bradley Fighting vehicle. To accompany field testing, the program test plans required that vulnerability models be used both to predict and, subsequently, to be upgraded by actual LFT results. As the test proceeded and the results were compared to model predictions, an apparent pattern of disagreement began to emerge. Critics in the Office of the Secretary of Defense (OSD) called into question the fidelity of existing ballistic vulnerability modeling. As the Vulnerability/Lethality Division (VLD) of the former Ballistic Research Laboratory (BRL) headed into the Abrams Live-Fire program, a goal was set to develop a new model — one designed to simulate actual live-fire events, including the statistical variations commonly encountered.

### (U) DEVELOPMENT OF THE SQuASH MODEL

(U) The SQuASH model was developed specifically for the purpose of providing a tool for predicting and understanding live-fire events. No existing model was adequate for this purpose; either they did not predict outcomes that could actually be measured in the field or they did not account for the variability of live-fire outcomes — or they were deficient in both of these areas.

### (U) Model Requirements to Address Live-Fire Testing

(U) When the need for vulnerability modeling to support live-fire testing arose in 1985, a number of insights

---

<sup>†</sup> Bradley live-fire actually began before the M113 tests, but the M113 firings were completed first.

UNCLASSIFIED

began to emerge:

- Many of the metrics commonly output by standard vulnerability models, such as *battlefield utility*, were not observable by vehicle assessors. In fact, none of the extant vulnerability models computed directly observable damage or vehicle capability. Vulnerability models have historically done a poor job of developing metrics which are observable in the field. The emphasis in vulnerability modeling today is on:
  - Direct Battle Damage (i.e. "killed" or non-functioning components) and
  - Platform Capability (the relationship between "killed" components and measurable platform function, rate-of-gun fire, top speed, etc.).

Battlefield utility, which is not an observable, is now seen to be the proper province of the force-on-force modeler.

- Few vulnerability models reflected the variability which is intrinsic to many ballistic interactions. When penetrators strike a target and perforate the skin, the armor spalls into numerous fragments of varying mass, velocity, shape and orientation. However, the existing models all converged on a single, expected-value for the final result, rather than yielding statistical distributions of possible outcomes. Some models attempted to calculate the probability of damaging components individually along a particular shotline, but said nothing about the probability of damaging components in combination with one another.

(U) In addition to establishing the need for a new model, this retrospection of existing vulnerability models also made it clear that:

- There is a dearth of information concerning many of the mechanisms of physical damage from ballistic interactions.
- There are many ballistic mechanisms which can cause significant damage which were not modeled at all. These typically included blast, shock, fire and toxic fumes.

(U) Another important by-product of this reexamination has been the establishment of a formal framework within which to understand and categorize the elements and properties of vulnerability/lethality. Termed the *V/L Taxonomy* (ref. 2), it provides a method to decompose the elements of V/L into a sequence of simpler constituent parts called *levels*. The levels relate to each other in a specific processing order and are fundamentally different. Each has its unique and appropriate use in the general scheme of V/L assessment and are related to each other by mapping operators. It can be seen that most (if not all) of these mapping operators must be stochastic in order to support the variability so intrinsic to many of the V/L processes. A further characterizing property of the vulnerability levels is the degree to which specific metrics are aggregated (i.e., lumped together) *versus* refined (i.e., subdivided into smaller elements). The word *granularity* is used to describe this property. Since the earliest notions of the V/L Taxonomy were first expressed (ref. 2), much progress has been made to formalize and extend this concept. The concept of the V/L Taxonomy has applicability ranging from how platform component damage relates to platform performance to how platform metrics should feed force-on-force models. (The reader is referred to ref. 2 for a current summary of this framework and its ramifications.)

#### (U) Need for a Stochastic Model

(U) To address the shortcomings described above, the Vulnerability/Lethality Division (VLD) of the Ballistic Research Laboratory embarked in 1985 on a significant initiative to establish a new kind of vulnerability code which would explicitly embody *observable model metrics supported by stochastic methods*. The new code, called *SQuASH* (for Stochastic Quantitative Analysis of System Hierarchies), was applied to some 48 Abrams shots performed in the 1986 time frame. SQuASH supported the following five sources of variability, subject to random sampling:

- Weapon Hit Point — sampled in the neighborhood of the intended impact point.
- Warhead Performance — from a Gaussian distribution with mean and standard deviation obtained from experimental data.

UNCLASSIFIED

- Residual Penetrator Deflection — from a Gaussian distribution with mean and standard deviation obtained from the variability of experimental data, width of the spall cone, and a Poisson distribution which controls the number of spall fragments. The parameters for these distributions were derived from experimental data.
- Component  $P_k$  Characterization — from a Poisson distribution to determine the number of impacts on a component and a uniform distribution to perform a Bernoulli trial on whether the component was “killed” or “not-killed.”

(U) Because of the paucity of knowledge for many sources of damage as well as insufficient time to code new algorithms, the only damage mechanisms modeled for this analysis were main penetrator (including residual penetrator) and behind-armor debris spall.

## (U) ASSESSMENT OF SQuASH — LESSONS LEARNED

(U) Following the Abrams program, a number of significant efforts were made to compare the model results with the field observables. This effort proved daunting as the SQuASH model exercise indicated the possibility of more than  $10^6$  individual combinations of component “kill” records for particular warhead-target encounters. A thousand, or even ten thousand, Monte Carlo replications with the model may not be sufficient to produce the exact sequence of damaged components observed in the field. Validation of a stochastic vulnerability model was — and still remains — problematical.

### (U) Early Assessment of SQuASH

(U) The initial published results addressing model validation for Abrams (refs. 3-5) live-fire shots resulted in the following conclusions (taken from ref. 5):

- Tests on the probability of armor perforation were in good agreement with model predictions.
- Tests on the probability of catastrophic “kill” were also in good agreement with model predictions.
- Tests on the Mobility “Kill” prediction were at the 85% agreement level with model predictions.
- Tests on the Fire Power “Kill” prediction were at the 33% level of agreement with model predictions.

(U) A number of other issues came to the fore. It was clear that fire, secondary spall, ricochet and blast sometimes played dominant roles. The absence of algorithms in the model to describe these potential sources of damage needed to be redressed. In addition, unless there were major disagreements between the model and the field tests, the very complexity of ballistic interactions — with the concomitant space of greater than  $10^6$  discrete outcomes to be compared with a small number of single test results — made statistical inference problematic.

(U) In the time since 1986, various upgrades to SQuASH have been made and the model has been used in a number of Army Live-Fire programs. These include M1A1, Paladin, M1A2 and T-72. To avoid confusion, note that the initial configuration of SQuASH used for the Abrams M1A1 live-fire program was written in Fortran. The version of SQuASH that is being incorporated into MUVES (described in subsequent sections) is written in the C language.

### (U) Independent Assessment of SQuASH

(U) In addition to the above in-house comparison, the VLD also contracted with The SURVICE Engineering Company in 1991 to perform an independent assessment of SQuASH. Their findings will be discussed below.

(U) Meanwhile, in 1993 the Army was involved in the Abrams M1A2 upgrade. In order to decrease the cost of testing, the Department of the Army (DA) proposed to substitute SQuASH predictions for a portion of live-fire testing. To estimate the risk associated with this strategy, OSD tasked the Institute for Defense Analyses (IDA) to perform an independent assessment of SQuASH. In a set of charts,<sup>†</sup> IDA appears to have utilized a novel strategy in which the probabilities of damaging particular components using *multiple* threats at *various* hit locations are aggregated over many tests. Via this strategy the paucity of field tests matching each model exercise would appear to have been somewhat mitigated. Based on these findings IDA drew the following three conclusions:

---

<sup>†</sup> To date, no formal report of the findings has been published by IDA.



- SQuASH is a poor predictor of damage at the component level.
- The number of components where the damage was *unexpected* ( $P_k \leq .05$ ) is comparable to or exceeds the number where the damage was *expected*.
- A large fraction of the damaged components was never reported by the model.

(U) Of the 259 “killed” components used in the IDA study, SQuASH correctly predicted damage to 49% (127) and incorrectly predicted no damage to 51% (132). The latter category can be further subdivided into two groups:

1. Component was hit but not predicted to be damaged — accounting for 21% (54 components) and
2. Component was not hit by a ray — accounting for 30% (78 components).

(U) IDA did not provide insight into the possible origins of SQuASH-Abrams LFT discrepancies. From our analyses, these two categories correspond to separate issues and are being addressed by different strategies. The first category illustrates a deficiency of modeling the vulnerability of critical components. Past modeling used an average probability of kill ( $P_k$ ), averaged over hit location and direction of penetration. Due to the inherent variability of component vulnerability, a distribution of possible outcomes rather than a single expected value may be more appropriate — and we are exploring this option. However, another factor which may contribute to the discrepancy — and may even be more important — is the use of a *single* draw on the component  $P_k$  to produce a binary kill/no-kill outcome. Even if the component is modeled extremely well, the expected number of Bernoulli trials required to realize a “kill” is  $1/P_k$ , where  $P_k$  is the component’s probability of “kill.” Thus an unintended result of the Bernoulli trial approach is to effectively under-sample the components having low  $P_k$  values. We now believe that a better approach may be to use the *actual*  $P_k$  value in the *Criticality Analysis* (see ref. 6, for an example of the latter) — and the methodology is being changed to accomplish this.

(U) The second category illustrates a geometric sampling problem: If SQuASH never samples a component, it can never be regarded as damaged. The methodology being developed in the new SQuASH model will be using a different approach altogether for generating spall fragments (see *Improvements to SQuASH* below), as well as modern recursive techniques to produce secondary burst points.

(U) In general, the conclusions of the SURVICE study (ref. 7) were not substantially different from the IDA study, although they do contain more detail. However, the SURVICE study used a more stringent statistical test called the *Modified Ordering of Probabilities* Test (ref. 8).

## (U) MUVES — NEW CONTEXT FOR SQuASH

(U) In 1986, concurrent with the development of SQuASH, the VLD initiated a project to develop a computer architecture, written in the C language, that would be modular in nature, strongly coupled to the UNIX operating system, and would minimize vulnerability code redundancy. This effort resulted in a computer environment called *MUVES* (ref. 9) (for *Modular UNIX-based Vulnerability Estimation Suite*). The development was made possible by a number of new insights including:

- The actual vulnerability process can be broken into specific building elements. These elements can calculate possible damage in uniform ways regardless of the threat-material class, can aggregate damage in consistent ways to estimate component “kill,” and can map component “kill” to platform capability in the same general fashion.
- Each vulnerability code is composed principally of support modules which are not threat-target specific. This 85% of the code includes modules, for example, to manage memory, interrogate geometry, interpolate tables, and draw random numbers. All of these modules should be applicable to many classes of vulnerability computation for many threats and many targets.
- The computer methods and techniques historically used to code vulnerability models are inadequate to the task of rapid upgrade, code VV&A, extensibility to new encounter conditions, and ability to share code among various threat-target classes.

UNCLASSIFIED

(U) Over the past six years, the Ballistic Vulnerability/Lethality Division has been moving its vulnerability codes under this single, consistent MUVES environment. The first code integrated into MUVES was the direct-fire, lumped-parameter, *Compartment Model*, historically called *VAMP* (ref. 10). The resulting code has supported many direct-fire studies over the past years. In the summer of 1995, an aircraft-missile model called *MAVEN* (ref. 11) (*Modular Air-system Vulnerability Estimation Network*) was placed in production. The first operational capability embodied armor piercing (AP) threats against aircraft and was used for live-fire predictions in the current Apache-Longbow program (ref. 12). Now in final beta testing is an indirect-fire model called *SAFE* (ref. 13) (*Statistical Analysis of Fragment Effects*). A major improvement for indirect-fire weapons including artillery munitions, *SAFE* can assess multiple burst points, proper target perspective, random fragments (including mass, velocity, shape and orientation) and aggregate damage correctly at the vehicle component level. *SQuASH* is also moving to the MUVES environment. Not only is the overhead in dealing with the *SQuASH* Fortran environment too high, it is incapable of supporting the proper inclusion of new damage mechanisms.

## (U) SQuASH IMPROVEMENTS AND APPLICATIONS

### (U) Methodology Improvements

(U) With the intent of redressing the modeling deficiencies that were identified previously (*see ASSESSMENT OF SQuASH — LESSONS LEARNED*), the following changes to the methodology are being implemented:

- **Upgraded Kinetic Energy (KE) Long Rod Armor Penetration:** Based on the research of Alekseevskii (ref. 14) and Tate (ref. 15), this methodology applies to a wide variety of threat-target interactions by accounting for hydrodynamic flow of both target and penetrator that can arise in the hypervelocity regime. This methodology also makes explicit use of physical quantities, such as Brinell hardness, that can be varied in a stochastic manner when it is appropriate to do so — such as when the penetrator is close to the ballistic limit  $v_{50}$  of perforation.
- **New Spall Characterization:** A substantial effort has been expended to improve (ref. 16) the *SQuASH* spall model. The upper section of Fig. 1 shows a flash radiograph of a shaped-charge jet following armor penetration. An elliptical debris cloud is evident. The lower section shows the geometric characterization of the shell shape and velocity field used to model this phenomenon.

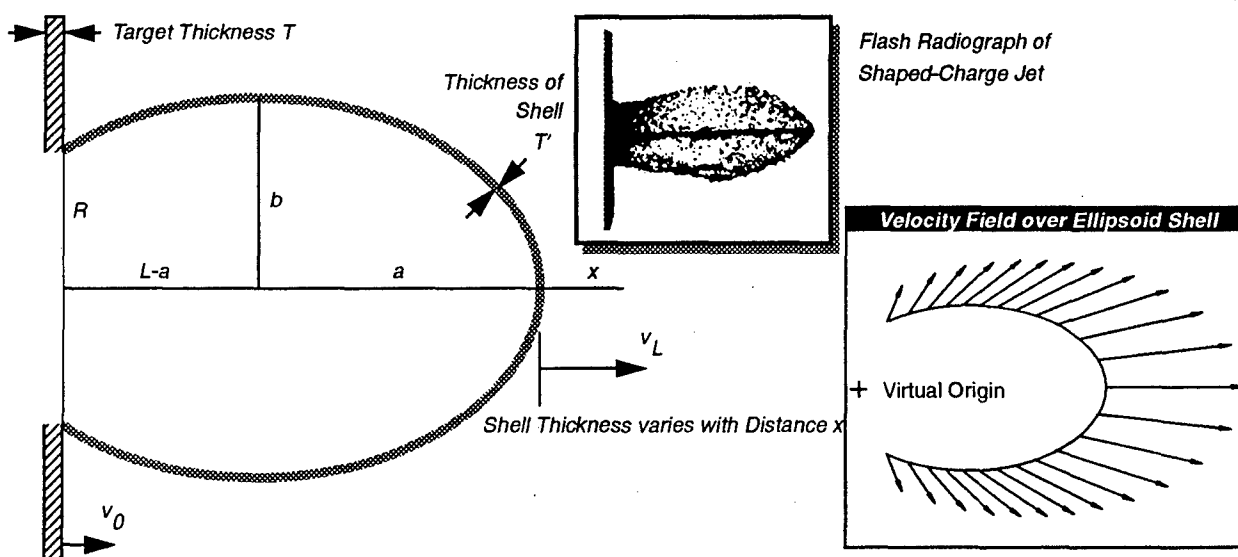
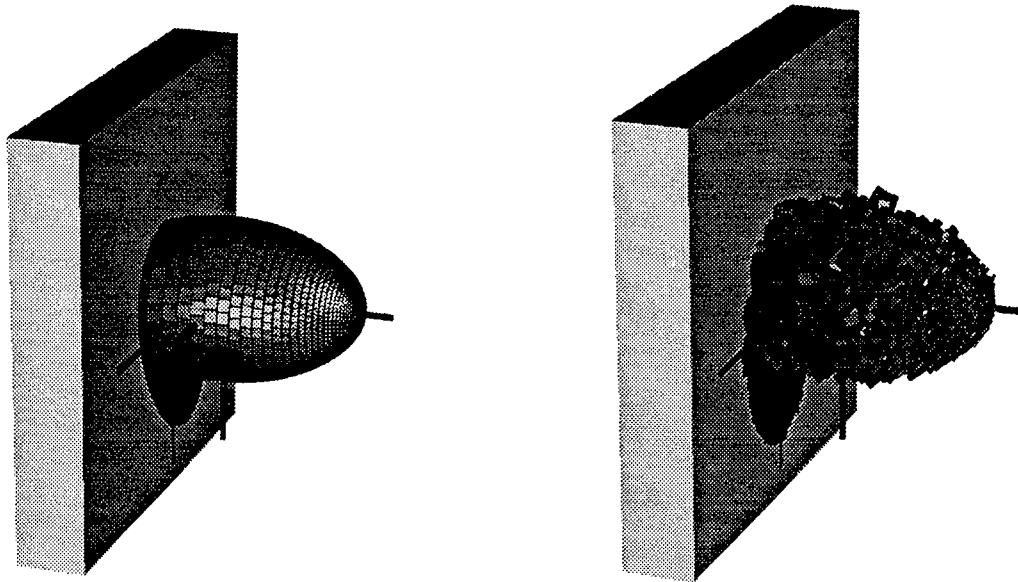


Figure 1. (U) Behind Armor Debris Characterization

UNCLASSIFIED

The image on the left in Figure 2 shows a three-dimensional rendering of a spall cloud computed with expected-value parameters for each surface element on the cloud topology. The image on the right in this figure shows the same plot with stochastic spall generation enabled.



**Figure 2.** (U) *Three-Dimensional Renderings of Spall Cloud* (Images due to Gary Moss, ARL/SLAD/BVLD)

- **Multiple Barrier Penetration:** The code will propagate the threat (spall or penetrator) until it comes to rest or exits the vehicle. The Fortran version of SQuASH did not track spall beyond the first barrier and broken penetrator pieces were not tracked beyond the sixth barrier.
- **Accounting for Ricochet:** Ricochet was not accounted for in the Fortran version of SQuASH, although the LFT assessors noted the occurrence of ricochet in the live-fire tests. SQuASH will be using a ricochet criterion published by Tate (ref. 17) that is based upon penetrator velocity and target obliquity. When the ricochet criterion is satisfied, the code will go on to compute the ricochet angle and residual velocity (ref. 18).
- **Upgraded Personnel Incapacitation:** The Fortran version of SQuASH used the Kokinakis-Sperrazza criteria for crew incapacitation (ref. 19). The MUVES version of SQuASH will use "Ballistic Dose" (ref. 20). This is a combination of mass, velocity and number of fragment hits that was formulated from extensive runs of the *ComputerMan* model (ref. 21). It removes a number of limitations of the older methodology.
- **New Component Characterization:** The Fortran version of SQuASH performed a Bernoulli trial on each component that was hit to get a binary "kill/no-kill" outcome. Since the  $P_k$  of the component will be known as a function of the encounter conditions, the MUVES version of SQuASH will output the  $P_k$  value itself. This value will then be passed along from each component and combined using fault-tree algebra. This change in methodology should go a long way toward alleviating the sampling problem that has been identified in the IDA and SURVICE studies.
- **New Sampling Procedures:** The Fortran version of SQuASH used the expected number of fragments along a trajectory whereas the MUVES version of SQuASH brings more fidelity to the process by specifically generating a ray for each fragment. This allows for more realism and a more natural application of stochasticism. The MUVES version of SQuASH will have a library of twenty continuous distributions and seven discrete distributions to simulate various random processes. Furthermore, this library is extensible so

that the user can use an empirical distribution or a user-specified function to represent a given stochastic process. Among the stochastic processes that the MUVES version of SQuASH will consider as the model is fine-tuned are:

- Hit Location
- Penetration Depth (based upon variation of material properties)
- Ballistic Limit Velocity (based upon spread about the  $v_{50}$  value)
- Penetrator Breakup (based on velocity, obliquity and yaw)
- Deflection of Kinetic Energy Long Rod Penetrators
- Ricochet Angle of KE Long Rod Penetrators
- Spall (fragment velocity, size, direction and orientation)
- Component  $P_k$

(U) We note again that neither the SURVICE nor IDA study was able to make a determination of specific causes for disagreement between SQuASH and the Abrams LFT program. Our diagnosis of the disagreement is based upon past experience, knowledge of the modeling methodology, and insight. As a result, we believe that the planned improvements outlined in this section are plausible cures for these deficiencies but, of course, it will be the actual application of the model to Live-Fire that will determine our degree of success.

(U) Application to the Armored Gun System (AGS)

(U) The first application for the MUVES version of SQuASH comes soon with the Armored Gun System (AGS) program. Figure 3 shows a shaded rendering of the BVLD-generated image. This image was generated with the BRL-CAD™ suite of supporting utilities.

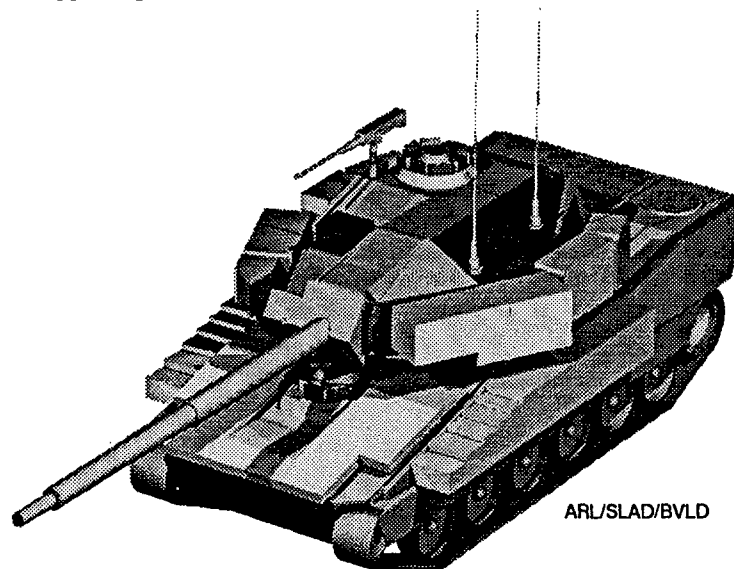


**Figure 3.** (U) A shaded rendering of the Armored Gun System (AGS) (Image due to Ted Muehl, ARL/SLAD/BVLD)

(U) AGS will constitute the Army's new combat vehicle, but in the form of a highly deployable, light-weight vehicle, with high fire-power and reconfigurable armor protection. Analysts are assembling the various required inputs including target description, fault-trees, penetration-fragment parameters and component  $P_k$  functions. This preparation phase is particularly challenging due to 1) the multiple armors being used on the AGS and 2) the paucity of relevant ballistic data bases, at least in comparison to that known at a comparable time in the Abrams program.

UNCLASSIFIED

(U) The MUVES environment is being upgraded with the software improvements previously discussed (see *IMPROVEMENTS TO SQuASH*). The application of the new MUVES version of SQuASH to the AGS will provide valuable information on the improvement strategy that we have outlined in this report.

#### (U) Future Improvements

(U) In addition, studies continue elsewhere in the ARL to bring insight into the ballistic phenomena of shock-blast loading and resulting component damage. As these complex damage mechanisms are gradually understood and modeled, the BVLD will integrate appropriate algorithms into the MUVES environment. This strategy has already resulted in great leveraging. First, mechanisms are easier to model and integrate into MUVES because the support structure already exists. Second, when a new mechanism is included one place in the MUVES environment, it is available for all other approximation methods sharing this environment. As the MUVES environment matures and these methods gain sophistication, we expect a gradual shift away from the long-existent problems of code implementation and towards the fidelity and calibration of specific ballistic phenomena and related platform dysfunction.

#### (U) NEED FOR STATISTICS

(U) A recurring theme throughout the application of SQuASH to LFT has been the need for statistical measures of comparison (see refs. 8, 22-24). Even the question of what test to use is not at all obvious. Different analysts apply different tests to judge the comparison between model predictions and field test results. Furthermore, there are various levels at which the comparison can be performed — ranging from component damage states to platform performance. Nor is this problem likely to be solved any time soon; it is an active, ongoing area of research.<sup>†</sup> Even if we didn't have the SQuASH model, we would still be faced with the problem of drawing statistically significant conclusions from an absolutely small number of live-fire tests. Of course the problem of inferring statistically significant conclusions from model predictions *vis-a-vis* live-fire tests extends beyond SQuASH to virtually all of the high-resolution V/L models whether within or without the MUVES environment.

#### (U) CONCLUSIONS

(U) In this paper we have reviewed a decade of Live-Fire V/L testing and modeling. The test programs have spurred substantial improvements to the extant suite of V/L codes, one of which is the SQuASH model. Comparisons of SQuASH model predictions with field tests indicate that fragment damage is underpredicted; other damage mechanisms must be added. A detailed strategy for code upgrade has been outlined including not just specific computational fixes, but the use of a general V/L computing environment called MUVES. Currently SQuASH is being upgraded in preparation for the AGS live-fire program. The next half year will provide a set of new opportunities to gauge progress in V/L model improvement.

### ACKNOWLEDGEMENTS

(U) The authors wish to thank Mr. Scott L. Henry, Mr. Gary S. Moss, Ms. Karen R. Murray, Ms. Lisa K. Roach, Mr. Richard S. Sandmeyer, Dr. Michael W. Starks, Dr. James J. Wade (all of ARL), and Mr. Richard E. Helmuth of Science Applications International Corporation for their comments and assistance in the preparation of this paper. The authors extend their special thanks to Dr. Benjamin W. Turner of the Institute for Defense Analyses for his detailed insights into the various statistical methods developed and applied by his organization. The IDA comparison of the SQuASH/Abrams modeling effort was sponsored by Mr. James F. O'Bryon, Operational Test and Evaluation, Office of Secretary of Defense.

---

<sup>†</sup> For example, an ARO/Academia/ARL Workshop was held September 11-12, 1995 at ARL/SLAD. Under the sponsorship of Dr. Jagdish Chandra, Director of the Army Research Office Division of Mathematics and Computer Science, a group of academic experts met to discuss various computer science and statistical issues in the area of vulnerability/lethality.

(U) REFERENCES

1. *Live Fire Testing*, National Defense Authorization Act for FY 1987, contained in Chapter 139, Section 2366 of Title 10, United States Code.
2. J. Terrence Klopac, Michael W. Starks and James N. Walbert, *A Taxonomy for the Vulnerability/Lethality Analysis Process*, **Ballistic Research Laboratory Memorandum Report BRL-MR-3972**, May 1992. These notions were first discussed in Paul H. Deitz and Aivars Ozolins, *Computer Simulations of the Abrams Live-Fire Field Testing*, **Proceedings of the XXVII Annual Meeting of the Army Operations Research Symposium**, 12-13 October, 1988, Ft. Lee, VA; also **Ballistic Research Laboratory Memorandum Report BRL-MR-3755**, May 1989.
3. Donald F. Menne, *Comparison of Abrams LF Data*, **Ballistic Research Laboratory White Paper**, December 1988.
4. Cynthia J. Dively, Scott L. Henry, John H. Suckling, Jill H. Smith, William E. Baker, David W. Webb and Paul H. Deitz, *Abrams Live Fire Test Program: Comparison Between SQuASH Predictions and Field Outcomes (U)*, **Ballistic Research Laboratory Special Report (SECRET)**, February, 1989.
5. Paul H. Deitz, Jill H. Smith and John H. Suckling, *Comparisons of Field Tests with Simulations: Abrams Program Lessons Learned*, **Proceedings of the XXVIII Annual Meeting of the Army Operations Research Symposium**, 11-12 October, 1989, Ft. Lee, VA, pp. 108-128; also **Ballistic Research Laboratory Memorandum Report BRL-MR-3814**, March 1990.
6. Joseph J. Ploskonka, Theodore M. Muehl and Cynthia J. Dively, *Criticality Analysis of the M1A1 Tank*, **Ballistic Research Laboratory Memorandum Report BRL-MR-3671**, June 1988.
7. *Comparison of SQuASH Predictions with Live-Fire Test Results for Three Combat Vehicles (U)*, **The SURVICE Engineering Company SURVICE-TR-94-015 (SECRET)**, May 1994.
8. David W. Webb, *Tests for Consistency of Vulnerability Models*, **Ballistic Research Laboratory Memorandum Report BRL-TR-3030**, August 1989.
9. Phillip J. Hanes, Scott L. Henry, Gary S. Moss, Karen R. Murray and Wendy A. Winner, *Modular UNIX-Based Vulnerability Estimation Suite (MUVES) Analyst's Guide*, **Ballistic Research Laboratory Memorandum Report BRL-MR-3954**, December 1991. Also, *Appendix B: "Compart" Approximation Method*, **Ballistic Research Laboratory Memorandum Report BRL-MR-3955**, December 1991.
10. C. L. Nail, T. E. Bearden and E. Jackson, *Vulnerability Analysis Methodology Program (VAMP): A Combined Compartment-Kill Vulnerability Model*, Computer Sciences Corporation Technical Manual, **CSC TR-79-5585**, October 1979.
11. Mark D. Burdeshaw, *The MAVEN Approximation Method in the MUVES Environment*, **Army Research Laboratory ARL-TR-787**, July 1995.
12. Lisa K. Roach, Ronald A. Bowers and James N. Walbert, *Ballistic Vulnerability Pre-Shot Predictions of the Hydraulic Systems of the AH-64D Modernized Apache (LONGBOW APACHE)*, **Draft in Publication**.
13. James E. Hunt, *An Indirect-Fire MUVES Approximation Method*, **Proceedings of the 6th Annual Combat Vehicle Survivability Symposium**, held in Monterey, CA, 28-30 March 1995; also available on the World Wide Web at the site <http://web.arl.mil/~jehunt/safe.html>.
14. V. P. Alekseevskii, *Penetration of a Rod into a Target at High Velocity*, **Fizika Goreniya i Vzryva**, Vol. 2, No. 2, pp 99-106, 1966. (Translated in **Combustion, Explosion and Shock Waves**, pp 63-66, 1966.)
15. A. Tate, *A Theory for the Deceleration of Long Rods After Impact*, **J. Mech. Phys. Solids**, Vol. 15, pp 387-399, 1967 and *Further Results in the Theory of Long Rod Penetration*, **J. Mech. Phys. Solids**, Vol. 17, pp 141-150, 1969.

UNCLASSIFIED

16. Richard Saucier, Robert Shnidman and Joseph C. Collins III, *A Stochastic Behind-Armor Debris Model*, **15th International Symposium on Ballistics**, held in Jerusalem, Israel, 21-24 May, 1995.
17. A. Tate, *A simple estimate of the minimum target obliquity required for the ricochet of a high speed long rod projectile*, **J. Phys. D: Appl. Phys.**, Vol. 12, pp 1825-1829, 1979.
18. R. F. Recht and T. W. Ipson, *The Dynamics of Terminal Ballistics*, **Denver Research Institute**, University of Denver, 1962; also, R. F. Recht, T. W. Ipson and E. P. Wittrock, *Transformation of Terminal Ballistic Threat Definitions into Vital Component Malfunction Predictions*, **Naval Weapons Center NWC TP 4871**, China Lake, CA, 1969.
19. William Kokinakis and J. Sperrazza, *Criteria for Incapacitating Soldiers with Fragments and Flechettes*, **Ballistic Research Laboratory BRL Report No. 1269**, January 1965.
20. Richard Saucier and Ada W. D. Gilman, *The Concept of Ballistic Dose and Its Use as a Predictor of Personnel Incapacitation and Survivability*, In Publication.
21. Richard Saucier and Howard M. Kash III, *ComputerMan Model Description*, **Army Research Laboratory ARL-TR-500**, August 1994. Also see the World Wide Web site <http://web.arl.mil/software/ComputerMan/index.html>.
22. William E. Baker and David W. Webb, *Applying Statistical Tests to Examine Consistency Between Abrams Live-Fire Data and SQuASH Simulation Output (U)*, **Ballistic Research Laboratory BRL-TR-3109 (SECRET)**, June 1990.
23. Lawrence D. Losie, *Examination of the Distribution of the Number of Component-Damage States*, **Ballistic Research Laboratory White Paper**, October 1991.
24. William E. Baker, David W. Webb, and Lawrence D. Losie, *Sampling Problems Pertaining to the Number of Replications for the Stochastic Simulation Models*, Army Research Office Report 93-2, **Proceedings of the Thirty-Eighth Conference on the Design of Experiments in Army Research, Development and Testing**, sponsored by the Army Research Office, 28-30 October 1992.

UNCLASSIFIED

## UNCLASSIFIED

### EVALUATION OF A FULL-SCALE ARMORED MULTILAYERED HULL-TURRET ASSEMBLY USING MODAL ANALYSIS

Aaron D. Gupta  
U.S. Army Research Laboratory  
Aberdeen Proving Ground, Maryland 21005-5066

#### ABSTRACT

In this paper a 3-D finite element (FE) model of an armored multilayered hull-turret assembly of the Armored Gun System (AGS) has been generated using a stepwise approach in which large components such as the Level 1 armored hull and turret models were independently developed in PATRAN3 and assembled using rigidlink elements in ADINA nonlinear dynamic FE code. A rigid block representing the engine and transmission assembly was attached to the rear of the hull, and a 105-mm tapered gun barrel was connected to the turret model. Comparison of the computational model with the experimental hull assembly indicated several component masses such as gun trunnions, rollers, sprockets, and idler wheels which were difficult to explicitly include in the computational assembly model. These components were included as concentrated masses attached to specific sets of nodes in the hull corresponding to the actual locations of these components. Addition of these masses resulted in improved correlation between computational and experimental modal analyses.

#### INTRODUCTION

Light combat vehicles and armored personnel carriers are being deployed in an increasingly important support role for both troops and other more heavily armored combat vehicles. As such, they are facing a higher risk of being subjected to severe battlefield environment. The analysis of the dynamic response of complex lightweight systems involving structural assemblies has become a subject of considerable research because of its practical significance in the evaluation of structural integrity [1-4] of fully assembled vehicles. The behavior of lightweight combat vehicle hull assemblies are of particular interest to the Army because of the need to ensure overall survivability and minimize degradation of performance of the entire vehicle.

Accuracy of prediction of dynamic response of an armored vehicle is directly dependent upon how well the model represents the actual experimental vehicle. Without being overburdened by nonessential detailed features of the vehicle, the model should attempt to capture the major characteristics of the vehicle assembly in an explicit manner. Improvement in modeling and prediction could then be achieved through grid refinement and incorporation of missing components with substantial masses through the addition of representative rigid blocks or concentrated nodal masses in selected regions approximating the location of such masses in the experimental vehicle. The current effort involves generation of three major component models of an armored vehicle; i.e., the hull, the turret, and the gun which were assembled together in PATRAN3 [5] pre- and post-processor code to generate the full-scale vehicle assembly. The

UNCLASSIFIED



assembled finite element model was used to simulate free vibrational response for the lowest 40 eigenfrequencies to facilitate comparison with experiments.

### PROBLEM CONFIGURATION

The particular vehicle selected for this simulation is the Level 1 armored hull-turret configuration of the Armored Gun System (AGS) vehicle assembly. This vehicle has multimaterial multilayered composite construction for both hull and turret. Overall specifications and geometric description of these two subassemblies were obtained from the United Defense Corporation master diagrams of the weldment construction. Overall length, width, and height of the assembled vehicle are 6.1 m, 2.69 m, and 2.55 m, respectively, while height of the hull alone is 1.77 m above the ground level. Level 1 combat weight of the vehicle is approximately 18,000 kg. Since the objective was to compare modal responses with those from the experimental hull-turret assembly, all extraneous components that are difficult to model explicitly such as tracks, wheels, track covers, sprockets, idlers, suspensions, and torsion bars and detailed internal equipments were excluded from the current model. An isometric frontal view of the fully assembled vehicle is shown in Figure 1.

### BASIC ASSUMPTIONS

The engine and transmission assembly contained substantial mass and remained attached to the rear of the vehicle during experiment. Although explicit modeling of these components was avoided as being too cumbersome, the influence of these masses on the overall response could not be ignored. As a result the total mass of the assembly was included as a rigid block of equivalent mass attached to the rear hull at four points using rigidlink elements in the ADINA [6] finite element analysis code. Only linear elastic isotropic homogeneous material properties were used during this study since the modal analysis was performed in the strictly linear elastic regime.

The computational model was unrestrained because this condition best approximated the experimental configuration where the vehicle assembly was mounted on inflatable rubber cushions laterally at the base. Hence, the computational model would result in generation of six rigid body modes with nearly zero frequencies initially, followed by the flexible modes which are of primary interest.

All hatches, covers, and access doors in the hull as well as in the turret were fully assembled to the mating cutouts in the computational model with the exception of the large circular hole centrally located in the roof plate of the hull to facilitate accommodation of the turret basket and the turret ring assembly. The hatches were included in the experimental assembly as reasonably tight-fitting elements. However, due to lack of data on spring stiffnesses and damping coefficients of the experimental attachments, we decided to rigidly attach these components as integral parts of the hull and turret structures during computational modal analysis.

### MODEL DESCRIPTION

Three separate models were employed during the course of this investigation. The initial 3-D model of the tight-fitting hull with closed hatches was assumed to have each wall made from a single-layer uniformly thick monolithic basic 5083 aluminum alloy for the hull as well as the turret assembly. The model was extended to include the multimaterial layered armored configuration for both the hull and the turret wall surfaces using the multilayer shell elements capability in the ADINA finite element analysis code. However, in accordance with weldment drawing directives, both bottom floor and horizontal sponsons of the hull were monolithic single-layer aluminum construction. A 105-mm tapered gun tube was subsequently modeled and attached to the turret using constrained rigidlink elements in ADINA to

generate the turret-gun assembly. The hull model was augmented with the addition of a rigid block representing the equivalent masses of the engine and transmission assembly at the rear of the vehicle.

The completed finite element models of the hull and the turret were reconfigured and the elements, nodes, and element groups were renumbered to avoid duplication and consequent deletion of redundant nodes and elements during final assembly. The two reconfigured finite element models were assembled using rigidlink elements in ADINA at the interface between the master hull nodes and the slave turret ring nodes to represent the full-scale vehicle assembly without tracks and rollers. The final configuration included the engine-transmission assembly modeled as an equivalent mass rigid block positioned above the bottom floor at the rear of the armored hull and connected to floor nodes with four rigidlink elements corresponding to locations of suspension points for engine mounts. Sufficient clearance between the front lower glacis and the rigid block was allowed to enable the block to vibrate freely without inadvertent load transfer due to contact or interference. Additionally, the cannon was modeled as a tapered cantilevered cylindrical tube section assembled to the frontal mating region of the turret assembly. The combined weight of these two components and supporting masses is approximately 4,500 kg, which could have substantial influence on the vibrational response of the vehicle assembly. All internal components with nonlinear attachments and small masses relative to the gross weight of the vehicle assembly were omitted from this simplified model to avoid generation of spurious local modes and unnecessary complexities. An isometric view of the undeformed finite element model of the hull-turret assembly is shown in Figure 2.

#### MATERIAL PROPERTIES AND THICKNESSES

The basic construction material for both hull and turret is 5083 aluminum with isotropic elastic material properties given as: Young's modulus = 68,950 Mpa, Poisson's ratio = .336, and mass density = 2.66 g/cm<sup>3</sup>. Thickness of plates varied from one section to another; e.g., 1.27 cm for the vertical sponsons, the bottom floor plate, and the horizontal sponsons, while the sidewalls and the front lower glacis are fabricated from 1.6-cm and 2.54-cm-thick plates, respectively. Additionally, in the Level 1 configuration, with the exception of the floor and the horizontal sponsons, a multimaterial multilayered design was used for all other walls for both the hull and the turret, utilizing varying thicknesses of steel, titanium, Kevlar, and silicon carbide (SiC) ceramic materials; isotropic homogeneous linear elastic properties of which are listed below:

##### Steel

Young's modulus = 206,840 Mpa, Poisson's ratio = .292  
Mass density = 7.833 g/cm<sup>3</sup>.

##### Kevlar

Young's modulus = 124,100 Mpa, Poisson's ratio = .300  
Mass density = 1.439 g/cm<sup>3</sup>.

##### Titanium

Young's modulus = 110,300 Mpa, Poisson's ratio = .300  
Mass density = 4.429 g/cm<sup>3</sup>.

##### SiC

Young's modulus = 437,800 Mpa, Poisson's ratio = .300  
Mass density = 3.488 g/cm<sup>3</sup>.

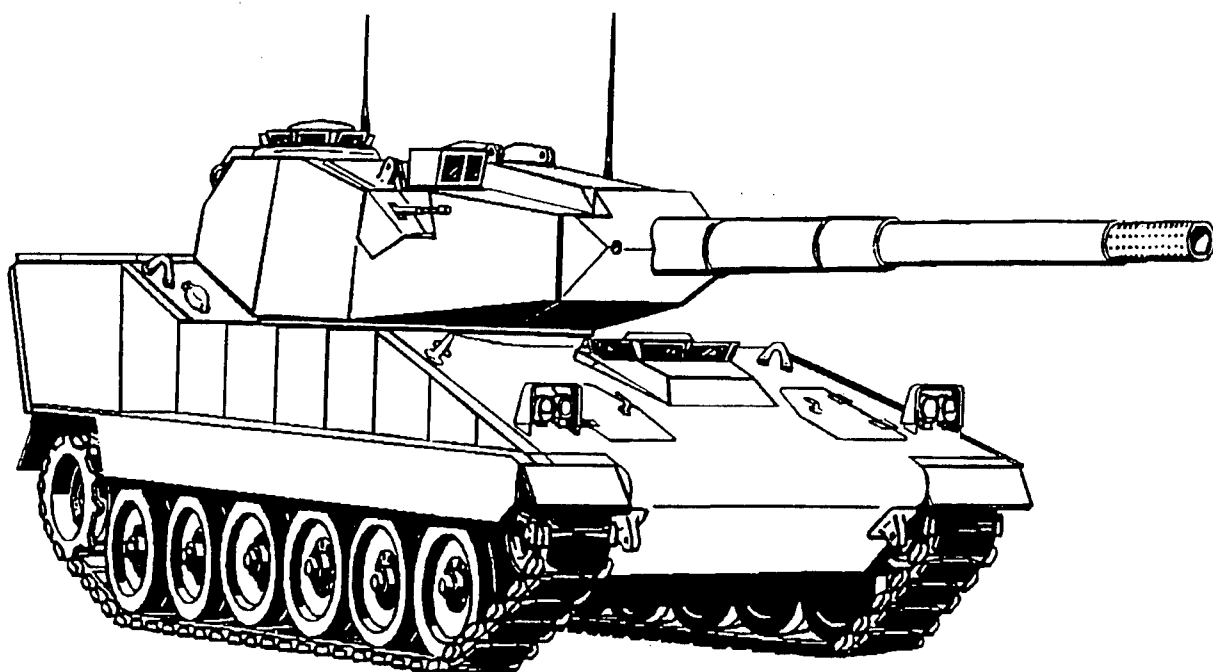


Figure 1. A pictorial view of the AGS.

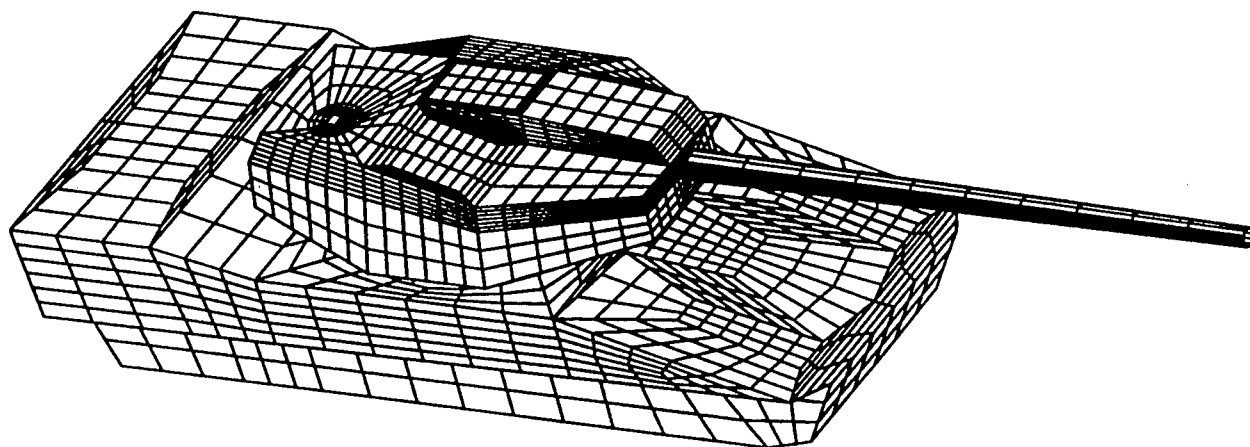


Figure 2. A fully assembled finite element model of the AGS.

The 105-mm gun tube has a constant inner bore and a tapered outer diameter and is made from AISI 4340 gun steel. Monolithic quad four-noded shell elements with varying thicknesses were used to model the gun barrel.

### NUMERICAL MODAL ANALYSIS

Fundamental frequency of vibration in bending or torsional mode for an undamped single degree-of-freedom system is given in closed form as:

$$f = [1/(2\pi)]\sqrt{k/m}$$

where  $f$  represents fundamental frequency of vibration and  $k$  and  $m$  are bending or torsional stiffness and mass of the system, respectively. Time period of oscillation is reciprocal of natural frequency. For a complex system such as the AGS assembly with approximately 12,000 degrees of freedom, simulation of 3-D oscillatory response of the entire system is rather complex, necessitating numerical analysis using a transient finite element code such as ADINA.

The finite element model of the AGS hull-turret assembly was represented by 2142 four-noded quad shell elements and 2,221 nodes subdivided into 35 element groups based on material properties and thicknesses of various wall surfaces. Addition of the engine block and the cannon increased the total number of shell elements to 2,409 corresponding to 2,499 nodes and 38 element groups. The updated model was run as a linear dynamic model using the ADINA finite element code to generate the first 40 modes of vibration and the corresponding modeshapes for each eigenfrequency. The frequencies solution employed lumped mass formulation and the subspace iteration method in ADINA. A minimum of 50 iterations was necessary to assure convergence of the first 40 natural frequencies. The magnification factor selected for modeshape deformation plots was 5.0. However, due to space limitation, detailed isometric top and bottom views of deformation modeshapes were omitted. Isometric frontal and bottom views for a typical deformed modeshape of the multilayered hull-turret-gun assembly are shown in Figures 3 and 4, respectively.

### RESULTS AND DISCUSSIONS

Comparison of modeshapes and frequencies between the basic monolithic and the multilayer shell models indicates noticeable increase in stiffness-to-mass ratio for the Level 1 layered structure, resulting in a 15-20% gain in magnitude of the fundamental and subsequent frequencies at higher modes for the AGS. All fitted hatches and covers rigidly connected to the structure appear to have minimal influence on modal response due to minimal change in stiffness-to-mass ratio. However, this may not be the case for loosely fitted hatches, where local modes of vibration can have considerable influence on the eigenfrequencies of the experimental vehicle.

During the stepped computational modal analysis approach where responses were computed at each stage of the assembly process, simulation of a massive turret as an equivalent rigid mass attached to the top of the hull appeared to be futile due to minimal change in stiffness-to-mass ratio. This necessitated detailed modeling of the turret, including the turret basket and turret ring as well as the 105-mm gun to facilitate step-by-step assemblage with the hull, resulting in a realistic model of the hull-turret-gun assembly.

The eigenfrequencies of the fully assembled configuration were substantially lower than those for either the hull or the turret and were closely spaced due to increased mass, resulting in a lower stiffness-to-mass ratio. Comparison of these eigenfrequencies and modeshapes with those from the experimental

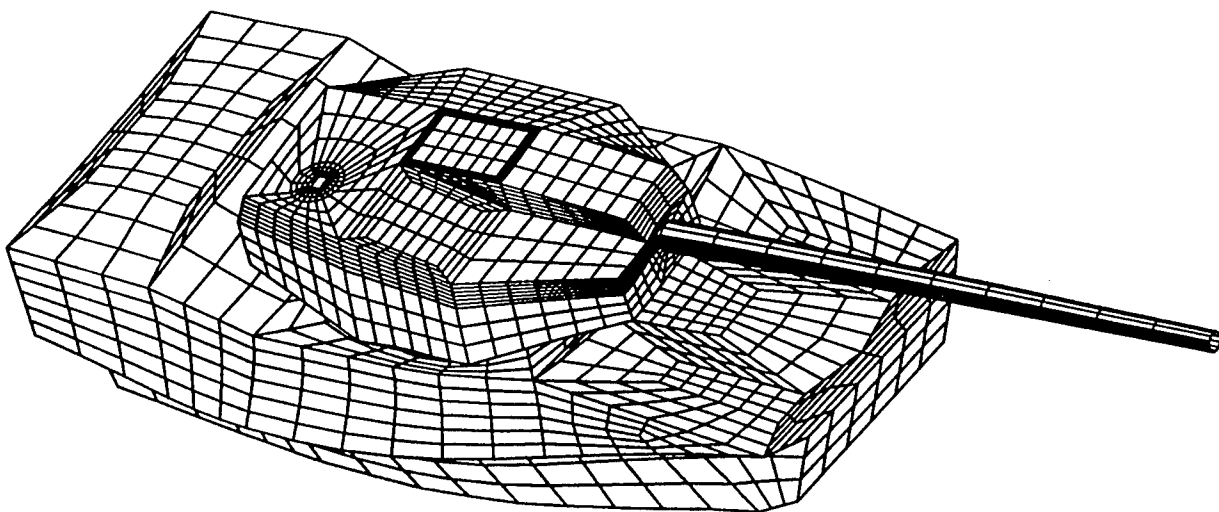


Figure 3. Isometric frontal view of a typical deformed modeshape of the AGS.

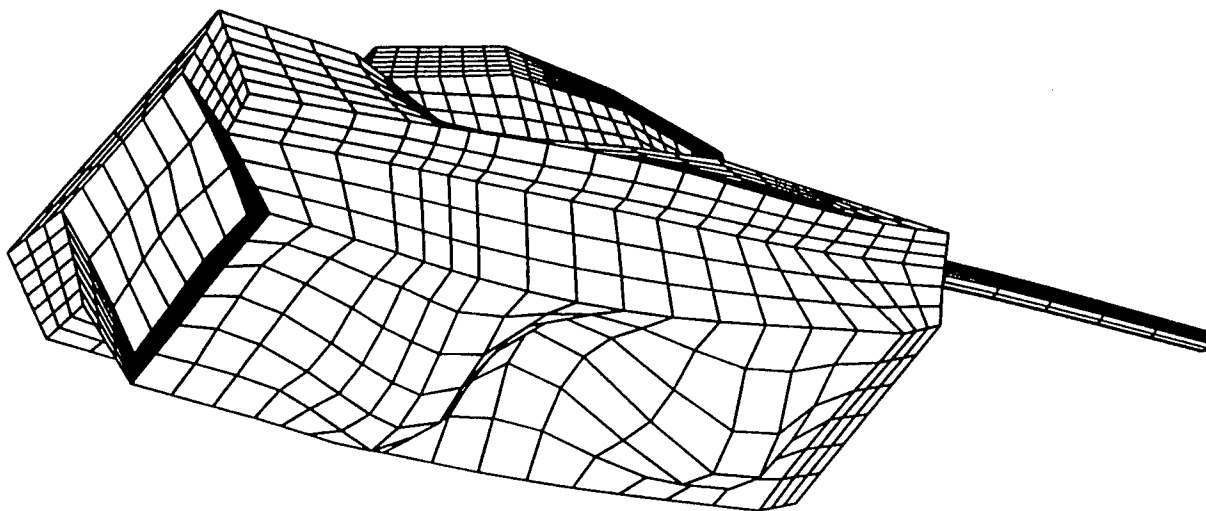


Figure 4. Isometric bottom view of a typical deformed modeshape of the AGS.

modal analysis indicated rather poor agreement at all modes since the computational eigenfrequencies were substantially higher than experimental values. A realistic assessment of the computational model and the experimental hull-turret assembly indicated several component masses which were not accounted for and proved to be rather difficult to include explicitly in the computational model due to additional complexity and modeling constraints. Combined effect of these masses on overall response was substantial and could not be ignored. Some of these missing masses were found to be inner and outer idler wheels and pivots, track adjusters, roadwheels, suspension support assemblies, shock absorbers, drive sprockets, guards, sprocket carrier and guide, torsion bars, anchors, autoloader assembly, gun breech mechanism assembly, trunnions, cradle assembly, left and right rails, yoke and adapter, recoil brake, recuperator, etc.

An implicit modeling approach with respect to missing component masses was adopted, using concentrated masses attached to corresponding nodes and uniformly distributed in the associated area in which these components are actually attached to the hull-turret assembly. Distribution of these masses can significantly influence the mass matrix, while the stiffness matrix remains relatively unaffected. Significant improvement in correlation between computational and experimental analyses may be feasible through careful modification of the mass matrix in the finite element model. Table I compares eigenfrequencies between the analysis and the experiment for the lowest 30 modes.

A reasonable comparison of computational and experimental modal analyses requires comparison of both modeshapes and eigenfrequencies, since addition of component masses can significantly alter both results. A careful comparison of both computational and experimental modeshapes at the fundamental frequency indicate satisfactory agreement in both modeshapes governed by the cantilever bending deformation mode of the gun barrel and corresponding frequencies. The next two computed frequencies are also influenced by gun vibrational modes which do not agree with the experiment. This vibrational mode is dominated by the commander hatch vibration at these frequencies. It appears that the hatch did not remain tightly fitted to the vehicle during the experiment, causing local hatch opening modes of vibration to be dominant and be picked up by the sensors. This is in sharp contrast to the computational model where all hatches were rigidly attached to the vehicle and local nonlinear hatch cover oscillations were insignificant. If these nonlinear oscillations could be filtered from the experimental data, correlation could be improved. The rigid link attachment of the gun barrel to the turret in the computational model differed sufficiently from the attachment mechanism of the gun to the turret of the experimental vehicle, which can account for variation in modal responses in the low-frequency regime.

At higher order modes, qualitative correlation of modeshapes between computation and experiment for sidewalls, bottom floor, rear door, and roof bending vibration, in addition to cantilever beam bending mode of oscillation of the gun barrel, could be achieved. At higher modes, some of the experimental frequencies were too closely spaced together, resulting in increased modal density which was probably caused by nonlinear oscillation modes of complex structural components. These multiple frequencies could not be accurately predicted by the simplified computational model. To facilitate a reasonable comparison between the computational and experimental modal analyses, these densely packed experimental eigenfrequencies have been lumped together as single modes. Higher order modes with eigenfrequencies in excess of 85 Hz were ignored since the experimental data were deemed to be unreliable beyond this range for effective comparative evaluation.

Cantilever beam bending type oscillation of the cannon at the fundamental frequency followed by sidewall, bottom floor, rear door, and roof vibrations at subsequent higher order modes and the frequency range predicted by the computational model were made available prior to the experiment to facilitate instrumentation of the vehicle assembly. Due to economic constraints, the experiment was conducted only once, using the fully assembled vehicle in Level 1 armored configuration instead of a logical stepped approach using three distinct configurations, i.e., stripped, tightly-fitted, and fully armored configurations. As a result, experimental identification of the influence of component masses on overall response and

Table I: Comparison of eigenfrequencies between computational analysis and experiment

Freq. No	Computation	Experiment
1	7.83e+00	7.92e+00
2	9.76/10.36	
3		1.45e+01
4	1.62e+01	1.61e+01
5	1.92e+01	1.97e+01
6		21.73/22.59
7	2.51e+01	2.49e+01
8		26.21/26.94
9	2.78e+01	2.79e+01
10		28.65/28.75
11		32.04/32.93
12	3.37e+01	33.09/33.47
13	3.50e+01	36.28/36.88
14	3.97e+01	3.86e+01
15	4.03e+01	4.06e+01
16	4.28e+01	4.21e+01
17		44.9/45.296
18	4.79e+01	47.23/48.25
19	4.98e+01	48.94/49.08
20		50.64/51.17
21	53.35/54.49	5.48e+01
22	5.81e+01	57.89/58.32
23	5.97e+01	59.26/59.43
24	6.01e+01	60.4/60.5
25		61.17/61.36
26	6.46e+01	63.23/64.31
27	6.83e+01	6.75e+01
28	7.31e+00	7.39e+01
29	79.37/80.27	8.06e+01
30	8.62e+01	8.52e+01

isolation or reduction of nonlinear effects due to local oscillation modes of fitted hatch covers could not be feasible.

In spite of several simplifying assumptions during generation and analysis of the computational model, it has been demonstrated that modeling and response analysis of 3-D fully assembled armored vehicles through a stepped finite element approach involving generation and linking of substructures and subassemblies and validation with experiments at each critical stage of assembly, leading to the fully assembled configuration, is a viable method at a low-frequency regime within limited time and budget constraints for most modern complex state-of-the-art vehicular structures. In addition to aiding the experimentalist in instrumentation such as gage and exciter locations for effective comparison, valuable insight can be obtained into the influence of subassemblies upon each other at different stages of

construction and on the overall response of the fully assembled vehicle. Major component masses included in the experiment must be accounted for in the computational model before any effective comparison could be made. Future work may involve realistic modeling of suspension systems and nonrigid linkage of subassemblies, as well as improving correlation between analysis and experiment using mass matrix modification methods based on better redistribution of component masses, while keeping the overall mass constant. Once the computational model is validated, realistic forcing functions from coupled distributed blast and concentrated impact loads generated by target-weapon interaction can be imposed in specific regions of the assembled model and nonlinear transient response, and occurrence of failure at critical locations could be predicted to aid in damage assessment and reinforcement of vulnerable sections from a structural integrity and vehicle survivability improvement standpoint.

#### REFERENCES

1. A. D. Gupta, H. L. Wisniewski, and R. L. Bitting, "Response of a Generic Vehicle Floor Model to Triangular Overpressure Loads," Computers and Structures, Vol. 32, No. 3/4, pp. 527-536, Elsevier Science Ltd., U.K, 1989.
2. A. D. Gupta, J. M. Santiago, and C. Meyer, "Comparison of Computational and Experimental Modal Analyses of an Armored Vehicle Hull with Multiple Access Openings," Computers and Structures, Vol. 62, No. 5-6, Elsevier Science Ltd., U.K, June 1995.
3. A. D. Gupta, "Evaluation of a Composite Armored Vehicle Hull Using Modal Analysis," Proceedings of the 3rd ADPA Ballistics Symposium on Classified and Controlled Topics, Johns Hopkins University, Applied Physics Laboratory, Laurel, MD, November 1995.
4. A. D. Gupta, "3-D Finite Element Modeling and Analysis of an Armored Vehicle Hull with Multiple Access Openings," Proceedings of the Sixth Annual TARDEC Combat Vehicle Survivability Symposium, Vol. 1, pp. 479-487, U.S. Naval Postgraduate School, Monterey, CA, 28-30 March 1995.
5. PATRAN 3 Users' Guide, PDA Engineering Inc., Costa Mesa, CA, 1993.
6. "ADINA—A Finite Element Program for Automatic Dynamic Incremental Nonlinear Analysis," ADINA Users' Manual, ARD 90-1, ADINA R & D Inc., Watertown, MA, September 1990.

#### ACKNOWLEDGMENTS

Experimental modal analysis results were provided by Morris Berman and Ami Frydman, Mechanics and Structures Branch, Adelphi site, U.S. Army Research Laboratory (ARL). Valuable assistance of Dr. A. Dietrich, Chief, Target Interaction Branch; C. Meyer, GWU-COL Student Apprentice in ARL; and Dan Blankenblair, CSTA, Aberdeen Proving Ground, MD during the course of this investigation is gratefully acknowledged.



**UNCLASSIFIED**

THIS PAGE INTENTIONALLY LEFT BLANK

**UNCLASSIFIED**

# THE DETERMINATION OF SHOCK LOADS ON ARMORED VEHICLES DURING THREAT ENGAGEMENT

Neil M. Gniazdowski and Frederick H. Gregory

U.S. Army Research Laboratory  
Weapons Technology Directorate  
Aberdeen Proving Ground, Maryland 21005

## ABSTRACT

This paper describes a number of analyses and experimental programs that are aimed at providing shock loading data for ballistic impacts and blast producing munitions on combat vehicles. This information is needed to perform shock vulnerability analyses for vehicle design and for Live Fire Test predictions. Descriptions of models and experiments used to develop shock loading functions for shaped charge jets, mine blast, artillery weapons, and kinetic energy projectiles are included herein.

## INTRODUCTION

In testing conducted under the aegis of the Army Live Fire Test Program, component damage has been observed in combat vehicles, in which the components were off-the-line of fire. The damage occurring in these instances was caused by the shock propagated from the site of the impact or blast location through the vehicle hull to a remote location where shock sensitive equipment or devices were mounted. In most cases, sensitive equipment can be shock mounted to provide an increased envelope of operability in shock environments. However, there are some components such as sights, resolvers, and gyroscopes that need to be hard mounted for reasons related to their function. Particular attention must be paid to the mounting and construction of these and certain other equipment (as well as shock mounted components) in combat vehicles in order that they be capable of operating in harsh shock environments.

An effort to predict the vulnerability of components to ballistic shock can logically be divided into several phases. These are (a) determination of loading functions for the various threat munitions and encounter scenarios, (b) structural characterization of the vehicle hull, armor components, and major subassemblies, (c) construction of a mathematical model for the propagation of the shock, (d) determination of failure criteria for components and structural elements, and (e) melding the four forgoing subtasks into an analysis that is capable of

Distribution is limited to U.S. Government agencies and their contractors; Critical Technology; 15 February 1996. Other requests for this document shall be referred to the Directorate Executive, U.S. Army Research Laboratory, WTD, AMSRL-WT, Aberdeen Proving Ground, MD 21005-5066.

predicting failures for components based on independent information on the shock hardness of various components.

Shock loading definition has been accomplished for four different threat/target combinations and two more are near completion. These shock loads have been determined by combined numerical and experimental techniques. The threats include mine blast, artillery attack, a kinetic energy projectile impact, combined HE/KE impact, and two different shaped charge attacks on reactive armor for light weight vehicles. The load definitions consist of force, surface acceleration and velocity histories, and shock response spectra (equivalent static acceleration vs. frequency).

## TYPE OF MODELS AND EXPERIMENTS AND THEIR RESULTS

Hydrocode calculations were performed for mine blast, artillery attack, kinetic energy projectile impact, and combined HE/KE impacts; whereas, experiments were conducted for the shaped charge attacks. The hydrocode used was an ARL modified version of DYNA3D<sup>1</sup>.

Figure 1 shows an 8,064 element finite element model of a light vehicle floor being subjected to a blast from an antipersonnel mine. A three-dimensional model was used in this calculation because the mine was located off center of the longitudinal axis of the vehicle. The blast loading was applied by a CONWEP<sup>2</sup> module which was incorporated as a subroutine in DYNA3D. In this model, the floor structure was characterized by a Johnson-Cook<sup>3</sup> material model and a Gruneisen equation of state. Figure 2 shows the resulting shock response spectrum of four points at increments of 13.6 cm away from the line of fire. The order of the nodes closest to the line of fire (LOF) to the furthest is wb9827, wb9841, wb9855, and wb9869. It can be seen that the response at each node has very high shock amplitudes below 3 kHz and that the shock decreases slightly above 3 kHz. The response at all four nodes would cause catastrophic damage to components mounted on the floor at these locations. The further away a node is from the LOF, the smaller its response is, as was expected.



**Figure 1.** Deformed Mesh Showing Penetration of Vehicle Floor by Mine Blast

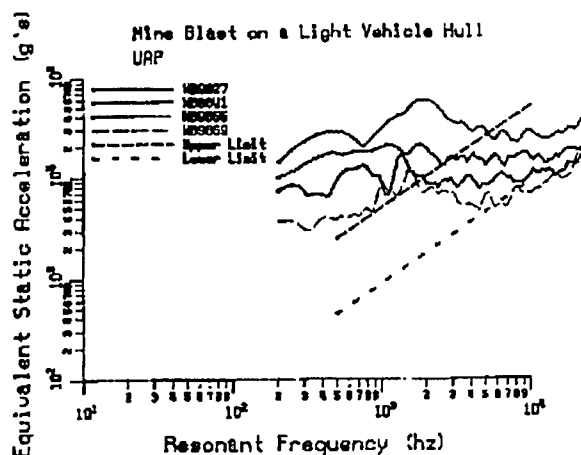


**Figure 2.** SRS of 4 Nodes on Floor Plate as a Result of Mine Detonation



Figure 3. 2-D Finite Element Model of Circular Plate being Impacted by FSP

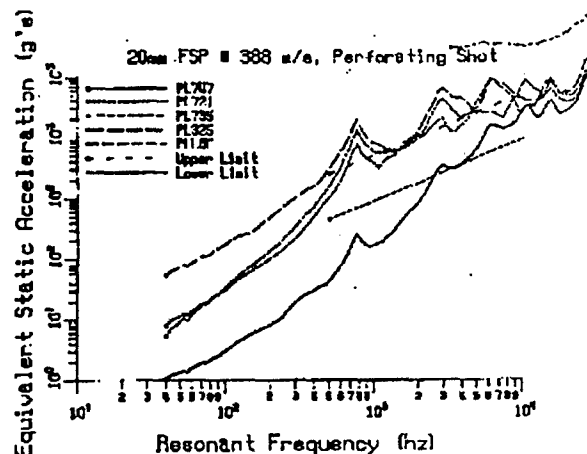


Figure 4. SRS of 4 Nodes at Spatial Increments of 4.4 cm from FSP Impact on Circular Plate

To simulate the impact of artillery fragments on the vehicle hull plates, a 20 mm Fragment Simulator Projectile (FSP) was used in a DYNA2D<sup>4</sup> calculation. Figure 3 shows an 840 element, two-dimensional finite element model of a circular plate being impacted by such a FSP. Circular plates of various sizes were used to approximate various size plates of an armored vehicle's hull. The velocity of the 20 mm FSP was adjusted to represent different size fragments of the artillery round. An elastic-plastic bi-linear stress strain model with

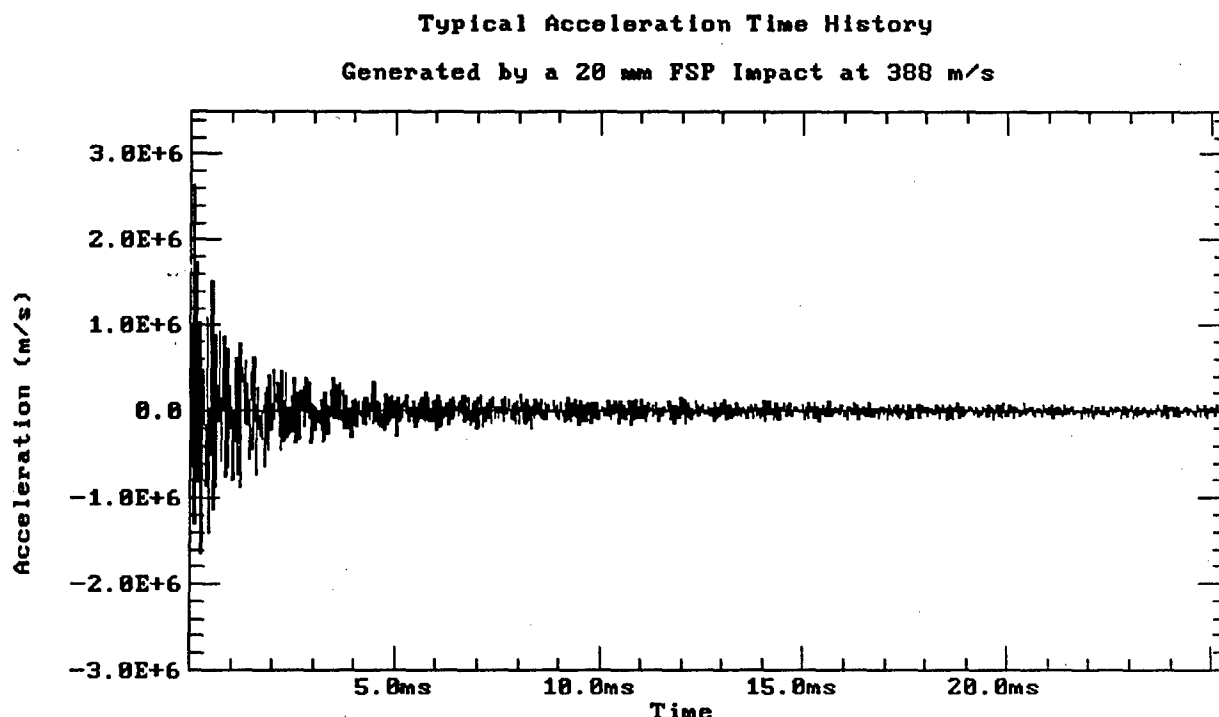


Figure 5. Typical Acceleration-Time History for Surface Node on Plate Impacted by FSP

failure was used in this simulation. Figure 4 shows the shock response spectrum of four points that are not uniformly spaced, but are at slightly different increments (of about 4.4 cm) away from the LOF. The nodes in order from closest to the LOF to furthest away are: PL325, PL721, PL735, and PL747. In this Figure, below 3 kHz the SRS are of the same shape, but the amplitude of their responses is shifted. It should be noted that this shift is not constant throughout the 0 to 3 kHz band. Above 3 kHz, the SRS overlap and the differences in amplitude of the responses at the nodes are less than those below 3 kHz. The large differences in amplitude below 1 kHz are due to the effects of the boundary conditions used in this model. This is also seen in experiments. Figure 5 shows a typical acceleration time history at one node in the model.

Figure 6 shows a 46,524 element model of an HE/KE impact on a multilayered armor package. Results from this model are still being processed and were not available at the time this report was written. A three-dimensional model was constructed because of the fact that the bullet impact is oblique in two planes.

Two experiments simulating shaped charge attacks on reactive armor were conducted. Two reactive armor configurations were tested, one a front glacis design, and the other was a side chassis design. Figure 7 shows the test fixture used for both tests. At the time of this report, only the data from the front glacis experiment was available.

Figure 8 shows the experimental setup for the front glacis reactive armor test. A wedge like fixture is used to simulate a portion of the front glacis of a light armored vehicle and allows measurement of the impact force on the shot line axis. This set up is also used to

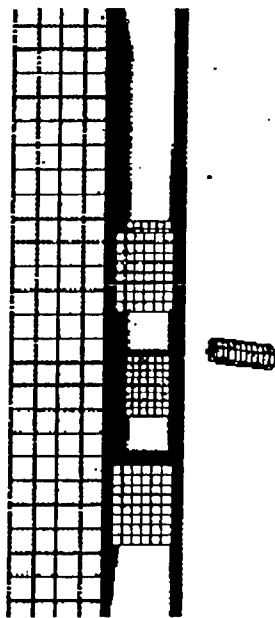


**Figure 6.** Finite Element Model of HE/KE Projectile Impact on a Multilayered Armor Package

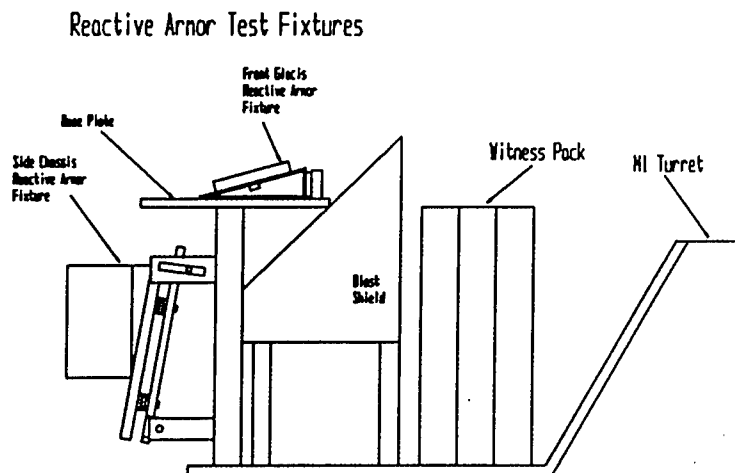


**Figure 7.** Fixture Used for SC Experiments to Measure Shock with Reactive Armor Packages

Front Glacis Reactive Armor Experiment

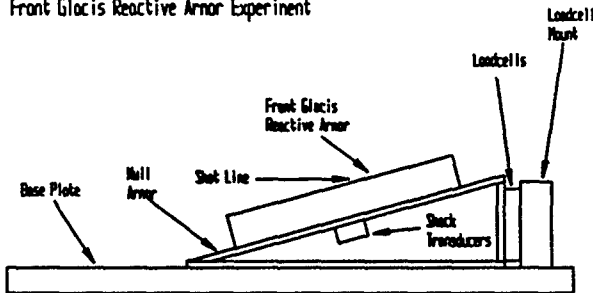


Figure 8. Setup for Front Glacis Reactive Armor Experiment Showing Instrumentation

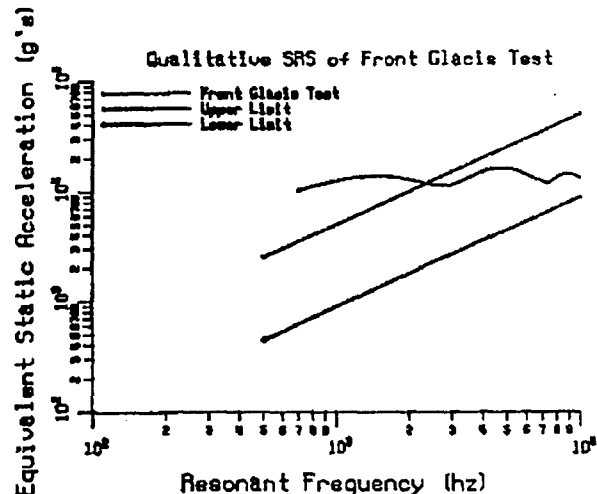
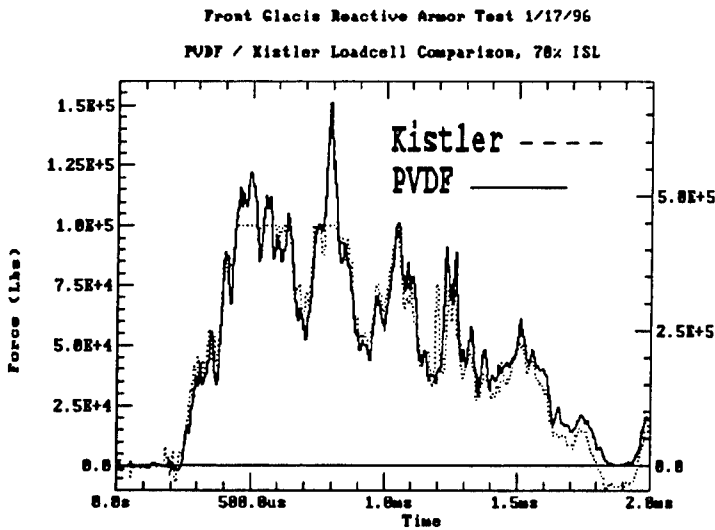


Figure 9. Qualitative SRS for Front Glacis SC Experiment Based on Part of BOBKAT Accelerometer Data

minimize off axis loading of the force transducers. Quartz and Polyvinylidene Fluoride (PVDF) loadcells were used to obtain force measurements. A Combat Systems Test Activity (CSTA) Type A velocity gauge, piezoresistive accelerometer mounted in a BOBKAT shock mount, and a piezoresistive accelerometer mounted in a Low-Frequency Foam Isolation (LOFFI) mount were used to obtain shock response spectrum data. Unfortunately, the shock levels experienced during the test far exceeded the expected values, so most of the gauge records were clipped. However, a portion of the BOBKAT's time history was used to generate a minimum qualitative shock spectrum as shown in Figure 9. Also, the load experienced by the loadcells was higher than expected. The quartz loadcell reading was clipped above the linear range of the transducer. The PVDF loadcell was able to capture the maximum load due to its higher measuring range. A comparison plot between the two loadcells out to a time of 2 ms is shown in Figure 10. The agreement between the two loadcells was excellent. Two different types of loadcells are used in series to lend confidence to the measurements obtained. This technique has proven reliable in past work with large frontal reactive armor boxes for main battle tanks<sup>5,6</sup>. Multiple transducers were also used to measure the shock environment of the front glacis plate. Reference 6 gives a more detailed description of the principles involved in obtaining reliable force and shock measurements. It is hoped that dynamic force loading data from both the front glacis and side chassis reactive armor tests and the tests discussed in References 5 and 6 can be used to develop "generic" loading functions for shaped charge / reactive armor interactions.

## LIMITATIONS OF MODELS AND EXPERIMENTS

The two biggest sources of error in our computational models are the choice of boundary conditions and material properties. The response at the "gauge" location is independent of the boundary conditions up until the shortest time that the shock (usually the longitudinal component) makes the transit from the excitation point to boundary and then back to the "gauge" location. During this period the response of the model is not affected by



**Figure 10.** Comparison of Loadcell Force vs. Time Records for Front Glacis SC Impact on RA Package

conditons selected. A more satisfying solution is to model a significantly larger part of the target geometry and compare the solution for the more geometrically complex model with the "smaller" model using several different boundary conditions in the smaller model. This would lend some credence to the boundary conditions selected in the smaller model. However, the larger model may lose some fidelity if joints and materials interfaces are not represented properly.

Parametric studies of response versus material properties can also be performed to assess the band width of loading values attributable to materials representations. One must select not only the materials constitutive model and equation of state models, but also the parameters that go into those models. These choices are typically influenced by computer run times and computer resources available.

The primary sources of error in experimental tests can be attributed to two sources. The first occurs when the mounting hardware used in a test does not mimic fielded conditions. The second occurs when the transducer is large enough that it affects the response of the system to which it is attached. To overcome these errors, actual mounting hardware used on prototype vehicles was used in the reactive armor experiments. As far as the physical size of the load transducers is concerned, they were selected not only for their measuring capabilities but also for their similarity in size and shape with spacers used on the prototype vehicle. By insuring that the ballast mass used to restrict the motion of the test fixture is close to the same mass as the intended target vehicle, one can properly account for inertial effects. In the case of the front glacis reactive armor fixture, the hull plate on which the reactive armor box lies was the same thickness as the hull of the vehicle. The size of the hull plate was made large enough so that it should allow similar flexing as the front glacis of the vehicle. Exact conditions cannot be matched totally with this type of setup but reasonably approximate results can be derived. By closely matching the size of loadcells with spacers used in the prototype vehicles armor package, the response of the armor system should not be greatly

the boundary condition imposed by the modeler. When the computational loading model consists of only a plate or structural section, which is actually a part of a complete assembly, such as a combat vehicle, then the signal received at the "gauge" location is affected by the actual boundary condition used after this round trip shock transit time. In order to gauge the magnitude of the effect of the boundary conditions on the late time shock response, we have chosen several different boundary conditions to determine the range of values of the load function as affected by various boundary

affected.

## GENERIC LOAD FUNCTIONS

To be able to characterize a certain class of threat / armor interaction with a generic, empirical load function would be an ideal outcome of this work. However, the variety of armor materials that are being used in modern armored vehicles makes this a difficult task that may require a large amount of modeling or experiments. Typically the same class of threat may be used in a variety of shotlines in a Live Fire Test. In each of these different shotlines, the same threat may impact totally different armor recipes. Another problem is the uncertainty of the effects of obliquity on loading functions. Very few if any shot lines used in Live Fire Testing impact normal to the target. In order to be able to make a generic load function which accounts for obliquity effects, more basic research and experimental data will be required. By knowing more about the effects of obliquity on loading functions, we will also be able to determine the necessity for large three-dimensional models. Despite the difficulty involved in accounting for numerous parameters affecting shock loading descriptions, a series of first generation guidelines and generic load functions for shape charge jet / reactive armor interactions may be available soon.

## CONCLUSIONS

Computer modeling and experiments can be used to determine the transient loads imposed on armor vehicles during threat engagement. Both modeling and experiments have their sources of error and limitations. The sources of error in experiments and limitations of models can be reduced by making reasonable assumptions and comparing the results of models while varying critical parameters to determine the maximum and minimum values of the loading functions. Reasonably accurate loading and response data can be obtained in experiments by ensuring that attachments mimic that of fielded conditions and by selecting the proper sensors that minimally affect the response of the test fixture.

Generic load functions require some more research, but are not necessarily beyond reach.

## REFERENCES

1. J. O. Hallquist, R. G. Whirley, and B. E. Engelmann, "DYNA3D, A Nonlinear, Explicit, Three-Dimensional Finite Element Code for Solid and Structural Mechanics, User's Manual," Lawrence Livermore National Laboratory, Livermore, CA, November 1993.
2. D. W. Hyde, "User's Guide for Microcomputer Programs CONWEP and FUNPRO, Applications of TM 5-855-1," *Fundamentals of Protective Design for Conventional Weapons*, U.S. Army Corps of Engineers, 20 Massachusetts Ave, NW, Washington, DC 20314-1000.



3. G. R. Johnson and W. H. Cook, "A Constitutive Model and Data for Metals Subjected to Large Strains, High Strain Rates, and High Temperatures," *Proceedings of the Seventh International Symposium on Ballistics*. The Hague, The Netherlands, April 1983.
4. Robert. G. Whirley and Bruce E. Engelmann, "DYNA2D, A Nonlinear, Explicit, Two-Dimensional Finite Element Code for Solid and Structural Mechanics, User's Manual," Lawrence Livermore National Laboratory, Livermore, CA, UCRL-MA-110630, April 1992.
5. John A. Condon, Neil M. Gniazdowski, and Frederick H. Gregory, "Testing and Analysis of Reactive Armor Containment Structures," ARL-TR-444, June 1994 (SECRET).
6. Neil M. Gniazdowski, Frederick H. Gregory, and John A. Condon, "Full Scale Testing of Conceptual Frontal Modular Armor for Future Main Battle Tanks", ARL-TR-987, February 1995 (CONFIDENTIAL).

**UNCLASSIFIED**

**BEHIND THE ARMOR SESSION**

**Ingersoll Auditorium  
Thursday, March 28, 1996**

**Session Chairman: Mr. Mark Ryzyi, Office of the Project Manager, Armored Systems Integration**

**UNCLASSIFIED**

**UNCLASSIFIED**

**THIS PAGE INTENTIONALLY LEFT BLANK**

**UNCLASSIFIED**

# ESTIMATING AMMUNITION AND AMMUNITION COMPARTMENT RESPONSE IN SUPPORT OF SURVIVABILITY ANALYSES

Gould Gibbons Jr., Jerry L. Watson, and Frederick H. Gregory

U.S. Army Research Laboratory  
Weapons Technology Directorate  
Aberdeen Proving Ground, Maryland 21005-5066

## ABSTRACT

With the development of new weapon systems and the increased emphasis on survivability, there is a need for improved techniques that can predict the response of ammunition compartments to external threats. This problem is aggravated by the need to increase the lethality of the ammunition for both new and current weapon systems. Ammunition fratricide, temperature effects, and other storage parameters increase the complexity of things that have to be understood if compartment response is to be predicted. Evaluation of every ammunition compartment issue by performing full-scale tests is cost prohibitive, and other approaches have been sought to minimize test requirements while optimizing predictive capabilities. Recent work directed at this issue has been performed employing small-scale, single-round tests to evaluate ammunition response to varying threat energy and the effect of temperature upon that response. The results are being reported as functional relationships that are applicable to compartment modeling used in assessing system survivability. Characterizing fratricide susceptibility has also been investigated by employing small-scale, two-round tests to evaluate ammunition response to varying threat energy and the effect of temperature upon that response. The results of these evaluations will be presented, and an example of their use in predictive compartment modeling will be demonstrated.

## INTRODUCTION

Historically, all compartmented ammunition response has been treated in the same way, using what has been called, "step functions". Given an overmatch of the compartment armor, there is a certain residual penetration (which may be threat dependent) above which catastrophic kills are assumed to occur, and below which less destructive damage occurs. When evaluating high-

Distribution limited to U.S. Government agencies and their contractors; Critical Technology; 15 February 1996. Other requests for this document shall be referred to the Directorate Executive, U.S. Army Research Laboratory, WTD, AMSRL-WT, Aberdeen Proving Ground, MD 21005-5066.

explosive (HE) warhead response, this technique is somewhat reasonable, in that HE response typically changes abruptly from very mild reactions to detonation. However, gun propellant does not usually demonstrate this type of threshold response (solid gun propellant will be the only propellant discussed in this paper). Propellant response, though quite varied, is more uniform, progressing in a steady, consistent fashion from mild deflagration to very violent events as the stimulus increases.

Modern solid propellants, some containing significant quantities of HE, are usually multibase materials and can be unpredictable in response to threat stimulus. This paper will discuss work completed to characterize the response of a single base (M1), a triple base (M30), and a nitramine base material (M43) at 75° F and -10° F. The lower temperature is below the glass transition temperature of M43, while neither M1 nor M30 demonstrates a typical glass transition. The M1 material does not exhibit an increased susceptibility to fracture at cold temperatures (not demonstrating a glass transition); whereas, M30 does demonstrate a change in mechanical properties without going through a true glass transition, and as it becomes cold, approaching 32° F, becomes more brittle and more susceptible to fracture.<sup>1</sup> The authors feel that embrittlement with lower temperatures is an important characteristic with respect to increased response to shaped charge (SC) attack.<sup>2</sup> The threat in our tests will be a conditioned SC jet and will provide a range of impact conditions, producing different response levels. From such data, response functions for the different propellants can be determined, thus supplying the survivability model with actual response data.

The work employed a modified ballistic pendulum to measure propellant response. The pendulum is not a traditional ballistic pendulum in that it does not trap an impacting projectile; but rather, the pendulum mass is displaced by reflected pressure from the energetic event.

## PENDULUM TESTS

### Test Configuration

The ballistic pendulum used by the U.S. Army Research Laboratory (ARL) at Aberdeen has been reported by Watson and will not be discussed further.<sup>3</sup> The pendulum has been calibrated, as a mechanical integrator, to provide displacement as equivalent pounds of detonating TNT. Response data, or pendulum displacement, is presented as equivalent pounds of TNT because the authors feel that the effect of a known mass of detonating TNT is well understood within the vehicle survivability community, and that presenting propellant response in those units simplifies the use of the data in predicting vehicle survivability.

The tests employed fielded, steel-cased, 105-mm ammunition.

The target cartridge was positioned 24 in from the pendulum face and centered on the face. Rolled homogeneous armor (RHA) was used to condition the SC jet from a basic TOW or Viper warhead, providing different residual jet velocities with a corresponding variation in deposited kinetic energy (KE). Single-round tests employed an inert cartridge positioned 1 in inboard from the target round, so that the test setups with one and two live rounds were physically the same. Two-round tests were used to characterize fratricide susceptibility with the more reactive M30 and M43 propellants. No fratricide effort was conducted with the M1 material because of its mild response to SC attack in the range tested (5.89 to 67.3 kJ of deposited KE).

Determination of deposited KE was achieved by treating the propellant bed as an inert, granular bed, with a bulk density of 1 g/cc; calculating the entrance and exit velocities of the SC jet impacting the propellant; and then using measured cumulative jet particle energy to determine the energy partitioned to the propellant in a given test. The deposited KE determination employed the following relationships:<sup>4</sup>

$$V_{ip} = V_i (S/S+T)^\gamma, \quad (1)$$

where

$V_{ip}$  = jet velocity into the propellant  
 $V_i$  = unconditioned jet velocity  
 $S$  = SC standoff to the conditioning armor from the virtual origin of the SC  
 $T$  = thickness of the conditioning armor  
 $\gamma$  = square root of the ratio of conditioning armor density to jet density (0.9387 for the work being reported).

$$V_o = V_{ip} (s/s+t)^\gamma, \quad (2)$$

where

$V_o$  = jet velocity exiting the propellant  
 $V_{ip}$  = same as Equation 1  
 $s$  = SC standoff to the impacted surface of the test cartridge from the virtual origin of the SC  
 $t$  = thickness of the test cartridge (133.35 mm for the work being reported)  
 $\gamma$  = square root of the ratio of propellant density to jet density (0.3348 for the work being reported).

$$KE_p = a + b(V_p)^c, \quad (3)$$

where

$KE_p$  = kinetic energy of a specified jet particle  
 $V_p$  = velocity of the specified jet particle  
 $a, b$ , and  $c$  are constants satisfying the equation

for a Viper SC jet  
 $a = 303.2822$ ,  $b = -0.8268$ ,  $c = 2.4952$

for a Basic TOW SC jet  
 $a = 2020.5767$ ,  $b = -94.0898$ ,  $c = 1.4225$ .

Equation 3 was obtained from a curve fit of jet particle velocity and cumulative particle energy. The velocity and energy values were experimentally determined for various SC jets and are maintained in an ARL database.<sup>5</sup> The "specified jet particle" is either the particle into the propellant ( $V_{ip}$ ) or the exit particle ( $V_o$ ). The difference in the two energies equals the deposited KE in a given test firing.

Plotting propellant response as a function of deposited KE, and fitting a linear relationship to the data sets, creates a family of curves that can be used to define a particular ammunition event, and thus predict ammunition compartment response.

#### Single-Round Test Data

Tables 1 and 2 present the response data obtained for three types of 105-mm cartridges, as centimeters of displacement, and as equivalent pounds of TNT. The individual data sets have been plotted as Figures 1 through 6, and a combined plot of curve fits is presented as Figure 7. The three deflagration-to-detonation transition points (DDT), observed with M43 at 9.4 and 16.2 kJ of deposited threat energy, have not been included in the curve fit effort (see Tables 1, 2, and Figure 5). These data points are an anomaly and represent a different reaction domain. The authors

Table 1: Corrected Pendulum Displacement Data (displacement of threat weapon has been removed from data).

Cart./ Prop.	Temp. (°F)	Displacement in Centimeters @ c.g. of Pendulum Mass Tabulated by Deposited Kinetic Energy (kJ)								
		5.89 (kJ)	9.40 (kJ)	16.2 (kJ)	23.0 (kJ)	30.7 (kJ)	31.3 (kJ)	38.8 (kJ)	46.1 (kJ)	67.3 (kJ)
M393/M1	75	0.1	0.57	0.93			1.08		3.25	
	-10			1.23			1.08		1.69	
M490/M30	75	0.1	1.12	2.51	3.29	4.73	5.06	6.13	5.78	14.6
	-10			12.0	21.1	21.1	16.9	23.4	21.5	26.7
M900/M43	75	1.79	40.3	23.0	6.61	7.06	6.75	8.0	8.89	19.3
	-10		4.23	25.9	12.2	12.5	12.5	12.5		24.1

believe that this DDT is controlled by physical properties of the M43 propellant bed, creating a "tuned" response at the defined threat stimulus. The hypothetical, tuned condition is that the detonation velocity in the propellant bed and the jet penetration velocity at 9.4 kJ of deposited KE are approximately equal; thus, the penetrating jet supports, or drives, the detonation. This hypothesis is being investigated and will be reported by ARL in the future.

As previously stated, the three sets of cartridge data were obtained with fielded rounds and, as such, contained their operational propellant loads. The M393 round contains 5.9 lb of M1 propellant, the M490 training round contains 12.1 lb of M30 propellant, and the M900 round contains 13.6 lb of M43 propellant. All three are granular propellants, and Table 3 summarizes their physical characteristics. Table 4 lists the equations resulting from the different curve fits.

Table 2: Propellant Response as Equivalent Pounds of TNT.

Cart./ Prop.	Temp. (°F)	Equivalent Pounds of TNT Tabulated by Deposited Kinetic Energy (kJ)								
		5.89 (kJ)	9.40 (kJ)	16.2 (kJ)	23.0 (kJ)	30.7 (kJ)	31.3 (kJ)	38.8 (kJ)	46.1 (kJ)	67.3 (kJ)
M393/M1	75	.002	.044	.104			.133		.763	
	-10			.166			.133		.279	
M490/M30	75	.002	.142	.518	.778	1.31	1.44	1.88	1.74	5.86
	-10			4.57	9.25	9.25	7.0	10.4	9.38	12.2
M900/M43	75	.306	19.7	10.2	2.09	2.28	2.15	2.70	3.10	8.26
	-10		1.12	11.8	4.64	4.79	4.80	4.79		10.8

Table 3: Physical Characteristics of Propellants Tested.

Cartridge/ Propellant	Lot #	Length (in)	Diameter (in)	# of Perfs/ WEB (in)	Bulk Den. (g/cc)
M393/M1	RAD77J-069777	0.432	0.196	7/0.036	
M490/M30	RAD82B-070197	0.629	0.312	7/0.059	1.03
M900/M43	IH91M-E00043	0.551	0.332	19/0.044	1.03

#### Two-Round Test Data

As stated previously, the two-live-round configuration was used to characterize fratricide susceptibility. Comparison of a single-round response curve and its corresponding two-round curve provides a means of visualizing the interaction of collocated ammunition. Given similar slopes, comparing the y intercepts of a set of linear response functions of one and two rounds approximately



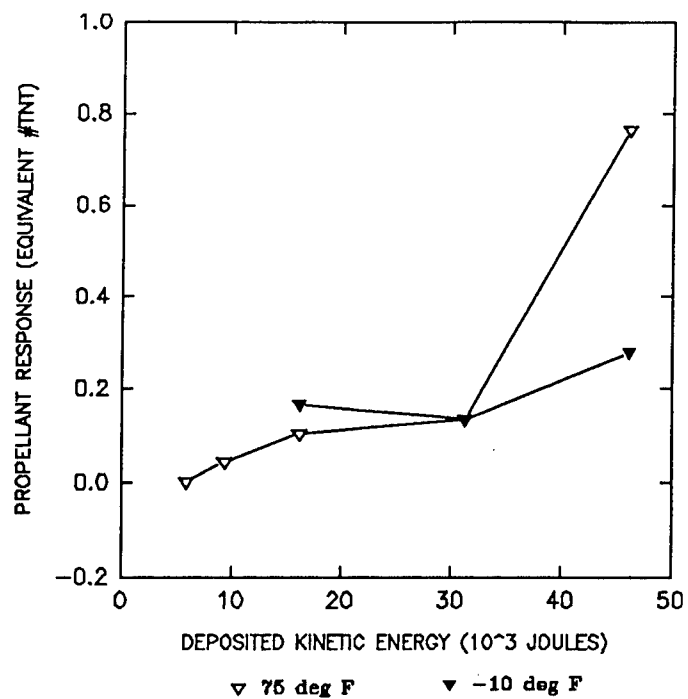


Figure 1: M1 SC Data at Two Temperatures.

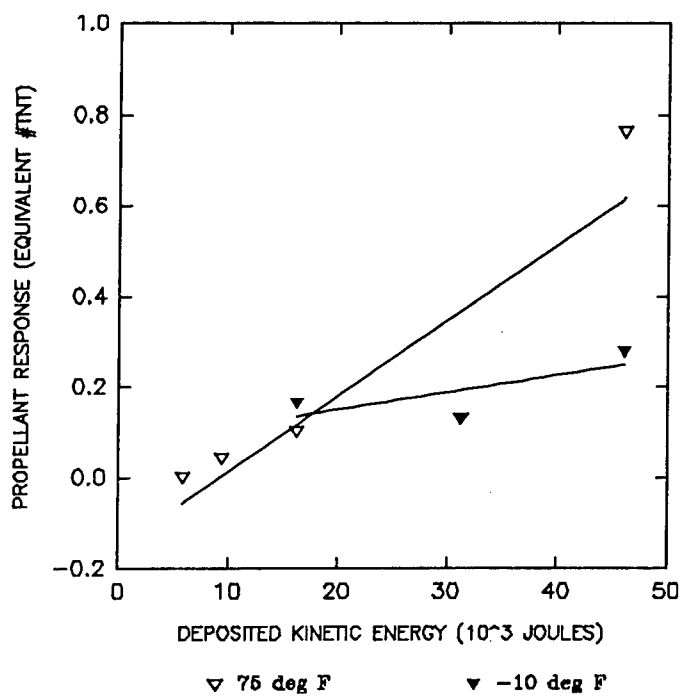


Figure 2: Linear Fit to M1 SC Data at Two Temperatures.

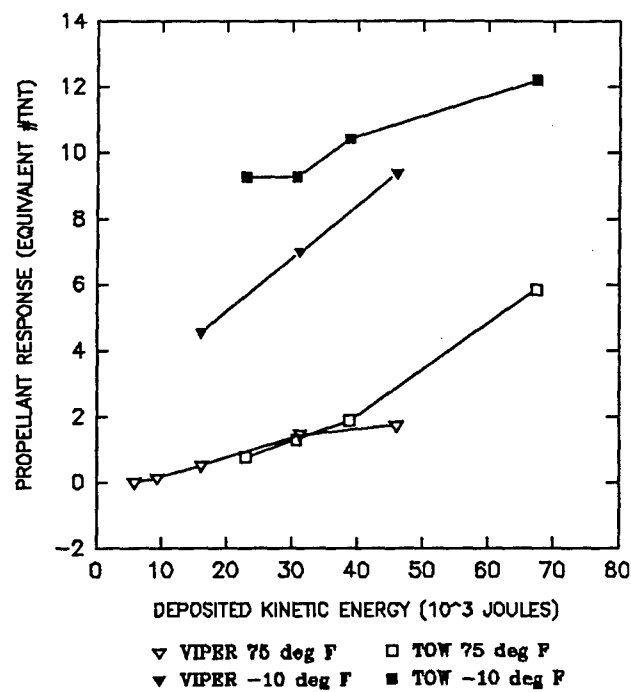


Figure 3: M30 SC Data at Two Temperatures.

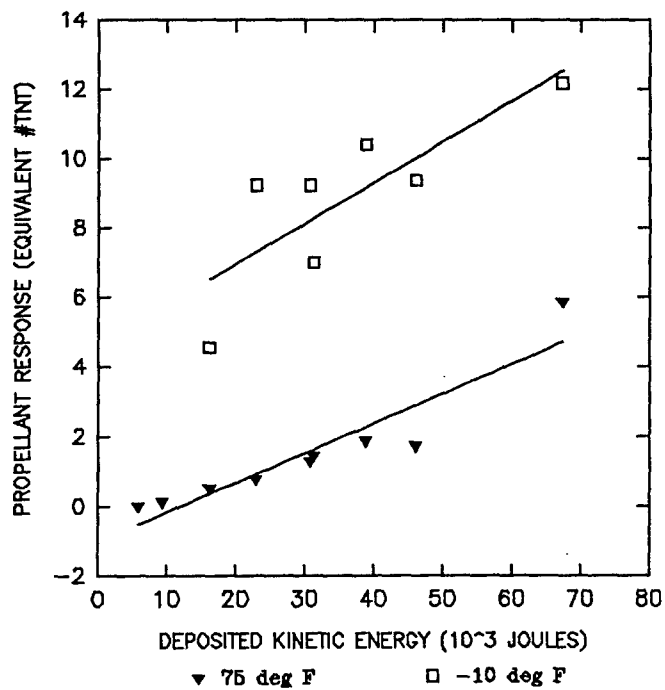


Figure 4: Linear Fit to M30 Data at Two Temperatures.

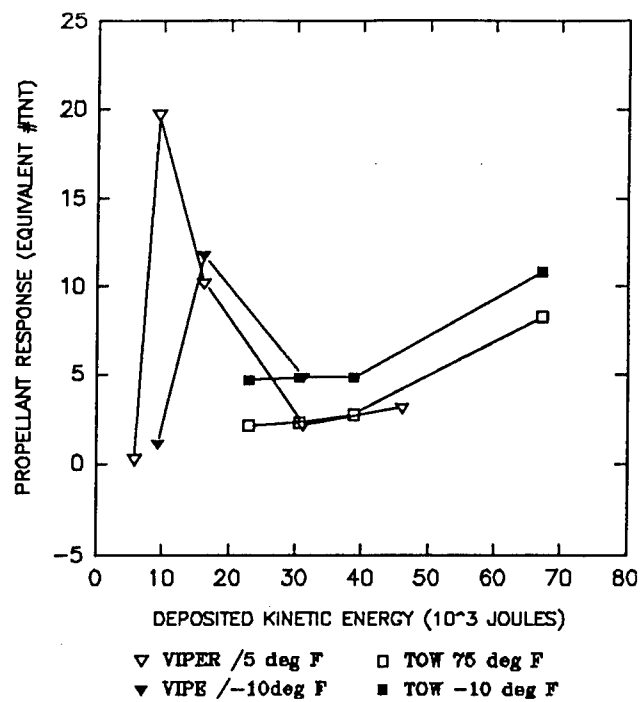


Figure 5: M43 SC Data at Two Temperatures.

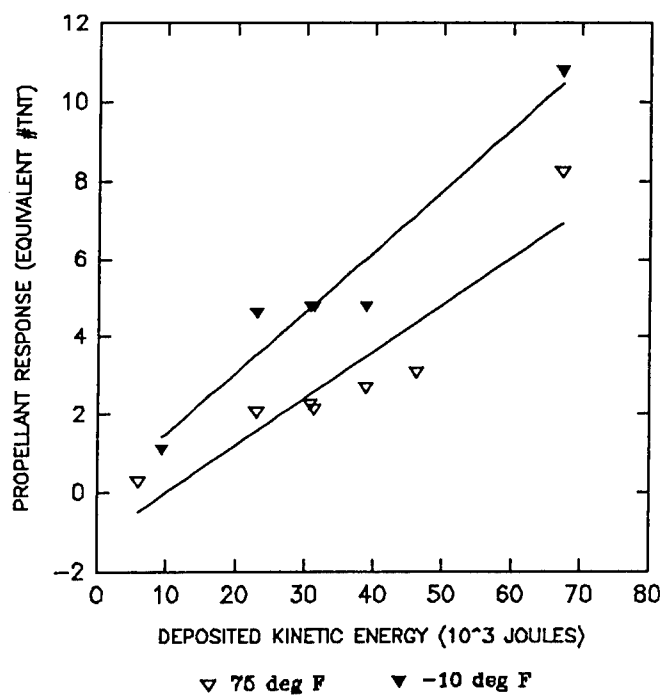


Figure 6: Linear Fit to M43 SC Data at Two Temperatures.

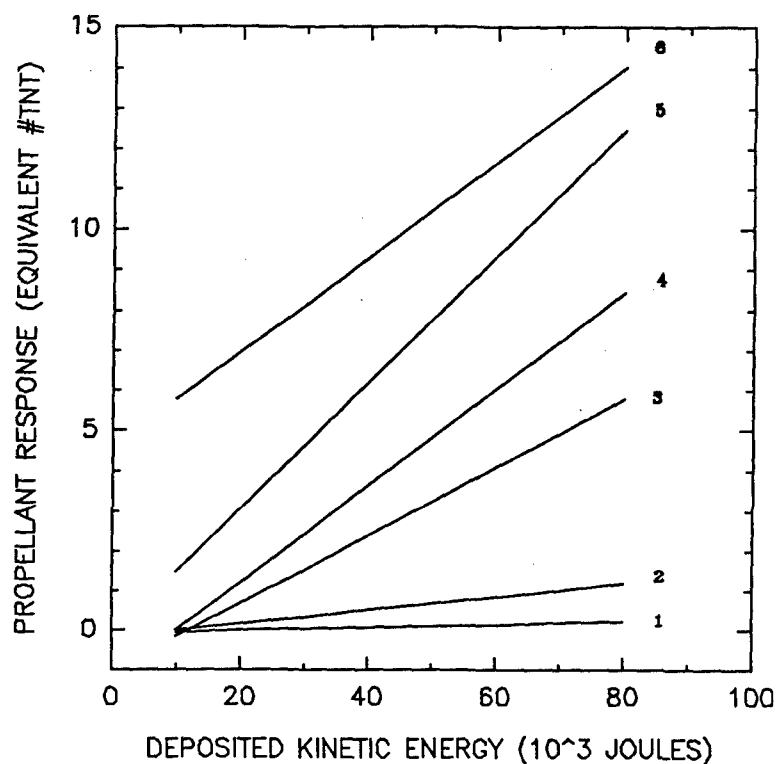


Figure 7: Summary of Linear Regressions for Three Propellants at Two Temperatures.

Table 4: List of Equations for Curves in Figure 7.

Cartridge/ Propellant	Temp. (°F)	Linear Fit for Response as Equivalent Pounds of TNT	Comments
M393/M1	75	$Y = 0.0167X - 0.155$	Curve #2
	-10	$Y = 0.00376X - 0.0755$	Curve #1
M490/M30	75	$Y = 0.0848X - 1.012$	Curve #3
	-10	$Y = 0.118X + 4.604$	Curve #6
M900/M43	75	$Y = 0.120X - 1.198$	Curve #4 No transition data
	-10	$Y = 0.157X - 0.0695$	Curve #5 No transition data

Table 5: Pendulum Displacement Data for Two-Live-Round Tests (pendulum shielded from blast of threat weapon).

Cart./ Prop.	Temp. (°F)	Displacement in Centimeters @ c.g. of Pendulum Mass Tabulated by Deposited Kinetic Energy (kJ)			
		23.0 (kJ)	30.7 (kJ)	38.8 (kJ)	67.3 (kJ)
M490/M30	75	3.54	5.10		11.3
	-10	31.4	32.6	31.2	39.6
M900/M43	75	6.36	11.6	43.9	12.6
	-10	12.2	12.7	12.9	26.9

Table 6: Propellant Response as Equivalent Pounds of TNT for Two-Live-Round Tests.

Cart./ Prop.	Temp. (°F)	Equivalent Pounds of TNT Tabulated by Deposited Kinetic Energy (kJ)			
		23.0 (kJ)	30.7 (kJ)	38.8 (kJ)	67.3 (kJ)
M490/M30	75	.867	1.46		4.23
	-10	14.7	15.4	14.6	19.3
M900/M43	75	1.98	4.38	21.8	4.85
	-10	4.64	4.92	5.0	12.3

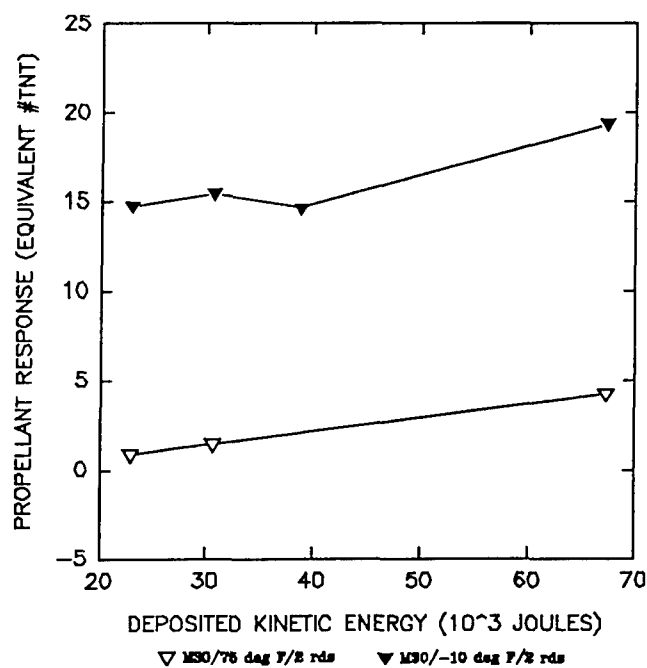


Figure 8: M30 SC Data at Two Temperatures for Two-Live-Round Tests.

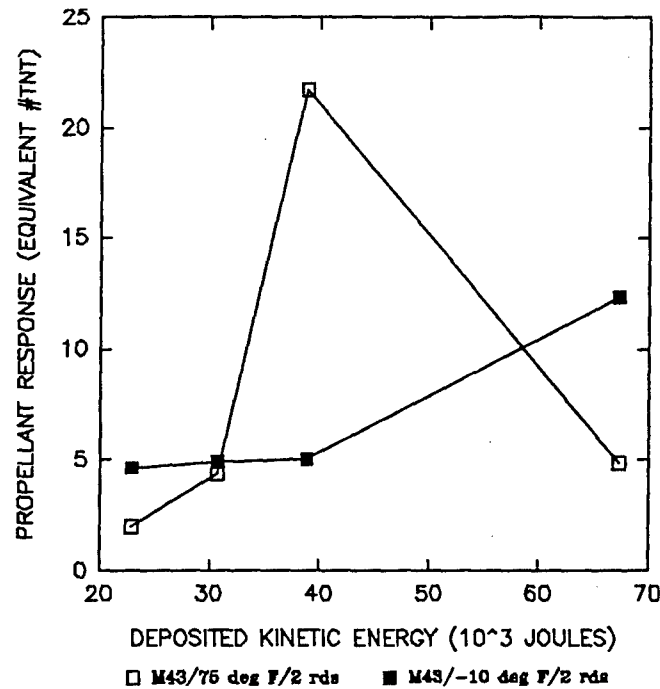


Figure 9: M43 SC Data at Two Temperatures for Two-Live-Round Tests.

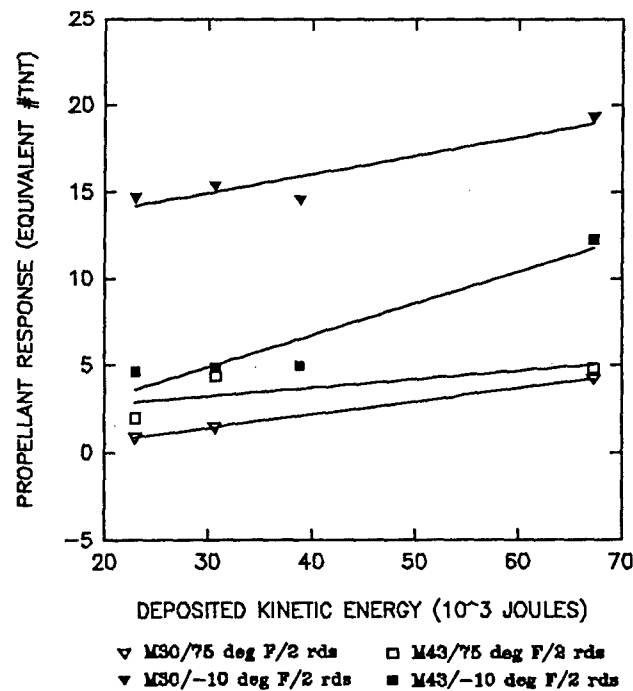


Figure 10: Summary of Linear Regressions for Two Propellants at Two Temperatures for Two-Live-Round Tests.

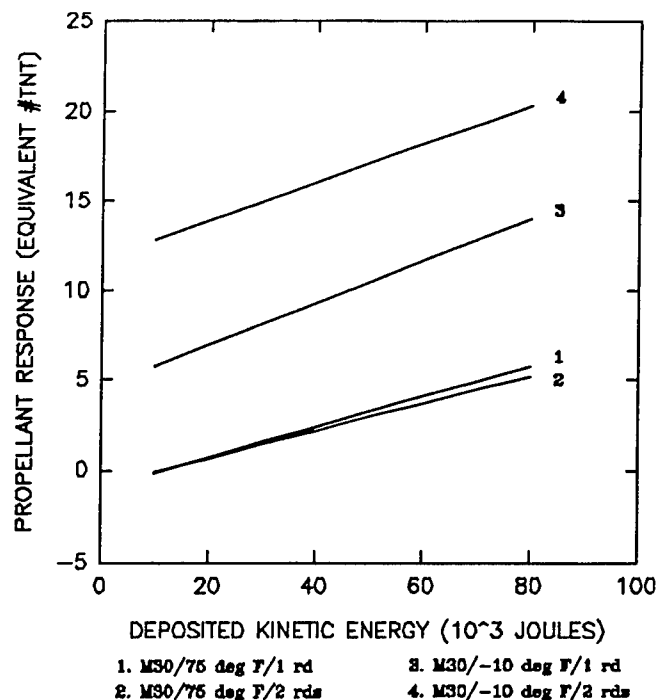


Figure 11: Summary of Linear Regressions for M30 One- and Two-Live-Round Tests.

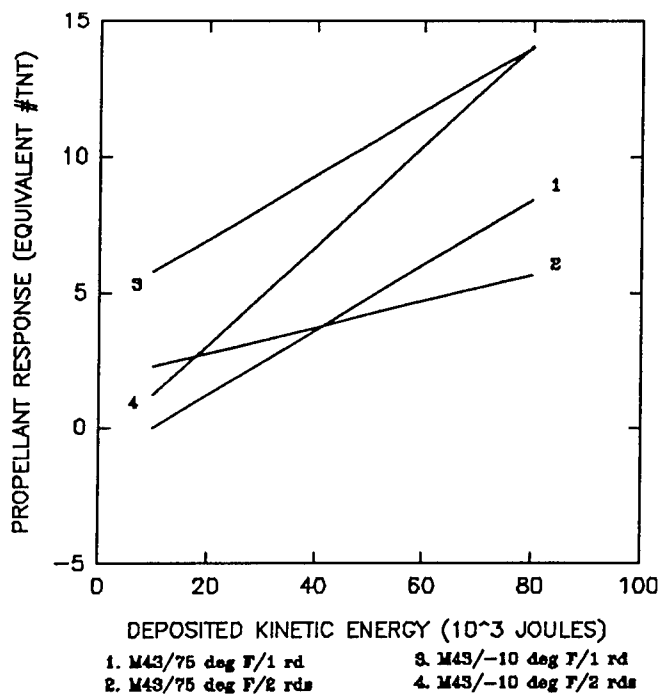


Figure 12: Summary of Linear Regressions for M43 One- and Two-Live-Round Tests.

quantifies the ammunition interaction. The corresponding change in response can be multiplied by the number of collocated rounds in the system configuration and then added to the donor response as an estimate of the total level of reaction in the system being analyzed.

Table 7: List of Equations for Curves in Figures 11 and 12.

Cartridge/ Propellant	Temp. (°F)	Linear Fit for Response as Equivalent Pounds of TNT	Comments
M490/M30	75	$Y = 0.07589X - 0.874$	Curve #2 Fig. 11
	-10	$Y = 0.1066X + 11.77$	Curve #4 Fig. 11
M900/M43	75	$Y = 0.04855X + 1.778$	Curve #2 Fig. 12 No transition data
	-10	$Y = 0.1836X - 0.6209$	Curve #4 Fig. 12 No transition data

The M43 SC data summarized in Figure 12 is not the precise fit observed with the M30 data seen in Figure 11. M43 has historically responded in an irregular fashion to SC jet impact and is probably due to the relationship of response and physical properties previously mentioned. The one- and two-round sets would probably match more precisely if additional tests were conducted in each set. This would provide a larger statistical population for the linear fits. However, as an evaluation of fratricide susceptibility, the two-round results confirm that M43 should not present a fratricide problem at either temperature, providing there is no DDT in the range of interest.

#### APPLICATION

Characterizing the residual SC jet, or the actual threat energy impacting the ammunition, is important to successful application of the response functions being reported. Defining the energy that exits modern armors is not a trivial exercise and is not being addressed in this paper. Our example application assumes a known stimulus of 35.5 kJ of deposited KE against M30 propellant.

#### Example

As an example of applying the presented technique in predictive compartment modeling, a finite element analysis was conducted to examine the dynamic response of an aluminum bulkhead separating the ammunition storage area from the crew area in a combat vehicle. The target round was an M456A2 HEAT round, containing M30 propellant. The residual SC jet was assigned a deposited KE of 35.5 kJ, and the round was at a temperature of 75° F. Applying the M30/75° F equation from Table 4, 35.5 kJ of deposited KE produces a 2-lb TNT event, and an examination of Figure 11 indicates that fratricide will not occur.



The finite element simulation included elastic-plastic material properties in a finite strain formulation using the DYNA3D code.<sup>6</sup> Actual transient pressure loads were obtained from the CONWEP blast prediction code,<sup>7</sup> which has been coupled to the DYNA3D code. The calculations simulated reaction of the target round 30 in from the bulkhead and 8 in from the base of a standing cartridge. Figure 13 is an overhead view of the turret of a fighting vehicle, with the dark line being the modeled bulkhead. Figure 14 is an isometric view of the finite element model. The model includes the 0.25-in-thick bulkhead being analyzed and approximately ten to twelve in of a surrounding, welded edge support that is fixed in the horizontal beam-line direction on the autoloader side of the model. The material is 5083 aluminum alloy. Table 8 summarizes the results of the analysis. CONWEP treats blast either as a hemispherical, surface burst, or as a spherical, free air blast; therefore, both results are summarized in Table 8. In a real compartment event, the results would be somewhere between the two. The authors recommend using the more severe, hemispherical prediction in assessing vehicle survivability because of the multitude of blast reflective surfaces near the impacted round.

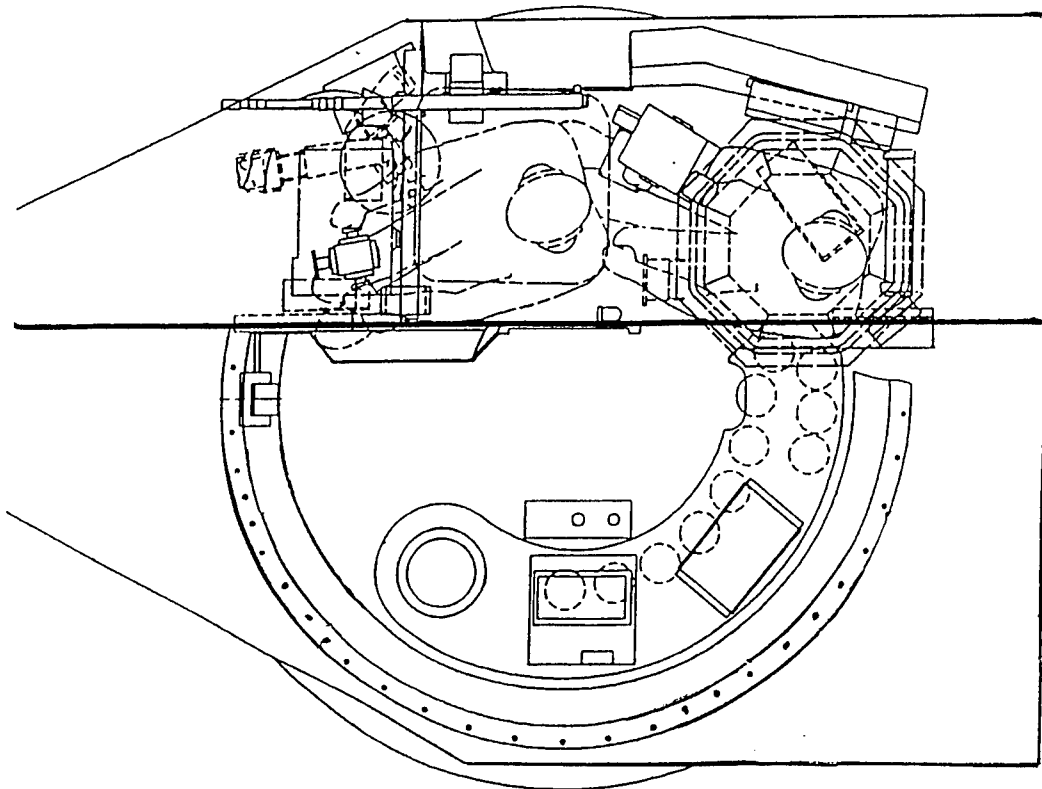


Figure 13: Top View of the Turret of a Combat Vehicle Showing the Bulkhead Being Modeled (dark line between crew and bottom two thirds of sketch).

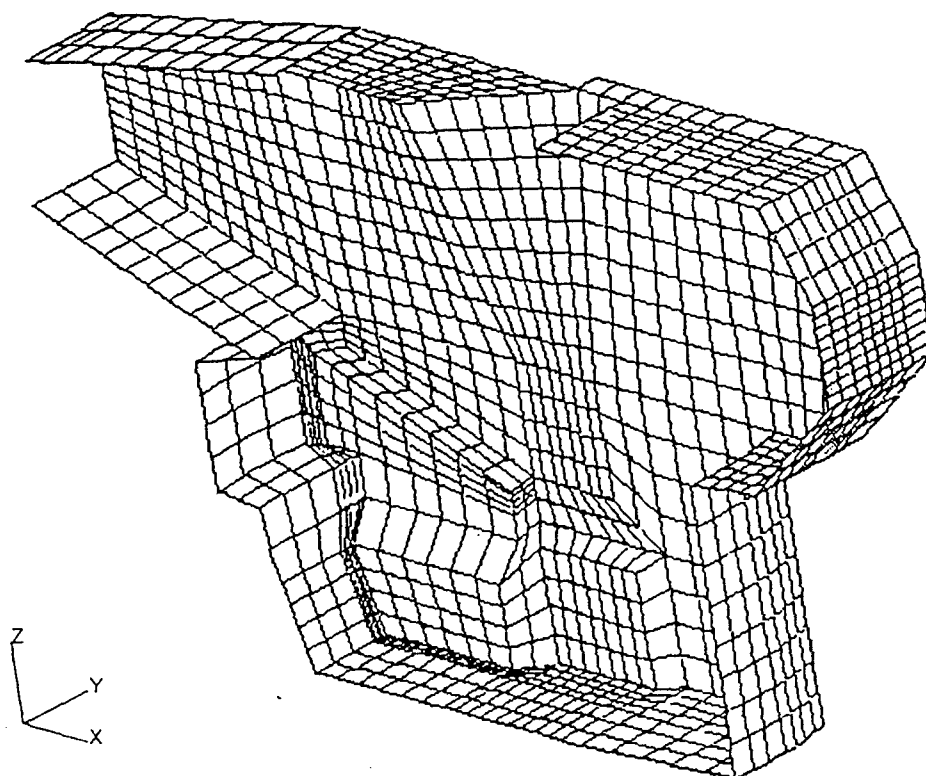


Figure 14: Isometric View of Finite Element Model.

Table 8: Results of the Finite Element Analysis.

CONWEP TYPE	MAX. Y DISPL.	MAX. STRAIN	BULKHEAD THICKNESS/ TYPE	ALLOWABLE FRACTURE STRAIN	RESULT
HEMISPHERICAL	3.3"	22% Plastic Strain	0.25"/ 5083	19%	Deformation and Fracture Likely
SPHERICAL	2.4"	6.2% Plastic Strain	0.25"/ 5083	19%	Deformation Without Fracture

The hemispherical blast model predicts that a 2-lb TNT event will cause permanent deformation of the bulkhead, accompanied by fracture. The fracture prediction is based upon the fact that the predicted plastic strain exceeds the allowable value for 5083

aluminum. These results could now be applied to the survivability algorithm, which is beyond the scope of this paper.

#### COMMENTS AND CONCLUSIONS

Small-scale, relatively inexpensive tests have been demonstrated that provide realistic response of ammunition to ballistic threat information. The technique can be used to investigate and quantify multiple storage, ammunition, and threat parameters. The resulting functions are applicable to existing survivability algorithms, providing the analyst with response information that is continuous over the range tested and specific to ammunition type and threat energy. The specific and continuous nature of the response data is an improvement over the step function technique, which is general to ammunition and makes decisions concerning ammunition response and vehicle survivability based upon defined, incremental response steps.

#### References

1. Personal communication with R. Lieb, U.S. ARL, Weapons Technology Directorate, Propulsion and Flight Division, AMSRL-WT-PD, Aberdeen Proving Ground, MD 21005-5066, February 1996.
2. G. Gibbons, Jr., J. L. Watson, P. J. Peregrino, II, "Evaluation of a Proposed Change in the Combat Stowage Plan for the M1 Abrams Tank (U)," BRL-MR-3981, U.S. Army Research Laboratory, Aberdeen Proving Ground, MD 21005-5066, June 1992.
3. J. L. Watson, "Technique for Measuring the Response of Gun Propellant to External Stimuli," presented at the JANNAF Propulsion Systems Hazards Subcommittee Meeting, The Johns Hopkins University Applied Physics Laboratory, Laurel, MD, April 1990.
4. R. DiPersio and J. Simon, "The Penetration-Standoff Relation for Idealized Shaped Charge Jets," BRL Memorandum Report No. 1542, U.S. Army Research Laboratory, Aberdeen Proving Ground, MD 21005-5066, February 1964.
5. Personal communication with R. Summers, U.S. ARL, Weapons Technology Directorate, Terminal Effects Division, AMSRL-WT-TC, Aberdeen Proving Ground, MD 21005-5066, February 1996.
6. J. O. Hallquist, R. G. Whirley, and B. E. Engelmann, "DYNA3D, A Nonlinear, Explicit, Three-Dimensional Finite Element Code for Solid and Structural Mechanics, User's Manual," Lawrence Livermore National Laboratory, Livermore, CA, November 1993.
7. D. W. Hyde, CONWEP, a collection of conventional weapons effects calculations from the equations and curves of TM 5-855-1, "Fundamentals of Protective Design for Conventional Weapons," U.S. Army Corps of Engineers, 20 Massachusetts Ave, NW, Washington, DC 20314-1000.

# UNCLASSIFIED

## INVESTIGATION OF FIRE-EXTINGUISHING POWDERS (U)

Anthony E. Finnerty  
U.S. Army Research Laboratory  
Aberdeen Proving Ground, MD 21005-5066

Lawrence Vande Kieft  
4258 Federal Hill Road  
Street, MD 21154-1127

### (U) ABSTRACT

(U) Four fire-extinguishing powders (aluminum oxide, Purple K dry powder, Ansul +50 [sodium bicarbonate], and Monnex) were examined in a scanning electron microscope. The aluminum oxide and the Monnex had the smallest particle sizes with estimated medium particle sizes of 10  $\mu\text{m}$  and 8  $\mu\text{m}$ , respectively. However, agglomeration of the Monnex was observed, which reduced its available surface area per unit weight. The Purple K and the Ansul +50 had medium particle sizes of about 40  $\mu\text{m}$ . The small particle size of the aluminum oxide helps explain how this inert material can be an effective fire-extinguishing agent.

(U) Common commercial grades of aluminum oxide and sodium bicarbonate had medium particle sizes of 80  $\mu\text{m}$  and 90  $\mu\text{m}$ , respectively. These materials could be suitable fire-extinguishing agents only if the particles were to be broken up during dissemination.

### (U) INTRODUCTION

(U) Many finely divided solids (nonflammable salts) have been used to quench hydrocarbon flames. Sodium bicarbonate was widely used into the 1950s as the primary fire-extinguishing powder. The U.S. Navy determined that potassium bicarbonate was superior to the sodium analog, and subsequently changed its hand-held extinguishers from sodium bicarbonate to potassium bicarbonate. Other solids, such as Monnex, have been proposed, but their fire-extinguishing ability is only marginally superior to the potassium bicarbonate. Because of the expense, there has been resistance to a changeover.

(U) It is widely believed that fire-extinguishing powders can function as both energy-absorbing materials and as solid surfaces on which free radicals can be destroyed. Heat may be absorbed by the heat capacity of the solid, the heat of fusion at the melting point, the heat capacity of the liquid, heat of dissociation from breaking of chemical bonds, and heat of vaporization. These all contribute to the total endothermacy of the fire-extinguishing powder (ref. 1).

(U) From a chemical aspect (ref. 2,3), it has been found that potassium salts are more effective than sodium salts, and iodide anions are more effective than chloride anions. Presumably, there is a catalytic path for destruction of free radicals, such as H, O, and OH, utilizing the potassium in the

UNCLASSIFIED

salts. It must be remembered that any powder that has a chemical fire-extinguishing capability will also have a heat-absorbing (endothermic) capability.

(U) Ewing (ref. 1) has shown that less weight of salt per unit volume of a fuel-air mixture is required for extinguishment if the salt is finely divided. Thus, micron-sized solids are more efficient as fire-extinguishing powders than larger particles are. Large surface areas are important in both the heat absorption and the chemical interference mechanisms.

(U) In many cases, there is a hesitation to use conventional fire-extinguishing powders such as Purple K, Monnex, and sodium bicarbonate, which can be corrosive to metals, especially aluminum. Therefore, aluminum oxide powder, which is chemically unreactive, has been chosen for aircraft applications. This material has no ability to melt or vaporize or undergo bond breaking at the temperatures encountered in hydrocarbon flames. Yet, tests have shown that aluminum oxide powder is effective in extinguishing fires even though it has only the heat capacity of the solid to serve as its heat sink. This fact prompted a decision to examine aluminum oxide powder in a scanning electron microscope (SEM) to determine if there was anything unusual about this material.

#### (U) EXPERIMENTAL

(U) We identify fire-extinguishing materials studied:

<u>Material</u>	<u>Source</u>
Aluminum oxide, anhydrous 99.4%	Pfaltz and Bauer
Aluminum oxide, powder panel grade for aircraft fire protection	Composite Structures
Sodium bicarbonate	Arm and Hammer
Ansul +50, micronized sodium bicarbonate (Desikarb)	Ansul
Monnex (potassium imido dicarboxamide with about 20% potassium bicarbonate)	ICI
Purple K (siliconized potassium bicarbonate)	Automated Protection Systems

(U) Magnified pictures of the powders were taken in an International Scientific Instruments SEM. The image of the powders at 100x, 300x, and 3,000x are given in Figures 1-6.

#### (U) DISCUSSION

##### (U) Aluminum Oxide

(U) Perhaps the most interesting of the powders is aluminum oxide. It can be seen in Figure 1 (100x magnification) that the normal chemical grade of aluminum oxide contains particles whose medium size is approximately 80  $\mu$ m. At higher magnification—300x and 3,000x—it can be seen that

the large particles are composed of an extensive array of platelets. The major dimension of these platelets is on the order of 3  $\mu\text{m}$  and their thickness is approximately an order of magnitude less than this. The platelets give the particle a much greater surface area than would be expected, based just on particle size.

(U) In the event this powder were to be used as a fire-extinguishing agent, it would need to be expelled under conditions that would ensure that the agglomerated particles were broken into their individual platelets. This would result in a very large surface area per unit mass. Such an increase would be necessary for this material to be a reasonable fire-extinguishing agent.

(U) In Figure 2, at 100 $\times$  magnification, it can be seen that the fire-extinguishing grade of aluminum oxide has much smaller particles, about 10  $\mu\text{m}$ . At 300 $\times$  and 3,000 $\times$  magnifications, the particle morphology is more apparent. The material appears to be a random collection of lumps, fragments with sharp edges, some almost single crystals, and at least some platelets. It has a broad size distribution whose medium value, as mentioned previously, is approximately 10  $\mu\text{m}$ . Some instrumental problems were encountered, but they did not invalidate the data.

(U) It was observed that there was little tendency of the particles to clump together. The high surface area of the powder helps explain how an inert material can act as an efficient fire-extinguishing agent.

#### (U) Sodium Bicarbonate

(U) The 100 $\times$  magnification in Figure 3 shows that the common grade of sodium bicarbonate has particles with a medium size of 90  $\mu\text{m}$ , very similar to that of the agglomerated form of the normal chemical grade aluminum oxide. Higher magnifications, 300 $\times$  and 3,000 $\times$ , show that while there are some small particles attached to the large particles, there is not a significant increase in surface area. The large particle size of the common sodium bicarbonate limits its fire-extinguishing effectiveness. However, there is some chemical contribution in its role as an extinguishing agent.

(U) Figure 4 shows that the Ansul +50 sodium bicarbonate has much smaller particles, about 40  $\mu\text{m}$ . There was insignificant agglomeration. These are larger than the fire-extinguishing grade of aluminum oxide. The higher magnifications, 300 $\times$  and 3,000 $\times$ , show that there is some increase in surface area due to the attachment of some small particles to the larger ones. However, there is less surface area than in the fire-extinguishing grade of aluminum oxide. The chemical contribution of sodium bicarbonate to its extinguishing role may be strong enough to overcome the difference in particle size.

#### (U) Potassium Bicarbonate

(U) Examination of Figure 5 shows that the Purple K dry powder (potassium bicarbonate) and the Ansul +50 have a similar particle size (40  $\mu\text{m}$ ), however, the Purple K has a much larger particle size distribution. It has some large pieces that reduce the overall surface area per unit mass. The higher magnification of 300 $\times$  and 3,000 $\times$  show that while there are some smaller particles adhering to the surface of the larger potassium bicarbonate particles, there is not a significant increase in surface area. The Purple K probably has less surface area than the Ansul +50 possesses. The increased chemical ability of potassium over sodium to quench flames will be an extra contribution for fire suppression. Whether the extra surface area of the Ansul +50 over Purple K is more important than the higher

chemical contribution of potassium over sodium is not obvious. It is probable that both will prove to be high quality fire-extinguishing agents.

(U) Monnex

(U) The 100× image in Figure 6 shows that the particles of Monnex powder are smaller than the particles of Ansul +50. At 300× and 3,000× magnifications, the Monnex particles appear to be agglomerates of small particles, not inherently large particles. The median size of the agglomerated particles appear to be about 90 μm, while that of their constituents and the non-agglomerated particles is about 8 μm. The surface area of Monnex should be greater than that of Ansul +50 and Purple K, while comparable to that of the fire-extinguishing grade of aluminum oxide. The presumed chemical role of Monnex, in addition to its small particle size, may well make it a superior fire-extinguishing agent.

(U) CONCLUSION

(U) Examination of four fire-extinguishing powders and two reference powders in a SEM showed that all the fire-extinguishing powders were of relatively small particle size, 40 μm maximum medium size. The reference powders had at least twice as large medium particle size. The fire-extinguishing grade aluminum oxide powder appeared to have the largest surface area due to the fact that it had non-agglomerated, small particles.

(U) The normal chemical grade of aluminum oxide consisted of agglomerated particles. If these were broken up during dissemination, this material could prove effective as a fire-extinguishing agent.

(U) The commercial grade of sodium bicarbonate consisted of inherently large particles that would likely be very inefficient as a fire-extinguishing agent.

(U) The Monnex powder appeared to have the smallest size of individual particles. However, Monnex had a tendency to form clumps. This agglomeration reduces the surface area of the particles and Monnex's potential effectiveness.

(U) Ansul +50 had particles larger than Monnex, but with very little agglomeration.

(U) Purple K dry powder had the largest particle size of the fire-extinguishing powders. There was little tendency for agglomeration.

(U) The commercial, non-fire-extinguishing grades of aluminum oxide and sodium bicarbonate appeared similar to the fire-extinguishing powders except for much larger particle size and the morphology of those large particles.

(U) REFERENCES

1. (U) Ewing, C. T., J. T. Hughes, and H. W. Carhart. Fire and Materials, vol. 8, p. 148, 1984.
2. (U) Dolan, J. E. Sixth Symposium on Combustion p. 787, Reinhold, NY, 1956
3. (U) Altman R. L., A. C. Teng, L. A. Mayer, and D. J. Myronuk. "Development and Testing of Dry Chemicals in Advanced Extinguishing Systems for Jet Engine Macelle Fires." Report JTCG/AS-82-T-002, 1983

UNCLASSIFIED

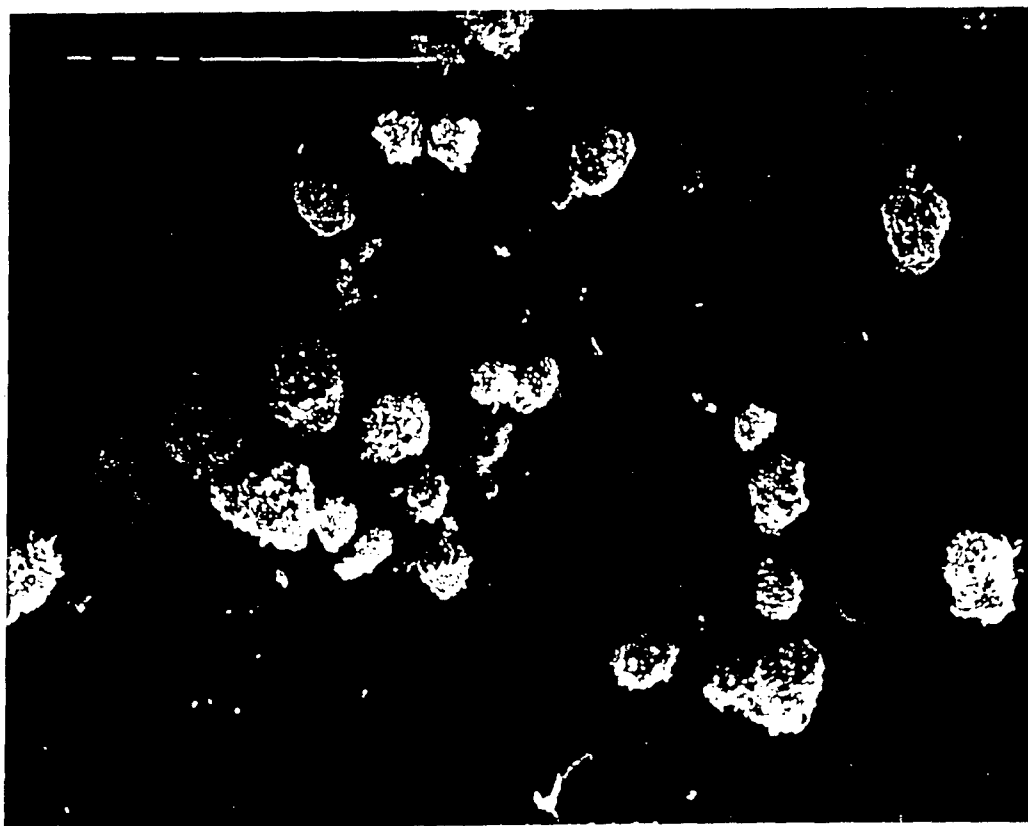


Figure 1. (U) Commercial grade aluminum oxide at 100x, 300x, and 3,000x.

UNCLASSIFIED



UNCLASSIFIED

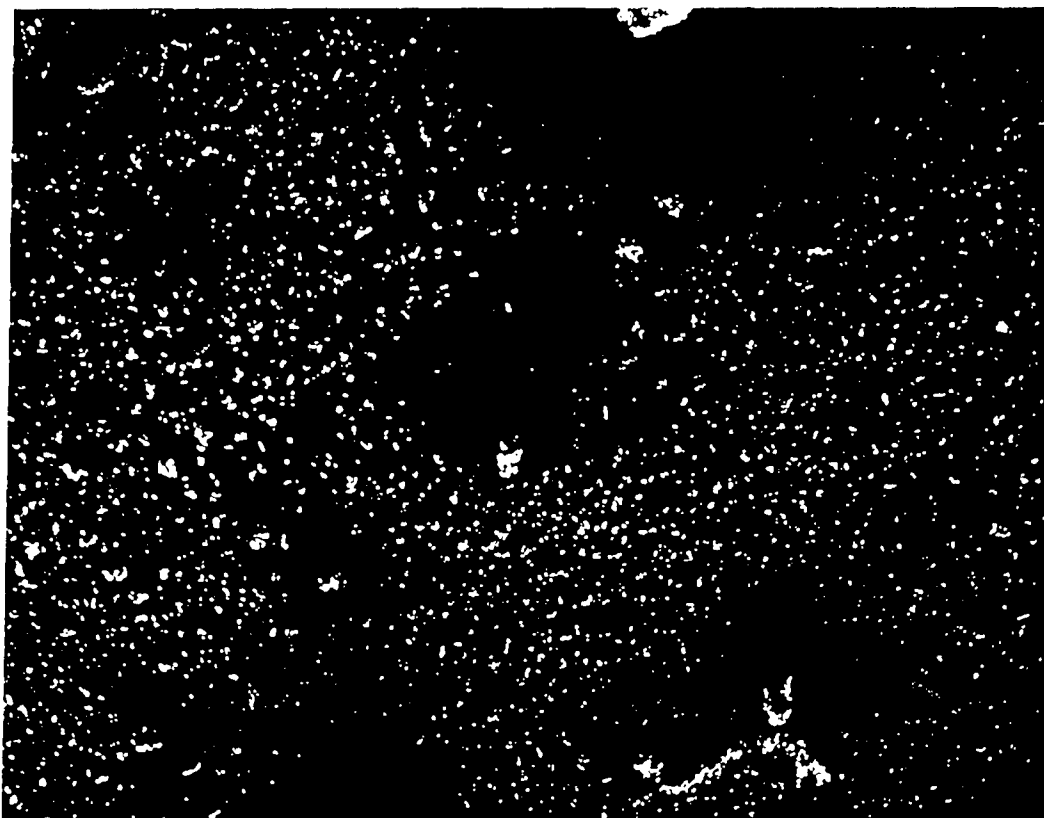
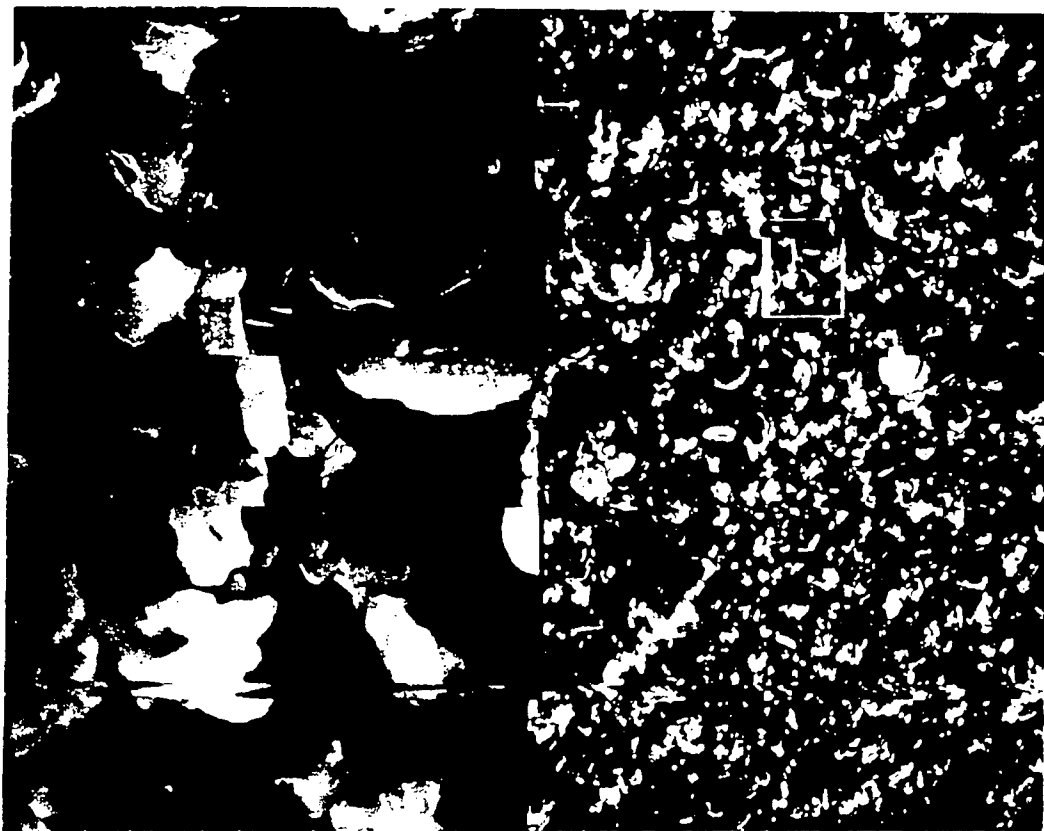


Figure 2. (U) Fire-extinguishing grade aluminum oxide at 100x, 300x, and 3,000x.

UNCLASSIFIED

UNCLASSIFIED

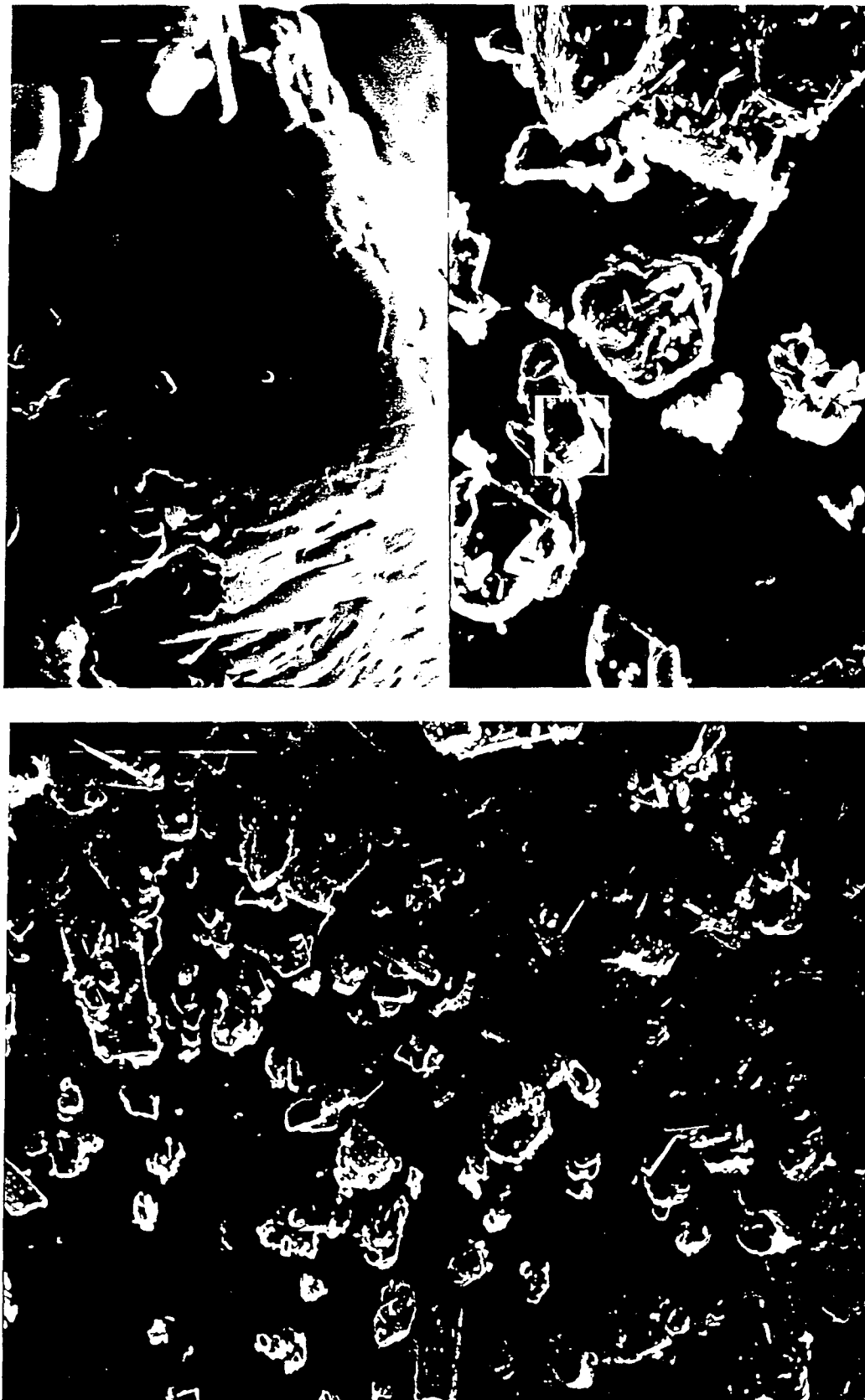


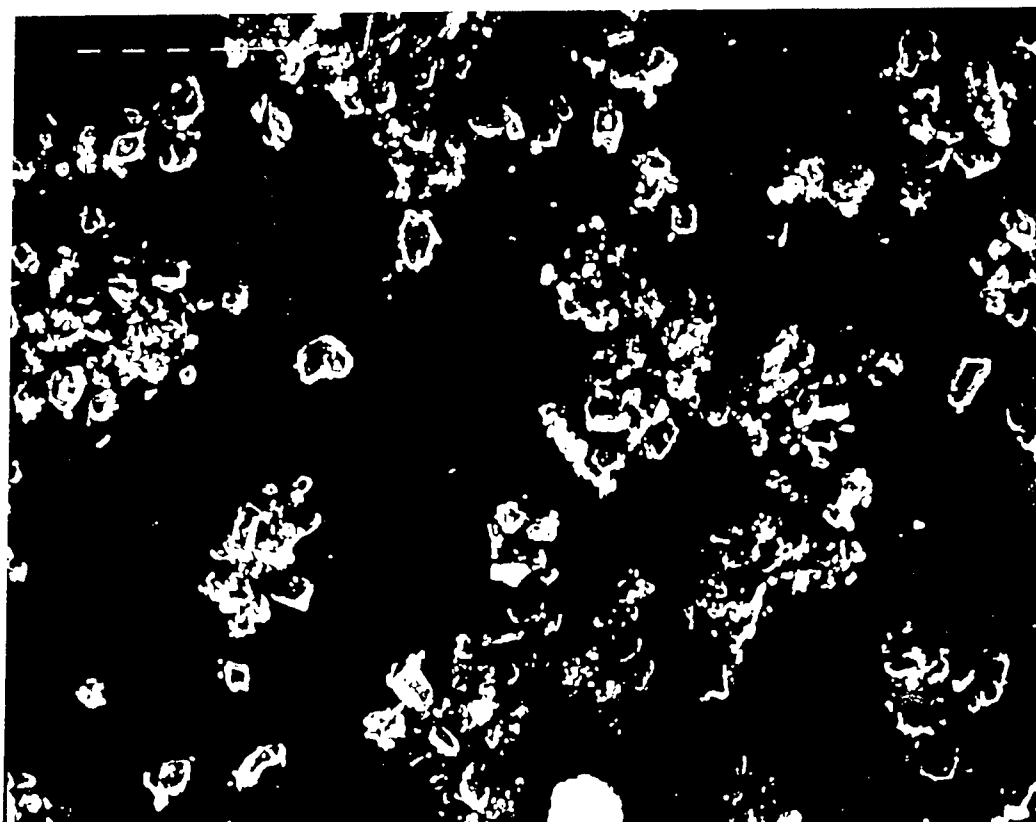
Figure 3. (U) Commercial grade sodium bicarbonate at 100x, 300x, and 3,000x.

UNCLASSIFIED

UNCLASSIFIED



Figure 4. (U) Ansul +50 at 100x, 300x, and 3,000x.



UNCLASSIFIED

UNCLASSIFIED

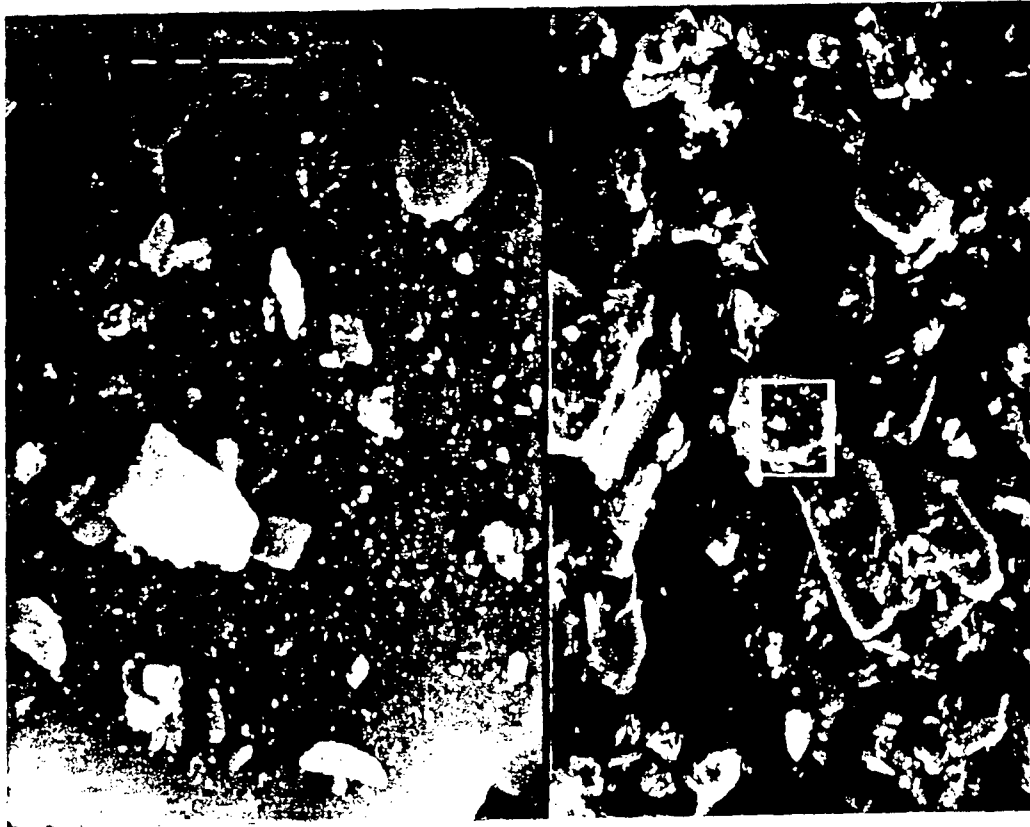
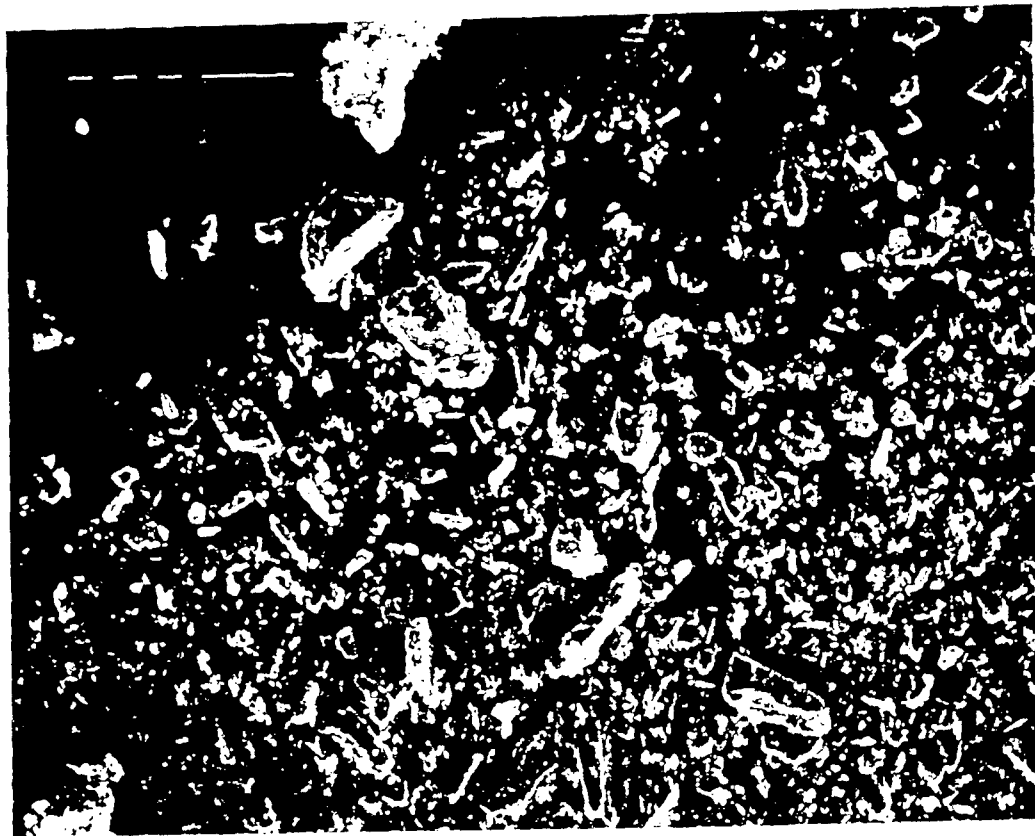


Figure 5. (U) Purple K at 100x, 300x, and 3,000x.



UNCLASSIFIED

UNCLASSIFIED

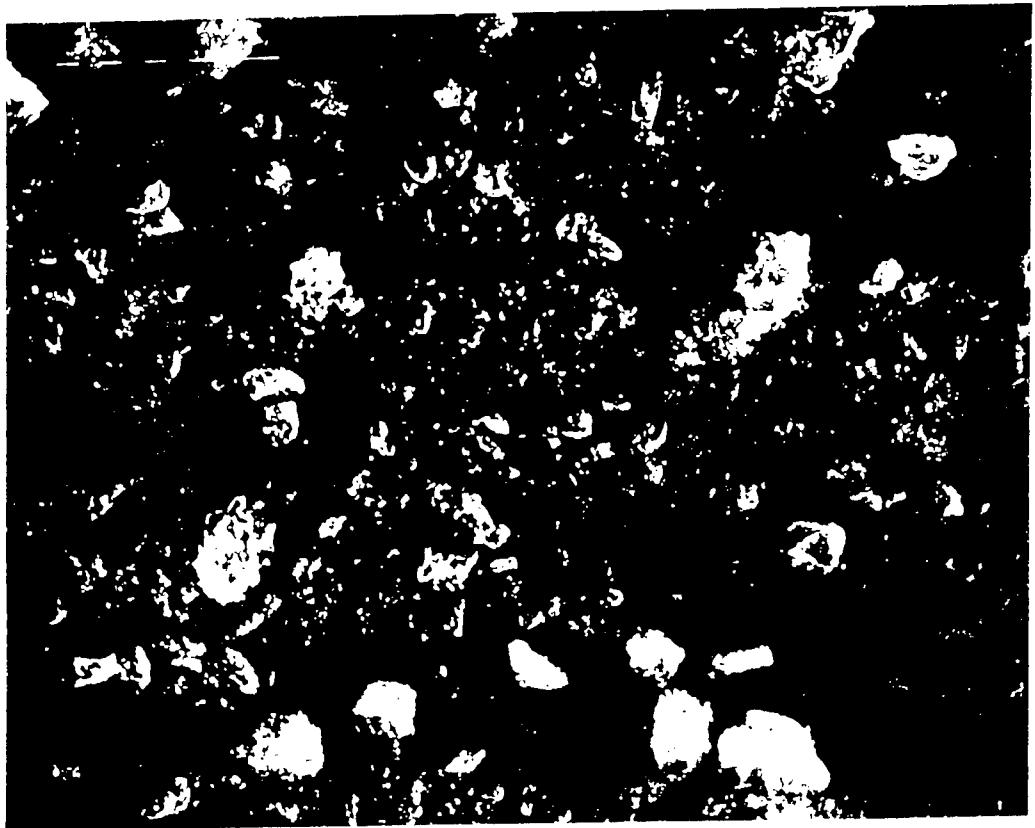
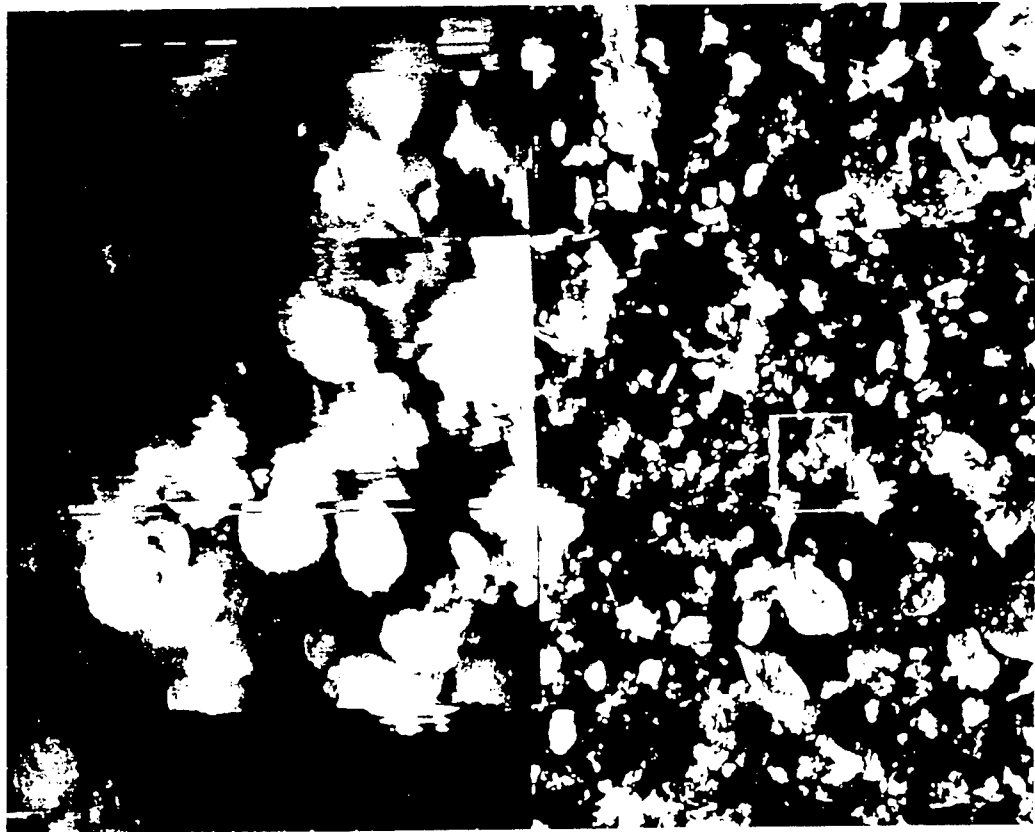


Figure 6. (U) Monnex at 100x, 300x, and 3,000x.

UNCLASSIFIED

UNCLASSIFIED

**NUCLEAR, BIOLOGICAL, AND CHEMICAL CONTAMINATION SURVIVABILITY  
(NBCCS)**

R. Andrew Blankenbiller

William S. Magee, Jr.

U. S. Army Chemical and Biological Defense Command  
Executive Office for the Joint Service Materiel Group  
Aberdeen Proving Ground, MD 21010-5423

**ABSTRACT**

(U) To address the hazards presented by NBC environments, two principal approaches are generally used: "Doctrinal" NBC Survivability and NBC Contamination Survivability (sometimes referred to as "Regulatory" NBCCS). Most developers are familiar with the former, which consists of the sub-categories of Avoidance, Protection, and Decontamination. Moreover, it is usually approached by integration of various types of items/systems into such materiel as combat and tactical vehicles. Less familiar (and indeed less "mature") is the latter principal approach, i.e. NBCCS, which consists of the sub-categories of Hardness, Compatibility, and Decontaminability. NBCCS is usually approached through incorporation of designs and materials within systems.

(U) This paper elaborates on the nature of NBCCS, its sub-categories, current regulations for implementation including the role of the Deputy Assistant to the Secretary of Defense (Atomic Energy) (Chemical/Biological Matters), how it is implemented in the Defense Acquisition Board processes, and the evolving efforts for its expression in performance vs fabrication standards. All will be discussed within the context of the initiative for Combined Battlefield Environmental Effects (CBEE) within the Department of Defense.

UNCLASSIFIED

Approved for public release; distribution is unlimited.

## UNCLASSIFIED

### (U) INTRODUCTION

(U) To ensure mission effectiveness in NBC contaminated environments, two complementary approaches are employed. The first, sometimes called "doctrinal" NBC survivability, is comprised of three tenets: avoidance, protection, and decontamination. In addition to the operational measures taken to effect these tenets, integration of NBC defensive materiel into host systems is also necessary. For example, avoidance involves inclusion of detection equipment for warning, monitoring, and reconnaissance. Protection, both individual and collective, is achieved by integration of masks, protective ensembles, and/or filtration equipment. Decontamination is accomplished by either carrying or having available items and materials to remove and "neutralize" the harmful effects of contamination. The second of the complementary approaches is NBC contamination survivability (NBCCS). It is often referred to as "regulatory" NBCCS and is also comprised of three tenets. NBCCS is the main subject of this paper.

### (U) SCOPE

(U) With the stated goal of acceptable mission effectiveness, NBCCS addresses three ways that missions may be degraded or fail. First, NBC environments (including decontaminants and/or decontamination processes) may result in degraded or failed mission critical/essential functions of materiel. NBCCS addresses this issue of acceptable functionality by requiring materiel to exhibit a characteristic called **Hardness**. Despite other uses of this term in survivability, within NBCCS it concerns the acceptable functioning of materiel.

(U) Second, the protective measures of personnel being at Mission Oriented Protective Posture (MOPP) Level IV, i.e. complete ensemble, mask, etc., can degrade performance of mission critical/essential tasks. NBCCS addresses this issue of acceptable performance of tasks by requiring materiel to exhibit a characteristic called **Compatibility**.

(U) Finally, because removal and "neutralization" of contamination is labor intensive and logistically burdening, missions may be unacceptably affected by materiel being "off-line" undergoing decontamination. Simplification of the process of decontamination is achieved by NBCCS through requiring materiel to be capable of efficient and effective decontamination. The characteristic of materiel to this end is called **Decontaminability**.

UNCLASSIFIED

## UNCLASSIFIED

(U) The goal, then, of NBCCS is to have materiel exhibit characteristics of hardness, compatibility, and decontaminability to complement the measures for avoidance, protection, and decontamination in order to ensure overall, acceptable mission effectiveness.

### (U) CRITERIA

(U) Currently the United States Army Nuclear and Chemical Agency located at Ft. Belvoir, VA issues Headquarters Department of Army (HQDA) Approved Quantitative NBCCS Criteria to developers of Army materiel in fulfillment of Army Regulation (AR) 70-75, "Survivability of Army Personnel and Materiel" (1995). These criteria are virtually identical (except for some administrative verbiage) to the international criteria of Quadripartite Standardization Agreement (QSTAG) 747. Both the latest HQDA and QSTAG documents are dated 1991. AR 70-75 is the Army implementation of Department of Defense Instruction (DoDI) 5000.2, Part 6F (1991).

(U) Needless to say in the current era of acquisition reform, many of these documents are being revised. At the time of writing of this paper, final revisions are not yet available. Therefore, we can not give definitive, updated information. However, we will offer comments on several of the initiatives now active. By the time this appears in print, we expect several of the initiatives to be completed.

### (U) SELECTED INITIATIVES

(U) The present-day environment in acquisition strategy is to buy commercial-off-the-shelf (COTS) or non-developmental items (NDI). If these are not feasible and development is necessary, then commercial rather than military standards/specifications are preferred. In any case, "performance" versus "fabrication" standards/specifications are to be used. "Performance" specifications characterize form/fit/function, functional requirements, and/or service (use) environmental conditions. On the other hand, "fabrication" specifications dictate designs, materials, and/or manufacturing processes. Because NBCCS is usually implemented by use of suggested or recommended designs and materials, citing NBCCS as a necessary requirement in acquisition is seen as requiring a "fabrication" type specification. In reality, citing NBCCS as a requirement meeting the criteria for hardness, compatibility, and decontaminability has always been a "performance" type requirement. That is, materiel must function acceptably (hardness), must be useable in NBC environments (compatibility), and must be restorable to use by unprotected personnel are clearly "performance" requirements. Note that the mandate to use Chemical Agent Resistant Coating (CARC) is not and never was part of the NBCCS program. Use of CARC is a separate requirement. Therefore, NBCCS is and has been a performance requirement. Implementation, however, has been expressed in "fabrication" terms.

UNCLASSIFIED



## UNCLASSIFIED

(U) Within the Department of Defense (DoD), there appears a number of standards, specifications, and other dictates for a bewildering number of survivability-like issues for a wide variety of threats. A DoD initiative exists to distill this number down to a minimal set. This initiative is the one on Combined Battlefield Environmental Effects (CBEE). NBCCS is included within this effort. A hierarchy of work groups is addressing the CBEE effort headed by the Office of the Assistant to the Secretary of Defense (Atomic Energy), OATSD(AE). Draft consolidated, performance-type specifications/standards are being prepared.

(U) The American Institute of Aeronautics and Astronautics (AIAA) in conjunction with the Joint Technical Coordinating Group - Aircraft Survivability (JTTCG/AS) is developing an overarching survivability performance specification/standard. Although the effort deals with aircraft, the form should be adaptable to other types of materiel.

(U) Also, under revision is the DoD capstone acquisition document DoD Directive 5000.1 and supporting materials. Although not published as of the date of this writing, some reforms to the acquisition process have already been instituted. One of these is the use of Overarching Integrated Product Teams (OIPT) to streamline the processes of the Defense Acquisition Board (DAB). The ATSD(AE) through his deputy for chemical/biological matters, DATSD(AE)(CB/M), supports the OIPTs for NBCCS matters. In fact, through the request of this deputy and with the concurrence of the Assistant Secretary of the Army for Research, Development, and Acquisition (ASA(RDA)), one of the authors (WSM) serves on the DoD OIPTs. Further strengthening of NBCCS in the acquisition process is expected in the revisions to 5000.1 and supporting documents.

### (U) JOINT NBC MANAGEMENT STRUCTURE

(U) Title XVII of the National Defense Authorization Act for Fiscal Year 1994 (Public Law 103-160) among other issues mandated that DoD consolidate management of (N)BC issues and have the Army serve as executive agent for (N)BC matters. In response to this the Secretary of Defense designated the ATSD(AE) and his DATSD(AE)(CB/M) as the single DoD element for NBC matters. Subsequently through a Joint Service Agreement (JSA), the Army serves as Executive Agent via a Joint NBC Defense Board (JNBCD Bd) co-chaired by the ASA(RDA) and Vice Chief of Staff of the Army. Per the JSA the JNBCD Bd oversees the efforts of a Joint Service Integration Group (JSIG) and Joint Service Materiel Group (JSMG). Throughout the development and approval of the management processes and structure via these organizational elements, the leadership has repeatedly supported the inclusion of NBCCS as an integral aspect. There are differing opinions, however, but to date NBCCS remains an important aspect of NBC defense.

UNCLASSIFIED

UNCLASSIFIED

(U) **CONCLUSION**

(U) NBCCS with its characteristics of hardness, compatibility, and decontaminability complements the familiar tenets of NBC defense: avoidance, protection, and decontamination. The criteria for NBCCS with appropriate interpretation (and perhaps minor modification) already fit into the trends of acquisition reform for performance versus fabrication standards. NBCCS issues are integral to DoD initiatives including revision of the 5000 series and the CBEE effort to minimize the number and type of required standards. NBCCS is integral to the Joint NBC defense management structure in accordance with Public Law 103-160. The authors of this paper are members of the Executive Office for the JSMG in support of the Joint NBC Defense Board with oversight by ATSD(AE).

UNCLASSIFIED

**UNCLASSIFIED**

THIS PAGE INTENTIONALLY LEFT BLANK

**UNCLASSIFIED**

# UNCLASSIFIED

## NUCLEAR PROTECTION FACTORS FOR THE COMPOSITE ARMORED VEHICLE\*

K. G. Kerris and G. K. Ovrebo  
U. S. Army Research Laboratory  
2800 Powder Mill Road, Adelphi, MD 20783-1197  
and  
J. O. Johnson  
Oak Ridge National Laboratory  
P. O. Box 2008, Oak Ridge, TN 37831-6363

### ABSTRACT

We modeled the major structural components of the Composite Armored Vehicle (CAV) using a simplified geometry that includes most of the important features of the current vehicle design. We calculated initial nuclear radiation protection factors for this simplified CAV model using the vehicle shielding code system MASH. Although the final vehicle structure is expected to be 33 percent lighter than that of a comparable aluminum vehicle, the neutron protection factor of this vehicle is considerably higher than that of a typical armored personnel carrier and even exceeds that of a typical main battle tank. We found that the total protection factor for the crew could be increased by 34 percent by replacing the present titanium hatch with an aluminum/Kevlar hatch of slightly lower mass. The addition of a small quantity of a boron compound to the hull resulted in a further increase of 18 percent, for an overall increase in the total protection factor of 59 percent with no increase in the gross vehicle weight.

### INTRODUCTION

The Composite Armored Vehicle Advanced Technology Demonstrator (CAV/ATD) is a technology test-bed vehicle that is designed to demonstrate critical materials technologies that might be used in designing a future armored vehicle that is lightweight, survivable, and deployable.

The CAV/ATD program included 16 technical goals that had to be met by the test-bed vehicle design. The first priority was to achieve a 33-percent reduction in the weight of the vehicle structure and armor relative to a similar vehicle of traditional metal design. The target maximum vehicle weight was 22 tons (19,958 kg) to make it air-transportable by C-130 cargo aircraft. This design goal mandated extensive use of composite and ceramic materials in the design of the vehicle structure and armor.

---

\* Research sponsored by Army Research Laboratory, Program AH-25, Nuclear Survivability.

# UNCLASSIFIED

## UNCLASSIFIED

Priority 13 required consideration of initial nuclear radiation protection for the crew of the test bed vehicle. The initial impression is that a lightweight vehicle would have lower initial nuclear radiation protection factors than a traditional heavier vehicle since radiation shielding tends to be a function of shield mass to a first approximation. On the other hand, the extensive use of hydrogenous materials (composite plastics) would tend to increase the neutron shielding effectiveness of the vehicle structure and thus increase the neutron and total protection factors.

The objective of this study was to develop an estimate of the initial nuclear radiation protection factors for the CAV/ATD and to make suggestions for increasing radiation protection by incorporating relatively simple, low-cost design changes while incurring negligible weight penalty.

### TECHNICAL APPROACH

We developed two simplified target descriptions of the CAV/ATD. The first one, designated Mark 1, was extremely simplified, being basically a rectangular parallelepiped, or box, consisting of only 14 regions and 10 materials. Initial radiation protection factors based on this simple model were reported at the 1995 Combat Vehicle Survivability Symposium (ref. 1).

Because the results of that study were very encouraging, we developed a much more detailed target description, designated Mark 2. The Mk. 2 target description contains 120 regions and 18 materials. The multiply-layered walls were much more accurately represented in this second model, as were the sloping front glacis and important interior detail.

### DEFINITION OF VEHICLE MODEL

The baseline Mk. 2 vehicle model was completely closed up, with no hatches or hatch openings. In addition to this baseline vehicle, we analyzed six variants of the baseline vehicle as defined below:

1. Baseline Vehicle  
Closed up: No Hatches, No Hatch Openings
2. Hatch Configuration Variants
  - 2.1 Open Hatches
  - 2.2 Titanium AGS Hatches  
(1.22 in. 6-4 Titanium)
  - 2.3 Aluminum-Kevlar Hatches  
(1.00 in. Aluminum + 2.00 in. Kevlar)
  - 2.4 RHA-Kevlar Hatches  
(0.50 in. RHA + 1.00 in. Kevlar)
3. Addition of Boron Compounds to the Hull
  - 3.1 Boron Carbide Loaded EPDM Rubber  
(All EPDM rubber contains 7.5 percent by weight B<sub>4</sub>C)
  - 3.2 Boron Carbide Paint on Exterior Surfaces  
(Thin coating of B<sub>4</sub>C paint)

UNCLASSIFIED

## UNCLASSIFIED

Hatch variant 2.2 (with titanium AGS hatches) represents the vehicle as presently configured. We analyzed a number of variants to attempt to identify a number of best- and worst-case designs to illustrate the impact of design details on initial nuclear radiation protection.

All seven vehicle variants were configured as an armored personnel carrier with two crew members and carrying a squad of six infantrymen. The squad was represented by either one or two typical soldiers in the squad compartment.

Figure 1 shows an exterior perspective view of the vehicle model used in this study. We modeled sprockets, road wheels, and skirt armor, but for the sake of simplicity did not model the tracks. This omission should have a minimal impact on any of the nuclear protection factor results. Figure 2 is a cut-away view showing the location of interior components.

All four hatch variants were expected to degrade the radiation protection of the closed-up (no hatch) baseline vehicle to various degrees. We therefore explored variants of the baseline vehicle that we expected would increase the radiation protection factors by the addition of boron compounds to the outside of the hull. Two relatively simple means for the addition of boron suggested themselves. Since most of the exterior hull materials, as well as the crew compartment vertical armor, include a layer of EPDM rubber, we replaced the pure EPDM rubber with a material consisting of EPDM rubber containing 7.5 percent by weight of finely powdered boron carbide,  $B_4C$ . Alternatively, instead of adding boron carbide to the EPDM rubber, we applied an equivalent thickness of boron, in the form of paint, to the exterior of the vehicle.

Table I defines all materials used in the Mk. 2 vehicle target description.

### CALCULATION OF PROTECTION FACTORS

As was the case for the Mk. 1 vehicle, we calculated protection and reduction factors for initial nuclear radiation for the seven target descriptions described above using the MASH version 1.0 computer code system (ref. 2). Five protection and reduction factors (NPF, GPF, TPF, NRF, and GRF) were calculated for the six detector locations (commander's mid-head and mid-gut, driver's mid-head and mid-gut, and soldier's mid-head and mid-gut) for each of the seven vehicle variants. All calculations were done for an empty vehicle with detectors positioned at the location of the crew members or soldier(s).

In all cases the radiation source was the USANCA reference environment for initial nuclear radiation (ref. 3, 4). For each of the seven vehicle variants and six detector locations, we calculated 100,000 histories of primary incident particles, resulting in a fractional standard deviation (fsd) of less than 5 percent. The results of the MASH calculations are summarized in tables II - IV. In these tables, "Crew" refers to protection factors averaged over the two crew positions (commander and driver, mid-head and mid-gut). "Squad" refers to protection factors averaged over the six typical squad positions.

UNCLASSIFIED

UNCLASSIFIED

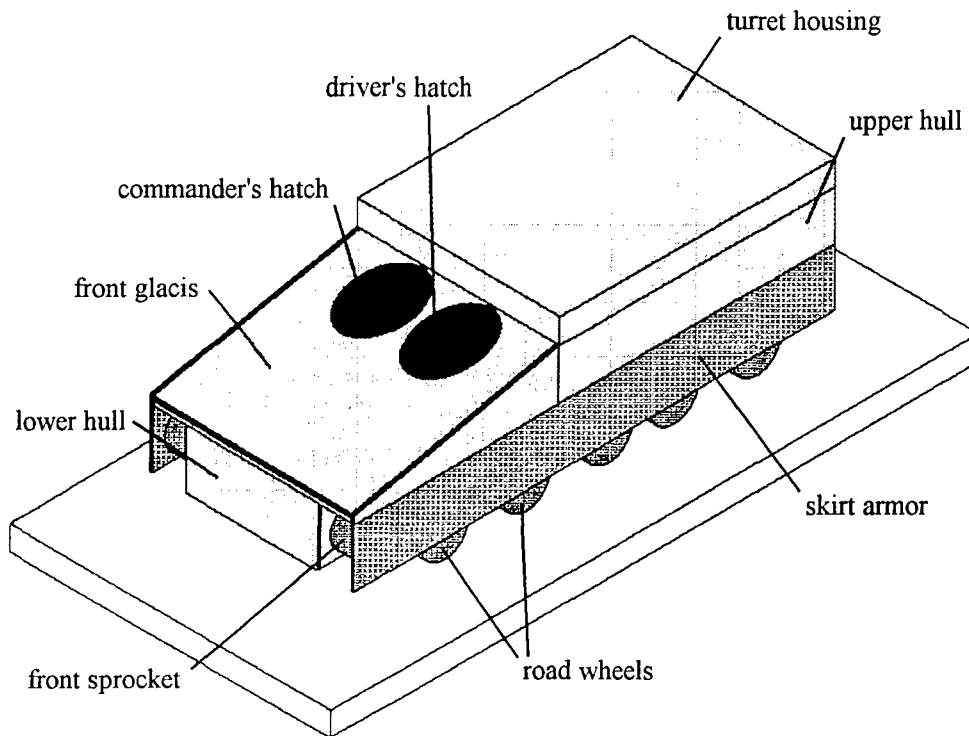


Figure 1. Exterior View of Simplified CAV Vehicle Model, Mk. 2.

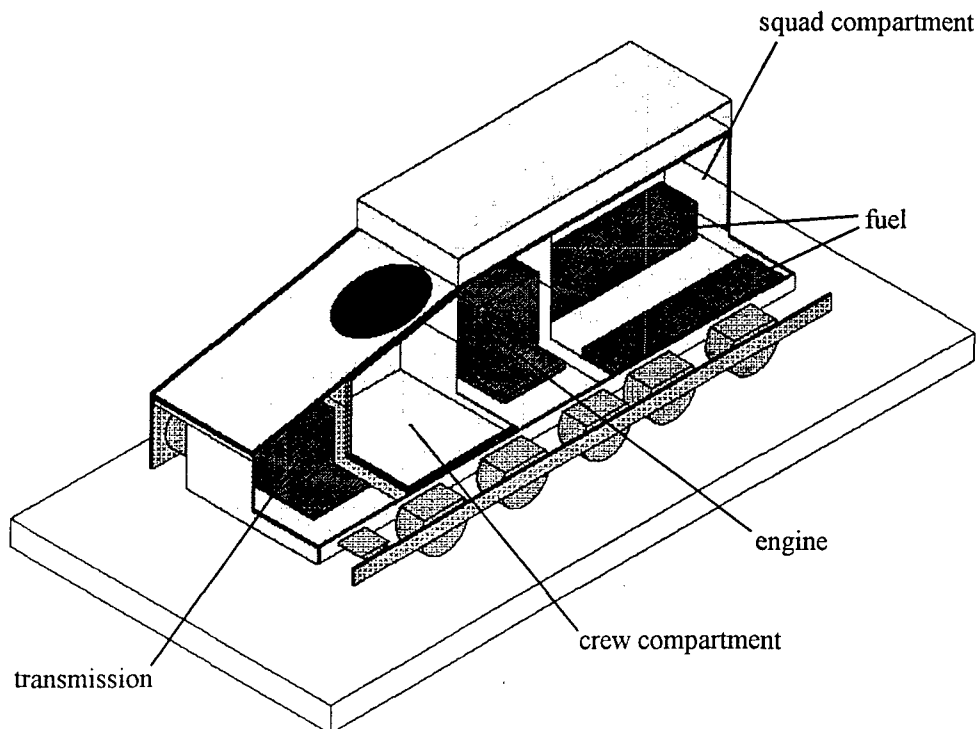


Figure 2. Cut-Away View of Simplified CAV Vehicle Model, Mk. 2.

UNCLASSIFIED

# UNCLASSIFIED

Table I. Material Composition of CAV Mk. 2 Vehicle Structure

Turret Housing	0.38 in.	S-2 Glass/PPS
Top & Sides of Upper Hull,	0.18 in.	S-2 Glass/Epoxy
Rear Upper Hull & Ramp,	0.60 in.	Alumina
Front Upper & Lower Hull	0.06 in.	EPDM Rubber
	0.50 in.	S-2 Glass/Epoxy
	0.12 in.	S-2 Glass/Phenolic
Front Glacis	0.18 in.	S-2 Glass/Epoxy
	0.60 in.	Alumina
	0.06 in.	EPDM Rubber
	0.50 in.	S-2 Glass/Epoxy
	0.12 in.	S-2 Glass/Phenolic
	0.50 in.	Titanium
Lower Hull Side, Rear, Bottom Front	1.00 in.	S-2 Glass/PPS
Crew Compartment Shell,	0.50 in.	S-2 Glass/PPS
Crew Capsule Bulkhead,		
Parts of Lower Hull, Lower Sponson		
Lower Hull Foam Panel	0.25 in.	S-2 Glass/PPS
(under Crew Compartment)	2.00 in.	Syntac 351 Foam
	0.25 in.	S-2 Glass/PPS
Crew Compartment Vertical Armor	1.13 in.	Silicon Carbide
	0.13 in.	EPDM Rubber
	1.00 in.	Titanium
	0.25 in.	No Spall
Crew Compartment Glacis Armor	0.75 in.	Titanium
	0.25 in.	No Spall
Skirt Armor	0.06 in.	Kevlar
	0.45 in.	Silicon Carbide
	0.56 in.	S-2/Polyester
	0.09 in.	Kevlar
AGS Hatch	1.22 in.	Titanium
Aluminum/Kevlar Hatch	1.00 in.	Aluminum 7039
	2.00 in.	Kevlar
RHA/Kevlar Hatch	0.50 in.	Steel 4340
	1.00 in.	Kevlar

UNCLASSIFIED



## UNCLASSIFIED

Table II. Neutron Protection Factors

Vehicle Configuration	Crew	Squad
Baseline (Closed-Up) Vehicle	2.322	1.844
Open Hatches	1.652	1.808
AGS (Titanium) Hatches	1.685	1.833
Al / Kevlar Hatches	2.347	1.848
RHA / Kevlar Hatches	2.031	1.852
Boron-Loaded EPDM Rubber	2.618	1.865
Boron Paint on Exterior	2.494	1.829

Table III. Gamma Protection Factors

Vehicle Configuration	Crew	Squad
Baseline (Closed-Up) Vehicle	4.624	2.160
Open Hatches	3.399	2.106
AGS (Titanium) Hatches	4.071	2.178
Al / Kevlar Hatches	4.055	2.150
RHA / Kevlar Hatches	4.072	2.164
Boron-Loaded EPDM Rubber	4.645	2.154
Boron Paint on Exterior	4.606	2.143

Table IV. Total Protection Factors

Vehicle Configuration	Crew	Squad
Baseline (Closed-Up) Vehicle	2.584	1.901
Open Hatches	1.846	1.862
AGS (Titanium) Hatches	1.913	1.894
Al / Kevlar Hatches	2.568	1.903
RHA / Kevlar Hatches	2.262	1.908
Boron-Loaded EPDM Rubber	2.874	1.917
Boron Paint on Exterior	2.751	1.885

UNCLASSIFIED

## UNCLASSIFIED

### DISCUSSION OF SQUAD PROTECTION FACTORS

The relative thicknesses and types of materials that surround the squad and the crew account for the significantly lower protection factors for the squad positions as compared to the crew positions. Neutron protection depends primarily on the areal density of hydrogen atoms surrounding a given detector position; gamma protection depends on the areal mass-density of material surrounding the detector. Because of the considerably thicker layers of armor and vehicle structure around the crew compartment, a typical crew position is surrounded by approximately 3.5 times as many hydrogen atoms per unit area and 3.5 times the mass per unit area than a typical squad position. The result is a 20 percent reduction in NPF and a 50 percent reduction in GPF for the squad compartment relative to the crew compartment. The squad compartment NPF and GPF are practically unaffected by any of the vehicle design variations that we considered. Changes in the hatch configurations affect the crew compartment but not the squad compartment. The addition of boron to the EPDM rubber affects primarily the crew compartment because its wall structure contains three times as much EPDM rubber than the squad compartment walls.

### DISCUSSION OF CREW GAMMA PROTECTION FACTORS

The crew compartment gamma protection factors for the baseline vehicle and the six variants are shown graphically in figure 3. Recall that gamma protection factors depend primarily on the areal density of the walls surrounding a given detector position. The areal density of material surrounding the crew positions is the same for all seven vehicle variants, *except for the hatches*. The lowest GPF occurs for the open hatch case (hatch areal density = 0). We deliberately chose the aluminum/Kevlar and RHA/Kevlar hatch thicknesses so that their areal density was approximately equal to that of the titanium hatch ( $\approx 27$  lbs./sq. ft.). Note that all three hatch variants have about the same GPF. Finally, since the very small amount of boron carbide adds negligible areal density, the three no-hatch, completely closed up variants (average areal density  $\approx 68$  lbs./sq. ft.) all have approximately equal GPF.

### DISCUSSION OF CREW NEUTRON PROTECTION FACTORS

The crew compartment neutron protection factors exhibit the most variation among the seven vehicle variants. This is shown graphically in figure 4 a. In order to understand the NPF, we must consider the relative contributions of penetrating neutron dose,  $D_{ni}$ , and armor-generated secondary gamma dose,  $D_{gn}$ . The definition of neutron protection factor is

$$NPF = D_{no} / (D_{ni} + D_{gn}).$$

The free-field neutron dose,  $D_{no}$ , is the same for all seven cases; all variation in NPF must therefore be attributed to  $D_{ni}$  and  $D_{gn}$ .  $D_{ni}$  and  $D_{gn}$  are shown in the form of a stacked bar graph in figure 4 b. The differences in NPF can best be understood by studying this figure.

Consider the "Open Hatches" case. Not surprisingly, the penetrating neutron dose,  $D_{ni}$ , is more

UNCLASSIFIED

UNCLASSIFIED

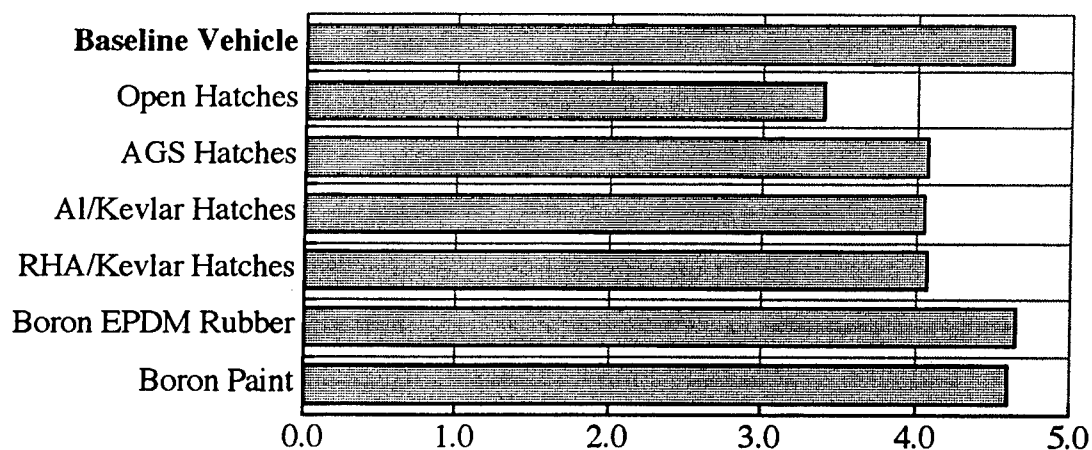


Figure 3. Gamma Protection Factors, Crew Average

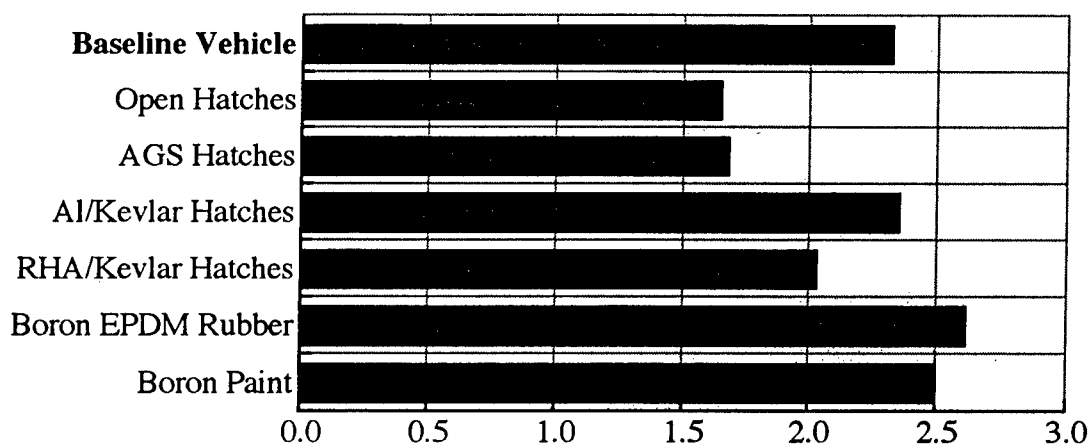


Figure 4 a. Neutron Protection Factors, Crew Average

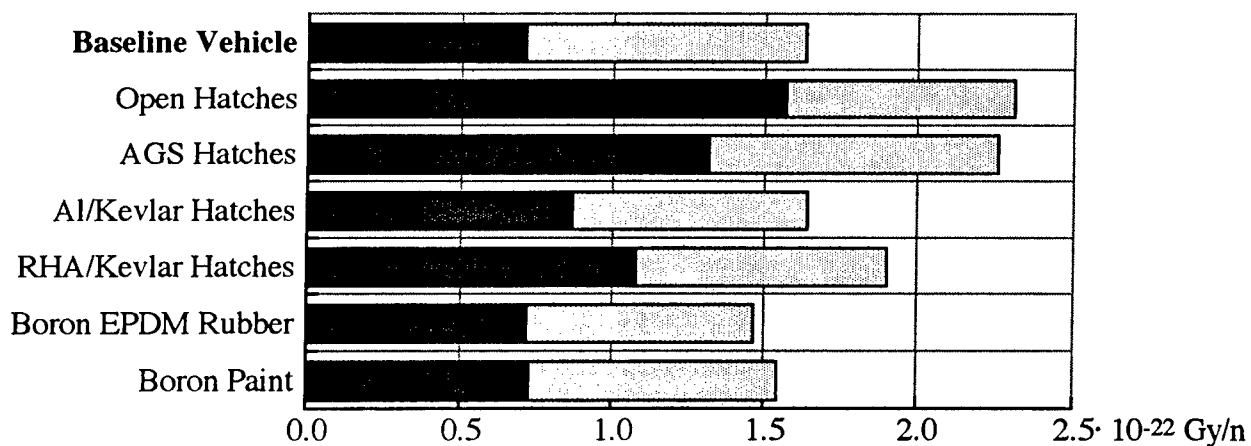


Figure 4 b. In-Vehicle Doses from Neutrons, Crew Average

$$D_{no} = 3.86 \cdot 10^{-22} \text{ Gy/n}$$

UNCLASSIFIED

## UNCLASSIFIED

than twice that for the baseline vehicle. The armor-generated secondary gamma dose,  $D_{gn}$ , is somewhat lower because there is less armor. However, the net result is an interior dose from neutrons that is 40 percent higher than for the baseline vehicle.

The "AGS Hatches" case is not much better, although the relative proportions of  $D_{ni}$  and  $D_{gn}$  are different. In this case, the armor-generated secondary gamma dose is about the same as for the baseline vehicle, but the transmitted neutron dose is 80 percent higher, yielding the 25 percent reduction in NPF.

The "Al/Kevlar Hatches" case has about the same NPF as the baseline vehicle. This is because although the transmitted neutron dose is somewhat higher, this increase is almost exactly offset by a lower secondary gamma dose.

The "RHA/Kevlar Hatches" case has a 12 percent lower NPF primarily because the transmitted neutron dose is higher than for the Al/Kevlar hatches (which have twice the thickness of Kevlar).

Finally, the two cases where boron was added to the hull have practically the same transmitted neutron dose as the baseline vehicle, but a lower secondary gamma dose, accounting for the higher NPF of these two cases. The secondary gamma dose reduction is higher for the case where the boron layer is buried deep within the hull structure in the EPDM rubber than for the case where the boron is applied to the outside surface of the vehicle. Boron reduces armor-generated secondary gamma dose by absorbing thermal neutrons that can produce secondary gamma rays by thermal neutron capture reactions. The thermal neutron flux is greater inside the hull structure than on the surface because the hull material thermalizes the incident fast neutron flux. The buried layer of boron is thus more effective in reducing secondary gamma rays.

### CONCLUSIONS

It is important to note again that these initial nuclear radiation protection factor results were derived for a very simple vehicle model that bears only a superficial resemblance to the likely final vehicle design. However, notwithstanding the preliminary nature of these data, we can draw certain conclusions for this particular CAV Mk. 2 model:

1. The average crew neutron protection factor, NPF, of 1.70 (baseline with AGS hatches) is quite high for an armored personnel carrier and is indeed higher than that of a typical main battle tank. Furthermore, considerable improvement of the NPF is possible by relatively simple means. It appears that an increase of greater than 50 percent in the NPF, to 2.62, could be realized by replacing the commander's and driver's hatches and by adding a boron compound to the EPDM rubber layers in the upper hull, front glacis, and vertical crew compartment armor. This increase could be achieved with a negligible change in the vehicle structure weight. A neutron protection factor of 2.62 compares very favorably with many modern main battle tanks.
2. The average crew gamma protection factor, GPF, of 4.02 (baseline with AGS hatches) is  $\approx 60$

UNCLASSIFIED

## UNCLASSIFIED

percent higher than for a typical armored personnel carrier. This GPF could be increased by another  $\approx 15$  percent to 4.65 by the same improvements suggested above. This remarkable result is due to the relatively large mass of material surrounding the crew compartment.

3. The squad NPF of 1.83 and GPF of 2.18 are considerably lower than corresponding crew protection factors. Nevertheless, they are still quite respectable when compared to protection factors of a 'typical' APC.

These comparisons are summarized in table V.

Table V. Comparison of Initial Nuclear Radiation Protection Factors

	Neutron Protection Factor, NPF	Gamma Protection Factor, GPF
Typical Armored Personnel Carrier:	1.0	2.5
Typical Main Battle Tank:	1.5	20.
<b>CAV Mk. 2 Vehicle</b>		
<u>CREW:</u>		
Baseline CAV with AGS Hatches:	1.70	4.02
Optimized CAV	2.62	4.65
<u>SQUAD:</u>		
Baseline CAV with AGS Hatches:	1.83	2.18
Optimized CAV	1.87	2.15

### REFERENCES

1. Proceedings of the 6th Annual TACOM Combat Vehicle Symposium, March 1995.
2. J. O. Johnson, ed., *A User's Manual for MASH 1.0 --A Monte Carlo Adjoint Shielding Code*, ORNL/TM-11778, Oak Ridge National Laboratory, January 1992.
3. "Standard USANCA Protocol for Determining the Protection Factor of a Combat Vehicle", USANCA Memo, signed for the Commander by A. M. Novotny, Jr., Major, FA, XO, 29 Aug 90.
4. NATO Allied Engineering Publication AEP-14, *Guidelines for the Armored Fighting Vehicle Designer to Improve Nuclear Radiation Protection*, Edition 3, February 1994.

UNCLASSIFIED

UNCLASSIFIED

## DEVELOPMENT OF A FALLOUT SIMULANT

Craig R. Heimbach, Mark A. Oliver, Michael B. Stanka  
Aberdeen Test Center  
Aberdeen Proving Ground, MD 21005-5059

### ABSTRACT

A radioactive simulant for fallout has been developed. its properties are compared to those of fallout from small fission weapons. This simulant was used to measure the protection factor of a BTR-80 whose top surface was contaminated. About half of the interior exposure will be due to fallout on the vehicle, about half from fallout on the ground.

### INTRODUCTION

The radioactive fallout from a nuclear weapon may cover an extremely large area. Weapons of 10-20 kilotons (kt) can easily cover tens of thousands of square miles with measurable radioactivity (ref. 1,2). Such a large area may encompass an entire combat region. If the armed forces are not prepared to manage this situation, an entire battle area may become off limits.

The potential for such an event in an uncertain world is real. The ability for hostile forces to cause such an event is increasing.

The Aberdeen Pulse Radiation Facility (APRF) is developing techniques to test military equipment in a fallout environment. The foundation of this effort is the development of a fallout simulant. This simulant should have appropriate physical and radiological properties to perform meaningful tests.

### SIMULATION OF FALLOUT

Fallout is not a constant, unvarying type of material. Its properties depend on the type of nuclear weapon generating it, the height of burst, the time after burst, the distance from ground zero, and local topography. The practice is to find a consistent environment to meaningfully rank potential equipments, and to predict behavior in an actual battlefield environment.

UNCLASSIFIED

Distribution authorized to U.S. Government agencies and their contractors, Test and Evaluation, April 1995. Other requests shall be referred to Commander, Aberdeen Test Center, STEAC-SE, Aberdeen Proving Ground, MD 21005-5059.

The simulant used by the APRF had been pioneered by the Nuclear Defense Laboratory (NDL, ref. 3).  $\text{La}_2\text{O}_3$  was chemically combined with sand of an appropriate particle size distribution. The mixture was then activated by exposure to neutrons. The activated material was diluted into non-radioactive sand and mixed to provide a uniform fallout simulant of the appropriate mass and activity.

### Size

The particle size of the sand was selected to provide a good match to the threat. From an actual weapon, the size distribution depends on the time after burst and distance from the event. Larger particles tend to fall sooner and closer to ground zero.

Figure 1 shows the particle sizes of the simulant versus the particle sizes from a "typical" weapon (ref. 1,4). The simulant shows relatively fewer small particles. Representative Nevada Test Site soil assumed by DELFIC (ref. 4) is  $130\text{ }\mu\text{m}$  for the median diameter by volume.

All of the particle size distributions are log-normal. With this distribution, the logarithms of the sizes are normally distributed.

Care must be taken in the interpretation of the particle size distributions on whether the number of particles, the mass (volume) or radioactivity of the distribution is being shown. The distribution of radioactivity will follow the mass if the particles are uniformly radioactive through the interior. It will follow the surface area if the radioactive material is deposited on the particle surface, as in the case with the simulant.

For particles from a weapon, the distribution is uniform through the volume for an air burst. For a near-ground burst, radioactivity tends to plate out on the surface of the particles. As the height of burst varies, the relative fraction will also vary.

### Mass

Approximately  $5.4 \times 10^{-3}\text{ mg/cm}^2$  of fallout material will give 1 R/hr at 1 hour after burst (ref. 2). To determine the amount of simulant to use in  $\text{mg/cm}^2$ , multiply the 1-hour threat in R/hr by  $5.4 \times 10^{-3}$ .

The radioactivity of the simulant need not equal the radioactivity of actual fallout. For example, the protection factor of a vehicle will be the ratio of the inside dose to the activity of the source. This ratio will be independent of the source intensity. To determine the amount of radioactivity in a clogged filter, the measured radioactivity must be scaled to account for the correct radioactivity per gram.

## UNCLASSIFIED

### Radioactive decay

The overall decay of radiation follows a

$$R_t = R_1 t^{-1.2} \quad (1)$$

where  $R_t$  and  $R_1$  are the dose rates at time  $t$  and at unit time after the burst (ref. 1). This equation may be used from 30 minutes to 6 months after the burst. Any units may be used for time in this equation, so long as  $R_1$  is the rate for  $t=1$ . Usually, hours are used and  $R_1$  is the dose rate at one hour after burst and  $R_t$  is the rate at  $t$  hours afterwards.

For the purpose of measuring protection factors, there is no need for the simulation to follow this decay mode. La-140 does not. It has a 40 hour half-life. This is long enough to perform experiments without the time variation of the field being a problem. It is short enough to ensure decay to background within a few weeks.

### Spectrum

The gamma-ray spectrum will largely follow that of fission of U-235 for a fission weapon. Additional components will include the activation of material surrounding the weapon and activation of soil sucked up into the fireball. This spectrum will change as a function of time, as different radioactive isotopes decay at different rates (ref. 5).

For standardization purposes, the spectrum at 1 hour after burst is used for protection-factor measurements (ref. 6). Figure 2 shows that this is quite conservative for times 1 to 5 days after burst.

The standard 1-hour spectrum gives about the same protection factors as Co-60 and La-140, making testing easier. Figure 3 shows transmission factors for Co-60 and La-140 versus the NATO reference.

### Chemistry

The chemistry of the simulant is not important for protection factor tests. It may become important for other tests, such as decontamination, if chemical washes are used.



UNCLASSIFIED

APPLICATION

Radioactive fallout will accumulate on the surface of a vehicle, causing exposure to personnel. This might arise from either a direct deposition of fallout on the vehicle, or from accumulation of radioactive dirt which might be thrown up by driving over a radioactive area. The accumulation of radioactivity on the outer surfaces of a vehicle may be a hazard to the crew. This paper describes a feasibility test which has demonstrated the ability of the APRF to generate and use a fallout simulant in the testing of military hardware. Additional details may be found in Reference 7.

A Russian armored personnel carrier, the BTR-80, was used for the demonstration. It had the advantages of being readily available, free, and of a boxy shape to simplify the analysis. Being relatively thin, it promised a low and easily measurable protection factor.

The effects of radiation on crew are typically reported in terms of protection factors. This is not directly applicable in this case. In the absence of a vehicle, there would be no accumulation of radiation, and no threat. The decision was made to evaluate the vehicle in terms of mRad/hr at crew locations for a given mCi/m<sup>2</sup> of fallout deposited. This will be further developed into a protection factor below.

To avoid spreading of contamination, a structure was erected inside the APRF silo. The dimensions (11.3 m long × 6.1 m wide × 4.1 m high) were large enough to allow 1.5 m clearance around all sides of the vehicle, including the top. The enclosure consisted of wood frame with a plastic liner. Any simulant which escaped the enclosure would still be inside the silo, and be caught with absolute filters to prevent release to the environment.

To distribute the simulant on the vehicle, a set of four air spreaders was used. Each spreader consisted of a feed bucket, a nozzle which sprayed the sand with pressurized air, and a connecting plastic tube. Eight collection dishes were located on the vehicle to measure the quality of the distribution. Their locations on the BTR-80 are shown in Figure 4.

The horizontal portions of the top surface accumulated the most of the fallout. Vertical surfaces accumulated little. For example, the turret sides retained little, but sand accumulated at the turret base.

The left front of the vehicle had little exposure. This was not due to the tank itself, but due to an apparent misalignment of one of the nozzles. This may have happened when the radioactive sand was loaded into the buckets. The left front corresponds to the driver's position, and explains why his exposure is less than the others.

## UNCLASSIFIED

Sample collection and removal of material from the floor required entry into the contaminated test area after spraying. Entry was made using full radiation protection equipment.

### INSTRUMENTATION

The BTR-80 was instrumented with eight Geiger counters. These were located in driver, turret, and two passenger locations, head and seat in each location. These determined radiation exposure levels inside the vehicle due to the fallout.

The eight samples from the top of the vehicle were analyzed with a high-purity Germanium gamma-ray detector. These determined the source intensity causing the personnel exposure. They also verified the uniformity of radiation mixture in the simulant.

### RESULTS

A total of 11.6 kg of fallout simulant was spread inside the containment shelter. Virtually all the sand was deposited on the tank, giving an average density of  $0.054 \text{ g/cm}^2$ . Very little fell to the floor, and this was removed before measurements were made. The mass corresponded to a one-hour dose rate of 10,000 R/hr, although the actual radioactivity was substantially less.

For purposes of comparison, all activities were decay-corrected to a common time of 12:00 on 16 Mar 1995. The activities, as measured per gram of simulant, were within about 15%, indicating a good mixing of the activated material with the carrier material. The activity of the simulant averaged  $0.55 \text{ mCi/m}^2$ . This was the threat to the crew.

The measured dose rates are given in Table I. As might be expected with the simulant on top of the vehicle, all the head positions gave a higher dose than the seat positions.

The driver shows substantially less dose than the other positions, but this is probably due to the distribution of simulant on the vehicle. Due to misalignment of one of the spray nozzles, the driver's area received only minimal coverage.

The extra protection given the turret location may be due to the raised turret keeping fallout at a greater distance from the personnel inside, or because the turret was thicker than the remainder of the top.

## UNCLASSIFIED

Table I. Dose rates measured inside BTR-80.

Decay-corrected dose rates in BTR-80	
Location	Dose Rate (mrad/hr)
Driver Head	2.7
Driver Seat	2.1
Turret Head	4.1
Turret Seat	2.9
Left Pass. Head	6.7
Left Pass. Seat	3.0
Right Pass. head	7.1
Right Pass. Seat	4.3

Averaging over all measured positions, gives a dose rate of 4.1 mRad/hr for the threat simulant of 0.55 mCi/m<sup>2</sup>, or a protection of 7.45 mr/hr per mCi/m<sup>2</sup>.

All openings were closed during the fallout exposure, and no vehicle systems were operating during the test. By visual inspection, no simulant penetrated into the vehicle.

### RADIOACTIVE SOURCES

In addition to the test described above, discrete Co-60 and Cs-137 sources were used to measure the protection factors of the BTR-80. A grid with 50 cm spacing was marked on the top surface of the vehicle. A source was placed at one grid point at a time, and the inside dose rates measured. This was done for all the grid points and the results averaged.

Detailed results are given in Reference 8. Table II gives results averaged over in-vehicle location. The Co-60 and Cs-137 distributions were adjusted to have the same distribution as the La-140 simulant.

The protection of the BTR-80 as reported in terms of mr/hr per mCi/m<sup>2</sup> is listed in the second column of the table. These differ artificially because the threat is not the same. For example, one mCi/m<sup>2</sup> of Co-60 delivers substantially more energy than one mCi/m<sup>2</sup> of Cs-137. The last column in the table adjusts for this by dividing the in-vehicle dose rate by

UNCLASSIFIED

the dose rate above an infinite plane contaminated with the same mCi/m<sup>2</sup> as the threat. The resulting number is dimensionless (mr/hr divided by mr/hr) and is titled here the "on-vehicle fallout protection factor". These numbers reflect the actual protection against the incident gamma rays.

Table II. BTR-80 fallout protection factors.

Fallout Simulant	$\frac{\text{mR/hr}}{\text{mCi/m}^2}$	On-vehicle FPF
Co-60 (0.5 m grid)	7.63	3.9
Co-60 (1 m grid)	7.12	4.2
Cs-137 (1 m grid)	1.28	6.7
La-140 (simulant)	7.38	3.8

The Co-60 and La-140 protection factors are quite similar. This is due to the Co-60 and La-140 gamma rays having about the same penetrating power. Cs-137 has reduced penetrating power, and thus a higher protection factor.

#### COMPARISON WITH FREE FIELD

If the BTR-80 were parked in an open area, and the area were covered with fallout, there would be two sources of radiation. The plane area would be covered uniformly and expose the vehicle from the sides and from below. The protection against this would be the standard fallout protection factor. The on-vehicle contamination would be attenuated by the on-vehicle fallout protection factor. The net dose would be the sum of the two.

$$\text{Dose} = \frac{\text{FF}}{\text{FPF}} + \frac{\text{FF}}{\text{on-Veh FPF}} = \frac{\text{FF}}{3} + \frac{\text{FF}}{3.8} \quad (2)$$

The standard FPF used here is not specific to the BTR-80, but generic to light armored vehicles. The net in-vehicle dose would be 50% of the free-field dose, with roughly half coming from the ground and half from the vehicle top.

If the vehicle were moving, or had moved, the relative distribution of fallout on the ground and on the vehicle would change.

UNCLASSIFIED

SUMMARY

A radioactive simulant for fallout has been developed and used. It has been applied to find the protection of a BTR-80 against fallout being deposited on the upper surface. Results have been compared to those found by using isotopic sources. Agreement was good. This may be due in part to the simple, boxy shape of the vehicle. A vehicle with more sloping surfaces might show a different distribution.

Other potential uses for the simulant would be the testing of filters, both in terms of assessing the radioactive hazard and in terms of verifying protection. The degree to which fallout adheres to equipment and clothing, and the ease of decontamination, may also be assessed using this simulant.

ACKNOWLEDGEMENTS

This work was supported by the Defense Nuclear Agency radiation environments program. The National Ground Intelligence Center allowed the use of the vehicle.

REFERENCES

1. "The Effects of Nuclear Weapons", Glasstone and Dolan, Ed., DA Pamphlet 50-3, 1977.
2. "Fallout: Its characteristics and management", K. P. Ferlic, AFRRRI Technical Report TR83-5, 1983.
3. "Cold Weather Decontamination Study - McCoy II", J.C. Maloney, J.L. Meredith, J. Barnard, and C.C. Kilmer, NDL-TR-32, 1962.
4. "DELFIC: Department of Defense Fallout Prediction System, Volume I - Fundamentals", H.G. Norment, DNA 5159F-1, 1979.
5. "Gamma-ray Energy and Angular Distributions above Fallout", R.L. French, Health Physics 11, pp 369-383, 1965.
6. "Guidelines for the Armored Fighting Vehicle Designer to Improve Nuclear Radiation Protection", Allied Engineering Publication AEP-14, Edition 3, 1994, NATO Restricted.
7. "Fallout Investigations on a BTR-80", C.R. Heimbach, CSTA-7706, 1995.
8. "Fallout Contamination Simulation Using Point Sources on a Light Armored Vehicle", M.A. Oliver and M.B. Stanka, ATC-7746, 1995.

UNCLASSIFIED

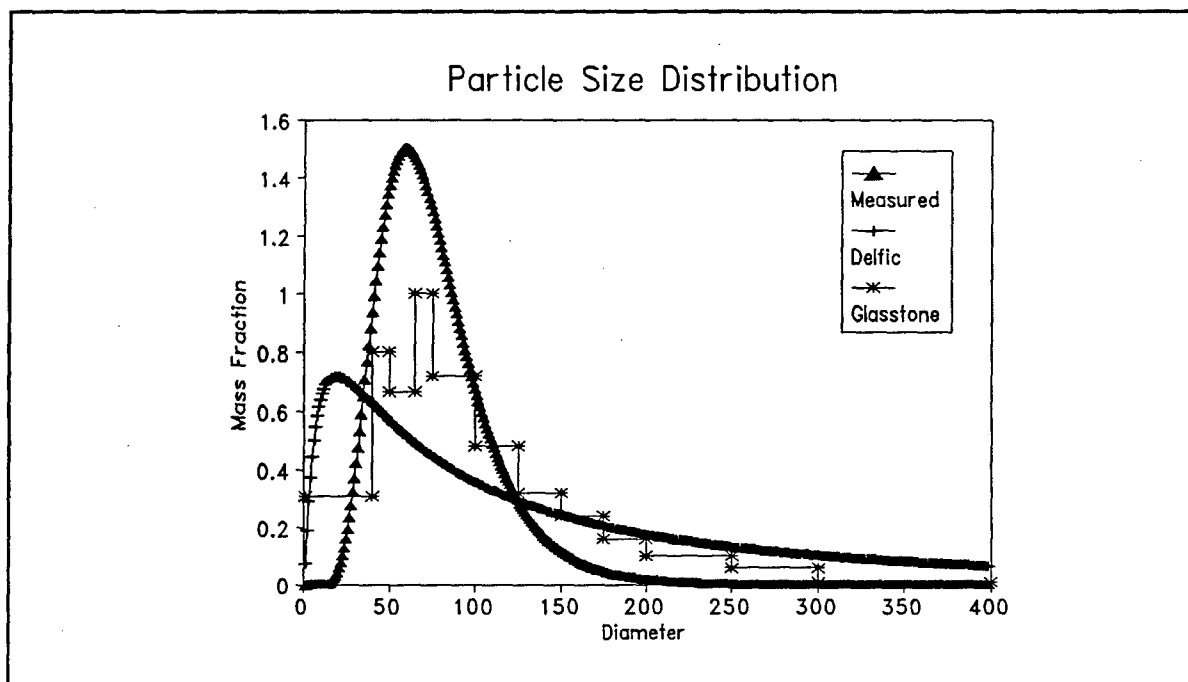


Figure 1. Particle size distribution. Sizes are in  $\mu\text{m}$ .

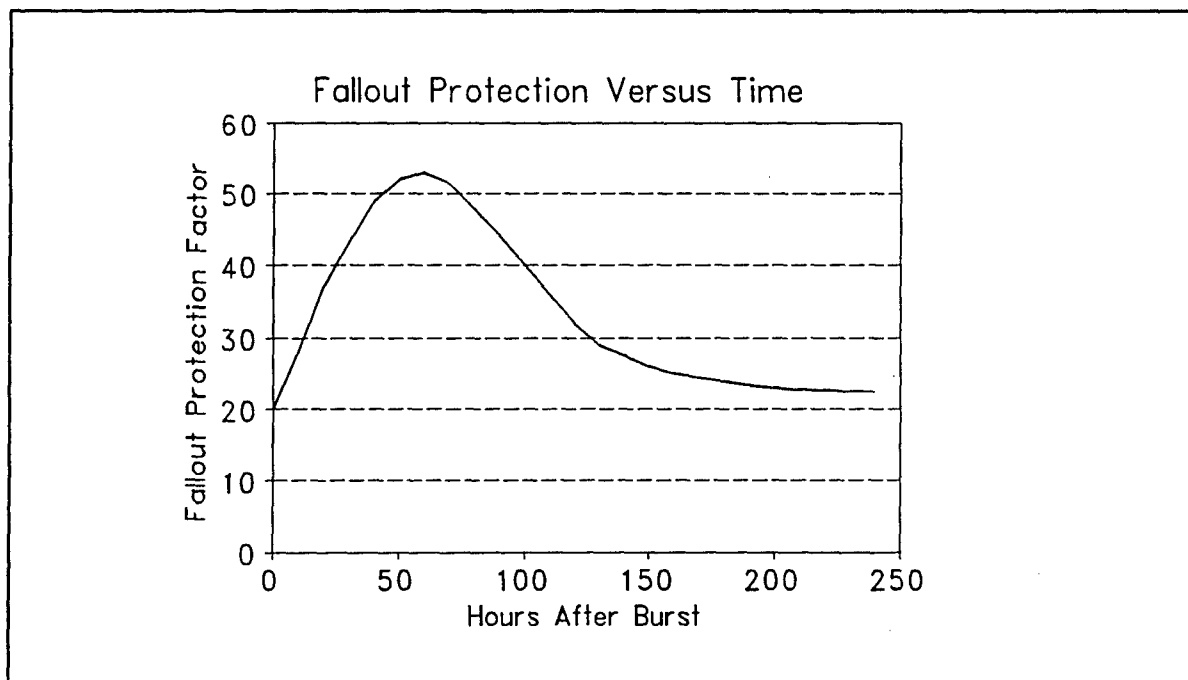


Figure 2. Protection factor versus time after burst.

UNCLASSIFIED

UNCLASSIFIED

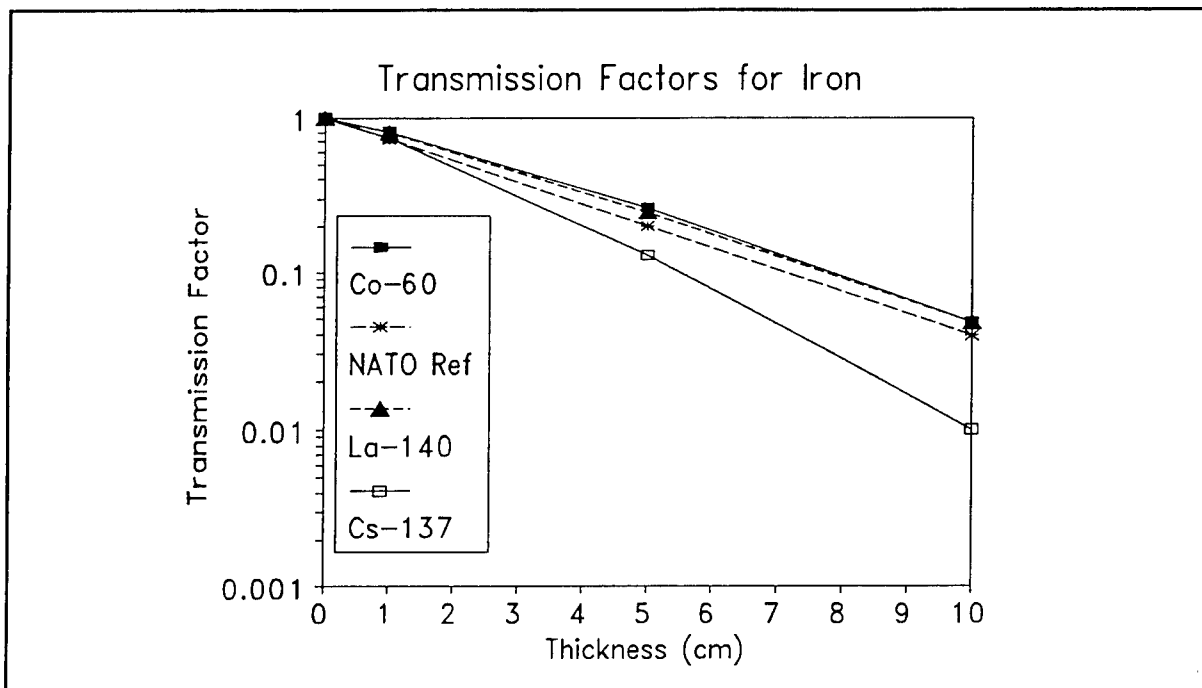


Figure 3. Transmission factors for iron.

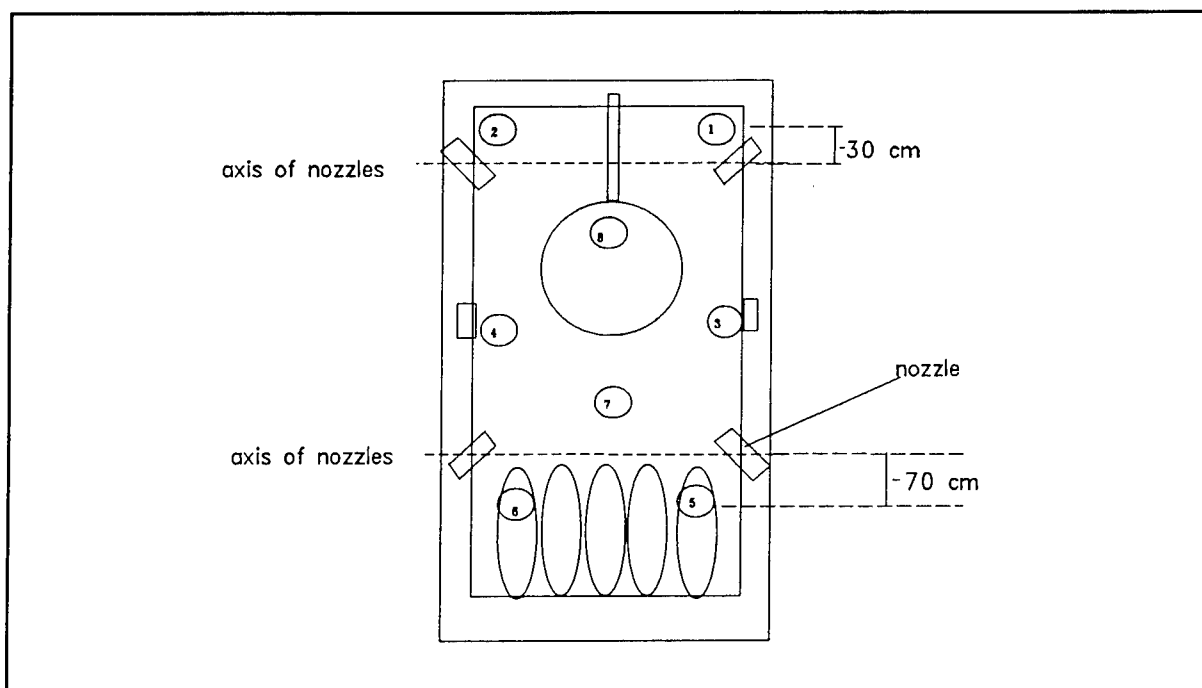


Figure 4. Overview of BTR-80.

UNCLASSIFIED

**UNCLASSIFIED**

**SURVIVABILITY MODEL INTEGRATION AND SYSTEM SURVIVABILITY OPTIMIZATION**  
**SESSION**

**Glasgow Auditorium  
Thursday, March 28, 1996**

**Session Chairman: Dr. William Jackson, TARDEC**

**UNCLASSIFIED**



**UNCLASSIFIED**

**THIS PAGE INTENTIONALLY LEFT BLANK**

**UNCLASSIFIED**

**UNCLASSIFIED**

**Hughes DSO  
Integrated Simulation Environment:  
A Signature Modeling and Analysis Toolset (U)**

Richard Bryant  
Milos Machacek  
Hughes-DSO  
Santa Barbara, Ca. 93117

**ABSTRACT (U)**

(U) The Hughes-DSO Integrated Simulation Environment (ISE) is a multi-spectral computer simulation environment that was developed to measure the effectiveness of computer modeled sensors on a variety of simulated ground targets set in natural background clutter.

(U) The ISE was developed around a small number of government simulation programs and Hughes-DSO developed programs. The government models have been incorporated into a multi-spectral integrated simulation environment through the use of common file formats and data visualization tools.

(U) Here we describe the ISE architecture, and discuss some of the salient integration issues that was addressed during development. Later, we describe the ISE simulation process and how it is used to process digital imagery to produce metrics that may be used to assess sensor effectiveness.

**INTRODUCTION**

(U) The Hughes-DSO Integrated Simulation Environment (ISE) is a multi-spectral computer simulation environment that was developed to measure the effectiveness of computer modeled sensors on a variety of simulated ground targets set in natural background clutter. Targets can be viewed at different aspect angles and can be sized to a set of possible sensor-target ranges. Given a set of calibrated background images that were recorded with far-infrared, near-infrared, and visual instruments, a ground target can be modeled in any of these bandpasses. The resultant test sensor image may be analyzed using a variety of classical and empirical metrics, or some other user derived image analysis methodology may be added.

Copyright (c) 1996 Hughes DSO

**UNCLASSIFIED  
Approved for public release**

## UNCLASSIFIED

(U) The ISE is based on a small number of validated government models that, together with Hughes-DSO developed software, create an integrated digital simulation environment that provides strong data visualization and analytical tools.

(U) Simulations of complex systems are of value when the characteristics of the system being analyzed do not lend themselves to a straight forward analytical model. Digital simulations of physical objects and processes are not, and should not be, intended to be complete reproductions of a physical system in every detail. Each model is intended to encapsulate those processes that are necessary and relevant to the system being modeled with the expectation that measurements of the modeled processes will provide useful information about how a real system would perform. And, of course, the results of modeling any physical process must be correlated to empirical data to validate the results. And the model itself must be calibrated with empirical data.

(U) The ISE has incorporated five government models to perform specific functions in the modeling process. The models required a certain amount of I/O and interface modifications to integrate them and provide consistency in data processing and data visualization across all the different spectral bandpasses. Several of the government models have also been functionally extended, sometimes extensively, to provide a multi-spectral capability. Many of the models were developed with only one bandpass in mind, such as infrared. However, some have been designed in a way which actually facilitated extending them for multiple bandpass usage. Within the ISE the original functionality of the individual models has not been compromised. Our development philosophy was to take what worked and build upon that foundation new functionality and capabilities.

### THE ISE PROGRAM COMPONENTS

(U) All of the government models in the ISE execute on an SGI (Silicon Graphics) Indigo II Extreme workstation. The Indigo II is configured with 96 MB RAM, 3 GB internal hard disk storage, and has an external 1 GB magneto-optical removable disk. It is currently networked to a file server. A 486 class PC serves as the second workstation and is used for video capture of backgrounds, and to run some metrics and perform the final correlation analysis. It is also possible to tie the SGI and PC together on their own private network when required.

(U) TTIM (TACOM Thermal Imaging Model) is used to model the sensor and sensor effects on an image representation of the real world. TTIM comes with three sensor modules, a scanning array, a focal plane array, and an image intensifier. The scanning and focal plane arrays are thermal sensors. The image intensifier module can be used for direct view optics and T.V. as well as for image intensifier near-infrared devices. Each of the sensor packages allows the user to modify sensor bandpass, frequency response, and other parameters to model a wide variety of sensors. Also the developer can write additional sensor modules to link to TTIM.

(U) FRED (Faceted Region EDitor) serves several functions within the ISE. Its original purpose was to convert BRL-CAD solid models of 3D targets to faceted models and to create

Copyright (c) 1996 Hughes DSO

UNCLASSIFIED

## UNCLASSIFIED

vehicle input files for PRISM (see below). This program has been extended to do several additional tasks. It reads the TIFF (Tagged Image File Format) which contains image calibration data; location and climate data; terrain description; and imaging sensor data. This data is used to generate the scenario, weather, terrain, and other input files required by PRISM.

(U) PRISM 3.2 (Physically Reasonable Infrared Simulation Model) provides discrete time steady state thermal simulation of a 3D model over a diurnal cycle by calculating simulated solar loads, and, conduction and convection radiation exchange between facets. Version 3.2 of PRISM incorporates LOWTRAN (see below). This has allowed us to extend PRISM's simulation capabilities into the near-infrared and visible frequency bandpasses. PRISM's thermal model has been augmented with a lambertian reflectance model that is used when near-infrared and visible bandpasses are specified. A surface material database has been added to FRED which defines color in CIE chromaticity coordinates, emissivity, and the variable reflectance of surfaces in eight frequency subbands for both visible and near-infrared. This database is imported by PRISM and used for reflection calculations. When an observer position is defined we can also generate specular reflections for facets.

(U) LOWTRAN 7 is the venerable atmospheric effects model. It is not used as a stand alone model but is integrated into other programs, TTIM, PRISM, and FRED. This model is important because it guarantees consistent solar irradiance and atmospheric effects calculations when they must be performed independently in the different models.

(U) TVM 2.0 (TARDEC Visual Model) is a recent model combining image analysis algorithms that simulates the color/feature extraction processes of human vision, and a observer search model, that is used as one of the image analysis tools.

(U) IFP 3.2 (Image Filter Program) is a Hughes-DSO developed program used for image capture of background scenes. It will encapsulate user defined climate, sensor, location, and terrain information about the background scene into image file. The IFP program also has the ability to calculate image metrics and perform other image analysis tasks.

Copyright (c) 1996 Hughes DSO

UNCLASSIFIED

# UNCLASSIFIED

## THE MODELING PROCESS

(U) The mechanics of the modeling process can be broken down into a small number of tasks.

1. Scenario Preparation (IFP, FRED)
2. Target Simulation (PRISM)
3. Target-Background Synthesis (FRED)
4. Sensor Predictive Model (TTIM)
5. Image Analysis And Sensor  
Predictive Performance (IFP, TVM)

(U) We will discuss each of the government models in the context of the modeling process tasks. Since some models are used in more than one task, their salient aspects will be discussed in the context of the modeling task at hand.

(U) The ISE process is described in Figure 1. through a data flow diagram. Circles in the diagram represent modeling processes and are labeled with the program name that executes the process. Rectangles represent input, output, and intermediate data objects. The Glyphs suggest the kind of data contained in each object and how each process may transform it.

## SCENARIO PREPARATION

(U) There are two aspects of scenario preparation. The first part involves selection of the background scene in the bandpass of interest. Digitized images of backgrounds have been generated that include a variety of topology, flora, clutter, and range. The image format used throughout is the 24-bit RGB TIFF (Tagged Image File Format) file. Along with the image information it contains image calibration data; location and climate data, and data about the originating sensor. This information is used at each step in the ISE to support each model's execution so results will be consistent with the background environment. With the information from the TIFF file, the Faceted Region Editor (FRED) generates all the input files necessary to run a PRISM scenario.

(U) The second part of scenario preparation involves creating the target model. This involves using an existing FRED faceted model of a vehicle or some other ground target, or deriving a faceted model from a BRL-CAD solid model design. After a target is chosen the PRISM vehicle file and related radiation exchange files must be created for the scenario.

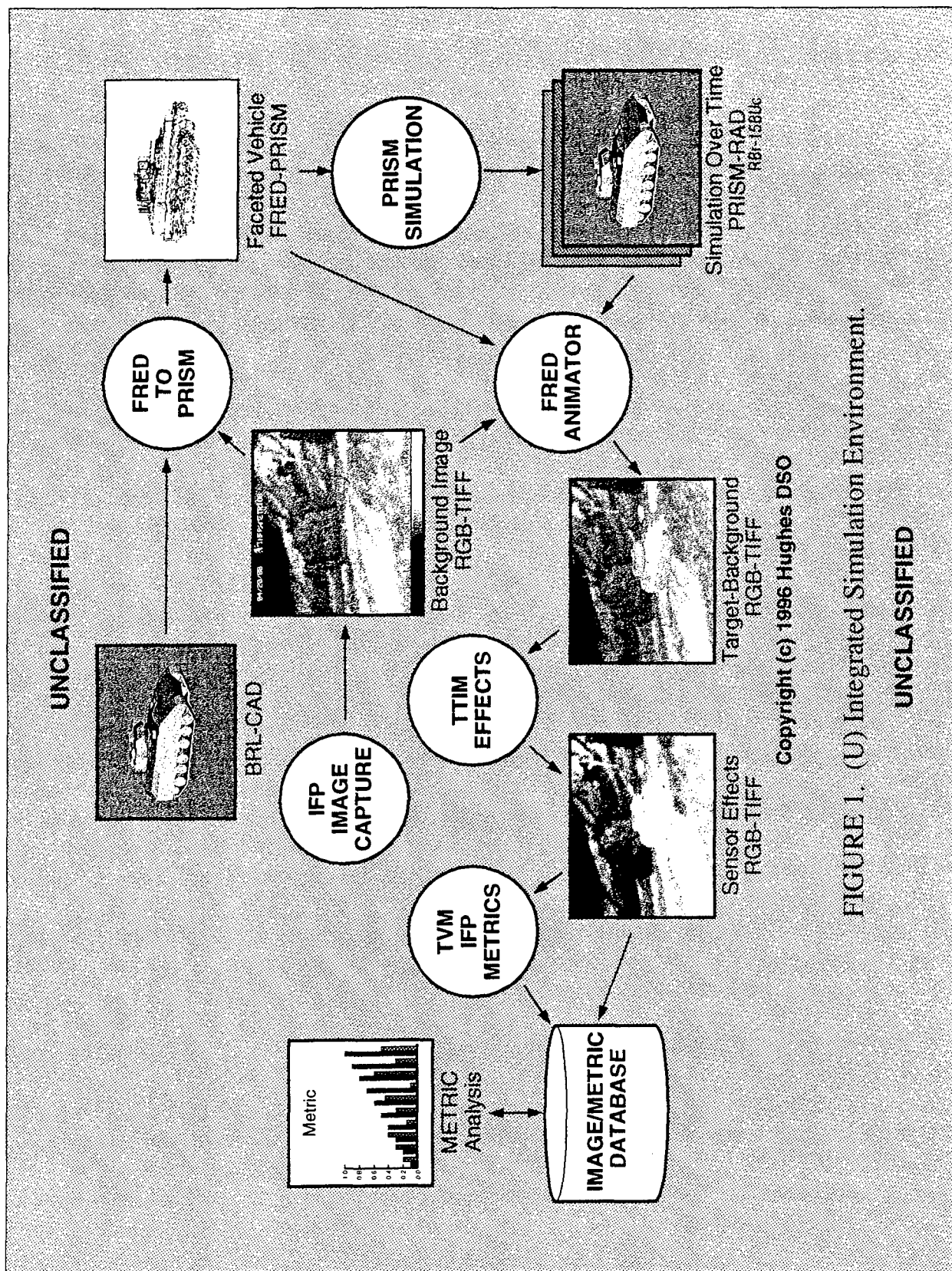


FIGURE 1. (U) Integrated Simulation Environment.

## UNCLASSIFIED

### TARGET SIMULATION

(U) For target simulation we use a version PRISM 3.2. that has been extended with a reflectance model. This new version of PRISM includes LOWTRAN which, for the infrared bandpasses, is used to determine band specific solar irradiance. PRISM is a steady state discrete time simulation of a 3D faceted target model. PRISM calculates solar loading, facet to facet convection and conduction, and reflection radiation exchange.

(U) The output from PRISM is the modeled target's per facet calculated radiation values, emitted radiance for thermal or reflected radiance for visual and near-infrared bandpass data. This is repeated for each time-slice during the simulation. Using PRISM to generate the simulated radiance values, we have a common multi-spectral data visualization tool for generating ground targets.

(U) We have taken advantage of the presence of LOWTRAN which has enabled us to augment PRISM with a lambertian reflectance model for the visible and near-infrared bands. We have also added a first order effect specular reflection capability to model potential glinting surfaces. This model is valid for both the visible and infrared bandpasses. The specular reflection information is saved in a separate file so the user can choose whether it will be used for target visualization in FRED. The information for the reflectance model comes from a reflectance database that was added to FRED and PRISM. The database is a collection of surface quality values including emissivity, color coordinate, and sub-band reflectance in multiple nanometer steps for the visible and near-infrared bands. Using the FRED editor a different surface quality value can be assigned to each PRISM facet.

(U) One concern which is central to the task of generating synthetic targets for use with actual real background images relates to the mutual conformity of the radiance and apparent temperature between the target and the background. Rigorous tests comparing pertinent data taken with a real target in a real background with those obtained from simulation of the same target superimposed on the same background is an ongoing effort. Every effort has been made to conduct sanity checks such as measuring the radiance of a multi-colored test board and using a light-dark calibration board making Minolta camera measurements at the time of recording for use as references, then measuring the spectral composition of incident radiation as function of time of day and comparing specimens recorded in the background to simulated targets with the same material and surface qualities.

### TARGET-BACKGROUND SYNTHESIS

(U) Target-background synthesis is accomplished in FRED. After PRISM simulation of the target, a selected frame corresponding to a particular time during the animation is incorporated into the background image by FRED. The target is sized to range, and the range dependent atmospheric effects are computed. The same version of LOWTRAN used in PRISM was added to FRED for this purpose. It is used to calculate the transmittance and in-path scattering

## UNCLASSIFIED

corresponding to the atmospheric conditions of the background, which are then applied to each facet of the target at range.

(U) The integration of LOWTRAN into FRED offers an example of the issues that arise in implementing extensions and modifications to the standard models. Unlike in PRISM, where all propagation paths are slant paths to space to derive solar loads, the computations of atmospheric effects due to range in FRED involve mostly horizontal paths. Since the atmosphere is modeled in LOWTRAN as spherical shells or layers, scattering is computed as a layer-by-layer summation along the line-of-sight of the scattered intensity evaluated at the layer boundaries (Ref. 5). Consequently, if both the target and the sensor are located within the same atmospheric layer, LOWTRAN returns no in-path radiance value. After consultations with one of the LOWTRAN coauthors at Hanscom AFB a work-around to this problem was implemented which assures that the target and the sensor always lie on opposite sides of a layer boundary.

(U) In the 0.4 - 0.8  $\mu\text{m}$  visible band the program is fully capable to treat color. Chromaticity coordinates of the facets are available in the surface material database that also contains reflectance data for up to eight sub-bands. To account for the range dependent color shift, LOWTRAN again is used to calculate color coordinates at the horizon, which then provide the basis for adjusting the color coordinates of each target facet.

(U) The composite TIFF image then goes to TTIM where sensor effects are applied.

### SENSOR EFFECTS

(U) TTIM (TACOM Thermal Imaging Model) is the model used to add sensor effects to the TIFF image composed in FRED for the spectral band of interest. TTIM comes with three sensor modules that can be tailored to simulate a wide number of sensors. The Image Intensifier TTIM will accommodate visual bandpass direct view optical and T.V., and near-infrared image intensifier tube sensors. Infrared sensor can be simulated with either the scanning or focal plane array TTIM sensors.

(U) The only alteration to TTIM has been to enable TTIM to read a TIFF scene file and output a TIFF sensor file.



# UNCLASSIFIED

## IMAGE ANALYSIS AND SENSOR PERFORMANCE

(U) At this point the user is free to apply any analysis tools of his/her choosing. An example of such a tool, which accepts the resulting data file as input, is the TACOM Visual Model (TVM), which performs scene analysis, includes its own search model, and outputs image metrics including Pd and Pr.

(U) Hughes-DSO has developed its own tool, the Image Filter Program (IFP), which is used for image capture and to generate the TIFF file with the sensor, location, climate and other information required for the target simulation. It also contains in excess of thirty classical and DSO-derived empirical metrics used in image analysis and system performance evaluation.

(U) All background images, target vehicles, radiation exchange files, scenario files, PRISM simulation output, TTIM image files, and metric output files are saved in a database which provides for the building of a set of scenarios which may be used as a knowledge base for comparison to new scenarios, or for multi-scenario correlation.

## CONCLUSION

(U) The ISE tool has been tested during various stages of its development, and exercised using several test scenarios. It is presently being applied in a realistic situation of immediate practical interest. As with any modeling tool, its value is in producing analytical results that are useful. The ISE has applicability in sensor design analysis, and vehicle design analysis. The ISE is even being used to help generate input values for large force-on-force computer simulation models.

(U) There are many potential areas for growth. One is for deriving and testing new image analysis metrics. Another is to add the ability to define and generate 3D simulated background scenes.

## UNCLASSIFIED

### BIBLIOGRAPHY

1. The Ballistic Research Laboratory CAD Package Release 3.0, SECAD/VLD Computing Consortium, U.S. Army Ballistic Research Laboratory, 1988.
2. FRED User's Manual, Version 3.1, U.S. Army Tank-Automotive Command and OptiMetrics, Inc., 1992.
3. PRISM User's Manual, Version 3.2, Keweenaw Research Center and U.S. Army Tank-Automotive Research, Development & Engineering Center, 1995.
4. TACOM Thermal Image Model, Version 3.1, Technical Reference and User Guide, OptiMetrics, Inc. and U.S. Army Tank-Automotive Command, 1989.
5. Atmospheric Transmittance/Radiance: Computer Code LOWTRAN 6, Air Force Geophysics Laboratory, AFGL-TR-83-0187, 1983.
6. Users Guide to LOWTRAN 7, Air Force Geophysics Laboratory, AFGL-TR-88-0177, 1988.
7. The Infrared and Electro-Optical Systems Handbook, Environmental Research Institute of Michigan and SPIE Optical Engineering Press, 1993.

**UNCLASSIFIED**

THIS PAGE INTENTIONALLY LEFT BLANK

**UNCLASSIFIED**

# UNCLASSIFIED

## VEHICLE SURVIVABILITY ANALYSES WITH THE MODEL LINKAGE PROCESS

Mr. Frank Briglia  
Teledyne Brown Engineering  
Huntsville, AL 35807-7007

### ABSTRACT

A tool has been developed to facilitate the analysis of vehicle survivability. Called the "Model Linkage Process" or MLP, the process was developed under the sponsorship of the Project Manager for Armored Systems Integration (PM-ASI).

Developed as a methodology for studying ground combat vehicle survivability at the force and system level, the MLP uses a combination of models, modeled data, and measured data to facilitate survivability treatment comparisons, treatment-versus-threat analyses and system and force level survivability benefit analyses. Where generic or explicit models exist they are used and when measured data are available those data are used in the process. For armor and some other survivability assets, a parametric analysis technique is used to characterize the survivability contributions of those assets.

The MLP was initially developed to support systems and force level survivability analyses addressing signature-managed land combat vehicles. The MLP was needed because a high fidelity method of assessing the effects of signature management on ground combat vehicles in a force context was not available. The process was developed also to increase the traceability of vehicle signature management modeling and survivability analyses to real threats, real vehicle signature treatment performance, and test data from real sensor-vehicle engagement tests.

The MLP has been used in several vehicle survivability studies for PM-ASI. In a recent analysis for PM-ASI, the MLP generated data that clearly indicated the benefit of applying signature treatments to a specific vehicle.

This paper presents the MLP, describes insights into its benefits to survivability analyses, and discusses its potential to perform weapons systems lethality analyses at the force level.

### Introduction

The Project Manager for Armored Systems Integration (PM-ASI) at the U.S. Army Tank Automotive and Armaments Command (TACOM) has the lead in developing and identifying the survivability assets needed by each ground combat vehicle in the Army's current and future inventory. To help survivability assets' developers and users evaluate the benefit of survivability measures at the system and force level, PM-ASI has sponsored the development of the Model Linkage Process (MLP). The development of the MLP was actually started by Teledyne Brown Engineering (TBE) under the Armored Systems Modernization program and TBE has continued to expand and refine the capabilities of the process with PM-ASI's support.

The MLP involves the use of Government developed and approved models (refer to Figure 1). Analysts use the models in a contiguous manner to generate data from which conclusions are made concerning the effectiveness of survivability treatments and lethality systems. Using the

UNCLASSIFIED

# UNCLASSIFIED

MLP, PM-ASI is determining those techniques that are required to defeat threats at the detection, hit, and penetration steps in the survivability process. Signature management is only one of the survivability methods used to defeat the killing process, i.e., to reduce or eliminate the probability of detection. The question is, How much signature reduction is enough to make a vehicle survivable yet affordable? The same is true for the other survivability assets and lethality systems. How much is required? Using the MLP facilitates answering the how much is enough questions for survivability treatments and lethality systems.

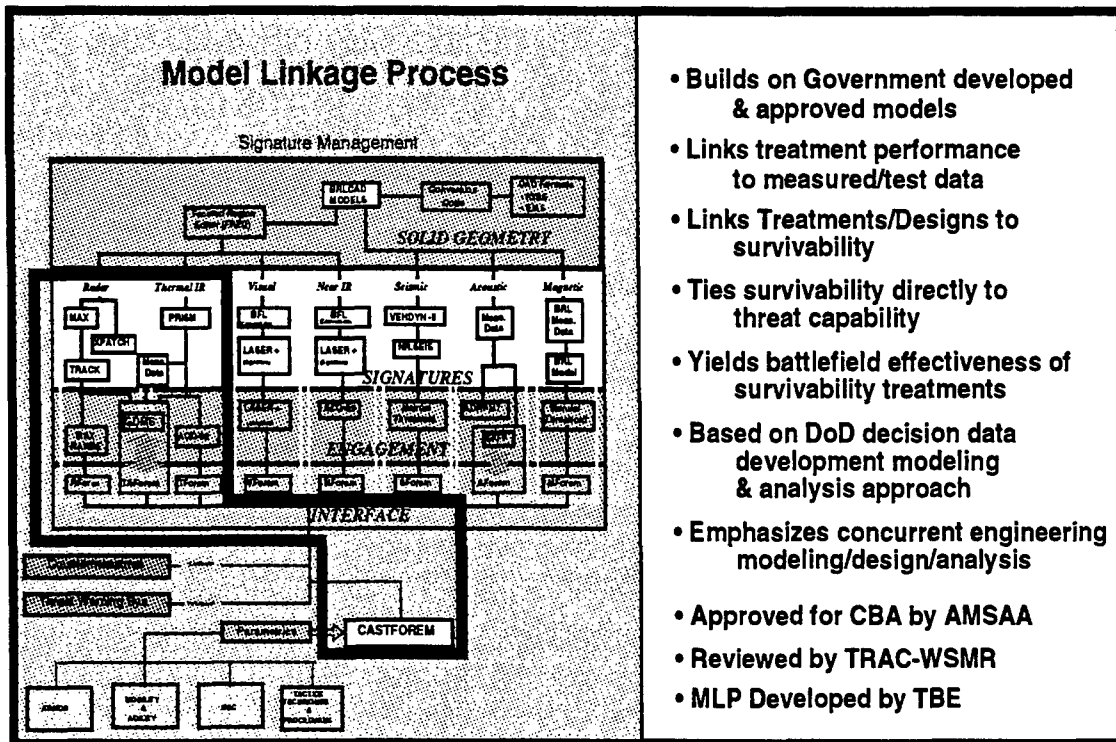


Figure 1. Block diagram of the models used in the MLP.

The name Model Linkage Process comes from the use of geometry data by signature models, the use of signature data by engagement models (sensor models developing probability of vehicle detection data), and in turn the use of engagement data by an operational model. Therefore, the MLP provides linkage and traceability from geometry and specific treatments to operational effectiveness information. The process also provides direct traceability to real threat performance because threats are modeled using data provided by the intelligence community.

## II. The Model Linkage Process

The MLP is an approach or method for improving evaluations of survivability and lethality treatments' benefits at the system and force levels. The first step completed in the development of the MLP was the collection of Government approved models and the data needed to perform survivability analyses of signature managed vehicles. The first analyses performed using the MLP were survivability studies of signature managed vehicles engaged by Man-Out-of-the-Loop (MOL) threats (indirect-fire smart munitions). The second step in the MLP's development, which is currently being taken, is the improvement of the capability to model and analyze Man-In-the-Loop (MIL) engagements of threats and vehicles and the capability to model and analyze other vehicle survivability assets such as armor, threat warning systems and countermeasures.

## UNCLASSIFIED

The MLP uses detailed data obtained from models or tests at four distinct levels to generate the information necessary to assess vehicle and force survivability. The four levels of the process are the geometry level, the signature level, the engagement level, and the operational level. In threat warning and countermeasures effects modeling, generic models do not exist so the MLP uses measured or predicted performance data. Where a specific warning system or countermeasure has an engineering model, that model is used to generate performance data in the absence of measured data. For armor and other survivability assets, parametric analyses are performed using the MLP to understand the benefits of specific performance levels of these assets. Data for the parametric studies are derived from testing or from complex models. In general, if measured data are available, they are used in the MLP.

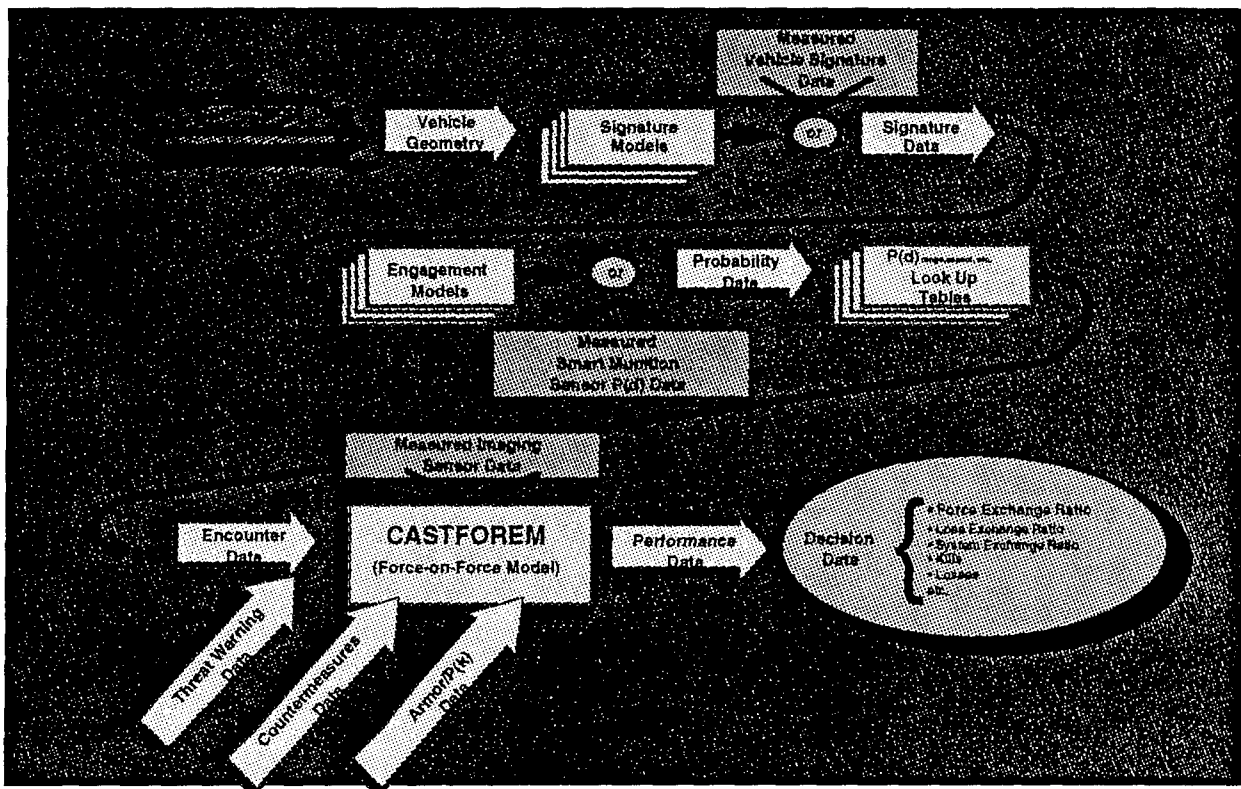


Figure 2. Flow block diagram of the MLP indicating measured data input points for signature, probability of detection, threat warning, countermeasures and armor data.

The MLP has been used only for signature management analyses, as of the end of February 1996. In the survivability evaluations of signature managed vehicles, the MLP uses signature modeled or measured data of treated and untreated vehicles. Engagement models use the signature data to determine the probability of vehicle detection by a specific threat sensor, given specific parameters which include vehicle signature(s) (aspect dependent), threat sensor performance, background signature, environmental conditions, and vehicle to threat-sensor range. Smart munitions' probabilities of detection are determined from generic sensor models and are formatted into data files called "Look Up Tables" (LUT) (refer to Figure 3). The LUT files are used by CASTFOREM in modeling sensor and target interactions in an operational context. The probability of detection and recognition data required for MIL sensors are generated currently by the ACQUIRE model which is embedded in CASTFOREM. In the MLP's application, the signature data used by the ACQUIRE model are derived from measured data. The signature data provided to the ACQUIRE model represent one elevation angle and 8 azimuth angles about the

# UNCLASSIFIED

vehicle (45 degree increments).

Sensor	Target	Background	Slant Range (m)	Altitude (m)	Azimuth (degrees)	Probability Det. x 1000
108	80	6007	25	21	0	946
108	80	6007	25	21	15	970
108	80	6007	25	21	30	973
					•	
					•	
108	80	6007	25	21	345	957
108	80	6007	50	43	0	666
108	80	6007	50	43	15	784
108	80	6007	50	43	30	792
					•	
					•	
108	80	6007	50	43	345	702
108	80	6007	75	64	0	332
			•		•	
			•		•	
108	80	6007	250	216	300	1
108	80	6007	250	216	315	0
108	80	6007	250	216	330	0
108	80	6007	250	216	345	0

Figure 3. Portion of a LUT file containing the probability of detection data for smart munitions.

Through February 1996, BRL-CAD has been the source of geometry data for the MLP. Measured signature data and models such as PRISM and XPATCH have been used to generate vehicle signature data (PRISM for IR signatures and XPATCH for RF signatures). Other models have been integrated into the MLP to generate signature data in the visible, near IR, magnetic, seismic, and acoustic spectra (refer to Figure 4). Depending on the threat sensor(s) being modeled, one of two generic sensor models have been used to produce probability of detection data. These engagement models are GDMS and VSAT. At the operational level, the high resolution combat model CASTFOREM has been used and is kept current with the version validated by AMSAA and developed, maintained, and used by TRAC-WSMR.

## III. Survivability Analysis Benefits From the MLP

The MLP's primary benefit is that it links force level performance to specific levels of survivability treatment and threat performance. In the case of signature management, vehicle survival has been shown to increase as vehicle signatures (in bands used by threat sensors) are reduced. Analyses have shown that a vehicle's signature must be reduced to a specific level before any substantial benefit at the force level is achieved and that lowering a vehicle's signature below a certain level does not provide a cost effective solution. These levels are threat dependent, which leads to another benefit of the MLP; the process models threats as specifically as possible based on the capability of available sensor models and CASTFOREM. (Threat performance and characteristics data are provided by NGIC, MSIC and other intelligence organizations, however, when data are not available from the intelligence community, sensor experts are consulted.)

The MLP also provides insight into the effects of survivability treatments at the one-on-one engagement level (treatment performance against a specific threat). This allows analysts to better understand the results of force level modeling. In the case of signature management, analysts can compare and analyze untreated and treated vehicles' shapes and signatures, threat engagements results, and force engagement results (refer to Figures 5, 6, and 7). An example of an untreated vehicle and a potential treated vehicle are shown in Figure 5; notice the reduction of the curved surfaces (replaced by flat surfaces) and the elimination of many small components in the treated case. Also notice the change in the vehicle's general shape; a few large specifically oriented flat

## UNCLASSIFIED

surfaces have replaced the curved surfaces used in the untreated vehicle. A few flat surfaces confines the vehicle's RF signature to specific portions of threat space where either potential threats do not operate or where threats can take minimal advantage of the signature.

	Short Titles	Model Description
X	ACQUIRE92	US Army, Night Vision & EO Directorate, EO Target Acq. Model, 23 March 1992
	ACQUIRE-X	US Army, Night Vision & Electronic Sensors Directorate, Acquire-X, Range Performance Model for Thermal Imaging Systems
	ADBP7	TACOM, Acoustic Detection Range Prediction Model 7, v1.3
	BRL-CAD	US Army, Ballistics Research Laboratory (BRL) CAD, v4.0
X	CASTFOREM	TRAC-WSMR, Combined Arms and Support Task Force Evaluation Model
	FRED	TACOM, Faceted Region Editor, v3.1
X	GDMS	MICOM, Generic Dual Mode Sensor Model, v1.0
	LASER+	I-Math Associates, Visual Signature Predictive Model, v5.2
X	MAX	Georgia Tech Research Institute (GTRI) Geometric Database Model, v6.6
	NB SEIS	US Army, Corps of Engineers WES, Seismic Signature Model, May 20, 1992
X	PRISM	TACOM, Physically Reasonable Infrared Signature Model, v3.0
	SFFP	ARL, Scanning Fast Field Program, Unknown Version, February 1993
X	TRACK	GTRI, Radar Cross Section and Tracking Simulation, v4.2
	TTIM	TACOM Thermal Image Model, v3.2
	VEHDYN2	TACOM, Vehicle Dynamics Model, v2.0
	XIPS	Image Processing System Supplement to ACQUIRE-X
X	XPATCH	Wright Patterson AFB (WPAFB), Radar Cross Section Prediction Code, v1.2
	ARTM	TACOM, Acoustic Requirement Translation Model, v2.0
	RSM	TACOM, Radar and Smart Munitions, v1.3
	TVM	TACOM, Visual Model, Beta 2.1
X	VSAT	TACOM, Vehicle Survivability Analysis Tool, v1.1

X = Used in the current CBA

\* Models used varies IAW analysis issues.

Figure 4. Models currently used in the MLP to evaluate signature management. The "x" beside certain models indicates they were approved by AMSAA for use in a recent analysis.

An example of potential changes in vehicle signature (given specific application of RF signature treatments) is shown in Figure 6. During an analysis, data such as those shown in the signature managed case of Figure 6 could be used to identify vehicle locations or vehicle aspects that exceed signature requirements (too low or too high). Because of the signature to vehicle design traceability and the data links maintained in the MLP, areas or aspects of a vehicle producing inappropriate signatures can be easily identified. This is beneficial because inappropriate signatures can be identified and corrections can be made early enough that the end product produces the desired performance and costly engineering design changes can be avoided.

An example of potential changes in vehicle probability of detection by a specific RF threat sensor is shown in Figure 7. The left side of the figure shows the probability of detection of a vehicle without RF signature treatments and the right side of the figure shows the probability of detection of the same vehicle with RF signature treatments applied. Analyzing the signature-managed case's data, areas or aspects of the vehicle can be identified which exceed requirements (too high). Because of the traceability of the probability of detection data to signatures and signatures to vehicle geometry, the areas or aspects of a vehicle producing inappropriate probability of detection can easily be identified.

The modular nature of the MLP allows it to be verified by verifying the individual models comprising it using the model test model (MTM) paradigm. When tests are conducted, each



## UNCLASSIFIED

applicable MLP model's performance is evaluated against the data acquired from the tests. When a model does not produce data similar to test data, the model is adjusted to make its output more closely reflect the results of the tests. As of February 1996, the only attempt at implementing the MTM paradigm with the MLP's models has been with the GDMS and VSAT models. Tests were conducted during 1995 and data were taken; unfortunately, the sensors used to represent actual sensor threats involving the infrared (IR) spectrum were multi-spectral (IR & MMW) and the individual spectral channel's data were not accessible. Therefore, the MTM paradigm could not be completed for the IR sensor models. However, the radar sensor used to represent actual radio frequency (RF) threat sensors provided appropriate data and the MLP's RF models' performance was verified for a select set of threats. Another set of tests are being planned and appropriate sensors are being sought to assure that proper equipment are used in those tests and appropriate data are recorded to verify vehicle signature and models' performance.

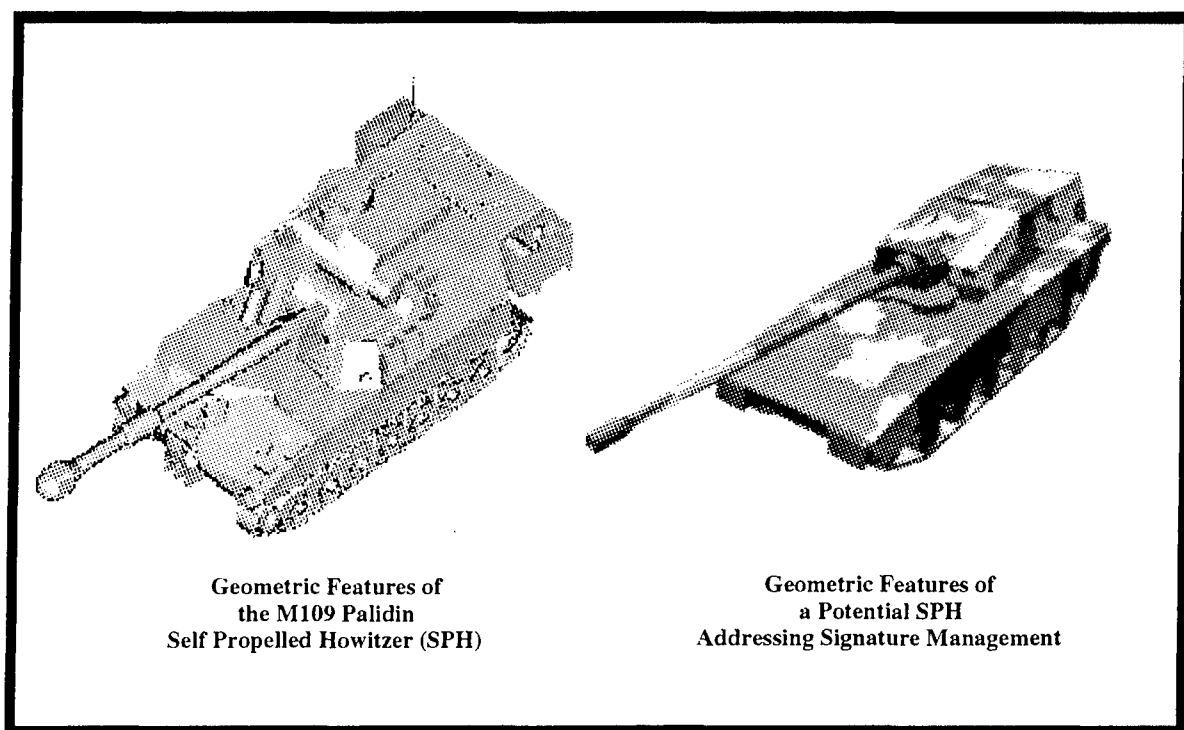


Figure 5. Example geometry representation of an untreated self propelled howitzer and a signature managed SPH..

One of the major benefits of the MLP lies in its ability to fully support the concurrent engineering design philosophy. As requirements are studied at the operational level for a system, requirements can be flowed down to the individual treatment areas and analyzed against designs, technology capability, performance, cost, manufacturability, etc. As design concepts or system performance is established, appropriate data can be integrated into the MLP and the force level benefit determined. The process of establishing and reevaluating operational and system requirements is iterative as illustrated in Figure 8 and the MLP supports this iterative process.

In a recent analysis where the MLP was used, operational results like those presented in Figure 9 were generated. In the recently completed analysis, a specific vehicle was studied to determine the benefit to the field commanders of reducing the vehicle's signature. The analysis included three different scenarios. Each scenario had a representative 1999 U.S. force and a representative 2005 threat force employing appropriate weapons and tactics for the time period.

## UNCLASSIFIED

However, in the analysis, two sets of threat sensors (FLIRs) and smart munitions (top attack indirect-fire IR, MMW, and dual mode systems) were used. The threat sensors (generation 1 FLIRs) and smart munitions used were those expected to be on the battlefield in the year 2005 and in the year 2012. This provided data on the capability of the system under investigation as a function of time.

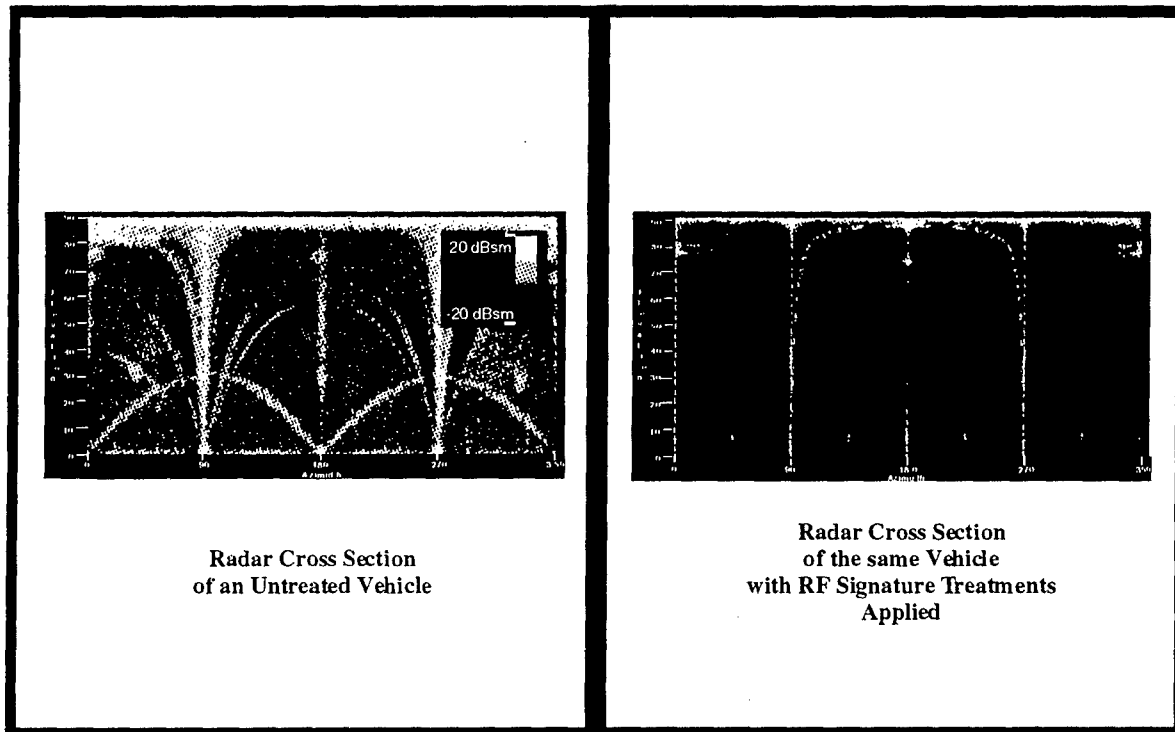


Figure 6. Example representations of RCS changes in vehicle signature with the application of specific signature treatments.

Files of LUTs were generated for the threat and U.S. smart munitions used in each scenario. The files included pertinent probability of detection data for each sensor used in the analysis. The probability of detection data addressed each vehicle and sensor encounter in each scenario, the environmental conditions of each scenario, the potential vehicle encounter aspects, two clutter levels, slant range between the sensor and the vehicle, etc. The two clutter levels were used to address the impact of clutter on the outcome of sensor vehicle engagements. The clutter values selected were those that represent a moderately high clutter and a moderately low clutter as a function of spectrum. When high clutter was used, all sensors were modeled as engaging targets in high clutter backgrounds and when low clutter was used, all sensors were modeled as engaging targets in low clutter backgrounds. No attempt was made to specifically address each sensor and vehicle engagement for high or low clutter conditions. All vehicles were either in high or low clutter backgrounds for each specific run as indicated in the analysis run matrix (see Figure 10).

The three scenarios used in the recent analysis were the CASTFOREM scenarios HRS 29 (a meeting engagement), HRS 25 (blue performing a mine field breaching maneuver with threat engagement), and HRS 35 (a Blue hasty defense engagement). Each of the scenarios were run with the 2005 threat in low and high clutter conditions and with the 2012 threat in high and low clutter conditions. Twenty-one runs were made with each scenario per condition.

UNCLASSIFIED

UNCLASSIFIED

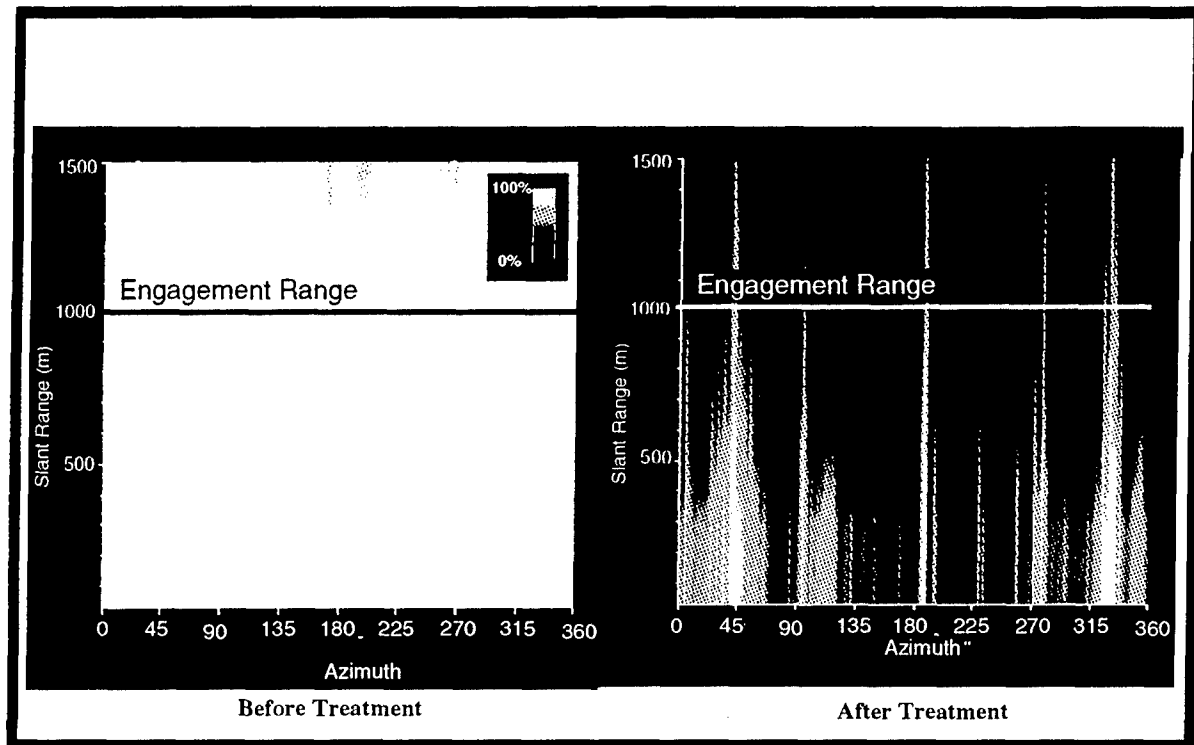


Figure 7. Example threat engagement probability of detection data illustrating the effect of the application of specific signature treatments.

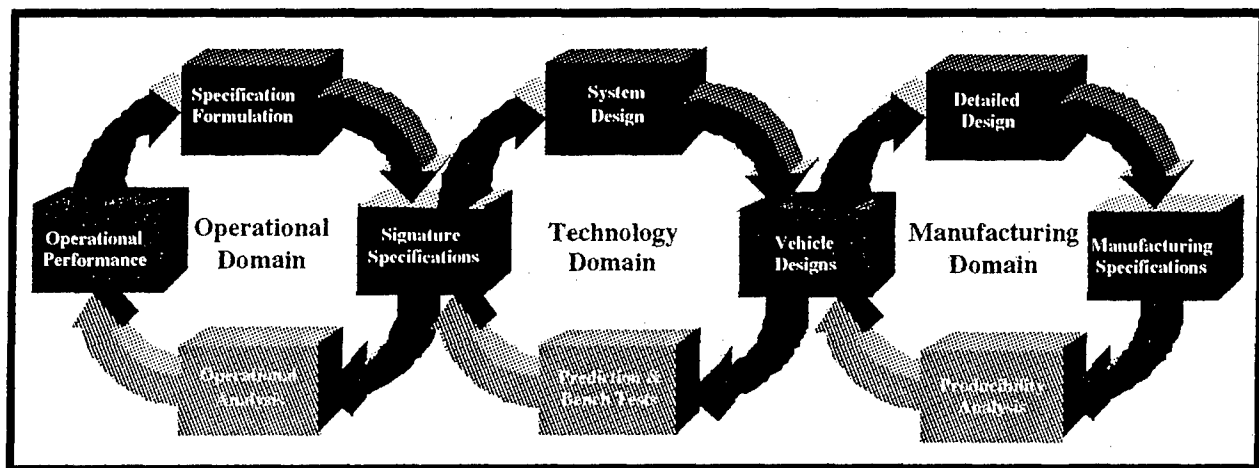


Figure 8. The MLP supports the concurrent engineering philosophy of system design.

The data from all of the CASTFOREM runs were studied first to ensure the results made operational sense. The investigated and reviewed data included system losses (or survivability), system-loss exchange ratio, force-exchange ratio, kills of systems by dumb indirect-fire weapons, detections and kills of systems by smart indirect-fire weapons, and detections and kills of systems by direct-fire weapons. Data were also evaluated for each weapon type employed (example -- indirect-fire IR top attack faller type smart munition) in each scenario. Data similar to that presented in Figure 9 represent only a portion of the different measures of effectiveness used to

UNCLASSIFIED

# UNCLASSIFIED

assess the benefit of the treatments under investigation in the recent study. Because of the fidelity and traceability of data provided by the MLP, the decision in the recent study concerning the signature treatments' benefit to the system and force commander was easily made.

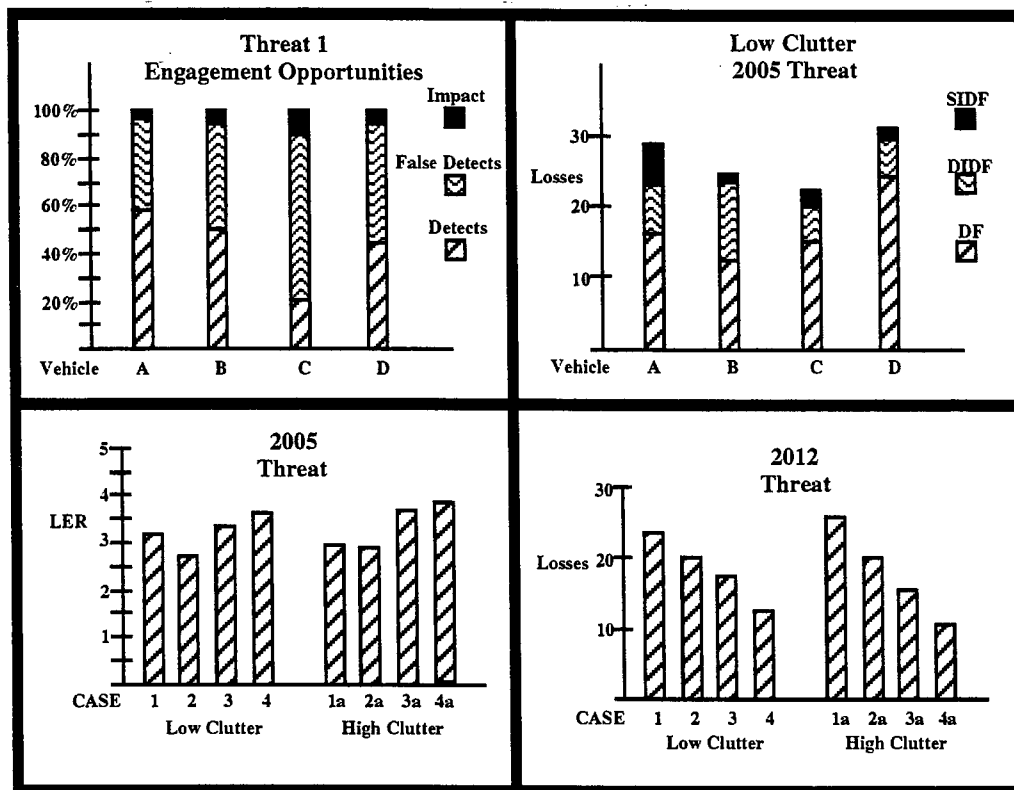


Figure 9. Data illustration of force and system measures of effectiveness generated with the MLP.

## IV. Potential For Weapons Lethality Analyses

As was done to a limited extent in recent analyses, the performance of specific weapons can be evaluated at the one-on-one and force perspectives. The fact that only survivability analyses using the MLP have been performed through February 1996 is an artifact that TBE's customers have been interested only in survivability of systems rather than the effectiveness of current or future weapon systems. The fidelity improvements made to CASTFOREM and the entire MLP are applicable to weapons effectiveness analyses too. The techniques used in system and force survivability analyses can easily be applied to understand weapons effectiveness by incorporating the appropriate weapon performance data and evaluating the changes in system kills and force effectiveness. Weapon systems such as Javelin, second generation FLIRs, Long Bow, SADARM, etc. could be studied to determine their benefit to the force commander. Combinations of weapon systems can also be addressed.

## V. Summary and Conclusions

A mature MLP is ready for use in vehicle survivability analyses involving signature management treatments. The MLP has proven itself in a recent Cost Benefit Analysis to be a valuable tool for generating useful information. The MLP has been reviewed by AMSAA and TRAC-WSMR personnel and approved for specific studies. The data produced using the MLP have been reviewed by Government agencies and found to be very good. The keys to the excellent

UNCLASSIFIED

# UNCLASSIFIED

results were the fidelity of the models comprising the MLP and the traceability of the modeling results to the real world.

Alternative	HRS 25		HRS 35		HRS 29	
Tactical Situation	Heavy Breach		Heavy Defense		Heavy Meeting	
2005 Threat	X - 1		X - 1, 2		X - 1	
2012 Threat	X - 3, 4, 5		X - 3, 6		X - 3, 4, 5	
Clutter	High	Low	High	Low	High	Low
Case 1	X	X	X	X	X	X
Case 2	X	X	X	X	X	X
Case 3	X	X	X	X	X	X
Case 4	X	X	X	X	X	X
Case 5	X	X	X	X	X	X

**Threat Munitions**

1. Threat 1, IR Faller/Flier	3. Threat 3, IR Faller	5. Threat 5, MMW Faller
2. Threat 2, Dual Mode	4. Threat 4, MMW	

**U.S. Munitions**

1. Multi-Mode Faller
----------------------

Figure 10. Run matrix used in a recent survivability analysis.

The Project Manager for Armored Systems Integration is the sponsor for the MLP. The Tool is currently being used to support PM-ASI customers' vehicle survivability analysis needs in the area of signature management but the tool is being expanded to address other survivability measures and weapons lethality systems as well.

The smart weapons and sensor communities have not yet used the MLP but it is directly applicable to system and force level studies of weapons and sensors which use target signatures to perform their tasks.

The MLP is a good tool for evaluating vehicle survivability treatments. With continued cooperation of several Government agencies, the MLP will provide a capability to evaluate a full complement of vehicle survivability treatments' and weapon systems at the force level. Because the MLP models both sides of an engagement, Red and Blue systems and forces equipment and performance can be evaluated.

## Acknowledgements

Teledyne Brown Engineering thanks the Project Manager for Armored Systems Integration for sponsoring the development of the MLP and the team of CASTFOREM experts at TRAC-WSMR for their support with TBE's use of CASTFOREM.

UNCLASSIFIED

UNCLASSIFIED

## THE THREAT ORIENTED SURVIVABILITY OPTIMIZATION MODEL (TOSOM).

Alan A. Anderson  
Teledyne Brown Engineering  
Huntsville, AL 35807

### ABSTRACT (U)

(U) In support of TARDEC and the Program Manager - Armored Systems Integration (PM-ASI), Teledyne Brown Engineering (TBE) has developed the TOSOM decision support tool. The TOSOM tool builds upon earlier TBE models which used linear programming techniques to determine an optimal countermeasure suite solution (should one exist) to counter a specified threat. A major feature of this model is the incorporation of a graphical user interface (GUI) to promote ease of use and quick turnaround time for "what if" analysis. The model includes extensive user documentation and was designed with the intent of providing a much needed trade off tool suitable for configuration management and widespread dissemination among the user community. This paper will provide a brief history of the model, the model methodology, the specific questions to be answered or explored by the model and the data required to run the model. The actual model formulation in terms of equations and definitions of variables will also be presented.

### (U) Model Summary

(U) TOSOM is a computer based decision support tool designed to assist the analyst in finding an optimal survivability strategy (realized as a suite of countermeasures) for a specific weapon system. Survivability requirements are usually a function of the distribution and lethality of expected threats. There are almost always multiple ways to satisfy these survivability requirements, and each solution will have "burdens" or costs such as dollars, power or weight. The problem that TOSOM is designed to solve is the generation of the requisite amount of survivability while remaining within the budget for the system's burdens. The TOSOM tool helps users provide structure to the complexities of this problem.

(U) TOSOM is a tool the analyst can use to gain insights into possible survivability trade-offs and solutions. The model does this by using mixed integer linear programming techniques to determine the optimum survivability suite solution (if one exists) based upon user defined threat lethality, available survivability technologies, and vehicle design constraints. TOSOM can consider all determinants of vehicle survivability except the frequency of attack. Recommended countermeasures are selected as a function of their effectiveness versus specific threats and the relative burdens they impose upon the system.

(U) In addition to the mixed integer formulation, TOSOM also provides an Exhaustive Enumeration (E<sup>2</sup>) option. The E<sup>2</sup> module calculates the countermeasure suite performance and burdens for all possible combinations of up to 15 countermeasures and provides the results as a database manipulatable by the user.

UNCLASSIFIED

Approved for public release; distribution is unlimited

## UNCLASSIFIED

(U) The process of conducting analysis with TOSOM starts with the identification of the relevant threats, the likelihood of encountering those threats and quantification of the threat performance against the system under study. This information defines the lethality of the threat environment which in turn is used to identify the survivability shortfall. The next step is to define the burden limits to be applied to the study system. Burdens typically include such items as cost, weight, space claim, risk, etc. The final step is to provide data for possible countermeasure systems and their associated burdens and effectiveness versus the specified threats. With this information the TOSOM is then applied using either (or both) the GAMS mixed integer optimization program or the E<sup>2</sup> module.

(U) TOSOM guides the analyst through this process with a graphical user interface (GUI). The GUI developed for TOSOM allows the user to rapidly and confidently describe the data to be used in solving the problem and provides several different solution options. It also contains embedded error trapping to insure that the data is mathematically valid, provides assistance in entering proper data, and provides a means for easily assessing the results of a model run. TOSOM is self contained, requiring only the PC Windows operating environment. However, the GAMS software must also be available if that solver option is desired.

### (U) Model Background

(U) In response to the need to organize and associate a wide range of survivability variables, Teledyne Brown Engineering (TBE) developed TOSOM. The government has contracted with TBE for the development, implementation, testing and training efforts associated with providing a standardized TOSOM decision support tool for combat system survivability technology assessment and trade-off. This effort has enhanced and formalized the existing TOSOM decision support tool, making it a viable and acceptable tool for conducting program management efforts and tradeoff studies.

(U) The overall goal of the TBE effort is to make TOSOM a configuration managed tool which is easy to use and provides answers to the survivability questions that are currently being asked. The problem "solved" by TOSOM is a multi-variable optimization problem. The model is prescriptive in nature, providing rapid turnaround "what if" type analysis. TOSOM (or any other survivability model) will NOT produce THE answer to the survivability question. This tool should be considered as only part of an analysis process that facilitates the development of requirements matching the spectrum of possible threats with the highest payoff treatments to counter those threats. TOSOM is designed to assist the analyst to prioritize the threats, focus on candidate countermeasure treatments, understand the tradeoffs required when choosing one countermeasure over another, and provide direction on preferred countermeasure treatment suites to be further investigated using such analytical tools as JANUS or CASTFOREM.

### (U) Problem Statement

(U) Given the war fighting scenarios that a candidate vehicle will be operating in, to include the possible threats and their respective effectiveness, the problem is to maximize the survivability of the vehicle by choosing which countermeasure treatments to employ while subject to constraints on added weight, internal volume, external volume, data requirements, cost, power requirements or other burdens on the vehicle. The problem can also be stated as a minimization of any of the burdens subject to constraints on obtaining a minimum level of survivability.

(U) Solving this problem will allow the performance of sensitivity analyses to determine which treatments have the biggest impact on improved survivability, how much survivability

UNCLASSIFIED

## UNCLASSIFIED

could be gained if allowed to violate specific constraints on burdens, and, just as important, which treatments contribute negligibly to survivability. Many times it's just as important to know which alternatives can be eliminated as it is to know which are the best.

### (U) Methodology

#### Assumptions.

- A critical assumption of this mixed integer / linear programming approach is that there is a direct, linear relationship between the weight, cost, power requirements and the other burdens of a survivability measure and its effectiveness, i.e. given two equally effective countermeasures one would select the lowest in cost, weight, or other burden.
- Using the TOSOM decision support tool to address the survivability question first requires an assessment of the likelihood of the vehicle being attacked. If no event requiring additional survivability is expected to take place, then no additional measures are required. In other words, if the threat system encountered is ineffective then minimal additional survivability measures are needed. With this in mind, the TOSOM tool starts with an assumption that an encounter will occur. This assumption is further restricted in that only the outcome of one "expected threat" encounter will be addressed. The threat profile (or tree) is designed to structure the process of determining encounter likelihood and to provide an "audit" trail for the threat encounter probabilities used within the formulation. The values resulting at the base of the tree provide the probability of encounter ( $P_{enc}$ ) for each of the threat systems modeled within the scenario. TOSOM provides the means to rapidly modify these values and re-run the model for sensitivity analysis.
- When combined, survivability systems do not have mutually exclusive benefits. If both systems A & B are used, the respective success probabilities must be combined conditionally. This means that there is no "synergy" or additional survivability effect generated by combining systems - the suite of systems will not perform better than the sum of the individual systems. Indeed, because the model combines the treatments as conditional probabilities, the suite will **ALWAYS perform less effectively than the sum of the individual systems.**

#### Limitations.

- TOSOM attempts to solve the survivability requirement for a single encounter. The model uses a threat tree structure to define (given an attack will take place) the likelihood of that attack being prosecuted by a particular type of enemy weapon system. The model **does not** maximize the likelihood of surviving an entire battle, only the probability of surviving one encounter/attack during a battle. Various techniques exist for expanding the one encounter result, but all rely on some estimate of the number and distribution of encounters expected.

### (U) Data Requirements

(U) TOSOM requires a variety of input data. This data includes threat distribution data, threat effectiveness data, countermeasure specifications and vehicle design constraints.

UNCLASSIFIED



# UNCLASSIFIED

## 1. Threat distribution information

(U) This is a structured description of the types of force, unit, system, and sensor threats that are to be arrayed as encounter threats against the candidate vehicle. Figure 1 presents, in a tree

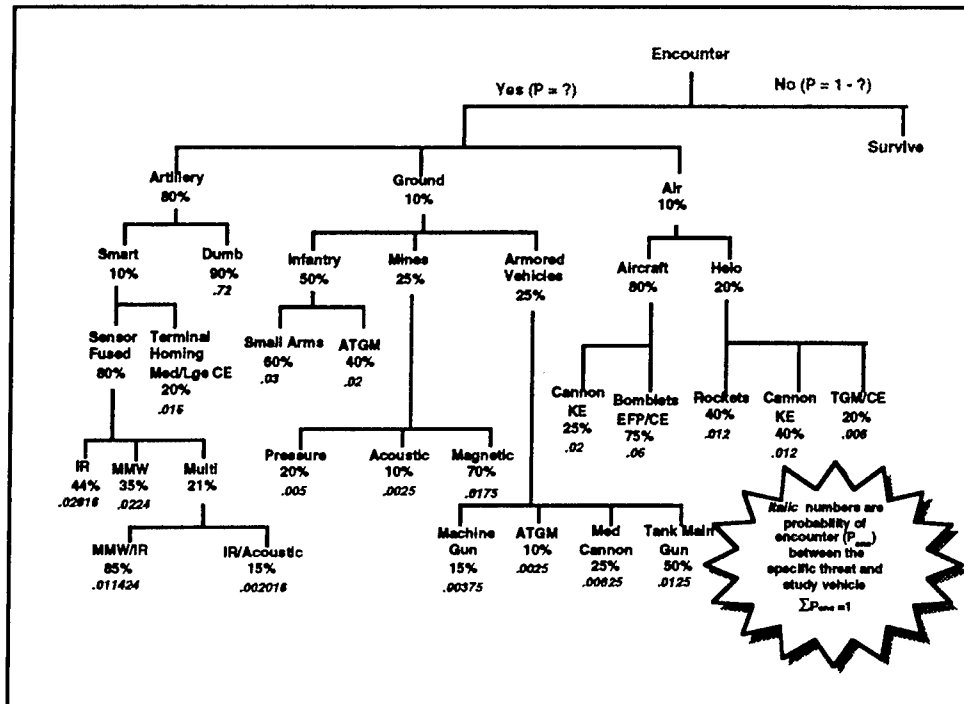


Figure 1. Force Structure/Threat Tree (U)

form, an example of a TOSOM threat distribution. The threat tree is used to define the likelihood of encounter between the system under study and the members of the specific threat array. The data reflects the likelihood of the threat systems presented participating in an encounter with the system under analysis. When complete, this information is used to determine the probability of an encounter between the candidate system and the various members of the threat array while at the same time providing an audit trail for the encounter information used within the model. Within the linear programming formulation which appears later in this paper, this data is defined by the variables  $enperj$ ,  $unitperj,k$ ,  $systemperj,k,l$  and  $sensorj,k,l,m$ .

(U) The threat tree can be thought of as a visual model of the threat information used by the TOSOM. The tree represents a threat scenario involving alternative enemy threats, chance events, and event outcomes as shown in Figure 1. The term tree is applied to this structure because situations are represented as a time-ordered series of decision points and chance events, with alternatives and event outcomes branching out to represent all the possible paths through the decision. This tree is specific to a threat - both the technology and forces available to the threat and the environment in which that threat is to be encountered.

## 2. Threat weapon system effectiveness information

(U) Threat weapon system effectiveness data describes the effectiveness of the threat systems encountered by the candidate vehicle. Threat weapon effectiveness is currently represented by three different probability values in the mixed integer objective function. These values are probability of acquisition or  $pa_{j,k,l,m}$ , probability of hit,  $ph_{j,k,l,m}$ , and probability of kill or  $pk_{j,k,l,m}$ . The  $j,k,l,m$  coefficients on each of the probabilities identify the unique threat weapon system being described (for a 4 tier tree). The probability values are multiplied together, in

UNCLASSIFIED

series (conditional probabilities) to determine the expected lethality of that weapon versus the candidate system. The result is then multiplied by the likelihood of encountering that system (data requirement #1 above) to determine the relative lethality of that particular threat to the candidate system. Figure 2 gives an overview of the TOSOM threat definition methodology.

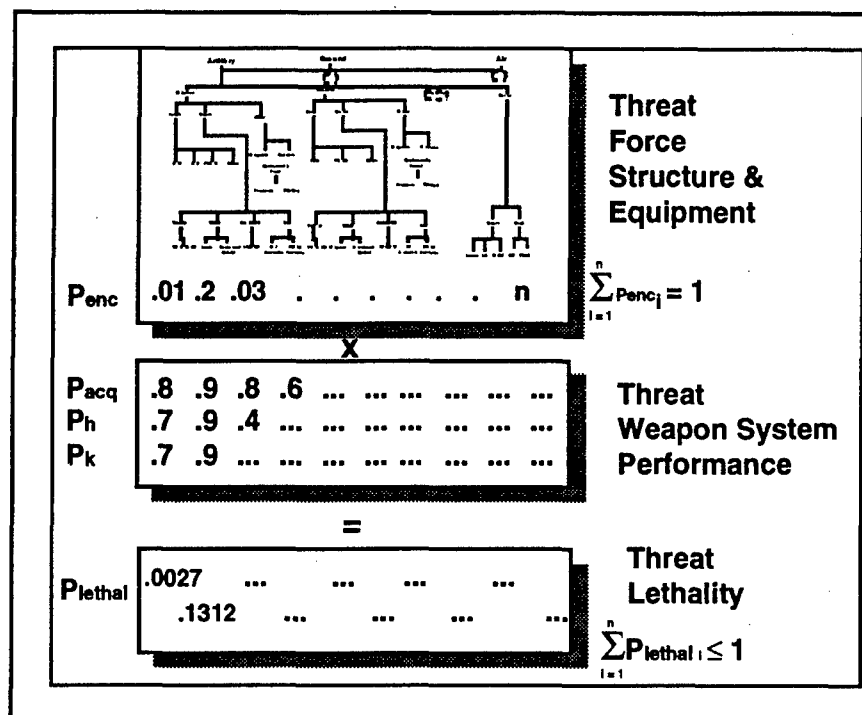


Figure 2. TOSOM Threat Data (U)

### 3. Survivability countermeasure effectiveness data

(U) Survivability countermeasure data describe the candidate systems for inclusion on the study vehicle. Each countermeasure must have information on its effectiveness against the specified threats. This value is represented in the formulation by the term  $eff_{i,j,k,l,m}$ , where the  $j,k,l,m$  coefficients again represent the specific threat system and the  $i$  is a specific countermeasure treatment. The value of  $eff$  is the percentage reduction of the threat weapon system lethality achieved by the treatment. Figure 3 displays the required relationship which must be developed between the different countermeasures, labeled as  $CM_1$ ,  $CM_2$ , etc., and the various threats to the system. The model requires that the effect of each countermeasure against each threat be defined (the effect may be 0).

		$CM_1$	$CM_2$	$CM_3$	$CM_4$	$CM_5$	....	$CM_n$
	$P_k$							
	$P_h$							
	$P_{acq}$							
Threat1		.04	.14	-	-	-	-	-
Threat2		-	-	.6	-	-	.5	-
Threat3		-	-	-	-	.8	-	-
:		-	-	-	-	-	-	-
Threatm		-	.3	-	-	-	-	-

Figure 3. Countermeasure Effectiveness Data (U)

UNCLASSIFIED

## UNCLASSIFIED

### 4. Countermeasure Burden Data

(U) The burdens of each treatment or countermeasure (cost, weight, data, power, etc. ) and the burden limits for each burden category must also be defined. In the mixed integer formulation this value is represented by the term  $BURDLIM_n$ . The relationship between countermeasures and burdens is displayed in Figure 4.

	CM <sub>1</sub>	CM <sub>2</sub>	CM <sub>3</sub>	CM <sub>4</sub>	CM <sub>5</sub>	....	CM <sub>n</sub>
Cost	10	12	8	14	9	...	7
Weight	22	.5	2	.7	8	...	11
Power	0	.1	.4	7	1	...	2
⋮	⋮	⋮	⋮	⋮	⋮	⋮	⋮
⋮	⋮	⋮	⋮	⋮	⋮	⋮	⋮

Figure 4. Countermeasure Burden Data (U)

(U) As can be seen, the TOSOM process requires considerable input data. However, it is very easy to modify the input data, and not unreasonable to require at least estimates for all of these items when designing survivability suites.

### (U) Solving the Problem

(U) Two methods of modeling the survivability benefits of applying countermeasure systems are currently available within TOSOM. Both use the same input data. The two techniques compliment each other in the analysis process.

- The first method is a mixed integer linear programming formulation which optimizes the benefits and burdens of the countermeasure(s) against the  $P_{lethal}$  value previously discussed. Up to two countermeasures per threat are applied in this formulation. This method finds a single optimal solution under the constraints provided.
- The second method provided within the TOSOM is exhaustive enumeration. The computer calculates the outcome of all possible combinations of countermeasures (up to 15), stores them into a relational database, and allows the user to conduct searches and queries.

(U) The lethal event probabilities used within TOSOM are modified by the specific countermeasures selected by the model for employment. For example, a "bare" blue system versus a red HE round may experience an untreated  $P_{lethal}$  of 0.8. If an armor countermeasure is employed the  $P_{lethal}$  of that threat may be reduced by 50% to 0.4 (or by some other percentage, but 50% for the sake of this example). Any additional countermeasures against this threat can only be applied against the remaining  $P_{lethal}$  of .4. The application of more than one countermeasure against a specific threat requires the multiplication of the probability reductions and the  $P_{lethal}$  value making the problem non-linear.

(U) Non-linearity brings a special set of problems to optimization models. Non-linear programming solvers are more complex (and expensive), operate slower, require more computer

## UNCLASSIFIED

resources and do not always produce global optimal solutions (there may be many "local" optimal solutions). A full discussion of the topic of non-linear optimization is beyond the scope of this paper. Suffice to say, the current implementation of TOSOM does not include a non-linear solver. Instead, the current formulation of the model performs a linear approximation allowing up to two countermeasures to be employed against any one threat system. Experiments have shown this approximation to typically be as accurate as the non-linear solution out to two decimal places. This degree of accuracy is deemed adequate given the coarse nature of most input data and the fact that TOSOM is designed for first order decision support.

(U) The  $E^2$  module of TOSOM precisely models the non-linear nature of combining countermeasures. The problem is not difficult for this module since no algorithm is applied and no optimal solution is sought. All possible solutions are generated and the database search tools are then used to sort and select the solutions of interest to the analyst.

### (U) Mixed Integer Formulation

(U) The following is a description of the TOSOM mixed integer formulation. This particular formulation produces an optimal solution under the assumptions of using up to two countermeasures for any particular threat. Other TOSOM formulations can produce higher resolution, more flexible responses at the possible cost of more computer run time, greater data requirements, possible infeasible situations or finding only a local optimum.

#### Indices

- i Survivability treatments
- ii Alias for i; again, all the survivability treatments
- j Encounter force type
- k Encounter unit type
- l Encounter system type
- m Encounter sensor type
- n Burdens on the vehicle (cost, weight, power, data, external/ internal volume)

#### Parameters

enper j	The likelihood of encounter of type j
unitper j,k	The percent of unit of type k within an encounter of type j
systemper j,k,l	The percent of systems of type l within a unit type k in encounter j
sensor j,k,l,m	The percent of sensor type m with system k
pa j,k,l,m	The probability of acquisition given a detection
ph j,k,l,m	The probability of a hit given acquisition
pk j,k,l,m	The probability of a kill given a hit
eff i,j,k,l,m	The effectiveness of treatment i against threat system j,k,l,m in terms of how much the treatment reduces one of the above 4 probabilities.
twoeff i,ii,j,k,l,m	The combined effectiveness of both treatments i and ii against threat system j,k,l,m. Calculated as $[1 - (1 - \text{eff}_{i,j,k,l,m}) * (1 - \text{eff}_{ii,j,k,l,m})]$ where i doesn't equal ii
burdeni,n	The value of the burden n for treatment i; e.g., treatment i adds 100 lb. of
weight	(burden n) to the vehicle
BURDLIM <sub>n</sub>	The allowable limit of increase of burden n attributable to all the treatments on the vehicle.
TKILL	Total kill potential. $\text{TKILL} = \sum_{j \in J} \sum_{k \in K} \sum_{l \in L} \sum_{m \in M} (\text{enper } j * \text{unitper } j,k * \text{systemper } j,k,l * \text{sensor } j,k,l,m * \text{pa } j,k,l,m * \text{ph } j,k,l,m * \text{pk } j,k,l,m)$

UNCLASSIFIED

Variables

treat <sub>i</sub>	Binary variable (0,1); 0 if the treatment is not used, 1 if the treatment is used
subtreat <sub>i,l,m</sub>	Binary variable to account for the treatment application against specific threat
pairtreat <sub>i,ii,l,m</sub>	Binary variable (1, if treatments i and ii are both used against threat system l,m, 0 otherwise)

(U) Problem Formulation

(U) The objective function can be written as:

Minimize  $Z = \text{TKILL} - \sum_{i \in I} \sum_{ii \in I} \sum_{j \in J} \sum_{k \in K} \sum_{l \in L} \sum_{m \in M} (\text{enper } j * \text{unitper } j,k * \text{systemper } j,k,l * \text{sensor } j,k,l,m * \text{pa } j,k,l,m * \text{ph } j,k,l,m * \text{pk } j,k,l,m) * [\text{subtreat}_{i,l,m} * \text{eff } i,j,k,l,m + \text{pairtreat}_{i,ii,l,m} * \text{twoeff } i,ii,j,k,l,m]$

subject to:

$$\sum_{i \in I} (\text{treat}_i * \text{burden}_{i,n}) \leq \text{BURDLIM}_n \quad \forall n$$

$$\sum_{ii \in I} (\text{pairtreat}_{i,ii,l,m} + \text{subtreat}_{i,l,m}) \leq 1 \quad \forall i, l, m$$

$$\sum_{ii \in I} \sum_{l \in L} \sum_{m \in M} \text{pairtreat}_{i,ii,l,m} / \text{RN} + \sum_{l \in L} \sum_{m \in M} \text{subtreat}_{i,l,m} / \text{TOTAL \# OF SUBTREATMENTS}_{i,l,m} \leq \text{treat}_i \quad \forall i$$

$$\sum_{ii \in I} \sum_{l \in L} \sum_{m \in M} \text{pairtreat}_{i,ii,l,m} + \sum_{l \in L} \sum_{m \in M} \text{subtreat}_{i,l,m} \geq \text{treat}_i \quad \forall i$$

(U) Because of the binary nature of the decision variables, this is a mixed-integer, linear program (MIP). After solving the MIP, we can look at the shadow prices and determine which are the binding constraints and what decrease in the objective functions one would get by relaxing the binding constraint; valuable information in sensitivity analysis. Also, with the single coefficient in the objective function that represents the probability of a lethal encounter,

$$(\text{enper } j * \text{unitper } j,k * \text{systemper } j,k,l * \text{sensor } j,k,l,m * \text{pa } j,k,l,m * \text{ph } j,k,l,m * \text{pk } j,k,l,m)$$

one can easily prioritize the threats for their impact on the objective function, survivability.

(U) We can make a constraint out of the current objective function so that we choose the treatments that guarantee we meet some specified level of survivability. We can similarly convert any of the constraints on 'burdens' to objective functions. This would allow us to determine the minimum cost ( or minimum weight, etc.) suite of treatments that meet specified survivability requirements.

(U) This TOSOM formulation can be used to produce a prioritized list of potential threats, i.e., which threats have the greatest probability of lethal encounters. The analyst can use it to select a set of countermeasure treatment suites or technologies to incorporate into higher level models such as CASTFOREM or JANUS to determine improved force effectiveness given inclusion of those suites. TOSOM can also provide sensitivity information to determine what design features and parameters have the most significant impact on improved survivability.

# UNCLASSIFIED

## (U) Exhaustive Enumeration (E<sup>2</sup>)

(U) The E<sup>2</sup> module is a straightforward application of conditional probability using the threat and countermeasure data provided by the user. Figure 5 provides an illustration of how conditional probability is applied within the module. The TOSOM calculates the probability of survival and the associated burdens for every possible combination of up to 15 countermeasures. The result is then stored in a database file and can be analyzed with a variety of tools which are also provided.

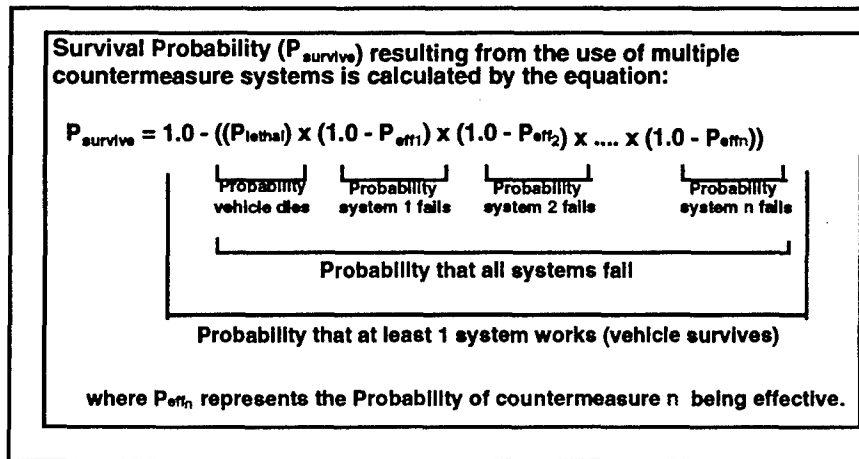


Figure 5. Conditional Probability (U)

(U) Figure 6 shows how the conditional probability calculations are implemented with the E<sup>2</sup> module. These calculations (and totals for the associated burdens) are performed for every combination of up to 15 countermeasures and the results written to a file. That file is then read by the TOSOM model and made available to the analyst, along with a variety of database tools, for study.

	$P_{\text{lethal}}$		CM <sub>1</sub>		CM <sub>4</sub>		CM <sub>5</sub>		$P_{\text{lethal (treated)}}$
Threat <sub>1</sub>	.187		(1 - .6 )		(1 - 0 )		(1 - 0 )		.075
Threat <sub>2</sub>	.457		(1 - .6 )		(1 - 0 )		(1 - 0 )		.183
Threat <sub>3</sub>	.011		(1 - 0 )		(1 - .8 )		(1 - 0 )		.002
Threat <sub>4</sub>	.155	X	(1 - .4 )	X	(1 - .0 )	X	(1 - .2 )	=	.074
.	.		(1 - . )		(1 - . )		(1 - . )		.
.	:		(1 - : )		(1 - : )		(1 - : )		:
Threat <sub>n</sub>	.005		(1 - 0 )		(1 - .48 )		(1 - .36 )		.001
$\Sigma =$ .872									
$\Sigma =$ .465									

Probability of  
**UNTREATED** system  
being killed

Probability of  
**TREATED** system  
being killed

Figure 6. E<sup>2</sup> Implementation (U)

## UNCLASSIFIED

(U) The E<sup>2</sup> approach has some advantages over the linear program. Rather than one "best" answer, the database can be searched for all solutions which meet user specified criteria. The countermeasures which show up in "many" acceptable combinations can be easily identified. A database can be generated and stored. Information will not change unless input parameters change so additional analysis is possible without rerunning the module. Finally, the E<sup>2</sup> provides robust and responsive "what if" analysis. The major drawback in this approach is its limitation with regard to the number of countermeasures which can be studied at one time. Currently the E<sup>2</sup> module will work for up to 15 countermeasures. This number of countermeasures generates over 32,000 records.

### (U) Conclusion

(U) TOSOM is a rapid, versatile, and reasonably comprehensive decision-making tool for selecting survivability measures for inclusion in a vehicle design. Its recommendations are based on the specific threats defined for the objective combat system. The tool can be effectively used in survivability concept development and requirements allocation to hardware. It provides survivability performance measurements for different sets of survivability suites against the defined threats. Because of its versatility and simplicity of computing platform (PC based) implementation, it can provide quick and inexpensive evaluations of evolving technologies, "what-if" and sensitivity analyses, and screening of alternatives for combat modeling and field demonstration.

(U) TOSOM provides a valuable and much needed capability to conduct tradeoff analysis and to explore the utility and limiting conditions surrounding survivability analysis. The greatest limitation with this and many other models is the volume and availability of data used by the program to reach a solution. Without solid operational and engineering analysis of the threat systems and the treatments necessary to produce the required data, this tool will produce answers which are meaningless.

(U) The tradeoff analysis should account for identified threats, possible alternative survivability suite architecture's / components, architecture / component performance and / or effectiveness against the examined threats, and the burdens (cost, weight, space, power, compatibility, safety, etc.) associated with each architecture / component. TOSOM provides a mechanism to conduct just such analysis in a quantifiable and repeatable process. Use of TOSOM can provide sensitivity analysis of key or major assumptions allowing a determination of the robustness of the identified solution.

UNCLASSIFIED

UNCLASSIFIED

## ORDER OF MAGNITUDE TRADEOFFS USING LANCHESTER EQUATIONS

John Reed, Daniel Hicks, David Fredrick, William Jackson  
Survivability Center

U.S. Army Tank-automotive and Armaments Command Research, Development and Engineering Center  
(TARDEC)  
Warren, MI 48397-5000

### ABSTRACT (U)

(U) Using the most common form of the Lanchester equations for modern warfare, order of magnitude tradeoffs between various survivability technologies and cost will be presented.

(U) The Lanchester equations are a pair of ordinary differential equations relating the rate of change of force size with force size and various parameters. The parameters include, for example, the time for the Red threat to acquire a Blue target, the single shot kill probability of a Red threat to kill a Blue target, and the symmetric parameters.

(U) The single shot probability of a Red threat killing a Blue target can be taken as a surrogate measure of the level of Blue armor or hit avoidance protection. Likewise, the time for a Red threat to acquire a Blue target can be taken as a surrogate measure of the level of Blue's signature or detectability. With these substitute measures, the Lanchester equations allow us to make order of magnitude tradeoffs between Blue detectability and Blue armor protection. Other similar tradeoffs, including cost, will be presented.

(U) The purpose of this paper is to elucidate an extremely quick and simple technique for providing order-of-magnitude answers to questions concerning the tradeoffs between various survivability capabilities and cost, and order of magnitude tradeoffs among various survivability capabilities, themselves. Historically, these quick and dirty tradeoffs have been determined sometimes by questionable methodologies or by some arbitrary rule-of-thumb (What percent of the unit cost should I spend towards survivability?). These "rough order" estimates have traditionally been beset by unquantifiable assumptions. The Lanchester differential equation approach, as opposed to other non-standardized methods, provides the decision maker with "back of the envelope" solutions backed up with a quantifiable, systematic, reliable methodology. This paper will provide a general discussion of the Lanchester differential equations followed by how they are applied utilizing a spreadsheet model of this simple technique. Additionally, a number of examples utilizing this method will also be presented.

(U) We take as our starting point the Lanchester differential equations of modern warfare (ref. 1). The Lanchester equations are a pair of ordinary differential equations relating the rate of change of force size with force size and other parameters, in a static battlefield environment. The parameters include, for example, the time for a Red threat to acquire a Blue target, the single shot probability of a Red threat killing a Blue target, and the same parameters with Red and Blue interchanged. Within each of these parameters lie various survivability

UNCLASSIFIED

DISTRIBUTION STATEMENT A. Approved for public release; distribution unlimited.



components of a weapons platform. For example, the time for a Red threat to acquire a Blue target can be taken as a surrogate measure of the level of Blue's signature or detectability. The single shot probability of a Red threat killing a Blue target can be taken as a surrogate measure of the level of Blue armor, Blue hit avoidance protection, or of Red lethality. These parameters can then be modeled in a spreadsheet as surrogate survivability characteristics of the platform. With these substitute measures, the Lanchester equations then allow us to make order of magnitude tradeoffs between Blue detectability, Blue armor protection, Blue hit avoidance, Blue lethality, and cost.

(U) Briefly, the Lanchester equations of modern warfare are:

$$dx/dt = -ry \text{ and } dy/dt = -bx$$

where  $x = x(t)$  is the size of the Blue force at time  $t$ ,  $y = y(t)$  is the size of the Red force at time  $t$ , with  $r$  and  $b$  being constants that measure the effectiveness of the Red and Blue forces, respectively. In this most elementary case of the Lanchester equations, it is of use to observe that the system of differential equations can be explicitly solved. The solution is given by the following pair of equations:

$$x(t) = \frac{1}{2} \left\{ \left[ x_0 - \sqrt{\frac{r}{b}} y_0 \right] e^{\sqrt{rb}t} + \left[ x_0 + \sqrt{\frac{r}{b}} y_0 \right] e^{-\sqrt{rb}t} \right\}$$

$$y(t) = \frac{1}{2} \left\{ \left[ -x_0 \sqrt{\frac{b}{r}} + y_0 \right] e^{\sqrt{rb}t} + \left[ x_0 \sqrt{\frac{b}{r}} + y_0 \right] e^{-\sqrt{rb}t} \right\}$$

The units of  $r$  and  $b$  are inverse units of time. The form of  $r$  is given by:

$$1/r = \text{trab} + 1/(rfr \times \text{ssprkb})$$

where  $\text{trab}$  is the time for Red to acquire Blue,  $rfr$  is the Red firing rate, and  $\text{ssprkb}$  is the single shot probability of Red killing Blue. Likewise, the form of  $b$  is given by:

$$1/b = \text{tbar} + 1/(bfr \times \text{sspbkr})$$

where  $\text{tbar}$ ,  $bfr$ , and  $\text{sspbkr}$  have interpretations similar to those for  $r$ . Thus, in addition to needing to know the red and blue platform costs (if we are using the model in a costing scenario), we have only the parameters  $x(0)$ ,  $y(0)$ ,  $\text{tbar}$ ,  $\text{trab}$ ,  $bfr$ ,  $rfr$ ,  $\text{sspbkr}$ , and  $\text{ssprkb}$  upon which to base our conclusions.

(U) Our general approach for using the equations is as follows: We fix all parameters except two. This effectively reduces the parameter space to two dimensions. Next, we draw the curve of parameter points which produce a draw in the battle between Red and Blue (it follows that on one side of the curve Blue wins the engagement while Red wins on the opposing side). See Figure 1 for an example. Then, given data for a baseline platform, we determine a point on the draw curve. This point is called the baseline point. Finally, one parameter is modified to reflect estimated future capability, and the other parameter is adjusted so as to remain on the draw curve. This then allows tradeoffs between the two parameters to be determined.

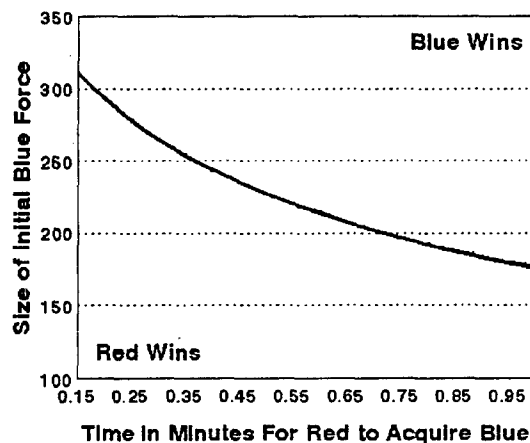
UNCLASSIFIED

(U) Several examples have been included which will illustrate the above approach. It should be noted here that the decision maker determines all the values for the variables and the initial values. As we will see, part of the simplistic beauty of the Lanchester equations spreadsheet model is the ease with which any of these variables can be adjusted.

(U) The first example will answer the question: For a \$5 million Blue main battle tank (MBT), what is a reasonable amount to spend on modifications which reduce its signature, if the time for Red to acquire Blue increases by 25%? Since we are interested in cost (which is derived at the conclusion of the battle by units saved) and the time for Red to acquire Blue, the two parameters which we will allow to vary are,  $x(0)$ , the initial size of the Blue force, and  $trab$ , the time for Red to acquire Blue.  $trab$  will be used as the x-axis variable,  $x(0)$  as the y-axis variable. These two varying parameters, as well as the fixed parameters, are as follows:

$x(0)$  = y-axis,  
 $y(0)$  = 300 vehicles, initial size of the Red force,  
 $tbar$  = 0.25 minutes, time for Blue to acquire Red,  
 $trab$  = x-axis (baseline value .38 minutes),  
 $bfr$  = 8 rounds per minute, Blue firing rate,  
 $rfr$  = 8 rounds per minute, Red firing rate,  
 $sspbkr$  = 0.70, single shot probability of Blue killing Red,  
 $ssprkb$  = 0.50, single shot probability of Red killing Blue.

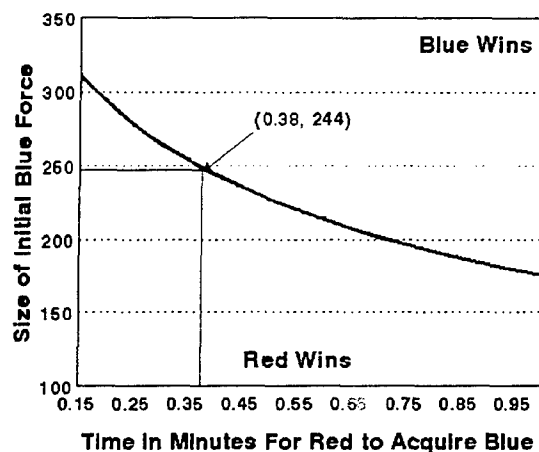
The two-dimensional parameter space, including the draw curve with Blue wins and Red wins regions, is shown in Figure 1.



(U) Figure 1

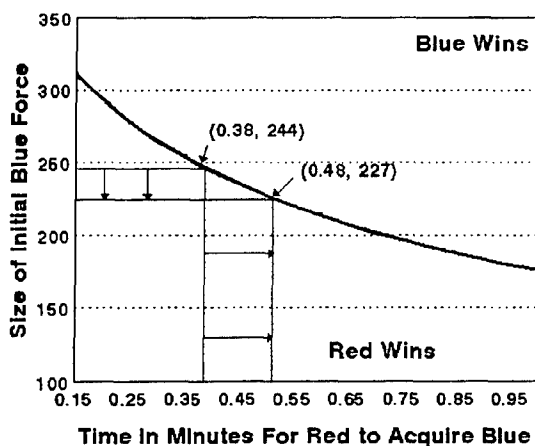
(U) To establish a baseline point, assume  $trab$  to be 0.38. This is approximately 50% worse than Blue's performance in acquiring Red, which is not an unreasonable assumption. Now, using this value for  $trab$  and the expression for  $x(t)$ , it can be calculated (or estimated from the draw curve) that  $x(0)$  will be 244 units. That is, the point (0.38, 244) will become the baseline point on the draw curve; if  $x(0)$  is larger than 244 with  $trab$  fixed, or,  $trab$  is larger than 0.38 with  $x(0)$  fixed, then Blue will win the engagement. Likewise, if  $x(0)$  is smaller than 244 with  $trab$  fixed, or,  $trab$  is smaller than 0.38 with  $x(0)$  fixed, then Red wins the battle. For other pairs of varied parameters, a calculation will determine on which side of the draw curve the parameter pair lies (or again by observing the graph). See Figure 2.

UNCLASSIFIED



(U) Figure 2

(U) Now, suppose that the Blue platform is modified in such a fashion that it will be more difficult to detect and that this modification forces Red to incur a 25% increase in time for detecting Blue. That is,  $t_{\text{red}}$  increases from 0.38 to approximately 0.48 minutes. This in turn reduces  $x(0)$  to 227 in order to remain on the draw curve. See Figure 3. Thus, by decreasing Blue detectability by 25%, up to \$85 million can be saved  $([244 \text{ platforms} - 227 \text{ platforms}] \times \$5 \text{ million})$ . We conclude "up to" \$85 million because we have not taken into account other factors which may be involved with determining unit costs such as learning curves, etc. These estimated dollars are now available to pay for the decreased Blue detectability. Spreading that savings over the 227 remaining vehicles we can invest nearly \$375,000 per platform to decrease Blue's detectability if it forces Red to increase his acquisition time by 25%.



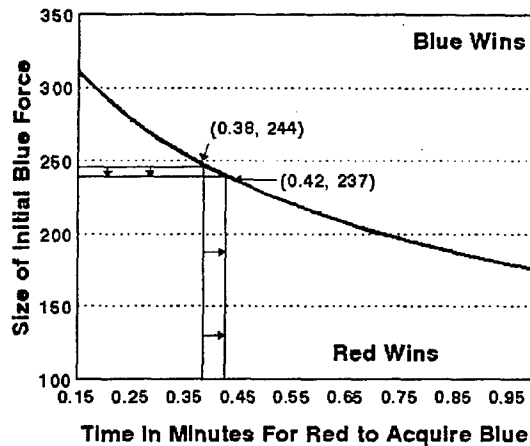
(U) Figure 3

(U) Pressing this example slightly further, suppose that the change in Blue detectability is a more modest 10% decrease, rather than the 25% decrease previously assumed. Then,  $t_{\text{red}}$  will only increase to approximately 0.42 rather than 0.48 minutes. This time  $x(0)$  will decrease from 244 to 237 vehicles so that 7 Blue vehicles are saved with a value of \$35 million. See Figure 4. Again spreading this savings over the 237 remaining

UNCLASSIFIED

UNCLASSIFIED

platform we can invest up to \$148,000 per vehicle to reduce detectability if it forces Red to increase his acquisition time by 10%.



(U) Figure 4

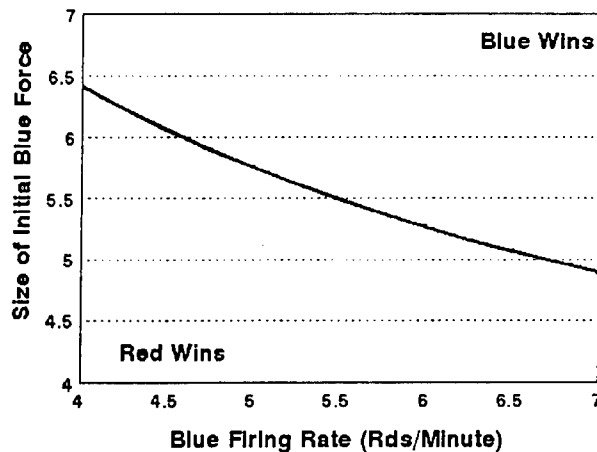
(U) Another example of a cost tradeoff is given in the following example and answers the question: For a \$4.5 million artillery platform, what are the investment costs associated with increasing Blue's firing rate 20%? This time, since we are interested in cost and the increase of Blue's firing rate; the two parameters which we will vary are,  $x(0)$ , the initial size of the Blue force, and  $bfr$ , the Blue firing rate in rounds per minute.  $bfr$  will be used as the x-axis variable,  $x(0)$  as the y-axis variable. These two varying parameters, as well as the remaining fixed parameters are as follows (modified from the first example to reflect the change in platform):

$x(0)$  = y-axis, initial size of the Blue force,  
 $y(0)$  = 6, initial size of the Red force,  
 $tbar$  = 1.0 minutes, time for Blue to acquire Red,  
 $trab$  = 4.0 minutes, time for Red to acquire Blue,  
 $bfr$  = x-axis, Blue firing rate (baseline value of 5 rounds per minute),  
 $rfr$  = 5 rounds per minute, Red firing rate,  
 $sspbkr$  = 0.006, single shot probability of Blue killing Red,  
 $ssprkb$  = 0.006, single shot probability of Red killing Blue,

(U) The two dimensional parameter space, including the draw curve with Blue and Red wins regions, is shown in Figure 5.

UNCLASSIFIED

UNCLASSIFIED



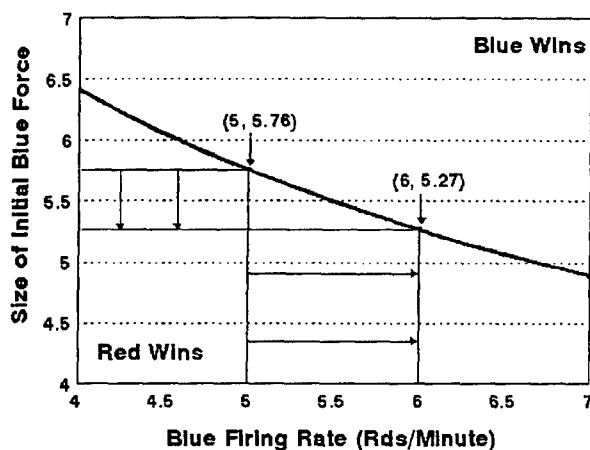
(U) Figure 5

(U) As in the previous example, to establish a baseline point, assume bfr is equal to rfr at 5 rounds per minute. Using this value for bfr and the expression for  $x(t)$ , it can be calculated (or estimated from the draw curve) that  $x(0)$  will be 5.76 units. The point (5, 5.76) will be the baseline point on the draw curve; if  $x(0)$  is larger than 5.76 units with bfr fixed, or, bfr is greater than 5 rpm with  $x(0)$  fixed, then Blue wins the battle. Similarly, if  $x(0)$  is smaller than 5.76 units with bfr fixed, or bfr is smaller than 5 rpm with  $x(0)$  fixed, then Red wins the battle. Like before, a calculation can easily determine which side of the draw curve other pairs of parameters will lie (or by observation of the graph).

(U) Next, we will assume that the Blue artillery unit is modified in such a way as to increase its firing rate 20%, from 5 to 6 rpm (i.e., increasing bfr from 5 to 6). Again it follows that to remain on the draw curve  $x(0)$  must be reduced by nearly half a platform (.49 units) to 5.27. See Figure 6. Hence, by increasing Blue's rate of fire 20%, we can recognize a savings of approximately \$2.21 million (that is, [5.76 units - 5.27 units] x \$4.5 million). This estimated savings can offset the cost of the increased firing rate to the amount of \$419,000 per platform.

UNCLASSIFIED

UNCLASSIFIED



(U) Figure 6

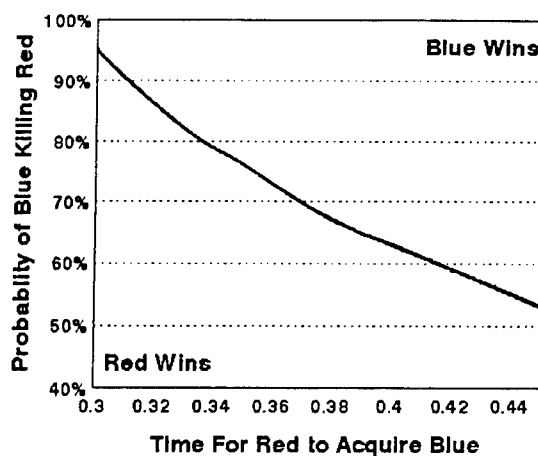
(U) A third example exemplifies the use of the Lanchester equation spreadsheet model from a strictly technological tradeoff standpoint; that is, not utilizing cost. This example begins by considering the question: Red has a new and improved armor package which decreases the sspbkr by 15%. If the technology does not presently exist to increase the lethality of Blue, but does exist to decrease Blue's detectability, how much must Blue reduce its signature to compensate for Red's increase in armor? In this example we are interested in playing the lethality of the Blue vehicle against the detectability of the Blue vehicle. The two parameters that we will let vary then, are, sspbkr, the single shot probability of Blue killing Red (for Blue's lethality), and trab, the time for Red to acquire Blue (for Blue's signature). The two varying parameters, as well as the remaining fixed parameters, are as follows:

$x(0)$  = 250 vehicles, initial size of the Blue force,  
 $y(0)$  = 300 vehicles, initial size of the Red force,  
 $tbar$  = 0.25 minutes, time for Blue to acquire Red,  
 $trab$  = x-axis, time for Red to acquire Blue,  
 $bfr$  = 8 rounds per minute, Blue firing rate,  
 $rfr$  = 8 rounds per minute, Red firing rate,  
 $sspbkr$  = y-axis, single shot probability of Blue killing Red (baseline value of 0.70),  
 $ssprkb$  = 0.50, single shot probability of Red killing Blue.

(U) The draw curve with the associated Blue and Red win regions is shown in Figure 7.

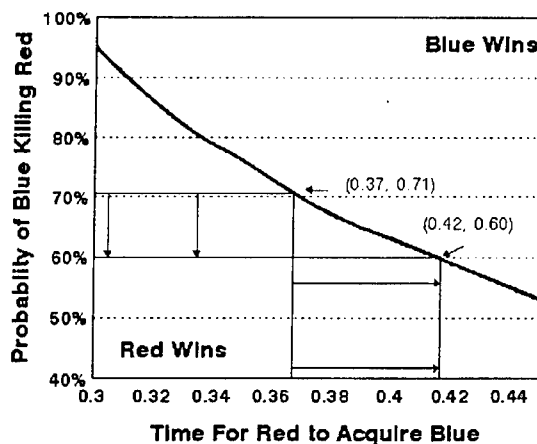
UNCLASSIFIED

UNCLASSIFIED



(U) Figure 7

(U) For this example the established sspbkr of 0.70 minutes will be assumed as the baseline value. Then, from either the draw curve or from the equations, a corresponding value of 0.37 minutes for trab can be determined (that is, a baseline point of (.37, .70)). This is followed by calculating the value which decreases sspbkr by 15%. This value is  $(.70 - (.70 \times .15)) = 0.60$ . That is, improved Red armor has reduced Blue's lethality to 0.60. Again, for this new value of sspbkr, the corresponding value of trab is determined from the draw curve or the equations; this value of trab is 0.42 minutes. See Figure 8. From the delta in sspbkr, a percentage can be determined which corresponds to the increase in trab required to compensate for the decrease in sspbkr. This required increase in trab is 14%. Hence, the punchline for the decision maker in this case is: "A 15% decrease of single shot lethality of the Blue platform can be compensated by a 14% reduction in Blue's signature."



(U) Figure 8

(U) The final example will briefly describe another technological tradeoff which answers the question: A MBT is presently capable of firing at a rate of 8 rounds per minute. If we are interested in conserving rounds,

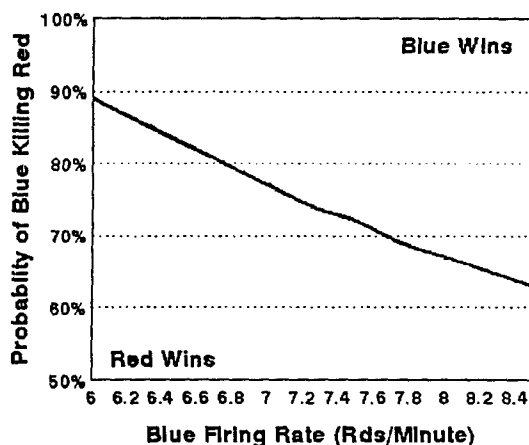
UNCLASSIFIED

# UNCLASSIFIED

how much must lethality be improved to recognize a savings of one round per minute? The two parameters to vary are, sspbkr, the single shot probability of Blue killing Red, and bfr, Blue firing rate. The two varying parameters, as well as the remaining fixed parameters, are as follows:

$x(0) = 250$  vehicles, initial size of the Blue force,  
 $y(0) = 300$  vehicles, initial size of the Red force,  
 $tbar = 0.25$  minutes, time for Blue to acquire Red,  
 $trab = 0.38$  minutes, time for Red to acquire Blue,  
 $bfr = x$ -axis, Blue firing rate (baseline value of 8 rounds per minute),  
 $rfr = 8$  rounds per minute, Red firing rate,  
 $sspbkr = y$ -axis, single shot probability of Blue killing Red,  
 $ssprkb = 0.50$ , single shot probability of Red killing Blue.

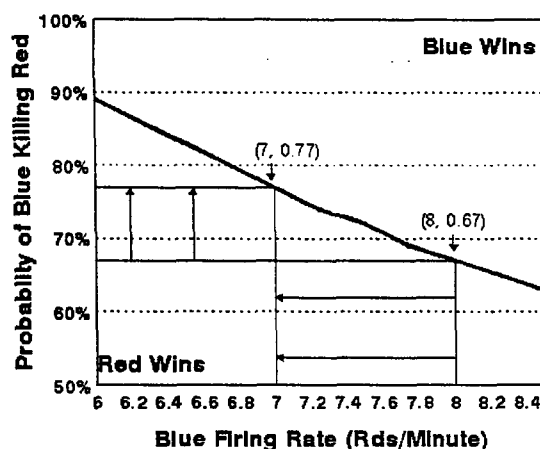
(U) The draw curve with the associated Blue and Red win region is shown in Figure 9.



(U) Figure 9

(U) From the draw curve or from the equations, utilizing a baseline value for bfr of 8 rpm, we can determine a baseline value for sspbkr of 0.67. Decreasing rpm to 7 (conserving one rpm), the corresponding sspbkr is 0.77 (again from the graph or from the equations). See Figure 10. The moral of the story for the decision maker is: "On an MBT on the battlefield, an increase of about 15% in lethality is required to conserve one round of ammunition per minute."





(U) Figure 10

(U) In summary the Lanchester differential equations spreadsheet model is a quick, easy, and quantifiable "what if" tool designed to assist the decision maker in playing rough order cost and technology tradeoffs for a given platform. The model is neither CASTFOREM or JANUS, but then it is not intended to be. However, the model may very well be utilized in conjunction with these larger, more sophisticated models, for fast pre-run reasonability checks, or to act as a filtering agent to reduce the number of scenarios required to be run using these more time consuming and more expensive models. And, as a matter of time and expense, the spreadsheet model can be developed using nearly any spreadsheet software package in a matter of hours, with differing scenarios developed and played out in minutes. The techniques discussed here, and the examples explained in this paper only begin to demonstrate to the decision maker the capabilities of this simple, yet powerful, tool.

(U) Reference

(U) James G. Taylor, "Force-on-Force Attrition Modeling," Operations Research Society of America, 1981.

## **TOSOM in Support of Crusader Survivability Suite Trade-Off Analyses**

Hugh Griffis  
Teledyne Brown Engineering  
Huntsville, AL 35805

### **ABSTRACT (U)**

(U) This paper presents the analysis methodology in use for ongoing Crusader Survivability Suite Trade-Off Analyses. The methodology and data analysis techniques, applied to both input and emerging results data, provide the reader valuable insights into one method of using TOSOM in support of survivability suite trade-off analyses.

(U) INTRODUCTION. The purpose of this document is to provide the reader some insight into one method of using the Threat Oriented Survivability Optimization Model (TOSOM) to conduct survivability suite trade-off analyses. The Crusader Program is currently in the Requirements Analysis / Concept Maturation phase of development. Team Crusader has been conducting survivability treatment concept trade-off analyses to determine the initial priorities to be set during the Demonstration and Validation (DEM / VAL) Phase of the Crusader Life Cycle. The analytical approach presented here is the methodology in use by Team Crusader to conduct these trade-off analyses.

(U) OVERVIEW. The purpose of this analysis was to focus the Crusader survivability suite development during the DEM/VAL Phase of the system life cycle. To accomplish this purpose the TOSOM-Like Model (TLM) was used to conduct the initial concept trades. The TLM is a slightly modified version of the Mixed Integer Program used as the formulation in the TOSOM model. The original model was modified to address some specific Crusader issues and renamed to avoid confusion. The basic premise behind the TLM methodology centers around threat lethality:

The lethality of any given threat against the Crusader system is a function of the number of times the given threat encounters the Crusader and the consequence of each of those encounters.

Mathematically:

$$\begin{aligned}\text{Total Threat Lethality} &= P(\text{encounter}) * P(\text{consequence}) \Rightarrow \\ \text{Total Threat Lethality} &= P(\text{encounter}) * P(\text{acq}) * P(\text{hit|lacq}) * P(\text{kill|hit})\end{aligned}$$

Threat encounter and one-on-one lethality data were transformed into multiple round engagement data and used to define the threat lethality. One-on-one treatment effectiveness data were provided by Team Crusader and combined into feasible sensor-countermeasure combinations (hereafter referred to as Threat Warning systems and CounterMeasures (TWACM)). One-on-one treatment effectiveness data were also provided for several armor, susceptibility reduction, and situational awareness concepts. These detection, hit, and kill avoidance concepts were combined in the TLM model and the optimal solution returned. The purpose of this optimization was to determine the best conceptual survivability suite solution for the

Crusader given the cost and weight constraints established by the program. The optimal solution; given the threat, program cost and weight constraints, and the treatment effectiveness and burden data; was a balanced survivability suite. This balanced solution consisted of TWACM, Armor, Susceptibility Reduction, and Situational Awareness technologies. The analysis results are used to establish the priorities for technology development and exploration during the DEM/VAL phase of the Crusader's life cycle. As technologies mature and knowledge is gained about candidate systems, this type of analysis will be repeated to either confirm or change the direction for technology development or integration. Figure 1 shows the Survivability Suite Analysis Methodology in use by Team Crusader. This methodology allows Crusader to utilize modeled and test data to define the treatment effectiveness, use the TLM model to determine the major survivability treatment "players", and develop the baseline force survivability expectations. The CASTFOREM modeling is done specifically to examine the effects of multiple threat engagements against multiple Crusaders. The TAFSM modeling examines the force level survivability benefits attributable to the modeled survivability suite.

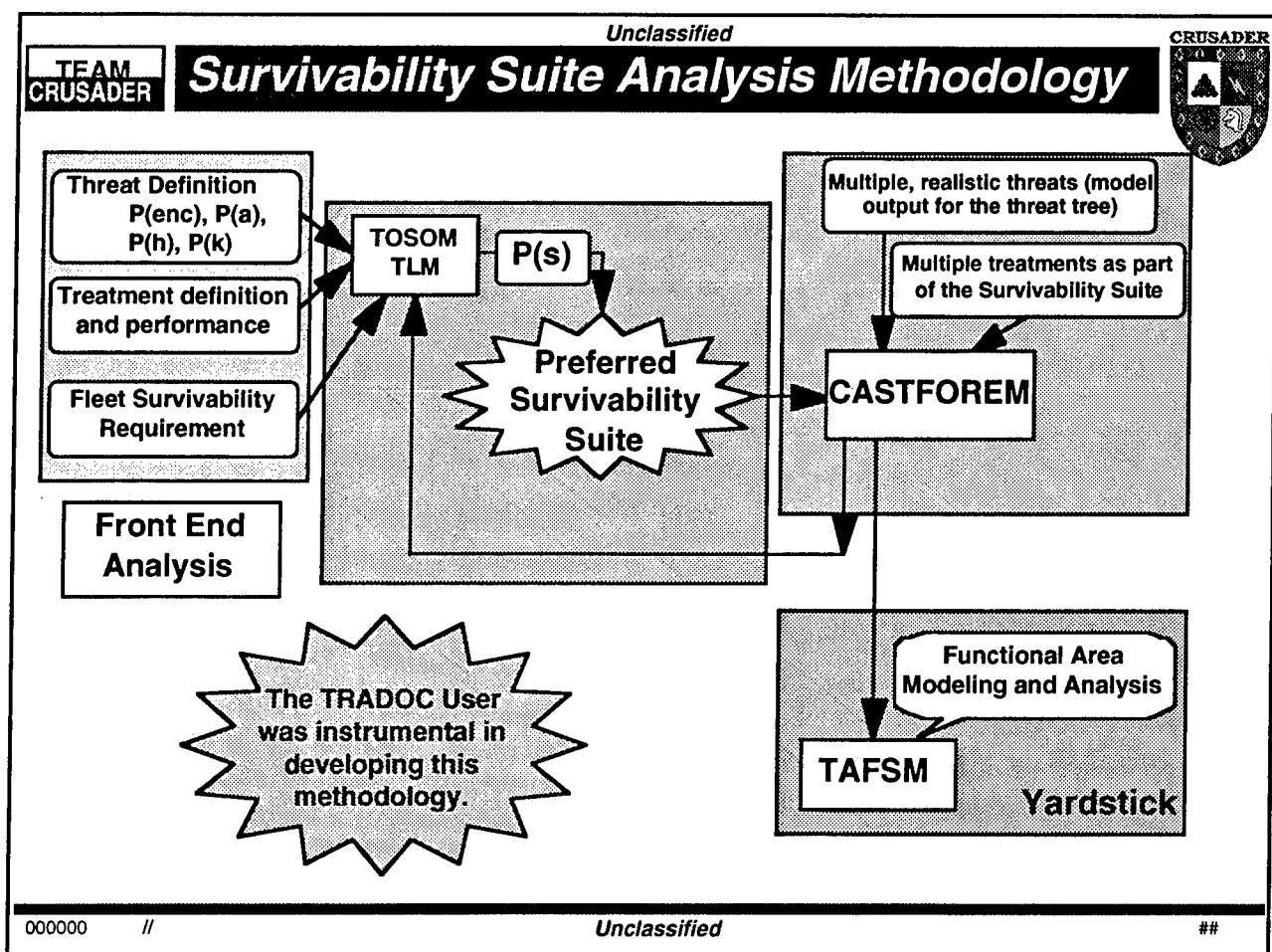


**Figure 1. Crusader Survivability Suite Analysis Methodology**

Key to this process is the fact that this methodology is iterative in nature. As data are refined and new TTP are developed, the TLM modeling and analysis must be repeated to insure technologies are correctly prioritized within the Crusader Program.

(U) TOSOM / TLM. To maximize survivability (minimize threat lethality), subject to cost and weight constraints, an optimization approach was used to allocate survivability treatments to the vehicle design. The TLM is a Mixed Integer Program (MIP) which maximizes the survivability of a single vehicle in a single expected value encounter. The TLM is a slightly modified version of the MIP used as the formulation in the TOSOM model. The original model was modified to address some specific Crusader issues and renamed to avoid confusion. The expected threat systems and their total lethality drive the solution, subject to burden constraints. The decision variables are the survivability treatments included in the vehicle's survivability suite to counter the threat. To maximize survivability the model chooses treatments that can counter the specific threats according to quantitative measures of each treatment's effectiveness at countering the threats. The assignments of the treatments are chosen such that the resulting suite does not exceed established burden limits. The Exhaustive Enumeration (E2) module of TOSOM was also used during this analysis. The E2 module calculates each possible combination of survivability treatments with associated burdens. This data allows a detailed understanding of the feasible solution space.

(U) Metrics. The primary metric from the TOSOM is the individual vehicle probability of survival (P(s)). P(s) is defined as the probability of a single Crusader surviving a single expected value encounter. The total threat lethality is the probability of a kill by that threat system given an encounter occurs. The sum of the total threat lethality of all threats is the total lethality inherent to the Crusader or the expected probability of a kill (M/F kill) of the Crusader given a single expected value encounter. Conversely, the inherent survivability of the system without treatments is:

$$P(s) = [1 - \{\sum_{(i=1, 30)} [\text{Total threat lethality (i)}]\}],$$

where (i) designates the threat systems.

The inherent survivability of a single Crusader against the threat represented in the analysis is approximately 70% (the sum of the lethality of all threats against the Crusader is approximately 30%). In other words, the Crusader achieves 70% survivability through Tactics, Techniques, and Procedures (TTP - survivability moves) and threat inefficiencies. The overall P(s) metric is the sum of the inherent survivability (70%) achieved through TTP and the amount of the total lethality the Crusader can eliminate with a survivability suite.

Other measures of performance were also used to assess suite performance. Cost and weight were significant discriminators. Cost was the constraining variable during the analysis. Weight turned out to be a discriminator but was not the constraining variable in most cases. The number of threats that were not countered at all was also another measure of performance used to choose suite components.

(U) DATA DEVELOPMENT. Figure 2, Data Development Process Overview, describes the engineering level thought process required to develop the input data for TLM. This analysis used a focused process to determine the data used to represent each of the threats and survivability treatments within the TLM model. The threats were defined in accordance with data provided by the TRADOC User and AMSAA. The program threat experts were consulted and threat data modified until consistency with program documentation, modeling efforts, and AMSAA data was achieved. Treatment data sheets were then prepared for each treatment-threat pairing. The treatment data sheets were used by each of the Team Crusader survivability treatment

engineers to provide the required data in support of the analysis. The treatment data sheets structure the engineering estimate by providing a description of the threat engagement and the threat effectiveness. The expectation is for the treatment to defeat a specific aspect (or multiple aspects) of the threat encounter chain.

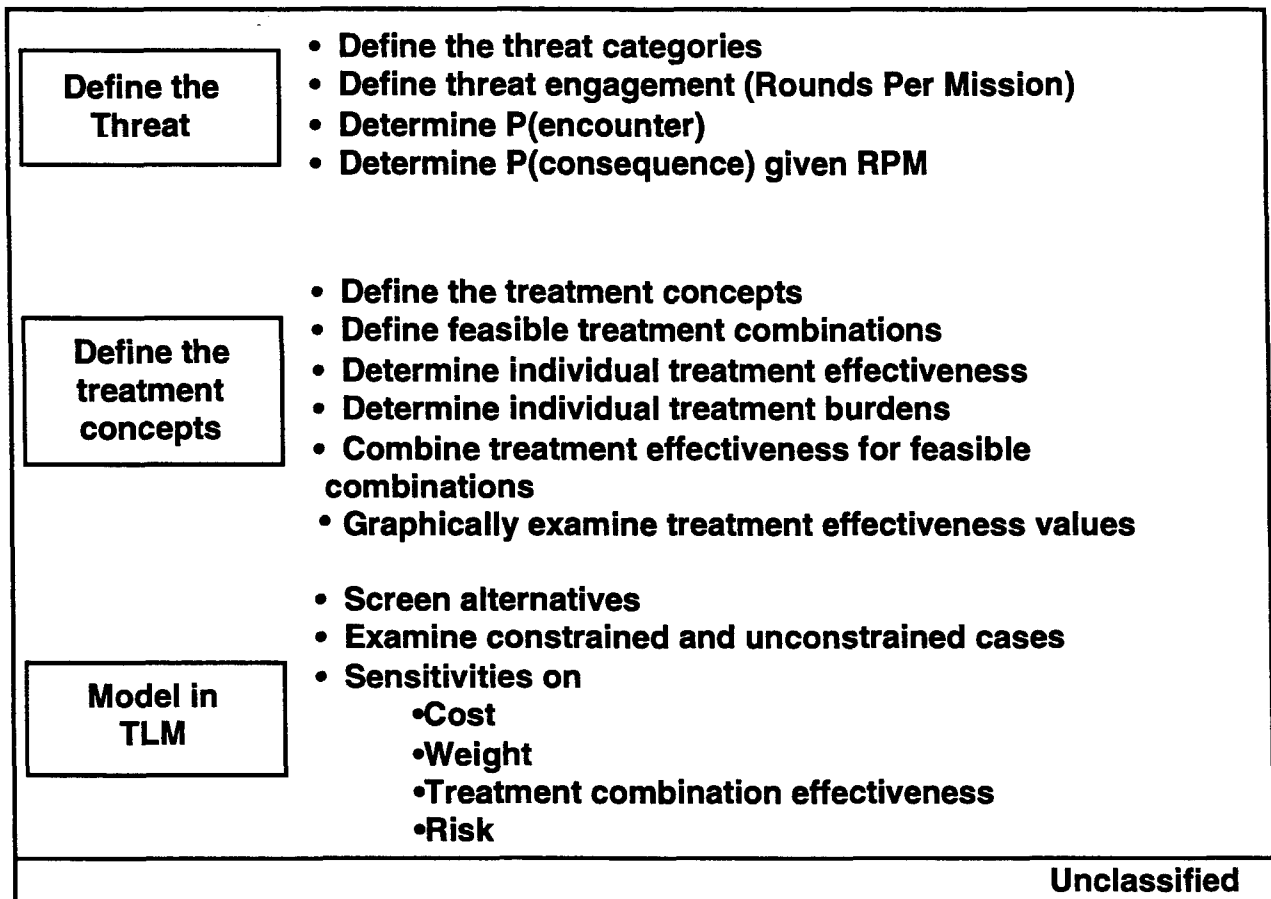


**Figure 2. Data Development Process Overview**

The following paragraphs describe each step of the process in greater detail.

(U) Threat Definition. The first step of the analysis was to define the threat. This step required extensive coordination with various threat agencies. The threat systems were defined in terms of two discrete metrics: (1) the probability of encounter ( $P(\text{enc})$ ), which is the probability that the Crusader is engaged by a specific threat system; and (2) the consequence probability, which consists of the probability of acquisition ( $P(a)$ ), probability of hit ( $P(h)$ ), and the probability of kill ( $P(k)$ ) versus the Crusader. An examination of the threat encounter distribution defines the frequency of encounter to specific types of threats for the Crusader. The consequence probability can be considered equivalent to the Single Shot Probability of Kill (SSPK) of the threat system against the Crusader. Note the probability of kill has been defined for this analysis as the probability of a mobility or firepower kill against the Crusader.

(U) Probability of Encounter. The probability of encounter data was derived from a compilation of model output and intelligence projections. The data was used to develop a hierarchical threat tree that contains representative threats from three types of threat platforms: (1) indirect fire, which include cannon, rocket, and mortar delivered munitions; (2) ground threats, which include armored vehicles and

dismounted infantry delivered munitions; and (3) air threats, which include fixed wing and rotary wing aircraft delivered munitions. Survivability moves (shoot & scoot) were integrated into the probability of encounter data. As a result of this exercise, a total of 30 threats (with a  $P(\text{enc})$  greater than zero) were defined for this study: 14 indirect fire threats, 10 ground threats, and six air threats. Each of these 30 threat categories has a "representative" threat system, selected as representative of the category, and identified in the Crusader Threat Support Plan. An example of the threat tree structure is shown in Figure 3.

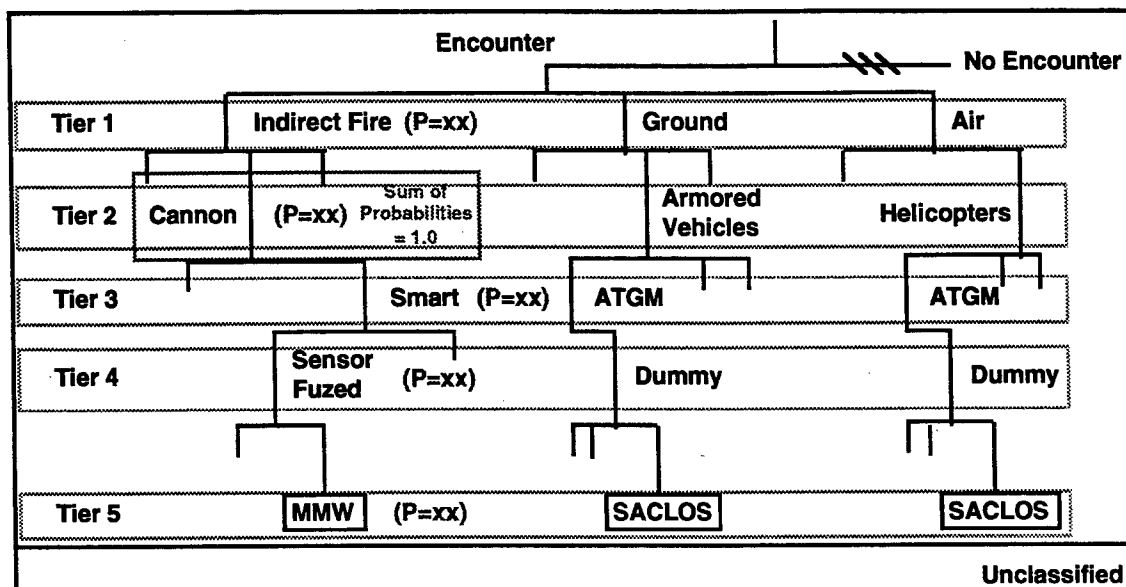


Figure 3. Structure of the threat tree

(U) **Consequence Probabilities.** The consequence data are comprised of three components;  $P(\text{acq})$ ,  $P(\text{hit})$ , and  $P(\text{kill})$ . The first component of the consequence data,  $P(\text{acq})$ , is the probability of acquisition. This data item refers to the probability of detection in the case of a smart munition, and the probability of acquisition in the case of a man in the loop sensor/sight.  $P(\text{acq})$  is defined as the likelihood of a munition/vehicle reaching a detection threshold and alerting on the Crusader given nominal range and background clutter values. The second component,  $P(h)$ , is the probability of a hit given a successful fusing/flyout.  $P(h)$  is the likelihood the munition will hit the target at a nominal range. The third component,  $P(k)$ , is the probability of kill given a hit, and is defined as the likelihood of a mobility or firepower kill given a hit.

The one-on-one consequence data were derived from AMSAA data. During early threat working group sessions, the team determined that single round engagements (specifically indirect fire area (dumb) munitions) are not typical against the Crusader. Consequently, the threat working group determined that the threat engagement must also be defined in terms of "rounds per mission". Several assumptions were made and the one-on-one consequence data were transformed from representative of a one-on-one engagement to representative of a multiple round engagement.

(U) **Treatment Data.** The second step of the analysis began by defining the set of possible treatment concepts available to counter the threat. Four different categories of treatments were considered: Threat Warning sensors and Countermeasures (TWACM), armor treatments, susceptibility reduction treatments (hypothetical), and

situational awareness sensors. NOTE: as described earlier, the individual sensor and countermeasures were combined into feasible sensor-countermeasure combinations. When these combinations were finalized, the effectiveness values were changed to reflect the effectiveness of multiple sensors, multiple countermeasures, or both against a specific threat. The treatments concept data were expressed in terms of effectiveness and burdens. The individual component effectiveness values were obtained from engineers at Team Crusader. These values were expressed as the percentage degradation of threat consequence. These values were a one-on-one treatment effectiveness and were combined assuming independence from other treatments on the vehicle. Burdens, on the other hand, represent constraints on the treatment components. For this analysis, only cost and weight burdens were addressed. Other constraints, such as power requirements and risk were examined but not used as constraints on the optimal solution.

#### THE TRADE-OFF ANALYSIS.

(U) Preparation. The analysis began with a thorough examination of the data to understand the treatment concepts and the expected performance of the treatments. Each of the treatments' effectiveness data were examined to gain appreciation for the performance of the treatment against each of the threats. Once a clear understanding of the treatments and associated effectiveness and burdens was achieved the analysis began. Figure 4 shows the starting conditions for the analysis.

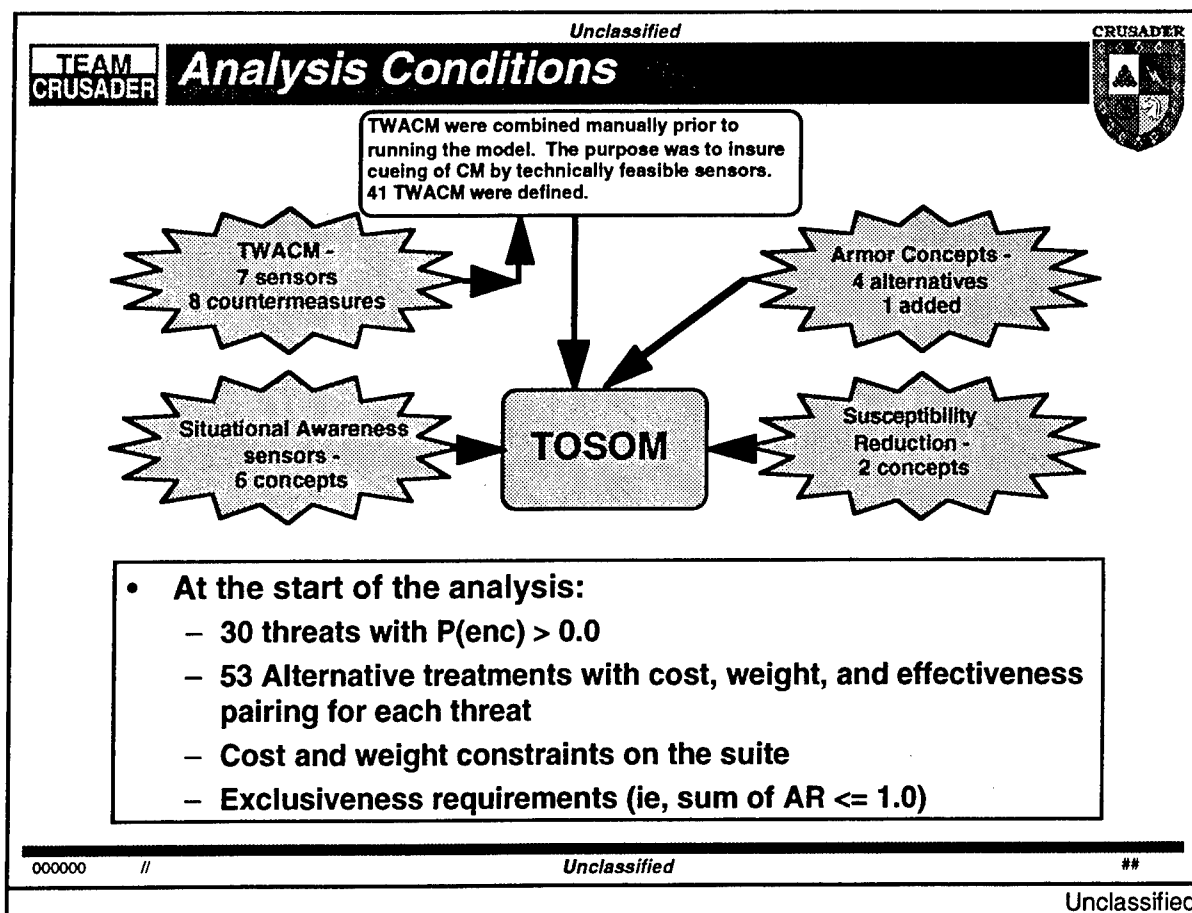
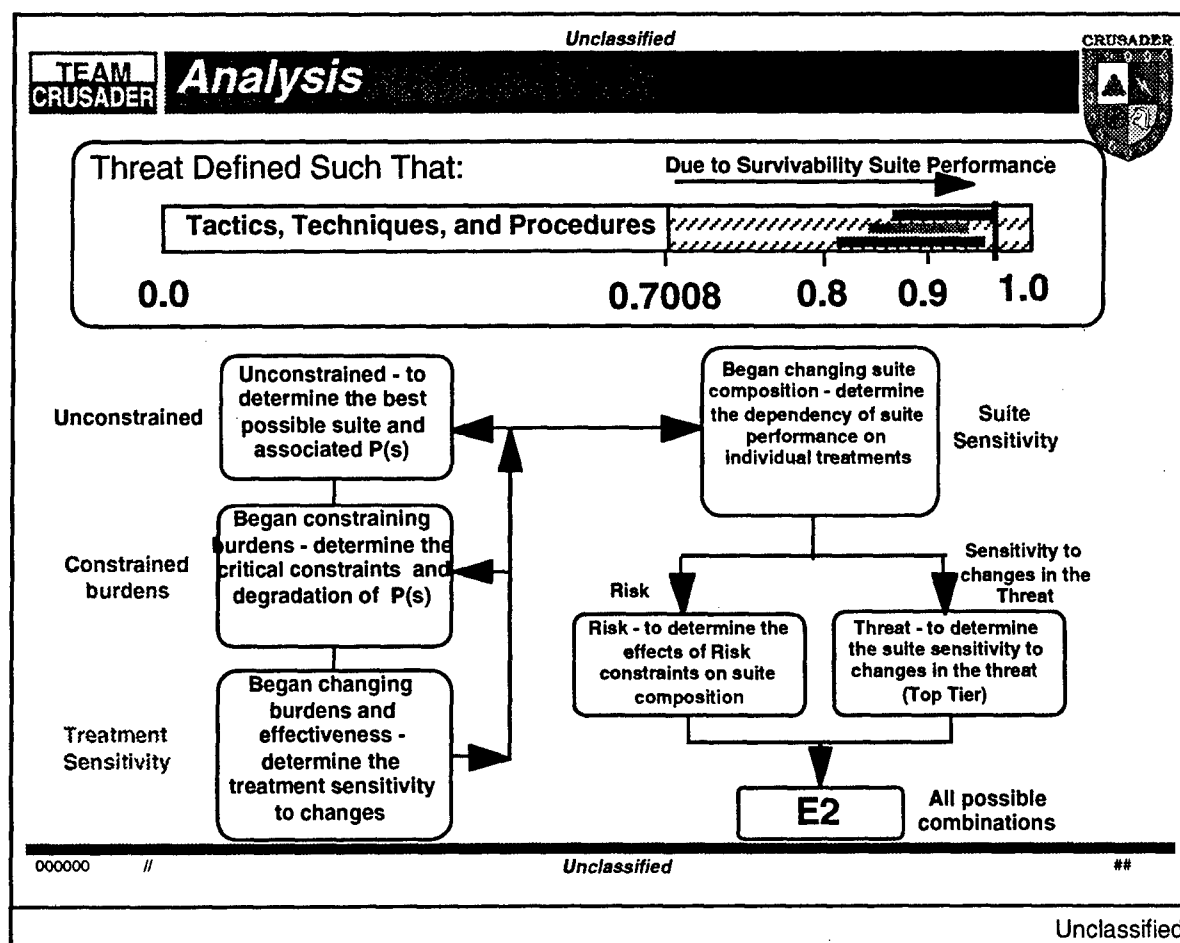


Figure 4. Conditions for the Analysis

(U) Execution of the Analysis. The analysis began by determining the best possible performance of any combination of survivability treatments against the defined threats. Figure 5 shows the scale of improved individual vehicle survivability due to addition of a survivability suite as well as the process for conducting the analysis. The scale of improved vehicle survivability shows the amount of survivability gained through tactics, techniques, and procedures and then the survivability gained through addition of a survivability suite. The upper limit of individual vehicle survivability shown on the line represents the best possible individual vehicle survivability performance achievable by any combination of these treatments against this particular threat.



**Figure 5. Conduct of the Analysis**

(U) Once the best possible individual vehicle survivability performance is determined, the cost and weight constraints were gradually reduced to identify those treatments that were consistently chosen as components of the suite. Those treatments that were consistently chosen were considered to be the high performers and, as such, were likely to be selected as part of the recommended suite. While constraining the burdens, several questions arose concerning treatment effectiveness and burden data, so a treatment sensitivity analysis was conducted on several of the treatments to determine if those treatments truly performed "head & shoulders" above the other treatments or if their selection was sensitive to either effectiveness or



burdens. Once a solid understanding of the model rationale for selecting each treatment was achieved, then a suite sensitivity analysis was done to determine what alternative treatments would be selected if certain treatments were not available for inclusion in the suite. This portion of the analysis demonstrated the high performers as well as those treatments that might, or might not, be selected under certain constraint conditions.

The analysts developed an initial recommended suite solution based on the analysis described above. Two distinct sensitivity analyses were then conducted to determine the effects of the initial recommended suite under changed threat conditions and determine the optimal suite under risk constraints. The result of these analyses demonstrated excellent recommended suite performance under a wide range of threat conditions. The threat ranged from an extremely high indirect fire threat to an extremely high direct fire threat and the recommended suite exceeded expectations in both cases. The optimal suite under high and medium risk constraints was the recommended suite. The optimal suite under low risk conditions replaced one high risk treatment with a lower risk solution with a sharp reduction in suite performance.

(U) Trade-Off Analysis Results. Figure 6, Example Results, shows several of the methods of examining the results data. The analysis demonstrated that a balanced solution consisting of TWACM, armor, susceptibility reduction, and situational awareness technologies is the optimal solution for the Crusader. Even with the optimal, balanced survivability suite solution for the Crusader, the force survivability requirement will be difficult to attain against a robust threat. The upper left quadrant of Figure 6 shows the value of each of each of the treatments in isolation (that one treatment alone). This Individual Treatment Contribution chart demonstrates the effectiveness of one treatment against all threats. The values are measured in terms of percentage increase of overall system survivability from a baseline of 70%.

The upper right quadrant of Figure 6 shows the percentage reduction of each threat system (indexed along the x-axis) by a specific survivability suite. The stacked bar for each threat shows the difference between the threat effectiveness against an untreated system and the threat effectiveness against a survivability suite equipped system. The lower right quadrant of Figure 6 shows the "knee in the curve" chart for the Cumulative Effects of All Treatments. The curve is indexed on both sides for cost, weight, and P(s). Consequently, it is relatively easy to identify the value of a specific suite; Cost & Weight vs. Performance. These example results analysis methods, along with other measures (cost per percentage point of survivability, response surface, etc.) demonstrate the value of this TOSOM mathematical programming methodology to both the analyst and the decision maker.

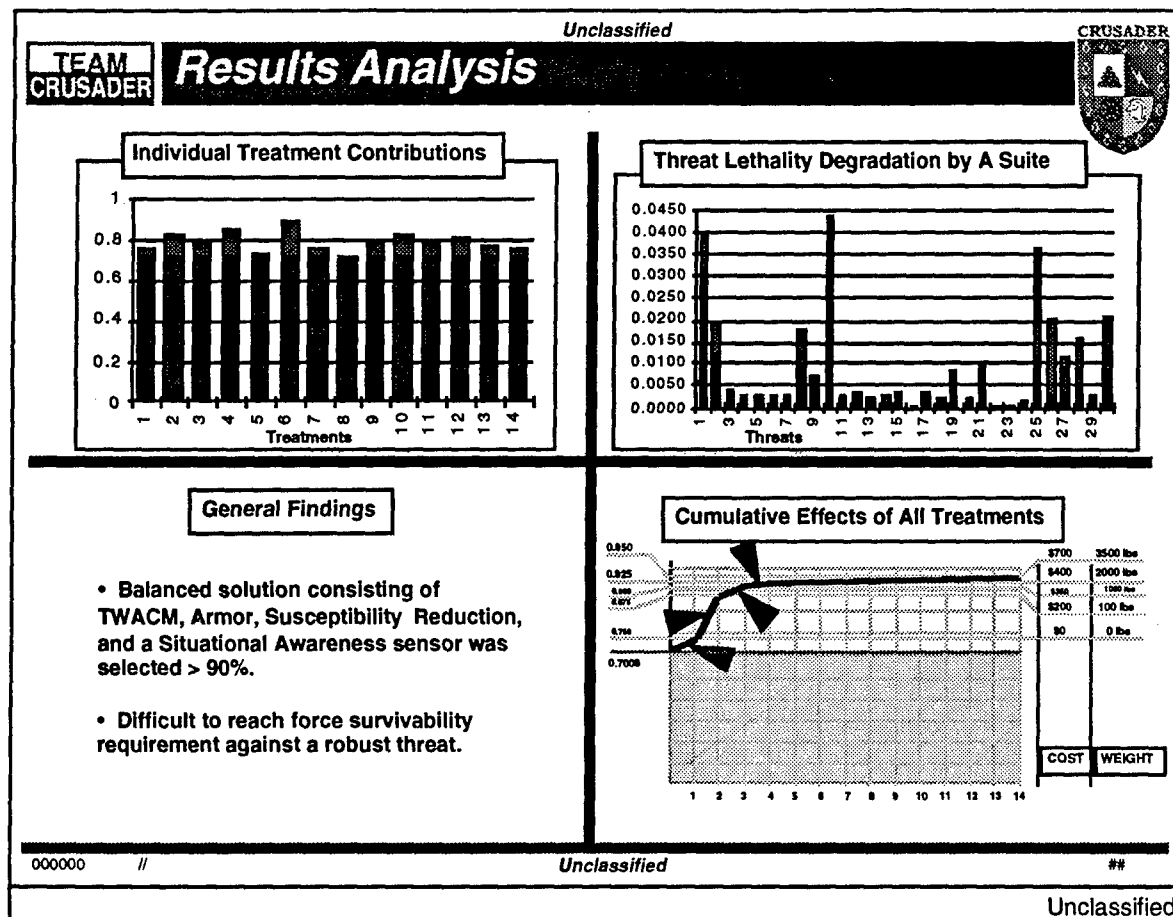


**Figure 6. Example Results**

(U) **SUMMARY.** The process described above is the survivability suite concept trade-off analysis methodology currently in use by Team Crusader. The results from these analyses are being used to establish the survivability treatment development priorities for the DEM / VAL phase of the system life cycle. A thorough understanding of the threat as well as treatment technologies is required prior to the start of the analysis. Additionally, data traceability from both source documents as well as during the course of the sensitivity analyses is absolutely essential. Community concurrence on threat and treatment input data is necessary to insure results are accepted throughout and defensible in front of the community as well as the decision maker(s).

This analysis methodology is iterative in that as hardware is developed and tests are conducted, the level of data fidelity increases significantly. As the data is refined, the analysis is repeated to insure the selected survivability technologies will provide the expected battlefield system survivability and meet fleet survivability requirements.

**UNCLASSIFIED**

**THIS PAGE INTENTIONALLY LEFT BLANK**

**UNCLASSIFIED**

**Verification, Validation and Accreditation (VV&A) Tests of the Bradley Simulator for the Anti-Armor Advanced Technology Demonstration (A2 ATD) Program**

**Bhuvdutt Jha**

Computer Engineer, VETRONICS Technology Center  
U.S. Army Tank-Automotive And Armaments Research, Development and Engineering Center, Warren, MI

**Floyd Wofford**

U.S. Army Material Systems Analysis Activity  
Aberdeen Proving Ground, MD

**TOPIC: Survivability Testing and Test Methodologies**

**ABSTRACT**

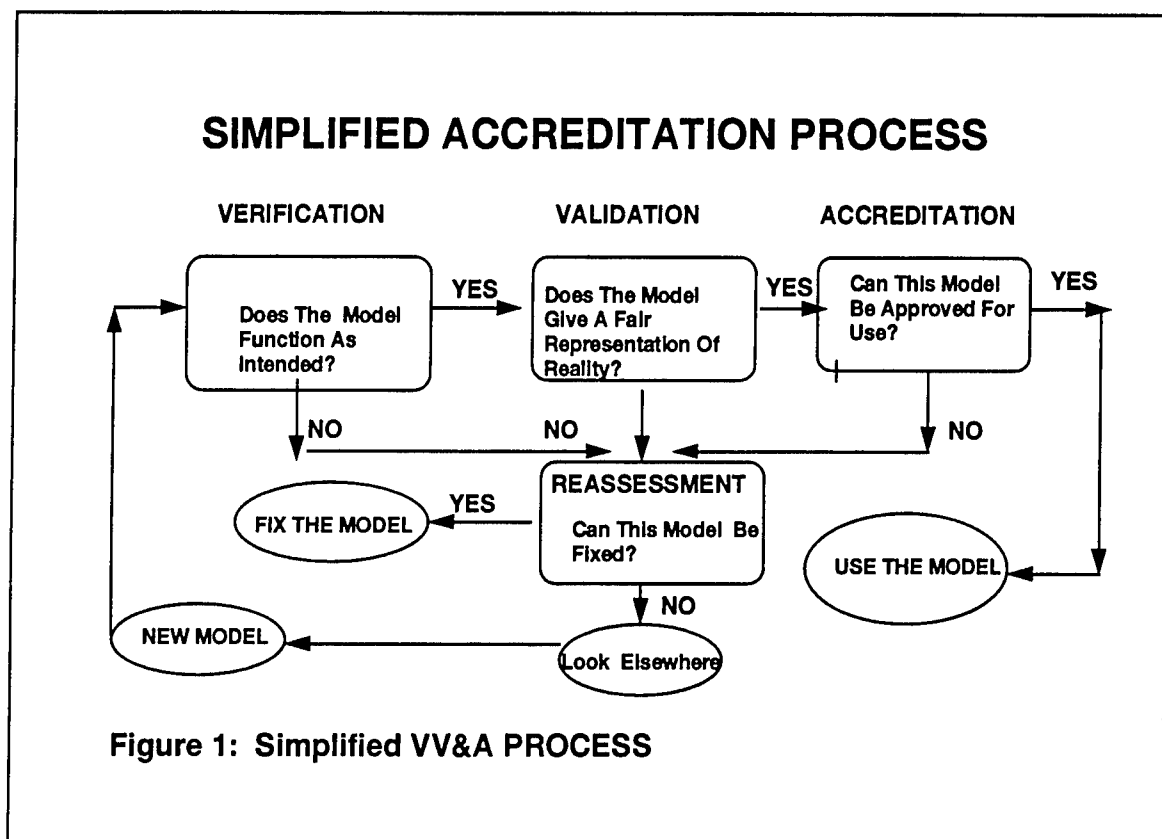
The analytical community has historically used constructive simulations such as JANUS and CASTFOREM to do analysis for the acquisition process. These simulations do not fully represent the impacts of human interactions with the system and their effect upon combat effectiveness of the system during the early phases of research and development. Research and development and the training communities have been using real time man-in-the-loop Distributed Interactive Simulation (DIS) for several years. However, the models and simulators used before have never been verified, validated and accredited. The objective of the Anti-Armor Advanced Technology Demonstration (A2 ATD) program is to develop and demonstrate a verified, validated and accredited (VV&A) DIS capability to assess and evaluate anti-armor weapon systems effectiveness on a combined arms synthetic environment at the battalion task force or brigade level. This paper will describe the verification and validation tests that were conducted on a Bradley simulator to ensure suitable functionality in the following areas: form, fit and function; direct-fire and indirect-fire vulnerability, target acquisition; main gun delivery accuracy; mobility; and timelines. Verification and validation tests were completed using soldiers from Ft. Benning and Aberdeen Proving Grounds. These tests identified discrepancies for which corrective measures were taken. The Bradley simulator was accredited in September '95 to take part in the A2 ATD experiment.

**Purpose of the Anti-Armor ATD Program**

A2 ATD is a joint DA/DOD program that was initiated with the goal of maturing DIS as a credible evaluation tool to support acquisition decisions. The purpose of the A2 ATD is to develop and demonstrate a verified, validated and accredited DIS capability to support anti-armor weapon system virtual prototyping, concept formulation, requirements definition, effectiveness evaluation, and mission area analysis on a combined arms battlefield at the Battalion Task Force or Brigade level.

UNCLASSIFIED

Verification, Validation and Accreditation is required for models, simulators, and simulations that are used to support ASARC/DAB managed programs. Verification is the process of determining that the Manned Simulators (MS) or Simulations (S) accurately represent the developer's conceptual description and specifications. Validation is the process of determining the extent that the MS or S represents the intended real world entity. Accreditation is an official certification that the MS or S has achieved an established level of credibility such that it can be used for a specific application. Figure 1. is an overview of the VV&A process.



### Bradley M2A2+ Simulator Description

The Bradley simulator verified and validated for A2 ATD experiment 3 was developed at the VETRONICS Simulation Facility (VSF) of the TACOM Research Development and Engineering Center (TARDEC) in Warren, MI. This simulator incorporated many, but not all, of the features of the proposed A3 system. During development of the simulator the final design for the A3 system had not been finalized. Features of the proposed live system which were well defined by the simulator design deadline were included in the A2+ simulator.

The A2+ simulator is partitioned into two stations, the driver's station which is operated by one soldier and the turret station which is operated by two soldiers. Both stations consist of detailed replications of the driver's, gunner's, and commander's areas. These areas contain crew seating, vision devices, controls, and panels with buttons,

switches, lamps, meters and/or physical devices. The layout of the crew stations is such to provide crew members with appropriate Bradley Fighting Vehicle System (BFVS) functionality while resembling the functional elements in the actual vehicle. It simulates a 25 mm gun, a TOW missile system and a coaxial 7.62 mm gun.

The Bradley A2+ simulator went through the VV&A process from June-September '95. This paper will describe briefly the verification and validation tests that were conducted on the simulator to ensure suitable functionality in the following areas: form, fit and function, direct-fire and indirect-fire vulnerability, target acquisition, main gun delivery accuracy and mobility. These tests were conducted by trained soldiers from Ft. Benning and Aberdeen Proving Grounds. These tests identified discrepancies for which corrective measures were taken. The Bradley simulator was accredited in September '95 to take part in the A2 ATD experiment 3.

The experiment 3 was run on the South West Asia terrain database. The manned simulator was part of a Bradley platoon and demonstrated its capabilities in a force on force type of exercise. The other manned simulators taking part in the experiment were at Ft. Benning and the computer generated forces were controlled from Ft. Knox. The three sites connected on the DSI network and conducted the real time battle exercises.

## **VV&A SUMMARY**

### **Form, Fit, and Function**

The objective of the form, fit and function tests was to determine how well does the simulator represent the look and feel of the proposed real vehicle. Functional tests were performed on all of the components of the simulator to ensure that they performed correctly. They did function as intended in all cases. For example, if a switch was intended to arm the TOW2B, it was checked and it did indeed arm the TOW2B. All of the stations were tested by trained soldiers and their assessment was that the simulated Bradley A2+ was a functional vehicle.

Some differences were noted such as the visual scene presented across the driver's vision blocks was not uniform. The elevation of the ground in the central vision block was several meters higher than the elevation of the ground in the right or left vision blocks. The elevation of the terrain in the left and right vision blocks appeared the same. The appearance of the gear shift control panel in the simulator was different than on the M2A2. However, all simulated gear movements corresponded correctly to the labeling in the simulator. The differences between the simulator were seen as minor and would not interfere with the driving functionality of the simulator. The differences in terrain elevation, although annoying, was not serious enough to impair the driver's vision nor did it affect his driving ability. The A2+ simulator was able to provide all the features required for experiment 3. The differences between what was simulated and what was proposed were viewed as to not adversely affect the experiment outcomes. The form, fit and function aspects of the A2+ simulator were accredited for use in experiment 3.

## **Mobility Model**

The Mobility model used in the A2 ATD experiment 3 is the SIMNET M2/3 vehicle simulation model. It was reengineered from C programming language structure to an object-oriented programming language (C++) for the VSF's reconfigurable simulator in order to provide plug and play model capability. This model was verified, validated and accredited through its software development life cycle by staff at the Simulation and Training System Division of BBN.

The A2 ATD required the reengineered model to be verified, validated and accredited using both qualitative and quantitative methods to ensure that the process of reengineering has not altered the original software in any way. The quantitative tests were conducted in the areas of acceleration, deceleration and braking, maximum and minimum speed, turning and pivoting and fuel consumption. Information transmitted over the network was collected to extract the state of the vehicle in order to calculate the performance measures. The PANDA tool read these time-stamped PDUs from the simulator network to extract the state of the vehicle, and either calculated various performance results or generated tables containing enough information to make a decision about the performance measures. PANDA is a verification and validation tool developed by the OASIS corporation. The results from PANDA were compared with the "Final Report - Production Qualification Test (PQT) of Bradley Fighting Vehicle Systems -A2 (BFVS - A2) 600 HP powertrain" provided by AMSAA. The qualitative tests were conducted by asking the soldiers the following questions: Does the simulator have the ride qualities and sense of handling as the actual Bradley vehicle?, As you drove on the terrain (various terrain slopes) did the simulator behave (e.g. quality of ride) as you would have expected?, Did the model's acceleration and deceleration characteristics respond like the actual Bradley vehicle?. The qualitative data were compared to the real-life driving experience of the trained soldiers from Ft. Benning and Aberdeen Proving Grounds.

Both the qualitative and quantitative VV&A tests verified and validated that the A2+ simulator appeared to maneuver, accelerate, decelerate and brake like a real vehicle. The maneuverability affected by dynamic terrain (e.g. varying slope) was apparent to the trained soldiers. These tests also proved that the right VV&A tool, such as PANDA, greatly reduces the manned numerical calculations required to derive the performance measures and therefore saves time and money. Overall, mobility model was a good representation of the real Bradley vehicle. The mobility model was accredited to take part in A2 ATD experiment 3.

## **Vulnerability Model**

One of the modules developed for the Bradley A2+ simulator was the Vulnerability module for both "Direct" and "Indirect" munitions. The Direct-fire methodology is used to predict damage when a munition hits the target directly. The Indirect-fire methodology is used to predict the damage when a munition detonates close to the target. In order to

verify and validate the Bradley A2+ Vulnerability module, Computer Generated Forces (CGF) were used to simulate friendly and enemy vehicles firing Direct fire and Indirect fire munitions. Direct fire munitions consist of Kinetic Energy (KE) or Heat rounds. Indirect fire rounds consisted of High Explosive (HE) and Improved Conventional Munitions (ICMs).

Prior to validating the Vulnerability module, the module had to be capable of loading 30 to 50 AMSAA data files. Also, the random number generated by the vulnerability module had to be from a uniform distribution. For Direct fire methodology tests were conducted to check that the correct tables were accessed; damage accrued and that the mutually exclusive PKs were calculated correctly. For Indirect fire munitions tests were conducted to check that the appropriate damage function was used; lethal area data table was accessed correctly; mutually exclusive PKs were calculated correctly and the kill thermometer was constructed correctly.

The results of both direct fire and indirect fire vulnerability assessment methodologies were consistent with AMSAA goals. Crew casualty data was not employed. Exposure scalars and environment scalars were not used in Experiment 3. Elements for the future employment of the exposure and environmental scalars were provided in the vulnerability code. One of the problems noticed during the VV&A of this module was that the MODSAF does not fill in the eventID (Fire PDU) field correctly for Indirect fire munitions. This made it difficult for the vulnerability module to detect a successful hit. In addition, the format of the AMSAA PKH data tables for Direct fire munitions was not consistent. The vulnerability assessment code was accredited for use in experiment 3.

### **Target Acquisition**

The target acquisition test was performed with the test subject sitting at the gunner's position. All test subjects were qualified Bradley gunners currently on active duty. Targets consisting of M1A2, T-72, Bradley and BMP were presented to the test subject on the simulated IBAS screen. The test subject would then have fifteen seconds to verbally respond with the highest level of target acquisition which could be performed for that target presentation. After the test subject responded or fifteen seconds elapsed the response would be recorded and another target would be presented.

The Bradley A2+ simulator IBAS display was capable of showing one of four scenes at any time. The four scenes correspond to each of the normally operational IBAS configurations; Day Sight - Wide Field of View, Day Sight - Narrow Field of View, Night Sight - Wide Field of View, and Night Sight - Narrow Field of View. During the target acquisition test one sensor display was chosen for the entire trial. After the successful completion of each trial the display was switched to one of the remaining. After all four configurations were successfully tested the target acquisition test ended.



The data collected were compared to sets of probability of acquisition curves for an IBAS type of sensor generated at AMSAA using the Night-Vision Laboratories Target Acquisition Model. The Night-Vision Target Acquisition Model generates probabilities of acquisition for four different levels of target acquisition for a variety of optical and thermal target acquisition sensors. The data collected from the simulator correlated well with the results expected from the Night-Vision model and the simulator was accredited for use in experiment 3.

### **Delivery Accuracy**

The verification and validation tests performed provided information on the TOW2B and 25 mm gun only. The coaxial machine gun was not tested. The test consisted of a target entity being displayed on the gunner's IBAS display, the test subject firing the designated weapon at the target, and counting the number of rounds fired at the target and hitting the target. The number of hits and shots were recorded. The ratio of hits over shots was derived for each trial and test subject. These ratios served as approximations to hitting probabilities. They were compared to AMSAA generated data.

None of the tests proved the 25mm gun fired rounds in a manner consistent with the proposed M2A3 system. This could not have been done since there exist no performance data as to how the system will behave. Some of the results for the tests seemed to follow closely what was expected from the system. There were several other points noticed during the tests. First, none of the performance were out of the bounds of expectation. Second, when firer-target ranges increased the probability of hit went down, which should be expected. Third, all gunners were questioned as to the performance of the main gun/fire control portion of the simulator. All of the soldiers in the simulator thought the simulation of the 25mm gun to be very much like the live Bradley. The 25mm chain gun was accredited to participate in experiment 3.

The TOW2B could not be sufficiently tested before experiment 3 to characterize performance. It was accepted as it was for use in experiment 3. Soldier subject matter experts had stated that the missile flyout appeared like the TOW II B and that the guide to hit phenomenology was similar. After experiment 3 a fast test of the TOW II B was performed. The data collected matched well with the expected probability of hit given a shot of .90 or greater for all ranges of concern and all engagement types. The delivery accuracy of the TOW2B was accredited for use in experiment 3 from a delivery accuracy perspective.

### **Lessons Learned**

Number of valuable lessons were learned from the VV&A of the Bradley A2+ simulator. One of the most important was that the methods used to VV&A a real vehicle are different than the methods used to VV&A a simulated vehicle. What is easy to do in the real world can sometimes be very difficult to do in a simulated world. The VSF team and AMSAA discovered that using the real terrain database for target acquisition tests

was very time consuming. A decision was made to develop a new terrain database that was one big polygon and had the same texture as the real terrain database. Using the VV&A test tool to place the targets on the battlefield for different ranges and angles was very easy with this new test terrain database. This saved a lot of time and effort.

It is also important to note that VV&A tests designed for one ground vehicle simulator cannot be automatically assumed to be reusable in another vehicle simulator. Vehicles are designed for different functions and their components may look similar but have unique characteristics such as distance from the ground to the vision blocks etc. that prevent us from using the same tests. During the VV&A of the vulnerability module we realized that it would be beneficial to develop new tools to place targets at exact distances and angles for direct and indirect fire munitions. The tests were performed using MODSAF which did not always provide the correct output for testing purposes. It is also important to involve the soldier early in the development process of a simulator and also to discuss the VV&A tests with subject matter experts to make sure that the tests being run will prove what the test was intended for.

## Conclusion

The US ARMY TACOM's participation in the Verification, Validation and Accreditation of the VSF Bradley A2+ simulator has proved to be a very valuable experience. The Anti-Armor (A2) ATD has provided a good foundation for the VV&A of DIS simulators, but there is still a lot to be learned. The DIS community needs to develop more tools and procedures to make the VV&A process easier to be accomplished. The DIS community needs to use the VV&A process developed by the A2 ATD project as a baseline. We need to take the lessons learned from the six experiments and all the participants involved to determine what else needs to be developed to make the VV&A process easier and more automated. The VV&A of DIS simulators will provide more opportunities for simulators in the material acquisition cycle.

It is clear that all simulators taking part in an experiment must go through the VV&A process. It gives us a chance to stress test the simulator and generate credible data to make critical decisions from an exercise. The VV&A effort undertaken for the A2 ATD program has been a good learning experience for all parties involved and is a big step forward in maturing the DIS technology as a viable analytical tool. DIS has already demonstrated its ability to generate new opportunities for the application of simulation to many areas such as training, operational analysis and concept & tactics development. It is constantly being enhanced to allow larger scale exercises to be carried with a more complete representation of the virtual battlefield. However, it is important to recognize some of the significant issues such as correlation, fidelity differentials and validation that must be addressed if DIS is to make a valid contribution.

UNCLASSIFIED

## REFERENCES

1. Jha, B., "Vulnerability Assessment For Survivability Modeling". Proceedings of the 6th TACOM Combat Vehicle Survivability Symposium, Monterey, CA., 1995.
2. Jha, B., "Vulnerability Assessment Based on Probability of Kill Given a Hit (P(K/H)) Estimates". Proceedings of the 11th DIS Simulation Conference, Orlando, FL., 1994.
3. "A2 ATD Bradley A3 Fighting Vehicle System Simulator VV&A Plan". Army Material Systems Analysis Activity (AMSAA), APG, MD., 1993.
4. Rayment, C, "Simulation And DIS: The Way Ahead," in Proc. Force Projection Through Technology - The Land Environment, Surrey, U.K., 1994.
5. Topper, P., A Compendium of Close Combat Tactical Trainer Data Structures, Algorithms, and Generic System Mappings. Technical Report, The U.S. Army Material Systems Analysis Activity (AMSAA), MD., 1993.
6. Yeakel, W., Harkrider, S., "Anti-Armor Advanced Technology Demonstration (A2 ATD) Experiment One". Proceedings of the 12th DIS Simulation Conference, Orlando, FL., 1995.

UNCLASSIFIED

UNCLASSIFIED

**POSTER PAPER PRESENTATIONS**

Spanagel Hall, Room 101 A  
Tuesday and Wednesday, March 26 & 27, 1996

UNCLASSIFIED

**UNCLASSIFIED**

THIS PAGE INTENTIONALLY LEFT BLANK

**UNCLASSIFIED**

UNCLASSIFIED

**THE CONFIGURATION MANAGEMENT OF DATA FOR SIGNATURE,  
COUNTERMEASURES, AND ARMOR MODELING OF SYSTEMS FOR THE  
RAPID FORCE PROJECTION INITIATIVE (RFPI) ADVANCED CONCEPT AND  
TECHNOLOGY DEMONSTRATION (ACTD)**

C. Kennamer  
Nichols Research Corporation  
Huntsville, AL

E. Vandiver  
U.S. Army Missile Command Research, Development, and Engineering Center  
Redstone Arsenal, AL

(U) THE RAPID FORCE PROJECTION INITIATIVE (RFPI) ADVANCED CONCEPT TECHNOLOGY DEMONSTRATION (ACTD) WILL PROVIDE AN ENVIRONMENT FOR USERS AND DEVELOPERS TO INTEGRATE AND TEST ADVANCED TECHNOLOGIES TO SUPPORT EARLY ENTRY FORCES. SEVERAL ADVANCED TECHNOLOGY DEMONSTRATIONS, TECHNOLOGY DEMONSTRATIONS, AND NON-DEVELOPMENTAL ITEMS WILL PROVIDE TECHNOLOGY PRODUCTS TO BE DEMONSTRATED VIA A SERIES OF INCREASINGLY MORE ROBUST FIELD TEST EXERCISES (LIVE SIMULATION). THE RFPI ACTD FOCUSES ON INTEGRATION OF A "SYSTEM OF SYSTEMS" OF FORWARD SENSORS (HUNTERS) AND ADVANCED WEAPON SYSTEMS (STANDOFF KILLERS) INTEGRATED THROUGH ROBUST COMMAND, CONTROL, AND COMMUNICATIONS (C3) SYSTEMS INCORPORATED INTO A HUNTER/STANDOFF KILLER OPERATIONAL CAPABILITY. THE RFPI ACTD EXPERIMENT AND LIVE AND VIRTUAL SIMULATION EXERCISES WILL PROVIDE THE USER COMMUNITY, XVIII ABN CORPS, AN OPPORTUNITY TO EVALUATE THE RFPI SYSTEM OF SYSTEMS CONCEPT IN AN OPERATIONAL ENVIRONMENT. DUE TO THE LARGE NUMBER OF ELEMENTS, ACTIVITIES, AND USERS, CONFIGURATION MANAGEMENT OF DATA SUPPORTING THIS PROGRAM IS CRUCIAL.

(U) THE RFPI ACTD RELIES ON EXTENSIVE SIMULATION ACTIVITIES TO SUPPORT DEVELOPMENT AND REFINEMENT OF OPERATIONAL CONCEPTS AND TECHNOLOGIES TO DEMONSTRATE AN INCREASE IN SURVIVABILITY AND LETHALITY. CONSTRUCTIVE SIMULATIONS ARE USED TO INVESTIGATE PLANNED SCENARIOS, PARTICIPANT LAYDOWNS, SYSTEM ENGAGEMENT AREAS, TARGET MOVEMENT, AND BOUND EXPECTED RESULTS FOR THE WEAPON SYSTEMS. DISMOUNTED BATTLESPACE BATTLE LAB HAS IDENTIFIED APPROPRIATE RFPI SCENARIOS AND EXCURSIONS FOR USE IN EVALUATING AND DEVELOPING REPRESENTATIVE EARLY ENTRY FORCE STRUCTURES. THESE ARE BASED ON THE EARLY ENTRY, LETHALITY, AND SURVIVABILITY (EELS) BATTLE LAB 2K

UNCLASSIFIED

UNCLASSIFIED

(U) STUDY, WITH MODIFICATIONS TO INCLUDE THE UNIQUE RFPI SYSTEMS. RFPI SCENARIOS ARE BASED ON USER APPROVED SCENARIOS, AND ARE GENERALLY EXCURSIONS FOR EARLY ENTRY FORCES BASED ON TRADOC-APPROVED HIGH RESOLUTION SCENARIOS (HRS).

(U) A CONFIGURATION MANAGEMENT TOOL (CMT), UNDER DEVELOPMENT BY THE RFPI PROGRAM MANAGEMENT OFFICE (PMO), WILL SUPPORT PLANNING AND IMPLEMENTATION OF THE CONSTRUCTIVE, VIRTUAL, AND LIVE SIMULATION EXERCISES. THIS PAPER DISCUSSES AND DEMONSTRATES THE RFPI PMO CONFIGURATION MANAGEMENT APPROACH. THIS CMT IS ACCESSIBLE BY ALL RFPI ELEMENTS, AND CONTAINS ACCREDITED SYSTEM DESCRIPTIONS, PERFORMANCE DATA, OPERATIONAL CONCEPTS, AND TACTICS, TECHNIQUES, AND PROCEDURES.

**THE CONFIGURATION MANAGEMENT OF DATA FOR SIGNATURE, COUNTERMEASURES, AND ARMOR MODELING OF SYSTEMS FOR THE RAPID FORCE PROJECTION INITIATIVE (RFPI) ADVANCED CONCEPT AND TECHNOLOGY DEMONSTRATION (ACTD) (U)**

I. (U) INTRODUCTION

(U) This paper discusses the configuration management of data supporting signature, countermeasures, and armor modeling activities for the Rapid Force Projection Initiative (RFPI) Advanced Concept and Technology Demonstration (ACTD). This effort is supported through the development of the MICOM Interactive Data Accreditation System (MIDAS), an automated tool that will facilitate the configuration management and data accreditation process.

II. (U) BACKGROUND

(U) U.S. contingency forces must have the ability to respond quickly to challenges to U.S. interest around the globe. To prioritize defense technology exploration, the Department of the Army (DA) has identified activities responsive to the needs of early entry forces. The objective of these activities is to ensure proper focus of individual Science and Technology (S&T) programs so that required military capabilities can be acquired to preserve peace, deter conflict, fight and win the battle into the next century. The Rapid Force Projection Initiative (RFPI) is one of these activities. The Department of Defense (DOD) has also implemented a series of ACTDs to provide Forces Command (FORSCOM)

UNCLASSIFIED

## UNCLASSIFIED

(U) troops with training, conduct a large scale experiment, and retain the technology for a two year follow-on residual period.

### II.A. RFPI ACTD

(U) The RFPI ACTD will provide an environment for users and developers demonstrate, via a series of increasingly robust field test exercises, advanced technologies for the U.S. Army early entry forces. To accomplish this mission, several Advanced Technology Demonstrations (ATDs), Technology Demonstrations (TDs), and Non-Developmental Items (NDI) will provide technology products which will be integrated into a "system of systems". The RFPI ACTD "system of systems" consists of forward sensors (hunters) and advanced technology weapon systems (standoff killers) integrated through robust command, control, and communications (C3) systems incorporated into a hunter/standoff killer operational capability for early entry forces. The RFPI system of systems will demonstrate the potential of advanced technologies to produce air deployable, helicopter-transportable light forces, that are more lethal and survivable against armor and are not dependent on advanced positioning.

(U) The RFPI ACTD will integrate 17 elements which are managed by U.S. Army Missile Command (MICOM), U.S. Army Communications and Electronics Command (CECOM), and U.S. Army Tank and Automotive Command (TACOM). The RFPI ACTD Exercise and live and virtual simulation exercises will provide the user community (XVIII ABN CORPS) an opportunity to evaluate the RFPI system of systems concept in an operational environment.

(U) The RFPI ACTD will demonstrate operational capability requirements, developed by U.S. Army Training and Doctrine command (TRADOC) for increased lethality and survivability of light early entry forces while maintaining the inherent strategic deployment of these forces. The RFPI ACTD will demonstrate technology solutions that expand the battle space of light forces; provide increased survivability, lethality, and target acquisition; and increase command tempo and control. The potential operational capability enhancements offered by RFPI will enable the light force commander to mass synchronize precision fires on threat forces at ranges beyond those of the enemy.

### II.B. (U) RFPI ACTD Demonstration and Simulation Activities

(U) The RFPI ACTD will rely on extensive simulation and demonstration activities to support the development and refinement of operational concepts and technologies. All RFPI scenarios are based on user approved scenarios, and are generally excursions for early entry forces based on various TRADOC-approved High Resolution Scenarios (HRS). Due to the large number of elements and users, configuration management of data supporting the simulation activities is crucial. Demonstrations associated with

UNCLASSIFIED



## UNCLASSIFIED

(U) the RFPI ACTD program include Early Version Demonstration (EVD), 4QFY94; JRTC (Joint Readiness Training Center) 96-2, 2QFY96; A2 ATD Experiment 6, 3QFY96; EFOG-M VPE BLWE, 3QFY96; RFPI ACTD PREP BLWE, 2QFY97; RFPI ACTD, FY98.

(U) The RFPI ACTD will rely on extensive simulation activities to support the development and refinement of operational concepts and technologies. Constructive simulations will be used to investigate the planned scenarios, participant laydowns, system engagement areas, target movement, and to bind the expected results for the weapon systems. These include BEWSS (Battlefield Environmental Weapon System Simulation), TAFSM (Target Acquisition and Fire Support Simulation), CASTFOREM (Combined Arms Task Force Effectiveness Model), and Janus. Virtual Simulations, utilizing Distributive Simulation Interfaces (DSI), will be used to evaluate the contribution of the Man-in-the-Loop, expand the "real" elements in live exercises, and to simulate missile firings in live exercises. Live exercises will include JRTC 94-02 and 96-05, RFPI Early Version Demonstrations, multiple Battle Lab Warfighting Experiments (BLWEs) leading to a capstone ACTD exercise. Using TRADOC and Dismounted Battlespace Battle Lab (DBBL) scenarios, representative early entry force structures are being developed based on the TRADOC Early Entry, Lethality, and Survivability (EELS) Battle Lab 2K Study encompassing appropriate modifications to include the unique RFPI sensor and weapon systems.

### III. (U) DATA ACCREDITATION AND CONFIGURATION MANAGEMENT

(U) The RFPI Program and the RFPI ACTD draws upon data from a variety of agencies and activities. The RFPI Program Office identified a need for an automated tool to support the configuration management and accreditation of this data. The MICOM Interactive Data Accreditation System (MIDAS) was developed to support these previously identified agencies and activities.

#### III.A. (U) Data Configuration Management (CM)

(U) The CM process includes configuration management of data associated with system and munitions descriptions and performance data; scenario information; force package data and operational information; descriptions of all simulations, models, experiments, and tests used by the RFPI program (including accreditation status). MIDAS will support the planning and implementation of the constructive, virtual, and live simulation exercises and will provide accredited data sets for all elements under development by the RFPI Program Office; organic elements that the RFPI systems will be integrated with; and an Integrated System of Systems. MIDAS will provide an automated process for tracking the development of system performance in support of the RFPI ACTD systems. It will also support the Independent Verification, Validation, and Accreditation (IVV&A) of the RFPI ACTD systems.

UNCLASSIFIED

## UNCLASSIFIED

(U)

This tool will streamline the accreditation process between the developer, user, and AMSAA.

(U) The goal of the RFPI CM process is to provide control over the information used to functionally and physically describe the systems identified in the RFPI operational concept. This data is organized into Automated System Design Notebooks (ASDNs) and used as inputs to all RFPI sponsored simulations, tests, experiments, and analyses. AMSAA, as the Government system performance accrediting agency, will have oversight of all approved RFPI data elements. All data elements must have RFPI PMO approved parentage before they can be included in the respective ASDN. Data will also be collected for the top level RFPI areas such as Force Structure and Scenarios. Information in these top level ASDNs will address areas of the RFPI concept that are dependent on a number of systems.

(U) An RFPI PMO approved configuration management plan will govern the inclusion of data in MIDAS. The data collected in MIDAS includes a reference or parent source. As system concepts are matured, test or experiment data are collected, or as actual hardware matures, updates to the physical and performance descriptions of the system can be expected. These updates must pass the MIDAS CM plan accreditation criteria and RFPI PMO approval before they will be included.

### III.B. (U) Data Accreditation

(U) To facilitate the accreditation of data used to support the RFPI ACTD program, the ASDNs developed for each system and the "system of systems" will contain the latest approved data. All entries to the ASDNs will be managed by the RFPI PMO so that only data that has been "certified" as correct and under configuration control will be entered. Accreditation statements will be developed for each major update to the ASDN. These statements will document the level to which the data in the notebook is considered valid. As an example, if the data in the notebook is based on a preliminary design, then the data will have very little "validity" beyond a concept design. Studies using this data will only be valid to that level. As the Preliminary Design Requirements (PDR) data matures through Critical Design Requirements (CDR) and then to prototype production, the data will become increasingly more valid. If the system matures to a point that it passes all elements of the Independent Verification and Validation (IV&V) for that system (PM RFPI managed), then the ASDN for that system will carry a full accreditation statement, allowing results of studies and demonstration using that system to be valid for the full spectrum of RFPI encounters. ***This accreditation will be issued jointly with AMSAA.***

UNCLASSIFIED

## UNCLASSIFIED

(U) An element critical to the accreditation of results is the certification of the demonstration or experiment. Detailed plans will be created to ensure that the goals of each participating element can be achieved. These plans will contain descriptions of the demonstration architecture, the level playing field requirements, the demonstration MOAs and the data collections process. Once fully planned, each of the systems participating in the demonstration will be verified to meet the demonstration requirements. This verification will be an additional entrance criteria for demonstration participation. The Scenario and Operational areas will be validated by the ACTD Warfighting Experiment Manager (AWEM). The V&V of the demonstration layout will be included as part of the final accreditation of the results of the exercise.

### IV. (U) MICOM INTERACTIVE DATA ACCREDIATION SYSTEM (MIDAS)

(U) The objective MIDAS system will allow a user, through local or remote connections, to select a type of analysis, a scenario, systems and force structures for analysis, and provide the user with a list of accredited models for that analysis. A super user will then have the capability to "set-up" the analysis to be performed. Users will also have the ability to post simulation, modeling, and test results to the MIDAS system.

(U) MIDAS will allow a user to have interactive access to the data collected as part of the CM efforts and will consist of three parts: ASDNs; Scenario(s); Simulation/Modeling, Test/Experiments, and Analyses. The user will access the data through predefined and ad-hoc queries that will run behind a graphical user interface enabling the user to comfortably and effortlessly search and utilize information stored in the database(s). The user can perform functions and commands without needing to know or understand how the database is structured, how to write SQL or query commands, or how to program and retrieve information inherent to the database program selected.

#### IV.A. (U) Automated System Design Notebooks (ASDNs)

(U) The ASDNs have been developed for each system participating in the RFPI ACTD. Each ASDN includes data item elements (<1200 elements/system) that were developed as a compilation of the data necessary to support most of the major models, simulation, test, and analysis tools envisioned for use by the RFPI program. The breakdown and storage of each system or unit will be by platform, munitions, and submunition. If a platform doesn't have munitions, and submunitions those data element will be listed as N/A.

UNCLASSIFIED

## UNCLASSIFIED

### IV.B. (U) Simulation And Analysis Worksheets

(U) MIDAS will allow a user to develop a worksheet to guide simulation, test or analysis activities. This worksheet establishes the data set and run matrix for the simulation, test or analysis activities. Most system and operational data elements will be modifiable by the user as he/she sets up the ground rules for the activity. For each simulation or analysis conducted for the RFPI project office, MIDAS will contain a data file with the following items: the data set provided to the modeler or analyst; the data set that was used by the modeler for analysis; the results, in raw data, of the analysis or simulation; the accredited results of the analysis of simulation (final report).

### V. (U) CONCLUSION

(U) The effective and efficient use of simulation (constructive and virtual), and test and experiments, will provide critical data to the material development process and operational information for the operational developer. The accuracy of the data used in these activities is critical to ensure that decisions made are based on realistic ATD/TD performance. RFPI will make extensive use of the Model-Test-Model (MTM) approach. The RFPI PMO will conduct these simulations; monitor, coordinate and integrate the development of technologies; and conduct the integrated demonstrations that allow an evaluation of proposed technologies and a validation of the models and simulations used fully develop the RFPI hunter/standoff killer concept.

### VI. (U) SUMMARY

(U) The RFPI HSOK concept will provide the 21st century warrior with significantly enhanced lethality and survivability by expanding the battle space for the early entry forces. The process of employing progressively more complex test will involve examination of technical and tactical development issues in simulation and the infusion of those findings into system design. This interactive simulation - demonstration process, MTM, supports continuous improvement through all phases of system development.

UNCLASSIFIED

**UNCLASSIFIED**

**THIS PAGE INTENTIONALLY LEFT BLANK**

**UNCLASSIFIED**

UNCLASSIFIED

## ADVANCED CONCEPT EVALUATION (ACE)

Patrick Buckley  
PMC Inc.  
Socorro, NM 87801  
Tel: (505)835-2951

Ken Lim  
US Army TARDEC  
Warren, MI

### ABSTRACT (U)

(U) ACE is a shotline code for evaluating shaped charges, long rod penetrators, and projectiles against armored vehicles. Designed to be highly interactive, ACE allows the user a great deal of flexibility in selecting threats, attack aspects, and shotlines. Individual shotlines can be examined in minute detail. It is also possible to modify shotlines and geometric models interactively.

### (U) INTRODUCTION

(U) ACE is a shotline analysis code built from the ground up as a native Microsoft Windows application. Native Windows programs offer the convenience of drop-down menus, dialog boxes for file selection, and the like, but more importantly they enable an "event-driven" computing model wherein the user controls the flow of events rather than following a rigid "batch-mode" protocol. This event-driven basis allows ACE to operate in a highly interactive fashion with the user; at almost any point in the analysis cycle the user can change threats, designate new impact locations, even modify the contents of an existing ray path through the target (add armor). With just a few mouse clicks the user can load and rotate a target geometric model, select a set of components for analysis, and generate shotlines through the components (Figure 1). With a few more mouse clicks the user can load a threat, compute the penetration of the threat along each shotline, then display the threat's residual speed, length, and so forth, measured at the point of intersection with the selected components. ACE displays the penetrator's residual properties as color maps, so the user has visual feedback on the performance of the armor in stopping the threat, or, conversely, on the ability of the penetrator to overmatch the armor. Figure 2 is an example color map displaying a penetrator's residual speed at the point of contact with the crew.

UNCLASSIFIED

UNCLASSIFIED

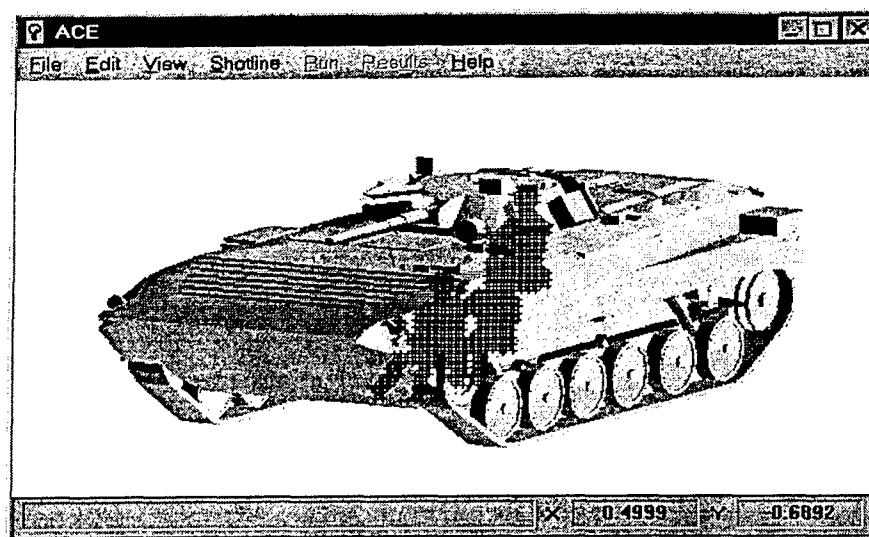


Figure 1. (U) Shotlines through crew components.

UNCLASSIFIED

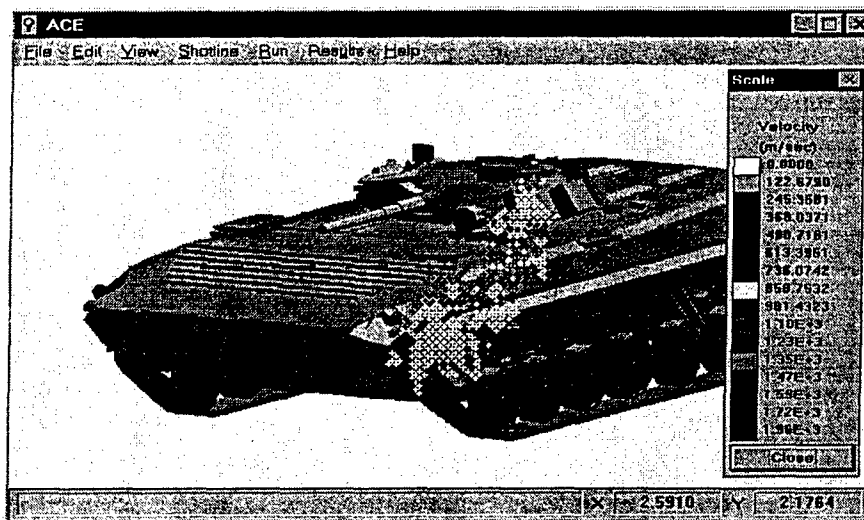


Figure 2. (U) Residual velocity plot.

UNCLASSIFIED

(U) Following a penetration analysis the user can elect to change the threat, or to rotate the target model to a new viewing position, etc., or he may choose to enter ACE's unique "shotline viewer." ACE's shotline viewer allows a user to examine in detail a "shotline" (ray path through the target). A complete description of the Shotline Viewer is beyond the scope of this introductory section, but Figure 3 illustrates the main features of the viewer. These main features include a graphical depiction of the shotline, windows displaying the threat's current state, and windows displaying target properties. Positioning the cursor in the shotline window and rolling it along the shotline dynamically updates the threat and target information. In the case of Figure 3, the shotline viewer depicts the situation at time

UNCLASSIFIED

UNCLASSIFIED

40 microseconds. The penetrator, which is displayed as a small cylinder, has almost reached the second target element along the shotline.

(U) Watching the state variables change along the shotline is interesting, but more importantly, the user is allowed to modify any target element along a shotline, to add new target elements along a shotline (new armor), and to recompute the penetration event along the modified shotline. For example, in Figure 4 the original shotline has been modified by adding two armor elements at the start of the shotline. The "Recompute" button evident in Figure 4 allows the user to run the penetration analysis for the modified shotline. Thus, the user can add or subtract armor until the desired level of protection is achieved.

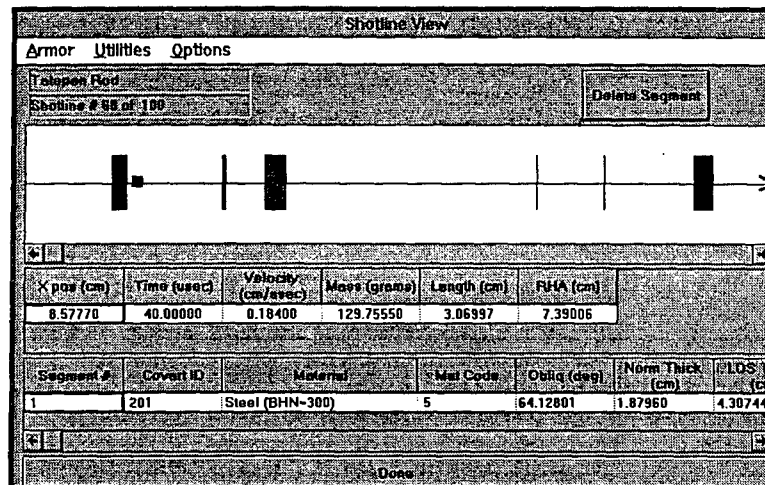


Figure 3. (U) Shotline Viewer display.

UNCLASSIFIED

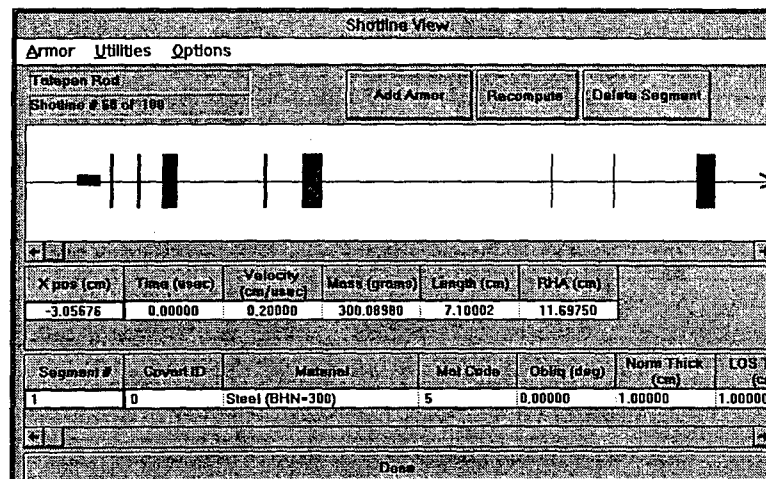


Figure 4. (U) Modified Shotline.

UNCLASSIFIED

UNCLASSIFIED



UNCLASSIFIED

(U) A basic block diagram for ACE is presented in Figure 5. This diagram includes blocks for the main features of ACE, and it indicates the main feedback loops available to the user. Penetration modules are included for shaped charge jets, long rod penetrators, armor piercing bullets, warhead fragments, and air blast.

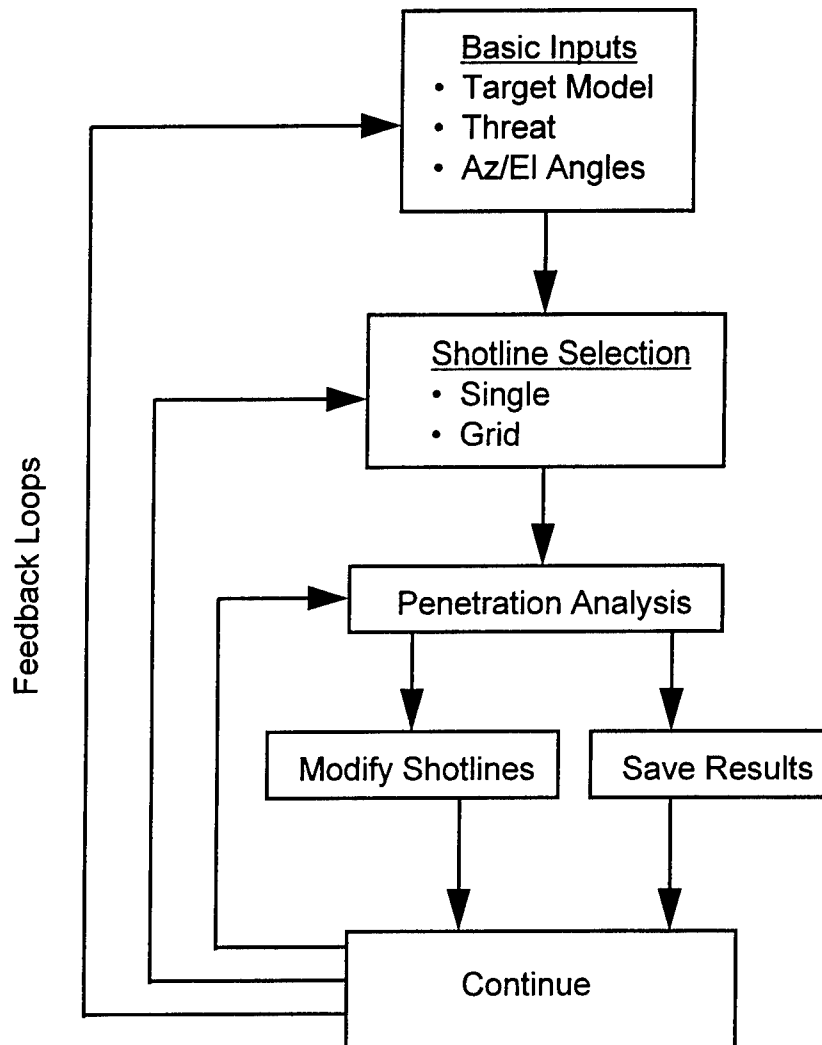


Figure 5. (U) Basic Flow Diagram for ACE  
UNCLASSIFIED

All threat modules are included as Windows DLL's (Dynamic Link Libraries) controlled by a central ACE core written in Visual Basic (Figure 6). Some of the DLL's are written in C and some are written in FORTRAN. Implementing the modules as DLL's allows mixed language support in ACE, and it also facilitates the addition of new DLL's in the future.

UNCLASSIFIED

UNCLASSIFIED

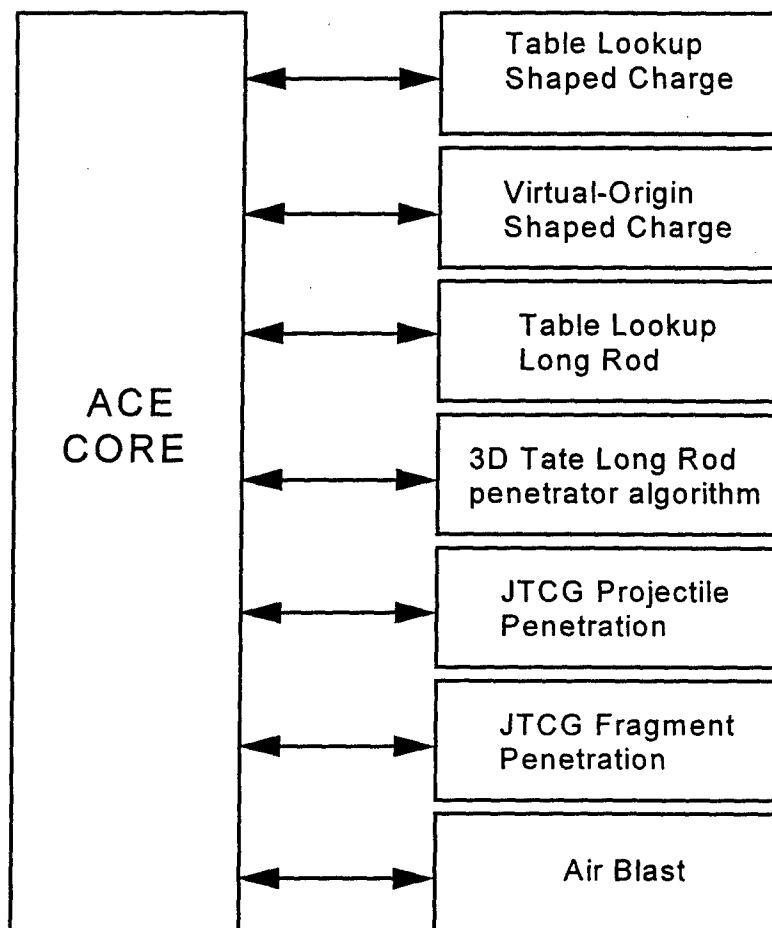


Figure 6. (U) ACE Core/DLL Architecture.

UNCLASSIFIED

(U) As Figure 6 indicates, routines are included for shaped charges, long rod penetrators, fragments, projectiles, and air blast. It is also possible to analyze a "point-burst" of a warhead. Thumbnail descriptions of the analysis modules follow.

(U) Shaped Charges. Two shaped charge routines are implemented. The first is a table lookup routine for which the user specifies a penetration vs. standoff curve and a set of penetration hole profiles at various standoff distances. Total penetration is interpreted linearly from the former, and hole profiles are interpreted linearly from the latter [1]. The second shaped charge routine models the jet in a "virtual origin" fashion by specifying tip speed, tail speed, average breakup time, particle length at breakup, and number of particles at breakup. The crater hole profile is then computed on a particle-by-particle impact basis. Particles are assigned randomized radial drift speeds after breakup, which induces reduced penetration at long standoff distances.

UNCLASSIFIED

## UNCLASSIFIED

(U) Long Rod Penetrators. Two methods are included for long rod penetrators. Method 1 is a table lookup routine for which the user specifies RHA penetration values as a function of impact speed and impact obliquity [1]. Method 2 is a modified version of Tate's classic method for rods [2]. The ACE version of Tate's method treats both the rod and the target as 3D objects. A number of shotlines are traced through the 3D representation of the rod and through the 3D target geometric model. Each shotline is then treated as a central streamline in the same fashion as [2].

(U) Armor Piercing Projectiles (Bullets). Projectiles are treated according to the method proscribed in the JTCG Handbook of Penetration Equations [3].

(U) Warhead Fragments. Two methods are supplied for fragment penetration analysis. The first is the standard method in the JTCG Handbook of Penetration Equations [3]. The second is the FATEPEN2 (Fast Air Target Penetration) method described in [4]. FATEPEN2 is an improvement over [3], especially for high speed fragment impacts.

(U) Free Air Blast. ACE employs the Speicher-Brode [5] empirical equations for free air blast. These equations predict a number of free air blast properties such as peak pressure and total reflected impulse as a function of the yield equivalent and the distance of the charge to the measuring location.

(U) The Visual Basic core handles all of the Windows message traffic and interactions with the user. Core tasks include the creation of shotlines, display of the target geometry, display of the computational results, file I/O, editing of threats and/or shotlines, saving results and so forth. The DLL's are strictly per-shotline computational modules; given a threat definition and a single shotline impact sequence they return results that are threat specific.

### (U) INTERACTIVE GEOMETRY EDITOR

(U) ACE follows the usual steps for shotline analysis, i.e., load a target, load a threat, generate shotlines, analyze the threat along each shotline, and display the results. ACE also allows the user to modify the target geometry description from within a shotline analysis session. So it is possible to analyze a set of shotlines, then modify the target geometry and re-analyze the shotlines in an iterative fashion. Modifying the geometry is done in cooperation with a companion program called ACE-STE (ACE Simple Target Editor). ACE-STE is a target geometry modeling code that can be launched as a stand-alone application, or it can be launched from within ACE. If ACE-STE is launched from ACE, then the two codes can share geometry data through a DDE (Dynamic Data Exchange) link that ACE sets up. Figures 7 through 10 show the basic operation of the DDE exchange between ACE and ACE-STE. In Figure 7 a target has been loaded into ACE and the user has selected the **Edit Target** menu item. Selecting this menu item

UNCLASSIFIED

causes ACE to launch ACE-STE and to send the geometry model to ACE-STE via the internal DDE link. ACE-STE then initializes itself and exposes its main window to the user (Figure 8). At this point the user can add geometry using the toolbar items to add spheres, boxes, plate arrays, and so forth. A skirt plate has been added to the model in Figure 9. When the modifications are complete the user returns control to ACE, at which point ACE-STE disappears and the new geometry now appears in ACE (Figure 10).

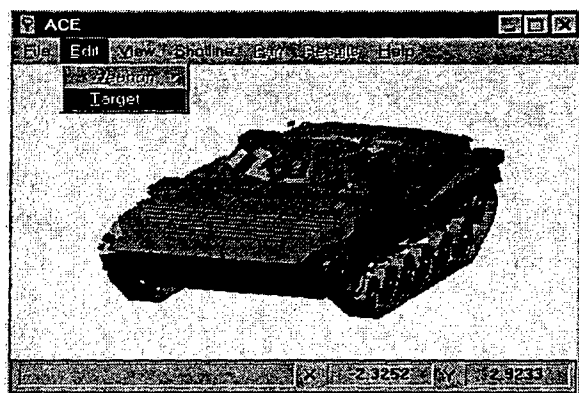


Figure 7. Ready to launch ACE-STE.

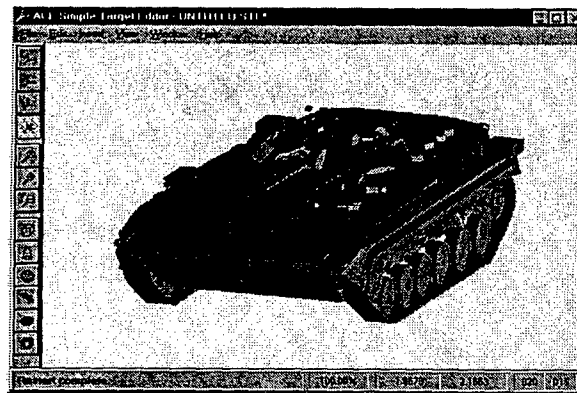


Figure 8. Initial Geometry in ACE-STE.

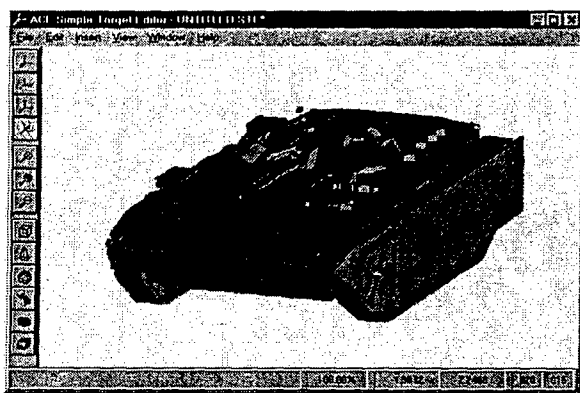


Figure 9. Skirt plate added to the model.

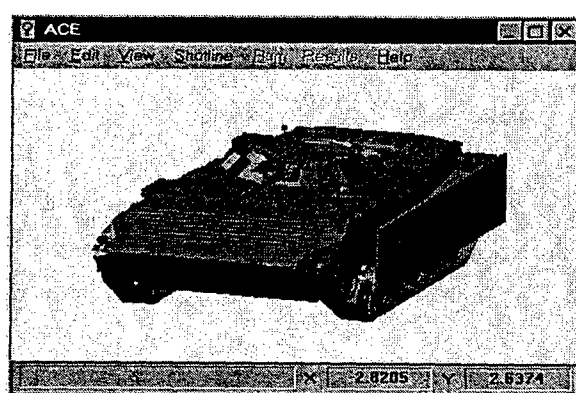


Figure 10. Modified geometry back in ACE.

(U) SUMMARY

(U) ACE is a new shotline analysis code that emphasizes user interaction up to and including geometry modification. Penetration routines are provided for long rod penetrators, shaped charge jets, projectiles, fragments, and air blast. ACE's modular architecture enables new penetration routines to be added as necessary.

UNCLASSIFIED

(U) Bibliography

- [1] P.J. Hanes, et al "MODULAR UNIX-BASED VULNERABILITY ESTIMATION SUITE (MUVES) ANALYST's GUIDE." Memorandum Report BRL-MR-3955, December 1991, Ballistic Research Laboratory, Aberdeen Proving Ground, Maryland.
- [2] A. Tate, "A Theory for the Deceleration of Long Rods After Impact," J. Mech. Phys. Solids 15, pp. 387-399 (1967).
- [3] None, "Penetration Equations Handbook for Kinetic-Energy Penetrators," JTCG/ME publication 61 JTCG/ME-77-16, October 1985.
- [4] Yatteau, Recht, and Dickinson "High Speed Penetration of Spaced Plates by Compact Fragments," Proceedings of the Ninth International Symposium on Ballistics, May 1986, Royal Military College of Science, Shrivenham, England.
- [5] Speicher, B.J., Brode, H.L., "Extremely High Overpressure Analytical Expression for Burst height, Range, and Time - Over an Ideal Surface", Pacific Sierra Research Corporation PSR Note 611, 1984.

UNCLASSIFIED

## WAVELET AND FRACTAL ANALYSIS OF GROUND VEHICLE VISUAL SIGNATURES(U)

David Gorsich, Charles R. Tolle, Robert Karlsen, and Grant Gerhart

US Army Tank-automotive and Armaments Command

Research, Development & Engineering Center

Survivability, MS263

Warren, MI 48397-5000

March 1, 1996

### ABSTRACT(U)

(U) This paper presents continuing work on analyzing visual signatures of ground vehicles using wavelet and fractal analysis techniques. The fractal dimension of an image is an important cue feature to human observers and SAR automatic target recognition systems. An important step in defeating automatic target recognition systems is to determine which features they look for and how to mask those features. This paper first validates and compares various algorithms to compute the fractal dimension. Various textures, both synthetic and natural are compared using the box algorithm and a wavelet decomposition. The value of these techniques are judged based on how well textures can be classified into groups.

### (U) 1 INTRODUCTION

(U) A common method used in automatic target detection or pattern recognition is image segmentation. Image segmentation is the process of separating images into regions which are similar in some way. Texture analysis of images is an important part of computer vision since the patterns provide important cue features to recognize objects. This paper considers the value of using the fractal dimension to segmenting images into different texture regions. Each smaller region is thus characterized by its fractal dimension. Human perception to changes in the fractal dimension of textures have been determined [1]. Lincoln Laboratory has looked at the fractal dimension as one of the best five cue features (out of thirteen studied) in automatic target recognition of SAR imagery [2]. When the fractal dimension is used as a cue feature along with several other cue features which are orthogonal to each other (uncorrelated), these features can be mapped into a multi-dimensional space and clustered, in order to classify the regions.

(U) A fractal is a set which has a non-integer fractal dimension. The fractal dimension is most commonly defined as the Hausdorff-Besicovitch (HB) dimension. There are a number of ways to determine the fractal dimension. These are a few of the methods: the box algorithm, the wavelet transform, the Fourier transform or power spectrum method, Hurst coefficients, and capacity dimension. Recent work has been done to determine which of the methods are efficient versus accurate [3]. There is even a web site (<http://life.csu.edu.au/fractop/>) which calculates the capacity dimension of a user supplied image, although we found this to give us an unreliable measure of dimension.

(U) In this paper we look at the box dimension algorithm and a wavelet method developed by Mallat [4]. Each method is checked initially in one dimension on Cantor sets with well known fractal dimensions. Then for the two dimension case, the algorithms were tested using the Seirpinski triangle. Values of the various methods were compared. Next, we used a texture generation program given by Ebert [5]. The texture generator can give us textures of a given fractal dimension with varying lacunarity. The algorithms were finally tested on these textures. We were then able to analyze the changes in the fractal dimension over various parts of images taken of a M1 tank and a 40 ton prototype tank, the FMBT40T, in front of a tree line. Changes in the fractal dimension over the image were determined. It was determined that the box algorithm was the best approach to estimate the fractal dimension for these sub-images.

## (U) 2 FRACTAL DIMENSIONS

(U) As discussed earlier, the fractal dimension is most commonly defined as the Hausdorff-Besicovitch (HB) dimension,  $D_h(A)$ , where  $A$  denotes the image/signal. In general the HB dimension of  $A$  is defined in the following manner [6]:

Let

$$(U) \quad R^n = \{x | x = (x_1, \dots, x_n), x_i \in R\} \quad (1)$$

for some natural number  $n$ . Then, define:

$$(U) \quad \text{diam}(C) = \sup\{d_e(x, y) | x, y \in C\}, \quad (2)$$

where  $d_e(x, y)$  denotes the euclidean distance function. Next, define an open cover of  $A$ :

$$(U) \quad A \subset \bigcup_{i=1}^{\infty} C_i \quad (3)$$

Then, define:

$$(U) \quad h_\epsilon^s(A) = \inf \left\{ \sum_{i=0}^{\infty} \text{diam}(C_i)^s \mid \{C_1, C_2, \dots\} \text{ open cover of } A \text{ with } \text{diam}(C_i) \leq \epsilon \right\} \quad (4)$$

Finally, define the  $s$ -dimensional Hausdroff measure of  $A$  as:

$$(U) \quad h^s(A) = \lim_{\epsilon \rightarrow 0} h_\epsilon^s(A) \quad (5)$$

And it follows that,

$$(U) \quad D_h(A) = \inf\{s \mid h^s(A) = 0\} = \sup\{s \mid h^s(A) = \infty\} \quad (6)$$

It should be noted that calculating the HB dimension is hard in general and thus there is a need for a more easily calculated dimension, i.e. the box dimension which is discussed next.

## (U) 2.1 Using The Box Counting Algorithm To Determine Fractal Dimension

(U) The box dimension,  $D_b(A)$ , which is normally calculated by the box counting algorithm, is a good estimator of the HB dimension. In general the box dimension can be defined as follows [6]:

(U) Let  $N_\delta(A)$  be the smallest number of closed balls (boxes) with size  $\delta$  that cover the set  $A$ . Then it follows that:

$$(U) \quad D_b(A) = \lim_{\delta \rightarrow 0} \frac{\log N_\delta(A)}{\log \frac{1}{\delta}} \quad (7)$$

At this point it is important to note that the box dimension does not always equal the HB dimension. There are several such examples. It can be shown that,  $D_b(A) = n$  for any dense subset  $A$  such that  $A \subset R^n = \{x \mid x = (x_1, \dots, x_n), x_i \in R\}$ , likewise for the same  $A$ ,  $D_h(A) \leq n$ , moreover  $D_h(A) = 0$  for any such countable set  $A$ . Therefore, given the set  $A$  of rational numbers on  $[0, 1]$ , the box dimension is  $D_b(A) = 1$  while the HB dimension is  $D_h(A) = 0$  [6]. Although the box dimension fails in some instances, the value it normally produces is a good approximation to the HB dimension.

(U) The major problem with the box dimension is in its calculation. In order to calculate the actual box dimension, one must first find the optimal (smallest number of boxes) covering of  $A$  for a given set of boxes with sides of size  $\delta$ . Note that finding such a cover is in



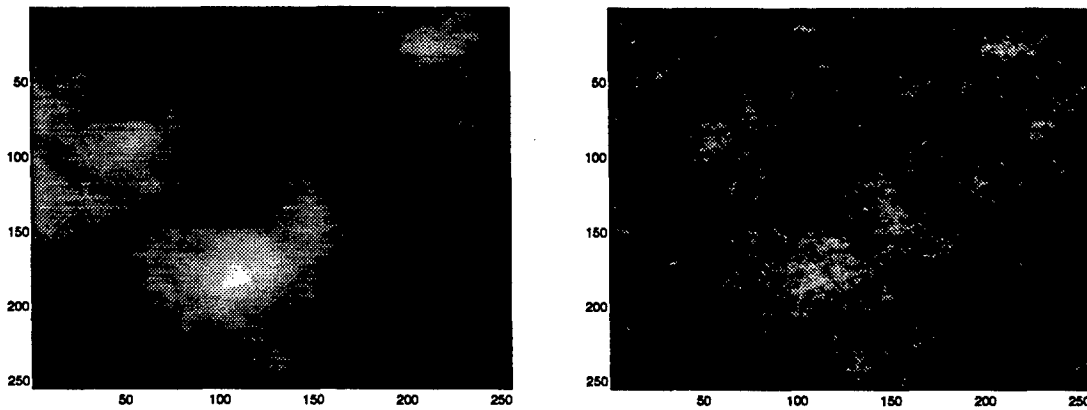


Figure 1. (U) This is an example of two Brownian motion textures with a fractal dimension of 2.1 on the left and 2.7 on the right.

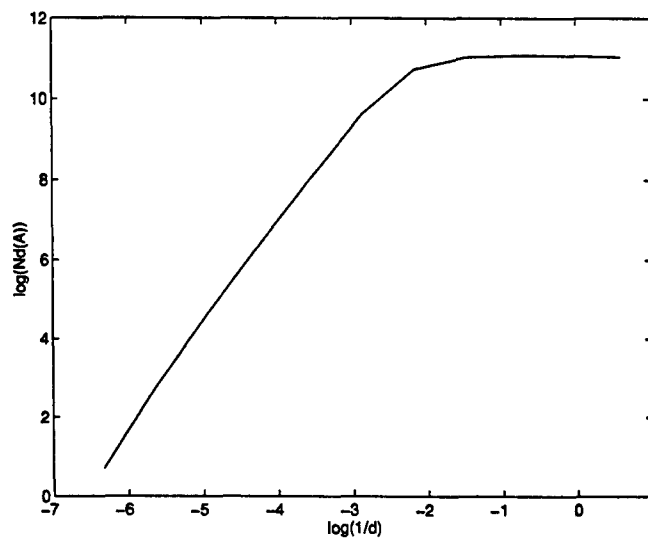


Figure 2. (U) The log-log plot of the results from the box counting algorithm for the texture with a fractal dimension of 2.7 shown in Figure 1.

general difficult. Therefore, the box dimension is normally estimated using the box counting algorithm. In short, the box counting algorithm places a standard set of rectangular grids (or set of boxes) upon the image/signal and counts the number of boxes that are filled by the image/signal. This count is then plotted on a *log-log* plot of the number of filled boxes versus the inverse of the box size, see Figure 2. Finally, the box dimension estimate is taken from the monotonically rising nonzero linear slope of the *log-log* plot. By examining this procedure closely one can see that the only difference between the results obtained using the box counting algorithm and the box dimension is in the choice of the cover. In other words, the box counting algorithm doesn't use the optimal cover in general. Furthermore, it has been shown that the box counting algorithm needs at least  $10^{D_h(A)}$  points to determine the fractal dimension of a set with dimension  $D_h(A)$  [7].

(U) 2.2 Using The Wavelet Transform To Find The Fractal Dimension

(U) The wavelet transform has been very popular over the last few years for its time-frequency localization ability, something the Fourier transform does not have. The use of the wavelet transform to decompose images and extract cue features is well established and documented. Here, we wish to demonstrate the ability of the wavelet transform to approximate the fractal dimension of signals and images. An appealing aspect of the wavelet transform is its ability to analyze images on different scales. By looking at the differences between scales, the self-similar properties of an image can become apparent. We implemented an approach given by Mallat [4] which looks at the power spectrum of a signal that has been decomposed several times in order to estimate the fractal dimension.

(U) The signal is decomposed several times using the wavelet transform. The wavelet transform is calculated by using a sub-band filtering scheme. The original signal is convolved with a low-pass filter representing a scaling function and a high-pass filter representing the wavelet. Then each convolved signal is down-sampled by two.

(U) The decomposition of a signal represented by the vector  $c^o(k)$  is determined by:

$$(U) \quad c^{j+1}(k) = \sum_n h(n - 2k)c^j(n) \quad (8)$$

$$(U) \quad d^{j+1}(k) = \sum_n g(n - 2k)c^j(n) \quad (9)$$

where  $j$  indicates the resolution level or the numbers of decompositions of the original signal. The  $h(n)$  are the low-pass filter coefficients and  $g(n)$  are the high-pass filter coefficients. In our implementation, we used a 6-tap Daubechies filter [8]. The high-pass filter coefficients are related to the low-pass filter coefficients by:

$$(U) \quad g(n) = (-1)^n h(5 - n) \quad \text{where } 0 \leq n \leq 5 \quad (10)$$

Fractal dimension is determined from the similarity parameter  $H$ :

$$(U) \quad D_w(A) = T + 1 - H \quad (11)$$

where  $T$  is the topological dimension of the space in which the set resides. For images,  $T$  is equal to two.  $H$  may be determined by the following ratio:

$$(U) \quad \frac{\sigma_{2^{j+1}}^2}{\sigma_{2^j}^2} = 2^{2H} \quad (12)$$

Table I. (U) Tabulated estimates of fractal dimension,  $D_w(A)$ , for known fractal dimension,  $D(A)$ , signals using the Wavelet method.

Signal Being Estimated	Wavelet Estimate	Actual Dimension	3% Error	Actual Error
Cantor $\frac{\log(2)}{\log(3)}$	0.6223	0.6309	0.0189	0.0086
Cantor $\frac{\log(3)}{\log(5)}$	0.6644	0.6826	0.02	0.0182
Sierpinski Triangle	1.6677	1.5850	0.0475	0.0827

Note: this ratio is constant for fractals. The energy of the details of the original signal  $d^j(k)$ , i.e. the high pass part, is  $\sigma_{2^j}^2$ .

$$(U) \quad \sigma_{2^j}^2 = \frac{1}{2\pi} \int_{-2^j\pi}^{2^j\pi} \sum_{k=1}^N P_{2^j}(\omega + 2^{j+1}k\pi) d\omega \quad (13)$$

$P_{2^j}$  is the absolute value of the Discrete Fourier Transform (DFT) of  $d^j(k)$  for  $1 \leq k \leq N$ .  $N$  is the length of the original signal.

(U) The approach was tested with two Cantor sets, the  $\frac{\log(2)}{\log(3)}$  and  $\frac{\log(3)}{\log(5)}$  sets. Three decompositions were performed and three ratios taken. Then these three ratios were averaged and tabulated in Table I. The errors fell within the maximum error bound of the algorithm given by Mallat to be 3%, except for the two dimensional images. For the images, we extended the above approach to two dimensions so that the fractal dimension of images could be determined. In doing this we simply extended the wavelet transform, Fourier transform and integration routines to their two dimensional forms. The wavelet method did not approximate the Brownian textures with fractal dimensions 2.1 and 2.9 very well. The energy ratios between successive decompositions were not constant, even though we were decomposing a fractal. This is potentially caused by the low resolution of the initial image, and/or in the way in which we extended the one dimensional case.

(U) It was strange to notice that when the low-pass filter coefficients were used instead of the high-pass filter coefficients, the values came as close and sometimes much closer to the actual fractal dimensions. For example, the  $\frac{\log(2)}{\log(3)}$  Cantor with the low-pass coefficient approach gave a fractal dimension of 0.6313, an error of only 0.0004! The theoretical reasons for this are unclear and require further study.

### (U) 3 RESULTS

(U) From the initial tests, the Fourier transform methods appears to be less reliable then the wavelet and box methods. For example, in the  $\frac{\log(2)}{\log(3)}$  Cantor set case, the Fourier method

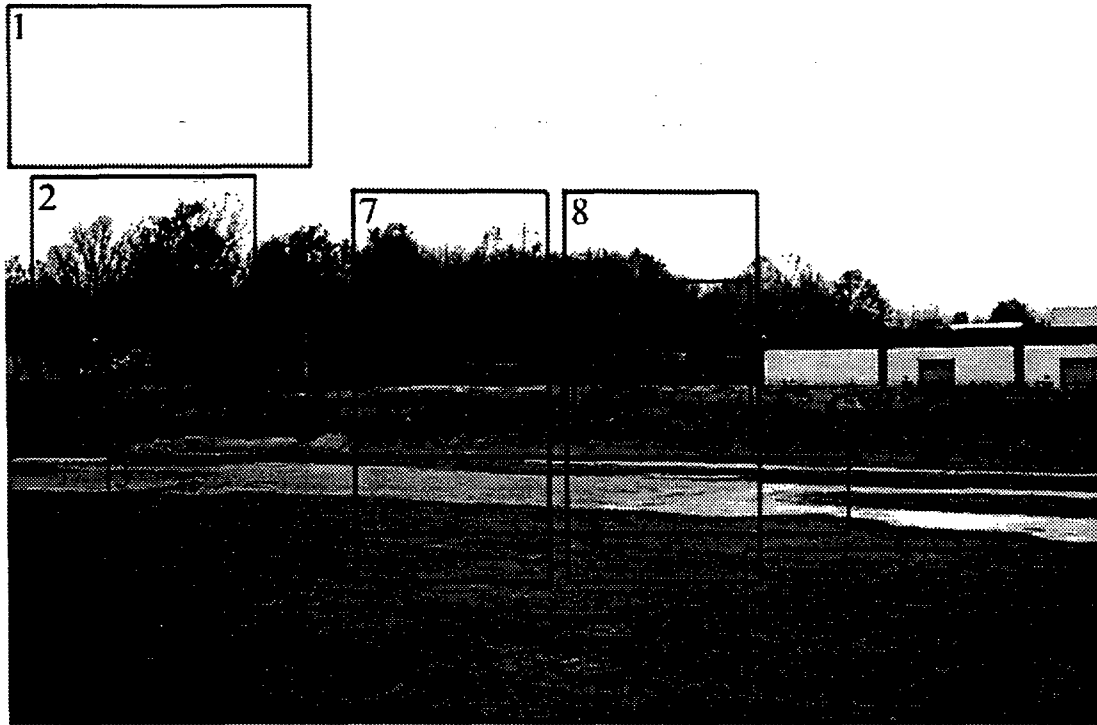


Figure 3. (U) This is the original photo of the FMBT40T and M1 tanks with the segmented regions shown.

gave approximate values of 0.2986 and 0.2379 while the actual value is 0.6309. In other cases, such as the  $\frac{\log(3)}{\log(5)}$  Cantor set, the Fourier method had a much more accurate fractal dimension estimate. However, due to this unreliability we choose not to use the Fourier method. Likewise, the wavelet method was much faster than the box algorithm, but did not accurately predict the values of the Brownian textures as well as the box algorithm. Therefore, the box algorithm was used on the tank image to classify the textures.

(U) The image that was analyzed was taken with a Kodak Digicam camera which took 756x504 pixel images and then saved them in the TIFF format, see Figure 3. The image is composed of two tanks side by side. On the left is a 40 ton prototype tank called FMBT40T and on the right is the M1. In order to analyze the image based on its fractal dimension, the image was partitioned into eight regions. Once partitioned, each region's individual fractal dimension estimate was calculated using the box algorithm, as stated above. The tabulated values for each region are listed in Table II. It is important to note that differences in the estimated fractal dimension for each region do occur. However, the differences are small for these examples. There are a number of possible reasons for this. One of the most visible possibilities is that these regions might be better characterized by their *lacunarity* rather than by their actual fractal dimension. How do we define lacunarity? The Latin word *lacuna*, which means gap [9], gives us the initial concept of what lacunarity means: a gap within a fractal. A better explanation is given by an example. Fractals aren't characterized by only their fractal dimension (their self similarity on different scales) but also by how widely spread their replicating parts are distributed. In Figure 4, two textures with the

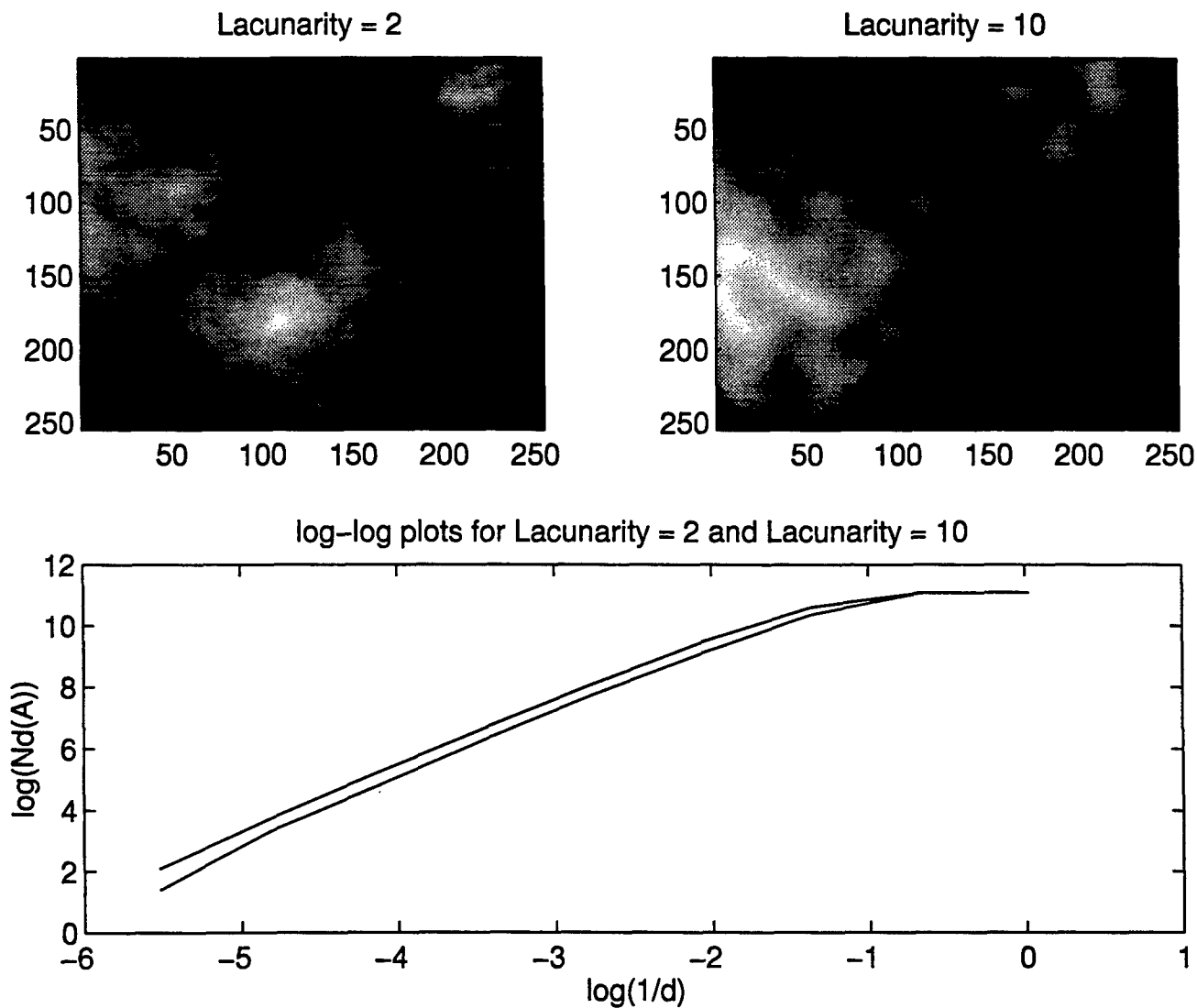


Table II. (U) Estimated fractal dimensions for the regions within Figure 3.

Region Number	Region Description	Estimated Fractal Dimension
1	sky	2.22
2	trees without leaves	2.30
3	smooth water	2.09
4	short grass	2.20
5	FMBT40T tank	2.15
6	M1 tank	2.16
7	Composite with FMBT40T	2.11
8	Composite with M1	2.19

same fractal dimension but with different lacunarities are shown. Note how different the two textures appear from each other. If one looks closely one can see that the texture with the higher lacunarity appears to have large gaps within its smoother textured regions. This is one reason the fractal dimension does not represent all of the differences between two textures with identical HB dimensions.

#### (U) 4 CONCLUSIONS AND FUTURE DIRECTIONS

(U) One problem in using the fractal dimension for image segmentation is the inability to always accurately calculate the fractal dimension. The box algorithm was found to be more versatile and accurate than the wavelet and Fourier methods to approximate the fractal dimension, but more research needs to be done with the wavelet approach. This includes questions about the effects of using different filter coefficients within the wavelet transform. In addition, after three or four decompositions, the images no longer contained enough information to support a fractal dimension calculation. The Seirpinksi image initially was 256x256 pixels, and after three decompositions, its size was 32x32 pixels. Thus, for the wavelet approach, higher resolution images are needed. The wavelet approach is very appealing since the image is actually analyzed on different scales, so that the differences between scales should highlight the scale invariant properties of the image.

(U) It was found in this paper that the fractal dimension can not classify textures in images - even Brownian motion. There are many different textures which have the same fractal dimension. For example, textures were generated with the same fractal dimension but different lacunarities. From the standpoint of defeating automatic target recognition systems, this is an important result. If a system uses a fractal dimension type cue feature (a statistical similarity property), the system could be defeated by matching the target's texture to the background texture via the fractal dimension, and this texture need not be the same texture as the background! From an estimate of the fractal dimension of a typical

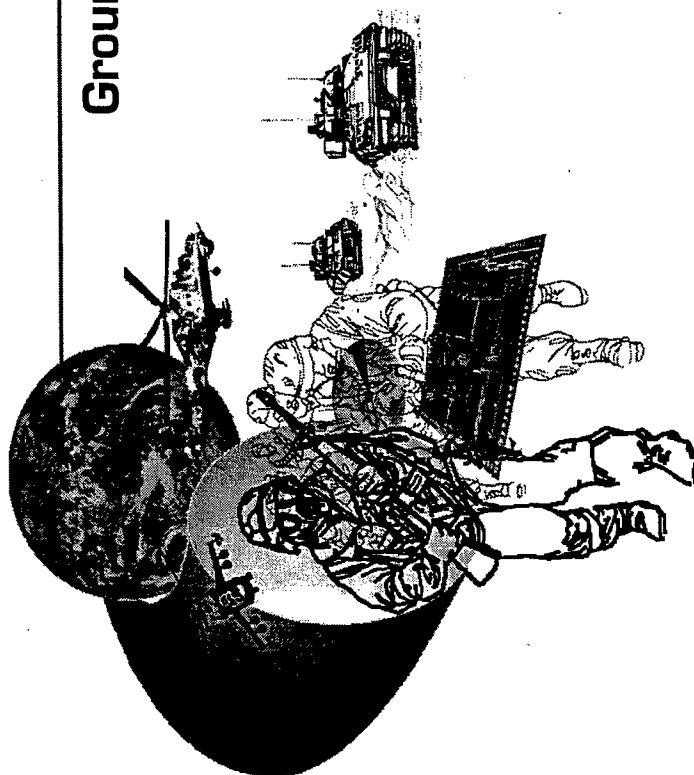
battlefield background, the fractal dimension could be used as an additional parameter for the design of the camouflage pattern of the vehicle. With lacunarity as a variable, it may still be possible to keep within the current US-GE camouflage guidelines. These topics provided some of the potential areas of future research.

### (U) References

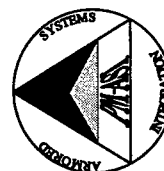
- [1] Lewis F. Jardine, "Fractal-based Analysis and Synthesis of Multispectral Visual Texture for Camouflage," *Applications of Fractals and Chaos*, Springer-Verlag, New York, NY, 1993, pp 101-116.
- [2] Daniel E. Kreithen, Shawn D. Halversen, and Gregory J. Owirka, "Discriminating Targets from Clutter," *MIT Lincoln Laboratory Journal*, Vol. 6, No. 1, Spring, 1993, pp. 25-52.
- [3] X.C. Jin, S.H. Ong, and Jayasooriah, "A practical method for estimating fractal dimension," *Pattern Recognition Letters*, Vol. 16, May, 1995, pp. 457-464.
- [4] Stephane G. Mallat, "A Theory for Multiresolution Signal Decomposition: The Wavelet Representation," *IEEE Transactions on Pattern Analysis and Machine Intelligence*, Vol. II, No. 7, July, 1989, pp. 674-693.
- [5] Editor David S. Ebert, *Texturing and Modeling: A Procedural Approach*, Academic Press Professional, Cambridge, MA, 1994, pp. 256-260.
- [6] Heinz-Otto Peitgen, Hartmut Jürgens, and Dietmar Saupe, *Chaos and Fractals: New Frontiers of Science*, Springer-Verlag New York, Inc., New York, NY, 1992.
- [7] James B. Bassingthwaighite, Larry S. Liebovitch, and Bruce J. West, *Fractal Physiology*, American Physiological Society, New York, NY, 1994.
- [8] Ingrid Daubechies, *Ten Lectures on Wavelets*, Society for Industrial and Applied Mathematics, Philadelphia, PA, 1992, pg. 195.
- [9] Editors: Heinz-Otto Peitgen, and Dietmar Saupe, *The Science of Fractal Images*, Springer-Verlag, New York, NY, 1989, pp.67-69.

# GCVSD

## Ground Combat Vehicle Survivability Database



Developed for the  
PEO-Armored Systems Modernization,  
PM-Armored Systems Integration  
by  
The Survivability/Vulnerability Information  
Analysis Center (SURVIAC)

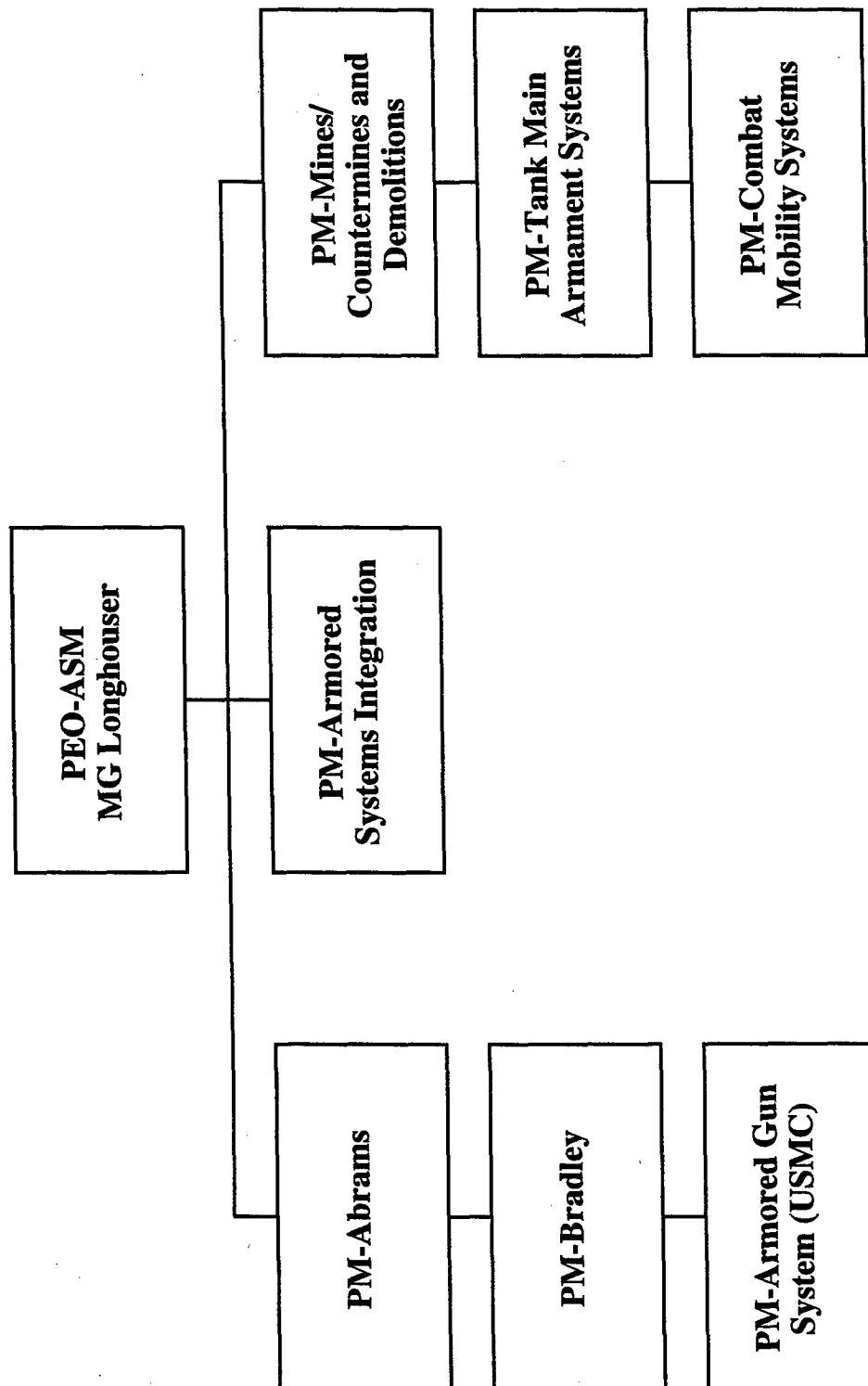




Who is Sponsoring this Database Effort?

Project Manager - Armored Systems Integration (PM-ASI)

## PEO-Armored Systems Modernization



## Who are We?

- SURVIAC is the DoD focal point for non-nuclear survivability/vulnerability data, information, methodologies, models and analysis relating to U.S. and foreign surface and aeronautical Systems
- SURVIAC is Sponsored by:
  - The Joint Technical Coordinating Group on Aircraft Survivability (JTCCG/AS)
  - The Joint Technical Coordinating Group for Munitions Effectiveness (JTCCG/ME)
- SURVIAC provides analysis and technical support to Government organizations through its Technical Area Task program

## Background

PM-ASI Identified a Need for a Ground Combat Vehicle (GCV) Survivability Database to Support Current and Ongoing Government R&D Projects

### Current Threat Data Limitations

- Not Concentrated in One Location
- Not Available in a Consistent Format
- Data Collection Must be Repeated
- Matching Threats to GCVs and Threats to CM's is Sometimes Difficult

The Current Data Gathering Process is Neither Time nor Cost Effective

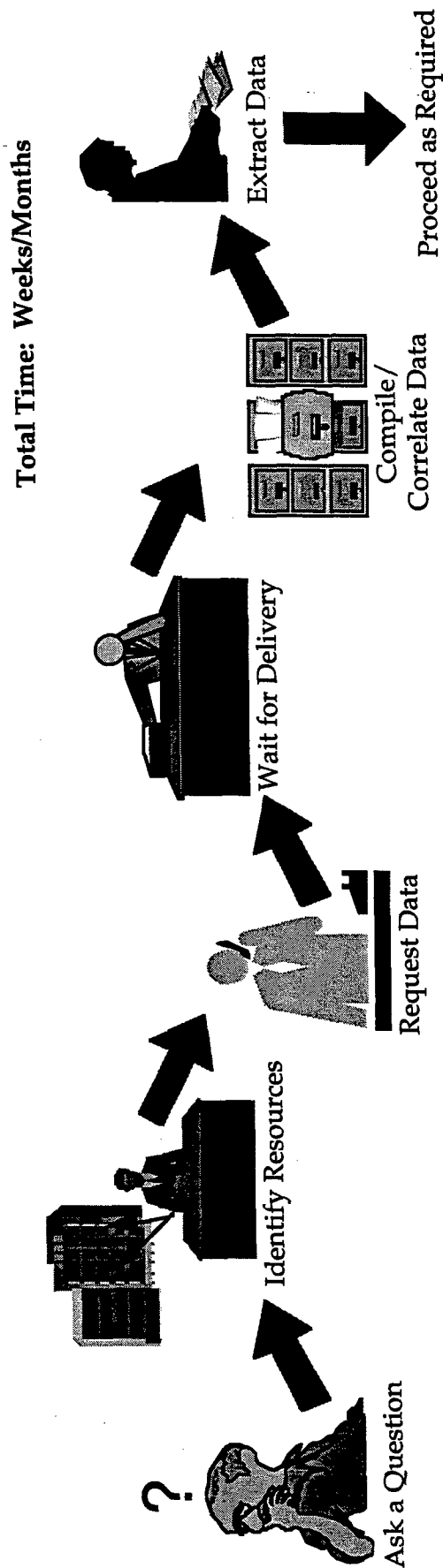
## Purpose

To Develop a User Friendly and Unique Relational Database System which will contain data on and provide easy access to:

- U.S. Ground Combat Vehicles
- Potential Threats to U.S. GCVs
  - Acquisition
  - Engagement
    - Conventional
    - Non-Conventional
- Delivery Systems/Platforms for Those Threats
- Potential Survivability Options Against Those Threats
  - Detection Avoidance
  - Hit Avoidance
  - Penetration Avoidance
  - Kill Avoidance

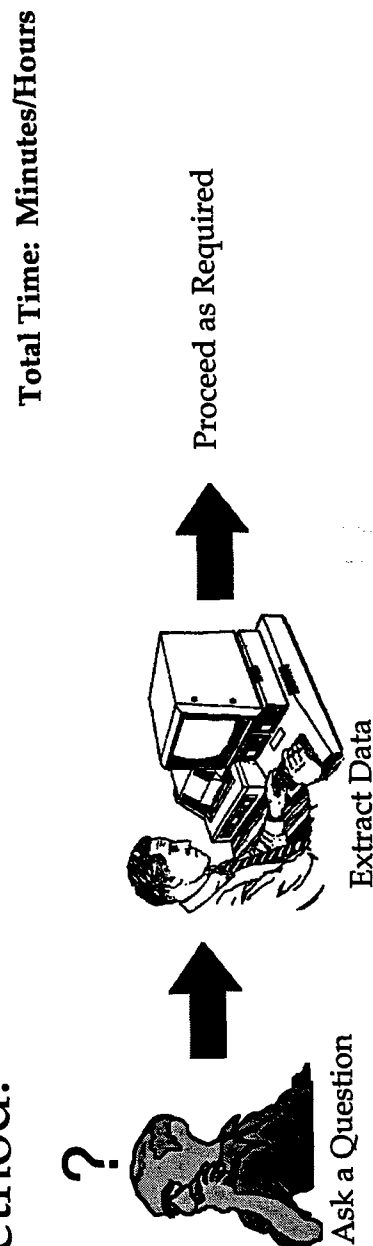
## Expected Benefits

### Conventional Method:



OR:

### Automated Method:



## Who Will Benefit?

- DoD Organizations
- Defense Contractors
- All Authorized Users can Obtain a Copy

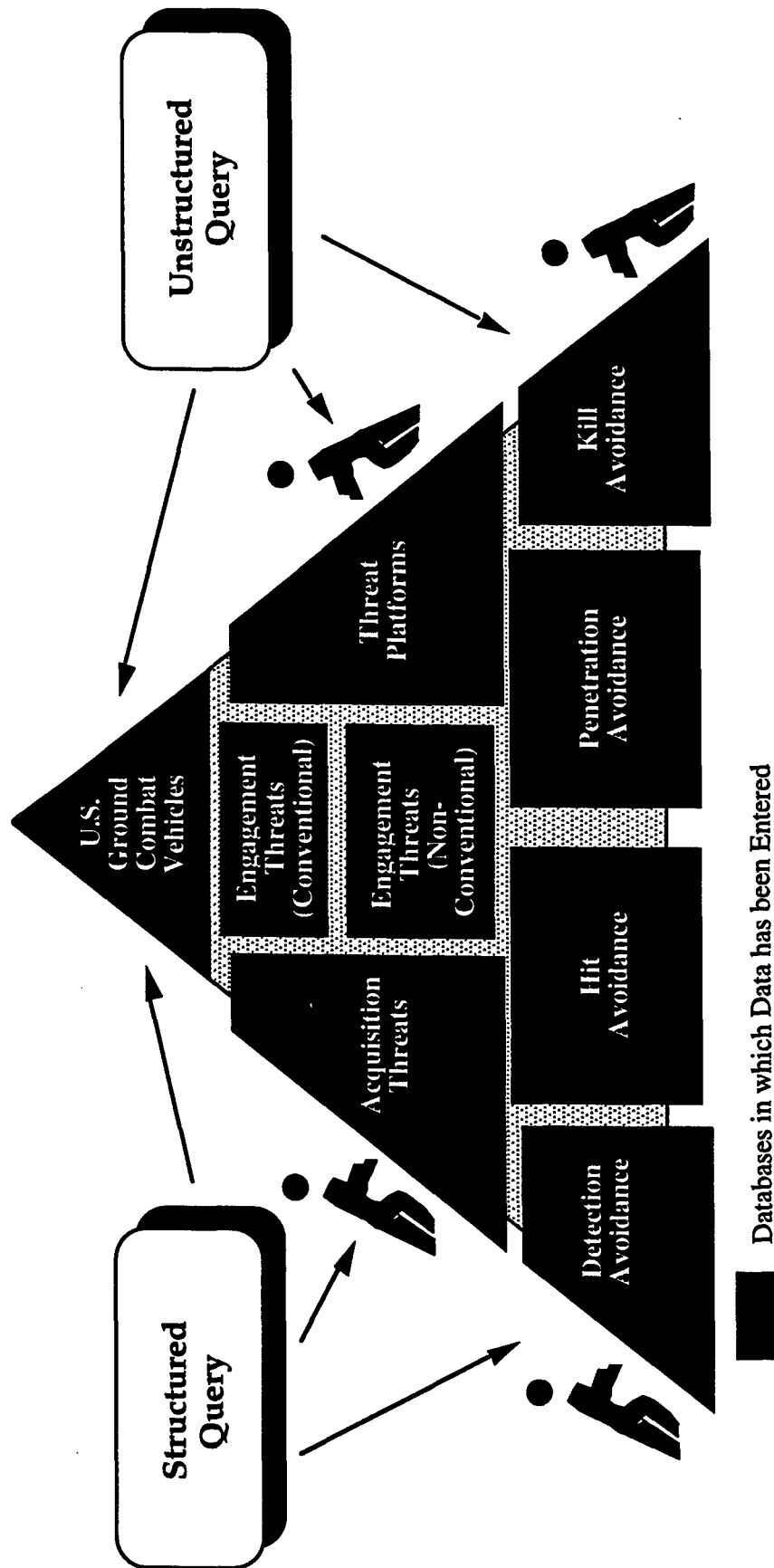
This Database is Not being Developed Solely for PM-ASI. It is Intended to Benefit All Authorized Users

## Database Supporters/Potential Users

- PEO-ASM (MG Longhouser)
- PEO-FAS (Mr. Dale Adams)
- Program Managers
  - PM-CRUSADER (Ms. Iris Edwards)
  - PM-ABRAMS (Mr. Latson)
  - PM-BRADLEY (Mr. Ben Demarco)
  - PM-AGS (Mr. Joe Godell)
  - PM-CMS (MAJ Stass)
  - PM-TMAS (MAJ Thorson)
- Centers
  - TRADOC, Ft. Monroe, VA (COL Reuss/COL O'Dawes)
  - DCD - Armor School, Ft. Knox (MAJ Hrdy)
  - DCD - Infantry School, Ft. Benning (COL Patterson)
  - TSM Cannon (COL Williams)
- HQDA
  - HQ AMC (Mr. Dale Adams)
  - AMC DCSINT (COL Kennedy)
  - DA DCSINT (LTG Mehnor)
  - SARD-CS (LTC Burton)
  - SARD-ZD (Dr. Fallin)
  - SARD-DE (Mr. Burdt)
  - DAMI-FIT (LTC Villare)
  - DCSOPS (LTC Bailly)
- Other Customers
  - TARDEC (Dr. Jack Parks)
  - TRAC-WSMR (Mr. Carl Powers)
  - SLAD/EWD (Mr. Joe Herman)
  - USMC Intelligence Activity (Mr. David Kositzke)



# Conceptual Database Design



## Data Sources

- Primary Sources

- Blue Vehicle Data

- PM for Each Ground Combat Vehicle (Data Approved by AMSAA)

- Threat Data

- Defense Intelligence Agency (DIA)
    - Missile and Space Intelligence Center (MSIC)
    - National Ground Intelligence Center (NGIC)
  - Survivability Data and Linkages
  - PM-Armored Systems Integration (PM-ASI)

- Secondary Sources

- U.S. Army Tank-automotive and Armaments Command (TACOM)
  - Army Research Laboratory (ARL)
  - Belvoir RD&E Center (BRDEC)
  - Edgewood RD&E Center (ERDEC)

TACOM, Foreign Intelligence Office is Coordinating All Data Gathering Efforts

## Long Term Maintenance

- SURVIAC will Maintain the Database  
(Requires Separate Technical Area Task)
  - The Database will be Continually Updated
  - New Versions of the Database will be Distributed Annually
  - Establishing Automated Updating Procedures with Intelligence Community
  - Establish Customer Support Phone Line
  - Establish User Group to Monitor Maintenance
- Chaired by PM-ASI
- Membership Opened to:
  - SURVIAC
  - TACOM, FIO
  - Interested Users
  - Data Sources
  - PM-ASI Invited Members

Points-of-Contact

PM-Armored Systems Integration (PM-ASI)

Mr. Jeffery Mosley  
(810) 574-7759

Booz•Allen & Hamilton Inc.  
McLean, VA

Mr. Charles Glausier  
(703) 902-5827

Booz•Allen & Hamilton Inc.  
Warren, MI

Mr. John Olejar  
(810) 978-3146

**UNCLASSIFIED**

**THIS PAGE INTENTIONALLY LEFT BLANK**

**UNCLASSIFIED**

UNCLASSIFIED

SURVIVABILITY ISSUES ASSOCIATED WITH POWER MANAGEMENT  
IN FUTURE ALL-ELECTRIC COMBAT VEHICLES

Dr. Scott Fish  
Institute for Advanced Technology, The University of Texas at Austin,  
Austin, Texas, 78759

ABSTRACT (U)

(U) With the proliferation of both advanced armors and smart projectiles, the U.S. Army has been motivated to explore new technologies for hypervelocity launchers and active or semi-active armor. Some of these concepts, such as electric guns, and electrically powered armor systems have been considered rather well suited for integration into a combat vehicle with electric propulsion. The resulting concepts have been referred to as "all-electric" combat vehicles despite the remaining presence of an internal combustion prime power source. The inclusion of these new technologies in a weight, volume, and cost minimized scheme however, will likely require some level of sharing available energy and power amongst the major electrical consumers onboard. This paper explores some of the basic issues associated with the resulting power management and its impact on vehicle survivability. Simulations of a combat vehicle in a complex maneuver which utilizes shared power between weapons, protection, and mobility systems will be used to illustrate these issues.

(U) INTRODUCTION

(U) The notion of an "all-electric" combat vehicle has been around for some time, but has become quite mature in the last decade through simultaneous advances in technologies associated with high power electric weapons and pulsed energy storage, as well as high power solid state switching and associated electric machine control systems. The resulting vehicle system configurations utilize electricity for the transmission of power from a prime mover or electro-chemical energy storage element to all the major power consumers onboard the combat vehicle. Some of the electrical power applications being considered in future combat vehicles are: electric weapons (both Electromagnetic EM, and Electro-Thermal-Chemical ETC guns), high power microwaves, active suspension, active protection, active signature reduction or deception, and mine clearing. Though some of these are still in the concept stages, others are showing great promise through laboratory demonstration of being fieldable in the time frame of a next generation combat vehicle. The feasibility of these and other applications of electrical power will ultimately hinge on the availability of low weight and volume power supplies. While development in the power supply technology is ongoing, it is important to examine what power system architectures lend themselves well to the efficient use of energy and power, thus reducing the required ratings for equipment and resulting in higher performance/lower weight vehicle concepts. The key in these

UNCLASSIFIED

## UNCLASSIFIED

architectures will be an overall energy/power management controller, which will monitor all power loads, sources, and energy storage components and optimize the allocation of energy and power to maximize overall performance. In this paper we will focus on that portion of performance related to survivability, though it will be shown, that this criterion is sufficient to influence most of the major components either directly or indirectly.

### (U) SURVIVABILITY ISSUES FOR ALL-ELECTRIC COMBAT VEHICLES

(U) Survivability of direct fire combat vehicles is usually couched in the well known trio of rules: (1) don't be seen (detected), (2) if seen, don't be hit, and (3) if hit, don't be killed. These three axioms can be translated into several more descriptive design constraints which are used in developing concept vehicles, and will not change with the introduction of all-electric configurations.

(U) *Don't be seen.* Typically this means keeping a low vehicle profile, but can be extended to include reducing other types of signatures such as thermal and radar cross sections (RCS). The visible and RCS signatures are most highly dependent on vehicle volume positioned higher than one meter above the ground. This is due to the way these vehicles typically use cover and maintain firing positions. Since this typically includes all the turret volume in tank-like vehicles, reducing turret size is usually a strong incentive in the overall design. Active suspension concepts could allow the vehicle to be lowered while stationary or traversing smooth terrain, thus reducing its visible signature. Thermal constraints are particularly important for the prime mover, which is typically a combustion engine that can produce significant thermal signature not only on the vehicle but in its wake through the exhaust plume. Though this wake may not allow identification, it can be a great aid in detection for an enemy with a thermal viewer. Thermal signature remains an issue for all-electric vehicles with many power loads, and must be demonstrated in a concept system before major procurements can begin. Another signature is acoustic, and we will see more emphasis on low noise operations particularly for reconnaissance vehicles. Operation of electric vehicles from batteries with the prime mover off will greatly enhance the survivability in this application if sufficient range can be accommodated by limited battery storage volume.

(U) *If seen, don't be hit.* This aspect of survivability is enhanced by two means. First, the vehicle should present as small a cross section to the enemy as possible. Obviously, this reduces his probability of hitting you since you are a smaller target. To aid in reducing the probability of being hit, one can implement decoys and active protection systems, which are particularly effective against slower moving "smart" threat projectiles. Both of these systems can show increased effectiveness in all-electric concept vehicles with appropriate allocation of power to their cause. The second means of survivability enhancement has to do with maneuvering to avoid being hit. Maneuvers can be directed at positioning for maximum cover, positioning to present minimum target area, or positioning to become invisible prior to being shot at (preferred), or changing position to create error in enemy fire control system. All of the above maneuver objectives are enhanced when vehicle power to weight ratio is increased. For all-electric vehicles, the issue is how to reduce the total weight of both prime power and energy storage while providing the requisite performance in all subsystems. This reduction is typically enhanced by the sharing of energy among subsystems, but requires some form of "energy management" to maintain the desired performance.

UNCLASSIFIED

## UNCLASSIFIED

(U) *If hit, don't be killed.* This part of survivability is the basis of work in armor mechanics and internal vehicle arrangements. All-electric vehicles can provide enhanced survivability if they reduce or eliminate propellants, which can often result in a kill if detonated. In addition, the use of EM guns can allow for storage of only the projectiles in the turret since no cartridge is required. The power supplies alluded to here are currently being considered for installation in the turret basket area and in the hull. Placement of the very high power components must be as close to the load as possible and the use of slip rings in this pulse-power to gun link must be avoided. Charging equipment may however be located outside the turret if necessary since the current values are within reason for slip ring connections. Reductions in required high turret volume may be used to implement more voluminous, but lighter armor concepts for greater hardness in the future.

### (U) POWER MANAGEMENT: WHAT DOES IT BUY YOU IN SURVIVABILITY?

(U) Many aspects of new weapon systems, armors, and drive systems will contribute to increased survivability in future all-electric combat vehicles, but the underlying key, as mentioned earlier, is the reduction in weight and volume required for the power system components. The sharing of power and energy among subsystems promises to reduce the required ratings on their components and result in smaller overall packages for the required performance than autonomous power systems. The interdependence, however, will require very careful monitoring and direction of the energy to effect this benefit.

(U) Where are these benefits in reduced ratings? The prime mover is a good example to begin with. Current engines are designed to operate over a wide speed range even with multi-speed gearboxes to provide power to the drive wheels. The use of hybrid electric drive with the transmission replaced by a generator/motor combination allows the prime mover to operate at a more confined speed, since the gear ratio can be varied continuously. This reduction in operating speed range can result in increases in efficiency of operation, which can be translated into reduced size for the same output power, and reduced required fuel capacity for the same range. This efficiency benefit becomes magnified when there are multiple transient loads and we can coordinate power from storage elements like flywheels and batteries to absorb the transients and allow the prime mover to operate at a more steady load. The exhaust system may also be more effectively optimized in reducing acoustic and chemical emissions in this confined operating range.

(U) The response time of the electric drive system will be increased by an order of magnitude over the mechanical system, since its inertia and drag are greatly reduced. The pulse duty performance can also be enhanced by the use of parallel energy storage devices working with the prime mover to provide very high power for brief periods, e.g., when dashing to new cover.

(U) Finally, the use of new high power devices such as microwaves, and active protection may only become feasible in the context of sharing a power supply with other consumers such as the drive or weapon systems. Likewise, the enhanced lethality expected for EM weapons may only be practical in a vehicle designed to use available energy for other functions when not using the gun.

UNCLASSIFIED



## UNCLASSIFIED

### (U) ALL-ELECTRIC VEHICLE POWER SYSTEM EVALUATION

(U) The evaluation of candidate power system concepts and technologies will be greatly facilitated by simulation (Ref. 1). A sample of such a simulation for a tank-type vehicle equipped with an EM gun and an active protection system is presented here. By examining the power and energy flow throughout the system, one can examine various combinations of subsystem performance ratings by looking at different ways a power system can meet the desired performance.

(U) The specific mission cycle studied here is approximately 15 minutes long and is illustrated in Figure 1. It begins with one minute in a firing position where the vehicle remains stationary for two minutes. Two salvos of two shots each are fired from this position with 5 seconds between shots, and 35 seconds between salvos. Each of these shots extracts 30 MJ from the pulsed energy store. The vehicle moves out 45 seconds after firing the last shot and travels at an average speed of 20 km/hr over cross country terrain to a second firing position (transit time = 10 min). While in transit, the vehicle fires a protection system twice, with discharges of 15 and 10 MJ respectively. A final twin 30 MJ shot salvo is fired as the vehicle slows to enter the second firing position.

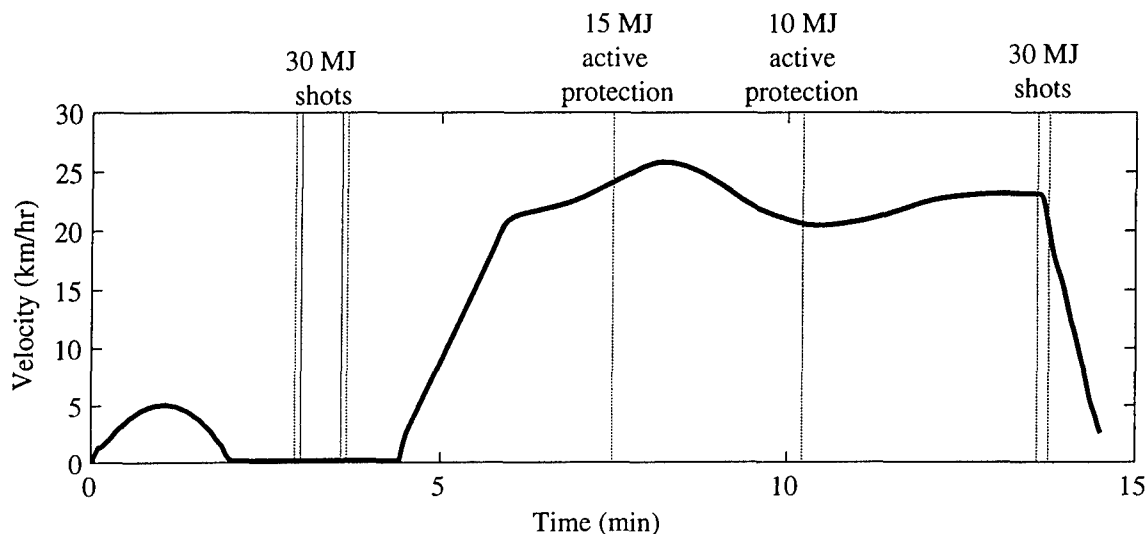


Figure 1. (U) Notional mission profile for combat vehicle.

(U) Figure 2 shows results of such a simulation for an all-electric combat vehicle with a 1.5 MW prime mover and an available pulsed energy storage capacity of 90 MJ. An intermediate energy store (battery) is used to augment the turbine/generator only during its transient periods when the turbine response time is limited by its inertia. The same performance could also be achieved by depleting the intermediate energy store to augment the prime power if a higher power weapon charger is used. The benefit of such an arrangement could be in reduced turbine size. The

UNCLASSIFIED

penalty is that the intermediate energy store must also be charged periodically during the mission to continue to provide power at critical times. If one neglects energy management completely and each of the systems used in this scenario were to operate autonomously, the total prime power required could have been over 2 MW.

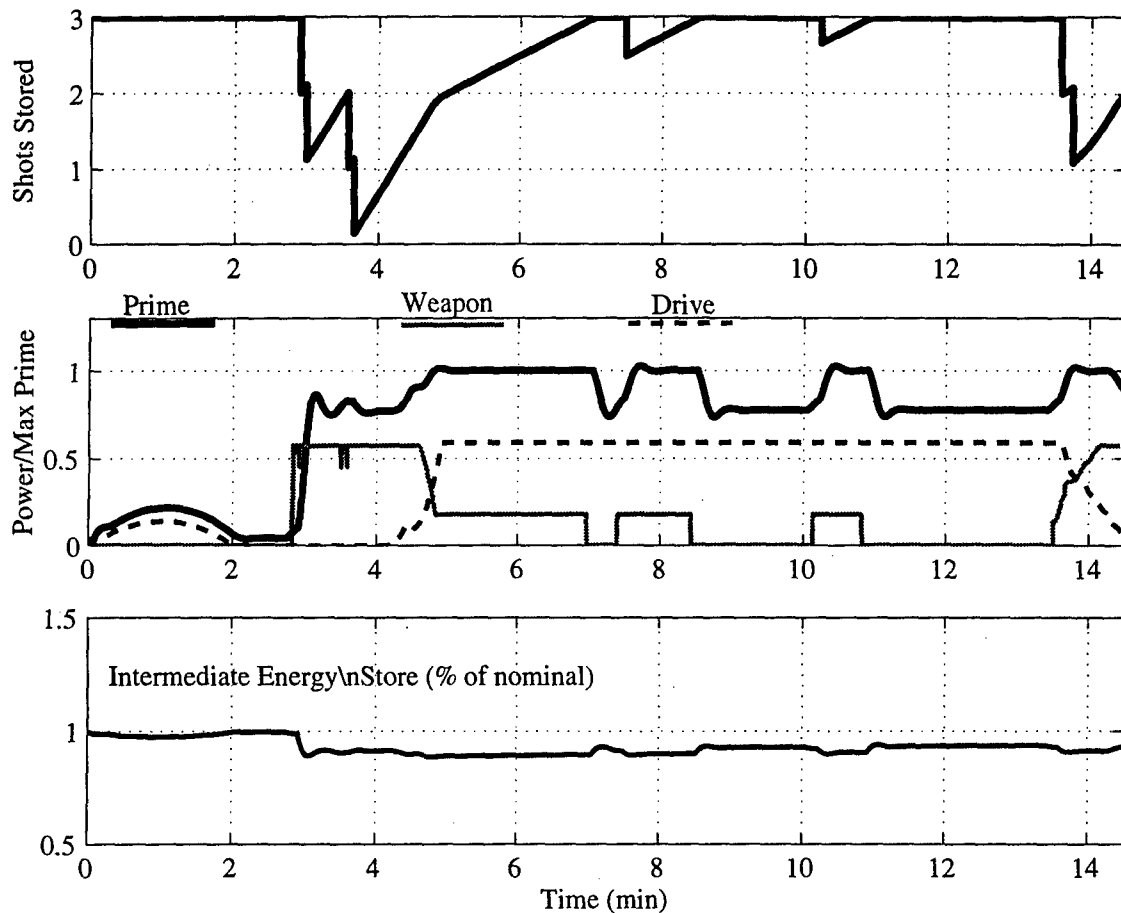


Figure 2. (U) Power system status over the mission cycle.

(U) CONCLUSIONS

(U) All-electric combat vehicles provide survivability benefits both from reduction or elimination of propellants, and from enhanced performance enabled by the electrical subsystems: weapons, drives, suspensions, and active protection. These performance benefits come with a penalty in volume related to the power supplies. Optimal use of these power supplies through the use of energy management will be required for practical vehicle concepts.

(U) The answers to many details alluded to in this paper will become more apparent as the Army directs more resources to the development of concept vehicle architectures and the

## UNCLASSIFIED

technologies required to bring the main systems online. The Mounted Battle Lab, in conjunction with the Directorate for Combat Developments at Ft Knox, ARDEC at Picatinny, and TARDEC are currently pursuing the development of an Electric Gun Equipped Main Battle Tank Virtual Prototype to allow for the ARMY to investigate new forms of armor fighting techniques with these new technologies, and appropriate vehicle requirements for a future tank combat vehicle (Ref. 2). ARL is conducting a program to demonstrate critical technology issues associated with electric weapons and their power systems (Ref. 3). ARPA is initiating work looking at hybrid electric vehicle architectures and technologies required for practical application to several combat vehicles (Ref. 4). ARPA also has ongoing efforts with industry looking at technologies being considered for commercial applications of hybrid electric vehicles with potential spin-offs for the military application. And finally, the U.S. Army armor school has expressed strong desire from the soldier to have an alternative to the current tank concepts in its next generation combat vehicle. All these developments indicate a push in the right direction to transition these electric vehicle concepts to the field.

### (U) ACKNOWLEDGMENTS

(U) This work was supported by the U.S. Army Research Laboratory (ARL) under contract DAAA21-93-C-0101.

### (U) REFERENCES

(U) (1) Fish, S., "Power Simulation for All-Electric Combat Vehicles," *Simulation*, vol. 65, no. 6, December 1995.

(U) (2) U.S. Army ARDEC Contract DAAE30-95-C0003 to Loral Vought Systems, "EM Gun Main Battle Tank Virtual Prototype."

(U) (3) U.S. Army ARDEC Contract DAA21-92-C-0105 to Science Applications International Corporation, "EM Gun Focused Technology Program."

(U) (4) ARPA Broad Agency Announcement 96-09, "Design and Analysis of Power Systems for Land Vehicles," January 1996.

UNCLASSIFIED

## COMPUTERIZED WIRING DAMAGE ASSESSMENT GROUND SYSTEMS

Matt Kolleck - Booz-Allen Hamilton, Inc., Dayton, Ohio

James Martin - The SURVICE Engineering Company, Aberdeen, Maryland

### INTRODUCTION

US Air Force combat experience and ABDR exercises have shown that the biggest battle damage factor in keeping aircraft grounded for maintenance is assessing wiring system damage and making suitable repairs. The problem is compounded by the fact that on many aircraft the wires are only marked where they terminate at connectors. The US Army is faced with similar problems. During the 1987/1988 Abrams Live Fire program, a tank crew, Organizational Maintenance Team (MT) and Maintenance Support Team (MST) used Battle Damage Assessment and Repair (BDAR) techniques to evaluate combat reparability of the M1/M1A1 tank. Assessments and repairs were conducted for 54 shot events on five different M1 and M1A1 tanks. While the BDAR teams were able to identify and repair much of the damage which resulted from the live fire shots, one of the most significant problem encountered by them was the difficulty in assessing and repairing electrical wire damage. Many of the M1/M1A1 wiring harnesses are 2 to 4 inches thick and contain up to 128 wires which are marked only at the connectors to the line replaceable units (LRUs).<sup>1</sup>

Two major reasons for the difficulty of repairs of wire damage are:

- The volume of technical data required to troubleshoot and evaluate electrical circuits.
- The skill level required to trace the wiring and identify the systems that each individual wire services.

Computer-based techniques may present a possible solution for electrical troubleshooting difficulties by presenting crews and technicians the capability to rapidly access wiring technical data now available only in technical manuals. An assessor-centered identification logic-flow program could produce significant payoffs to users as follows:

- reduce skill level dependency for wiring assessment tasks to the lowest maintenance level forward on the battlefield.
- prove a simple means to quickly identify mission critical wires so that damaged vehicles can be expeditiously repaired and returned to combat.
- reduce the time required for assessing wiring damage.
- reduce the time required for repairing wiring damage.
- reduce the dependency on hard copy troubleshooting and repair manuals.

---

<sup>1</sup> Battle Damage Repair of Tactical Weapons: An Assessment, Logistics Management Institute Report RE801R1, August 1989.

- reduce the time required for troubleshooting and damage repair of inoperable wiring components during normal training and peacetime maintenance operations.
- provide for the integration of data management program into existing troubleshooting tools.
- easy to update and distribute changes to the maintenance aid program.

## STATEMENT OF THE PROBLEM

The application of electronic technology to manage and control critical combat functions of a vehicle has significantly increased. Electrical systems of modern weapon systems are extremely complex and, therefore, difficult to assess and repair quickly when they are damaged. Rapid assessment of combat-induced damage is a major requirement of the BDAR program. Advanced analysis tools and techniques for wiring systems are required to ensure a timely and responsive BDAR program. As more sophisticated systems are fielded, the problem can only be exacerbated. Electronic management of firepower, mobility and command and control components requires a large number of wires and wire bundles. As the technologies advance however new or retrofitted weapon systems become dependent on electronics, the survivability and fightability of these vehicles becomes very much a factor of how efficiently maintenance personnel can quickly and correctly troubleshoot and repair electrical wire harnesses.

## UNDERSTANDING THE PROBLEM

The purpose of battlefield damage assessment and repair (BDAR) is to rapidly return disabled combat vehicles to the operational commander by expediently fixing, bypassing, or jerry-rigging components to restore the minimum essential systems required for the vehicle to be mission capable, or at a minimum, to be capable of self-recovery. Battlefield damage can be caused by a number of sources or conditions: random failures due to material fatigue, operator errors, accident, and the most severe, hostile fire.

The way electrical wiring harnesses are currently routed through ground vehicles has caused them to be susceptible to hits by penetrators and spall from practically attack aspects. The position of LRUs requires wiring harnesses to be strung around the interior of the vehicles and attached to the inside walls of the hull and turret. As a result, the total presented area for all wiring harnesses installed in the vehicles is large. Recent live fire programs have identified these long exposed spans of wire harnesses and bundles between the LRUs as a vulnerability problem. Unprotected wires running throughout the vehicle are very susceptible to being hit from all attack aspects and from a variety of damage mechanisms which might perforate the interior volume of a vehicle.

Because of the amount of wires, their routing, and the complexity of the electrical system, assessment of vehicle damage is difficult. A computerized assessor aid or tool to assist the vehicle crew and maintenance crews in evaluating and identifying damage to

wiring harnesses so that they may be repaired as required. The assessor aid should, at a minimum, provide identification of each wire and terminal connectors/pins and their locations, wire gage, wire length, and the critical components they service. The aid should be vehicle specific and be part of a man portable test set that is sufficiently rugged to be useful in a hostile environment, or it should be hosted with the vehicles built-in-test equipment.

For such an aid to be useful and effective, it must be usable at the lowest maintenance level where the first assessment of damage occurs. The lowest level of maintenance is at the crew. By providing an initial assessment of the damage to the vehicle, the crew can provide a more accurate assumption of requirements for repairing the vehicle and putting it back into the battle. The immediacy of the assessment and any subsequent report, is very important to a unit's mission. A computerized wiring aid would help the crew to make a quick determination as to the extent of repairs required to damaged wiring harnesses which could help commanders judge the amount of time the vehicle will be unavailable to fight. Furthermore, if the vehicle is damaged in a forward battle area, it is imperative that the crew attempt to move the vehicle to a position where additional combat damage cannot be inflicted. Such an aid could be used to assist the crew in determining a possible "quick-fix" solution that will allow the vehicle to be moved into a protected area.

## APPROACH

A computerized wiring aid as described above has been successfully developed and tested for the US Air Force.<sup>2</sup> The prototype system was demonstrated on an F-15 aircraft during a field test at the Joint Command Aircraft Battle Damage Repair Exercise held at Davis Monthan Air Force Base, AZ on October 31, 1994. For the exercise, five wires in the aircraft were selected at random location and cut. The primary objective of the demonstration was to quantify the amount of time saved in locating endpoints (connector and pin) of the five wires cut. Two teams of technicians were assigned to troubleshoot and locate the wire damage; one team used doctrinal troubleshooting procedures, the other used the computerized maintenance aid. The team using normal troubleshooting procedures were able to identify the connectors/pins to one end of the cut wires in 90 minutes but after four hours could not locate the other ends. By contrast, the team utilizing the computerized maintenance aid found all connectors/pins to both ends of the five cut wires in 35 minutes. This clearly demonstrates that when wiring damage is addressed using the ABDR tool, significant time savings result.<sup>3</sup> Wiring in many types of weapon platforms have common components and attributes.

The same processes and procedures used to develop the aircraft computerized maintenance aid may very easily be applied to ground systems. To initiate the development

---

<sup>2</sup> Development of a Computerized Aircraft Wiring Maintenance Aid, WL-TR-92-3077, April 1992.

<sup>3</sup> Computerized Maintenance Aid Provides A Faster Way to Repair Aircraft Wiring Damage, SURVIAC Bulletin, March 1995.

of such an aid for ground systems an extensive library of vehicle specific data are required. For most recent production vehicles, the data require for implementing a computerized wiring aid are available in technical manuals, engineering drawings, test equipment manuals, and training material. This data can be extremely detailed and includes information like vehicle serial numbers, electrical system schematics, wire harness numbers, routing data for all wires and wire harnesses, mission essentiality of each function supported by the individual wires, terminal locations, connector pin numbers, connector numbers, and connector locations. Results of the Air Force effort found that a significant quantity of the data described above is available in automated form for many of the recently fielded weapon systems. After data has been assembled, construction of the assessor aid follows a very straight forward process as listed below.

1. Divide the vehicle into zones so that the evaluation of damage may be isolated into a small manageable area.
2. Develop mission critical component lists for each wire, wire harness, and bundle.
3. Populate and modify the current aircraft maintenance software with the wire data based on the mission critical list.
4. Test, correct errors, and verify the system functionality.

The program's troubleshooting logic flow is assembled for two levels of assessment. The crew-centered logic flow is designed to focus the crew on the fault indications that are observed during the normal operation of a vehicle. This logic flow, depicted in Figure 1, will lead the crew through a series of questions that require them to evaluate the weapon system operation from the wires located in the damage zone to components serviced by the damaged wires.

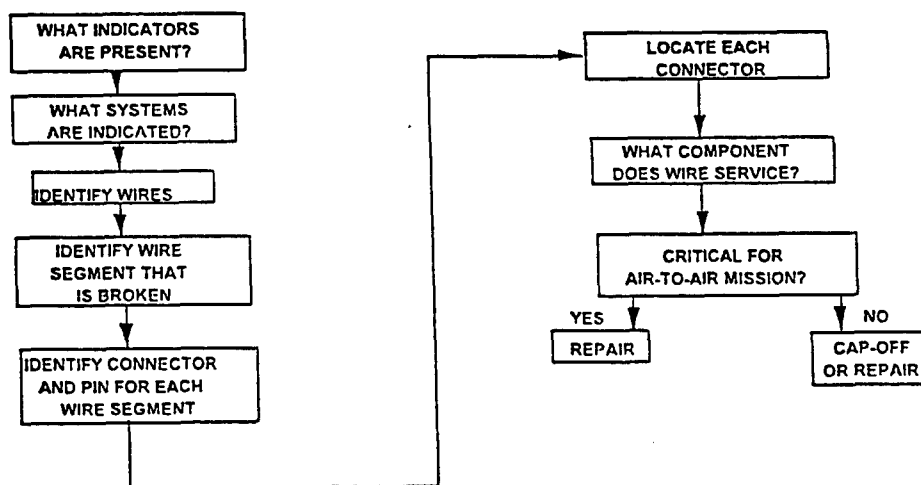


Figure 1. Logic Flow (Crew-Centered).

A second logic flow is designed to focus on the higher level of maintenance assessment where a crew may not be available to explain fault symptoms which occur as a

result of the damage. The assessor-centered logic, shown in Figure 2, initiates the troubleshooting process at the point of damage and leads the assessor through a troubleshooting process designed to identify termination points of damaged mission critical wires. The user identifies and selects the problem being experienced, enters the information, and the aid returns the connector information needed to initiate the repair process.

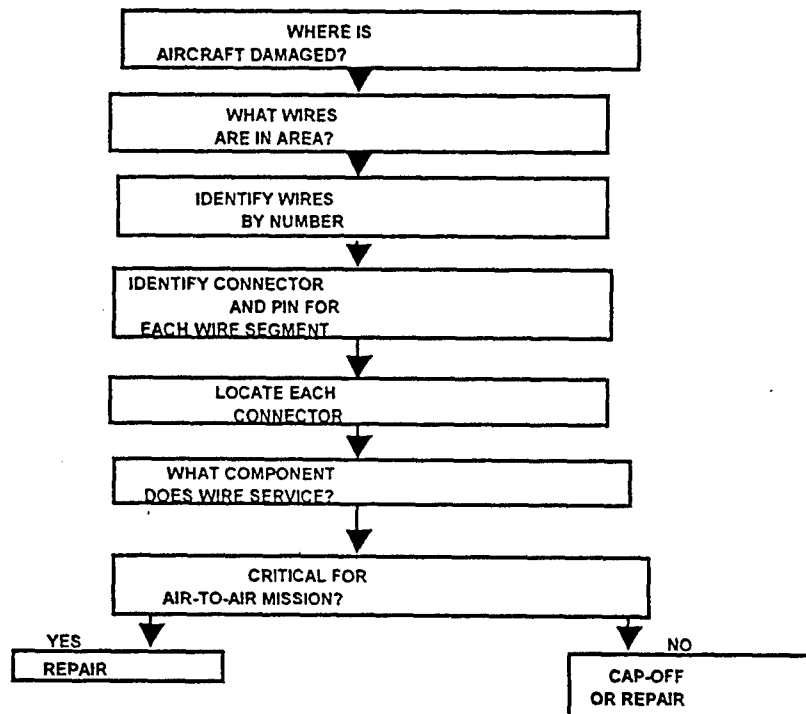


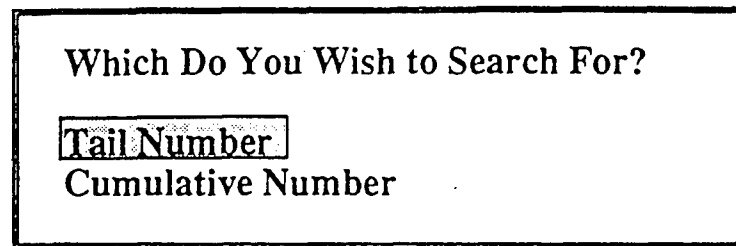
Figure 2. Logic Flow (Assessor -Centered).

## PROTOTYPE COMPUTER WIRING AID

The prototype computer wiring aid software program was developed and tested for the US Air Force. The program was written in C++ language and is currently installed on an IBM 286, PC-compatible microcomputer with 640K RAM, 20 MB hard drive. There are five database files in the program which contain wire data, wire bundle data, end connector/pin data, and aircraft data. Eight screens are used to prompt the assessors and to identify information necessary for evaluating damaged aircraft wiring. All tables and output screens could be modified to accommodate a specific ground weapon system.

When the wiring aid program is started, a title screen (Figure 3) appears requesting the user to specify either an aircraft identification number or a cumulative number. This allows the user to choose the method of designating the aircraft.





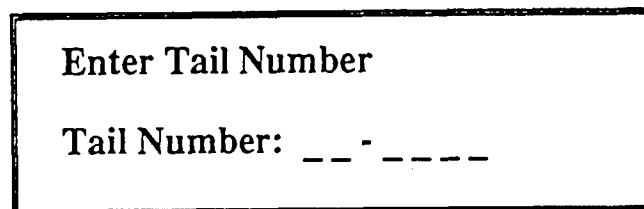
Which Do You Wish to Search For?

**Tail Number**

Cumulative Number

Figure 3. Title Screen.

The most common method is by choosing the tail number (Figure 4). This choice initiates the program and by using the <UP> and <DOWN> arrow keys choose between the tail number or the cumulative number.

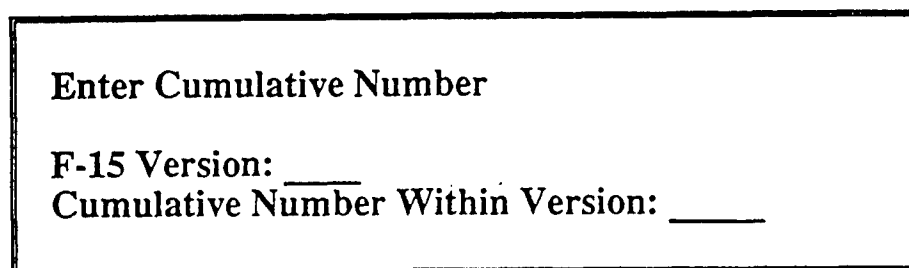


Enter Tail Number

Tail Number: \_\_ - \_\_\_\_

Figure 4. Tail Number Search Screen.

If the cumulative number is selected, the prompt (Figure 5) will require a version of the aircraft and cumulative number within the version to be input.



Enter Cumulative Number

F-15 Version: \_\_\_\_

Cumulative Number Within Version: \_\_\_\_

Figure 5. Cumulative Number Search Screen.

Should the user incorrectly enter an identification, the "Aircraft not found!" screen (Figure 6) will be displayed.



— ERROR —

Aircraft Not Found!

(Press Any Key)

Figure 6. Incorrect Identification Screen.

After the program has selected the requested aircraft from the database, a screen defining the aircraft sections appears (Figure 7) and the user selects the section based on the location of damage.

Please Enter the Section of the Aircraft Which was Damaged:

Nose (L) [2-L]	ECS Area (L) [6-L]
Nose (R) [2-R]	ESC Area (R) [6-R]
No. 2 Equipment Bay (L) [4-L]	<u>Center Fuselage (L) [7,9 L]</u>
No. 2 Equipment Bay (R) [4-R]	Center Fuselage (R) [7,9 R]
No. 3 Equipment Bay (L) [4-L]	Acft Fuselage and Fin (L) [12,13,14-L]
No. 3 Equipment Bay (R) [4-R]	Acft Fuselage and Fin (R) [12,13,14-R]
Nose Wheelwell [5]	Wing (L) [11-L]
Cockpit (L) [3-L]	Wing (R) [11-R]
Cockpit (R) [3-R]	Inboard Pylons
No. 5 Equipment Bay (L) [4-L]	Outboard Pylons
No. 5 Equipment Bay (R) [4-R]	Miscellaneous
	Centerline Pylon

Figure 7. Aircraft Section Selection Menu.

With the section identified, the program searches the database and displays the bundle numbers (Figure 8) for each wire located in the selected area.

Select Bundle in Center Fuselage (L) [7,9-L]

68A752094	68A752441	68A752443	68A755026
68A755027	68A755208	68A755210	68A755212
68A755223	68A755234	68A755237	68A755239
68A755251	68A755270	68A755274	68A755277
68A755401	68A755402	68A755403	68A755404
68A755405	<u>68A755407</u>	68A755408	68A755409
68A755413	68A755414	68A755417	68A755421
68A755422	68A755424	68A755426	68A755428
68A755431	68A755433	68A755434	68A755435
68A755436	68A755438	68A755439	68A755440
68A755441	68A755443	68A755445	68A755446
68A755447	68A755449	68A755450	68A755451
68A755452	68A755453	68A755454	68A755455
68A755457	68A755459	68A755461	68A755462
68A755463	68A755466	68A760214	68A760401

Figure 8. Wire Bundle Selection Menu.

The user determines which bundle has been damaged, chooses the appropriate bundle number on the wire select screen, and the program will display the individual wires that are part of the bundle (Figure 9, top window). By using the arrow keys the, the user can highlight each individual wire and the critical mission and maintenance information will appear in the bottom window.

Select Wire in Bundle 68A755407 in Section P:			
*A174A	*A174AIN	*A174AOU	<b>*A185C20</b>
*A189C20	*A222C20	*A2406D22	*A2407E16
*A2407F12	*A2408E16	*A2408F12	*A2424M24
*A2424P24	*A2424MSH	*A2424PSH	*A2425M24
*A2425P24	*A2426MSH	*A2426PSH	*A2426M24
*A2426P24	*A2427M24	*A2427P24	*A2502B24

A185C20
MISSION CRITICAL
Function: Armament
Gage: 20
Wire type: Single conductor, stranded silver coated copper
Connection 1: 52P-P151 Pin: FF
Door: 83, 85L
LRU: PLUG L AMAD FIREWALL DISC
Connection 2: 52P-R156 Pin: H
Door: 83, 85L
LRU: PLUG AMAD BAY/CL PYLON DISC

Figure 9. Wire Selection Menu.

To move to a different zone or to identify a different bundle, the user presses the <ESCAPE> key to display an option menu (Figure 10). The selection may be changed by moving the highlight bar to a desired option and pressing the <ENTER> bar.

Select Wire in Bundle 68A755407 in Section P:

Select Option	*A174AIN	*A174AOU	*A185C20
Bundle	*A222C20	*A2406D22	*A2407E16
Section	*A2408E16	*A2408F12	*A2424M24
Aircraft	*A2424MSH	*A2424PSH	*A2425M24
Quit	*A2426MSH	*A2426PSH	*A2426M24
	*A2427M24	*A2427P24	*A2502B24

A185C20

MISSION CRITICAL  
Function: Armament  
Gage: 20  
Wire type: Single conductor, stranded silver coated copper  
Connection 1: 52P-P151 Pin: FF  
Door: 83, 85L  
LRU: PLUG L AMAD FIREWALL DISC

Connection 2: 52P-R156 Pin: H  
Door: 83, 85L  
LRU: PLUG AMAD BAY/CL PYLON DISC

Figure 10. Option Menu.

The connectors and pins of each damage wire are located by working through the information provided in the wire select screen. Based on the mission critical definition provided for each particular wire, the user may initiate repair to return a function or "cap" the wire ends until normal maintenance can be afforded.

Changes in threat, support concepts, and weapon system technology are taking place that will radically alter the way maintenance must be performed. Combat units will be forced to depend less on bulky test equipment and large scale support operations to maintain their technologically complex weapon system. Computerized devices and integrated databases will be used to reduce the information burden placed on the crew and technicians performing maintenance tasks. The computerized wiring maintenance aid is one such device which may help ground forces maintain a superior operational edge on the battlefield of tomorrow.

**UNCLASSIFIED**

**THIS PAGE INTENTIONALLY LEFT BLANK**

**UNCLASSIFIED**

**UNCLASSIFIED**

## **INTEGRATED SURVIVABILITY ANALYSES (ISA) - REAL TIME (U)**

Bahram Fatemi, PhD  
and  
James Wiederrich, PhD  
United Defense L.P.  
Santa Clara, CA 95052

### **ABSTRACT (U)**

(U) Trends in ground vehicle weight and anti-armor penetration preclude armor as the sole solution for survivability. Vehicle survivability solutions require the proper selection of several survivability technologies to give the combined effect necessary to meet technical and cost requirements. This presentation gives an overview of the Integrated Survivability Analyses (ISA) approach being developed at United Defense to run in real time on engineering graphic workstations. This ISA approach accounts for the synergy and combined effect of survivability technologies, and the real time computation capability allows rapid evaluation of many design alternatives to be performed during the concept development phase. This ISA real time approach thus facilitates the selection of the proper mix of survivability technologies necessary to meet the technical and cost measures.

**UNCLASSIFIED**

Approved for public release

UNCLASSIFIED

UNCLASSIFIED

**United Defense**

**FMC/BMY**

# **Integrated Survivability Analyses (ISA) - Real Time**

Bahram Fatemi, PhD  
James L. Wiederrich, PhD  
United Defense  
Santa Clara, CA 95052

UNCLASSIFIED

UNCLASSIFIED

## **Why ISA?**

### **Armor Alone Won't Do It**

- Approaching Practical Weight Limits
- Increasing Anti-Armor Penetration

**Require Proper "MIX" of Survivability  
Technologies to Meet Technical &  
Cost Requirements**

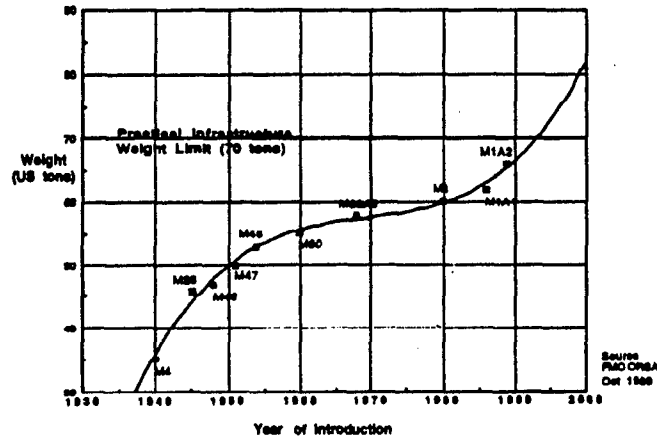
UNCLASSIFIED

UNCLASSIFIED

UNCLASSIFIED

UNCLASSIFIED

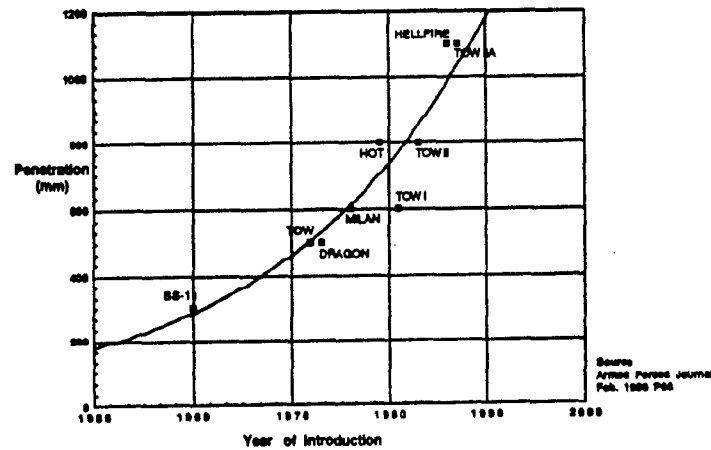
## US Tank Weight Trends



UNCLASSIFIED

UNCLASSIFIED

## Anti-Armor Penetration Trends



UNCLASSIFIED

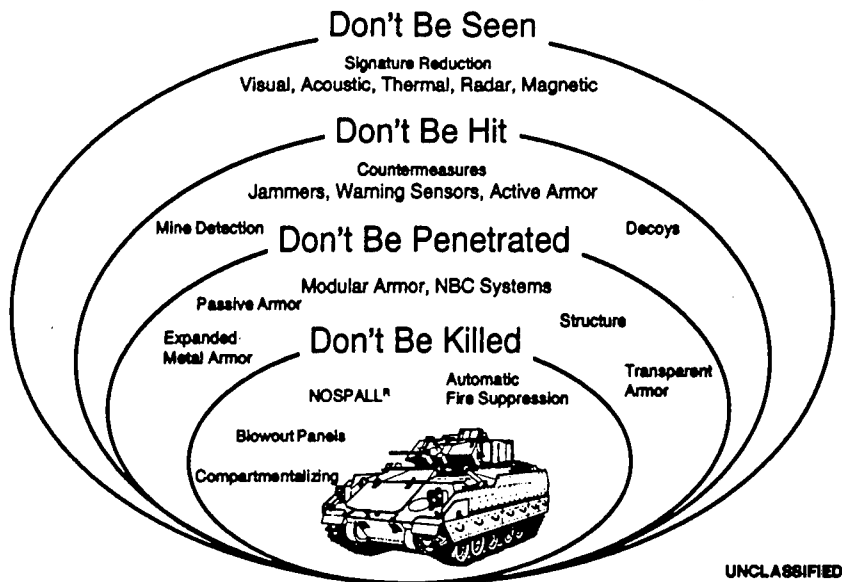
UNCLASSIFIED



UNCLASSIFIED

UNCLASSIFIED

## Layered Survivability



UNCLASSIFIED

## Ground Vehicle Survivability Focus

Survivability is the Combined Effect of:

- Detection Avoidance
- Acquisition / Hit Avoidance
- Damage Avoidance
- Kill Avoidance

Probability of Survival,  $P_s$

$$P_s = 1 - \{P_{\text{det}} \times P_{\text{acq/det}} \times P_{\text{hit/acq}} \times P_{\text{pen/hit}} \times P_{\text{kill/pen}}\}$$

UNCLASSIFIED

UNCLASSIFIED

UNCLASSIFIED

UNCLASSIFIED

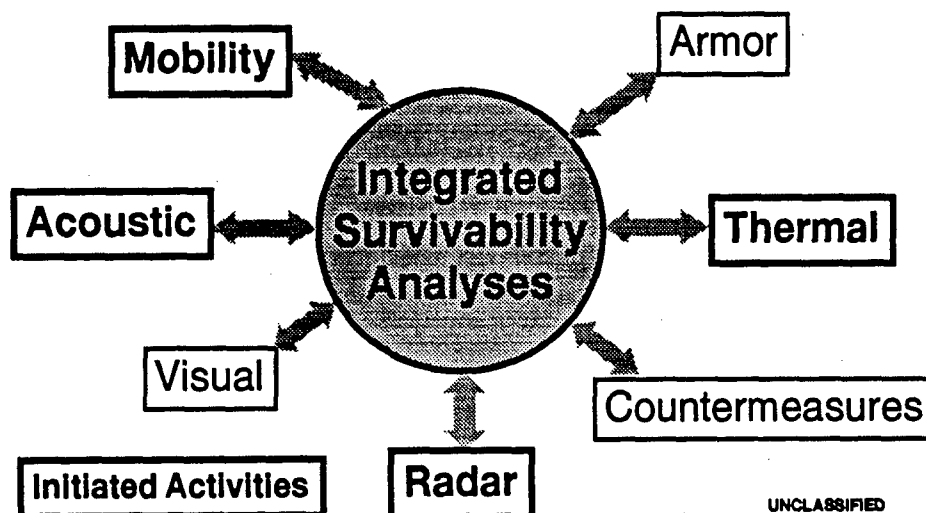
## Why ISA - Real Time ?

- Rapid Evaluation of Design Alternatives in Virtual Prototype
- Evaluate the Synergy and Combined Effect of Design Variables
- Visual and Graphical Presentation of Results
- Interactive Investigation of "What If" Scenario
- Applicable to Simulators and Virtual Environments

UNCLASSIFIED

UNCLASSIFIED

## Current UDLP ISA Activities



UNCLASSIFIED

UNCLASSIFIED

**UNCLASSIFIED**

UNCLASSIFIED

## **Real Time Thermal Signature Model**

- Dynamic Modeling of "Hot Spots" on the Bradley Fighting Vehicle
  - Roadwheel
  - Shock Absorber
  - Track, Sprocket and Idler
  - Gun Barrel
  - Exhaust Gas
- Thermal Model Validated Against UDLP's Lab Test Data
- Integrated into Dynamic Model of Vehicle to Provide Real-Time Transient Temperature Profile of Vehicle Hot Spots

UNCLASSIFIED

UNCLASSIFIED

## **Real Time Radar Signature Modeling**

- Predict the Radar Cross Section (RCS) of a Vehicle
- Basic Scattering Types Included are: Polygons, Cavities, Cylinder, Noise Sources and Wires
- RCS is a Function of Vehicle Position and Orientation and Position and Frequency of the Radar Sensor
- Integrated into Interactive Vehicle Dynamic Model to Provide Real-Time Prediction of RCS
- RCS Output Values Compare Favorably with Unclassified RCS Data Collected by UDLP

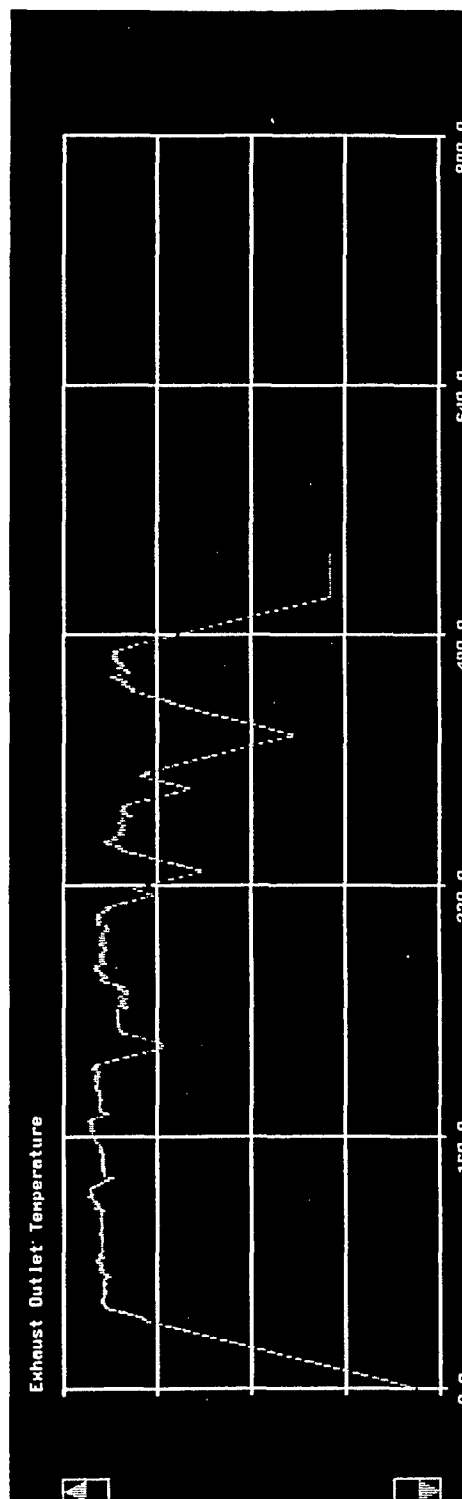
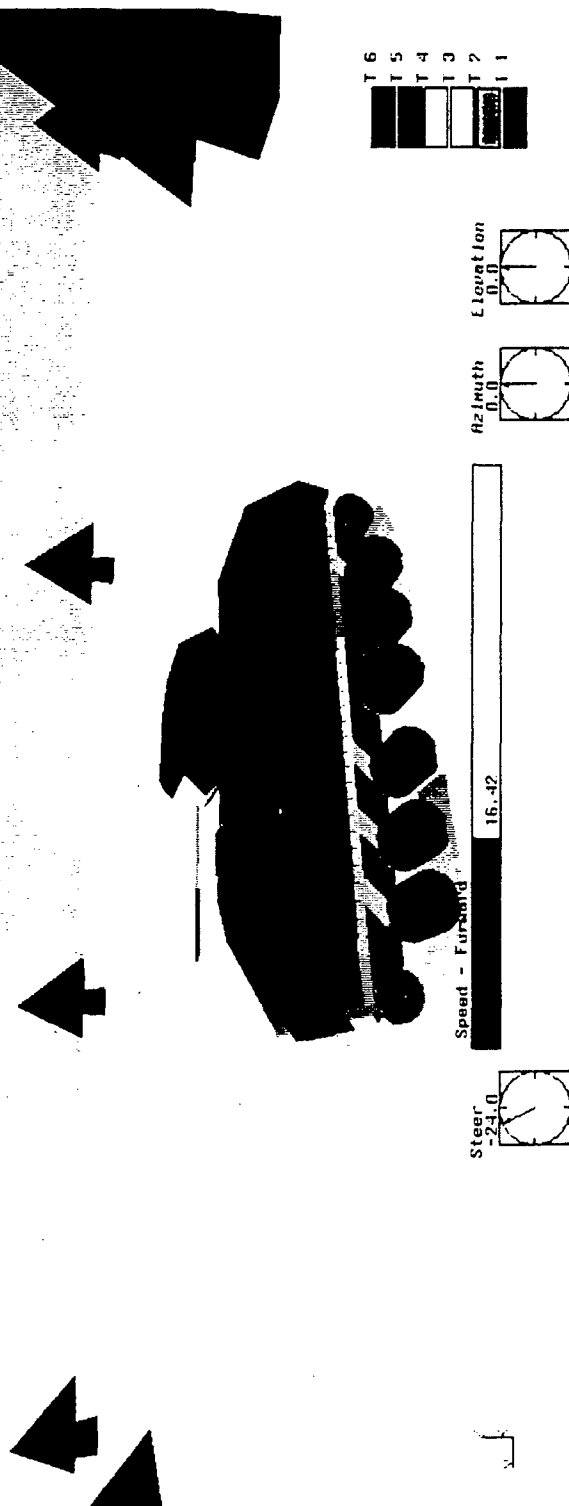
UNCLASSIFIED

**UNCLASSIFIED**

# Real Time Thermal Signature Model

Display Radar Thermal BeamCue

TIME = 532.79999  
FRAME NO. 3552  
FRAME RATE = 4.55



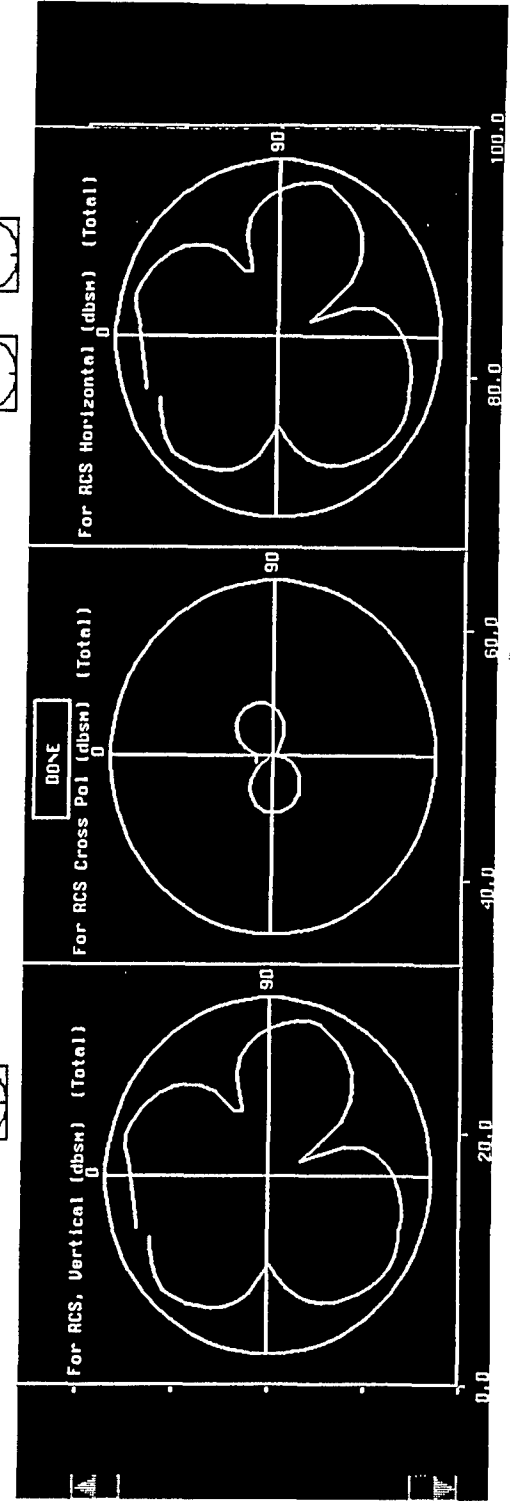
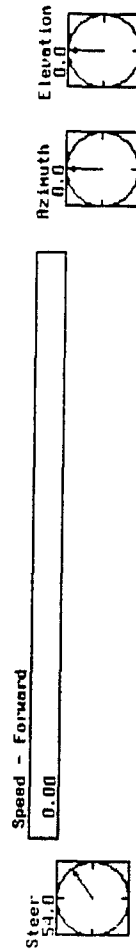
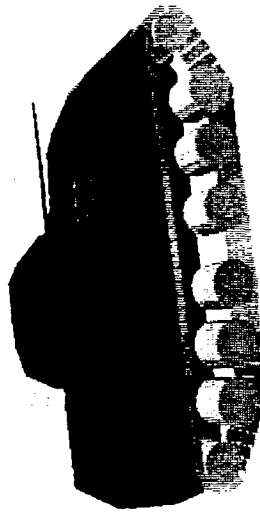
UNCLASSIFIED

UNCLASSIFIED

# Real Time Radar Signature Model

00 Load 00 Image Record 1/00 00 Display 00 Analysis Type Radar Thermal Remote

TIME = 64.85000  
FRAME NO. 433  
FRAME RATE = 3.03



UNCLASSIFIED

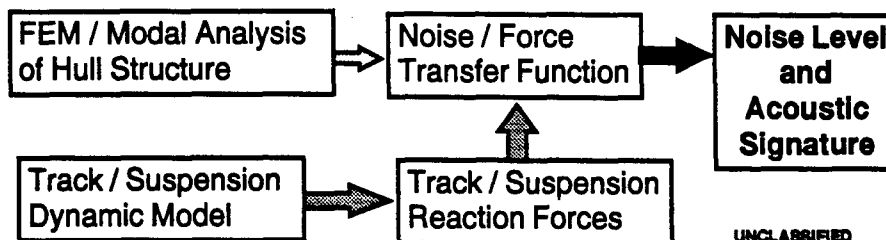
UNCLASSIFIED

UNCLASSIFIED

UNCLASSIFIED

## Real Time Acoustic Signature Modeling

- Procedure to Calculate Interior and Exterior Noise of Tracked Vehicles Based on Speed and Distance
- Acoustic Modeling Integrated into Dynamic Vehicle Model to Display Noise Level & Signature in Real-Time
- Good Correlation with Test Data from Quiet Components for Land Vehicles Contract



UNCLASSIFIED

## Conclusions

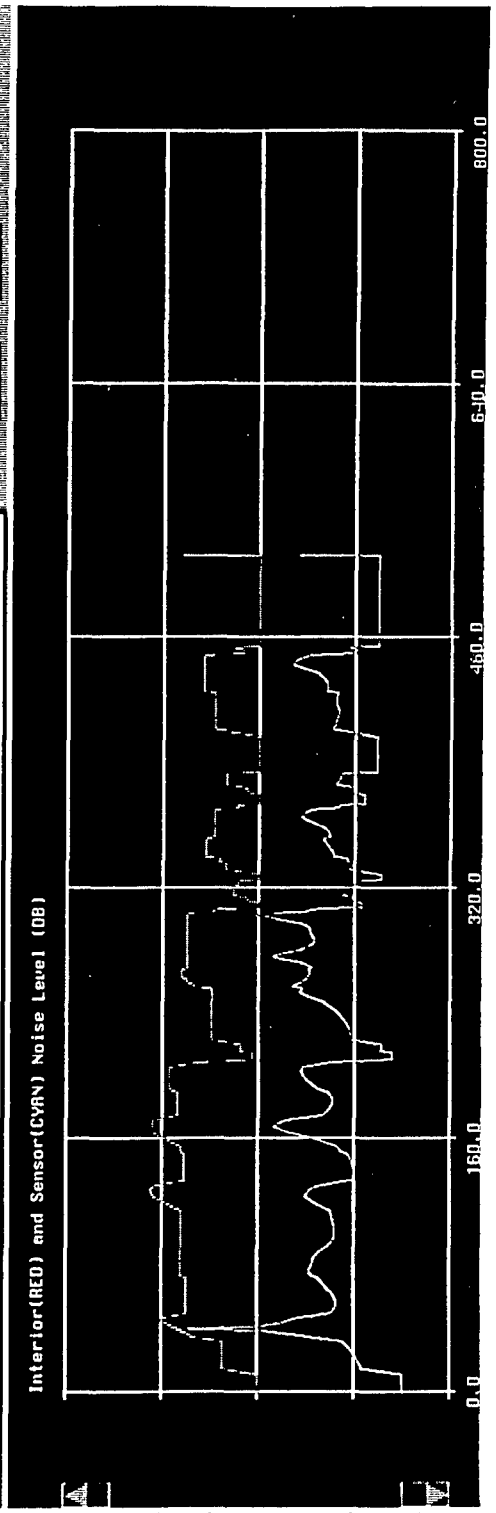
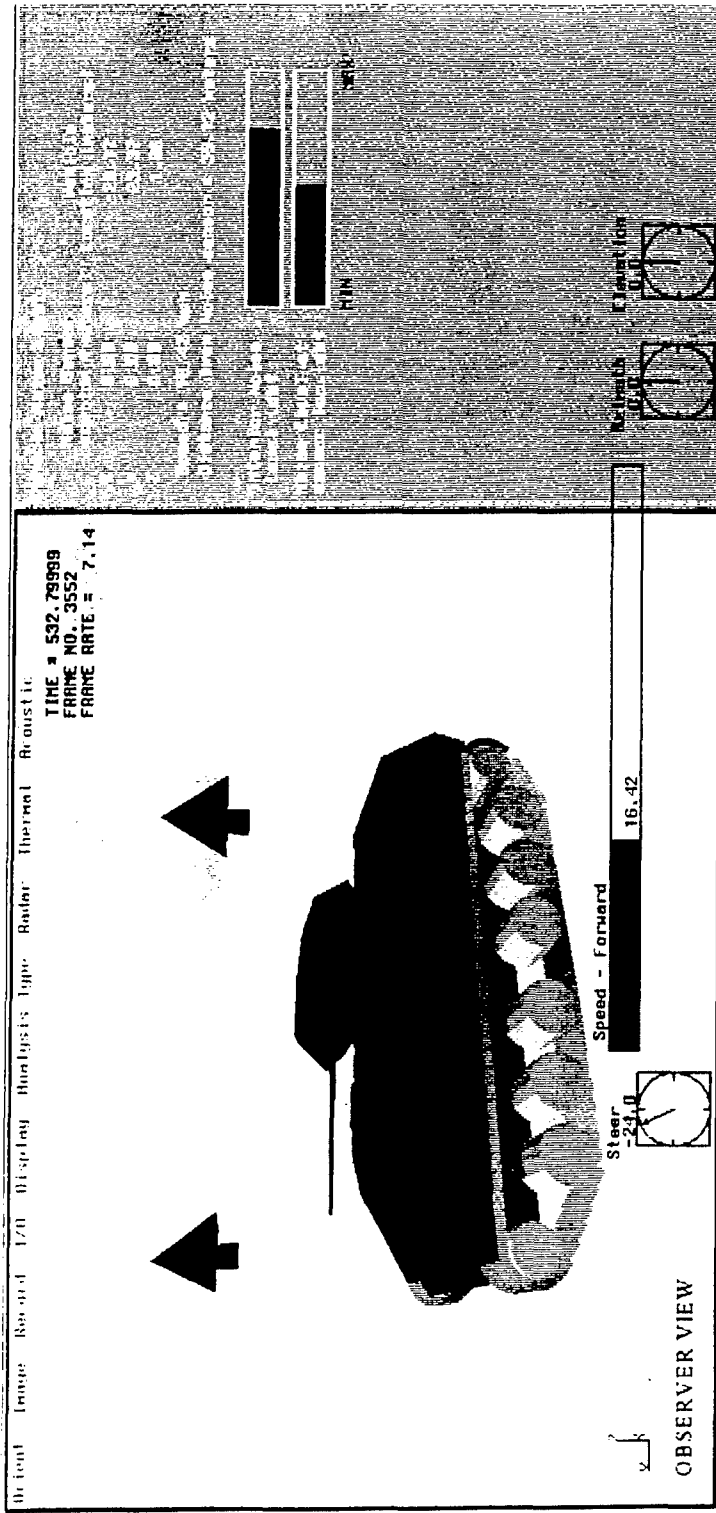
- ISA Approach is Being Developed for Vehicle Concept Evaluation
- Real Time Simulation of Vehicle Mobility and Thermal, Radar and Acoustic Signatures
- ISA Capability Facilitates Evaluating the Synergy and Combined Effect of Design Alternatives
- Methodology Allows Rapid Selection of the Proper Mix of Survivability Technologies to Meet Technical & Cost Requirements

UNCLASSIFIED

UNCLASSIFIED

# Real Time Acoustic Signature Modeling

UNCLASSIFIED



UNCLASSIFIED